



Nikon
100th
anniversary

A1ways Evolving

NEW High Definition 1K Resonant Scanner

Open up a world of new imaging strategies and possibilities with the latest upgrade to Nikon's always evolving A1R+ confocal microscope system. The all-new High Definition 1K Resonant Scanner delivers high resolution images at ultra-high speed. The new scanner also provides 4x the field of view at the same resolution usually generated by a normal 512x512 scanner. The wide dynamic range and reduced noise level raises the bar for image quality in resonant scanners.

For more information, go to www.nikoninstruments.com/a1r
or call 1-800-52-NIKON.



Cell

Best of 2017



Featuring a Collection of SnapShots

DISCOVER THE FUTURE OF CELL ANALYSIS

Seahorse Bioscience is now Agilent, providing the same proven technologies that help scientists make groundbreaking discoveries about the role of metabolism in disease. These technologies also enable researchers to open new windows of discovery and do more in less time:

- Rapidly measure both mitochondrial and glycolytic function in live cells in real-time
- Quickly connect physiological traits of cells with genomic and proteomic data
- Create new insights into immunology and diseases like cancer, obesity, and diabetes

See what's possible.

Learn more about Agilent Seahorse XF products at www.agilent.com/chem/discoverxf

David Ferrick, PhD, Agilent Technologies



Accuracy by Design; Not by Chance.

Human XL Cytokine Discovery Luminex® High Performance Assay

- Broad selection – 45 analytes
- Superior accuracy – see the data
- Flexible – choose your analytes
- Easy to order – save time

NEW



Learn more | rndsystems.com/human-xl

Antibody Validation

DEFINE the Intended Antibody Application

Determine the type of immunoassay required.

Consider how the target protein may be modified in sample preparation. Consider how the antigen is identified by an antibody in a given application (e.g. cell type differentiation, protein localization, protein expression, or quantification).

UNDERSTAND the Attributes of an Antigen

Find approved nomenclature of an antigen. Confirm protein sequence and molecular weight. Identify isoforms or variants.

Identify PTMs and other protein processing. Examine the presence of proteins closely related to target protein. Identify cellular localization.

ESTABLISH the Controls for Antigen Detection

Evaluate peer-reviewed literature for intended target detection. Review databases for expression levels of intended target.

Determine types of cell lines, tissues, stimulation agents, transgenic or knockout models to use for confirmation. Establish the best controls for the intended antigen.

REVIEW Antibody Vendor Information

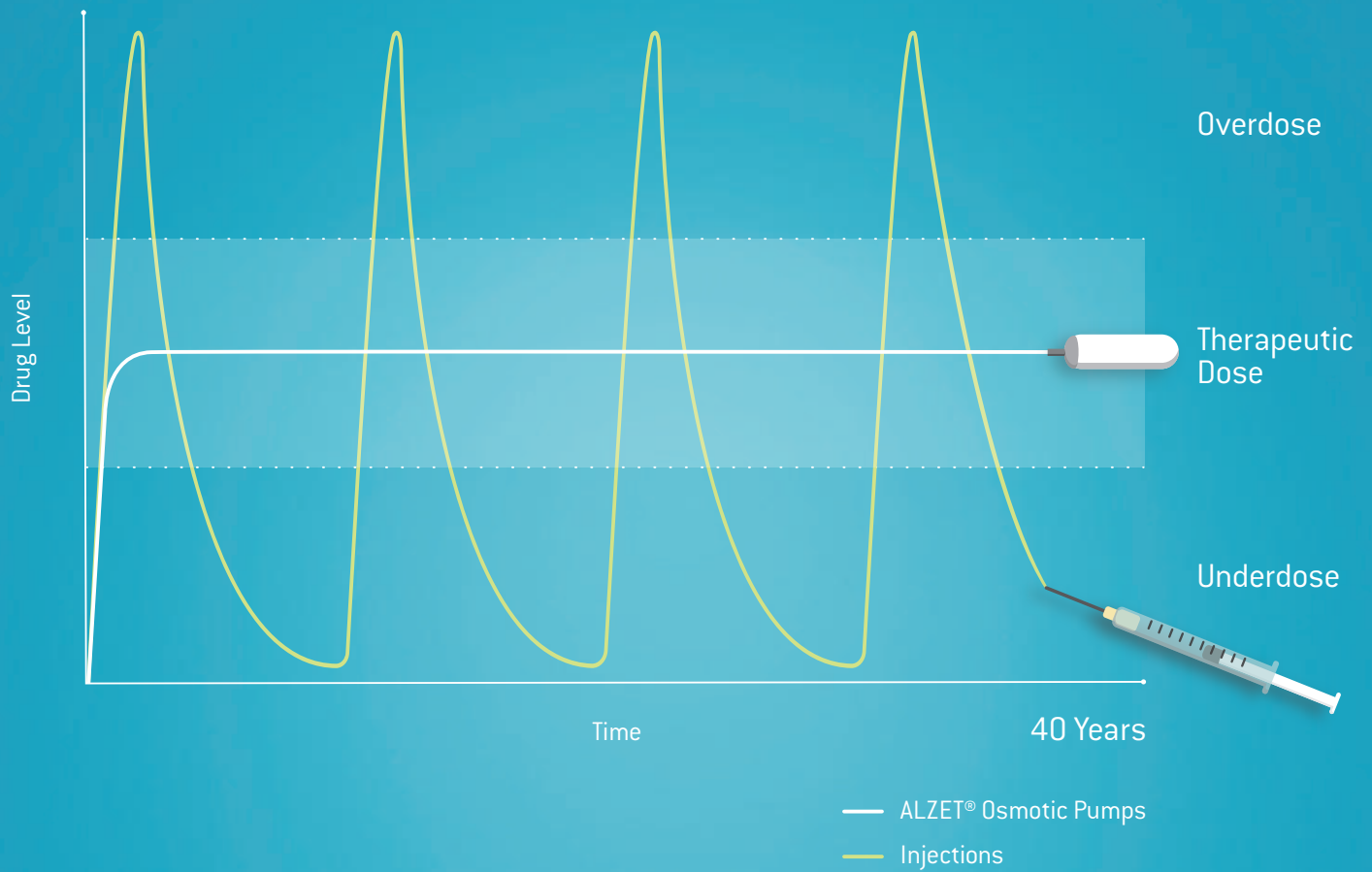
Determine the type of immunogen used for antibody production. Establish whether monoclonal or polyclonal. Determine antibody isotype. Identify clone name or product code.

Establish host species. Find species reactivity. Analyze performance data on tested applications.

PERFORM In-house Validation

Determine whether existing validation data is available. If data is unavailable, perform additional validation using the appropriate controls. Optimize the antibody concentrations and buffer conditions. Start with conditions suggested by the vendor.

Test the antibody against established controls to ensure specificity and reproducibility.



40 years of consistent dosing



ALZET Osmotic Pump, 100 µl
[actual size]

alzet[®]
OSMOTIC PUMPS

Find out more at
alzet.com/40years

A product of



©2017 DURECT Corporation
All Rights Reserved

Light re-engineered

An Employee-Owned Company

Multiline Laser Illuminator - High Power, Low Cost

LDI^{*}

- Up to 1W of power per channel
- Feedback controlled stability
- Up to 7 wavelengths
- Ultimate price to performance ratio

LDI Applications

- Spinning Disk Confocal
- Photoactivation
- Optogenetics
- TIRF
- PALM / STORM

Works with X-Light V2 & OptoTIRF

www.89north.com
sales@89north.com
+1.802.881.0302
1.877.417.8313

The World's Finest Optical Filters

TIRF Filter Sets

- Highest possible signal to noise
- Custom filter cubes for precise dichroic alignment

New Multiband Filter Sets

- Dedicated LED engine sets
- 5-band set for new Brilliant Violet™ dyes

Lifetime
Warranty

Filter sets optimized for the LDI

www.chroma.com
sales@chroma.com
+1.802.428.2500
1.800.824.7662

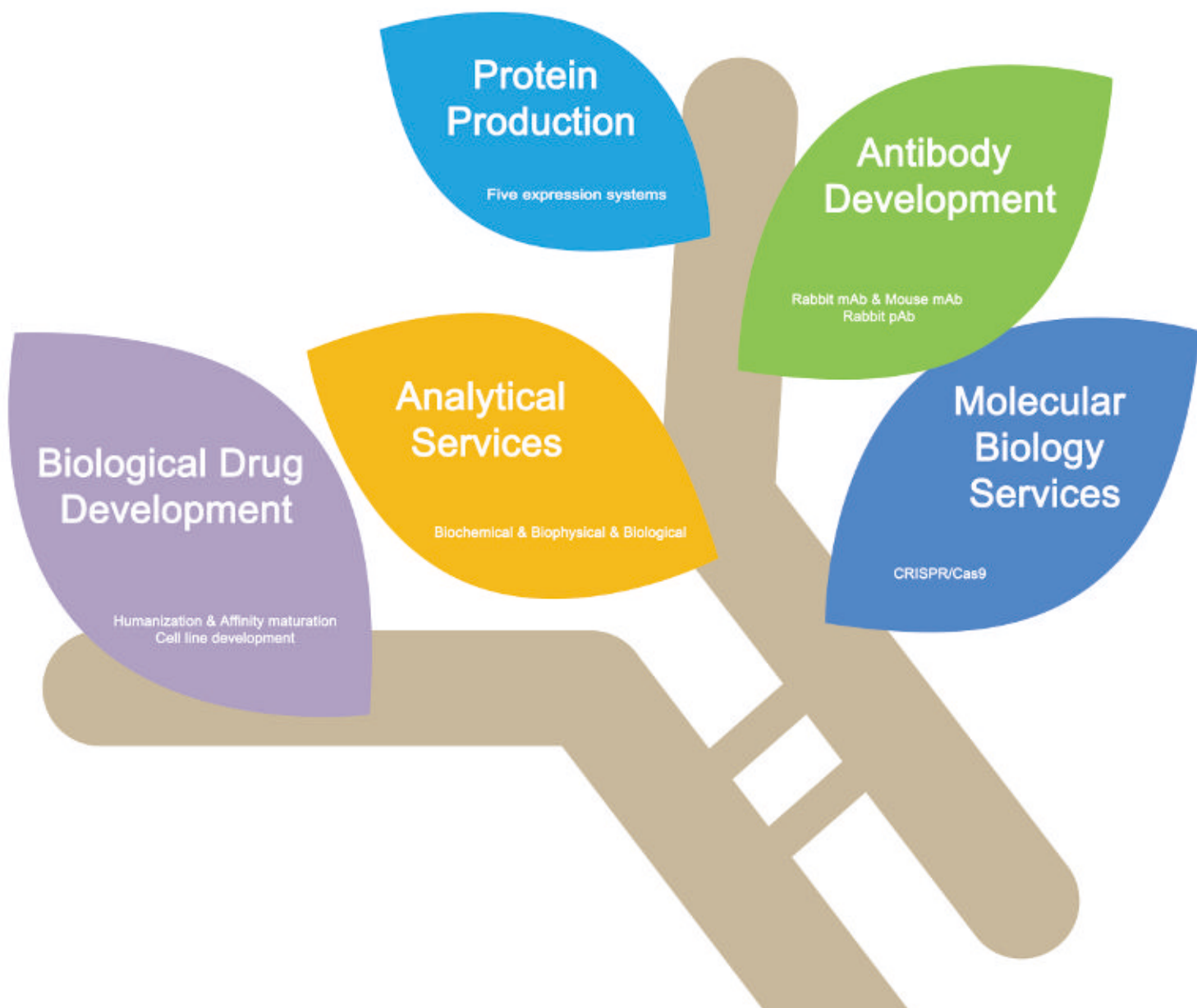


CRO & CMO Services

>16,000 Projects Accomplished; >99% Success Rate

Previous Achievements

- 12 days for protein production from DNA seq by HEK293
- 2600 liters cell culture within one week
- 99.9% monomer
- 0.01EU/mg endotoxin level





IT'S LIGHTING THE WAY TO A NEW LEVEL OF UNDERSTANDING

Your everyday and innovative cellular assays can reveal deep biological understanding, if you've got the sensitive imaging and intuitive data analysis to uncover it. The Operetta CLS™ high-content analysis system features a unique combination of microscopy technologies – automated water-immersion objectives, high-power 8x LED

illumination, true confocal optics, and an ultrasensitive sCMOS camera – to deliver all the speed, sensitivity, and resolution you need to reveal subcellular details. And with our simple, powerful Harmony™ 4.5 software, Operetta CLS lets you discover subtle phenotypic changes. Operetta CLS: When great technologies combine, what happens is illuminating.



Operetta CLS High-Content Analysis System

Check out the new Operetta CLS HCA System at www.perkinelmer.com/LightTheWay

Foreword

In 2012, Cell Press launched the “Best of” reprint collections across a number of journals, most notably *Cell*. Now, we are happy to bring you a new *Best of Cell* that focuses on articles published over the course of 2017.

For this edition, we made our selection by looking at reviews and research articles that garnered wide attention or captured editorial interest for their conceptual impact and then selecting a representative group from each of the year’s four published volumes and a broad range of topics. In addition, we’ve included a collection of SnapShots that present up-to-date, quick-read summaries to highlight several key areas of biology; we hope these SnapShots will be useful reference tools for the scientific community. The papers collected here also feature exciting methodologies and experimental procedures—including single-cell analysis of lung adenocarcinoma, engineering modified mRNA vaccines against Zika, and using gut microbiota to model neuroinflammation in a model of Parkinson’s disease.

We hope these highlighted articles will provide an overview of the different perspectives of the science we published during 2017. We recognize that no single measurement can be indicative of the “best” papers over a given period of time, especially when the articles are relatively new and their true significance may still need time to be established. Regardless of whether these papers will be highly cited in their fields, we believe they are noteworthy, and we hope you enjoy reading them.

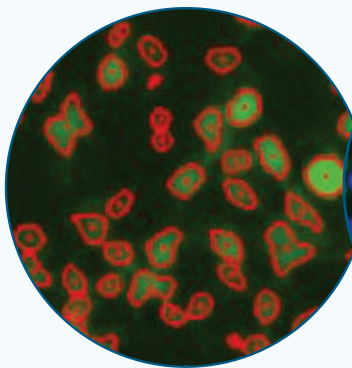
You can access the entire “Best of” collection online at www.cell.com/bestof. Also visit www.cell.com/cell to learn about the latest findings that *Cell* has had the privilege to publish and www.cell.com to find other high-quality life science papers published in the full portfolio of Cell Press journals. Please feel free to contact us at cell@cell.com to tell us about your latest work or to provide feedback. We look forward to working with you in 2018 and beyond!

As a final note, we are grateful for the generosity of our sponsors, who helped to make this reprint collection possible.

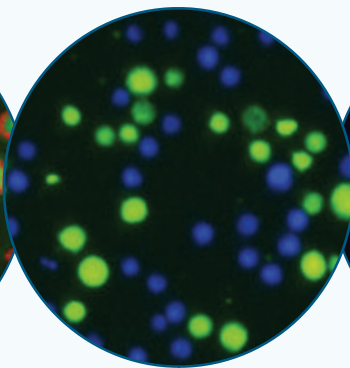
For information for the Best of Series, please contact:

Jonathan Christison
Program Director, Best of Cell Press
e: jchristison@cell.com
p: 617-397-2893
t: @CellPressBiz

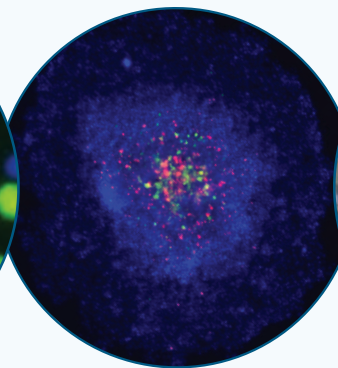
Pioneers in Automated Cell Counting and Analysis



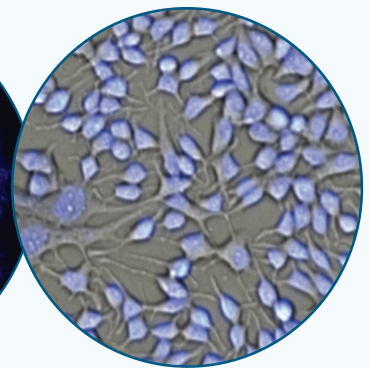
VIROLOGY



IMMUNO-ONCOLOGY



3D MODELS



SINGLE CELL ANALYSIS

Making your analysis count and your research excel in:

- ✓ High throughput foci and plaque counting
- ✓ 3D multicellular tumor-spheroid screening
- ✓ Cell mediated cytotoxicity assays for Immuno-Oncology
- ✓ Imaging, identification and quantification for single cell analyses

Learn more at www.nexcelom.com

REDEFINING more

FLUORESCENCE | CHEMILUMINESCENCE | PHOSPHOR IMAGING

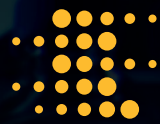


With three imaging modalities and outstanding performance, the **Sapphire™ Biomolecular Imager** expands what you can accomplish with a single image scanning instrument.

Find out what more really means—visit
azurebiosystems.com/sapphire







sartorius

No matter the time of day or night,
see exactly what happened
to your cells and when.

Biological processes are dynamic, and a single snapshot in time may not capture rare or transient events, causing you to miss a relevant response. With the IncuCyte® S3 live-cell analysis system and reagents, automatically follow the sequence of biological events continuously, then 'rewind and replay' the experiment to see what really happened to your cells while you were away.

The IncuCyte S3 combines image-based measurements, a physiologically relevant environment, and microplate throughput to enable researchers to visualize and analyze cell behaviors at a scale and in ways that were previously not possible—all without ever removing cells from the incubator.

Visit www.essenbio.com/IncuCyte to learn about the next-generation IncuCyte S3 System and the benefits of real-time, automated live-cell analysis.



IncuCyte®
by SARTORIUS

Your neurons are
talking.

Are you listening?



Maestro Pro MEA platform showing real-time neural activity across a 48-well plate.

Maestro Pro™ microelectrode array (MEA) *in vitro* neural activity analysis

Record network-level neural activity directly on the benchtop with Maestro. Over minutes or months, gain unprecedented access to electrical network function from cultured neural populations.

Straightforward and easy to use, any researcher can measure activity from neurons in 12-, 24-, 48- or 96-well plates. With a Maestro system for every budget, now there's nothing stopping you from exploring life's circuitry.

Connect to your network.

Snapshots

Class 1 CRISPR-Cas Systems

Kira S. Makarova, Feng Zhang, and Eugene V. Koonin

Class 2 CRISPR-Cas Systems

Kira S. Makarova, Feng Zhang, and Eugene V. Koonin

Epigenomic Assays

Martin Krzywinski and Martin Hirst

The Noncanonical Inflammasome

Jingjin Ding and Feng Shao

Cellular Senescence Pathways

Ricardo Iván Martínez-Zamudio, Lucas Robinson, Pierre-Francois Roux, and Oliver Bischof

Subcellular mRNA Localization

Mohammad Mofatteh and Simon L. Bullock

Nucleo-cytoskeletal Interactions

Cátia S. Janota, Francisco J. Calero-Cuenca, Judite Costa, and Edgar R. Gomes

Reviews

Emerging Biological Principles of Metastasis

Arthur W. Lambert, Diwakar R. Pattabiraman, and Robert A. Weinberg

mTOR Signaling in Growth, Metabolism, and Disease

Robert A. Saxton and David M. Sabatini

Metabolic Instruction of Immunity

Michael D. Buck, Ryan T. Sowell, Susan M. Kaech, and Erika L. Pearce

Putting p53 in Context

Edward R. Kasthuber and Scott W. Lowe

Articles and Resources

Mapping the Neural Substrates of Behavior

Alice A. Robie, Jonathan Hirokawa, Austin W. Edwards, Lowell A. Umayam, Allen Lee, Mary L. Phillips, Gwyneth M. Card, Wyatt Korff, Gerald M. Rubin, Julie H. Simpson, Michael B. Reiser, and Kristin Branson

Mutation of the Human Circadian Clock Gene *CRY1* in Familial Delayed Sleep Phase Disorder

Alina Patke, Patricia J. Murphy, Onur Emre Onat, Ana C. Krieger, Tayfun Özçelik, Scott S. Campbell, and Michael W. Young

Innate Immune Landscape in Early Lung Adenocarcinoma by Paired Single-Cell Analyses

Yonit Lavin, Soma Kobayashi, Andrew Leader, El-ad David Amir, Naama Elefant, Camille Bigenwald, Romain Remark, Robert Sweeney, Christian D. Becker, Jacob H. Levine, Klaus Meinhof, Andrew Chow, Seunghee Kim-Shulze, Andrea Wolf, Chiara Medaglia, Hanjie Li, Julie A. Rytlewski, Ryan O. Emerson, Alexander Solovyov, Benjamin D. Greenbaum, Catherine Sanders, Marissa Vignali, Mary Beth Beasley, Raja Flores, Sacha Gnjatich, Dana Péer, Adeeb Rahman, Ido Amit, and Miriam Merad

(continued)

Crystal Structure of the Human Cannabinoid Receptor CB₁

Tian Hua, Kiran Vemuri, Mengchen Pu, Lu Qu, Gye Won Han, Yiran Wu, Suwen Zhao, Wenqing Shui, Shanshan Li, Anisha Korde, Robert B. Laprairie, Edward L. Stahl, Jo-Hao Ho, Nikolai Zvonok, Han Zhou, Irina Kufareva, Beili Wu, Qiang Zhao, Michael A. Hanson, Laura M. Bohn, Alexandros Makriyannis, Raymond C. Stevens, and Zhi-Jie Liu

Interspecies Chimerism with Mammalian Pluripotent Stem Cells

Jun Wu, Aida Platero-Luengo, Masahiro Sakurai, Atsushi Sugawara, Maria Antonia Gil, Takayoshi Yamauchi, Keiichiro Suzuki, Yanina Soledad Bogliotti, Cristina Cuello, Mariana Morales Valencia, Daiji Okumura, Jingping Luo, Marcela Vilariño, Inmaculada Parrilla, Delia Alba Soto, Cristina A. Martinez, Tomoaki Hishida, Sonia Sánchez-Bautista, M. Llanos Martinez-Martinez, Huili Wang, Alicia Nohalez, Emi Aizawa, Paloma Martinez-Redondo, Alejandro Ocampo, Pradeep Reddy, Jordi Roca, Elizabeth A. Maga, Concepcion Rodriguez Esteban, W. Travis Berggren, Estrella Nuñez Delicado, Jeronimo Lajara, Isabel Guillen, Pedro Guillen, Josep M. Campistol, Emilio A. Martinez, Pablo Juan Ross, and Juan Carlos Izpisua Belmonte

Oncolytic Virotherapy Promotes Intratumoral T Cell Infiltration and Improves Anti-PD-1 Immunotherapy

Antoni Ribas, Reinhard Dummer, Igor Puzanov, Ari VanderWalde, Robert H.I. Andtbacka, Olivier Michielin, Anthony J. Olszanski, Josep Malvehy, Jonathan Cebon, Eugenio Fernandez, John M. Kirkwood, Thomas F. Gajewski, Lisa Chen, Kevin S. Gorski, Abraham A. Anderson, Scott J. Diede, Michael E. Lassman, Jennifer Gansert, F. Stephen Hodi, and Georgina V. Long

Modified mRNA Vaccines Protect against Zika Virus Infection

Justin M. Richner, Sunny Himansu, Kimberly A. Dowd, Scott L. Butler, Vanessa Salazar, Julie M. Fox, Justin G. Julander, William W. Tang, Sujun Shresta, Theodore C. Pierson, Giuseppe Ciaramella, and Michael S. Diamond

Gut Microbiota Regulate Motor Deficits and Neuroinflammation in a Model of Parkinson's Disease

Timothy R. Sampson, Justine W. Debelius, Taren Thron, Stefan Janssen, Gauri G. Shastri, Zehra Esra Ilhan, Collin Challis, Catherine E. Schretter, Sandra Rocha, Viviana Gradinaru, Marie-Francoise Chesselet, Ali Keshavarzian, Kathleen M. Shannon, Rosa Krajmalnik-Brown, Pernilla Wittung-Stafshede, Rob Knight, and Sarkis K. Mazmanian

Fasting-Mimicking Diet Promotes Ngn3-Driven β -Cell Regeneration to Reverse Diabetes

Chia-Wei Cheng, Valentina Villani, Roberta Buono, Min Wei, Sanjeev Kumar, Omer H. Yilmaz, Pinchas Cohen, Julie B. Sneddon, Laura Perin, and Valter D. Longo

UV Irradiation Induces a Non-coding RNA that Functionally Opposes the Protein Encoded by the Same Gene

Laura Williamson, Marco Saponaro, Stefan Boeing, Phillip East, Richard Mitter, Theodoros Kantidakis, Gavin P. Kelly, Anna Lobley, Jane Walker, Bradley Spencer-Dene, Michael Howell, Aengus Stewart, and Jesper Q. Svejstrup

Accelerate your drug discovery research at every step

GE Healthcare provides innovative tools and analytics to support therapeutic development from target identification, all the way through bioprocessing. Confidently move through the drug development pipeline while reducing costs and maximizing productivity throughout development and biomanufacturing. Learn more at gelifsciences.com.





Enhancing human research since 1999

Whole Genome/Exome Sequencing

Targeted Sequencing

Single-Cell RNA-Seq

SNP Genotyping

Synthetic Libraries

CLIA-Compliant Sanger Sequencing

 genewiz.com

NEW! Amplicon-EZ

Delivers fast, cost-effective, ultra-deep sequencing of PCR products/amplicons via next generation sequencing.

Experience the GENEWIZ Difference

- Superior data quality
- Starting at just \$50 a sample
- Complete sample-to-answer workflows
- Interactive reports
- Results in as few as three days!

 [Visit web.genewiz.com/amplicon-ez](http://web.genewiz.com/amplicon-ez)

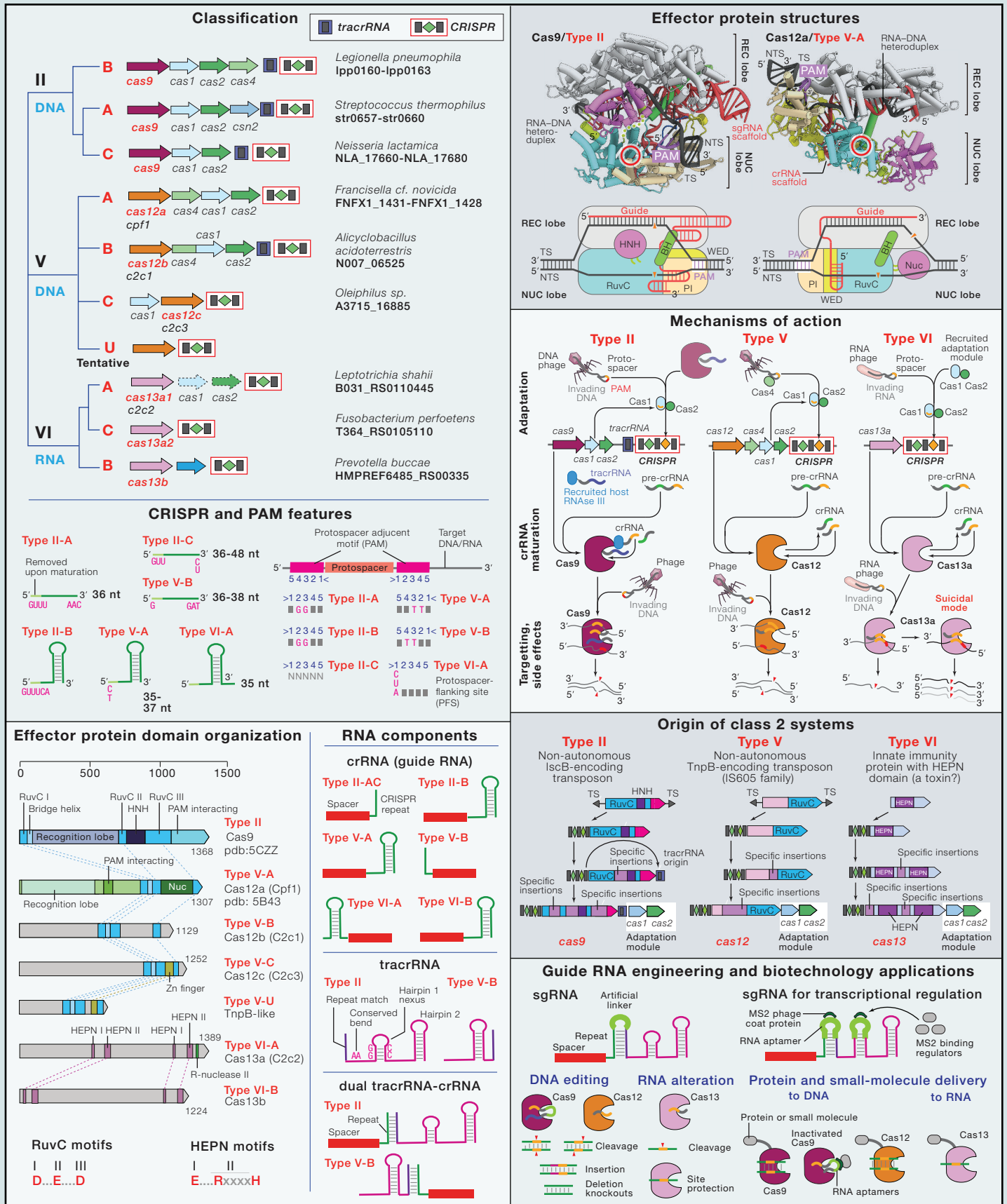
SnapShot: Class 2 CRISPR-Cas Systems Cell

Kira S. Makarova,¹ Feng Zhang,^{2,3} and Eugene V. Koonin¹

¹National Center for Biotechnology Information, National Institutes of Health, Bethesda, MD 20894, USA;

²Broad Institute of MIT and Harvard, Cambridge, MA 02142, USA; ³McGovern Institute for Brain Research,

Massachusetts Institute of Technology, Cambridge, MA 02139, USA



Focus on Results not Preparing Samples

New Bioluminescent Assays for Energy Metabolism

- In-well detection with no sample preprocessing
- Detect small metabolic changes in cells
- Use many sample types including: *media, tissue, plasma, serum and cells*

Metabolite Detection Assays: *Glucose, Glucose Uptake, Lactate, Glutamate, Glutamine*

Nucleotide/Co-Factor Detection Assays

Oxidative Stress Assays

Sample an Assay Today:

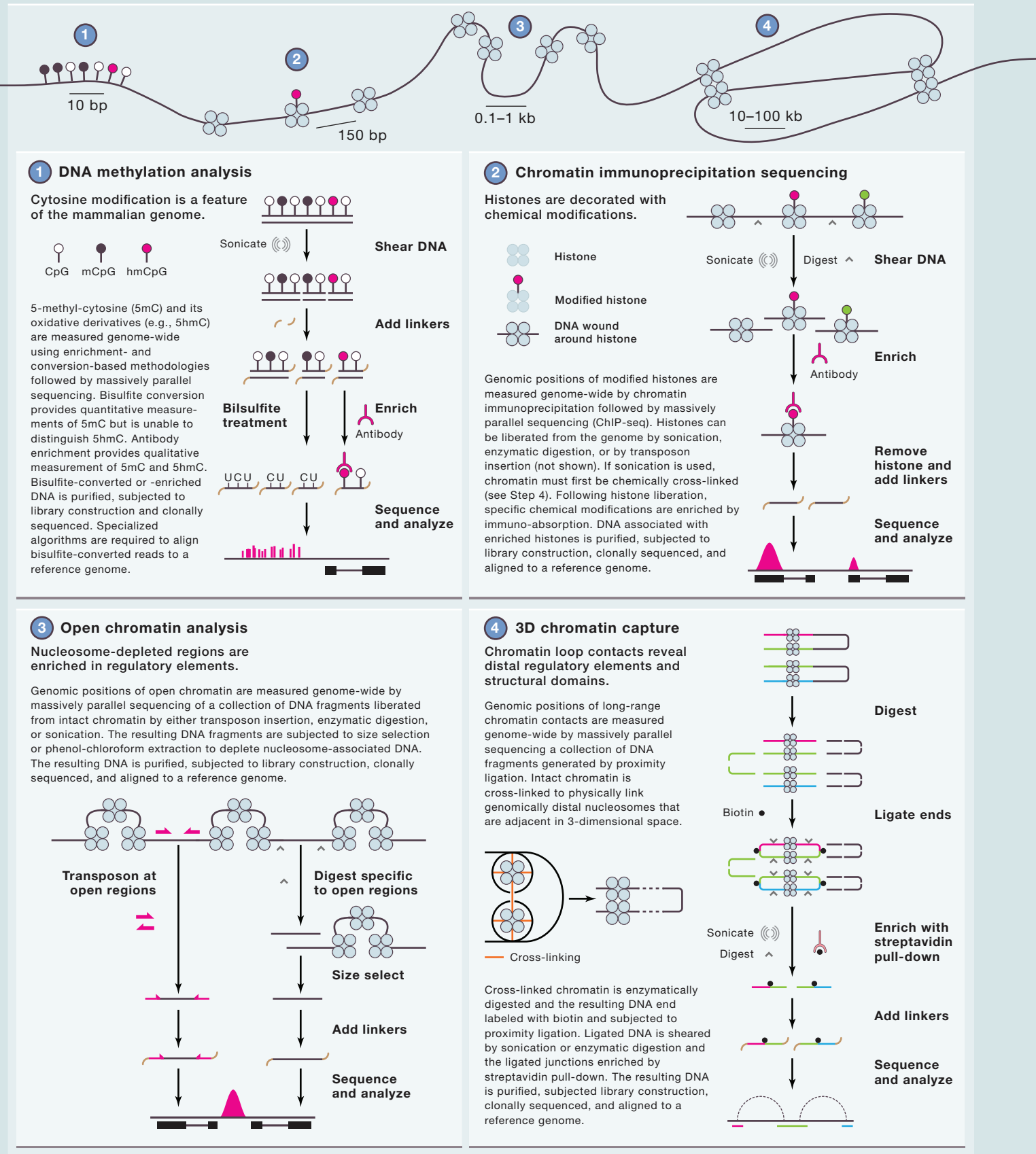
www.promega.com/Energy

SnapShot: Epigenomic Assays

Cell

Martin Krzywinski¹ and Martin Hirst^{1,2}

¹Canada's Michael Smith Genome Sciences Centre, BC Cancer Agency Research Centre, BC Cancer Agency, Vancouver, BC V5Z 1L3, Canada; ²Department of Microbiology and Immunology, Michael Smith Laboratories Centre for High-Throughput Biology, University of British Columbia, Vancouver, BC V6T 1Z4, Canada



Quantitative & Qualitative Data for the Total Cell Picture



Microplate Reader & Imager

DO MORE | GROW IT, READ IT, SEE IT, COUNT IT.

Cytation™5 Cell Imaging Multi-Mode Reader combines ultra-sensitive microplate detection *and* digital imaging in one compact instrument. Now with Gen5™ Image+ software, you have remarkable reader control and data analysis. Isn't it time you got the whole picture?

Get the whole picture, visit www.cytation5.com

Think Possible

 **BioTek**®



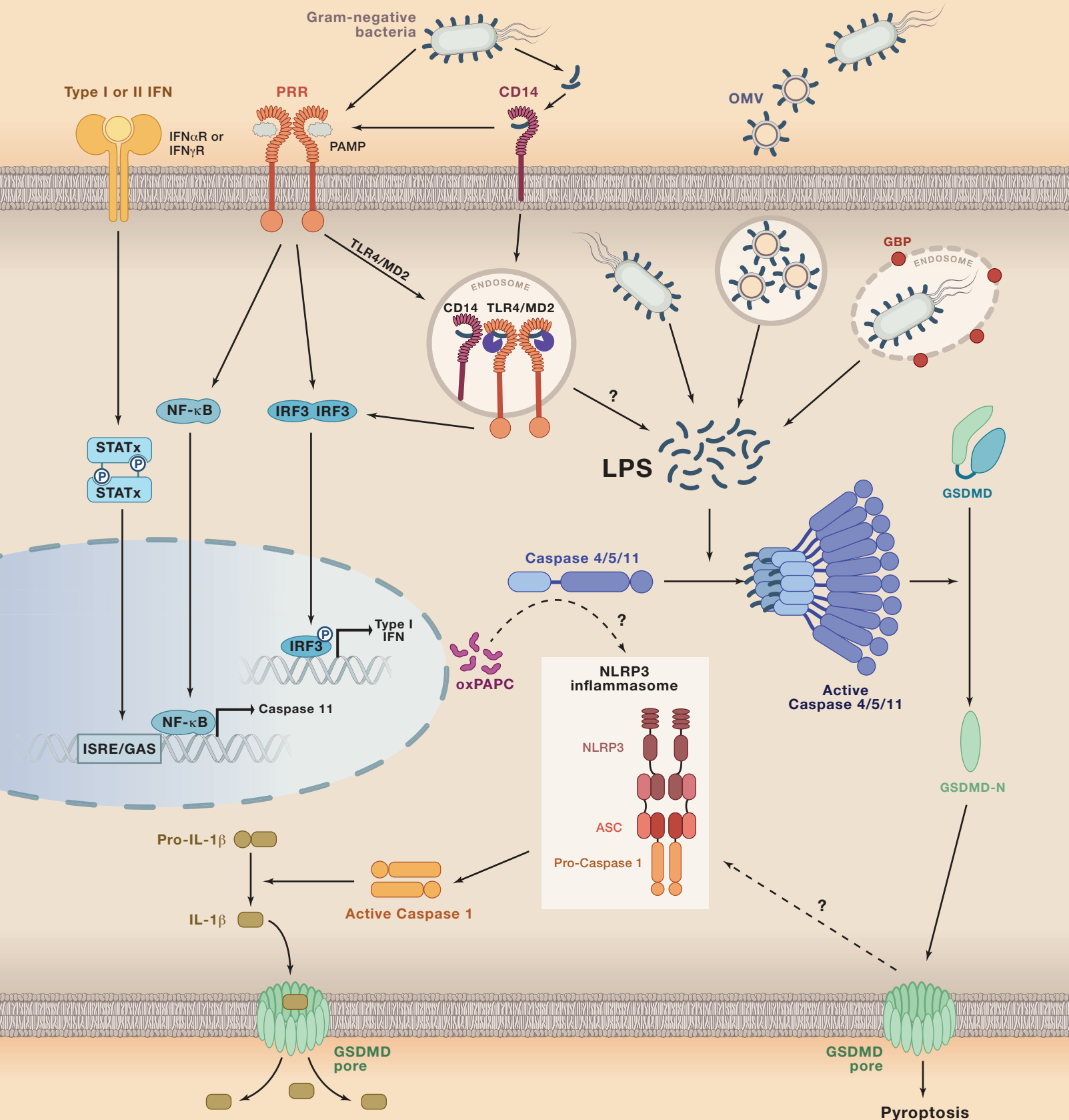
www.biotek.com

SnapShot: The Noncanonical Inflammasome

Jingjin Ding^{1,2} and Feng Shao²

¹National Laboratory of Biomacromolecules, Institute of Biophysics, Chinese Academy of Sciences, Beijing, 100101, China

²National Institute of Biological Sciences, Beijing, 102206, China



Revolutionizing your confocal imaging.

ZEISS LSM 880 with Airyscan



// INNOVATION
MADE BY ZEISS

Your new standard for fast and gentle confocal imaging

Discover ZEISS LSM 880 with Airyscan: this unique confocal laser scanning microscope delivers perfect optical sections with 120 nm resolution in x/y and 350 nm in z. You get 4–8× higher sensitivity for gentle superresolution imaging. Use the additional Fast mode with acquisition speeds of 27 fps (at 480 × 480 pixels) to follow even the most dynamic processes in your samples.

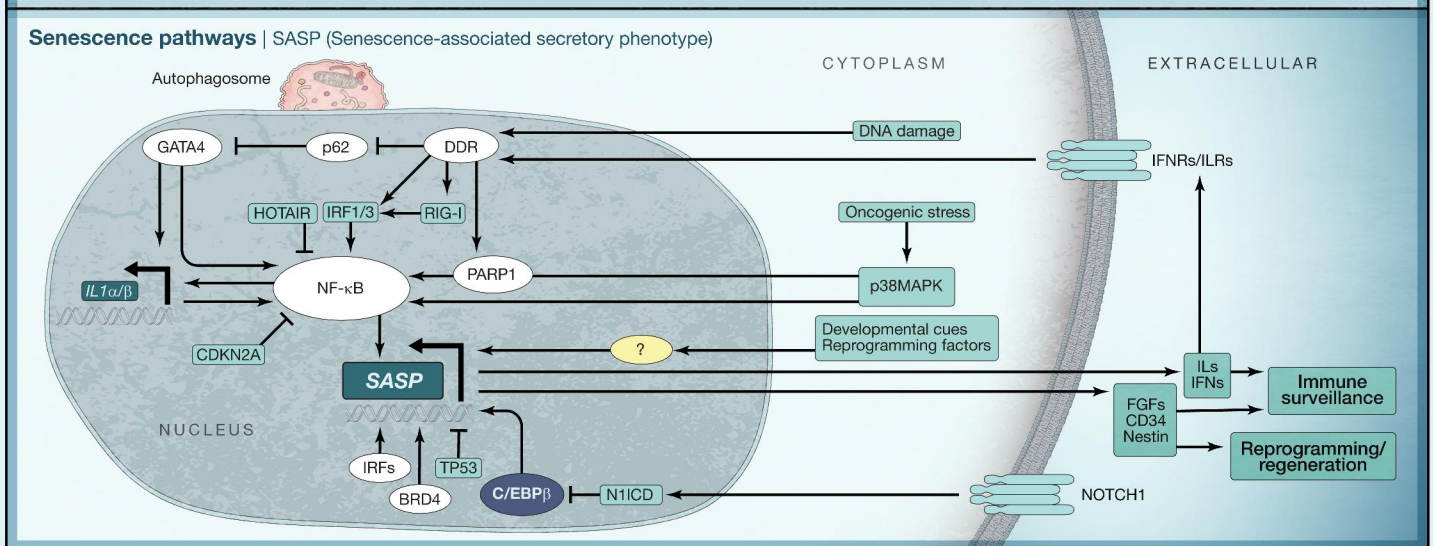
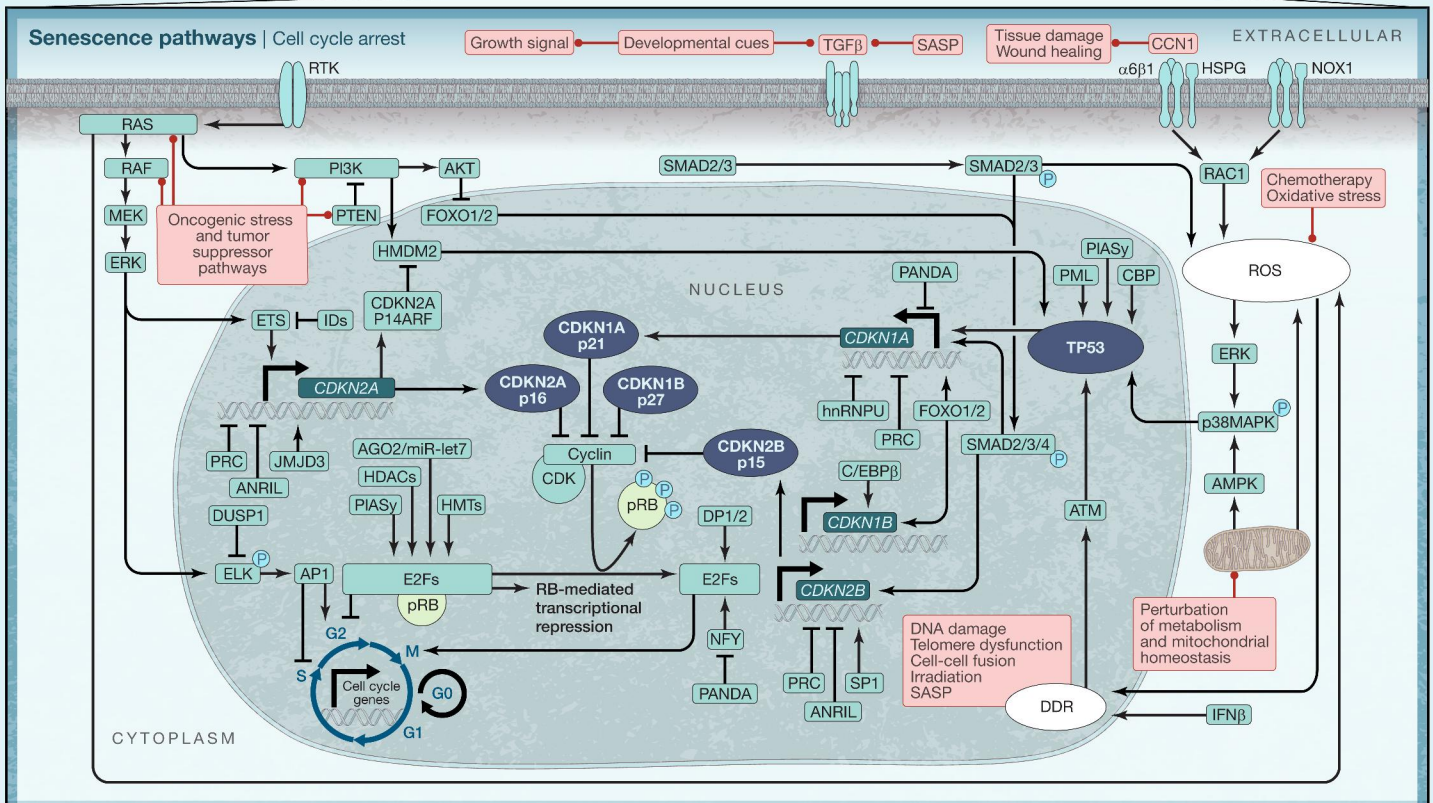
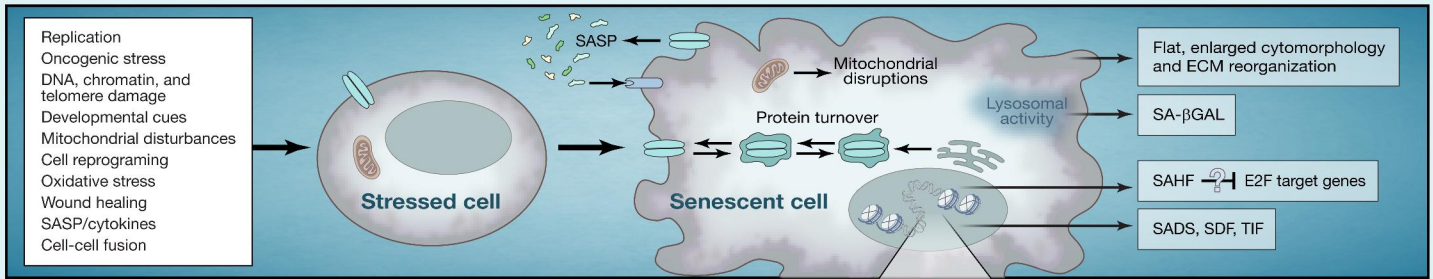


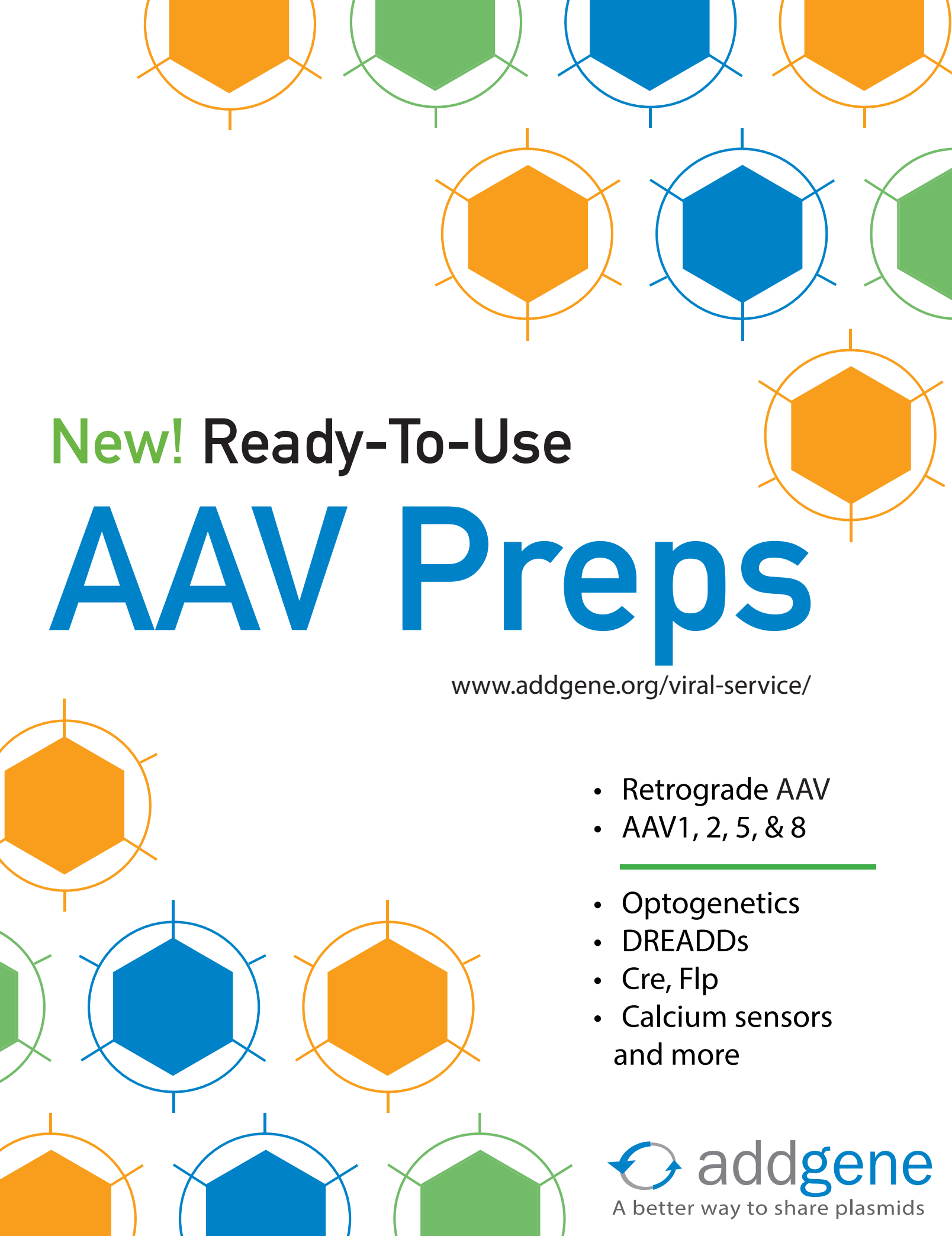
www.zeiss.com/lsm880



SnapShot: Cellular Senescence Pathways

Ricardo Iván Martínez-Zamudio, Lucas Robinson, Pierre-Francois Roux, Oliver Bischof
 INSERM, U993, 75015 Paris, France; Equipe Labellisée Fondation ARC pour la recherche sur le cancer, 94803 Villejuif;
 Institut Pasteur, Molecular and Cellular Biology of Cellular Senescence and Age-Related Pathologies Group,
 Nuclear Organization and Oncogenesis Unit, Department of Cell Biology and Infection, 75015 Paris, France





New! Ready-To-Use

AAV Preps

www.addgene.org/viral-service/

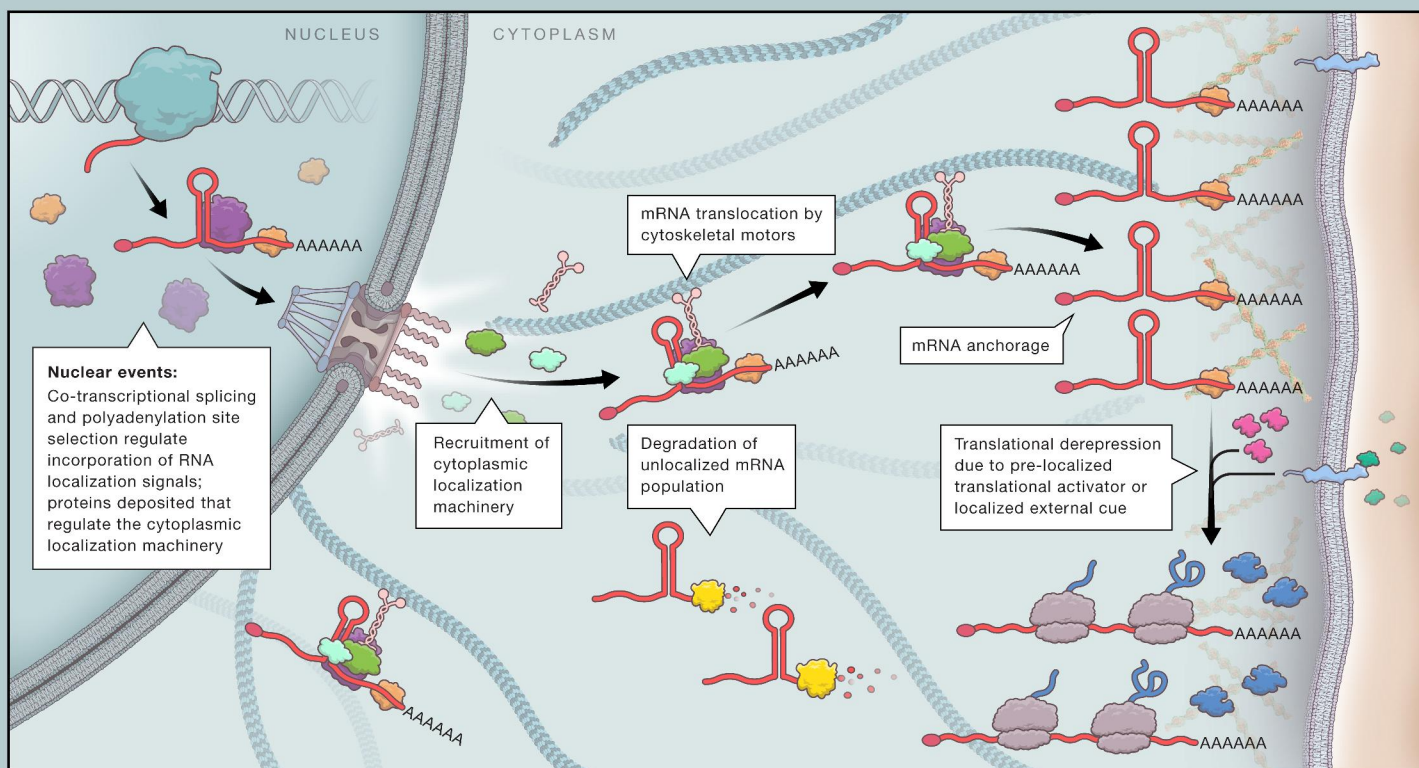
- Retrograde AAV
- AAV1, 2, 5, & 8

-
- Optogenetics
 - DREADDs
 - Cre, Flp
 - Calcium sensors
and more

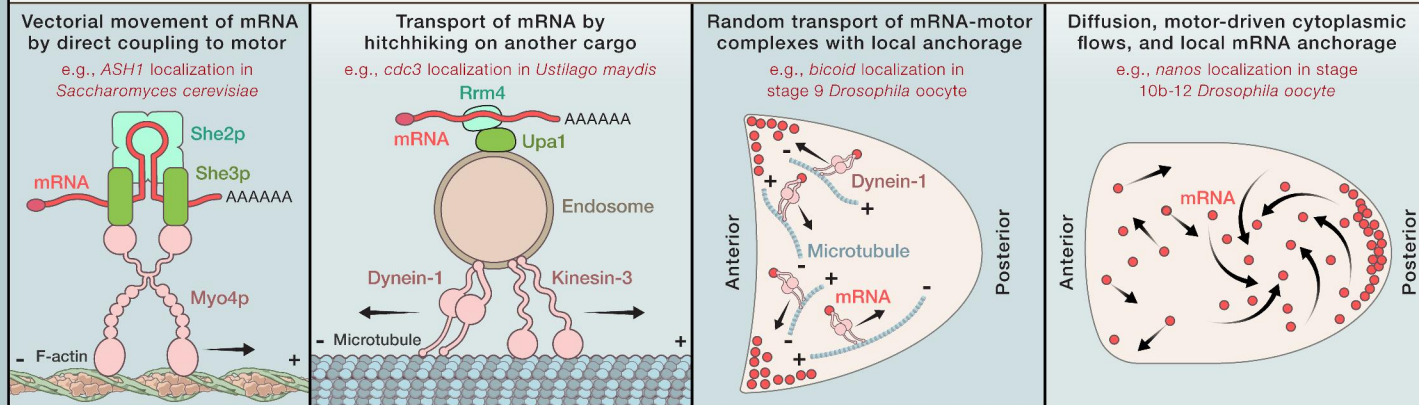
SnapShot: Subcellular mRNA Localization

Mohammad Mofatteh and Simon L. Bullock

Cell Biology Division, MRC Laboratory of Molecular Biology, Francis Crick Avenue, Cambridge CB2 0QH, UK



mRNA translocation strategies



Examples of mRNA transport complexes

Cell type	Example RNAs	Pattern	Function	RNA binding adaptor	Other adaptors	Motor(s)	Cytoskeletal filament
<i>S. cerevisiae</i>	<i>ASH1</i>	Bud cortex in mitosis	Segregation of protein product regulates mating type in daughter cell	She2p	She3p	Myo4p	F-actin
<i>U. maydis</i>	<i>cdc3</i>	Along hyphae	Transport of septin mRNAs and encoded proteins for assembly in higher-order structures; distribution of ribosomes	Rrm4	Upa1/ Endosome	Dynein-1, Kinesin-3	Microtubule
<i>Drosophila</i> egg chamber	<i>K10</i> , <i>oskar</i>	Oocyte	Delivery from the nurse cells of factors important for axial patterning	Egl	BicD/Dynactin	Dynein-1	Microtubule
<i>Drosophila</i> stage 9 oocyte	<i>oskar</i>	Posterior pole	Localized protein product specifies the site of abdomen and germ cell formation	Tm1-I/C	?	Kinesin-1	Microtubule
<i>Xenopus</i> oocyte	<i>Vg1</i>	Vegetal cortex	Mesoderm and endoderm specification in the embryo	ZBP1 (VgRBP1)	Staufen, ?	Kinesin-1, Kinesin-2	Microtubule
Chicken and mouse fibroblasts	β -actin	Leading edge	Encoded β -actin stabilizes focal adhesions and promotes persistent cell migration	ZBP1	?	Myo-Va, Myo-IIb	F-actin
				ZBP1	-	KIF11	Microtubule
Dendrites of mammalian neurons	<i>MAP1B</i>	Activity-stimulated dendritic localization	Targeting of regulators of synapse formation and maturation	FMRP	?	Kinesin-1	Microtubule

F · S · T[®]

FINE SCIENCE TOOLS

ADVANCING THE FIELD OF RESEARCH

Scissors • Retractors • Magnifiers • Probes & Hooks • Bone Instruments • Animal Identification
Hemostats • Forceps • Surgical & Laboratory Equipment • Feeding Needles • Spatulae & Spoons
Wound Closure • Surgical Plates • Instrument Care & Sterilization • Rongeurs • Scalpels & Knives
Clamps • Pins & Holders • Needles & Needle Holders • Student Quality Instruments & Much More



FINE SURGICAL INSTRUMENTS FOR RESEARCH™

VISIT US AT FINESCENCE.COM OR CALL 800 521 2109

slas
2018

INTERNATIONAL
CONFERENCE & EXHIBITION

FEB. 3-7 | SLAS2018.ORG
SAN DIEGO, CA
SAN DIEGO CONVENTION CENTER

WHERE DISCOVERY MEETS TECHNOLOGY

SHORT COURSES: FEBRUARY 3-4 | **CONFERENCE:** FEBRUARY 3-7 | **EXHIBITS:** FEBRUARY 5-7 | SLAS2018.ORG

Keynote Speakers



OPENING KEYNOTE
Benjamin F. Cravatt



CLOSING KEYNOTE
Marc Abrahams

Educational Tracks

SLAS2018 offers participants a world-class scientific program that showcases the top life sciences discovery and technology education from industry leaders. Podium and poster presentations offer SLAS2018 participants compelling content, best practice and new perspectives on emerging scientific technologies from a broad range of industries and academic research perspectives.

The SLAS2018 scientific program features 10 educational tracks, including three tracks making their debut in San Diego:

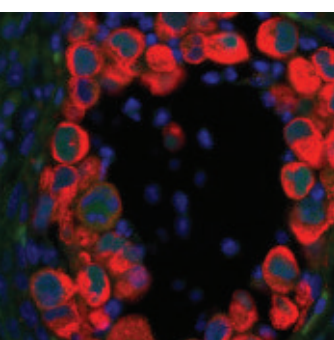
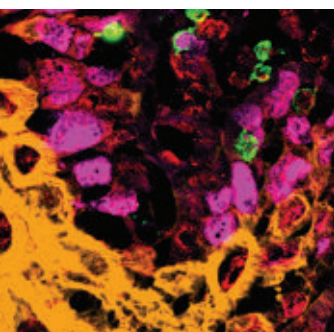
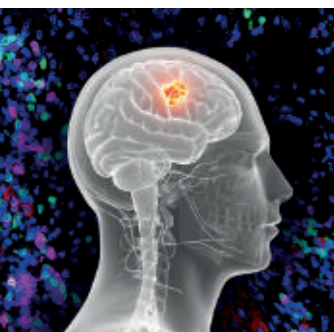
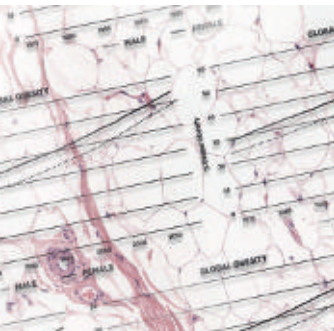
- Advances in Bioanalytics and Biomarkers
- Assay Development and Screening
- Automation and High-Throughput Technologies
- Biologics Discovery **(NEW!)**
- Cellular Technologies
- Chemical Biology **(NEW!)**
- Data Analysis and Informatics
- Drug Target Strategies
- High-Definition Biotechnology **(NEW!)**
- Micro- and Nanotechnologies

REGISTER NOW

Complete information about SLAS2018 can be found at SLAS2018.ORG.

LIFE SCIENCES

 **slas**



2018 SCIENTIFIC CONFERENCES

Presenting the most significant research on cancer etiology, prevention, diagnosis, and treatment

Fifth AACR-IASLC International Joint Conference: Lung Cancer Translational Science from the Bench to the Clinic

*Conference Cochairs: Charles M. Rudin
and Charles Swanton*

January 8-11, 2018 | San Diego, CA

Obesity and Cancer: Mechanisms Underlying Etiology and Outcomes

*Conference Cochairs: Lewis C. Cantley,
Michael N. Pollak, and Elizabeth A. Platz*

January 27-30, 2018 | Austin, TX

Immunobiology of Primary and Metastatic CNS Cancer: Multidisciplinary Science to Advance Cancer Immunotherapy

*Conference Cochairs: Hideho Okada, Robyn S. Klein,
Ignacio Melero, and Patricia S. Steeg*

February 12-15, 2018 | San Diego, CA

Third AACR-SNMMI Joint Conference on State-of-the-Art Molecular Imaging in Cancer Biology and Therapy

*Conference Cochairs: Todd E. Peterson
and David R. Piwnica-Worms*

February 14-17, 2018 | San Diego, CA

Targeting DNA Methylation and Chromatin for Cancer Therapy

*Conference Cochairs: Stephen B. Baylin,
Margaret A. Goodell, and Peter A. Jones*

March 1-4, 2018 | Atlanta, GA

AACR Annual Meeting 2018

Program Committee Chair: Elaine R. Mardis
April 14-18, 2018 | Chicago, IL

Cancer Dormancy and Residual Disease

*Conference Cochairs: Julio A. Aguirre-Ghiso,
Ann F. Chambers, Cyrus M. Ghajar,*

Christoph A. Klein, and Dorothy A. Sipkins

June 19-22, 2018 | Montreal, QC, Canada

Advances in Malignant Lymphoma: Maximizing the Basic-Translational Interface for Clinical Application

Scientific Committee Chair: Ari M. Melnick

June 22-26, 2018 | Boston, MA

Sixth JCA-AACR Special Joint Conference on the Latest Advances in Lung Cancer Research: From Basic Science to Therapeutics

*Organizing Committee: Hiroyuki Mano,
Seiji Yano, Hiroyoshi Nishikawa, Alice T. Shaw,
Roy S. Herbst, and Charles M. Rudin*

July 10-12, 2018 | Kyoto, Japan

Intestinal Stem Cells and Colon Cancer: Biology to Therapy

*Conference Cochairs: Anil K. Rustgi, Johanna Bendell,
Hans Clevers, Christina Curtis, and Owen Sansom*

September 27-30, 2018 | Washington, DC

Metabolism and Cancer

*Conference Cochairs: Ralph J. Deberardinis,
Tak W. Mak, Joshua D. Rabinowitz,
and M. Celeste Simon*

September 28-October 1, 2018 | New York, NY

Fourth CRI-CIMT-EATI-AACR International Cancer Immunotherapy Conference: Translating Science into Survival

September 30-October 3, 2018 | New York, NY

Tumor Immunology and Immunotherapy

*Conference Cochairs: James P. Allison,
Lisa M. Coussens, Ira Mellman, and Drew M. Pardoll*

November 27 - 30, 2018 | Miami Beach, FL

Learn more and register at
AACR.org/Calendar

AACR American Association
for Cancer Research®

FINDING CURES TOGETHER®

Emerging Biological Principles of Metastasis

Arthur W. Lambert,¹ Diwakar R. Pattabiraman,¹ and Robert A. Weinberg^{1,2,*}

¹Whitehead Institute for Biomedical Research, 9 Cambridge Center, Cambridge, MA 02142, USA

²Department of Biology, Massachusetts Institute of Technology and the MIT Ludwig Center for Molecular Oncology, Cambridge, MA 02142, USA

*Correspondence: weinberg@wi.mit.edu

<http://dx.doi.org/10.1016/j.cell.2016.11.037>

Metastases account for the great majority of cancer-associated deaths, yet this complex process remains the least understood aspect of cancer biology. As the body of research concerning metastasis continues to grow at a rapid rate, the biological programs that underlie the dissemination and metastatic outgrowth of cancer cells are beginning to come into view. In this review we summarize the cellular and molecular mechanisms involved in metastasis, with a focus on carcinomas where the most is known, and we highlight the general principles of metastasis that have begun to emerge.

Introduction

The diversity of cancers that arise in humans exceeds 200 distinct disease entities—reflecting differences in the normal cells of origin, acquired somatic mutations, variably altered transcriptional networks, and influences of local tissue microenvironments. Attempts have been made to distill this complexity into a unifying set of organizing principles termed cancer hallmarks (Hanahan and Weinberg, 2000, 2011). In spite of significant advances in the study, diagnosis, and treatment of cancer, the vast majority of patients with advanced metastatic disease confront a terminal illness that is, with rare exception, incurable by current therapeutic regimens. Stated differently, the overwhelming majority of cancer-associated deaths (about 90%) are caused by metastatic disease rather than primary tumors.

The dissemination of cancer cells from primary tumors and their subsequent seeding of new tumor colonies in distant tissues involves a multi-step process known as the invasion-metastasis cascade (Fidler, 2003; Gupta and Massagué, 2006; Talmadge and Fidler, 2010). This sequence of events involves the local invasion of primary tumor cells into surrounding tissues; intravasation of these cells into the circulatory system and survival during hematogenous transit; arrest and extravasation through vascular walls into the parenchyma of distant tissues; formation of micrometastatic colonies in this parenchyma; and the subsequent proliferation of microscopic colonies into overt, clinically detectable metastatic lesions, this last process being termed colonization.

In contrast to the large body of findings that have revealed the detailed pathogenetic mechanisms leading to primary tumor formation, the biological underpinnings of metastatic disease remain poorly understood. Furthermore, relatively few principles have emerged that would unify our understanding of how diverse types of metastases arise and how similar or different each may be relative to the behavior of its corresponding primary tumor. Nonetheless, over the past 15 years significant progress has been made in elucidating various aspects of the metastatic program, particularly for carcinomas, which in aggregate account for ~80% of cancer cases and thus the majority of cancer deaths.

Here we summarize important advances that have revealed some of the mechanisms that underlie the dissemination and metastatic outgrowth of carcinoma cells. Drawing from this increasingly large and complex body of work, we suggest that a few key biological principles have begun to emerge for certain aspects of the metastatic cascade, while for other steps of the cascade a unifying conceptual framework remains more elusive.

Dissemination of Carcinoma Cells

The process of dissemination subsumes the initial steps of the invasion-metastasis cascade that enable malignant tumor cells to acquire traits that equip them with the ability to leave the primary site and travel to distant tissues (Figure 1A). As with almost all of the discussions in this review, we describe these processes in the context of the intensively studied carcinomas. One centrally important process enabling these steps is the cell-biological program termed the epithelial-mesenchymal transition (EMT), a developmental program that is normally employed during embryogenesis (and in adults for the healing of epithelial tissues) and is hijacked by carcinoma cells, endowing them with multiple malignant traits associated with the loss of epithelial properties and the acquisition of certain mesenchymal features in their stead (Thiery, 2002).

The Epithelial-Mesenchymal Transition

The EMT program confers on epithelial cells, both normal and neoplastic, properties that are critical to invasion and metastatic dissemination, notably increased motility, invasiveness, and the ability to degrade components of the extracellular matrix (ECM) (Kalluri and Weinberg, 2009; Nieto et al., 2016; Thiery, 2002). In fact, the EMT is really a group of cell-biological programs that share features in common but differ in certain critical details, depending on the tissue site, the degree of malignancy, and the contextual signals experienced by individual neoplastic cells. These complex programs are orchestrated and coordinated by a series of master EMT-inducing transcription factors (EMT-TFs), notably Snail, Slug, Twist, and Zeb1, which have been explored in great experimental detail (De Craene and Berx, 2013; Lamouille et al., 2014). Yet other TFs capable of inducing components of the EMT program have also been described (e.g., Zeb2,

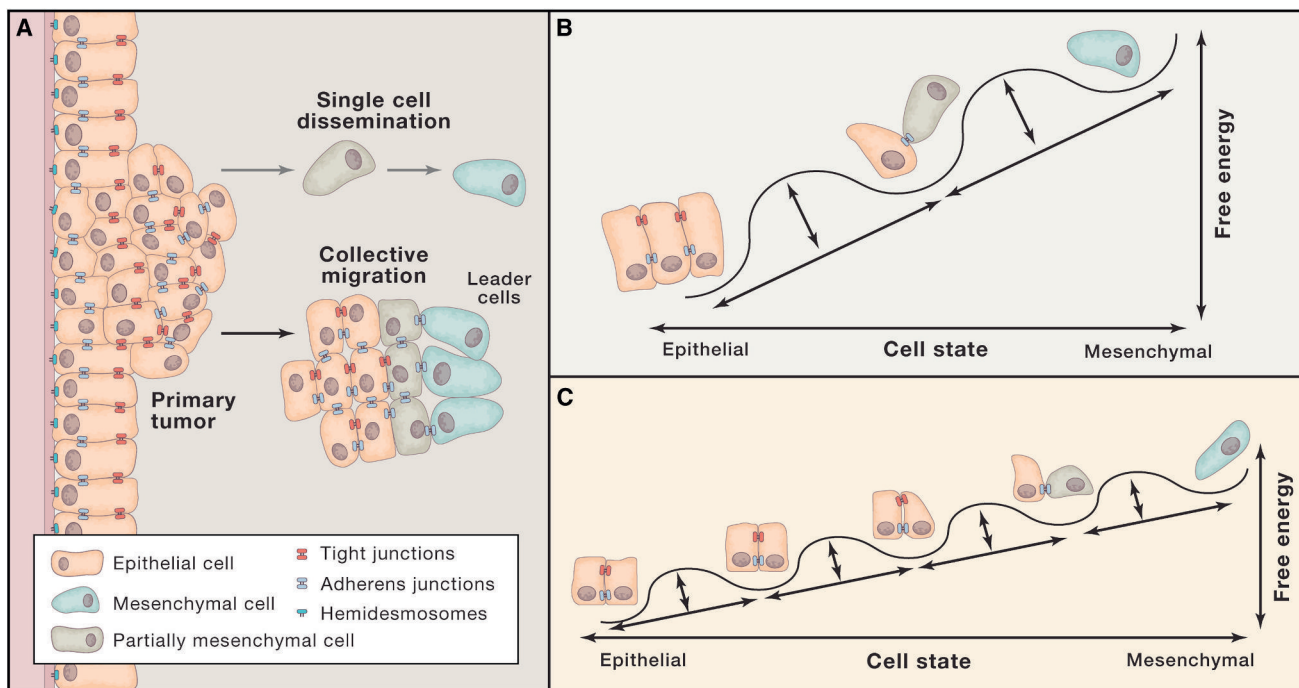


Figure 1. Dissemination of Carcinoma Cells

(A) Carcinoma cell dissemination occurs via two mechanisms: single-cell dissemination through an EMT (gray arrow) or the collective dissemination of tumor clusters (black arrow). Recent evidence suggests that the leader cells of tumor clusters also undergo certain phenotypic changes associated with the EMT. (B) The epithelial state can be portrayed as the default state of residence; as cells undergo an EMT they enter into a succession of multiple epigenetic states, depicted here as free energy wells, with each state moving toward a more mesenchymal phenotype representing a higher energy state. (C) However, the barriers between states, depicted here again as free energy wells, may be relatively low, resulting in substantial spontaneous interconversion between them, this being manifested as phenotypic plasticity.

Foxc2, Prrx1, among others), but their roles in cancer pathogenesis remain less well documented. Although traditional models of tumorigenesis posit that metastasis is a late event during the course of multi-step tumor progression, some studies have shown that acquisition of EMT-associated traits and the process of dissemination can actually occur relatively early, being evident even in certain preneoplastic lesions (Hüsemann et al., 2008; Rhim et al., 2012; Harper et al., 2016).

Of additional relevance is the fact that several types of carcinoma cells have been found to acquire tumor-initiating capability after induction of EMT programs. These include breast (Mani et al., 2008; Morel et al., 2008), colorectal (Brabletz et al., 2005; Fan et al., 2012; Pang et al., 2010), ovarian (Long et al., 2015), pancreatic (Rasheed et al., 2010), prostate (Kong et al., 2010), and renal (Zhou et al., 2016), among other types of carcinomas. Tumor-initiating ability, usually depicted as the defining trait of cancer stem cells (CSCs), is generally gauged by implantation of populations of neoplastic cells in appropriate mouse hosts. Such tests indicate that CSCs are almost always present as relatively small subpopulations of neoplastic cells residing within individual tumors among larger populations of cancer cells that lack tumor-initiating powers. Residence of a disseminating carcinoma cell in the CSC state would seem to be critical for progression through the invasion-metastasis cascade, since disseminated tumor cells must presumably be endowed with tumor-initiating ability in order to

function as the founders of new metastatic colonies. Moreover, acquisition of more mesenchymal traits, as driven by an EMT program, has been found to elevate the resistance of carcinoma cells to various types of cytotoxic treatments, including both radio- and chemotherapies (Gupta et al., 2009; Kurrey et al., 2009), providing one explanation of the often-observed phenomenon that CSCs tend to be more therapy resistant than their non-CSC counterparts (Singh and Settleman, 2010).

While the EMT program might be depicted as operating much like a binary switch, in which cancer cells reside either in an epithelial or a mesenchymal state, the truth is more complex, in that EMT programs activated in carcinoma cells usually drive the acquisition of certain mesenchymal traits while permitting the retention of some epithelial traits, leaving carcinoma cells with mixed epithelial/mesenchymal phenotypes (Figures 1B and 1C).

EMT programs seem almost invariably to be triggered in carcinoma cells by heterotypic signals that these cells receive from the nearby tumor-associated stroma. Thus, during the course of tumor progression, the stroma—which is composed of a variety of fibroblasts, myofibroblasts, endothelial, myeloid, and lymphoid cells recruited from host tissues—increasingly takes on the appearance of a stroma that typically forms during the healing of wounded epithelial tissues. Such a “reactive” stroma releases various signals, including TGF- β s, Wnts, and certain interleukins that impinge on nearby carcinoma cells, inducing the latter to activate their previously silent EMT

programs. This activation is generally reversible, and indeed carcinoma cells that have activated EMT programs may revert via a mesenchymal-epithelial transition (MET) to the phenotypic state in which their ancestors resided prior to induction of the EMT program.

While the EMT program appears to be critical to invasion and dissemination of most and possibly all carcinoma types (see below), to date there have been no rules formulated to predict expression of its various components in different tissue contexts. Among the unresolved fundamental issues are: (1) the nature of the heterotypic signals that converge on carcinoma cells and collaborate to activate previously silent EMT programs in these cells; (2) the extent to which these programs are activated at various stages of carcinoma progression; (3) the extent to which the differentiation programs of normal cells of origin influence the expression of various components of the EMT program; (4) the respective roles of the various EMT-TFs cited above in collaborating with one another in choreographing various types of EMT programs; (5) the influence of somatic mutations sustained during primary tumor formation on the activation and expression of EMT programs; and (6) the roles of intracellular and extracellular signaling pathways in sustaining the expression of already-activated EMT programs.

Invasion by Collective Migration

Although the EMT is widely embraced as an important mode of carcinoma cell dissemination, its precise roles in primary tumor behavior remain unresolved. For example, invasion by primary tumor cells generally involves the collective migration of large, cohesive cohorts of cells into adjacent tissues rather than the dispersal of individual carcinoma cells (Figure 1A; Friedl et al., 2012). The organization of these cohorts appears to conflict with the behavior of cells that have passed through an EMT and have lost cohesive cell-cell interactions, notably those mediated by adherens junctions. Thus, these cohorts provoke the question of whether EMT programs are indeed central to eventual carcinoma cell dissemination, as implied above, or instead represent only one of several alternative cell-biological programs that enable dissemination to occur.

Collective migration involving groups of cells, which is commonly seen at the borders of invasive carcinomas, is best documented in the case of carcinomas of the breast and lungs (Friedl et al., 2012); similar invasive cohorts undoubtedly participate in invasion by other types of carcinoma cells as well (Chung et al., 2016; Veracini et al., 2015). Cells residing within these invasive cell phalanxes continue to express key epithelial markers such as E-cadherin, which helps to sustain the cohesion between the individual epithelial cells within these cohorts. Moreover, the polyclonal nature of metastatic colonies of certain breast cancers raises the possibility that they arose from genetically heterogeneous clusters of disseminated cells, rather than arising clonally from single disseminated cells (Cheung et al., 2016). This raises the question of whether collective migration represents an alternative to EMT and whether the two cell-biological programs are essentially mutually exclusive.

In fact, detailed histopathological analyses of invasive cohorts often suggest that the EMT does indeed participate in collective migration (Ye et al., 2015). Thus, these cohorts are themselves internally complex, with invading cells at the leading edges

paving the way for large populations of followers to which they remain attached via cell-cell junctions (Cheung et al., 2013). In some cases, careful examination has revealed that certain mesenchymal traits are exhibited by the leading cells at the invasive fronts during collective migration (Revenu and Gilmour, 2009; Westcott et al., 2015; Ye et al., 2015). Such invading leaders are likely to release various proteases that degrade the extracellular matrix that would otherwise impede the forward progress of the cohort as a whole. Moreover, such leader cells may also possess the EMT-associated motility to enable forward motion of the cohort as a whole. Together, the cells at invasive edges may therefore pave the way for the followers that constitute the bulk of the cell phalanxes.

Unresolved is a key experimental test of this model: can collective invasion occur if activation of EMT programs is totally blocked? Yet other studies report the presence of cancer-associated fibroblasts, rather than carcinoma cells that have undergone an EMT, as leader cells at the invasive edges of carcinomas (Gaggioli et al., 2007). Thus, additional experimental evidence is required to address and clarify more precisely the events occurring at the invasive edges of carcinomas and the nature of the normal and neoplastic cell types involved.

An Essential Role of the EMT Program in Metastasis

Two studies have recently undertaken to refute the essential role of the EMT program in the process of metastasis (Fischer et al., 2015; Zheng et al., 2015). In both instances, the proofs that EMTs did not occur while metastasis proceeded were not supported by the evidence presented, leaving open the continuing question of whether EMT is indeed critical to the metastatic ability of all types of carcinoma cells. Moreover, the reports of these findings coincide with a time when the definition of the EMT is undergoing re-evaluation, as suggested above. Thus, EMT programs are increasingly viewed as generating cells residing in a spectrum of multiple intermediate states lying between epithelial and mesenchymal poles (Figures 1B and 1C; Bednarz-Knoll et al., 2012; Grosse-Wilde et al., 2015; Li and Kang, 2016; Nieto et al., 2016). It is therefore likely that in some cases, metastasizing carcinomas may exhibit overt mesenchymal properties that aid in metastatic spread (Bonnomet et al., 2012; Trimboli et al., 2008), whereas in other cases they may not require the same suite of EMT-associated traits (Celià-Terrassa et al., 2012).

In fact, a large number of reports highlight the existence of the “partial EMT” state and its propensity to enhance tumor progression and metastasis (Bednarz-Knoll et al., 2012; Grosse-Wilde et al., 2015; Hong et al., 2015; Jordan et al., 2011; Lundgren et al., 2009; Sampson et al., 2014; Schliekelman et al., 2015). In contrast, induction of a fully mesenchymal state, as achieved experimentally through the actions of introduced, highly expressed EMT-TFs and resulting completion of an entire EMT program, yields cells that have lost tumor-initiating ability and thus the power to found metastatic colonies (Ocaña et al., 2012; Tsai et al., 2012). Stated differently, the phenotypic plasticity associated with carcinoma cells inhabiting the middle of the epithelial-mesenchymal spectrum appears to be critical to the founding of metastatic colonies and their subsequent robust outgrowth. Unaddressed by this discussion is the behavior of ovarian carcinomas, whose spread through the peritoneal space

operates through principles very different from those characteristic of most solid tumors.

Circulating Tumor Cells

Individual invasive carcinoma cells and invasive cohorts arising from primary tumors may, sooner or later, invade into the vasculature either of adjacent normal tissues or the neovasculature that has been assembled within the tumors themselves. The resulting intravasation provides access to an avenue for circulating tumor cells (CTCs) to travel to distant sites, where they may seed new metastatic colonies (Kang and Pantel, 2013). Such travelers may move as individual cells or as multi-cellular clumps that can persist in the circulation until they encounter the small-bore microvessels of distant tissues (which often possess luminal diameters as small as $\sim 8 \mu\text{m}$). The consequent physical trapping would seem to ensure that the vast majority of intravasated CTCs dwell in the general circulation for only seconds or minutes after their initial entry into the vasculature. Although most CTCs may be rapidly cleared, it has been recently reported that even clusters of CTCs are capable of maneuvering through capillary-sized vessels, doing so as a single-cell chain still held together through adhesive interactions (Au et al., 2016). CTC clusters introduced experimentally into the venous circulation are far more efficient than individual carcinoma cells in seeding metastatic colonies, ostensibly because, relative to single CTCs, they are more resistant to apoptosis and may have an advantage in physically lodging in the lumen of vessels (Aceto et al., 2014). In addition, these clusters might be shielded from various types of attacks, such as those launched by natural killer (NK) cells, and may benefit from certain poorly understood advantages in post-extravasation proliferation that could contribute to their increased metastatic efficiency.

Nonetheless, single CTCs have been extensively studied in recent years because of technical improvements in their isolation from the blood of cancer patients (Aceto et al., 2015). Implicit in these surveys is the notion that these cells represent intermediaries between primary tumors and eventually formed metastatic colonies. However, in light of the considerations discussed above, it remains unclear which types of CTCs (single versus clusters) are actually responsible for the lion's share of metastasis formation. Indeed, the probability of a single CTC successfully founding a metastatic colony is vanishingly small (Baccelli et al., 2013). Independent of these considerations is the notion that single and clustered CTCs released by primary tumors could often be produced in a certain ratio, in which case the solitary CTCs may serve as surrogate markers of the cell clusters that may indeed be responsible for the formation of the great majority of metastatic colonies.

Of additional relevance here is the fact the CTCs, traveling either as individual cells or as clusters, often exhibit combinations of epithelial and mesenchymal traits, reinforcing the role of the EMT program in the process of intravasation and cancer cell dissemination (Yu et al., 2013). Moreover, in longitudinal studies of individual patients, the fraction of mesenchymal CTCs has been found to increase progressively with acquired treatment resistance and disease progression. One concern here derives from the fact that CTC enrichment methods that rely on the display by CTCs of cell-surface epithelial markers may well miss capturing a sizeable, clinically relevant portion of the

CTCs that are responsible for seeding distant metastases but have shed the bulk of their epithelial cell-surface markers as a consequence of extensive progression through EMT programs.

All of these provisos do not detract from certain already-proven uses of CTC technology. Single CTCs may indeed be useful for certain types of diagnoses, since the presence of CTCs has been repeatedly found in commonly occurring carcinomas, including those of the breast, prostate, lung, and colon (Aceto et al., 2015). In particular, the longitudinal monitoring of CTC concentrations through "liquid biopsies" may provide highly useful information about the responses of a patient's tumor to various types of therapies. Another clearly useful application is the measurement of CTCs in patients whose primary tumors have been removed in order to determine whether residual, occult metastatic deposits persist and continue to empty carcinoma cells into the circulation.

In addition, the isolation, *ex vivo* expansion, and analysis of viable CTCs can be used to profile genetic mutations and drug sensitivities of the cells residing within primary tumors (Yu et al., 2014). This may allow the prediction of patient responses to various types of therapy, especially when the lesions being treated are not readily biopsied, for example those in the brain. Indeed, one already published report demonstrates that CTCs isolated from prostate cancer patients can be harbingers of eventually acquired drug resistance, such as those carrying molecular changes that can confer resistance to androgen receptor antagonists (Miyamoto et al., 2015). Ideally, early detection and characterization of CTCs prior to the appearance of clinically detectable metastatic growths could be used to initiate or switch treatment before the eruption of life-threatening metastases. At present, however, this seems to be impractical, given the fact that even actively growing, aggressive tumors tend to release relatively low numbers of detectable CTCs into the circulation.

Interactions in Transit: Fates of Intravasated Carcinoma Cells

In fact, carcinoma cells that have successfully invaded stromal environments surrounding primary tumors can intravasate either into blood or lymphatic vessels. The dissemination of cancer cells to draining lymph nodes represents an important clinical parameter that is incorporated into the histopathological staging of the disease and thus is associated with particular prognoses (de Boer et al., 2010). While carcinoma cells may promote the growth of lymphatic vessels through the process of lymphangiogenesis (Karaman and Detmar, 2014)—a process that is correlated with disease progression (Skobe et al., 2001)—there is scant evidence for the notion that the draining lymph nodes represent temporary staging areas that enable significant numbers of cancer cells to pause before proceeding further into the bloodstream and thereafter to distant sites in the body. Hence, these small metastatic deposits probably represent dead ends for cancer cells and primarily function as surrogate markers that reveal the extent of parallel, concomitant dissemination from the primary tumor into the general circulation. For this reason, the discussion below is focused on the hematogenous transport of carcinoma cells, as this is likely the main route that metastatic cancer cells traverse prior to entering and colonizing distant tissues.

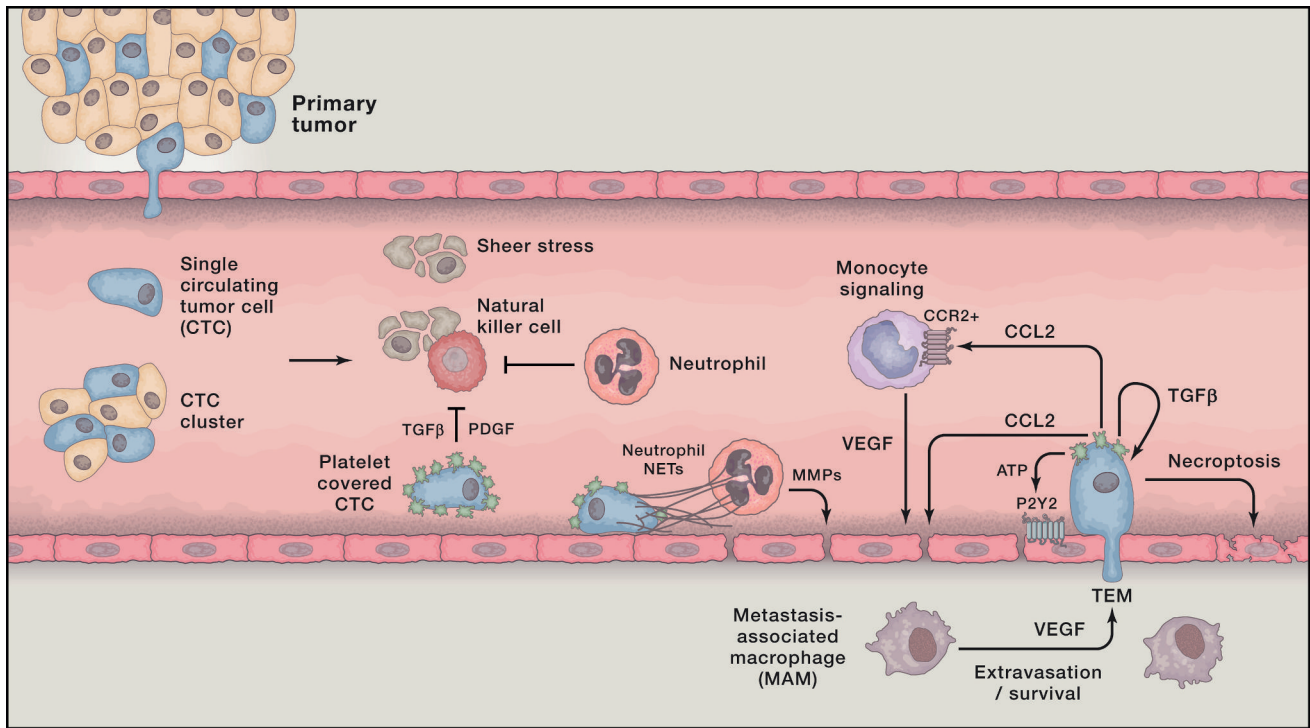


Figure 2. Interactions in Transit

Carcinoma cells escaping from primary tumors can intravasate into the circulation, either as single circulating tumor cells (CTCs) or as multicellular CTC clusters. The bloodstream represents a hostile environment for CTCs, exposing them to rapid clearance by natural killer (NK) cells or fragmentation due to the physical stresses encountered in transit through the circulation. Carcinoma cells gain physical and immune protection through the actions of platelets, which coat CTCs shortly after intravasation. Neutrophils can provide protection from NK cell attacks as well, while also contributing to the physical entrapment and extravasation of CTCs. Once lodged in a capillary, activated platelets and carcinoma cells secrete a number of bioactive factors that can act on monocytes, endothelial cells, and the carcinoma cells themselves. The collective effects of these interactions promote the transendothelial migration (TEM) of carcinoma cells, which can be aided by metastasis-associated macrophages (MAMs) in the target parenchyma. In lieu of TEM, arrested carcinoma cells may also proliferate intraluminally (not shown) or induce necroptosis in endothelial cells.

The safe passage of intravasated cancer cells to distant anatomical sites is hardly guaranteed. Although the transit time of a cancer cell through the bloodstream may amount to only a few minutes, CTCs encounter multiple obstacles en route to the parenchyma of distant tissues. Foremost here are the physical challenges associated with life in circulation, which include loss of attachment to a substrate, hydrodynamic flow, and shear stress (Headley et al., 2016). In addition, carcinoma cells in the circulation are vulnerable to an immune attack, notably by NK cells that target them for rapid elimination. However, certain interactions between circulating carcinoma cells and other cell types in the circulation can actually facilitate their passage to and extravasation at distant sites, notably those involving platelets, neutrophils, monocytes/macrophages, and endothelial cells (Figure 2).

Interactions with Platelets

Once in the circulation, CTCs rapidly associate with platelets, an interaction that is triggered by tissue factor displayed on the surface of the carcinoma cells (Labelle and Hynes, 2012). Depending on the rate of CTC introduction into the circulation, this can lead to imbalances in the normal homeostatic controls on coagulation, which can result in certain clotting symptoms that are seen in patients with cancer, specifically microthrombi,

disseminated intravascular coagulation, and even large pulmonary emboli (Gay and Felding-Habermann, 2011).

At the same time, platelets facilitate tumor metastasis. Indeed, the contribution of platelets to the metastatic process has been appreciated since the 1960s, when studies revealed that experimental induction of thrombocytopenia can exert an anti-metastatic effect (Gasic et al., 1968), while a high platelet count has for years been known to be associated with a poor clinical prognosis across diverse types of carcinomas (Gay and Felding-Habermann, 2011). Platelets contain a plethora of bioactive molecules that can potentially impact cancer progression and work in more recent years has revealed a number of mechanisms by which platelets can alter the fate of carcinoma cells in transit (Franco et al., 2015; Gay and Felding-Habermann, 2011).

Of relevance here is the fact that platelets can protect CTCs from elimination by cellular arms of the immune system. More specifically, adhered platelets can prevent tumor cell recognition and lysis by NK cells (Kopp et al., 2009; Nieswandt et al., 1999; Palumbo et al., 2005). This effect can be mediated by soluble factors derived from platelets, including TGF- β and PDGF that inhibit NK cell activity (Labelle and Hynes, 2012), and, quite possibly, by physically shielding cancer cells from NK cells

through the formation of protective cloaks around CTCs and the deposition of fibrinogen on the cancer cells (Palumbo et al., 2005, 2007). Such protection specifically against NK cell-mediated attack may represent the most important benefit conferred on intravascular carcinoma cells by platelets, since the pro-metastatic effects of the thrombocytes are no longer apparent in mice depleted of NK cells (Palumbo et al., 2005).

In addition to protecting circulating tumor cells from external insults, platelets can also alter intracellular signaling pathways within carcinoma cells that ultimately affect the ability of the latter to establish metastatic growths. Notably, TGF- β secreted by degranulating platelets can act in coordination with contact-dependent signals that activate the NF- κ B pathway in carcinoma cells, thereby inducing or sustaining the expression of EMT programs in the CTCs (Labelle et al., 2011). This direct signaling between platelets and carcinoma cells can presumably substitute for the absence of stroma-derived signals that previously led, in the context of the primary tumor, to the induction of an EMT. In the absence of such heterotypic interactions, CTCs may revert via a MET to the epithelial state of their ancestors in the primary tumor, thereby losing the invasive traits and tumor-initiating ability that would seem to be critical for subsequent extravasation and the founding of metastatic colonies.

Once activated by cancer cells, platelets can signal to nearby endothelial cells as well. Tumor cells elicit ATP secretion from activated platelets, which can proceed to render the vasculature more permeable by acting on P2Y2 receptors expressed by endothelial cells (Schumacher et al., 2013). Moreover, physical interactions between platelets and endothelial cells, for example those mediated by selectins, have been proposed to be important for the adhesion of platelet-cancer cell clusters to the walls of the vasculature (Köhler et al., 2010). It remains unclear, however, whether such adhesive interactions are actually critical to the intraluminal arrest and eventual entrance by the neoplastic cells into the parenchyma of various tissues.

Interactions with Neutrophils

Neutrophils can exist in distinct and dynamically changing phenotypic states that can be shaped by the primary tumor as well as other host cells (Coffelt et al., 2016; Fridlender et al., 2009; Sagiv et al., 2015). We focus here on their actions in circulation, where evidence is beginning to clarify their role during this phase of the metastatic cascade. In certain instances neutrophils have been found to inhibit metastasis. For example, primary tumors can educate neutrophils via CCL2 secretion, giving rise to tumor-entrained neutrophils (Granot et al., 2011). These cells appear to accumulate in the circulation and the lungs of tumor-bearing mice even prior to metastatic progression and have been found to prevent carcinoma cells from seeding the lungs. Neutrophils mobilized by G-CSF treatment lack this power (Granot et al., 2011), highlighting the fact that neutrophils can be primed to adopt different functional states.

In large part, however, the molecular and cellular physiology of neutrophils appears to dictate that their predominant role is one that favors metastatic seeding. For example, neutrophil extracellular traps (NETs), which are formed from released DNA molecules, are designed to entangle pathogens during a response to infection but can also be deployed by neutrophils to capture

tumor cells in the circulation (Cools-Lartigue et al., 2013). Such entangled CTCs may be more apt to survive intraluminally, adhere to endothelial cells, and extravasate. Neutrophils can directly interact with tumor cells trapped in the vasculature, prolonging their retention in the lung after intravenous injection (Huh et al., 2010). In a similar manner, neutrophils can facilitate adhesive interactions within liver sinusoids, thereby serving as physical platforms on which CTCs can dock prior to extravasation (Spicer et al., 2012). Additionally, neutrophils enhance the extravasation of tumor cells after arrest, mainly through the secretion of various matrix metalloproteinases (MMPs) (Spiegel et al., 2016).

Neutrophils have also been shown to exert immunosuppressive functions. Often mobilized through systemic signaling by a primary tumor, neutrophils can inhibit both cytotoxic CD8⁺ T cell responses (Coffelt et al., 2015) and the intraluminal clearance of carcinoma cells by NK cells (Spiegel et al., 2016). Such protection from attack by arms of the innate and adaptive immune system offers a clear advantage to tumor cells in transit. Finally, some of the effects mediated by neutrophils may occur in response to the aggregation of platelets and tumor cells noted previously. Thus, the release of platelet-derived chemokines can recruit neutrophils, which can then, as described here, enhance the seeding and metastatic outgrowth of carcinoma cells in circulation (Labelle et al., 2014).

Extravasation

Many of the intravascular interactions described above influence the ability of CTCs to extravasate and thereby enter into the parenchyma of distant tissues. Extravasation requires carcinoma cells to traverse the endothelial wall through a process that is termed transendothelial migration (TEM) (Reymond et al., 2013). Earlier we cited the ability of ATP released by activated platelets to render the capillary walls more permeable; in more detail, this is achieved by causing endothelial cells to retract from one another. In addition, breast carcinoma cells primed by TGF- β in the primary tumor acquire the ability to produce angiopoietin-like 4 (ANGPTL4), which enhances the permeability of the lung vasculature, promotes TEM of carcinoma cells, and leads to an increased capacity for metastatic outgrowth (Padua et al., 2008). Several other proteins produced by carcinoma cells have been reported to function as disruptors of vascular integrity, including VEGF, MMPs, and ADAM12; these secreted molecules seem to enhance both intravasation as well as extravasation (Gupta et al., 2007; Reymond et al., 2013), indicating that certain traits that were advantageous previously in the course of primary tumor invasion may also prove useful at later steps in the invasion-metastasis cascade.

The recruitment of monocytes has also been demonstrated to play a functional role in tumor cell extravasation. In particular, the recruitment of CCR2⁺ inflammatory monocytes in response to CCL2 secretion by carcinoma or host cells can facilitate extravasation and subsequent metastatic growth in the lung parenchyma (Qian et al., 2011; Wolf et al., 2012). These inflammatory monocytes may differentiate into metastasis-associated macrophages, which similarly enhance the seeding, survival, and growth of carcinoma cells in the lung through the release of VEGF (Qian et al., 2009, 2011). CCL2 can also act directly on endothelial cells to enhance vascular permeability (Wolf et al.,

2012). Although inhibition of the CCL2-CCR2 axis would seem to represent an ideal anti-metastatic therapy, the termination of anti-CCL2 therapy actually leads to an enhanced monocyte infiltration of tumors and lungs with a corresponding acceleration of disease progression (Bonapace et al., 2014), underscoring the dynamic and unpredictable nature of targeting such microenvironmental interactions.

Most experimental models of metastasis have, for various reasons, focused on the lungs as destination sites of disseminated tumor cells. However, the requirements for successful extravasation and the relevant interactions that facilitate this process are likely to be quite different in various tissue sites. For instance, the fenestrated sinusoids of the bone marrow and liver are more likely to permit the passive entry of CTCs, obviating many of the complex interactions and mechanisms enumerated above. In the case of the brain, the dissemination of carcinoma cells would seem to require passage through the blood-brain barrier, which may in fact necessitate the actions of a tissue-specific program for extravasation that is very different from those enabling metastatic seeding elsewhere in the body. Indeed, breast cancer cells selected for preferential metastasis to the brain express at high levels a number of genes that are known to facilitate passage through the blood-brain barrier (Bos et al., 2009; Sevenich et al., 2014).

In certain cases, TEM migration may not be required at all, as arrested carcinoma cells have been found to proliferate in the lumina of blood vessels, leading to the growth of large intraluminal tumor colonies that eventually rupture nearby endothelial walls, enabling direct access to the tissue parenchyma (Al-Mehdi et al., 2000). Finally, a novel mechanism has recently been described, in which tumor cells can extravasate and generate lung metastases via induction of programmed necrosis (necroptosis) in endothelial cells (Strilic et al., 2016).

Metastatic Colonization

The growth of an overt metastatic colony represents the final and most deadly phase in the malignant progression of a tumor. Still, the vast majority of carcinoma cells in circulation seem ill prepared for growth in a distant organ environment; some experimental evidence has yielded estimates of the efficiency of metastasis after intravenous injection of tumor cells as low as 0.01% (Chambers et al., 2002). Even carcinoma cells that have managed to extravasate seem almost invariably destined to either be eliminated from the tissue parenchyma or to enter into a state of dormancy (Luzzi et al., 1998), in which they persist in an indolent state as single disseminated tumor cells (DTCs) or as small micrometastatic clusters—sometimes for weeks, months, even years.

Having traveled far from the primary tumor, DTCs find themselves in a new tissue microenvironment that is devoid of the familiar stromal cells, growth factors, and ECM constituents that previously sustained the lives of their predecessors in the primary site. Hence, their inability to continue proliferating and the resulting entrance into a prolonged growth-arrested state may often be attributable to a microenvironment to which these cells are poorly adapted when they first arrive after extravasation. When portrayed in this way, metastatic dormancy reflects a failure of DTCs to adapt to and colonize a given tissue. Importantly,

a dormant state can also be actively imposed by certain anti-proliferative signals encountered by recently arrived cells in the parenchyma of foreign tissues. We first consider the programs operative in dormant DTCs before turning to those that enable colonization.

Dormancy Programs

The latent, clinically inapparent phase of metastasis might well be the result of factors beyond those cited here that render carcinoma cells unable to proliferate, such as an inability to induce angiogenesis or active suppression by the immune system (Aguirre-Ghiso, 2007). These two particular mechanisms are thought to permit a low level of proliferation that is counterbalanced by ongoing elimination, resulting in no net increase in the sizes of micrometastatic clusters.

From a clinical perspective, patients successfully treated for their primary tumors but potentially harboring such dormant cancer cells are considered to have asymptomatic minimal residual disease (MRD) (Figure 3A). For certain carcinomas, such as those of the breast, prostate, and kidney, this period of dormancy may last for many years, even decades after ostensibly successful courses of initial therapy. And while it is difficult to formally prove that a metastatic colony directly developed from a preexisting dormant DTC, the presence of DTCs in the bone marrow is clearly correlated with an increased risk of eventual clinical recurrence (Braun et al., 2005). This reveals why an understanding of the biologic bases of dormancy is of utmost clinical importance, if only because the period of dormancy represents a critical time window during which therapeutic interventions directed at DTCs—either targeting them for elimination or restraining their proliferation—may well succeed in preventing the eventual eruption of life-threatening metastatic disease.

Dormancy programs (Figure 3B) can be initiated from either an active response to signals encountered in the new tissue microenvironment or from an absence of contextual cues that carcinoma cells previously depended on while residing in their sites of origin within primary tumors (Giancotti, 2013; Sosa et al., 2014). As an example, DTCs that respond to survival signals present in the microenvironment can avoid destruction and persist for extended periods within a tissue parenchyma. In one well-studied case, breast cancer cells that have lodged in the bone marrow and possess high SRC activity and expression of CXCR4 are able to activate pro-survival pathways in response to bone-derived CXCL12 (Zhang et al., 2009). DTCs capable of sensing and responding to these survival cues are able to counteract TRAIL-induced apoptosis, a conserved tissue defense mechanism that can work in the opposite direction to eliminate DTCs. The survival of DTCs may also be related to their ability to withstand anoikis, for example through the expression of the tyrosine kinase receptor TrkB (Douma et al., 2004) or through non-canonical Wnt signaling mediated by WNT2 (Yu et al., 2012).

Even if DTCs benefit from such survival signals in their new tissue environment, in the absence of additional mitogenic cues, including interactions with the extracellular matrix (ECM), these cells may languish in a dormant state. Thus, dormancy has been reported to ensue when disseminated carcinoma cells fail to engage integrin β_1 and the downstream activation of focal adhesion kinase (FAK) (Aguirre Ghiso et al., 1999; Barkan et al., 2008; Shibue and Weinberg, 2009). The ability of DTCs

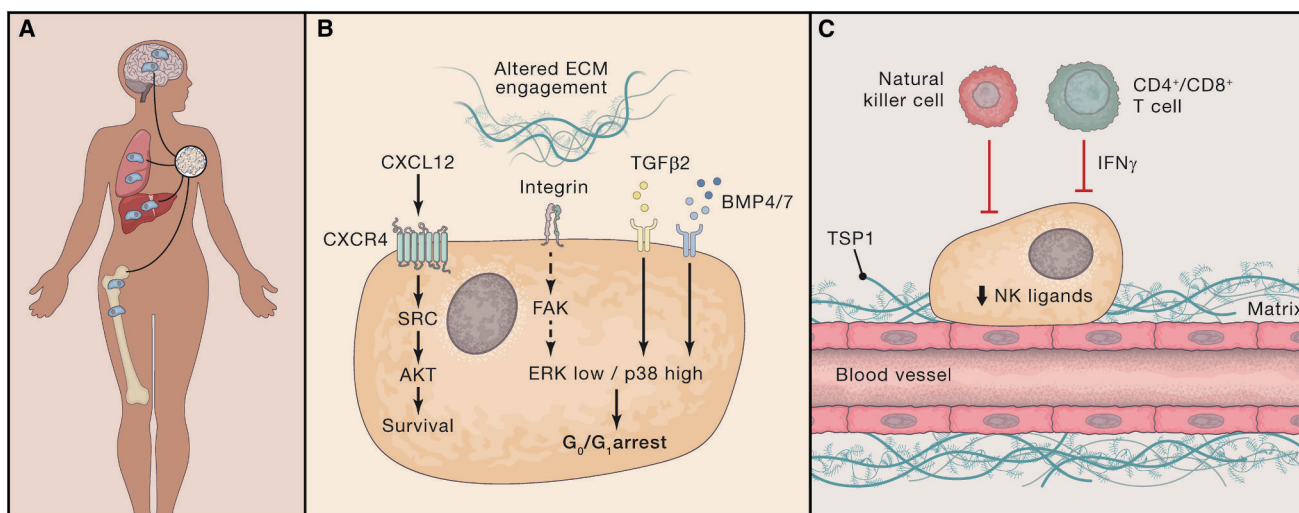


Figure 3. Dormancy Programs and Niches

(A) Carcinoma cells that have disseminated prior to the surgical removal of the primary tumor may persist in distant tissue environments as dormant disseminated tumor cells (DTCs). Patients harboring such reservoirs of occult carcinoma cells are considered to have minimal residual disease and are at increased risk of eventual metastatic recurrence. Although DTCs are most frequently examined in the bone, the delayed outgrowth of metastases in other organs suggests that they, too, can harbor dormant DTCs.

(B) Dormant DTCs rely on unique biochemical signaling pathways that sustain their survival and impose programs of quiescence. Signals from the microenvironment, such as CXCL12, can activate SRC and AKT to promote DTC survival. Reduced integrin-mediated mitogenic signaling, coupled with the actions of certain dormancy-inducing cytokines, enacts a quiescent program in DTCs that is associated with an ERK^{low}/p38^{high} signaling state.

(C) DTCs may reside in dormant niches such as the hematopoietic stem cell niche (not shown) or the perivascular niche illustrated here. Thrombospondin-1 (TSP1), present in the basement membrane surrounding mature blood vessels, promotes dormancy. Dormant cells can evade detection by NK cells through the repression of NK cell-activating ligands and are likely subject to surveillance by the adaptive immune system, which may keep cancer cells in a dormant state through the actions of IFN γ .

to productively interact with the matrix, at least in the context of the lung, appears to be contingent upon the formation of filopodium-like protrusions (FLPs) that are coated with integrin β_1 (Shibue et al., 2012, 2013). DTCs that are unable to sense or respond to such adhesive signals fail to activate proliferative programs that are primarily driven by FAK, SRC, and ERK signaling (Barkan et al., 2010; Shibue et al., 2012). Accordingly, combined inhibition of both the SRC and ERK pathways blocks the escape of DTCs from dormancy and thus prevents their subsequent success in metastatic colonization (El Touny et al., 2014).

Several dormancy-inducing signals found in the microenvironment of certain target tissues have been identified as well. For instance, TGF- β 2, present in high concentrations in the bone marrow and acting through stimulation of TGF- β -RI and TGF- β -RIII displayed by DTCs, can impose a state of dormancy upon head-and-neck squamous carcinoma cells (Bragado et al., 2013). Members of the related BMP ligand family have also been linked to metastatic dormancy. BMP7, which can be produced by bone stromal cells, can induce dormancy in prostate cancer cells (Kobayashi et al., 2011). In the lung, too, a number of alternative BMP ligands are expressed, including BMP4, and these have been implicated as factors that maintain a state of dormancy in disseminated mammary carcinoma cells (Gao et al., 2012). Many of these dormancy-inducing cytokines lead to activation of the p38 MAPK pathway; coupled with the absence of mitogenic signals, this has the net effect of promoting an ERK^{low}/p38^{high} state in DTCs, which leads in turn to arrest in the G₀/G₁ phases of the cell cycle and associated quiescence (Sosa et al., 2011).

The Dormant Niche

Dormant DTCs may reside in specialized niches (Figure 3C) that support their survival, restrain their proliferation, and quite possibly provide resistance to therapeutic agents (Ghajar, 2015). Of particular interest here is the idea that dormant DTCs can co-opt a niche that is otherwise reserved for tissue-resident stem cell populations. A compelling demonstration of this phenomenon is provided by the case of prostate cancer cells that metastasize to the bone, where these carcinoma cells have been found to compete with hematopoietic stem cells (HSCs) for occupancy of sites in the endosteal niche; this occurs via the CXCL12-CXCR4 signaling axis that is normally reserved for the physiologic regulation of HSCs (Shiozawa et al., 2011). The fact that DTCs can specifically target a stem-cell niche suggests that they may be poised to respond to the quiescent and survival signals present within the HSC microenvironment.

In multiple organs—including the lung, bone, and brain—DTCs have been found to reside in the microenvironment surrounding the vasculature, a region known as the perivascular niche (Ghajar, 2015). Whether this represents their active retention in this niche or simply indicates an inability to move farther from the vasculature after initial extravasation is unclear. An alternative mechanism is suggested by the finding that factors present in the perivascular niche have been demonstrated to actively promote dormancy. Thus, thrombospondin-1, produced from mature endothelial cells and deposited in the microvascular basement membrane, is able to confine DTCs to residence in a quiescent state (Ghajar et al., 2013). Moreover, in a study using

real-time imaging to examine the process of brain metastasis, the rare solitary DTCs that achieved long-term dormancy were invariably localized to the perivascular region (Kienast et al., 2010), suggesting a critical role for this niche in sustaining dormant DTCs in the brain as well.

DTCs must protect themselves from immune attack when dwelling as isolated single cells lodged far from the confines of the immunosuppressive primary tumor microenvironment. Breast and lung carcinoma cells selected for their ability to persist in a latent state after seeding of distant organ sites succeed in evading clearance by NK cells through the repression of various NK cell-activating ligands, a program that appears to be tightly coupled with entrance into a quiescent state (Malladi et al., 2016). Indeed, these latency-competent cells have been observed to grow out when injected into mice that lack NK cells, indicating that the innate immune system is an important component of the dormant niche that effectively forces many cancer cells into a quiescent state. A quite different process is suggested by the observation that antigen-presenting dendritic cells can protect against metastasis (Headley et al., 2016), implying a role of the adaptive immune system in controlling the growth of metastatic deposits. Both CD4⁺ and CD8⁺ T cells have been implicated in the control of dormant primary tumor cells through the secretion of IFN γ (Koebel et al., 2007; Müller-Hermelink et al., 2008) and there is evidence that CD8⁺ T cells can hold disseminated uveal melanoma cells in a dormant state (Eyles et al., 2010). However, at present very little is known about such immune-mediated dormancy mechanisms in the context of DTCs originating from carcinomas.

Cancer Stem Cell Programs and the Initiation of Metastatic Colonization

As mentioned above, activation of the EMT program, which is capable of driving the physical dissemination of carcinoma cells to distant anatomical sites, can also confer upon these cells important stem cell traits (Mani et al., 2008; Morel et al., 2008) that would appear to be highly relevant to metastatic colonization. Thus, an apparent prerequisite to the successful formation of a metastatic colony is the property of tumor initiation as embodied in CSCs. At least in principle, it is only those DTCs that reside in the CSC state that are qualified to serve as the founders of metastatic colonies.

Accumulating evidence, mostly from animal models, largely supports this notion. In the MMTV-PyMT mammary tumor model, a rare population of CSCs has been shown to be responsible for the initiation of metastatic growths in the lung and, accordingly, the ability of these tumors to metastasize is dependent on the maintenance of this stem cell population through enhanced Wnt signaling (Malanchi et al., 2011). In human breast cancer cells, the activation of key stem cell pathways, such as Wnt and Notch signaling, is also important for supporting their colonization in xenograft mouse models (Oskarsson et al., 2011). And mouse models of lung adenocarcinoma have revealed that metastatic progression is associated with a dedifferentiation program, mediated by loss of Nkx2-1 expression, which resembles programs operating in stem-like states (Li et al., 2015; Winslow et al., 2011). Thus, it appears that the metastatic potential of a carcinoma is closely related to its ability to dispatch populations of CSCs that can re-initiate tumor growth

after arrival at distant sites (Oskarsson et al., 2014). This notion implies that cell state is a critical determinant of successful metastasis, more specifically residence in the epigenetic state associated with CSCs.

As discussed extensively above, an alternative to metastatic outgrowth proceeding immediately after dissemination is the entrance of DTCs into an indolent state in which they may persist for extended periods of time before their progeny eventually erupt into readily detectable macroscopic metastases. Such persistence may be favored by the acquisition of stem cell characteristics. Thus, DTCs detected in the bone marrow of breast cancer patients exhibit features of CSCs (Balic et al., 2006). Consistent with this, cells that remain in a latent state in distant tissues also show CSC attributes, including expression of the SOX2 and SOX9 transcription factors (Malladi et al., 2016). In addition, single-cell expression analyses have been applied to DTCs isolated from the organs of patient-derived xenograft (PDX) models of breast cancer; some organs harbored low-burden metastatic disease due to the presence of small numbers of ostensibly dormant carcinoma cells (Lawson et al., 2015). These cells exhibited a distinctive gene expression profile, relative to carcinoma cells from advanced metastatic lesions, that was characterized by the expression of EMT, stem cell, and survival/dormancy genes. Most intriguingly, when neoplastic cells isolated from such low-burden tissues were implanted into new recipient animals, they retained their tumorigenic potential and could readily generate more differentiated carcinomas (Lawson et al., 2015). These studies provide further evidence in support of the notion that stem-like cancer cells often serve as the founders of metastatic colonies, even when such colonies appear only after great delay.

This scheme implicating the EMT and stem-cell programs as critical prerequisites to the successful founding of metastatic colonies must be reconciled with the commonly observed fact that carcinoma metastases tend to recapitulate key histopathological traits of their corresponding primary tumors. Among other traits, this usually includes significant epithelial features (Brabletz, 2012). On its surface, this notion would seem incompatible with the proposition that EMT plays a central role in launching carcinoma metastases through its ability to impart mesenchymal and stem cell attributes to the disseminating cells. In fact, this paradox is resolved by numerous studies, some cited here in passing, that have found that the disseminated progeny of carcinoma cells appear to undergo the reverse of the EMT program at some point after dissemination, i.e., they pass through a MET. This reversion to an epithelial state should restore many of the cellular traits that were lost during the prior passage through an EMT (Brabletz, 2012) and enable reconstruction of hierarchical cell organizations similar to those present in the initial primary tumors. Indeed, such reversals by many cells within an early metastatic growth to a more epithelial state may actually be essential for metastatic colonization (Del Pozo Martin et al., 2015; Korpál et al., 2011; Ocaña et al., 2012; Tsai et al., 2012). Of note, it remains unclear precisely why highly mesenchymal CSCs cannot generate robustly growing metastatic colonies in the absence of the epithelial progeny generated by such METs.

Mechanisms of Colonization

Metastatic colonization appears, at least as presently understood, to depend critically on two preconditions of the disseminated carcinoma cells: they must possess tumor-initiating ability, as argued above, and they must in some fashion contrive adaptive programs that enable them to thrive in the microenvironment present in the parenchyma of distant tissues. The “seed and soil” hypothesis, put forth by Paget in the late 19th century, suggested a complementary notion—essentially, that certain types of carcinoma cells are more able to generate metastases in certain foreign tissue microenvironments than are others (Fidler, 2003). Unspoken by Paget was the notion that even in such favored metastatic sites, DTCs must still undergo some form of phenotypic adaptation in order to proliferate robustly in those sites. Thus, the proclivity of prostate and breast carcinomas to metastasize to the bone would seem to imply some preexisting ability of the corresponding DTCs to more readily assemble adaptive programs suited to that tissue, whereas other less-favored tissue sites might require more elaborate, less readily assembled adaptive programs.

To be sure, in certain cases, the organ-specific tropism of metastatic cells is influenced by the design of the circulatory system. Colorectal carcinoma (CRC) metastasis to the liver is strongly favored simply because the portal vein draining the gut empties directly into the liver (Gupta and Massagué, 2006). Hence, even if disseminated CRC cells were intrinsically poorly adaptable for liver colonization, the sheer numbers of these cells that are trapped in the liver after passage through the portal vein may, on its own, pre-ordain metastases eventually arising at this site.

Importantly, the layout of the circulatory system explains only a small proportion of the organ-specific metastases commonly observed in the oncology clinic. Often cited in this context is the proclivity of breast and prostate cancer cells, as mentioned above, to colonize the bone marrow, usually termed osteotropic metastasis. We highlight below specific examples that illustrate the nature of the adaptive programs that seem critical to successful metastatic outgrowth.

To begin, we note that some of these programs may act generally by conferring a survival advantage in a number of distinct target organs. For instance, cancer cells have been shown to experience higher levels of oxidative stress both in the circulation and in the parenchyma of a distant tissue (Piskounova et al., 2015). As a consequence, metabolic adaptations, including the synthesis of antioxidants, may promote the survival and eventual metastatic outgrowth in diverse sites. Adhesive interactions that substitute for those encountered in the primary tumor, such as homotypic cell-cell interactions in the case of disseminating CTC clusters (Aceto et al., 2014) or FLP-ECM interactions in the case of single DTCs (Shibue et al., 2012), may be capable of activating crucial survival pathways in a manner that could be independent of specific target organs and would thus qualify as more general adaptations promoting colonization.

These general adaptive programs may be nothing more than preludes to the challenging tasks of contriving more narrowly applicable, tissue-specific adaptations. Indeed, a diverse array of organ-specific metastatic programs that mediate colonization of the bone, lung, liver, and brain have been reported and studied in mechanistic detail (Nguyen et al., 2009; Obenauf and Mas-

sague, 2015; Sethi and Kang, 2011). In the brain, for example, cancer cells encounter reactive astrocytes that produce plasminogen activator, leading to the production of plasmin that induces carcinoma cell death (Valiente et al., 2014). The ability of carcinoma cells to survive in this hostile environment is dependent upon the expression of serpins, which are typically produced by neurons and protect against plasminogen activator-mediated cell death. In the lung, VCAM-1-expressing carcinoma cells are able to activate their own AKT signaling by physically engaging with integrin α_4 on macrophages that are particularly abundant in the pulmonary microenvironment (Chen et al., 2011). The survival of carcinoma cells in the liver has been linked to an ability to utilize creatine and ATP present in the extracellular microenvironment to generate and import phosphocreatine, which may confer a significant survival advantage on DTCs subject to metabolic stress (Loo et al., 2015). The diversity of these survival mechanisms is a clear reflection of the varied cellular and molecular determinants of successful colonization that operate within different target organs.

More generally, the mechanisms that permit and/or promote the proliferation of various types of cancer cells in diverse distant tissue microenvironments remain obscure. Arguably, the best-understood example to date involves the metastatic colonization of the bone, which has been documented in the case of the osteolytic metastases formed by breast cancers (Nguyen et al., 2009; Obenauf and Massague, 2015; Weilbaecher et al., 2011). Breast carcinoma cells produce a number of molecules, including parathyroid hormone-related protein (PTHrP), IL-11, and MMPs, that favor RANKL stimulation of osteoclast activity, which in turn liberates growth factors from the bone matrix that reciprocally promote tumor cell proliferation and the secretion of even more factors that enhance osteoclast activity. The resulting self-reinforcing positive-feedback loop has been termed the “vicious cycle” of osteolytic metastasis (Mundy, 2002). In contrast, prostate carcinoma cells tend to spawn predominantly osteoblastic metastases that occur as a result of induced osteoblast differentiation (Weilbaecher et al., 2011). Presumably, the appearance of macroscopic metastases in other target organs is similarly dependent on the ability of carcinoma cells to subvert normal cell types residing within these organs, but the details of these heterotypic interactions largely remain to be defined. In one recent example, breast carcinoma cells that colonize the brain have been found to benefit from communication with astrocytes through the assembly of gap junctions established between cancer cells and astrocytes (Chen et al., 2016).

The growth of a metastatic colony may also ensue when dormant DTCs are awakened from their indolent state. The awakening of previously dormant micrometastases may depend on the successful assembly of functional adaptive programs, which may be achieved only rarely per cell generation, explaining the extraordinary low efficiency of metastasis formation. For example, we note that dormant micrometastases in the bone that somehow gain expression of VCAM-1 can transition to an active colonization phase through the recruitment of osteoclast progenitor cells expressing integrin $\alpha_4\beta_1$, a receptor for VCAM-1, which enables bone resorption and initiation of the vicious cycle described above (Lu et al., 2011). Carcinoma cells in the lung are able to escape dormancy through the production of

Coco, a secreted inhibitor of BMP signaling that promotes colonization (Gao et al., 2012). Unspoken here are the mechanisms by which such adaptive programs are actually acquired. Thus, it seems likely that continuous, low-level proliferation of the cells within individual micrometastatic deposits—this occurring over extended periods of time—is essential to the ability of DTCs to stumble through trial and error on highly effective gene expression programs and adaptive behaviors that enable them to thrive in the tissue microenvironment in which they happen to have landed.

Programs that confer multi-organ colonization potential may exist as well. Interestingly, the few examples of these programs that have been described center on interactions between DTCs and the ECM. For example, carcinoma cells selected in vivo for their ability to re-initiate tumor growth in subsequent xenotransplantation injections are also highly competent in establishing metastatic growths in multiple different organs (Ross et al., 2015). In this case, the capacity for multi-organ colonization has been traced to the production of the matrix protein laminin- α 4 (LAMA4), which seems to be critical for the initial proliferation of DTCs. Similarly, the collagen receptor DDR1, in collaboration with the TM4SF1 adaptor protein, has recently been identified as a signaling axis that regulates CSCs and thereby enables the outgrowth of otherwise-dormant carcinoma cells in multiple organ sites (Gao et al., 2016). The activation of such programs could account for the apparently synchronous appearance of metastases in various organs—metastatic showers—that are occasionally observed in patients.

The Metastatic Microenvironment

The above discussions fail to address in any detail the nature of the resident cells within various types of normal tissues that sprout metastatic colonies. At least in the case of carcinomas, these residents are essentially the various types of more mesenchymal cells that constitute the tissue-associated stroma together with the ECM laid down by these cells. To begin, in the same way that primary tumors are highly dependent on their recruited stromal microenvironment, metastatic growths seem equally reliant on stromal support (Hanahan and Coussens, 2012; Quail and Joyce, 2013; Wan et al., 2013). Indeed, the transition of carcinoma cells from a dormant state to one of robust outgrowth may be provoked by changes in their local environment. For example, the apparent dormancy-inducing actions of the perivascular niche noted above seem to be reversed during neo-vascularization as sprouting endothelial tip cells secrete TGF- β 1 and periostin (POSTN), which can break dormancy and promote tumor cell proliferation (Ghajar et al., 2013). Consistent with this idea, the outgrowth of dormant DTCs in the brain also seems to be dependent on angiogenesis (Kienast et al., 2010). Another recent report describes the outgrowth of previously latent DTCs in the lungs being provoked by inflammation (as mediated by pro-inflammatory cells) induced in this tissue (De Cock et al., 2016).

Other findings suggest that metastatic colonization requires, or at least can be aided by, a supportive ECM. This idea is bolstered by the identification of specific ECM components, such as tenascin C (TNC) (Oskarsson et al., 2011) and POSTN (Malanchi et al., 2011), that drive colonization of the lung by

breast carcinoma cells. Tumor cells may themselves produce these ECM components or, alternatively, they may evoke their secretion by resident stromal fibroblasts. In addition, separate but complementary lines of evidence have reported a connection between fibrosis and metastasis (Barkan et al., 2010; Cox and Erler, 2014), suggesting that the local fibroblast and ECM composition can influence the ability of carcinoma cells to colonize an organ. ECM stiffness (Levental et al., 2009; Mouw et al., 2014), which can be modulated by the collagen-crosslinking enzyme lysyl oxidase (LOX), may also be important for the creation of pro-metastatic microenvironment (Erler et al., 2006, 2009). Indeed, the well-described contribution of hypoxia to metastasis may be substantially related to the production of LOX downstream of the transcription driven by hypoxia-inducible factor (Rankin and Giaccia, 2016).

Metastatic colonization is also likely to be impacted by cells of both the innate and adaptive immune system (Kitamura et al., 2015; Quail and Joyce, 2013). Thus, both NK cells and CD8⁺ T cells have been implicated in the suppression of metastasis (Bidwell et al., 2012; Malladi et al., 2016). Conversely, the oxygen-rich environment in the lung acts to restrain T cell responses and induces tolerance against innocuous antigens, but in the context of cancer this actually provides a more hospitable environment for metastatic colonization (Clever et al., 2016). Myeloid cells have also been identified as important contributors to the formation of a favorable metastatic microenvironment (Kitamura et al., 2015), where a unique population of metastasis-associated macrophages may be responsible for not only provoking but also sustaining metastatic growth, perhaps by stimulation of angiogenesis (Qian et al., 2009). Finally, acute inflammatory responses have been found to trigger the outgrowth of carcinoma cells, an effect that may be primarily driven by neutrophils (De Cock et al., 2016).

The establishment of a supportive metastatic environment may occur prior to the arrival of any carcinoma cells, through the formation of what has been termed a pre-metastatic niche. This niche formation may involve the actions of VEGFR⁺ bone marrow progenitors (Kaplan et al., 2005), myeloid-derived suppressor cells (MDSCs) (Psaila and Lyden, 2009), or neutrophils (Wculek and Malanchi, 2015). Some have also reported that tumor-derived exosomes—small tumor-derived vesicles that contain DNA, mRNAs, microRNAs, and protein—can re-shape the pre-metastatic environment in preparation for the arrival of carcinoma cells (Costa-Silva et al., 2015; Peinado et al., 2012). Thus, the formation of a pre-metastatic niche may represent one consequence of far-ranging systemic effects induced by primary tumors. More generally, the presence of a primary tumor can lead to the production of numerous systemic signaling factors that, by acting on distant tissues, can elicit responses that may thereafter affect primary tumor growth, pre-metastatic niches, and the outgrowth of previously latent micrometastases (McAllister and Weinberg, 2014).

Genetic and Epigenetic Drivers of Colonization

The classic description of multi-step tumorigenesis implies that the successive accumulation of genetic and/or epigenetic alterations drives primary tumor progression (Fearon and Vogelstein, 1990). A logical extension of this concept would suggest that the outgrowth of a metastatic colony depends on the acquisition of

yet another somatic mutation or set of mutations that empower cancer cells to disseminate and thereafter proliferate in a distant organ. However, more than 25 years after the pioneering work on multi-step progression of colorectal carcinoma (Fearon and Vogelstein, 1990), no genetic mutations have been identified that are characteristically associated with progression to metastatic disease. Indeed, even large-scale genomic sequencing efforts have yet to uncover recurrent genetic mutations that can adequately explain the eruption of metastatic growths (Garraway and Lander, 2013; Vogelstein et al., 2013). This suggests that the development of metastasis is not contingent upon the accumulation of somatic driver mutations beyond those selected for during primary tumor formation.

In particular, these findings have focused attention on non-genetic mechanisms enabling colonization. According to one idea, colonization may depend on the amplification in metastatic cells of oncogenic signaling pathways that were previously activated in the cells of primary tumors (Vanharanta and Massagué, 2013), for example, through the enrichment of existing clones with elevated signaling through the MAP kinase pathway (Campbell et al., 2010; Jacob et al., 2015). Metastatic carcinoma cells may also need to evade the actions of metastasis suppressor genes, which have been proposed to specifically block the later stages of the invasion-metastasis cascade (Steeg, 2003). Another alternative mechanism may involve defined epigenetic alterations that drive colonization, such as aberrant DNA methylation patterns (Ozturk et al., 2016).

In addition to the actions of individual genes, recent data suggest that metastatic carcinoma cells often exhibit global changes in the structure of their chromatin. Thus, in a mouse model of small cell lung cancer pathogenesis, carcinoma cells competent for metastasis displayed a distinct open chromatin configuration at distal regulatory regions, which were established and bound by the transcription factor Nfib; this change in chromatin structure facilitated, in turn, a shift toward expression of a pro-metastatic neuronal gene expression program (Denny et al., 2016). Such altered epigenetic states may ease the adaptation of DTCs to foreign microenvironments. These advances notwithstanding, the difficulties involved in the procurement and analysis of metastatic samples have led to a continued dearth of information concerning the genetic and epigenetic landscapes found within the neoplastic cells that form human metastases.

To summarize, in spite of the findings described above, metastatic colonization continues to represent the most puzzling phase of malignant progression and the most challenging to model experimentally. The physical dissemination of tumor cells from the primary tumor into the parenchyma of distant tissues can, at least in the context of many carcinomas, be largely understood through the actions of a single cell-biological program—the EMT. This contrasts starkly with the extraordinary complexity of the last step of the invasion-metastasis cascade—colonization. This complexity, highlighted by the apparently myriad heterotypic interactions between populations of disseminated carcinoma cells and constituents of their newfound homes in distant tissues, has complicated attempts at deriving broadly applicable mechanistic principles underlying colonization. Nevertheless, we suggest that the weight of current evi-

dence points to three main prerequisites that must be met in order for metastatic colonization to succeed (Figure 4): (1) the capacity to seed and maintain a population of tumor-initiating cancer stem cells; (2) the ability to contrive adaptive, often organ-specific, colonization programs; and (3) the development of a supportive microenvironmental niche.

Metastatic Evolution

The process of multi-step tumor progression and the subsequent seeding of metastases appears, at least superficially, to operate as a linear path beginning in the primary tumor and ending in macroscopic metastatic colonies. In truth, however, each of the intervening steps is confounded by multiple factors, many discussed above. Similarly, the processes that occur subsequent to the establishment of metastatic colonies and the mechanisms by which they evolve have been a subject of research and discussion over the past few decades. The notion that tumor progression operates according to the Darwinian model of evolutionary growth has become widely accepted and influential in our thinking about metastatic progression (Cairns, 1975; Nowell, 1976). Recent genomic studies have often revealed close genetic relationships between primary tumors and metastases in a variety of cancer types, implying that, at least in certain cases, the cells forming a metastatic colony derive from a dominant clonal subpopulation within the primary tumor that managed to complete all of the steps required both for primary tumor formation and the subsequent multi-step invasion-metastasis cascade (Naxerova and Jain, 2015). Implicit in this depiction once again is the notion that the genetic alterations required for completion of the invasion-metastasis cascade are already present in the genomes of disseminating tumor cells and that completion of this cascade depends only on non-genetic changes, specifically epigenetically organized programs that complement the previously acquired genetic mutations.

Unanswered by such a scheme is the nature of the genetic and epigenetic alterations that render neoplastic cells especially fit to thrive within the context of the primary tumors and how such alterations affect the proclivity of primary tumor cells to disseminate. Thus, it may be that phenotypic changes (of genetic and epigenetic origin) that are selectively advantageous within the context of primary tumor formation may, through happenstance, also make primary carcinoma cells more capable of disseminating. If so, the resulting metastases may arise as incidental side products of primary tumor progression. Alternatively, many of the traits selected during primary tumor formation may prove irrelevant to the success of metastasis formation.

Such logic forces consideration of the genetic and non-genetic factors operating within primary tumors that favor the process of metastatic dissemination. To date, little attention has been placed on these factors. As a specific mechanistic example: what combination of epigenetic programs and somatic mutations render a primary carcinoma cell especially responsive to EMT-inducing heterotypic signals, enabling it to advance to a state of high-grade malignancy? Among important non-genetic factors may be the nature of the normal cells of origin and the differentiation programs that they bequeath to their neoplastic progeny (Latil et al., 2016). At present, we possess relatively little information on the fidelity with which preexisting differentiation

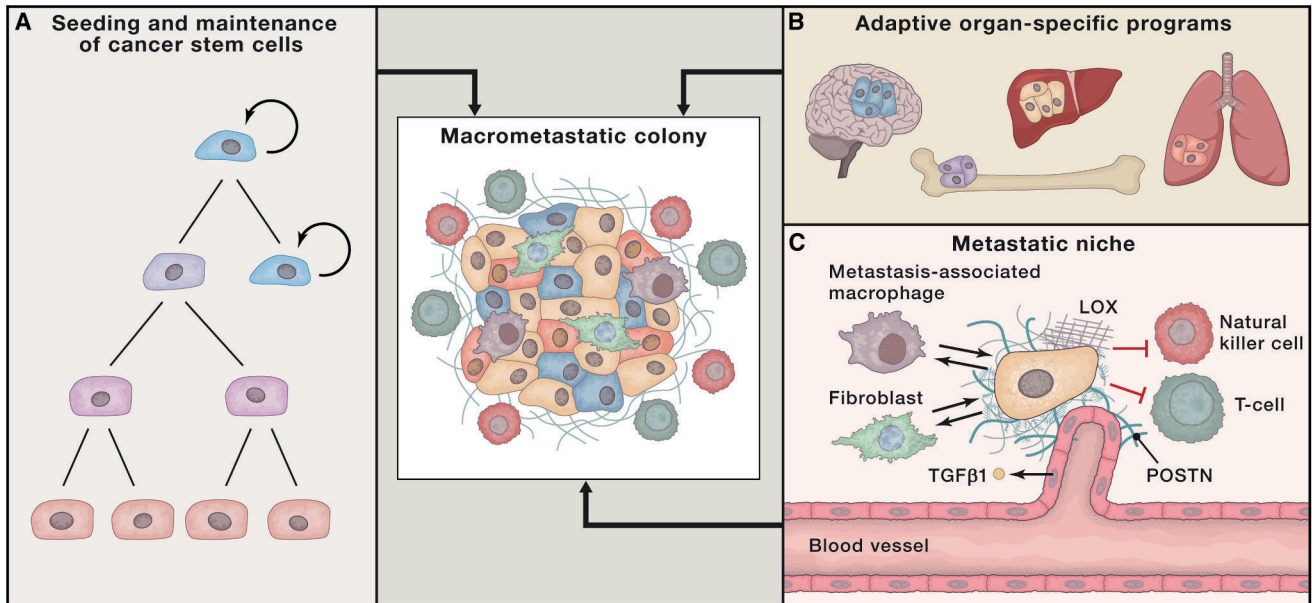


Figure 4. Prerequisites for Metastatic Colonization

The ability of carcinoma cells to outgrow as lethal metastases appears to be dependent on three essential conditions.

(A) The capacity to seed and maintain a population of cancer stem cells, which are competent to re-initiate tumor growth, appears to be an initial prerequisite for metastatic growth. Dormant DTCs also exhibit key cancer stem cell attributes that probably contribute to their prolonged persistence in a quiescent state and their ability to eventually spawn a metastatic colony.

(B) Although cancer stem cells are endowed with the potential to re-initiate tumor growth, the proliferative expansion to an overt metastatic colony is dependent on the ability to contrive organ-specific colonization programs that allow these cells to thrive in a foreign tissue microenvironment. An array of organ-specific metastatic programs has been described in the literature but there is also evidence for the existence of colonization programs that confer multi-organ metastatic potential.

(C) During many stages of metastatic growth, cancer cells depend on interactions with their microenvironmental niche and cross talk with various stromal cells, including endothelial cells, fibroblasts, and cells of the innate and adaptive immune system. The ECM is also an important component of the niche and can be modified in ways that support metastatic colonization. In some cases the formation of a metastatic niche may actually precede the arrival of cancer cells, in what is referred to as a pre-metastatic niche. Selected niche interactions discussed in the text are depicted here.

programs operating in cells of origin are transmitted in a cell-heritable fashion to the distant descendants of the founders of neoplastic cell clones. Such programs could well represent the dominant determinants of metastatic dissemination and may explain why certain subtypes of human cancers disseminate characteristically with predictable frequency to specific sites of metastatic colony formation (Gupta et al., 2005; Ince et al., 2007; Lim et al., 2009; Molyneux et al., 2010; Proia et al., 2011). Unanswered by all of this is another question of great interest: is metastatic ability a trait that is selected for during multi-step primary tumor evolution, or is it nothing more than an unselected, incidental consequence of primary tumor progression?

Dynamics of Tumor Progression and Metastasis

The development of metastasis has traditionally been considered as a relatively late event in multi-step tumor progression. More recent reports, however, suggest that dissemination can often occur early during the process of neoplastic transformation, perhaps even before departing cells are fully transformed (Hüsemann et al., 2008; Podsypanina et al., 2008; Rhim et al., 2012). At least in certain cases, this has been attributed to the presence of pre-neoplastic cells residing within inflammatory microenvironments that are able, via heterotypic signaling, to activate EMT programs, resulting in expression of invasive phenotypes (Rhim et al., 2012). Embedded in this thinking is the notion that EMTs operate both in fully normal epithelial cells

and in neoplastic epithelial cells, suggesting that EMTs may also function in all of the intermediate cell states that define the multi-step progression of primary tumors.

Additionally, the kinetics of metastasis formation in certain mouse models of breast cancer are in line with the idea that dissemination, and hence metastasis, are early events during tumor progression (Weng et al., 2012). The mechanistic details of this early dissemination program have recently been described in murine models of HER2⁺ breast cancer, where in the early stages of primary tumor formation a migratory and stem-like program predominates, before the well-established proliferative pathways take hold during the later stages of tumor growth (Hosseini et al., 2016; Harper et al., 2016). Both studies suggest the possibility that such early disseminated cells may subsequently generate overt metastases. However, in other cases the actual formation of distant metastases appears to be a late event, taking place many years or decades after initial neoplastic transformation (Yachida et al., 2010). Although physical dissemination itself could be an early event, it may have little bearing on the remaining steps of the cascade that result in the generation of macrometastatic foci. Stated differently, it is unclear whether early-disseminated carcinoma cells are ever able to evolve at distant anatomical sites to states of high-grade malignancy and spawn metastatic colonies, this situation representing the “parallel progression” model of metastasis formation.

Two general models of metastatic dissemination have been proposed: the parallel progression model and the linear progression model. According to the latter, clones capable of spawning metastases arise at the later stages of tumorigenesis with a small degree of genetic divergence between those cells in the primary tumor that actually spawned a metastasis and the cells in the metastasis itself (Turajlic and Swanton, 2016). However, such genetic divergence may, in real life, be very difficult to gauge, given the clonal diversity that may have arisen within a primary tumor (Gerlinger et al., 2012) and the fact that various genetically distinct clonal subpopulations may be represented within the primary tumor in dramatically different sizes. Given the possibility that a minor subpopulation within a primary tumor can serve as the source of a metastasis (Haffner et al., 2013), how can one know with any certainty that a sampling of the genomes of primary tumor cells has been able to detect and gauge the genome of this minority population responsible for metastasis and its somatic mutations?

Yet another confounding factor when assessing the linear progression of metastasis is the difference in time between resection and sampling of the primary tumor and that of the metastasis. In fact, a majority of studies have carried out comparisons between primary and secondary (metastatic) tissues that were resected synchronously, while others have compared metastases sampled up to 17 years after resection of the corresponding primary tumors; both have found genetic similarities between the two tissues (Campbell et al., 2010; Ding et al., 2010; Haffner et al., 2013; Liu et al., 2009). These studies favor the linear progression model rather than the parallel progression model, which posits that metastasis occurs as an early event during tumorigenesis, after which the primary tumor and disseminated colonies evolve independently at sites far removed from one another (Klein, 2009).

The parallel progression model, for its part, is encumbered with its own complications. It assumes that the cells disseminating early from the primary tumor are able to proliferate sufficiently to allow for the acquisition of additional mutations that would render them fully transformed and thus capable of forming significant tumor masses. Given that metastatic colonization is a highly inefficient process and given the complexity of essential adaptive programs, it seems unlikely that disseminated preneoplastic cells will actually continuously proliferate after their arrival in distant tissue microenvironments; in the absence of ongoing proliferation, it seems implausible that such cells can acquire, via stochastically occurring mutations, the complex repertoire of mutant alleles that are needed, in aggregate, for continuous growth and clonal expansion. Resolving between these models of metastatic progression may be further complicated by the fact that metastases have been reported to result from polyclonal populations ostensibly derived from CTC clusters (Cheung et al., 2016) and by the observation that metastatic clones may be transferred between different metastatic lesions in the same patient (Gundem et al., 2015).

Treatment and Resistance

Metastatic cancer most often represents a terminal illness and patients eventually succumb to the disease or from complications that result from their course of treatment, indicating the

current dearth of effective therapies (Steeg, 2016). Moreover, it remains unclear precisely whether the cells within metastases are intrinsically more resistant to therapy or whether they respond to therapies at rates comparable to the cells in their corresponding primary tumors. Comparable rates of responsiveness of metastases would certainly be compatible with the known genetic similarities between primary tumors and their derived metastases. Any heightened resistance might be explained by the fact that metastases derive from especially aggressive subpopulations of cells that resided within primary tumors or, alternatively, from further evolution to higher grades of malignancy after dissemination to distant sites.

Treatment of Primary Tumors and Metastatic Growths

Current therapeutic strategies for eliminating metastases are essentially the same as those directed at the corresponding primary tumors, the exception being surgery, which is infrequently employed to remove metastatic deposits. While cells that have succeeded in colonizing distant tissue microenvironments have often and perhaps always evolved adaptive programs that enable their robust proliferation at these secondary sites, it remains unclear whether this additional evolution, much of it achieved through epigenetic reprogramming, confers elevated therapeutic resistance. The alternative is that successful colonization of distant sites depends on the acquisition of adaptive traits that ultimately have no direct effect on therapeutic resistance.

The fact that metastatic lesions represent the progeny of minority subpopulations of the neoplastic cells present in a primary tumor (Ding et al., 2010; Yachida et al., 2010; Yates et al., 2015) suggests that metastatic colonies could be quite different from the primary tumor in terms of their clonal architecture and biology. And while numerous studies have examined the genetic and phenotypic diversity of the neoplastic cells that compose primary tumors (Marusyk et al., 2012), the level of genetic and epigenetic heterogeneity and phenotypic plasticity that operates in metastatic growths is still in question.

A formidable obstacle to treating the minimal residual disease (MRD) that may remain after initial chemo- or radiotherapy derives from the fact that dormant carcinoma cells appear to perpetuate this disease and form the precursors of eventual metastatic relapses. Unfortunately, almost all currently deployed cytotoxic therapies preferentially kill proliferating cells rather than those that have exited the active cell cycle, rendering dormant cells intrinsically more resistant to almost all currently available therapies (Ghajar, 2015; Goss and Chambers, 2010). This stark contrast in the behavior of these dormant DTCs and the actively cycling cells of the primary tumor may ultimately prove to be far more critical in determining susceptibility to therapeutic elimination than any genetic or epigenetic differences distinguishing MRD from the corresponding primary tumors. Further complicating the development of novel agents directed at dormant metastatic deposits is the fact that, for various types of cancer, true efficacy can be judged only after extremely long follow-up periods when the much-feared relapses may appear (Steeg, 2016). Still, preventative adjuvant therapies directed at dormant DTCs and their ability to spawn clinical relapses arguably offer the best opportunity to prevent these outcomes.

Therapeutic Resistance

The mechanisms of therapeutic resistance acquired by metastatic growths may closely parallel those operating within corresponding tumors. In the context of targeted adjuvant therapy, drug-resistant clones may emerge in primary tumors and metastatic lesions, as has been observed, for example, in ER⁺ breast cancer patients receiving hormone therapy (Alluri et al., 2014) and patients with EGFR mutant non-small-cell lung cancer treated with targeted kinase inhibitors (Gazdar, 2009). Of special interest to the present discussion are resistance mechanisms that are particular to the sites of dissemination. One possibility is that the metastatic microenvironment favors the induction of biological programs that confer drug resistance. For example, it has been reported that CXCL1/2, which actively supports the establishment of metastases through the recruitment of myeloid cells, can also mediate resistance to chemotherapy (Acharyya et al., 2012), providing support for the idea that certain traits involved in metastatic dissemination may also contribute to therapeutic resistance.

More generally, the effect of chemotherapy on either primary or metastatic growths may elicit the secretion of various paracrine mediators from the surrounding stromal cells that can promote resistance, including CXCL1/2 (Acharyya et al., 2012), IL-6 and Timp1 (Gilbert and Hemann, 2010), WNT16B (Sun et al., 2012), and HGF (Straussman et al., 2012). Resistance to targeted kinase inhibitors can also be conferred by a host of secreted factors that are produced by carcinoma cells after exposure to a drug (Lee et al., 2014; Obenauf et al., 2015). Although such effects may indeed promote the emergence of drug-resistant cell clones within primary tumors, they may operate even more strongly in sites of metastasis.

According to an alternative view, the cells forming metastases are intrinsically no more or less resistant to therapies than their counterparts in primary tumors. Hence, if drug-resistant ancestral metastatic clones were present in the original neoplasm, then such cells would render this tumor as well as its derived metastases equally resistant to therapy. Following such thinking, a major benefit of surgically eliminating primary tumors derives from reducing the sheer number and diversity of neoplastic cells, thereby increasing the chance that any therapy-resistant variant clones are removed from the body of a patient. In the context of metastatic disease this is, it seems, often not possible.

Conclusion: Principles and Outlook

As the preceding discussions have indicated, significant progress has been made over the past decade in elucidating the cellular and molecular programs that drive cancer metastasis. Although our understanding of metastasis remains quite incomplete, we see a number of common biological principles beginning to emerge. Thus, we suggest that one can take stock of the information that is currently at hand and conclude that:

1. Metastasis occurs mainly through a sequential, multi-step process that can be conceptualized as the invasion-metastasis cascade.
2. In the case of carcinomas, the EMT program enables primary tumor cells to accomplish most if not all of the steps

involved in the physical dissemination of tumor cells to a distant site.

3. The fate of disseminating carcinoma cells is strongly influenced by interactions that they experience during transit through the circulatory system.
4. Disseminated carcinoma cells must escape clearance by the arms of the immune system and subvert the cellular programs that impose a state of dormancy.
5. The process of active metastatic colonization is contingent upon the dissemination of cancer stem cells that can re-initiate tumor growth; the ability of their progeny to assemble adaptive, organ-specific colonization programs; and the establishment of a microenvironment conducive to metastasis.

The processes that enable the physical translocation of cancer cells from primary tumors to the parenchyma of distant tissues are within sight and relatively small in number; in contrast, the adaptive programs allowing cancer cells arising from diverse primary tumors to thrive in various tissue microenvironments may be large in number and not readily reducible to a common set of underlying mechanistic principles.

While these principles articulate general concepts, a number of key mechanistic details related to these ideas remain to be established. For example, we are beginning to appreciate that the EMT program is capable of generating a wide spectrum of carcinoma cells with various complements of mesenchymal traits, but there is little information on the functional role of these different phenotypic states in the metastatic process. Yet other critical questions about metastasis fall outside the bounds of the points outlined above. For one, it is not yet clear what specific factors determine the efficiency of clinical metastatic disease and why some patients present with metastatic cancer, while in other patients many years may lapse before the disease advances to this stage. The literature holds some provocative hints that could account for this variability (Figure 5), such as different cells of origin whose differentiation programs strongly predispose to an aggressive malignancy or to the dissemination of CTC clusters that may more readily establish a metastatic colony. Additionally, the fact that many patients experience metastatic spread to multiple organs suggests the existence of more universal, multi-organ metastatic programs, but the extent to which such programs operate is unclear and their biological details have just begun to be described. Finally, the clinical and biological impact of various immunotherapies, particularly checkpoint inhibitors (Sharma and Allison, 2015), on metastases is certain to be a continued area of active research, even offering the hope of seeking out and eliminating metastatic deposits.

Perhaps most pressing is a better understanding of the biological similarities and differences between primary tumors and their metastatic descendants, especially in regard to the extent of heterogeneity, plasticity, and resistance that they exhibit. We believe that an accurate comparison of the principles that govern primary tumor growth with those that govern the dissemination and outgrowth of metastases will be essential in order to enable the development of new approaches and therapies that are specifically designed to prevent or treat metastatic disease.

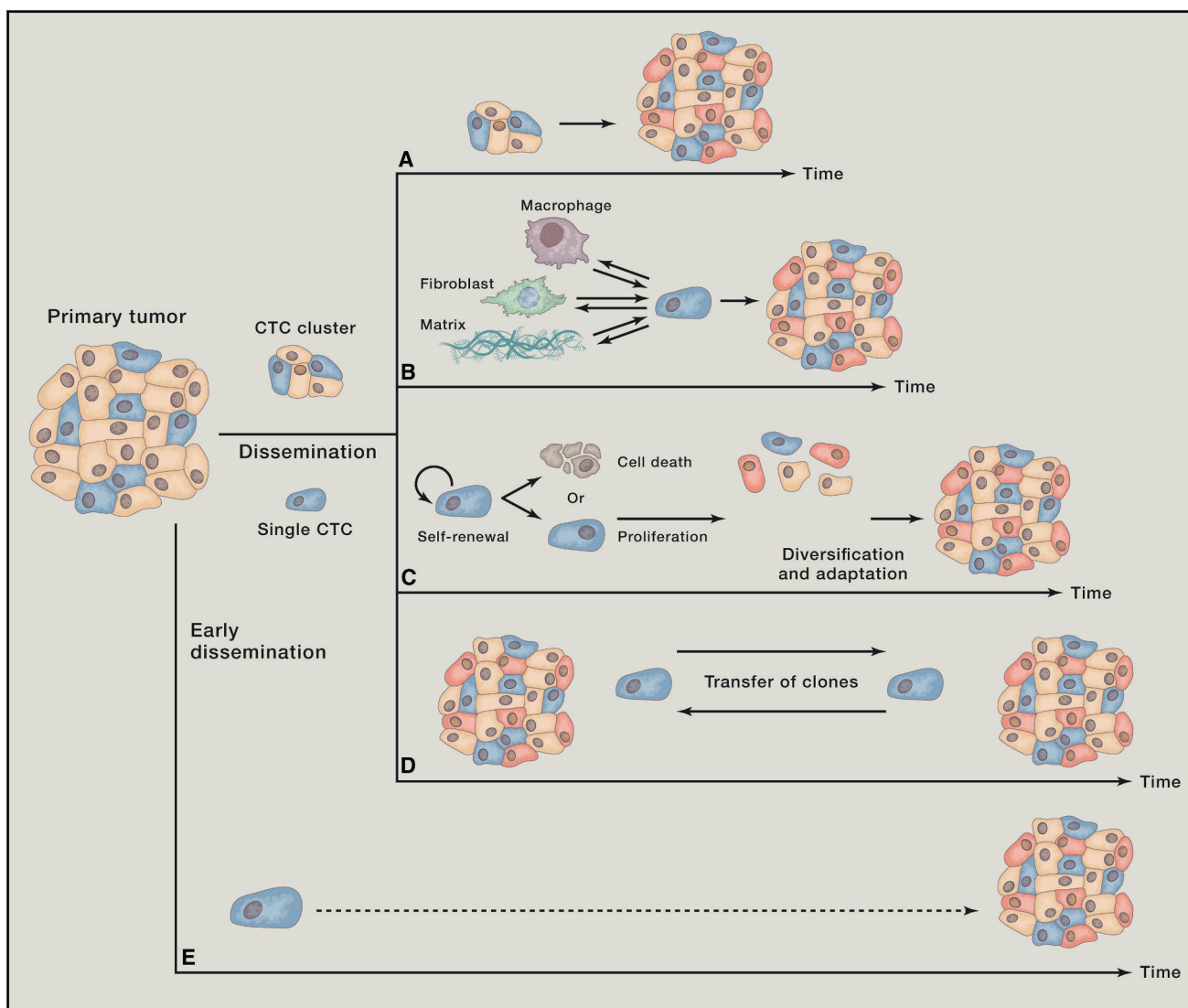


Figure 5. Dynamics of Metastatic Evolution

The progression and evolution of metastatic disease is highly variable, manifesting in ways that must affect the kinetics of metastatic colonization. Five hypothetical alternatives are presented here.

(A) The dissemination of CTC clusters to distant sites may generate overt metastases with a relatively short latency, since such clusters are highly efficient at spawning metastatic growths. Their efficiency in forming metastases may derive from advantages during transit in the circulation or because they benefit from homotypic cell-cell interactions in a foreign tissue environment.

(B) Solitary disseminated carcinoma cells that are adept at recruiting and establishing a supportive metastatic niche, or that are able to generate a microenvironmental niche themselves, may be better able to survive and initiate programs of proliferation.

(C) While the dissemination of tumor-initiating cancer stem cells may be a prerequisite for metastasis, the generation and evolution of progeny that are well adapted to the local microenvironment could take many months or years.

(D) At later stages of metastatic progression, other dynamics come into play, such as the exchange of metastatic cell clones between different metastatic lesions in the same patient. The biological and clinical impact of such transfer, however, remains to be firmly established.

(E) Tumor cells may disseminate during the early stages of tumorigenesis and even from pre-malignant lesions, but it remains unclear how such cells are able to evolve, in parallel with the primary tumor, the full complement of genetic mutations and malignant traits required for successful metastatic colonization.

ACKNOWLEDGMENTS

We would like to thank all members of the R.A.W. laboratory for fruitful discussions and especially Tsukasa Shibue for critical review of the manuscript. We would also like to thank Meredith Leffler for preparation of the figures. A.W.L. is supported by an American Cancer Society – New England Division – Ellison Foundation Postdoctoral Fellowship (PF-15-131-01-CSM). D.R.P. was supported by a C.J. Martin Overseas Biomedical Fellowship

from the National Health and Medical Research Council of Australia (NHMRC APP1071853) and is currently supported by a K99/R00 Pathway to Independence Award (NIH/NCI 1K99CA201574-01A1). Work in the R.A.W. laboratory is supported by grants from the NIH (R01-CA078461), the Breast Cancer Research Foundation, the Advanced Medical Research Foundation, and the Ludwig Center for Molecular Oncology. R.A.W. is an American Cancer Society Research Professor and a Daniel K. Ludwig Cancer Research Professor.

REFERENCES

- Aceto, N., Bardia, A., Miyamoto, D.T., Donaldson, M.C., Wittner, B.S., Spencer, J.A., Yu, M., Pely, A., Engstrom, A., Zhu, H., et al. (2014). Circulating tumor cell clusters are oligoclonal precursors of breast cancer metastasis. *Cell* 158, 1110–1122.
- Aceto, N., Toner, M., Maheswaran, S., and Haber, D.A. (2015). En Route to Metastasis: Circulating Tumor Cell Clusters and Epithelial-to-Mesenchymal Transition. *Trends Cancer* 1, 44–52.
- Acharyya, S., Oskarsson, T., Vanharanta, S., Malladi, S., Kim, J., Morris, P.G., Manova-Todorova, K., Leversha, M., Hogg, N., Seshan, V.E., et al. (2012). A CXCL1 paracrine network links cancer chemoresistance and metastasis. *Cell* 150, 165–178.
- Aguirre-Ghiso, J.A. (2007). Models, mechanisms and clinical evidence for cancer dormancy. *Nat. Rev. Cancer* 7, 834–846.
- Aguirre Ghiso, J.A., Kovalski, K., and Ossowski, L. (1999). Tumor dormancy induced by downregulation of urokinase receptor in human carcinoma involves integrin and MAPK signaling. *J. Cell Biol.* 147, 89–104.
- Al-Mehdi, A.B., Tozawa, K., Fisher, A.B., Shientag, L., Lee, A., and Muschel, R.J. (2000). Intravascular origin of metastasis from the proliferation of endothelium-attached tumor cells: a new model for metastasis. *Nat. Med.* 6, 100–102.
- Alluri, P.G., Speers, C., and Chinnaiyan, A.M. (2014). Estrogen receptor mutations and their role in breast cancer progression. *Breast Cancer Res.* 16, 494.
- Au, S.H., Storey, B.D., Moore, J.C., Tang, Q., Chen, Y.L., Javaid, S., Sarioglu, A.F., Sullivan, R., Madden, M.W., O'Keefe, R., et al. (2016). Clusters of circulating tumor cells traverse capillary-sized vessels. *Proc. Natl. Acad. Sci. USA* 113, 4947–4952.
- BacCELLI, I., Schneeweiss, A., Riethdorf, S., Stenzinger, A., Schillert, A., Vogel, V., Klein, C., Saini, M., Bäuerle, T., Wallwiener, M., et al. (2013). Identification of a population of blood circulating tumor cells from breast cancer patients that initiates metastasis in a xenograft assay. *Nat. Biotechnol.* 31, 539–544.
- Balic, M., Lin, H., Young, L., Hawes, D., Giuliano, A., McNamara, G., Datar, R.H., and Cote, R.J. (2006). Most early disseminated cancer cells detected in bone marrow of breast cancer patients have a putative breast cancer stem cell phenotype. *Clin. Cancer Res.* 12, 5615–5621.
- Barkan, D., Kleinman, H., Simmons, J.L., Asmussen, H., Kamaraju, A.K., Hoehnorhoff, M.J., Liu, Z.Y., Costes, S.V., Cho, E.H., Lockett, S., et al. (2008). Inhibition of metastatic outgrowth from single dormant tumor cells by targeting the cytoskeleton. *Cancer Res.* 68, 6241–6250.
- Barkan, D., El Touny, L.H., Michalowski, A.M., Smith, J.A., Chu, I., Davis, A.S., Webster, J.D., Hoover, S., Simpson, R.M., Gaudie, J., and Green, J.E. (2010). Metastatic growth from dormant cells induced by a col-1-enriched fibrotic environment. *Cancer Res.* 70, 5706–5716.
- Bednarz-Knoll, N., Alix-Panabières, C., and Pantel, K. (2012). Plasticity of disseminating cancer cells in patients with epithelial malignancies. *Cancer Metastasis Rev.* 31, 673–687.
- Bidwell, B.N., Slaney, C.Y., Withana, N.P., Forster, S., Cao, Y., Loi, S., Andrews, D., Mikeska, T., Mangan, N.E., Samarajiva, S.A., et al. (2012). Silencing of *Irf7* pathways in breast cancer cells promotes bone metastasis through immune escape. *Nat. Med.* 18, 1224–1231.
- Bonapace, L., Coissieux, M.M., Wyckoff, J., Mertz, K.D., Varga, Z., Junt, T., and Bontres-Alj, M. (2014). Cessation of CCL2 inhibition accelerates breast cancer metastasis by promoting angiogenesis. *Nature* 515, 130–133.
- Bonnomet, A., Syne, L., Brysse, A., Feyereisen, E., Thompson, E.W., Noël, A., Foidart, J.M., Birembaut, P., Polette, M., and Gilles, C. (2012). A dynamic in vivo model of epithelial-to-mesenchymal transitions in circulating tumor cells and metastases of breast cancer. *Oncogene* 31, 3741–3753.
- Bos, P.D., Zhang, X.H., Nadal, C., Shu, W., Gomis, R.R., Nguyen, D.X., Minn, A.J., van de Vijver, M.J., Gerald, W.L., Foekens, J.A., and Massagué, J. (2009). Genes that mediate breast cancer metastasis to the brain. *Nature* 459, 1005–1009.
- Brabletz, T. (2012). To differentiate or not—routes towards metastasis. *Nat. Rev. Cancer* 12, 425–436.
- Brabletz, T., Jung, A., Spaderna, S., Hlubek, F., and Kirchner, T. (2005). Opinion: migrating cancer stem cells - an integrated concept of malignant tumour progression. *Nat. Rev. Cancer* 5, 744–749.
- Bragado, P., Estrada, Y., Parikh, F., Krause, S., Capobianco, C., Farina, H.G., Schewe, D.M., and Aguirre-Ghiso, J.A. (2013). TGF- β 2 dictates disseminated tumour cell fate in target organs through TGF- β -RIII and p38 α / β signalling. *Nat. Cell Biol.* 15, 1351–1361.
- Braun, S., Vogl, F.D., Naume, B., Janni, W., Osborne, M.P., Coombes, R.C., Schlimok, G., Diel, I.J., Gerber, B., Gebauer, G., et al. (2005). A pooled analysis of bone marrow micrometastasis in breast cancer. *N. Engl. J. Med.* 353, 793–802.
- Cairns, J. (1975). Mutation selection and the natural history of cancer. *Nature* 255, 197–200.
- Campbell, P.J., Yachida, S., Mudie, L.J., Stephens, P.J., Pleasance, E.D., Stebbings, L.A., Morsberger, L.A., Latimer, C., McLaren, S., Lin, M.L., et al. (2010). The patterns and dynamics of genomic instability in metastatic pancreatic cancer. *Nature* 467, 1109–1113.
- Celià-Terrassa, T., Meca-Cortés, O., Mateo, F., Martínez de Paz, A., Rubio, N., Arnal-Estapé, A., Eil, B.J., Bermudo, R., Díaz, A., Guerra-Rebollo, M., et al. (2012). Epithelial-mesenchymal transition can suppress major attributes of human epithelial tumor-initiating cells. *J. Clin. Invest.* 122, 1849–1868.
- Chambers, A.F., Groom, A.C., and MacDonald, I.C. (2002). Dissemination and growth of cancer cells in metastatic sites. *Nat. Rev. Cancer* 2, 563–572.
- Chen, Q., Zhang, X.H., and Massagué, J. (2011). Macrophage binding to receptor VCAM-1 transmits survival signals in breast cancer cells that invade the lungs. *Cancer Cell* 20, 538–549.
- Chen, Q., Boire, A., Jin, X., Valiente, M., Er, E.E., Lopez-Soto, A., Jacob, L.S., Patwa, R., Shah, H., Xu, K., et al. (2016). Carcinoma-astrocyte gap junctions promote brain metastasis by cGAMP transfer. *Nature* 533, 493–498.
- Cheung, K.J., Gabrielson, E., Werb, Z., and Ewald, A.J. (2013). Collective invasion in breast cancer requires a conserved basal epithelial program. *Cell* 155, 1639–1651.
- Cheung, K.J., Padmanaban, V., Silvestri, V., Schipper, K., Cohen, J.D., Fairchild, A.N., Gorin, M.A., Verdone, J.E., Pienta, K.J., Bader, J.S., and Ewald, A.J. (2016). Polyclonal breast cancer metastases arise from collective dissemination of keratin 14-expressing tumor cell clusters. *Proc. Natl. Acad. Sci. USA* 113, E854–E863.
- Chung, Y.C., Wei, W.C., Hung, C.N., Kuo, J.F., Hsu, C.P., Chang, K.J., and Chao, W.T. (2016). Rab11 collaborates E-cadherin to promote collective cell migration and indicates a poor prognosis in colorectal carcinoma. *Eur. J. Clin. Invest.* 46, 1002–1011.
- Clever, D., Roychoudhuri, R., Constantinides, M.G., Askenase, M.H., Sukumar, M., Klebanoff, C.A., Eil, R.L., Hickman, H.D., Yu, Z., Pan, J.H., et al. (2016). Oxygen sensing by T cells establishes an immunologically tolerant metastatic niche. *Cell* 166, 1117–1131.
- Coffelt, S.B., Kersten, K., Doornebal, C.W., Weiden, J., Vrijland, K., Hau, C.S., Versteegen, N.J., Ciampricotti, M., Hawinkels, L.J., Jonkers, J., and de Visser, K.E. (2015). IL-17-producing $\gamma\delta$ T cells and neutrophils conspire to promote breast cancer metastasis. *Nature* 522, 345–348.
- Coffelt, S.B., Wellenstein, M.D., and de Visser, K.E. (2016). Neutrophils in cancer: neutral no more. *Nat. Rev. Cancer* 16, 431–446.
- Cools-Lartigue, J., Spicer, J., McDonald, B., Gowing, S., Chow, S., Giannias, B., Bourdeau, F., Kubes, P., and Ferri, L. (2013). Neutrophil extracellular traps sequester circulating tumor cells and promote metastasis. *J. Clin. Invest.* 123, 3446–3458.
- Costa-Silva, B., Aiello, N.M., Ocean, A.J., Singh, S., Zhang, H., Thakur, B.K., Becker, A., Hoshino, A., Mark, M.T., Molina, H., et al. (2015). Pancreatic cancer exosomes initiate pre-metastatic niche formation in the liver. *Nat. Cell Biol.* 17, 816–826.
- Cox, T.R., and Eler, J.T. (2014). Molecular pathways: connecting fibrosis and solid tumor metastasis. *Clin. Cancer Res.* 20, 3637–3643.

- de Boer, M., van Dijk, J.A., Bult, P., Borm, G.F., and Tjan-Heijnen, V.C. (2010). Breast cancer prognosis and occult lymph node metastases, isolated tumor cells, and micrometastases. *J. Natl. Cancer Inst.* *102*, 410–425.
- De Cock, J.M., Shibue, T., Dongre, A., Keckesova, Z., Reinhardt, F., and Weinberg, R.A. (2016). Inflammation triggers Zeb1-dependent escape from tumor latency. *Cancer Res.* *76*, 6778–6784.
- De Craene, B., and Bex, G. (2013). Regulatory networks defining EMT during cancer initiation and progression. *Nat. Rev. Cancer* *13*, 97–110.
- Del Pozo Martin, Y., Park, D., Ramachandran, A., Ombrato, L., Calvo, F., Chakravarty, P., Spencer-Dene, B., Derzsi, S., Hill, C.S., Sahai, E., and Malanchi, I. (2015). Mesenchymal cancer cell-stroma crosstalk promotes niche activation, epithelial reversion, and metastatic colonization. *Cell Rep.* *13*, 2456–2469.
- Denny, S.K., Yang, D., Chuang, C.H., Brady, J.J., Lim, J.S., Grüner, B.M., Chiou, S.H., Schep, A.N., Baral, J., Hamard, C., et al. (2016). Nfib promotes metastasis through a widespread increase in chromatin accessibility. *Cell* *166*, 328–342.
- Ding, L., Ellis, M.J., Li, S., Larson, D.E., Chen, K., Wallis, J.W., Harris, C.C., McLellan, M.D., Fulton, R.S., Fulton, L.L., et al. (2010). Genome remodelling in a basal-like breast cancer metastasis and xenograft. *Nature* *464*, 999–1005.
- Douma, S., Van Laar, T., Zevenhoven, J., Meuwissen, R., Van Garderen, E., and Peeper, D.S. (2004). Suppression of anoikis and induction of metastasis by the neurotrophic receptor TrkB. *Nature* *430*, 1034–1039.
- El Touny, L.H., Vieira, A., Mendoza, A., Khanna, C., Hoenerhoff, M.J., and Green, J.E. (2014). Combined SFK/MEK inhibition prevents metastatic outgrowth of dormant tumor cells. *J. Clin. Invest.* *124*, 156–168.
- Erler, J.T., Bennewith, K.L., Nicolau, M., Dornhöfer, N., Kong, C., Le, Q.T., Chi, J.T., Jeffrey, S.S., and Giaccia, A.J. (2006). Lysyl oxidase is essential for hypoxia-induced metastasis. *Nature* *440*, 1222–1226.
- Erler, J.T., Bennewith, K.L., Cox, T.R., Lang, G., Bird, D., Koong, A., Le, Q.T., and Giaccia, A.J. (2009). Hypoxia-induced lysyl oxidase is a critical mediator of bone marrow cell recruitment to form the premetastatic niche. *Cancer Cell* *15*, 35–44.
- Eyles, J., Puaux, A.-L., Wang, X., Toh, B., Prakash, C., Hong, M., Tan, T.G., Zheng, L., Ong, L.C., Jin, Y., et al. (2010). Tumor cells disseminate early, but immunosurveillance limits metastatic outgrowth, in a mouse model of melanoma. *J. Clin. Invest.* *120*, 2030–2039.
- Fan, F., Samuel, S., Evans, K.W., Lu, J., Xia, L., Zhou, Y., Sceusi, E., Tozzi, F., Ye, X.C., Mani, S.A., and Ellis, L.M. (2012). Overexpression of snail induces epithelial-mesenchymal transition and a cancer stem cell-like phenotype in human colorectal cancer cells. *Cancer Med.* *1*, 5–16.
- Fearon, E.R., and Vogelstein, B. (1990). A genetic model for colorectal tumorigenesis. *Cell* *61*, 759–767.
- Fidler, I.J. (2003). The pathogenesis of cancer metastasis: the ‘seed and soil’ hypothesis revisited. *Nat. Rev. Cancer* *3*, 453–458.
- Fischer, K.R., Durrans, A., Lee, S., Sheng, J., Li, F., Wong, S.T., Choi, H., El Rayes, T., Ryu, S., Troeger, J., et al. (2015). Epithelial-to-mesenchymal transition is not required for lung metastasis but contributes to chemoresistance. *Nature* *527*, 472–476.
- Franco, A.T., Corken, A., and Ware, J. (2015). Platelets at the interface of thrombosis, inflammation, and cancer. *Blood* *126*, 582–588.
- Fridlender, Z.G., Sun, J., Kim, S., Kapoor, V., Cheng, G., Ling, L., Worthen, G.S., and Albelda, S.M. (2009). Polarization of tumor-associated neutrophil phenotype by TGF-beta: “N1” versus “N2” TAN. *Cancer Cell* *16*, 183–194.
- Friedl, P., Locker, J., Sahai, E., and Segall, J.E. (2012). Classifying collective cancer cell invasion. *Nat. Cell Biol.* *14*, 777–783.
- Gaggioli, C., Hooper, S., Hidalgo-Carcedo, C., Grosse, R., Marshall, J.F., Harrington, K., and Sahai, E. (2007). Fibroblast-led collective invasion of carcinoma cells with differing roles for RhoGTPases in leading and following cells. *Nat. Cell Biol.* *9*, 1392–1400.
- Gao, H., Chakraborty, G., Lee-Lim, A.P., Mo, Q., Decker, M., Vonica, A., Shen, R., Brogi, E., Brivanlou, A.H., and Giancotti, F.G. (2012). The BMP inhibitor Coco reactivates breast cancer cells at lung metastatic sites. *Cell* *150*, 764–779.
- Gao, H., Chakraborty, G., Zhang, Z., Akalay, I., Gadiya, M., Gao, Y., Sinha, S., Hu, J., Jiang, C., Akram, M., et al. (2016). Multi-organ site metastatic reactivation mediated by non-canonical discoidin domain receptor 1 signaling. *Cell* *166*, 47–62.
- Garraway, L.A., and Lander, E.S. (2013). Lessons from the cancer genome. *Cell* *153*, 17–37.
- Gasic, G.J., Gasic, T.B., and Stewart, C.C. (1968). Antimetastatic effects associated with platelet reduction. *Proc. Natl. Acad. Sci. USA* *61*, 46–52.
- Gay, L.J., and Felding-Habermann, B. (2011). Contribution of platelets to tumour metastasis. *Nat. Rev. Cancer* *11*, 123–134.
- Gazdar, A.F. (2009). Activating and resistance mutations of EGFR in non-small-cell lung cancer: role in clinical response to EGFR tyrosine kinase inhibitors. *Oncogene* *28*(Suppl 1), S24–S31.
- Gerlinger, M., Rowan, A.J., Horswell, S., Larkin, J., Endesfelder, D., Gronroos, E., Martinez, P., Matthews, N., Stewart, A., Tarpey, P., et al. (2012). Intratumor heterogeneity and branched evolution revealed by multiregion sequencing. *N. Engl. J. Med.* *366*, 883–892.
- Ghajar, C.M. (2015). Metastasis prevention by targeting the dormant niche. *Nat. Rev. Cancer* *15*, 238–247.
- Ghajar, C.M., Peinado, H., Mori, H., Matei, I.R., Evason, K.J., Brazier, H., Almeida, D., Koller, A., Hajjar, K.A., Stainier, D.Y., et al. (2013). The perivascular niche regulates breast tumour dormancy. *Nat. Cell Biol.* *15*, 807–817.
- Giancotti, F.G. (2013). Mechanisms governing metastatic dormancy and reactivation. *Cell* *155*, 750–764.
- Gilbert, L.A., and Hemann, M.T. (2010). DNA damage-mediated induction of a chemoresistant niche. *Cell* *143*, 355–366.
- Goss, P.E., and Chambers, A.F. (2010). Does tumor dormancy offer a therapeutic target? *Nat. Rev. Cancer* *10*, 871–877.
- Granot, Z., Henke, E., Comen, E.A., King, T.A., Norton, L., and Benezra, R. (2011). Tumor entrained neutrophils inhibit seeding in the premetastatic lung. *Cancer Cell* *20*, 300–314.
- Grosse-Wilde, A., Fouquier d’Hérouël, A., McIntosh, E., Ertylan, G., Skupin, A., Kuestner, R.E., del Sol, A., Walters, K.A., and Huang, S. (2015). Stemness of the hybrid epithelial/mesenchymal state in breast cancer and its association with poor survival. *PLoS ONE* *10*, e0126522.
- Gundem, G., Van Loo, P., Kremeyer, B., Alexandrov, L.B., Tubio, J.M., Papaemmanuil, E., Brewer, D.S., Kallio, H.M., Högnäs, G., Annala, M., et al.; ICGC Prostate UK Group (2015). The evolutionary history of lethal metastatic prostate cancer. *Nature* *520*, 353–357.
- Gupta, G.P., and Massagué, J. (2006). Cancer metastasis: building a framework. *Cell* *127*, 679–695.
- Gupta, P.B., Kuperwasser, C., Brunet, J.P., Ramaswamy, S., Kuo, W.L., Gray, J.W., Naber, S.P., and Weinberg, R.A. (2005). The melanocyte differentiation program predisposes to metastasis after neoplastic transformation. *Nat. Genet.* *37*, 1047–1054.
- Gupta, G.P., Nguyen, D.X., Chiang, A.C., Bos, P.D., Kim, J.Y., Nadal, C., Gomis, R.R., Manova-Todorova, K., and Massagué, J. (2007). Mediators of vascular remodeling co-opted for sequential steps in lung metastasis. *Nature* *446*, 765–770.
- Gupta, P.B., Onder, T.T., Jiang, G., Tao, K., Kuperwasser, C., Weinberg, R.A., and Lander, E.S. (2009). Identification of selective inhibitors of cancer stem cells by high-throughput screening. *Cell* *138*, 645–659.
- Haffner, M.C., Mosbrugger, T., Esopi, D.M., Fedor, H., Heaphy, C.M., Walker, D.A., Adejola, N., Gürel, M., Hicks, J., Meeker, A.K., et al. (2013). Tracking the clonal origin of lethal prostate cancer. *J. Clin. Invest.* *123*, 4918–4922.
- Hanahan, D., and Coussens, L.M. (2012). Accessories to the crime: functions of cells recruited to the tumor microenvironment. *Cancer Cell* *21*, 309–322.
- Hanahan, D., and Weinberg, R.A. (2000). The hallmarks of cancer. *Cell* *100*, 57–70.
- Hanahan, D., and Weinberg, R.A. (2011). Hallmarks of cancer: the next generation. *Cell* *144*, 646–674.

- Harper, K.L., Sosa, M.S., Entenberg, D., Hosseini, H., Cheung, J.F., Nobre, R., Avivar-Valderas, A., Nagi, C., Girmius, N., Davis, R.J., et al. (2016). Mechanism of early dissemination and metastasis in Her2+ mammary cancer. *Nature*. Published online December 14, 2016. <http://dx.doi.org/10.1038/nature20609>.
- Headley, M.B., Bins, A., Nip, A., Roberts, E.W., Looney, M.R., Gerard, A., and Krummel, M.F. (2016). Visualization of immediate immune responses to pioneer metastatic cells in the lung. *Nature* 531, 513–517.
- Hong, T., Watanabe, K., Ta, C.H., Villarreal-Ponce, A., Nie, Q., and Dai, X. (2015). An *Ovol2-Zeb1* mutual inhibitory circuit governs bidirectional and multi-step transition between epithelial and mesenchymal states. *PLoS Comput. Biol.* 11, e1004569.
- Hosseini, H., Obradović, M.M., Hoffmann, M., Harper, K.L., Sosa, M.S., Werner-Klein, M., Nanduri, L.K., Werno, C., Ehrl, C., Maneck, M., et al. (2016). Early dissemination seeds metastasis in breast cancer. *Nature*. Published online December 14, 2016. <http://dx.doi.org/10.1038/nature20785>.
- Huh, S.J., Liang, S., Sharma, A., Dong, C., and Robertson, G.P. (2010). Transiently entrapped circulating tumor cells interact with neutrophils to facilitate lung metastasis development. *Cancer Res.* 70, 6071–6082.
- Hüsemann, Y., Geigl, J.B., Schubert, F., Musiani, P., Meyer, M., Burghart, E., Forni, G., Eils, R., Fehm, T., Riethmüller, G., and Klein, C.A. (2008). Systemic spread is an early step in breast cancer. *Cancer Cell* 13, 58–68.
- Ince, T.A., Richardson, A.L., Bell, G.W., Saitoh, M., Godar, S., Karnoub, A.E., Iglehart, J.D., and Weinberg, R.A. (2007). Transformation of different human breast epithelial cell types leads to distinct tumor phenotypes. *Cancer Cell* 12, 160–170.
- Jacob, L.S., Vanharanta, S., Obenauf, A.C., Pirun, M., Viale, A., Socci, N.D., and Massagué, J. (2015). Metastatic competence can emerge with selection of preexisting oncogenic alleles without a need of new mutations. *Cancer Res.* 75, 3713–3719.
- Jordan, N.V., Johnson, G.L., and Abell, A.N. (2011). Tracking the intermediate stages of epithelial-mesenchymal transition in epithelial stem cells and cancer. *Cell Cycle* 10, 2865–2873.
- Kalluri, R., and Weinberg, R.A. (2009). The basics of epithelial-mesenchymal transition. *J. Clin. Invest.* 119, 1420–1428.
- Kang, Y., and Pantel, K. (2013). Tumor cell dissemination: emerging biological insights from animal models and cancer patients. *Cancer Cell* 23, 573–581.
- Kaplan, R.N., Riba, R.D., Zacharoulis, S., Bramley, A.H., Vincent, L., Costa, C., MacDonald, D.D., Jin, D.K., Shido, K., Kerns, S.A., et al. (2005). VEGFR1-positive haematopoietic bone marrow progenitors initiate the pre-metastatic niche. *Nature* 438, 820–827.
- Karaman, S., and Detmar, M. (2014). Mechanisms of lymphatic metastasis. *J. Clin. Invest.* 124, 922–928.
- Kienast, Y., von Baumgarten, L., Fuhrmann, M., Klinkert, W.E., Goldbrunner, R., Herms, J., and Winkler, F. (2010). Real-time imaging reveals the single steps of brain metastasis formation. *Nat. Med.* 16, 116–122.
- Kitamura, T., Qian, B.Z., and Pollard, J.W. (2015). Immune cell promotion of metastasis. *Nat. Rev. Immunol.* 15, 73–86.
- Klein, C.A. (2009). Parallel progression of primary tumours and metastases. *Nat. Rev. Cancer* 9, 302–312.
- Kobayashi, A., Okuda, H., Xing, F., Pandey, P.R., Watabe, M., Hirota, S., Pai, S.K., Liu, W., Fukuda, K., Chambers, C., et al. (2011). Bone morphogenetic protein 7 in dormancy and metastasis of prostate cancer stem-like cells in bone. *J. Exp. Med.* 208, 2641–2655.
- Koebel, C.M., Vermi, W., Swann, J.B., Zerafa, N., Rodig, S.J., Old, L.J., Smyth, M.J., and Schreiber, R.D. (2007). Adaptive immunity maintains occult cancer in an equilibrium state. *Nature* 450, 903–907.
- Köhler, S., Ullrich, S., Richter, U., and Schumacher, U. (2010). E-/P-selectins and colon carcinoma metastasis: first in vivo evidence for their crucial role in a clinically relevant model of spontaneous metastasis formation in the lung. *Br. J. Cancer* 102, 602–609.
- Kong, D., Banerjee, S., Ahmad, A., Li, Y., Wang, Z., Sethi, S., and Sarkar, F.H. (2010). Epithelial to mesenchymal transition is mechanistically linked with stem cell signatures in prostate cancer cells. *PLoS ONE* 5, e12445.
- Kopp, H.G., Placke, T., and Salih, H.R. (2009). Platelet-derived transforming growth factor-beta down-regulates NKG2D thereby inhibiting natural killer cell antitumor reactivity. *Cancer Res.* 69, 7775–7783.
- Korpai, M., Ell, B.J., Buffa, F.M., Ibrahim, T., Blanco, M.A., Celià-Terrassa, T., Mercatali, L., Khan, Z., Goodarzi, H., Hua, Y., et al. (2011). Direct targeting of *Sec23a* by miR-200s influences cancer cell secretome and promotes metastatic colonization. *Nat. Med.* 17, 1101–1108.
- Kurrey, N.K., Jalgaonkar, S.P., Joglekar, A.V., Ghanate, A.D., Chaskar, P.D., Doiphode, R.Y., and Bapat, S.A. (2009). Snail and slug mediate radioresistance and chemoresistance by antagonizing p53-mediated apoptosis and acquiring a stem-like phenotype in ovarian cancer cells. *Stem Cells* 27, 2059–2068.
- Labelle, M., and Hynes, R.O. (2012). The initial hours of metastasis: the importance of cooperative host-tumor cell interactions during hematogenous dissemination. *Cancer Discov.* 2, 1091–1099.
- Labelle, M., Begum, S., and Hynes, R.O. (2011). Direct signaling between platelets and cancer cells induces an epithelial-mesenchymal-like transition and promotes metastasis. *Cancer Cell* 20, 576–590.
- Labelle, M., Begum, S., and Hynes, R.O. (2014). Platelets guide the formation of early metastatic niches. *Proc. Natl. Acad. Sci. USA* 111, E3053–E3061.
- Lamouille, S., Xu, J., and Derynck, R. (2014). Molecular mechanisms of epithelial-mesenchymal transition. *Nat. Rev. Mol. Cell Biol.* 15, 178–196.
- Latil, M., Nassar, D., Beck, B., Boumahdi, S., Wang, L., Brisebarre, A., Dubois, C., Nkusi, E., Lenglez, S., Checinska, A., et al. (2016). Cell-Type-Specific Chromatin States Differentially Prime Squamous Cell Carcinoma Tumor-Initiating Cells for Epithelial to Mesenchymal Transition. *Cell Stem Cell*. Published online November 16, 2016. <http://dx.doi.org/10.1016/j.stem.2016.10.018>.
- Lawson, D.A., Bhakta, N.R., Kessenbrock, K., Prummel, K.D., Yu, Y., Takai, K., Zhou, A., Eyob, H., Balakrishnan, S., Wang, C.Y., et al. (2015). Single-cell analysis reveals a stem-cell program in human metastatic breast cancer cells. *Nature* 526, 131–135.
- Lee, H.J., Zhuang, G., Cao, Y., Du, P., Kim, H.J., and Settleman, J. (2014). Drug resistance via feedback activation of Stat3 in oncogene-addicted cancer cells. *Cancer Cell* 26, 207–221.
- Levental, K.R., Yu, H., Kass, L., Lakins, J.N., Egeblad, M., Erler, J.T., Fong, S.F., Csiszar, K., Giaccia, A., Wenginger, W., et al. (2009). Matrix crosslinking forces tumor progression by enhancing integrin signaling. *Cell* 139, 891–906.
- Li, W., and Kang, Y. (2016). Probing the fifty shades of EMT in metastasis. *Trends Cancer* 2, 65–67.
- Li, C.M., Gocheva, V., Oudin, M.J., Bhutkar, A., Wang, S.Y., Date, S.R., Ng, S.R., Whittaker, C.A., Bronson, R.T., Snyder, E.L., et al. (2015). *Foxa2* and *Cdx2* cooperate with *Nkx2-1* to inhibit lung adenocarcinoma metastasis. *Genes Dev.* 29, 1850–1862.
- Lim, E., Vaillant, F., Wu, D., Forrest, N.C., Pal, B., Hart, A.H., Asselin-Labat, M.L., Gyorki, D.E., Ward, T., Partanen, A., et al.; kConFab (2009). Aberrant luminal progenitors as the candidate target population for basal tumor development in BRCA1 mutation carriers. *Nat. Med.* 15, 907–913.
- Liu, W., Laitinen, S., Khan, S., Vihinen, M., Kowalski, J., Yu, G., Chen, L., Ewing, C.M., Eisenberger, M.A., Carducci, M.A., et al. (2009). Copy number analysis indicates monoclonal origin of lethal metastatic prostate cancer. *Nat. Med.* 15, 559–565.
- Long, H., Xiang, T., Qi, W., Huang, J., Chen, J., He, L., Liang, Z., Guo, B., Li, Y., Xie, R., and Zhu, B. (2015). CD133+ ovarian cancer stem-like cells promote non-stem cancer cell metastasis via CCL5 induced epithelial-mesenchymal transition. *Oncotarget* 6, 5846–5859.
- Loo, J.M., Scherl, A., Nguyen, A., Man, F.Y., Weinberg, E., Zeng, Z., Saltz, L., Paty, P.B., and Tavazoie, S.F. (2015). Extracellular metabolic energetics can promote cancer progression. *Cell* 160, 393–406.

- Lu, X., Mu, E., Wei, Y., Riethdorf, S., Yang, Q., Yuan, M., Yan, J., Hua, Y., Tiede, B.J., Lu, X., et al. (2011). VCAM-1 promotes osteolytic expansion of indolent bone micrometastasis of breast cancer by engaging $\alpha 4\beta 1$ -positive osteoclast progenitors. *Cancer Cell* 20, 701–714.
- Lundgren, K., Nordenskjöld, B., and Landberg, G. (2009). Hypoxia, Snail and incomplete epithelial-mesenchymal transition in breast cancer. *Br. J. Cancer* 101, 1769–1781.
- Luzzi, K.J., MacDonald, I.C., Schmidt, E.E., Kerkvliet, N., Morris, V.L., Chambers, A.F., and Groom, A.C. (1998). Multistep nature of metastatic inefficiency: dormancy of solitary cells after successful extravasation and limited survival of early micrometastases. *Am. J. Pathol.* 153, 865–873.
- Malanchi, I., Santamaria-Martínez, A., Susanto, E., Peng, H., Lehr, H.A., Dela-loye, J.F., and Huelsken, J. (2011). Interactions between cancer stem cells and their niche govern metastatic colonization. *Nature* 481, 85–89.
- Malladi, S., Macalinao, D.G., Jin, X., He, L., Basnet, H., Zou, Y., de Stanchina, E., and Massagué, J. (2016). Metastatic latency and immune evasion through autocrine inhibition of WNT. *Cell* 165, 45–60.
- Mani, S.A., Guo, W., Liao, M.J., Eaton, E.N., Ayyanan, A., Zhou, A.Y., Brooks, M., Reinhard, F., Zhang, C.C., Shiptsin, M., et al. (2008). The epithelial-mesenchymal transition generates cells with properties of stem cells. *Cell* 133, 704–715.
- Marusyk, A., Almendro, V., and Polyak, K. (2012). Intra-tumour heterogeneity: a looking glass for cancer? *Nat. Rev. Cancer* 12, 323–334.
- McAllister, S.S., and Weinberg, R.A. (2014). The tumour-induced systemic environment as a critical regulator of cancer progression and metastasis. *Nat. Cell Biol.* 16, 717–727.
- Miyamoto, D.T., Zheng, Y., Wittner, B.S., Lee, R.J., Zhu, H., Broderick, K.T., Desai, R., Fox, D.B., Brannigan, B.W., Trautwein, J., et al. (2015). RNA-Seq of single prostate CTCs implicates noncanonical Wnt signaling in antiandrogen resistance. *Science* 349, 1351–1356.
- Molyneux, G., Geyer, F.C., Magnay, F.A., McCarthy, A., Kendrick, H., Natrajan, R., Mackay, A., Grigoriadis, A., Tutt, A., Ashworth, A., et al. (2010). BRCA1 basal-like breast cancers originate from luminal epithelial progenitors and not from basal stem cells. *Cell Stem Cell* 7, 403–417.
- Morel, A.P., Lièvre, M., Thomas, C., Hinkal, G., Ansieau, S., and Puisieux, A. (2008). Generation of breast cancer stem cells through epithelial-mesenchymal transition. *PLoS ONE* 3, e2888.
- Mouw, J.K., Yui, Y., Damiano, L., Bainer, R.O., Lakins, J.N., Acerbi, I., Ou, G., Wijekoon, A.C., Levental, K.R., Gilbert, P.M., et al. (2014). Tissue mechanics modulate microRNA-dependent PTEN expression to regulate malignant progression. *Nat. Med.* 20, 360–367.
- Müller-Hermelink, N., Braumüller, H., Pichler, B., Wieder, T., Mailhammer, R., Schaak, K., Ghoreschi, K., Yazdi, A., Haubner, R., Sander, C.A., et al. (2008). TNFR1 signaling and IFN- γ signaling determine whether T cells induce tumor dormancy or promote multistage carcinogenesis. *Cancer Cell* 13, 507–518.
- Mundy, G.R. (2002). Metastasis to bone: causes, consequences and therapeutic opportunities. *Nat. Rev. Cancer* 2, 584–593.
- Naxerova, K., and Jain, R.K. (2015). Using tumour phylogenetics to identify the roots of metastasis in humans. *Nat. Rev. Clin. Oncol.* 12, 258–272.
- Nguyen, D.X., Bos, P.D., and Massagué, J. (2009). Metastasis: from dissemination to organ-specific colonization. *Nat. Rev. Cancer* 9, 274–284.
- Nieswandt, B., Hafner, M., Echtenacher, B., and Männel, D.N. (1999). Lysis of tumor cells by natural killer cells in mice is impeded by platelets. *Cancer Res.* 59, 1295–1300.
- Nieto, M.A., Huang, R.Y., Jackson, R.A., and Thiery, J.P. (2016). EMT: 2016. *Cell* 166, 21–45.
- Nowell, P.C. (1976). The clonal evolution of tumor cell populations. *Science* 194, 23–28.
- Obenauf, A.C., and Massagué, J. (2015). Surviving at a distance: organ specific metastasis. *Trends Cancer* 1, 76–91.
- Obenauf, A.C., Zou, Y., Ji, A.L., Vanharanta, S., Shu, W., Shi, H., Kong, X., Bosenberg, M.C., Wiesner, T., Rosen, N., et al. (2015). Therapy-induced tumour secretomes promote resistance and tumour progression. *Nature* 520, 368–372.
- Ocaña, O.H., Córcoles, R., Fabra, A., Moreno-Bueno, G., Acloque, H., Vega, S., Barrallo-Gimeno, A., Cano, A., and Nieto, M.A. (2012). Metastatic colonization requires the repression of the epithelial-mesenchymal transition inducer Prrx1. *Cancer Cell* 22, 709–724.
- Oskarsson, T., Acharyya, S., Zhang, X.H., Vanharanta, S., Tavazoie, S.F., Morris, P.G., Downey, R.J., Manova-Todorova, K., Brogi, E., and Massagué, J. (2011). Breast cancer cells produce tenascin C as a metastatic niche component to colonize the lungs. *Nat. Med.* 17, 867–874.
- Oskarsson, T., Batlle, E., and Massagué, J. (2014). Metastatic stem cells: sources, niches, and vital pathways. *Cell Stem Cell* 14, 306–321.
- Ozturk, S., Papageorgis, P., Wong, C.K., Lambert, A.W., Abdolmaleky, H.M., Thiagalingam, A., Cohen, H.T., and Thiagalingam, S. (2016). SDPR functions as a metastasis suppressor in breast cancer by promoting apoptosis. *Proc. Natl. Acad. Sci. USA* 113, 638–643.
- Padua, D., Zhang, X.H., Wang, Q., Nadal, C., Gerald, W.L., Gomis, R.R., and Massagué, J. (2008). TGF β primes breast tumors for lung metastasis seeding through angiopoietin-like 4. *Cell* 133, 66–77.
- Palumbo, J.S., Talmage, K.E., Massari, J.V., La Jeunesse, C.M., Flick, M.J., Kombrinck, K.W., Jirousková, M., and Degen, J.L. (2005). Platelets and fibrin(ogen) increase metastatic potential by impeding natural killer cell-mediated elimination of tumor cells. *Blood* 105, 178–185.
- Palumbo, J.S., Talmage, K.E., Massari, J.V., La Jeunesse, C.M., Flick, M.J., Kombrinck, K.W., Hu, Z., Barney, K.A., and Degen, J.L. (2007). Tumor cell-associated tissue factor and circulating hemostatic factors cooperate to increase metastatic potential through natural killer cell-dependent and-independent mechanisms. *Blood* 110, 133–141.
- Pang, R., Law, W.L., Chu, A.C., Poon, J.T., Lam, C.S., Chow, A.K., Ng, L., Cheung, L.W., Lan, X.R., Lan, H.Y., et al. (2010). A subpopulation of CD26+ cancer stem cells with metastatic capacity in human colorectal cancer. *Cell Stem Cell* 6, 603–615.
- Peinado, H., Alečković, M., Lavotshkin, S., Matei, I., Costa-Silva, B., Moreno-Bueno, G., Hergueta-Redondo, M., Williams, C., García-Santos, G., Ghajar, C., et al. (2012). Melanoma exosomes educate bone marrow progenitor cells toward a pro-metastatic phenotype through MET. *Nat. Med.* 18, 883–891.
- Piskounova, E., Agathocleous, M., Murphy, M.M., Hu, Z., Huddlestun, S.E., Zhao, Z., Leitch, A.M., Johnson, T.M., DeBerardinis, R.J., and Morrison, S.J. (2015). Oxidative stress inhibits distant metastasis by human melanoma cells. *Nature* 527, 186–191.
- Podsypanina, K., Du, Y.C., Jechlinger, M., Beverly, L.J., Hambardzumyan, D., and Varmus, H. (2008). Seeding and propagation of untransformed mouse mammary cells in the lung. *Science* 321, 1841–1844.
- Proia, T.A., Keller, P.J., Gupta, P.B., Klebba, I., Jones, A.D., Sedic, M., Gilmore, H., Tung, N., Naber, S.P., Schnitt, S., et al. (2011). Genetic predisposition directs breast cancer phenotype by dictating progenitor cell fate. *Cell Stem Cell* 8, 149–163.
- Psaila, B., and Lyden, D. (2009). The metastatic niche: adapting the foreign soil. *Nat. Rev. Cancer* 9, 285–293.
- Qian, B., Deng, Y., Im, J.H., Muschel, R.J., Zou, Y., Li, J., Lang, R.A., and Pollard, J.W. (2009). A distinct macrophage population mediates metastatic breast cancer cell extravasation, establishment and growth. *PLoS ONE* 4, e6562.
- Qian, B.Z., Li, J., Zhang, H., Kitamura, T., Zhang, J., Campion, L.R., Kaiser, E.A., Snyder, L.A., and Pollard, J.W. (2011). CCL2 recruits inflammatory monocytes to facilitate breast-tumour metastasis. *Nature* 475, 222–225.
- Quail, D.F., and Joyce, J.A. (2013). Microenvironmental regulation of tumor progression and metastasis. *Nat. Med.* 19, 1423–1437.
- Rankin, E.B., and Giaccia, A.J. (2016). Hypoxic control of metastasis. *Science* 352, 175–180.
- Rasheed, Z.A., Yang, J., Wang, Q., Kowalski, J., Freed, I., Murter, C., Hong, S.M., Koorstra, J.B., Rajeshkumar, N.V., He, X., et al. (2010). Prognostic

- significance of tumorigenic cells with mesenchymal features in pancreatic adenocarcinoma. *J. Natl. Cancer Inst.* **102**, 340–351.
- Revenu, C., and Gilmour, D. (2009). EMT 2.0: shaping epithelia through collective migration. *Curr. Opin. Genet. Dev.* **19**, 338–342.
- Reymond, N., d'Água, B.B., and Ridley, A.J. (2013). Crossing the endothelial barrier during metastasis. *Nat. Rev. Cancer* **13**, 858–870.
- Rhim, A.D., Mirek, E.T., Aiello, N.M., Maitra, A., Bailey, J.M., McAllister, F., Reichert, M., Beatty, G.L., Rustgi, A.K., Vonderheide, R.H., et al. (2012). EMT and dissemination precede pancreatic tumor formation. *Cell* **148**, 349–361.
- Ross, J.B., Huh, D., Noble, L.B., and Tavazoie, S.F. (2015). Identification of molecular determinants of primary and metastatic tumour re-initiation in breast cancer. *Nat. Cell Biol.* **17**, 651–664.
- Sagiv, J.Y., Michaeli, J., Assi, S., Mishalian, I., Kisos, H., Levy, L., Damti, P., Lumbroso, D., Polyansky, L., Sionov, R.V., et al. (2015). Phenotypic diversity and plasticity in circulating neutrophil subpopulations in cancer. *Cell Rep.* **10**, 562–573.
- Sampson, V.B., David, J.M., Puig, I., Patil, P.U., de Herrerros, A.G., Thomas, G.V., and Rajasekaran, A.K. (2014). Wilms' tumor protein induces an epithelial-mesenchymal hybrid differentiation state in clear cell renal cell carcinoma. *PLoS ONE* **9**, e102041.
- Schliekelman, M.J., Taguchi, A., Zhu, J., Dai, X., Rodriguez, J., Celiktas, M., Zhang, Q., Chin, A., Wong, C.H., Wang, H., et al. (2015). Molecular portraits of epithelial, mesenchymal, and hybrid states in lung adenocarcinoma and their relevance to survival. *Cancer Res.* **75**, 1789–1800.
- Schumacher, D., Strilic, B., Sivaraj, K.K., Wettschureck, N., and Offermanns, S. (2013). Platelet-derived nucleotides promote tumor-cell transendothelial migration and metastasis via P2Y2 receptor. *Cancer Cell* **24**, 130–137.
- Sethi, N., and Kang, Y. (2011). Unravelling the complexity of metastasis - molecular understanding and targeted therapies. *Nat. Rev. Cancer* **11**, 735–748.
- Sevenich, L., Bowman, R.L., Mason, S.D., Quail, D.F., Rapaport, F., Elie, B.T., Brogi, E., Brastianos, P.K., Hahn, W.C., Holsinger, L.J., et al. (2014). Analysis of tumour- and stroma-supplied proteolytic networks reveals a brain-metastasis-promoting role for cathepsin S. *Nat. Cell Biol.* **16**, 876–888.
- Sharma, P., and Allison, J.P. (2015). Immune checkpoint targeting in cancer therapy: toward combination strategies with curative potential. *Cell* **161**, 205–214.
- Shibue, T., and Weinberg, R.A. (2009). Integrin beta1-focal adhesion kinase signaling directs the proliferation of metastatic cancer cells disseminated in the lungs. *Proc. Natl. Acad. Sci. USA* **106**, 10290–10295.
- Shibue, T., Brooks, M.W., Inan, M.F., Reinhardt, F., and Weinberg, R.A. (2012). The outgrowth of micrometastases is enabled by the formation of filopodium-like protrusions. *Cancer Discov.* **2**, 706–721.
- Shibue, T., Brooks, M.W., and Weinberg, R.A. (2013). An integrin-linked machinery of cytoskeletal regulation that enables experimental tumor initiation and metastatic colonization. *Cancer Cell* **24**, 481–498.
- Shiozawa, Y., Pedersen, E.A., Havens, A.M., Jung, Y., Mishra, A., Joseph, J., Kim, J.K., Patel, L.R., Ying, C., Ziegler, A.M., et al. (2011). Human prostate cancer metastases target the hematopoietic stem cell niche to establish footholds in mouse bone marrow. *J. Clin. Invest.* **121**, 1298–1312.
- Singh, A., and Settleman, J. (2010). EMT, cancer stem cells and drug resistance: an emerging axis of evil in the war on cancer. *Oncogene* **29**, 4741–4751.
- Skobe, M., Hawighorst, T., Jackson, D.G., Prevo, R., Janes, L., Velasco, P., Riccardi, L., Alitalo, K., Claffey, K., and Detmar, M. (2001). Induction of tumor lymphangiogenesis by VEGF-C promotes breast cancer metastasis. *Nat. Med.* **7**, 192–198.
- Sosa, M.S., Avivar-Valderas, A., Bragado, P., Wen, H.C., and Aguirre-Ghiso, J.A. (2011). ERK1/2 and p38 α / β signaling in tumor cell quiescence: opportunities to control dormant residual disease. *Clin. Cancer Res.* **17**, 5850–5857.
- Sosa, M.S., Bragado, P., and Aguirre-Ghiso, J.A. (2014). Mechanisms of disseminated cancer cell dormancy: an awakening field. *Nat. Rev. Cancer* **14**, 611–622.
- Spicer, J.D., McDonald, B., Cools-Lartigue, J.J., Chow, S.C., Giannias, B., Kubes, P., and Ferri, L.E. (2012). Neutrophils promote liver metastasis via Mac-1-mediated interactions with circulating tumor cells. *Cancer Res.* **72**, 3919–3927.
- Spiegel, A., Brooks, M.W., Houshyar, S., Reinhardt, F., Ardolino, M., Fessler, E., Chen, M.B., Krall, J.A., DeCock, J., Zervantonakis, I.K., et al. (2016). Neutrophils suppress intraluminal NK cell-mediated tumor cell clearance and enhance extravasation of disseminated carcinoma cells. *Cancer Discov.* **6**, 630–649.
- Steeg, P.S. (2003). Metastasis suppressors alter the signal transduction of cancer cells. *Nat. Rev. Cancer* **3**, 55–63.
- Steeg, P.S. (2016). Targeting metastasis. *Nat. Rev. Cancer* **16**, 201–218.
- Straussman, R., Morikawa, T., Shee, K., Barzily-Rokni, M., Qian, Z.R., Du, J., Davis, A., Mongare, M.M., Gould, J., Frederick, D.T., et al. (2012). Tumour micro-environment elicits innate resistance to RAF inhibitors through HGF secretion. *Nature* **487**, 500–504.
- Strlic, B., Yang, L., Albarrán-Juárez, J., Wachsmuth, L., Han, K., Müller, U.C., Pasparakis, M., and Offermanns, S. (2016). Tumour-cell-induced endothelial cell necroptosis via death receptor 6 promotes metastasis. *Nature* **536**, 215–218.
- Sun, Y., Campisi, J., Higano, C., Beer, T.M., Porter, P., Coleman, I., True, L., and Nelson, P.S. (2012). Treatment-induced damage to the tumor microenvironment promotes prostate cancer therapy resistance through WNT16B. *Nat. Med.* **18**, 1359–1368.
- Talmadge, J.E., and Fidler, I.J. (2010). AACR centennial series: the biology of cancer metastasis: historical perspective. *Cancer Res.* **70**, 5649–5669.
- Thiery, J.P. (2002). Epithelial-mesenchymal transitions in tumour progression. *Nat. Rev. Cancer* **2**, 442–454.
- Trimboli, A.J., Fukino, K., de Bruin, A., Wei, G., Shen, L., Tanner, S.M., Creasap, N., Rosol, T.J., Robinson, M.L., Eng, C., et al. (2008). Direct evidence for epithelial-mesenchymal transitions in breast cancer. *Cancer Res.* **68**, 937–945.
- Tsai, J.H., Donaher, J.L., Murphy, D.A., Chau, S., and Yang, J. (2012). Spatio-temporal regulation of epithelial-mesenchymal transition is essential for squamous cell carcinoma metastasis. *Cancer Cell* **22**, 725–736.
- Turajlic, S., and Swanton, C. (2016). Metastasis as an evolutionary process. *Science* **352**, 169–175.
- Valiente, M., Obenauf, A.C., Jin, X., Chen, Q., Zhang, X.H., Lee, D.J., Chaff, J.E., Kris, M.G., Huse, J.T., Brogi, E., and Massagué, J. (2014). Serpins promote cancer cell survival and vascular co-option in brain metastasis. *Cell* **156**, 1002–1016.
- Vanharanta, S., and Massagué, J. (2013). Origins of metastatic traits. *Cancer Cell* **24**, 410–421.
- Veracini, L., Grall, D., Schaub, S., Beghelli-de la Forest Divonne, S., Etienne-Grimaldi, M.C., Milano, G., Bozec, A., Babin, E., Sudaka, A., Thariat, J., and Van Obberghen-Schilling, E. (2015). Elevated Src family kinase activity stabilizes E-cadherin-based junctions and collective movement of head and neck squamous cell carcinomas. *Oncotarget* **6**, 7570–7583.
- Vogelstein, B., Papadopoulos, N., Velculescu, V.E., Zhou, S., Diaz, L.A., Jr., and Kinzler, K.W. (2013). Cancer genome landscapes. *Science* **339**, 1546–1558.
- Wan, L., Pantel, K., and Kang, Y. (2013). Tumor metastasis: moving new biological insights into the clinic. *Nat. Med.* **19**, 1450–1464.
- Wculek, S.K., and Malanchi, I. (2015). Neutrophils support lung colonization of metastasis-initiating breast cancer cells. *Nature* **528**, 413–417.
- Weilbaecher, K.N., Guise, T.A., and McCauley, L.K. (2011). Cancer to bone: a fatal attraction. *Nat. Rev. Cancer* **11**, 411–425.
- Weng, D., Penzner, J.H., Song, B., Koido, S., Calderwood, S.K., and Gong, J. (2012). Metastasis is an early event in mouse mammary carcinomas and is associated with cells bearing stem cell markers. *Breast Cancer Res.* **14**, R18.
- Westcott, J.M., Prechtel, A.M., Maine, E.A., Dang, T.T., Esparza, M.A., Sun, H., Zhou, Y., Xie, Y., and Pearson, G.W. (2015). An epigenetically distinct breast

- cancer cell subpopulation promotes collective invasion. *J. Clin. Invest.* 125, 1927–1943.
- Winslow, M.M., Dayton, T.L., Verhaak, R.G., Kim-Kiselak, C., Snyder, E.L., Feldser, D.M., Hubbard, D.D., DuPage, M.J., Whittaker, C.A., Hoersch, S., et al. (2011). Suppression of lung adenocarcinoma progression by Nkx2-1. *Nature* 473, 101–104.
- Wolf, M.J., Hoos, A., Bauer, J., Boettcher, S., Knust, M., Weber, A., Simonavicius, N., Schneider, C., Lang, M., Stürzl, M., et al. (2012). Endothelial CCR2 signaling induced by colon carcinoma cells enables extravasation via the JAK2-Stat5 and p38MAPK pathway. *Cancer Cell* 22, 91–105.
- Yachida, S., Jones, S., Bozic, I., Antal, T., Leary, R., Fu, B., Kamiyama, M., Hruban, R.H., Eshleman, J.R., Nowak, M.A., et al. (2010). Distant metastasis occurs late during the genetic evolution of pancreatic cancer. *Nature* 467, 1114–1117.
- Yates, L.R., Gerstung, M., Knappskog, S., Desmedt, C., Gundem, G., Van Loo, P., Aas, T., Alexandrov, L.B., Larsimont, D., Davies, H., et al. (2015). Subclonal diversification of primary breast cancer revealed by multiregion sequencing. *Nat. Med.* 21, 751–759.
- Ye, X., Tam, W.L., Shibue, T., Kaygusuz, Y., Reinhardt, F., Ng Eaton, E., and Weinberg, R.A. (2015). Distinct EMT programs control normal mammary stem cells and tumour-initiating cells. *Nature* 525, 256–260.
- Yu, M., Ting, D.T., Stott, S.L., Wittner, B.S., Oszolak, F., Paul, S., Ciciliano, J.C., Smas, M.E., Winokur, D., Gilman, A.J., et al. (2012). RNA sequencing of pancreatic circulating tumour cells implicates WNT signalling in metastasis. *Nature* 487, 510–513.
- Yu, M., Bardia, A., Wittner, B.S., Stott, S.L., Smas, M.E., Ting, D.T., Isakoff, S.J., Ciciliano, J.C., Wells, M.N., Shah, A.M., et al. (2013). Circulating breast tumor cells exhibit dynamic changes in epithelial and mesenchymal composition. *Science* 339, 580–584.
- Yu, M., Bardia, A., Aceto, N., Bersani, F., Madden, M.W., Donaldson, M.C., Desai, R., Zhu, H., Comaills, V., Zheng, Z., et al. (2014). Cancer therapy. Ex vivo culture of circulating breast tumor cells for individualized testing of drug susceptibility. *Science* 345, 216–220.
- Zhang, X.H., Wang, Q., Gerald, W., Hudis, C.A., Norton, L., Smid, M., Foekens, J.A., and Massagué, J. (2009). Latent bone metastasis in breast cancer tied to Src-dependent survival signals. *Cancer Cell* 16, 67–78.
- Zheng, X., Carstens, J.L., Kim, J., Scheible, M., Kaye, J., Sugimoto, H., Wu, C.C., LeBleu, V.S., and Kalluri, R. (2015). Epithelial-to-mesenchymal transition is dispensable for metastasis but induces chemoresistance in pancreatic cancer. *Nature* 527, 525–530.
- Zhou, D., Kannappan, V., Chen, X., Li, J., Leng, X., Zhang, J., and Xuan, S. (2016). RBP2 induces stem-like cancer cells by promoting EMT and is a prognostic marker for renal cell carcinoma. *Exp. Mol. Med.* 48, e238.

mTOR Signaling in Growth, Metabolism, and Disease

Robert A. Saxton^{1,2,3,4} and David M. Sabatini^{1,2,3,4,*}

¹Whitehead Institute for Biomedical Research, 455 Main Street, Cambridge, MA 02142, USA

²Department of Biology, Howard Hughes Medical Institute, Massachusetts Institute of Technology, Cambridge, MA 02139, USA

³Koch Institute for Integrative Cancer Research, 77 Massachusetts Avenue, Cambridge, MA 02139, USA

⁴Broad Institute of Harvard and Massachusetts Institute of Technology, 415 Main Street, Cambridge, MA 02142, USA

*Correspondence: sabatini@wi.mit.edu

<http://dx.doi.org/10.1016/j.cell.2017.02.004>

The mechanistic target of rapamycin (mTOR) coordinates eukaryotic cell growth and metabolism with environmental inputs, including nutrients and growth factors. Extensive research over the past two decades has established a central role for mTOR in regulating many fundamental cell processes, from protein synthesis to autophagy, and deregulated mTOR signaling is implicated in the progression of cancer and diabetes, as well as the aging process. Here, we review recent advances in our understanding of mTOR function, regulation, and importance in mammalian physiology. We also highlight how the mTOR signaling network contributes to human disease and discuss the current and future prospects for therapeutically targeting mTOR in the clinic.

In 1964, a Canadian expedition to the isolated South Pacific island of Rapa Nui (also known as Easter Island) collected a set of soil samples with the goal of identifying novel antimicrobial agents. In bacteria isolated from one of these samples, Sehgal and colleagues discovered a compound with remarkable antifungal, immunosuppressive, and antitumor properties (Eng et al., 1984; Martel et al., 1977; Vézina et al., 1975). Further analysis of this compound, named rapamycin after its site of discovery (clinically referred to as sirolimus), revealed that it acts in part by forming a gain of function complex with the peptidyl-prolyl-isomerase FKBP12 to inhibit signal transduction pathways required for cell growth and proliferation (Chung et al., 1992).

Despite these insights, the full mechanism of action of rapamycin remained elusive until 1994, when biochemical studies identified the mechanistic (formerly “mammalian”) target of rapamycin (mTOR) as the direct target of the rapamycin-FKBP12 complex in mammals (Brown et al., 1994; Sabatini et al., 1994; Sabers et al., 1995) and revealed it to be the homolog of the yeast TOR/DRR genes that had previously been identified in genetic screens for rapamycin resistance (Cafferkey et al., 1993; Heitman et al., 1991; Kunz et al., 1993).

In the more than 2 decades since these discoveries, studies from dozens of labs across the globe have revealed that the mTOR protein kinase nucleates a major eukaryotic signaling network that coordinates cell growth with environmental conditions and plays a fundamental role in cell and organismal physiology. Many aspects of mTOR function and regulation have only recently been elucidated, and many more questions remain unanswered. In this review, we provide an overview of our current understanding of the mTOR pathway and its role in growth, metabolism, and disease.

mTORC1 and mTORC2

mTOR is a serine/threonine protein kinase in the PI3K-related kinase (PIKK) family that forms the catalytic subunit of two

distinct protein complexes, known as mTOR Complex 1 (mTORC1) and 2 (mTORC2) (Figure 1A). mTORC1 is defined by its three core components: mTOR, Raptor (regulatory protein associated with mTOR), and mLST8 (mammalian lethal with Sec13 protein 8, also known as GβL) (Figure 1B; Kim et al., 2002, 2003; Hara et al., 2002). Raptor facilitates substrate recruitment to mTORC1 through binding to the TOR signaling (TOS) motif found on several canonical mTORC1 substrates (Nojima et al., 2003; Schalm et al., 2003) and, as described later, is required for the correct subcellular localization of mTORC1. mLST8 by contrast associates with the catalytic domain of mTORC1 and may stabilize the kinase activation loop (Yang et al., 2013), though genetic studies suggest it is dispensable for the essential functions of mTORC1 (Guertin et al., 2006). In addition to these three core components, mTORC1 also contains the two inhibitory subunits PRAS40 (proline-rich Akt substrate of 40 kDa) (Sancak et al., 2007; Vander Haar et al., 2007; Wang et al., 2007) and DEPTOR (DEP domain containing mTOR interacting protein) (Peterson et al., 2009).

Structural studies of mTORC1 have yielded significant insights into its assembly, function, and perturbation by rapamycin. Cryo-EM reconstructions of both mTORC1 and yeast TORC1 have revealed that the complex forms a 1-mDa “lozenge”-shaped dimer, with the dimerization interface comprising contacts between the mTOR HEAT repeats as well as between Raptor and mTOR (Figure 1B; Aylett et al., 2016; Baretic et al., 2016; Yip et al., 2010). In addition, a crystal structure of the mTOR kinase domain bound to mLST8 showed that the rapamycin-FKBP12 complex binds to the FRB domain of mTOR to narrow the catalytic cleft and partially occlude substrates from the active site (Yang et al., 2013).

While the rapamycin-FKBP12 complex directly inhibits mTORC1, mTORC2 is characterized by its insensitivity to acute rapamycin treatment. Like mTORC1, mTORC2 also contains mTOR and mLST8 (Figure 1C). Instead of Raptor, however,

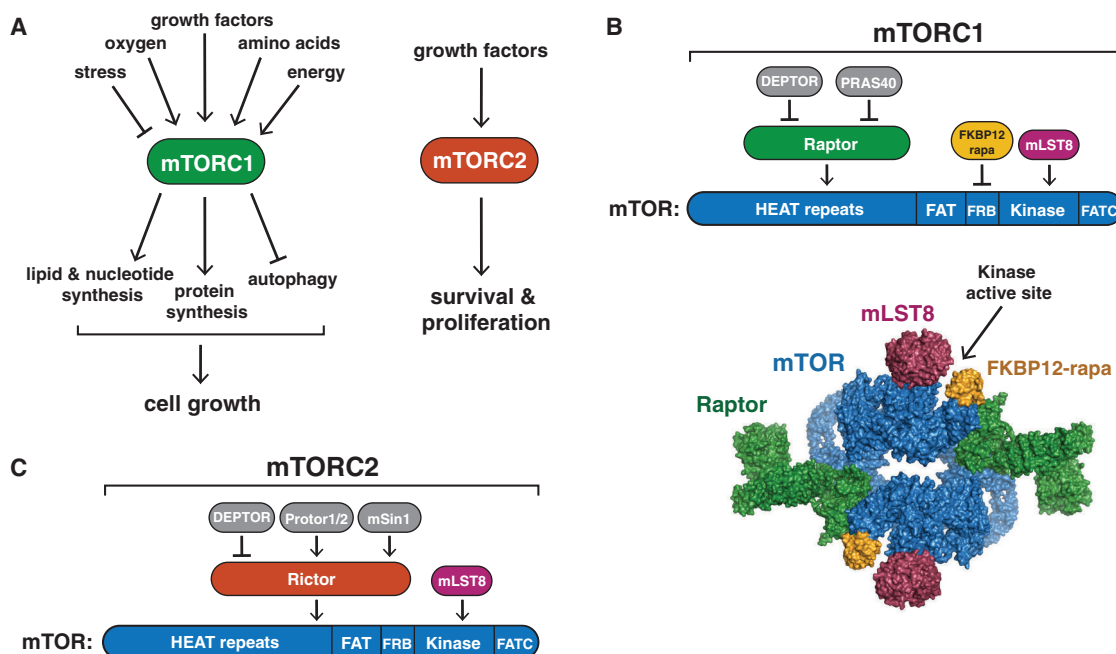


Figure 1. mTORC1 and mTORC2

(A) The mTORC1 and mTORC2 signaling pathways.

(B) mTORC1 subunits and respective binding sites on mTOR. The 5.9-Å cryo-EM structure of mTORC1 in complex with the FKBP12-*rapamycin* complex (without DEPTOR and PRAS40, PDB: 5FLC) is depicted as a space filling model and colored by subunit.

(C) mTORC2 subunits and respective binding sites on mTOR.

mTORC2 contains Rictor (*rapamycin* insensitive companion of mTOR), an unrelated protein that likely serves an analogous function (Jacinto et al., 2004; Sarbassov et al., 2004). mTORC2 also contains DEPTOR (Peterson et al., 2009), as well as the regulatory subunits mSin1 (Frias et al., 2006; Jacinto et al., 2006; Yang et al., 2006) and Protor1/2 (Pearce et al., 2007; Thedieck et al., 2007; Woo et al., 2007). Although *rapamycin*-FKBP12 complexes do not directly bind or inhibit mTORC2, prolonged *rapamycin* treatment does abrogate mTORC2 signaling, likely due to the inability of *rapamycin*-bound mTOR to incorporate into new mTORC2 complexes (Lamming et al., 2012; Sarbassov et al., 2006).

The mTOR Signaling Network Downstream of mTORC1

In order to grow and divide, cells must increase production of proteins, lipids, and nucleotides while also suppressing catabolic pathways such as autophagy. mTORC1 plays a central role in regulating all of these processes and therefore controls the balance between anabolism and catabolism in response to environmental conditions (Figures 2A and 2B). Here, we review the critical substrates and cellular processes downstream of mTORC1 and how they contribute to cell growth. Most of the functions discussed here were identified and characterized in the context of mammalian cell lines, while the physiological context in which these processes are important will be discussed in greater detail below.

Protein Synthesis

mTORC1 promotes protein synthesis largely through the phosphorylation of two key effectors, p70S6 Kinase 1 (S6K1) and

eIF4E Binding Protein (4EBP) (Figure 2B). mTORC1 directly phosphorylates S6K1 on its hydrophobic motif site, Thr389, enabling its subsequent phosphorylation and activation by PDK1. S6K1 phosphorylates and activates several substrates that promote mRNA translation initiation, including eIF4B, a positive regulator of the 5' cap binding eIF4F complex (Holz et al., 2005). S6K1 also phosphorylates and promotes the degradation of PDCD4, an inhibitor of eIF4B (Dorrello et al., 2006), and enhances the translation efficiency of spliced mRNAs via its interaction with SKAR, a component of exon-junction complexes (Ma et al., 2008).

The mTORC1 substrate 4EBP is unrelated to S6K1 and inhibits translation by binding and sequestering eIF4E to prevent assembly of the eIF4F complex. mTORC1 phosphorylates 4EBP at multiple sites to trigger its dissociation from eIF4E (Brunn et al., 1997; Gingras et al., 1999), allowing 5' cap-dependent mRNA translation to occur. Although it has long been appreciated that mTORC1 signaling regulates mRNA translation, whether and how it affects specific classes of mRNA transcripts has been debated. Global ribosome footprinting analyses, however, revealed that, while acute mTOR inhibition moderately suppresses general mRNA translation, it most profoundly affects mRNAs containing pyrimidine-rich 5' TOP or "TOP-like" motifs, which includes most genes involved in protein synthesis (Hsieh et al., 2012; Thoreen et al., 2012).

Lipid, Nucleotide, and Glucose Metabolism

Growing cells require sufficient lipids for new membrane formation and expansion. mTORC1 promotes *de novo* lipid synthesis through the sterol responsive element binding protein (SREBP)

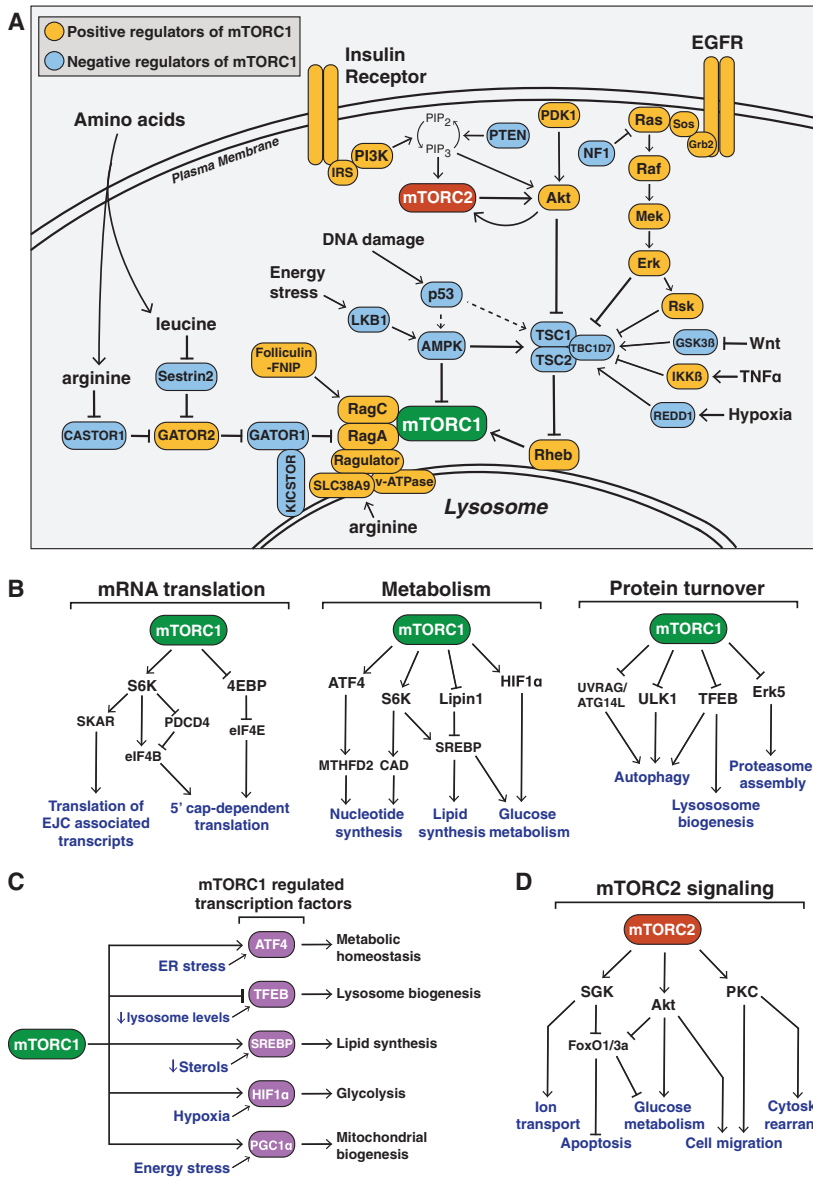


Figure 2. The mTOR Signaling Network

(A) The signaling pathways upstream of mTORC1 and mTORC2. Positive regulators of mTORC1 signaling are shown in yellow, while negative regulators are shown in blue. mTORC1 and mTORC2 are shown in green and red, respectively.

(B) The major pathways downstream of mTORC1 signaling in mRNA translation, metabolism, and protein turnover.

(C) mTORC1 controls the activity of several transcription factors that can also be independently regulated by cell stress.

(D) The major pathways downstream of mTORC2 signaling.

moyl-phosphate synthetase (CAD), a critical component of the de novo pyrimidine synthesis pathway (Ben-Sahra et al., 2013; Robitaille et al., 2013).

mTORC1 also facilitates growth by promoting a shift in glucose metabolism from oxidative phosphorylation to glycolysis, which likely facilitates the incorporation of nutrients into new biomass. mTORC1 increases the translation of the transcription factor HIF1α (Figure 2C), which drives the expression of several glycolytic enzymes such as phosphofructo kinase (PFK) (Düvel et al., 2010). Furthermore, mTORC1-dependent activation of SREBP leads to increased flux through the oxidative pentose phosphate pathway (PPP), which utilizes carbons from glucose to generate NADPH and other intermediary metabolites needed for proliferation and growth.

Regulation of Protein Turnover

In addition to the various anabolic processes outlined above, mTORC1 also promotes cell growth by suppressing protein catabolism (Figure 1B), most notably autophagy. An important early step in autophagy is the activation of ULK1, a kinase that forms a complex

transcription factors, which control the expression of metabolic genes involved in fatty acid and cholesterol biosynthesis (Porstmann et al., 2008). While SREBP is canonically activated in response to low sterol levels, mTORC1 signaling can also activate SREBP independently through both an S6K1-dependent mechanism (Düvel et al., 2010) as well as through the phosphorylation of an additional substrate, Lipin1, which inhibits SREBP in the absence of mTORC1 signaling (Peterson et al., 2011).

Recent studies established that mTORC1 also promotes the synthesis of nucleotides required for DNA replication and ribosome biogenesis in growing and proliferating cells. mTORC1 increases the ATF4-dependent expression of MTHFD2, a key component of the mitochondrial tetrahydrofolate cycle that provides one-carbon units for purine synthesis (Ben-Sahra et al., 2016). Additionally, S6K1 phosphorylates and activates carba-

with ATG13, FIP2000, and ATG101 and drives autophagosome formation. Under nutrient replete conditions, mTORC1 phosphorylates ULK1, thereby preventing its activation by AMPK, a key activator of autophagy (Kim et al., 2011). Thus, the relative activity of mTORC1 and AMPK in different cellular contexts largely determines the extent of autophagy induction. mTORC1 also regulates autophagy in part by phosphorylating and inhibiting the nuclear translocation of the transcription factor EB (TFEB), which drives the expression of genes for lysosomal biogenesis and the autophagy machinery (Martina et al., 2012; Rocznik-Ferguson et al., 2012; Settembre et al., 2012).

The second major pathway responsible for protein turnover is the ubiquitin-proteasome system (UPS), through which proteins are selectively targeted for degradation by the 20S proteasome following covalent modification with ubiquitin. Two recent

studies found that acute mTORC1 inhibition rapidly increases proteasome-dependent proteolysis through either a general increase in protein ubiquitylation (Zhao et al., 2015), or an increased abundance of proteasomal chaperones via inhibition of Erk5 (Figure 2B; Rousseau and Bertolotti, 2016). However, another study found that genetic hyperactivation of mTORC1 signaling also increases proteasome activity, through elevated expression of proteasome subunits downstream of Nrf1 (Zhang et al., 2014). One possible explanation for this discrepancy is that while acute mTORC1 inhibition promotes proteolysis to restore free amino acid pools, prolonged mTORC1 activation also triggers a compensatory increase in protein turnover to balance the increased rate of protein synthesis. Given that the UPS is responsible for the majority of protein degradation in human cells, precisely how mTORC1 regulates this process is an important question going forward.

Downstream of mTORC2

While mTORC1 regulates cell growth and metabolism, mTORC2 instead controls proliferation and survival primarily by phosphorylating several members of the AGC (PKA/PKG/PKC) family of protein kinases (Figure 2D). The first mTORC2 substrate to be identified was PKC α , a regulator of the actin cytoskeleton (Jacinto et al., 2004; Sarbassov et al., 2004). More recently, mTORC2 has also been shown to phosphorylate several other members of the PKC family, including PKC δ (Gan et al., 2012), PKC ζ (Li and Gao, 2014), as well as PKC γ and PKC ϵ (Thomanetz et al., 2013), all of which regulate various aspects of cytoskeletal remodeling and cell migration.

The most important role of mTORC2, however, is likely the phosphorylation and activation of Akt, a key effector of insulin/PI3K signaling (Sarbassov et al., 2005). Once active, Akt promotes cell survival, proliferation, and growth through the phosphorylation and inhibition of several key substrates, including the FoxO1/3a transcription factors, the metabolic regulator GSK3 β , and the mTORC1 inhibitor TSC2. However, while mTORC2-dependent phosphorylation is required for Akt to phosphorylate some substrates *in vivo*, such as FoxO1/3a, it is dispensable for the phosphorylation of others, including TSC2 (Guertin et al., 2006; Jacinto et al., 2006). Finally, mTORC2 also phosphorylates and activates SGK1, another AGC-kinase that regulates ion transport as well as cell survival (García-Martínez and Alessi, 2008).

Upstream of mTORC1

The mTORC1-dependent shift toward increased anabolism should only occur in the presence of pro-growth endocrine signals as well as sufficient energy and chemical building blocks for macromolecular synthesis. In mammals, these inputs are largely dependent on diet, such that mTORC1 is activated following feeding to promote growth and energy storage in tissues such as the liver and muscle but inhibited during fasting to conserve limited resources. Here, we discuss the cellular pathways upstream of mTORC1 and the mechanisms through which they control mTORC1 activation.

Growth Factors

Studies of rapamycin in the early 1990s revealed that mTORC1 is a downstream mediator of several growth factor and mitogen-

dependent signaling pathways, all of which inhibit a key negative regulator of mTORC1 signaling known as the Tuberous Sclerosis Complex (TSC). TSC is a heterotrimeric complex comprising TSC1, TSC2, and TBC1D7 (Dibble et al., 2012) and functions as a GTPase activating protein (GAP) for the small GTPase Rheb (Inoki et al., 2003a; Tee et al., 2003), which directly binds and activates mTORC1 (Long et al., 2005; Sancak et al., 2007). Although Rheb is an essential activator of mTORC1, exactly how it stimulates mTORC1 kinase activity remains unknown.

Numerous growth factor pathways converge on TSC (Figure 2A), including the insulin/insulin-like growth factor-1 (IGF-1) pathway, which triggers the Akt-dependent multisite phosphorylation of TSC2 (Inoki et al., 2002; Manning et al., 2002). This phosphorylation inhibits TSC by dissociating it from the lysosomal membrane, where at least some fraction of cellular Rheb localizes (Menon et al., 2014). Similarly, receptor tyrosine kinase-dependent Ras signaling activates mTORC1 via the MAP Kinase Erk and its effector p90^{RSK}, both of which also phosphorylate and inhibit TSC2 (Ma et al., 2005; Roux et al., 2004). It is unclear, however, whether these inputs also control the localization of TSC or rather inhibit its GAP activity through a distinct mechanism. Additional growth factor pathways upstream of TSC include Wnt and the inflammatory cytokine TNF α , both of which activate mTORC1 through the inhibition of TSC1 (Inoki et al., 2006; Lee et al., 2007). Precisely how the TSC integrates these numerous signals and their relative impact on mTORC1 activity in various contexts, however, remains an open question.

Energy, Oxygen, and DNA Damage

mTORC1 also responds to intracellular and environmental stresses that are incompatible with growth such as low ATP levels, hypoxia, or DNA damage. A reduction in cellular energy charge, such as during glucose deprivation, activates the stress responsive metabolic regulator AMPK, which inhibits mTORC1 both indirectly, through phosphorylation and activation of TSC2, as well as directly, through the phosphorylation of Raptor (Gwinn et al., 2008; Inoki et al., 2003b; Shaw et al., 2004). Interestingly, glucose deprivation also inhibits mTORC1 in cells lacking AMPK, through inhibition of the Rag GTPases, suggesting that mTORC1 senses glucose through more than one mechanism (Efeyan et al., 2013; Kalender et al., 2010). Similarly, hypoxia inhibits mTORC1 in part through AMPK activation, but also through the induction of REDD1 (Regulated in DNA damage and development 1), which activates TSC (Brugarolas et al., 2004). Finally, the DNA damage-response pathway inhibits mTORC1 through the induction of p53 target genes, including the AMPK regulatory subunit (AMPK β), *PTEN*, and *TSC2* itself, all of which increase TSC activity (Feng et al., 2007).

Amino Acids

In addition to glucose-dependent insulin release, feeding also leads to an increase in serum amino acid levels due to the digestion of dietary proteins. As amino acids are not only essential building blocks of proteins, but also sources of energy and carbon for many other metabolic pathways, mTORC1 activation is tightly coupled to diet-induced changes in amino acid concentrations.

A breakthrough in the understanding of amino acid sensing by mTORC1 came with the discovery of the heterodimeric Rag GTPases as components of the mTORC1 pathway (Kim et al.,

2008; Sancak et al., 2008). The Rags are obligate heterodimers of RagA or RagB with RagC or RagD and are tethered to the lysosomal membrane through their association with the pentameric Ragulator complex comprising MP1, p14, p18, HBXIP, and C7ORF59 (Sancak et al., 2010; Bar-Peled et al., 2012). Amino acid stimulation converts the Rags to their active nucleotide-bound state, allowing them to bind Raptor and recruit mTORC1 to the lysosomal surface, where Rheb is also located. This pathway architecture therefore forms an “AND-gate,” whereby mTORC1 signaling is only on when both the Rags and Rheb are activated, explaining why both growth factors and amino acids are required for mTORC1 activation.

Despite these insights, the identities of the direct amino acid sensors upstream of mTORC1 have been elusive until very recently. It is now clear that mTORC1 senses both intra-lysosomal and cytosolic amino acids through distinct mechanisms. Amino acids inside the lysosomal lumen alter the Rag nucleotide state through a mechanism dependent on the lysosomal v-ATPase, which interacts the Ragulator-Rag complex to promote the guanine-nucleotide exchange factor (GEF) activity of Ragulator toward RagA/B (Zoncu et al., 2011; Bar-Peled et al., 2012). The lysosomal amino acid transporter SLC38A9 interacts with the Rag-Ragulator-v-ATPase complex and is required for arginine to activate mTORC1, making it a promising candidate to be a lysosomal amino acid sensor (Jung et al., 2015; Rebsamen et al., 2015; Wang et al., 2015).

Cytosolic leucine and arginine signal to mTORC1 through a distinct pathway comprising the GATOR1 and GATOR2 complexes (Bar-Peled et al., 2013). GATOR1 consists of DEPDC5, Nprl2, and Nprl3 and inhibits mTORC1 signaling by acting as a GAP for RagA/B. The recently identified KICSTOR complex (consisting of Kaptin, ITFG2, C12orf66, and SZT2) tethers GATOR1 to the lysosomal surface and is necessary for the appropriate control of the mTORC1 pathway by nutrients (Peng et al., 2017; Wolfson et al., 2017). GATOR2 by contrast is a pentameric complex comprising Mios, WDR24, WDR59, Seh1L, and Sec13 and is a positive regulator of mTORC1 signaling that interacts with GATOR1 at the lysosomal membrane (Bar-Peled et al., 2013).

An important insight into the mechanism of cytosolic amino acid sensing came with the identification of Sestrin2 as a GATOR2 interacting protein that inhibits mTORC1 signaling under amino acid deprivation (Chantranupong et al., 2014; Parmigiani et al., 2014). Subsequent biochemical and structural analyses established that Sestrin2 is a direct leucine sensor upstream of mTORC1 that binds and inhibits GATOR2 function in the absence of leucine, and dissociates from it upon leucine binding (Saxton et al., 2016a; Wolfson et al., 2016). Furthermore, the affinity of Sestrin2 for leucine determines the sensitivity of mTORC1 signaling to leucine in cultured cells, demonstrating that Sestrin2 is the primary leucine sensor for mTORC1 in this context. It remains to be seen whether and in what tissues leucine concentrations fluctuate within the relevant range to be sensed by Sestrin2 *in vivo*, as the levels of interstitial or cytosolic leucine are unknown. Interestingly, another recent study found that Sestrin2 is transcriptionally induced upon prolonged amino acid starvation via the stress-responsive transcription factor ATF4 (Ye et al., 2015), suggesting that Sestrin2 functions as both an acute leucine

sensor as well as an indirect mediator of prolonged amino acid starvation.

Cytosolic arginine also activates mTORC1 through the GATOR1/2-Rag pathway by directly binding the recently identified arginine sensor CASTOR1 (Cellular Arginine Sensor for mTORC1). Much like Sestrin2, CASTOR1 binds and inhibits GATOR2 in the absence of arginine, and dissociates upon arginine binding to enable the activation of mTORC1 (Chantranupong et al., 2016; Saxton et al., 2016b). Thus, both leucine and arginine stimulate mTORC1 activity at least in part by releasing inhibitors from GATOR2, establishing GATOR2 as a central node in the signaling of amino acids to mTORC1. Importantly, however, the molecular function of GATOR2 and the mechanisms through which Sestrin2 and CASTOR1 regulate it are unknown.

Several additional mechanisms through which amino acids regulate mTORC1 signaling have also recently been reported, including the identification of the Folliculin-FNIP2 complex as a GAP for RagC/D that activates mTORC1 in the presence of amino acids (Petit et al., 2013; Tsun et al., 2013). Another study found that the amino acid glutamine, which is utilized as a nitrogen and energy source by proliferating cells, activates mTORC1 independently of the Rag GTPases through the related Arf family GTPases (Jewell et al., 2015). Finally, a recent report found that the small polypeptide SPAR associates with the v-ATPase-Ragulator complex to suppress mTORC1 recruitment to lysosomes, though how this occurs is unclear (Matsumoto et al., 2017).

Upstream of mTORC2

In contrast to mTORC1, mTORC2 primarily functions as an effector of insulin/PI3K signaling (Figure 2A). Like most PI3K regulated proteins, the mTORC2 subunit mSin1 contains a phosphoinositide-binding PH domain that is critical for the insulin-dependent regulation of mTORC2 activity. The mSin1 PH domain inhibits mTORC2 catalytic activity in the absence of insulin, and this autoinhibition is relieved upon binding to PI3K-generated PIP₃ at the plasma membrane (Liu et al., 2015). mSin1 can also be phosphorylated by Akt, suggesting the existence of a positive-feedback loop whereby partial activation of Akt promotes the activation of mTORC2, which, in turn, phosphorylates and fully activates Akt (Yang et al., 2015). Another study found that PI3K promotes the association of mTORC2 with ribosomes to activate its kinase activity, although the mechanistic basis for this is unclear (Zinzalla et al., 2011).

Unexpectedly, mTORC2 signaling is also regulated by mTORC1, due to the presence of a negative feedback loop between mTORC1 and insulin/PI3K signaling. mTORC1 phosphorylates and activates Grb10, a negative regulator of insulin/IGF-1 receptor signaling upstream of Akt and mTORC2, (Hsu et al., 2011; Yu et al., 2011), while S6K1 also suppresses mTORC2 activation through the phosphorylation-dependent degradation of insulin receptor substrate 1 (IRS1) (Harrington et al., 2004; Shah et al., 2004). This negative feedback regulation of PI3K and mTORC2 signaling by mTORC1 has numerous implications for the pharmacological targeting of mTOR in disease, discussed below.

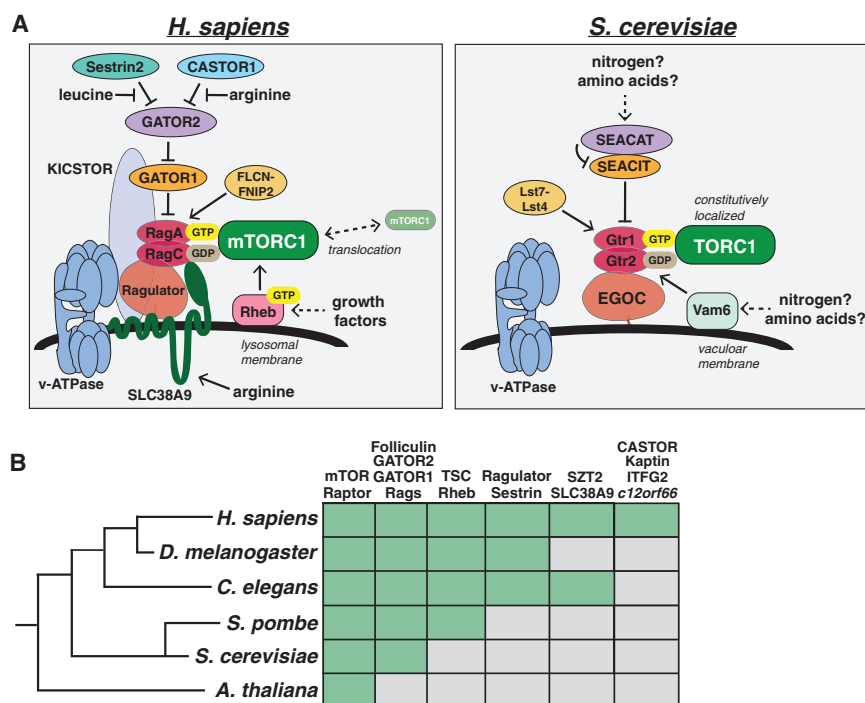


Figure 3. Evolutionary Conservation of the TOR Pathway

(A) The nutrient sensing pathway upstream of mammalian mTORC1 (left) and yeast TORC1 (right).

(B) Phylogenetic tree depicting the presence (green box) of key mTORC1 regulators in various model organisms.

GATOR1/2 complexes are present in *S. cerevisiae* in the form of Gtr1/2 and the SEACIT/SEACAT complexes, respectively (Figure 3A; Panchaud et al., 2013), while the yeast EGO Complex is a structural homolog of Ragulator that interacts with Gtr1/2 and likely serves an analogous function (Powis et al., 2015; Zhang et al., 2012). In contrast to mammals, however, amino acids do not affect the localization of yeast TORC1, which is constitutively bound to the Gtr-Ego complex at the vacuolar membrane (Binda et al., 2009), suggesting an alternative sensing mechanism exists. Consistent with this, the mammalian amino acid sensors SLC38A9, Sestrin2, and CASTOR1 all lack clear homologs in yeast.

Evolutionary Conservation of the TOR Pathway

One remarkable feature of the TOR pathway is its conservation as a major growth regulator in virtually all eukaryotes. Like mammals, *S. cerevisiae* also have two distinct TOR containing complexes, TORC1 and TORC2 (reviewed in Loewith and Hall, 2011) as well as homologs of Raptor (Kog1), mLST8 (Lst8), Rictor (Avo3), and mSin1 (Avo1), although several additional components are yeast or mammal specific. Furthermore yeast TORC1 also primarily controls cell growth and anabolic metabolism, including the activation of protein synthesis and inhibition of autophagy, while yeast TORC2 primarily functions to activate AGC family kinases such as YPK1, the homolog of mammalian SGK1.

As with mTORC1, yeast TORC1 also senses and responds to a diverse array of environmental stimuli, although the specific inputs and upstream signaling components differ in several respects, as one would expect given the vastly different environmental conditions that are relevant for these organisms (Figure 3A). For example, hormone and growth factor receptor signaling are developments specific to multicellular organisms, and the mTORC1 regulator TSC is not found in *S. cerevisiae*. Instead, yeast TORC1 appears to be primarily sensitive to direct biosynthetic inputs such as carbon, nitrogen, and phosphate sources.

Unlike mammals, yeast are able to synthesize all 20 amino acids, and starvation of individual amino acids like leucine or arginine does not inhibit TORC1 signaling in wild-type strains. Leucine deprivation does, however, inhibit TORC1 in leucine-auxotrophs (Binda et al., 2009), suggesting there may be a mechanism for signaling amino acid levels to TORC1, although this could also be due to the sensing of nitrogen sources that are perturbed in this context. Both the Rag GTPases and the

sensors SLC38A9, Sestrin2, and CASTOR1 all lack clear homologs in yeast.

While most of the TORC1 pathway components are also well conserved in other multicellular model organisms, the direct amino acid sensors appear to have diverged (Figure 3B). For example, although both SLC38A9 and CASTOR1 are conserved throughout many metazoan lineages, they are absent in *D. melanogaster*, suggesting that this organism either does not sense arginine or does so through a distinct mechanism. Both *D. melanogaster* and *C. elegans* do have a Sestrin homolog, however, and dmSestrin also binds leucine (Wolfson et al., 2016). Interestingly, both ceSestrin and dmSestrin contain subtle differences in their leucine binding pockets predicted to reduce their affinity for leucine relative to human Sestrin2, likely enabling the sensing of physiologically relevant leucine levels in these organisms (Saxton et al., 2016a).

Physiological Roles of mTOR

Changes in available energy sources following fasting or feeding require alterations in whole-body metabolism to maintain homeostasis. Under starvation, levels of nutrients and growth factors drop, inducing a catabolic state in which energy stores are mobilized to maintain essential functions (Figure 4A). Alternatively, high levels of nutrients in the fed-state trigger a switch toward anabolic growth and energy storage. Consistent with its role in coordinating anabolic and catabolic metabolism at the cellular level, physiological studies in mice have revealed that mTOR signaling is essential for proper metabolic regulation at the organismal level as well. Importantly, however, constitutive mTOR activation is also associated with negative physiological outcomes, indicating that the proper modulation of mTOR signaling in response to changing environmental conditions is crucial (Figure 4B).

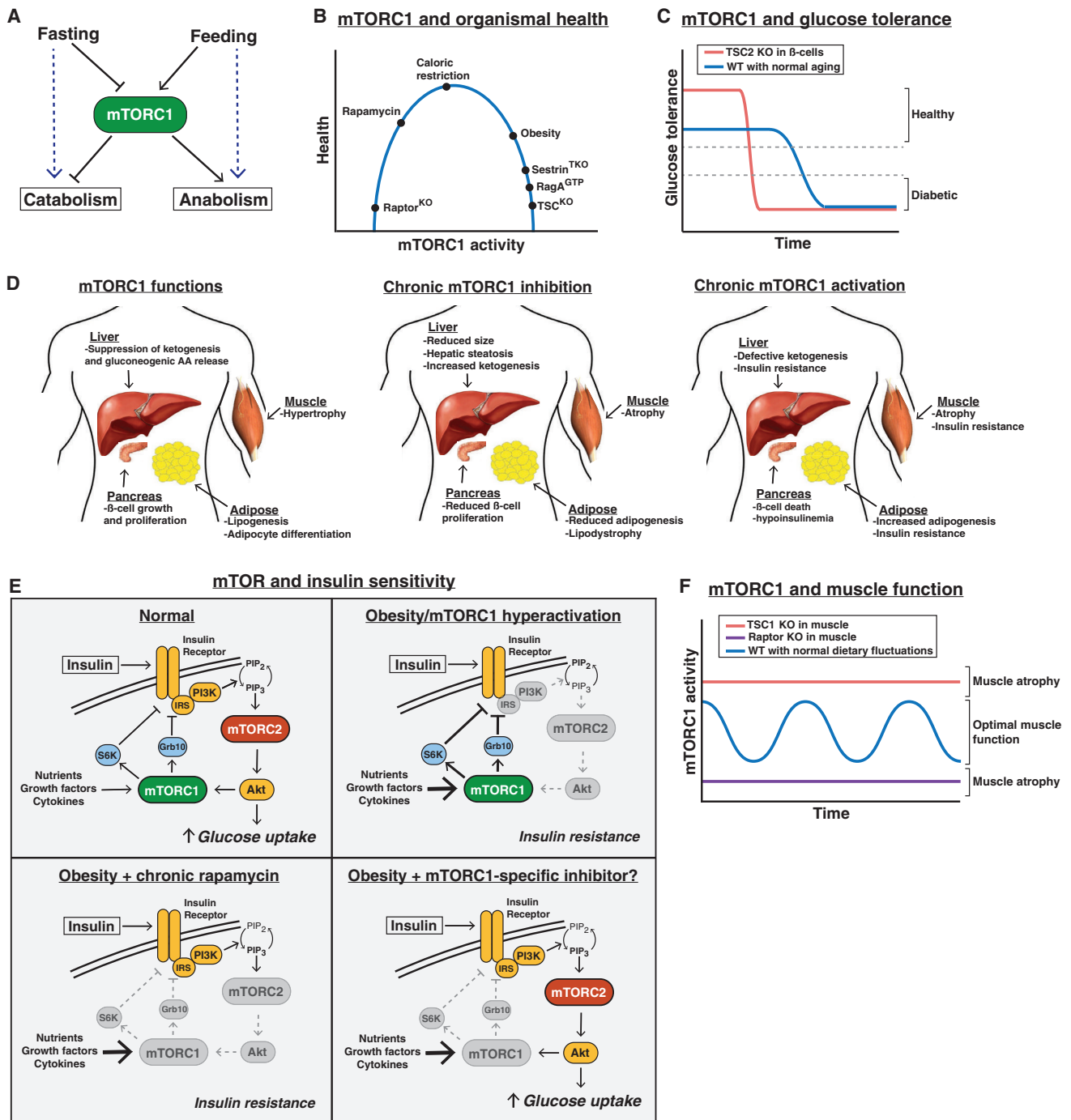


Figure 4. Physiological Roles of mTOR

(A) mTORC1 controls the balance between anabolism and catabolism in response to fasting and feeding.
 (B) The effect of cumulative mTORC1 activity on overall health.
 (C) The effect of mTORC1 hyperactivation in pancreatic β cells on glucose tolerance over time.
 (D) The normal functions of mTORC1 in the liver, muscle, pancreas, and adipose tissue (left), and the consequences of chronic mTORC1 inhibition (middle) or activation (right).
 (E) Deregulation of mTORC1 signaling in insulin resistance/diabetes, and the effect of rapamycin or a theoretical mTORC1-specific inhibitor.
 (F) Constitutive activation (red) and inhibition (purple) of mTORC1 signaling in the muscle leads to atrophy, whereas optimal muscle growth and function requires alternating periods of high and low mTORC1 activity (blue).

Glucose Homeostasis

When blood glucose levels drop, the liver activates a compensatory response involving the induction of autophagy, gluconeogenesis, and the release of alternative energy sources in the form of ketone bodies. Several lines of evidence suggest that regulation of mTORC1 signaling is crucial for the response of the liver to diet. For example, mice with liver-specific deletion of TSC1, which have constitutively activated mTORC1 signaling, fail to generate ketone bodies during fasting due to sustained mTORC1-dependent suppression of PPAR α , a transcriptional activator of ketogenic genes (Sengupta et al., 2010). The importance of inhibiting mTORC1 in the liver during fasting has also been observed through the generation of mice expressing a constitutively active allele of RagA (RagA^{GTP}). Although they develop normally, these mice die rapidly after birth due to an inability to maintain blood glucose levels during the perinatal fasting period (Efeyan et al., 2013). A similar phenotype was also observed in mice lacking the leucine sensor Sestrin2 and its paralogs, Sestrin1 and Sestrin3 (Sestrin^{TKO}) (Peng et al., 2014). Further analysis of these mice revealed that sustained mTORC1 activity during this fasting period prevents the induction of autophagy in the liver, which is critical for supplying free amino acids for gluconeogenesis. As a result, RagA^{GTP} mice display fatal hypoglycemia in response to fasting, consistent with a similar phenotype in autophagy-deficient mice (Kuma et al., 2004).

mTORC1 signaling also plays an important role in glucose homeostasis by regulating pancreatic β cell function. Studies using β cell-specific TSC2 knockout (β -TSC2^{KO}) mice revealed that hyperactivation of mTORC1 has a biphasic effect on β cell function, with young β -TSC2^{KO} mice exhibiting increased β cell mass, higher insulin levels and improved glucose tolerance (Mori et al., 2009; Shigeyama et al., 2008). This effect is reversed in older β -TSC2^{KO} mice, which more rapidly develop reduced β cell mass, lower insulin levels, and hyperglycemia. Thus, high mTORC1 activity in the pancreas is initially beneficial for glucose tolerance but also leads to a faster decline in β cell function over time (Figure 4C).

This biphasic effect of mTORC1 signaling is reminiscent of diet-induced (type 2) diabetes progression, in which pancreatic β cells initially expand and produce more insulin to compensate for an increased glycemic load, but eventually undergo exhaustion. Indeed, obese or high-fat diet (HFD)-treated mice have high mTORC1 signaling in many tissues, including the pancreas, likely due to increased levels of circulating insulin, amino acids, and pro-inflammatory cytokines (Khamzina et al., 2005). Increased mTORC1 signaling in these tissues also contributes to peripheral insulin resistance due to enhanced feedback inhibition of insulin/PI3K/Akt signaling, which is prevented in mice lacking S6K1/2 (Figure 4D; Um et al., 2004).

That mTORC1 hyperactivation from genetic or dietary manipulation results in insulin resistance has led many to speculate that mTORC1 inhibitors could improve glucose tolerance and protect against type 2 diabetes. Paradoxically, however, chronic pharmacological inhibition of mTORC1 using rapamycin has the opposite effect, causing insulin resistance and impaired glucose homeostasis (Figure 4D; Cunningham et al., 2007). This result is explained at least in part by the fact that prolonged rapamycin treatment also inhibits mTORC2 signaling in vivo (Lamming

et al., 2012). As mTORC2 directly activates Akt downstream of insulin/PI3K signaling, it is not surprising that mTORC2 inhibition disrupts the physiological response to insulin. Consistent with this, liver-specific Rictor knockout mice have severe insulin resistance and glucose intolerance (Hagiwara et al., 2012; Yuan et al., 2012), as do mice lacking Rictor in the muscle or fat (Kumar et al., 2008, 2010).

Muscle Mass and Function

Although the importance of mTOR signaling in promoting muscle growth is well appreciated by basic scientists and bodybuilders alike, the mechanisms underlying this process are still poorly understood, in part due to the difficulty of genetically manipulating multinucleate myocytes in vivo. Nonetheless, early studies of mTOR signaling in the muscle revealed that mTORC1 activation is associated with muscle hypertrophy (Bodine et al., 2001) and that both IGF-1 and leucine promote hypertrophy through the activation of mTORC1 signaling in cultured cells and in mice (Anthony et al., 2000; Rommel et al., 2001). Moreover, muscle-specific Raptor knockout mice display severe muscle atrophy and reduced body weight leading to early death (Bentzinger et al., 2008). This dramatic phenotype is also observed in muscle-specific mTOR knockout mice, but not Rictor-deficient mice, suggesting that the critical functions of mTOR in skeletal muscle are through mTORC1 (Bentzinger et al., 2008; Risson et al., 2009).

While acute activation of mTORC1 signaling in vivo does promote muscle hypertrophy in the short term (Bodine et al., 2001), chronic mTORC1 activation in the muscle through loss of TSC1 also results in severe muscle atrophy, low body mass, and early death, primarily due to an inability to induce autophagy in this tissue (Figure 4D; Castets et al., 2013). Considering that turnover of old or damaged tissue plays a critical role in muscle growth, these results suggest that alternating periods of high and low mTORC1 activity, as occurs with normal feeding and fasting cycles, is essential for maintaining optimal muscle health and function (Figure 4F).

An accumulating body of evidence suggests that muscle contraction also activates mTORC1 in the muscle, potentially explaining at least in part how increased muscle use promotes anabolism (Baar and Esser, 1999). A recent study found that mechanical stimuli activate mTORC1 signaling by inducing the phosphorylation of Raptor (Frey et al., 2014), although how this occurs is not clear. Understanding how mTORC1 can integrate the distinct signals from insulin, amino acids, and mechanical force in the muscle will be an important goal going forward and may inform approaches for treating muscle wasting disorders such as those associated with disuse and aging.

Adipogenesis and Lipid Homeostasis

Many studies over the last two decades also reveal a role for mTOR in promoting adipocyte formation and lipid synthesis in response to feeding and insulin (Figure 4D, reviewed in Lamming and Sabatini, 2013). mTORC1 promotes adipogenesis and enhanced lipogenesis in cell culture and in vivo, consistent with adipocyte-specific raptor knockout (Ad-Rap^{KO}) mice displaying lipodystrophy and hepatic steatosis (Lee et al., 2016). However, the role of mTORC1 in adipose is complicated by the fact that Ad-Rap^{KO} mice are also resistant to diet-induced

obesity due to reduced adipogenesis, suggesting mTORC1 inhibition in this tissue can have both positive and negative effects (Polak et al., 2008).

The loss of mTORC2 activity in adipocytes results not only in insulin resistance due to reduced Akt activity (Kumar et al., 2010), but also in less lipid synthesis in part due to reduced expression of ChREBP β , a master transcription factor for lipogenic genes (Tang et al., 2016). mTORC2 has also been shown to promote lipogenesis in the liver as well, suggesting a general role for mTORC2 in lipid synthesis (Hagiwara et al., 2012; Yuan et al., 2012). Thus, both mTORC1 and mTORC2 play important roles in multiple aspects of adipocyte function and lipid metabolism.

Immune Function

Early studies into the biological properties of rapamycin revealed a role in blocking lymphocyte proliferation, leading to its eventual clinical approval as an immunosuppressant for kidney transplants in 1999. The immunosuppressive action of rapamycin is largely attributed to its ability to block T cell activation, a key aspect of the adaptive immune response (reviewed in Powell et al., 2012). Mechanistically, mTORC1 facilitates the switch toward anabolic metabolism that is required for T cell activation and expansion and lies downstream of several activating signals present in the immune microenvironment, including interleukin-2 (IL-2), the co-stimulatory receptor CD28, as well as amino acids. Interestingly, mTORC1 inhibition during antigen presentation results in T cell anergy, whereby cells fail to activate upon subsequent antigen exposure (Zheng et al., 2007). As the induction of T cell anergy via nutrient depletion or other inhibitory signals is a mechanism utilized by tumors in immune evasion, these data suggest that promoting mTORC1 activation in immune cells may actually be beneficial in some contexts, such as cancer immunotherapy.

Recent studies have also found a role for mTORC1 in influencing T cell maturation, as rapamycin promotes the differentiation and expansion of CD4⁺FoxP3⁺ Regulatory T cells and CD8⁺ memory T cells while suppressing CD8⁺ and CD4⁺ effector T cell populations (Araki et al., 2009; Haxhinasto et al., 2008), consistent with the metabolic profiles of these cell types. Indeed, a recent report found that during the asymmetric division of activated CD8⁺ T cells, mTORC1 activity is high in the “effector-like” daughter cell, but low in the “memory-like” daughter cell, due to the asymmetric partitioning of amino acid transporters (Pollizzi et al., 2016; Verbist et al., 2016). Thus, the role of mTOR signaling in the immune system is clearly more complex than previously thought. Given the current clinical use of mTOR inhibitors in both immunosuppression and cancer, a more comprehensive understanding of how mTOR signaling influences overall immune responses in vivo will be a critical goal going forward.

Brain Function

mTOR has also emerged as an important regulator of numerous neurological processes, including neural development, circuit formation, and the neural control of feeding (reviewed in Lipton and Sahin, 2014). The deletion of either Raptor or Rictor in neurons causes reduced neuron size, and early death, suggesting

that signaling by both mTORC1 and mTORC2 is important for proper brain development. Conversely, the impact of hyperactive mTORC1 signaling in the brain is best observed in human patients with TSC, who exhibit a range of debilitating neurological disorders, including epilepsy, autism, and the presence of benign brain tumors.

The fact that mTORC1 hyperactivation in TSC patients correlates with a high occurrence of epileptic seizures (90% of TSC patients) and autistic traits (50%) suggests that deregulated mTORC1 signaling may also be involved in epilepsy and autism more generally. Indeed, mTORC1 hyperactivation in mice through neural loss of *Tsc1* or *Tsc2* leads to severe epileptic seizures that are prevented by rapamycin treatment (Zeng et al., 2008), and mutations in components of the GATOR1 and KICSTOR complexes have been linked to epilepsy in humans (Basel-Vanagaite et al., 2013; Ricos et al., 2016).

The importance of mTORC1 in this tissue stems in part from its role in promoting activity-dependent mRNA translation near synapses, a critical step in neuronal circuit formation. Consistent with this, the NMDA receptor antagonist ketamine acutely activates mTORC1 signaling in mouse neurons, which coincides with an increased translation of synaptic proteins (Li et al., 2010). The role of mTORC1 in regulating autophagy is likely also important, as autophagy dysfunction is strongly implicated in the pathogenesis of neurodegenerative disorders, including Parkinson's disease and Alzheimer's disease (AD). Inhibiting mTOR signaling has beneficial effects on mouse models of AD (Spilman et al., 2010), and it remains to be seen whether similar results will be seen in humans.

mTOR in Cancer

As discussed above, mTORC1 functions as a downstream effector for many frequently mutated oncogenic pathways, including the PI3K/Akt pathway as well as the Ras/Raf/Mek/Erk (MAPK) pathway, resulting in mTORC1 hyperactivation in a high percentage of human cancers (Figure 5A). Furthermore, the common tumor suppressors *TP53* and *LKB1* are negative regulators of mTORC1 upstream of TSC1 and TSC2, which are also tumor suppressors originally identified through genetic analysis of the familial cancer syndrome TSC. Several components of the nutrient sensing input to mTORC1 have also been implicated in cancer progression, including all three subunits of the GATOR1 complex, which are mutated with low frequency in glioblastoma (Bar-Peled et al., 2013), as well as RagC, which was recently found to be mutated at high frequency (~18%) in follicular lymphoma (Okosun et al., 2016). Additionally, mutations in the gene encoding folliculin (*FLCN*) are the causative lesion in the Birt-Hogg-Dube hereditary cancer syndrome (Nickerson et al., 2002), which manifests similarly to TSC. Finally, mutations in *MTOR* itself are also found in a variety of cancer subtypes, consistent with a role for mTOR in tumorigenesis (Grabiner et al., 2014; Sato et al., 2010).

mTORC2 signaling is also implicated in cancer largely due to its role in activating Akt, which drives pro-proliferative processes such as glucose uptake and glycolysis while also inhibiting apoptosis. Indeed, at least some PI3K/Akt-driven tumors appear to rely on mTORC2 activity, as Rictor is essential in mouse models of prostate cancer driven by *PTEN* loss, as well as in

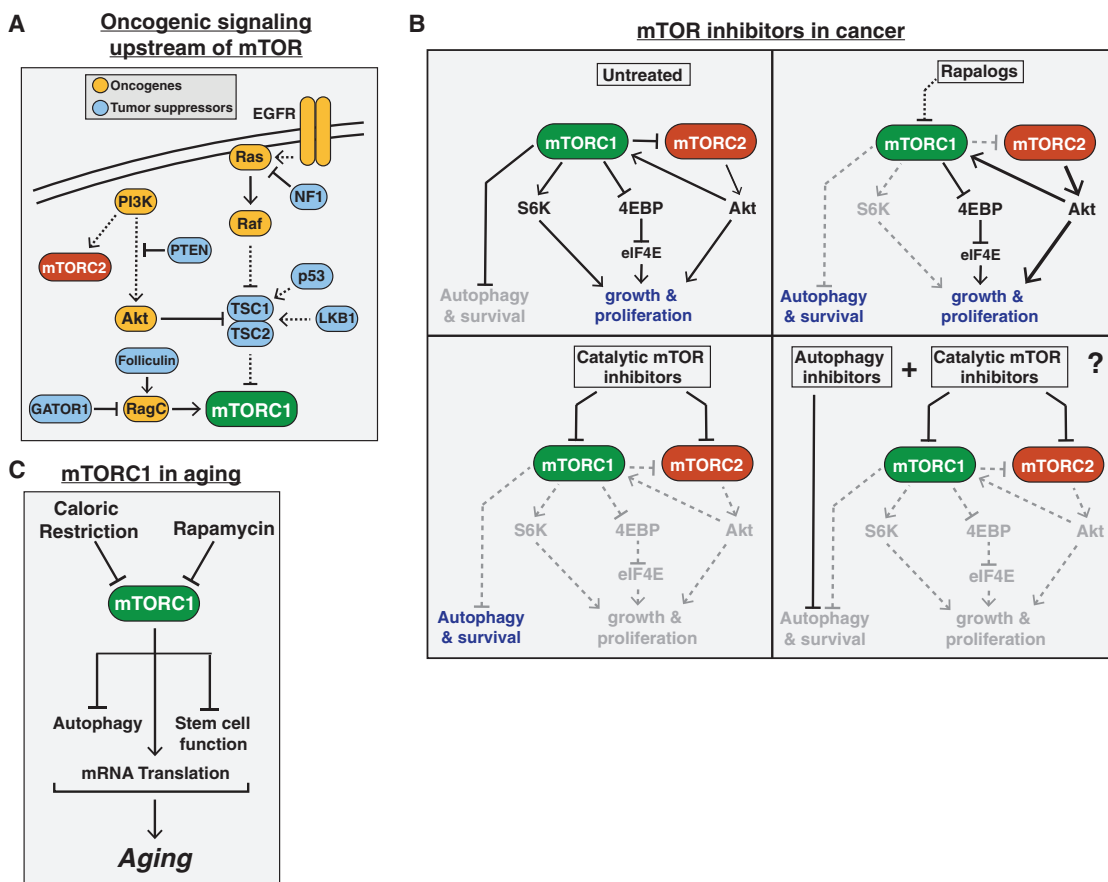


Figure 5. mTOR in Cancer and Aging

(A) The common tumor suppressors and oncogenes upstream of mTORC1 leading to increased mTORC1 signaling in a wide variety of cancers.

(B) The varying effects of rapalogs, catalytic mTOR inhibitors, or a combination of an mTOR inhibitor and autophagy inhibitor on cancer proliferation and survival.

(C) The role of mTORC1 signaling in aging.

human prostate cancer cell lines that lack *PTEN* (Guertin et al., 2009; Hietakangas and Cohen, 2008).

While many mTORC1-driven processes likely contribute to tumorigenesis, the translational program initiated by the phosphorylation of 4EBP is likely the most critical, at least in mouse models of Akt-driven prostate cancer and T cell lymphoma (Hsieh et al., 2010, 2012). Consistent with this, a variety of Akt- and Erk-driven cancer cell lines are dependent on 4EBP phosphorylation, and the ratio of 4EBP to eIF4E expression correlates well with their sensitivity to mTOR inhibitors (Alain et al., 2012; She et al., 2010).

The first mTOR inhibitors approved for use in cancer were a class of rapamycin derivatives known as “rapalogs.” The rapalog temsirolimus (Pfizer) was first approved for treatment of advanced renal cell carcinoma in 2007, followed by everolimus (Novartis) in 2009. Although a small number of “extraordinary responders” have been reported, these rapalogs have been less successful in the clinic than anticipated from pre-clinical cancer models.

Several explanations for this lack of efficacy have been suggested. The first came with the realization that, as allosteric inhibitors, the rapalogs block the phosphorylation of some but

not all mTORC1 substrates (Figure 5B, Choo et al., 2008; Feldman et al., 2009; Kang et al., 2013; Thoreen et al., 2009). In particular, the phosphorylation of 4EBP is largely insensitive to rapamycin. Second, inhibiting mTORC1 releases the negative feedback on insulin/PI3K/Akt signaling and therefore may paradoxically promote cell survival and prevent apoptosis in some contexts. Indeed, increased Akt signaling has been observed in biopsies of cancer patients following everolimus treatment and may help explain why rapalogs have largely cytostatic, but not cytotoxic, effects on tumors (Tabernero et al., 2008). Finally, mTORC1 inhibition also induces autophagy, which can help maintain cancer cell survival poorly vascularized, nutrient poor microenvironments such as in pancreatic tumors. Indeed, mTORC1 inhibition also promotes macropinocytosis, whereby extracellular proteins are internalized and degraded to provide amino acids for nutrient-starved tumors (Palm et al., 2015). These data suggest that combining rapalogs with autophagy inhibitors may improve efficacy, consistent with a recent phase 1 clinical trial using temsirolimus and the autophagy inhibitor hydrochloroquine in melanoma patients, which showed an improvement over temsirolimus alone (Rangwala et al., 2014).

In order to address some of the drawbacks of the rapalogs, “second-generation,” ATP-competitive catalytic inhibitors against mTOR have also been developed and are now in clinical trials. Unlike rapamycin, these compounds directly inhibit the catalytic activity of mTOR and therefore fully suppress both mTORC1 and mTORC2 (Figure 5B), making them more effective than rapalogs in a variety of preclinical cancer models. Although these second-generation mTOR inhibitors initially suppress Akt signaling due to inhibition of mTORC2, the release of negative feedback on Insulin/PI3K signaling eventually overcomes this blockade and Akt is reactivated following long-term treatment (Rodrik-Outmezguine et al., 2011). One possible solution to this problem may be the utilization of dual PI3K/mTOR inhibitors, which inhibit the closely related catalytic domains of both PI3K and mTOR, thereby more fully blocking phosphorylation of both Akt and 4EBP (Figure 5B). These inhibitors have also shown some promise in preclinical and early clinical trial data but have raised concerns over dose-limiting toxicities.

The cases where rapalogs have had the most success to date have generally involved mutations in the mTOR pathway itself, such as in *TSC1* or *MTOR* (Iyer et al., 2012; Wagle et al., 2014a). Even in these cases, however, an exquisite initial response has been followed by additional mutations in the kinase or FRB domains of *MTOR*, leading to acquired resistance (Wagle et al., 2014b). One creative way to overcome these resistance mutations may be with the recently described “third-generation” mTOR inhibitor called “RapaLink,” in which the ATP-competitive mTOR inhibitor is chemically linked to rapamycin, enabling inhibition of mTOR mutants that are resistant to either MLN0128 or rapamycin alone (Rodrik-Outmezguine et al., 2016).

mTOR in Aging

mTOR signaling is strongly implicated in the aging process of diverse organisms, including yeast, worms, flies, and mammals. This was first observed through studies in the nematode *C. elegans*, which found that reduced expression of the homologs of mTOR (ceTOR, formerly *let-363*) or Raptor (*daf-15*) extend lifespan (Vellai et al., 2003; Jia et al., 2004). Subsequent genetic studies found that reduced TOR signaling also promotes longevity in *Drosophila* (Kapahi et al., 2004), budding yeast (Kaeberlein et al., 2005) as well as mice (Lamming et al., 2012; Wu et al., 2013). Consistent with this, the mTOR inhibitor rapamycin is currently the only pharmacological treatment proven to extend lifespan in all of these model organisms (Bjedov et al., 2010; Harrison et al., 2009; Powers et al., 2006; Robida-Stubbs et al., 2012).

The only other intervention shown to extend lifespan in such a wide range of organisms is caloric restriction (CR), defined as a reduction in nutrient intake without malnutrition. Given the critical role of mTORC1 in sensing nutrients and insulin, this has led many to speculate that the beneficial effects of CR on lifespan are also due to reduced mTORC1 signaling. Indeed, CR-like regimens do not further extend lifespan in yeast, worms, or flies with reduced mTOR signaling, suggesting an overlapping mechanism (Kaeberlein et al., 2005; Hansen et al., 2007; Kapahi et al., 2004).

While there is now a general consensus that mTOR signaling plays a key role in mammalian aging, the mechanism through

which this occurs is still unclear. Several lines of evidence suggest that the general reduction in mRNA translation during mTORC1 inhibition slows aging by reducing the accumulation of proteotoxic and oxidative stress, consistent with the observation that loss of the mTORC1 substrate S6K1 also extends lifespan in mammals (Selman et al., 2009). A related possibility is that inhibition of mTORC1 slows aging by increasing autophagy, which helps clear damaged proteins and organelles such as mitochondria, the accumulation of which are also associated with aging and aging-related diseases. Finally, another model suggests that the attenuation of adult stem cells in various tissues plays a central role in organismal aging, and mTOR inhibition boosts the self-renewal capacity of both hematopoietic and intestinal stem cells in mice (Chen et al., 2009; Yilmaz et al., 2012). Ultimately, the importance of mTORC1 signaling in aging likely reflects its unique capacity to regulate such a wide variety of key cellular functions (Figure 5C).

The observation that mTOR inhibition extends lifespan and delays the onset of age-associated diseases in mammals has led many to speculate that mTOR inhibitors could be used to enhance longevity in humans. The major drawback of prolonged rapamycin treatment in humans, however, is the potential for side effects such as immunosuppression and glucose intolerance. There is reason for optimism, however, as a trial in healthy elderly humans using everolimus showed safety and even improved immune function (Mannick et al., 2014), and alternative dosing regimens have been proposed that can promote longevity with reduced side effects (Arriola Apelo et al., 2016). Given that many of the negative metabolic side effects associated with mTOR inhibitors are due to inhibition of mTORC2, while the anti-aging effects are due to inhibition of mTORC1, the development of mTORC1-specific inhibitors would be particularly beneficial.

Perspectives

It is now clear that the mTOR pathway plays a central role in sensing environmental conditions and regulating nearly all aspects of metabolism at both the cellular and organismal level. In just the last several years, many new insights into both mTOR function and regulation have been elucidated, and extensive genetic and pharmacological studies in mice have enhanced our understanding of how mTOR dysfunction contributes to disease.

While many inputs to mTORC1 have now been identified and their mechanisms of sensing characterized, an integrated understanding of the relative importance of these signals and the contexts in which they are important remains largely unclear. For example, it remains mysterious which inputs to TSC are dominant and how this depends on the physiological context. Similar questions exist for nutrient sensing by the Rag GTPases, specifically regarding the purpose of sensing of both lysosomal and cytosolic amino acids, as well as the tissues in which the nutrient sensors such as Sestrin2, CASTOR1, and SLC38A9 are most important. Such insights will likely require both deeper biochemical studies of these complexes in vitro as well as improved mouse models that enable more nuanced perturbation and monitoring of these sensors in vivo.

The major focus of mTOR research going forward, however, will be to address whether these molecular insights can improve

the therapeutic targeting of mTOR in the clinic. Although rapalogs and catalytic mTOR inhibitors have been successful in the context of immunosuppression and a small subset of cancer types, clear limitations have arisen that limit their utility. Specifically, given the critical functions of mTOR in most human tissues, complete catalytic inhibition causes severe dose-limiting toxicities, while rapalogs also suffer from the drawbacks associated with lack of tissue specificity and unwanted disruption of mTORC2. Future work should focus on the development of mTOR-targeting therapeutics outside of these two modalities, such as truly mTORC1-specific inhibitors for use in diabetes, neurodegeneration, and life-span extension, or tissue-specific mTORC1 agonists for use in muscle wasting diseases and immunotherapy. Such approaches will likely require going beyond targeting mTOR directly to instead developing compounds that modulate tissue-specific receptors or signaling molecules upstream of mTOR, such as the recently characterized amino acid sensors Sestrin2 and CASTOR1, which contain small-molecule binding pockets and specifically regulate mTORC1. Ultimately, such insights may enable the rational targeting of mTOR signaling to unlock the full therapeutic potential of this remarkable pathway.

ACKNOWLEDGMENTS

We thank all members of the Sabatini Lab for helpful discussions; in particular, W.C. Comb, T. Wang, R.L. Wolfson, and G.A. Wyant for critical reading of the manuscript. We apologize to everyone in the mTOR field whose work could not be included due to space constraints. This work was supported by grants from the NIH (R01CA103866, R01CA129105, and AI47389) and the U.S. Department of Defense (W81XWH-07- 0448) to D.M.S. and fellowship support to R.A.S. from the David H. Koch Graduate Fellowship Fund. D.M.S. is a founder and a member of the scientific advisory board for Navitor Pharmaceuticals, which targets the mTORC1 pathway for therapeutic benefit. D.M.S. is an Investigator of the Howard Hughes Medical Institute.

REFERENCES

- Alain, T., Morita, M., Fonseca, B.D., Yanagiya, A., Siddiqui, N., Bhat, M., Zammit, D., Marcus, V., Metrakos, P., Voyer, L.A., et al. (2012). eIF4E/4E-BP ratio predicts the efficacy of mTOR targeted therapies. *Cancer Res.* *72*, 6468–6476.
- Anthony, J.C., Yoshizawa, F., Anthony, T.G., Vary, T.C., Jefferson, L.S., and Kimball, S.R. (2000). Leucine stimulates translation initiation in skeletal muscle of postabsorptive rats via a rapamycin-sensitive pathway. *J. Nutr.* *130*, 2413–2419.
- Araki, K., Turner, A.P., Shaffer, V.O., Gangappa, S., Keller, S.A., Bachmann, M.F., Larsen, C.P., and Ahmed, R. (2009). mTOR regulates memory CD8 T-cell differentiation. *Nature* *460*, 108–112.
- Arriola Apelo, S.I., Neuman, J.C., Baar, E.L., Syed, F.A., Cummings, N.E., Brar, H.K., Pumper, C.P., Kimple, M.E., and Lamming, D.W. (2016). Alternative rapamycin treatment regimens mitigate the impact of rapamycin on glucose homeostasis and the immune system. *Aging Cell* *15*, 28–38.
- Aylett, C.H., Sauer, E., Imseng, S., Boehringer, D., Hall, M.N., Ban, N., and Maier, T. (2016). Architecture of human mTOR complex 1. *Science* *351*, 48–52.
- Baar, K., and Esser, K. (1999). Phosphorylation of p70(S6k) correlates with increased skeletal muscle mass following resistance exercise. *Am. J. Physiol.* *276*, C120–C127.
- Bar-Peled, L., Schweitzer, L.D., Zoncu, R., and Sabatini, D.M. (2012). Ragulator is a GEF for the rag GTPases that signal amino acid levels to mTORC1. *Cell* *150*, 1196–1208.
- Bar-Peled, L., Chantranupong, L., Cherniack, A.D., Chen, W.W., Ottina, K.A., Grabiner, B.C., Spear, E.D., Carter, S.L., Meyerson, M., and Sabatini, D.M. (2013). A Tumor suppressor complex with GAP activity for the Rag GTPases that signal amino acid sufficiency to mTORC1. *Science* *340*, 1100–1106.
- Baretić, D., Berndt, A., Ohashi, Y., Johnson, C.M., and Williams, R.L. (2016). Tor forms a dimer through an N-terminal helical solenoid with a complex topology. *Nat. Commun.* *7*, 11016.
- Basel-Vanagaite, L., Hershkovitz, T., Heyman, E., Raspall-Chaure, M., Kakar, N., Smirin-Yosef, P., Vila-Pueyo, M., Kornreich, L., Thiele, H., Bode, H., et al. (2013). Biallelic SZT2 mutations cause infantile encephalopathy with epilepsy and dysmorphic corpus callosum. *Am. J. Hum. Genet.* *93*, 524–529.
- Ben-Sahra, I., Howell, J.J., Asara, J.M., and Manning, B.D. (2013). Stimulation of de novo pyrimidine synthesis by growth signaling through mTOR and S6K1. *Science* *339*, 1323–1328.
- Ben-Sahra, I., Hoxhaj, G., Ricoult, S.J., Asara, J.M., and Manning, B.D. (2016). mTORC1 induces purine synthesis through control of the mitochondrial tetrahydrofolate cycle. *Science* *351*, 728–733.
- Bentzinger, C.F., Romanino, K., Cloëtta, D., Lin, S., Mascarenhas, J.B., Oliveri, F., Xia, J., Casanova, E., Costa, C.F., Brink, M., et al. (2008). Skeletal muscle-specific ablation of raptor, but not of rictor, causes metabolic changes and results in muscle dystrophy. *Cell Metab.* *8*, 411–424.
- Binda, M., Péli-Gulli, M.P., Bonfils, G., Panchaud, N., Urban, J., Sturgill, T.W., Loewith, R., and De Virgilio, C. (2009). The Vam6 GEF controls TORC1 by activating the EGO complex. *Mol. Cell* *35*, 563–573.
- Bjedov, I., Toivonen, J.M., Kerr, F., Slack, C., Jacobson, J., Foley, A., and Partridge, L. (2010). Mechanisms of life span extension by rapamycin in the fruit fly *Drosophila melanogaster*. *Cell Metab.* *11*, 35–46.
- Bodine, S.C., Stitt, T.N., Gonzalez, M., Kline, W.O., Stover, G.L., Bauerlein, R., Zlotchenko, E., Scrimgeour, A., Lawrence, J.C., Glass, D.J., and Yancopoulos, G.D. (2001). Akt/mTOR pathway is a crucial regulator of skeletal muscle hypertrophy and can prevent muscle atrophy in vivo. *Nat. Cell Biol.* *3*, 1014–1019.
- Brown, E.J., Albers, M.W., Shin, T.B., Ichikawa, K., Keith, C.T., Lane, W.S., and Schreiber, S.L. (1994). A mammalian protein targeted by G1-arresting rapamycin-receptor complex. *Nature* *369*, 756–758.
- Brugarolas, J., Lei, K., Hurley, R.L., Manning, B.D., Reiling, J.H., Hafen, E., Witters, L.A., Ellisen, L.W., and Kaelin, W.G., Jr. (2004). Regulation of mTOR function in response to hypoxia by REDD1 and the TSC1/TSC2 tumor suppressor complex. *Genes Dev.* *18*, 2893–2904.
- Brunn, G.J., Hudson, C.C., Sekulic, A., Williams, J.M., Hosoi, H., Houghton, P.J., Lawrence, J.C., Jr., and Abraham, R.T. (1997). Phosphorylation of the translational repressor PHAS-I by the mammalian target of rapamycin. *Science* *277*, 99–101.
- Cafferkey, R., Young, P.R., McLaughlin, M.M., Bergsma, D.J., Koltin, Y., Sathe, G.M., Faucette, L., Eng, W.K., Johnson, R.K., and Livi, G.P. (1993). Dominant missense mutations in a novel yeast protein related to mammalian phosphatidylinositol 3-kinase and VPS34 abrogate rapamycin cytotoxicity. *Mol. Cell. Biol.* *13*, 6012–6023.
- Castets, P., Lin, S., Rion, N., Di Fulvio, S., Romanino, K., Guridi, M., Frank, S., Tintignac, L.A., Sinnreich, M., and Rüegg, M.A. (2013). Sustained activation of mTORC1 in skeletal muscle inhibits constitutive and starvation-induced autophagy and causes a severe, late-onset myopathy. *Cell Metab.* *17*, 731–744.
- Chantranupong, L., Wolfson, R.L., Orozco, J.M., Saxton, R.A., Scaria, S.M., Bar-Peled, L., Spooner, E., Isasa, M., Gygi, S.P., and Sabatini, D.M. (2014). The Sestrins interact with GATOR2 to negatively regulate the amino-acid-sensing pathway upstream of mTORC1. *Cell Rep.* *9*, 1–8.
- Chantranupong, L., Scaria, S.M., Saxton, R.A., Gygi, M.P., Shen, K., Wyant, G.A., Wang, T., Harper, J.W., Gygi, S.P., and Sabatini, D.M. (2016). The CASTOR Proteins Are Arginine Sensors for the mTORC1 Pathway. *Cell* *165*, 153–164.
- Chen, C., Liu, Y., Liu, Y., and Zheng, P. (2009). mTOR regulation and therapeutic rejuvenation of aging hematopoietic stem cells. *Sci. Signal.* *2*, ra75.
- Choo, A.Y., Yoon, S.O., Kim, S.G., Roux, P.P., and Blenis, J. (2008). Rapamycin differentially inhibits S6Ks and 4E-BP1 to mediate cell-type-specific repression of mRNA translation. *Proc. Natl. Acad. Sci. USA* *105*, 17414–17419.

- Chung, J., Kuo, C.J., Crabtree, G.R., and Blenis, J. (1992). Rapamycin-FKBP specifically blocks growth-dependent activation of and signaling by the 70 kd S6 protein kinases. *Cell* 69, 1227–1236.
- Cunningham, J.T., Rodgers, J.T., Arlow, D.H., Vazquez, F., Mootha, V.K., and Puigserver, P. (2007). mTOR controls mitochondrial oxidative function through a YY1-PGC-1 α transcriptional complex. *Nature* 450, 736–740.
- Dibble, C.C., Elis, W., Menon, S., Qin, W., Klekota, J., Asara, J.M., Finan, P.M., Kwiatkowski, D.J., Murphy, L.O., and Manning, B.D. (2012). TBC1D7 is a third subunit of the TSC1-TSC2 complex upstream of mTORC1. *Mol. Cell* 47, 535–546.
- Dorrello, N.V., Peschiaroli, A., Guardavaccaro, D., Colburn, N.H., Sherman, N.E., and Pagano, M. (2006). S6K1- and betaTRCP-mediated degradation of PDCD4 promotes protein translation and cell growth. *Science* 314, 467–471.
- Düvel, K., Yecies, J.L., Menon, S., Raman, P., Lipovsky, A.I., Souza, A.L., Triantafellow, E., Ma, Q., Gorski, R., Cleaver, S., et al. (2010). Activation of a metabolic gene regulatory network downstream of mTOR complex 1. *Mol. Cell* 39, 171–183.
- Efeyan, A., Zoncu, R., Chang, S., Gumper, I., Snitkin, H., Wolfson, R.L., Kirak, O., Sabatini, D.D., and Sabatini, D.M. (2013). Regulation of mTORC1 by the Rag GTPases is necessary for neonatal autophagy and survival. *Nature* 493, 679–683.
- Eng, C.P., Sehgal, S.N., and Vézina, C. (1984). Activity of rapamycin (AY-22,989) against transplanted tumors. *J. Antibiot.* 37, 1231–1237.
- Feldman, M.E., Apsel, B., Uotila, A., Loewith, R., Knight, Z.A., Ruggero, D., and Shokat, K.M. (2009). Active-site inhibitors of mTOR target rapamycin-resistant outputs of mTORC1 and mTORC2. *PLoS Biol.* 7, e38.
- Feng, Z., Hu, W., de Stanchina, E., Teresky, A.K., Jin, S., Lowe, S., and Levine, A.J. (2007). The regulation of AMPK beta1, TSC2, and PTEN expression by p53: Stress, cell and tissue specificity, and the role of these gene products in modulating the IGF-1-AKT-mTOR pathways. *Cancer Res.* 67, 3043–3053.
- Frey, J.W., Jacobs, B.L., Goodman, C.A., and Hornberger, T.A. (2014). A role for Raptor phosphorylation in the mechanical activation of mTOR signaling. *Cell. Signal.* 26, 313–322.
- Frias, M.A., Thoreen, C.C., Jaffe, J.D., Schroder, W., Sculley, T., Carr, S.A., and Sabatini, D.M. (2006). mSin1 is necessary for Akt/PKB phosphorylation, and its isoforms define three distinct mTORC2s. *Curr. Biol.* 16, 1865–1870.
- Gan, X., Wang, J., Wang, C., Sommer, E., Kozasa, T., Srinivasula, S., Alessi, D., Offermanns, S., Simon, M.I., and Wu, D. (2012). PRR5L degradation promotes mTORC2-mediated PKC- δ phosphorylation and cell migration downstream of G α 12. *Nat. Cell Biol.* 14, 686–696.
- García-Martínez, J.M., and Alessi, D.R. (2008). mTOR complex 2 (mTORC2) controls hydrophobic motif phosphorylation and activation of serum- and glucocorticoid-induced protein kinase 1 (SGK1). *Biochem. J.* 416, 375–385.
- Gingras, A.C., Gygi, S.P., Raught, B., Polakiewicz, R.D., Abraham, R.T., Hoekstra, M.F., Aebersold, R., and Sonenberg, N. (1999). Regulation of 4E-BP1 phosphorylation: A novel two-step mechanism. *Genes Dev.* 13, 1422–1437.
- Grabiner, B.C., Nardi, V., Birsoy, K., Possemato, R., Shen, K., Sinha, S., Jordan, A., Beck, A.H., and Sabatini, D.M. (2014). A diverse array of cancer-associated MTOR mutations are hyperactivating and can predict rapamycin sensitivity. *Cancer Discov.* 4, 554–563.
- Guertin, D.A., Stevens, D.M., Thoreen, C.C., Burds, A.A., Kalaany, N.Y., Mofatt, J., Brown, M., Fitzgerald, K.J., and Sabatini, D.M. (2006). Ablation in mice of the mTORC components raptor, rictor, or mLST8 reveals that mTORC2 is required for signaling to Akt-FOXO and PKC α , but not S6K1. *Dev. Cell* 11, 859–871.
- Guertin, D.A., Stevens, D.M., Saitoh, M., Kinkel, S., Crosby, K., Sheen, J.H., Mullholland, D.J., Magnuson, M.A., Wu, H., and Sabatini, D.M. (2009). mTOR complex 2 is required for the development of prostate cancer induced by Pten loss in mice. *Cancer Cell* 15, 148–159.
- Gwinn, D.M., Shackelford, D.B., Egan, D.F., Mihaylova, M.M., Mery, A., Vasquez, D.S., Turk, B.E., and Shaw, R.J. (2008). AMPK phosphorylation of raptor mediates a metabolic checkpoint. *Mol. Cell* 30, 214–226.
- Hagiwara, A., Cornu, M., Cybulski, N., Polak, P., Betz, C., Trapani, F., Terracciano, L., Heim, M.H., Rüegg, M.A., and Hall, M.N. (2012). Hepatic mTORC2 activates glycolysis and lipogenesis through Akt, glucokinase, and SREBP1c. *Cell Metab.* 15, 725–738.
- Hansen, M., Taubert, S., Crawford, D., Libina, N., Lee, S.J., and Kenyon, C. (2007). Lifespan extension by conditions that inhibit translation in *Caenorhabditis elegans*. *Aging Cell* 6, 95–110.
- Hara, K., Maruki, Y., Long, X., Yoshino, K., Oshiro, N., Hidayat, S., Tokunaga, C., Avruch, J., and Yonezawa, K. (2002). Raptor, a binding partner of target of rapamycin (TOR), mediates TOR action. *Cell* 110, 177–189.
- Harrington, L.S., Findlay, G.M., Gray, A., Tolkacheva, T., Wigfield, S., Rebholz, H., Barnett, J., Leslie, N.R., Cheng, S., Shepherd, P.R., et al. (2004). The TSC1-2 tumor suppressor controls insulin-PI3K signaling via regulation of IRS proteins. *J. Cell Biol.* 166, 213–223.
- Harrison, D.E., Strong, R., Sharp, Z.D., Nelson, J.F., Astle, C.M., Flurkey, K., Nadon, N.L., Wilkinson, J.E., Frenkel, K., Carter, C.S., et al. (2009). Rapamycin fed late in life extends lifespan in genetically heterogeneous mice. *Nature* 460, 392–395.
- Haxhinasto, S., Mathis, D., and Benoist, C. (2008). The AKT-mTOR axis regulates de novo differentiation of CD4+Foxp3+ cells. *J. Exp. Med.* 205, 565–574.
- Heitman, J., Movva, N.R., and Hall, M.N. (1991). Targets for cell cycle arrest by the immunosuppressant rapamycin in yeast. *Science* 253, 905–909.
- Hietakangas, V., and Cohen, S.M. (2008). TOR complex 2 is needed for cell cycle progression and anchorage-independent growth of MCF7 and PC3 tumor cells. *BMC Cancer* 8, 282.
- Holz, M.K., Ballif, B.A., Gygi, S.P., and Blenis, J. (2005). mTOR and S6K1 mediate assembly of the translation preinitiation complex through dynamic protein interchange and ordered phosphorylation events. *Cell* 123, 569–580.
- Hsieh, A.C., Costa, M., Zollo, O., Davis, C., Feldman, M.E., Testa, J.R., Meyuhas, O., Shokat, K.M., and Ruggero, D. (2010). Genetic dissection of the oncogenic mTOR pathway reveals druggable addiction to translational control via 4EBP-eIF4E. *Cancer Cell* 17, 249–261.
- Hsieh, A.C., Liu, Y., Edlind, M.P., Ingolia, N.T., Janes, M.R., Sher, A., Shi, E.Y., Stumpf, C.R., Christensen, C., Bonham, M.J., et al. (2012). The translational landscape of mTOR signalling steers cancer initiation and metastasis. *Nature* 485, 55–61.
- Hsu, P.P., Kang, S.A., Rameseder, J., Zhang, Y., Ottina, K.A., Lim, D., Peterson, T.R., Choi, Y., Gray, N.S., Yaffe, M.B., et al. (2011). The mTOR-regulated phosphoproteome reveals a mechanism of mTORC1-mediated inhibition of growth factor signaling. *Science* 332, 1317–1322.
- Inoki, K., Li, Y., Zhu, T., and Guan, K.L. (2002). TSC2 is phosphorylated and inhibited by Akt and suppresses mTOR signalling. *Nat Cell Biol.* 4, 648–657.
- Inoki, K., Li, Y., Xu, T., and Guan, K.L. (2003a). Rheb GTPase is a direct target of TSC2 GAP activity and regulates mTOR signaling. *Genes Dev.* 17, 1829–1834.
- Inoki, K., Zhu, T., and Guan, K.L. (2003b). TSC2 mediates cellular energy response to control cell growth and survival. *Cell* 115, 577–590.
- Inoki, K., Ouyang, H., Zhu, T., Lindvall, C., Wang, Y., Zhang, X., Yang, Q., Bennett, C., Harada, Y., Stankunas, K., et al. (2006). TSC2 integrates Wnt and energy signals via a coordinated phosphorylation by AMPK and GSK3 to regulate cell growth. *Cell* 126, 955–968.
- Iyer, G., Hanrahan, A.J., Milowsky, M.I., Al-Ahmadie, H., Scott, S.N., Janakiraman, M., Pirun, M., Sander, C., Socci, N.D., Ostrovskaya, I., et al. (2012). Genome sequencing identifies a basis for everolimus sensitivity. *Science* 338, 221.
- Jacinto, E., Loewith, R., Schmidt, A., Lin, S., Rüegg, M.A., Hall, A., and Hall, M.N. (2004). Mammalian TOR complex 2 controls the actin cytoskeleton and is rapamycin insensitive. *Nat. Cell Biol.* 6, 1122–1128.
- Jacinto, E., Facchinetti, V., Liu, D., Soto, N., Wei, S., Jung, S.Y., Huang, Q., Qin, J., and Su, B. (2006). SIN1/MIP1 maintains rictor-mTOR complex integrity and regulates Akt phosphorylation and substrate specificity. *Cell* 127, 125–137.

- Jewell, J.L., Kim, Y.C., Russell, R.C., Yu, F.X., Park, H.W., Plouffe, S.W., Tagliabracchi, V.S., and Guan, K.L. (2015). Metabolism. Differential regulation of mTORC1 by leucine and glutamine. *Science* *347*, 194–198.
- Jia, K., Chen, D., and Riddle, D.L. (2004). The TOR pathway interacts with the insulin signaling pathway to regulate *C. elegans* larval development, metabolism and life span. *Development* *131*, 3897–3906.
- Jung, J., Genau, H.M., and Behrends, C. (2015). Amino Acid-Dependent mTORC1 Regulation by the Lysosomal Membrane Protein SLC38A9. *Mol. Cell. Biol.* *35*, 2479–2494.
- Kaeberlein, M., Powers, R.W., 3rd, Steffen, K.K., Westman, E.A., Hu, D., Dang, N., Kerr, E.O., Kirkland, K.T., Fields, S., and Kennedy, B.K. (2005). Regulation of yeast replicative life span by TOR and Sch9 in response to nutrients. *Science* *310*, 1193–1196.
- Kalender, A., Selvaraj, A., Kim, S.Y., Gulati, P., Brûlé, S., Viollet, B., Kemp, B.E., Bardeesy, N., Dennis, P., Schlager, J.J., et al. (2010). Metformin, independent of AMPK, inhibits mTORC1 in a rag GTPase-dependent manner. *Cell Metab.* *11*, 390–401.
- Kang, S.A., Pacold, M.E., Cervantes, C.L., Lim, D., Lou, H.J., Ottina, K., Gray, N.S., Turk, B.E., Yaffe, M.B., and Sabatini, D.M. (2013). mTORC1 phosphorylation sites encode their sensitivity to starvation and rapamycin. *Science* *341*, 1236566.
- Kapahi, P., Zid, B.M., Harper, T., Koslover, D., Sapin, V., and Benzer, S. (2004). Regulation of lifespan in *Drosophila* by modulation of genes in the TOR signaling pathway. *Curr. Biol.* *14*, 885–890.
- Khamzina, L., Veilleux, A., Bergeron, S., and Marette, A. (2005). Increased activation of the mammalian target of rapamycin pathway in liver and skeletal muscle of obese rats: Possible involvement in obesity-linked insulin resistance. *Endocrinology* *146*, 1473–1481.
- Kim, D.H., Sarbassov, D.D., Ali, S.M., King, J.E., Latek, R.R., Erdjument-Bromage, H., Tempst, P., and Sabatini, D.M. (2002). mTOR interacts with raptor to form a nutrient-sensitive complex that signals to the cell growth machinery. *Cell* *110*, 163–175.
- Kim, D.H., Sarbassov, D.D., Ali, S.M., Latek, R.R., Guntur, K.V., Erdjument-Bromage, H., Tempst, P., and Sabatini, D.M. (2003). GbetaL, a positive regulator of the rapamycin-sensitive pathway required for the nutrient-sensitive interaction between raptor and mTOR. *Mol. Cell* *11*, 895–904.
- Kim, E., Goraksha-Hicks, P., Li, L., Neufeld, T.P., and Guan, K.L. (2008). Regulation of TORC1 by Rag GTPases in nutrient response. *Nat. Cell Biol.* *10*, 935–945.
- Kim, J., Kundu, M., Viollet, B., and Guan, K.L. (2011). AMPK and mTOR regulate autophagy through direct phosphorylation of Ulk1. *Nat. Cell Biol.* *13*, 132–141.
- Kuma, A., Hatano, M., Matsui, M., Yamamoto, A., Nakaya, H., Yoshimori, T., Ohsumi, Y., Tokuhisa, T., and Mizushima, N. (2004). The role of autophagy during the early neonatal starvation period. *Nature* *432*, 1032–1036.
- Kumar, A., Harris, T.E., Keller, S.R., Choi, K.M., Magnuson, M.A., and Lawrence, J.C., Jr. (2008). Muscle-specific deletion of rictor impairs insulin-stimulated glucose transport and enhances Basal glycogen synthase activity. *Mol. Cell. Biol.* *28*, 61–70.
- Kumar, A., Lawrence, J.C., Jr., Jung, D.Y., Ko, H.J., Keller, S.R., Kim, J.K., Magnuson, M.A., and Harris, T.E. (2010). Fat cell-specific ablation of rictor in mice impairs insulin-regulated fat cell and whole-body glucose and lipid metabolism. *Diabetes* *59*, 1397–1406.
- Kunz, J., Henriquez, R., Schneider, U., Deuter-Reinhard, M., Movva, N.R., and Hall, M.N. (1993). Target of rapamycin in yeast, TOR2, is an essential phosphatidylinositol kinase homolog required for G1 progression. *Cell* *73*, 585–596.
- Lamming, D.W., and Sabatini, D.M. (2013). A central role for mTOR in lipid homeostasis. *Cell Metab.* *18*, 465–469.
- Lamming, D.W., Ye, L., Katajisto, P., Goncalves, M.D., Saitoh, M., Stevens, D.M., Davis, J.G., Salmon, A.B., Richardson, A., Ahima, R.S., et al. (2012). Rapamycin-induced insulin resistance is mediated by mTORC2 loss and uncoupled from longevity. *Science* *335*, 1638–1643.
- Lee, D.F., Kuo, H.P., Chen, C.T., Hsu, J.M., Chou, C.K., Wei, Y., Sun, H.L., Li, L.Y., Ping, B., Huang, W.C., et al. (2007). IKK beta suppression of TSC1 links inflammation and tumor angiogenesis via the mTOR pathway. *Cell* *130*, 440–455.
- Lee, P.L., Tang, Y., Li, H., and Guertin, D.A. (2016). Raptor/mTORC1 loss in adipocytes causes progressive lipodystrophy and fatty liver disease. *Mol. Metab.* *5*, 422–432.
- Li, X., and Gao, T. (2014). mTORC2 phosphorylates protein kinase C ζ to regulate its stability and activity. *EMBO Rep.* *15*, 191–198.
- Li, N., Lee, B., Liu, R.J., Banas, M., Dwyer, J.M., Iwata, M., Li, X.Y., Aghajanian, G., and Duman, R.S. (2010). mTOR-dependent synapse formation underlies the rapid antidepressant effects of NMDA antagonists. *Science* *329*, 959–964.
- Lipton, J.O., and Sahin, M. (2014). The neurology of mTOR. *Neuron* *84*, 275–291.
- Liu, P., Gan, W., Chin, Y.R., Ogura, K., Guo, J., Zhang, J., Wang, B., Blenis, J., Cantley, L.C., Toker, A., et al. (2015). PtdIns(3,4,5)P₃-Dependent Activation of the mTORC2 Kinase Complex. *Cancer Discov.* *5*, 1194–1209.
- Loewith, R., and Hall, M.N. (2011). Target of rapamycin (TOR) in nutrient signaling and growth control. *Genetics* *189*, 1177–1201.
- Long, X., Lin, Y., Ortiz-Vega, S., Yonezawa, K., and Avruch, J. (2005). Rheb binds and regulates the mTOR kinase. *Curr. Biol.* *15*, 702–713.
- Ma, L., Chen, Z., Erdjument-Bromage, H., Tempst, P., and Pandolfi, P.P. (2005). Phosphorylation and functional inactivation of TSC2 by Erk implications for tuberous sclerosis and cancer pathogenesis. *Cell* *121*, 179–193.
- Ma, X.M., Yoon, S.O., Richardson, C.J., Jülich, K., and Blenis, J. (2008). SKAR links pre-mRNA splicing to mTOR/S6K1-mediated enhanced translation efficiency of spliced mRNAs. *Cell* *133*, 303–313.
- Mannick, J.B., Del Giudice, G., Lattanzi, M., Valiante, N.M., Praestgaard, J., Huang, B., Lonetto, M.A., Maecker, H.T., Kovarik, J., Carson, S., et al. (2014). mTOR inhibition improves immune function in the elderly. *Sci. Transl. Med.* *6*, 268ra179.
- Manning, B.D., Tee, A.R., Logsdon, M.N., Blenis, J., and Cantley, L.C. (2002). Identification of the tuberous sclerosis complex-2 tumor suppressor gene product tuberlin as a target of the phosphoinositide 3-kinase/akt pathway. *Mol Cell* *10*, 151–162.
- Martel, R.R., Klicius, J., and Galet, S. (1977). Inhibition of the immune response by rapamycin, a new antifungal antibiotic. *Can. J. Physiol. Pharmacol.* *55*, 48–51.
- Martina, J.A., Chen, Y., Gucek, M., and Puertollano, R. (2012). mTORC1 functions as a transcriptional regulator of autophagy by preventing nuclear transport of TFEB. *Autophagy* *8*, 903–914.
- Matsumoto, A., Pasut, A., Matsumoto, M., Yamashita, R., Fung, J., Monteleone, E., Saghatelian, A., Nakayama, K.I., Clohessy, J.G., and Pandolfi, P.P. (2017). mTORC1 and muscle regeneration are regulated by the LINC00961-encoded SPAR polypeptide. *Nature* *541*, 228–232.
- Menon, S., Dibble, C.C., Talbott, G., Hoxhaj, G., Valvezan, A.J., Takahashi, H., Cantley, L.C., and Manning, B.D. (2014). Spatial control of the TSC complex integrates insulin and nutrient regulation of mTORC1 at the lysosome. *Cell* *156*, 771–785.
- Mori, H., Inoki, K., Opland, D., Münzberg, H., Villanueva, E.C., Faouzi, M., Ike-noue, T., Kwiatkowski, D.J., Macdougall, O.A., Myers, M.G., Jr., and Guan, K.L. (2009). Critical roles for the TSC-mTOR pathway in β -cell function. *Am. J. Physiol. Endocrinol. Metab.* *297*, E1013–E1022.
- Nickerson, M.L., Warren, M.B., Toro, J.R., Matrosova, V., Glenn, G., Turner, M.L., Duray, P., Merino, M., Choyke, P., Pavlovich, C.P., et al. (2002). Mutations in a novel gene lead to kidney tumors, lung wall defects, and benign tumors of the hair follicle in patients with the Birt-Hogg-Dubé syndrome. *Cancer Cell* *2*, 157–164.
- Nojima, H., Tokunaga, C., Eguchi, S., Oshiro, N., Hidayat, S., Yoshino, K., Hara, K., Tanaka, N., Avruch, J., and Yonezawa, K. (2003). The mammalian target of rapamycin (mTOR) partner, raptor, binds the mTOR substrates p70

- S6 kinase and 4E-BP1 through their TOR signaling (TOS) motif. *J. Biol. Chem.* **278**, 15461–15464.
- Okosun, J., Wolfson, R.L., Wang, J., Araf, S., Wilkins, L., Castellano, B.M., Escudero-Ibarz, L., Al Seraihi, A.F., Richter, J., Bernhart, S.H., et al. (2016). Recurrent mTORC1-activating RRAGC mutations in follicular lymphoma. *Nat. Genet.* **48**, 183–188.
- Palm, W., Park, Y., Wright, K., Pavlova, N.N., Tuveson, D.A., and Thompson, C.B. (2015). The Utilization of Extracellular Proteins as Nutrients Is Suppressed by mTORC1. *Cell* **162**, 259–270.
- Panchaud, N., Péli-Gulli, M.P., and De Virgilio, C. (2013). Amino acid deprivation inhibits TORC1 through a GTPase-activating protein complex for the Rag family GTPase Gtr1. *Sci. Signal.* **6**, ra42.
- Parmigiani, A., Nourbakhsh, A., Ding, B., Wang, W., Kim, Y.C., Akopiants, K., Guan, K.L., Karin, M., and Budanov, A.V. (2014). Sestrins inhibit mTORC1 kinase activation through the GATOR complex. *Cell Rep.* **9**, 1281–1291.
- Pearce, L.R., Huang, X., Boudeau, J., Pawlowski, R., Wullschlegel, S., Deak, M., Ibrahim, A.F., Gourlay, R., Magnuson, M.A., and Alessi, D.R. (2007). Identification of Protor as a novel Rictor-binding component of mTOR complex-2. *Biochem. J.* **405**, 513–522.
- Peng, M., Yin, N., and Li, M.O. (2014). Sestrins function as guanine nucleotide dissociation inhibitors for Rag GTPases to control mTORC1 signaling. *Cell* **159**, 122–133.
- Peng, M., Yin, N., and Li, M.O. (2017). SZT2 dictates GATOR control of mTORC1 signalling. *Nature*. Published online February 15, 2017. <http://dx.doi.org/10.1038/nature21378>.
- Peterson, T.R., Laplante, M., Thoreen, C.C., Sancak, Y., Kang, S.A., Kuehl, W.M., Gray, N.S., and Sabatini, D.M. (2009). DEPTOR is an mTOR inhibitor frequently overexpressed in multiple myeloma cells and required for their survival. *Cell* **137**, 873–886.
- Peterson, T.R., Sengupta, S.S., Harris, T.E., Carmack, A.E., Kang, S.A., Balderas, E., Guertin, D.A., Madden, K.L., Carpenter, A.E., Finck, B.N., and Sabatini, D.M. (2011). mTOR complex 1 regulates lipin 1 localization to control the SREBP pathway. *Cell* **146**, 408–420.
- Petit, C.S., Rocznik-Ferguson, A., and Ferguson, S.M. (2013). Recruitment of folliculin to lysosomes supports the amino acid-dependent activation of Rag GTPases. *J. Cell Biol.* **202**, 1107–1122.
- Polak, P., Cybulski, N., Feige, J.N., Auwerx, J., Rüegg, M.A., and Hall, M.N. (2008). Adipose-specific knockout of raptor results in lean mice with enhanced mitochondrial respiration. *Cell Metab.* **8**, 399–410.
- Pollizzi, K.N., Sun, I.H., Patel, C.H., Lo, Y.C., Oh, M.H., Waickman, A.T., Tam, A.J., Blosser, R.L., Wen, J., Delgoffe, G.M., and Powell, J.D. (2016). Asymmetric inheritance of mTORC1 kinase activity during division dictates CD8(+) T cell differentiation. *Nat. Immunol.* **17**, 704–711.
- Porstmann, T., Santos, C.R., Griffiths, B., Cully, M., Wu, M., Leever, S., Griffiths, J.R., Chung, Y.L., and Schulze, A. (2008). SREBP activity is regulated by mTORC1 and contributes to Akt-dependent cell growth. *Cell Metab.* **8**, 224–236.
- Powell, J.D., Pollizzi, K.N., Heikamp, E.B., and Horton, M.R. (2012). Regulation of immune responses by mTOR. *Annu. Rev. Immunol.* **30**, 39–68.
- Powers, R.W., 3rd, Kaerberlein, M., Caldwell, S.D., Kennedy, B.K., and Fields, S. (2006). Extension of chronological life span in yeast by decreased TOR pathway signaling. *Genes Dev.* **20**, 174–184.
- Powis, K., Zhang, T., Panchuad, N., Wang, R., De Virgilio, C., and Ding, J. (2015). Crystal structure of the Ego1-Ego2-Ego3 complex and its role in promoting Rag GTPase-dependent TORC1 signaling. *Cell Res.* **25**, 1043–1059.
- Rangwala, R., Chang, Y.C., Hu, J., Algazy, K.M., Evans, T.L., Fecher, L.A., Schuchter, L.M., Torigian, D.A., Panosian, J.T., Troxel, A.B., et al. (2014). Combined MTOR and autophagy inhibition: Phase I trial of hydroxychloroquine and temsirolimus in patients with advanced solid tumors and melanoma. *Autophagy* **10**, 1391–1402.
- Rebsamen, M., Pochini, L., Stasyk, T., de Araújo, M.E., Galluccio, M., Kandasamy, R.K., Snijder, B., Fauster, A., Rudashevskaya, E.L., Bruckner, M., et al. (2015). SLC38A9 is a component of the lysosomal amino acid sensing machinery that controls mTORC1. *Nature* **519**, 477–481.
- Ricos, M.G., Hodgson, B.L., Pippucci, T., Saidin, A., Ong, Y.S., Heron, S.E., Licchetta, L., Bisulli, F., Bayly, M.A., Hughes, J., et al.; Epilepsy Electroclinical Study Group (2016). Mutations in the mammalian target of rapamycin pathway regulators NPRL2 and NPRL3 cause focal epilepsy. *Ann. Neurol.* **79**, 120–131.
- Risson, V., Mazelin, L., Roceri, M., Sanchez, H., Moncollin, V., Corneloup, C., Richard-Bulteau, H., Vignaud, A., Baas, D., Defour, A., et al. (2009). Muscle inactivation of mTOR causes metabolic and dystrophin defects leading to severe myopathy. *J. Cell Biol.* **187**, 859–874.
- Robida-Stubbs, S., Glover-Cutter, K., Lamming, D.W., Mizunuma, M., Narasimhan, S.D., Neumann-Haefelin, E., Sabatini, D.M., and Blackwell, T.K. (2012). TOR signaling and rapamycin influence longevity by regulating SKN-1/Nrf and DAF-16/FoxO. *Cell Metab.* **15**, 713–724.
- Robitaille, A.M., Christen, S., Shimobayashi, M., Cornu, M., Fava, L.L., Moes, S., Prescianotto-Baschong, C., Sauer, U., Jenoe, P., and Hall, M.N. (2013). Quantitative phosphoproteomics reveal mTORC1 activates de novo pyrimidine synthesis. *Science* **339**, 1320–1323.
- Rocznik-Ferguson, A., Petit, C.S., Froehlich, F., Qian, S., Ky, J., Angarola, B., Walther, T.C., and Ferguson, S.M. (2012). The transcription factor TFEB links mTORC1 signaling to transcriptional control of lysosome homeostasis. *Sci. Signal.* **5**, ra42.
- Rodrik-Outmezguine, V.S., Chandralapaty, S., Pagano, N.C., Poulikakos, P.I., Scaltriti, M., Moskatel, E., Baselga, J., Guichard, S., and Rosen, N. (2011). mTOR kinase inhibition causes feedback-dependent biphasic regulation of AKT signaling. *Cancer Discov.* **1**, 248–259.
- Rodrik-Outmezguine, V.S., Okaniwa, M., Yao, Z., Novotny, C.J., McWhirter, C., Banaji, A., Won, H., Wong, W., Berger, M., de Stanchina, E., et al. (2016). Overcoming mTOR resistance mutations with a new-generation mTOR inhibitor. *Nature* **534**, 272–276.
- Rommel, C., Bodine, S.C., Clarke, B.A., Rossman, R., Nunez, L., Stitt, T.N., Yancopoulos, G.D., and Glass, D.J. (2001). Mediation of IGF-1-induced skeletal myotube hypertrophy by PI(3)K/Akt/mTOR and PI(3)K/Akt/GSK3 pathways. *Nat. Cell Biol.* **3**, 1009–1013.
- Rousseau, A., and Bertolotti, A. (2016). An evolutionarily conserved pathway controls proteasome homeostasis. *Nature* **536**, 184–189.
- Roux, P.P., Ballif, B.A., Anjum, R., Gygi, S.P., and Blenis, J. (2004). Tumor-promoting phorbol esters and activated Ras inactivate the tuberous sclerosis tumor suppressor complex via p90 ribosomal S6 kinase. *Proc Natl Acad Sci USA* **101**, 13489–13494.
- Sabatini, D.M., Erdjument-Bromage, H., Lui, M., Tempst, P., and Snyder, S.H. (1994). RAFT1: A mammalian protein that binds to FKBP12 in a rapamycin-dependent fashion and is homologous to yeast TORs. *Cell* **78**, 35–43.
- Sabers, C.J., Martin, M.M., Brunn, G.J., Williams, J.M., Dumont, F.J., Wiederrecht, G., and Abraham, R.T. (1995). Isolation of a protein target of the FKBP12-rapamycin complex in mammalian cells. *J. Biol. Chem.* **270**, 815–822.
- Sancak, Y., Thoreen, C.C., Peterson, T.R., Lindquist, R.A., Kang, S.A., Spooner, E., Carr, S.A., and Sabatini, D.M. (2007). PRAS40 is an insulin-regulated inhibitor of the mTORC1 protein kinase. *Mol. Cell* **25**, 903–915.
- Sancak, Y., Peterson, T.R., Shaul, Y.D., Lindquist, R.A., Thoreen, C.C., Bar-Peled, L., and Sabatini, D.M. (2008). The Rag GTPases bind raptor and mediate amino acid signaling to mTORC1. *Science* **320**, 1496–1501.
- Sancak, Y., Bar-Peled, L., Zoncu, R., Markhard, A.L., Nada, S., and Sabatini, D.M. (2010). Ragulator-Rag complex targets mTORC1 to the lysosomal surface and is necessary for its activation by amino acids. *Cell* **141**, 290–303.
- Sarbassov, D.D., Ali, S.M., Kim, D.H., Guertin, D.A., Latek, R.R., Erdjument-Bromage, H., Tempst, P., and Sabatini, D.M. (2004). Rictor, a novel binding partner of mTOR, defines a rapamycin-insensitive and raptor-independent pathway that regulates the cytoskeleton. *Curr. Biol.* **14**, 1296–1302.
- Sarbassov, D.D., Guertin, D.A., Ali, S.M., and Sabatini, D.M. (2005). Phosphorylation and regulation of Akt/PKB by the rictor-mTOR complex. *Science* **307**, 1098–1101.

- Barbassov, D.D., Ali, S.M., Sengupta, S., Sheen, J.H., Hsu, P.P., Bagley, A.F., Markhard, A.L., and Sabatini, D.M. (2006). Prolonged rapamycin treatment inhibits mTORC2 assembly and Akt/PKB. *Mol. Cell* 22, 159–168.
- Sato, T., Nakashima, A., Guo, L., Coffman, K., and Tamanoi, F. (2010). Single amino-acid changes that confer constitutive activation of mTOR are discovered in human cancer. *Oncogene* 29, 2746–2752.
- Saxton, R.A., Knockenhauer, K.E., Wolfson, R.L., Chantranupong, L., Pacold, M.E., Wang, T., Schwartz, T.U., and Sabatini, D.M. (2016a). Structural basis for leucine sensing by the Sestrin2-mTORC1 pathway. *Science* 351, 53–58.
- Saxton, R.A., Chantranupong, L., Knockenhauer, K.E., Schwartz, T.U., and Sabatini, D.M. (2016b). Mechanism of arginine sensing by CASTOR1 upstream of mTORC1. *Nature* 536, 229–233.
- Schalm, S.S., Fingar, D.C., Sabatini, D.M., and Blenis, J. (2003). TOS motif-mediated raptor binding regulates 4E-BP1 multisite phosphorylation and function. *Curr. Biol.* 13, 797–806.
- Selman, C., Tullet, J.M., Wieser, D., Irvine, E., Lingard, S.J., Choudhury, A.I., Claret, M., Al-Qassab, H., Carmignac, D., Ramadani, F., et al. (2009). Ribosomal protein S6 kinase 1 signaling regulates mammalian life span. *Science* 326, 140–144.
- Sengupta, S., Peterson, T.R., Laplante, M., Oh, S., and Sabatini, D.M. (2010). mTORC1 controls fasting-induced ketogenesis and its modulation by ageing. *Nature* 468, 1100–1104.
- Settembre, C., Zoncu, R., Medina, D.L., Vetrini, F., Erdin, S., Erdin, S., Huynh, T., Ferron, M., Karsenty, G., Vellard, M.C., et al. (2012). A lysosome-to-nucleus signalling mechanism senses and regulates the lysosome via mTOR and TFEB. *EMBO J.* 31, 1095–1108.
- Shah, O.J., Wang, Z., and Hunter, T. (2004). Inappropriate activation of the TSC/Rheb/mTOR/S6K cassette induces IRS1/2 depletion, insulin resistance, and cell survival deficiencies. *Curr. Biol.* 14, 1650–1656.
- Shaw, R.J., Bardeesy, N., Manning, B.D., Lopez, L., Kosmatka, M., DePinho, R.A., and Cantley, L.C. (2004). The LKB1 tumor suppressor negatively regulates mTOR signaling. *Cancer Cell* 6, 91–99.
- She, Q.B., Halilovic, E., Ye, Q., Zhen, W., Shirasawa, S., Sasazuki, T., Solit, D.B., and Rosen, N. (2010). 4E-BP1 is a key effector of the oncogenic activation of the AKT and ERK signaling pathways that integrates their function in tumors. *Cancer Cell* 18, 39–51.
- Shigeyama, Y., Kobayashi, T., Kido, Y., Hashimoto, N., Asahara, S., Matsuda, T., Takeda, A., Inoue, T., Shibutani, Y., Koyanagi, M., et al. (2008). Biphasic response of pancreatic beta-cell mass to ablation of tuberous sclerosis complex 2 in mice. *Mol. Cell. Biol.* 28, 2971–2979.
- Spilman, P., Podlutska, N., Hart, M.J., Debnath, J., Gorostiza, O., Bredesen, D., Richardson, A., Strong, R., and Galvan, V. (2010). Inhibition of mTOR by rapamycin abolishes cognitive deficits and reduces amyloid-beta levels in a mouse model of Alzheimer's disease. *PLoS ONE* 5, e9979.
- Tabernero, J., Rojo, F., Calvo, E., Burris, H., Judson, I., Hazell, K., Martinelli, E., Ramon y Cajal, S., Jones, S., Vidal, L., et al. (2008). Dose- and schedule-dependent inhibition of the mammalian target of rapamycin pathway with everolimus: A phase I tumor pharmacodynamic study in patients with advanced solid tumors. *J. Clin. Oncol.* 26, 1603–1610.
- Tang, Y., Wallace, M., Sanchez-Gurmaches, J., Hsiao, W.Y., Li, H., Lee, P.L., Vernia, S., Metallo, C.M., and Guertin, D.A. (2016). Adipose tissue mTORC2 regulates ChREBP-driven de novo lipogenesis and hepatic glucose metabolism. *Nat. Commun.* 7, 11365.
- Tee, A.R., Manning, B.D., Roux, P.P., Cantley, L.C., and Blenis, J. (2003). Tuberous sclerosis complex gene products, Tuberlin and Hamartin, control mTOR signaling by acting as a GTPase-activating protein complex toward Rheb. *Curr. Biol.* 13, 1259–1268.
- Thedieck, K., Polak, P., Kim, M.L., Molle, K.D., Cohen, A., Jenö, P., Arriemerlou, C., and Hall, M.N. (2007). PRAS40 and PRR5-like protein are new mTOR interactors that regulate apoptosis. *PLoS ONE* 2, e1217.
- Thomanetz, V., Anglikler, N., Cloëtta, D., Lustenberger, R.M., Schweighauser, M., Oliveri, F., Suzuki, N., and Rüegg, M.A. (2013). Ablation of the mTORC2 component rictor in brain or Purkinje cells affects size and neuron morphology. *J. Cell Biol.* 201, 293–308.
- Thoreen, C.C., Kang, S.A., Chang, J.W., Liu, Q., Zhang, J., Gao, Y., Reichling, L.J., Sim, T., Sabatini, D.M., and Gray, N.S. (2009). An ATP-competitive mammalian target of rapamycin inhibitor reveals rapamycin-resistant functions of mTORC1. *J. Biol. Chem.* 284, 8023–8032.
- Thoreen, C.C., Chantranupong, L., Keys, H.R., Wang, T., Gray, N.S., and Sabatini, D.M. (2012). A unifying model for mTORC1-mediated regulation of mRNA translation. *Nature* 485, 109–113.
- Tsun, Z.Y., Bar-Peled, L., Chantranupong, L., Zoncu, R., Wang, T., Kim, C., Spooner, E., and Sabatini, D.M. (2013). The folliculin tumor suppressor is a GAP for the RagC/D GTPases that signal amino acid levels to mTORC1. *Mol. Cell* 52, 495–505.
- Um, S.H., Frigerio, F., Watanabe, M., Picard, F., Joaquin, M., Sticker, M., Fumagalli, S., Allegrini, P.R., Kozma, S.C., Auwerx, J., and Thomas, G. (2004). Absence of S6K1 protects against age- and diet-induced obesity while enhancing insulin sensitivity. *Nature* 431, 200–205.
- Vander Haar, E., Lee, S.I., Bandhakavi, S., Griffin, T.J., and Kim, D.H. (2007). Insulin signalling to mTOR mediated by the Akt/PKB substrate PRAS40. *Nat. Cell Biol.* 9, 316–323.
- Vellai, T., Takacs-Vellai, K., Zhang, Y., Kovacs, A.L., Orosz, L., and Müller, F. (2003). Genetics: Influence of TOR kinase on lifespan in *C. elegans*. *Nature* 426, 620.
- Verbist, K.C., Guy, C.S., Milasta, S., Liedmann, S., Kamiński, M.M., Wang, R., and Green, D.R. (2016). Metabolic maintenance of cell asymmetry following division in activated T lymphocytes. *Nature* 532, 389–393.
- Vézina, C., Kudelski, A., and Sehgal, S.N. (1975). Rapamycin (AY-22,989), a new antifungal antibiotic. I. Taxonomy of the producing streptomycete and isolation of the active principle. *J. Antibiot.* 28, 721–726.
- Wagle, N., Grabiner, B.C., Van Allen, E.M., Hodis, E., Jacobus, S., Supko, J.G., Stewart, M., Choueiri, T.K., Gandhi, L., Cleary, J.M., et al. (2014a). Activating mTOR mutations in a patient with an extraordinary response on a phase I trial of everolimus and pazopanib. *Cancer Discov.* 4, 546–553.
- Wagle, N., Grabiner, B.C., Van Allen, E.M., Amin-Mansour, A., Taylor-Weiner, A., Rosenberg, M., Gray, N., Barletta, J.A., Guo, Y., Swanson, S.J., et al. (2014b). Response and acquired resistance to everolimus in anaplastic thyroid cancer. *N. Engl. J. Med.* 371, 1426–1433.
- Wang, L., Harris, T.E., Roth, R.A., and Lawrence, J.C., Jr. (2007). PRAS40 regulates mTORC1 kinase activity by functioning as a direct inhibitor of substrate binding. *J. Biol. Chem.* 282, 20036–20044.
- Wang, S., Tsun, Z.Y., Wolfson, R.L., Shen, K., Wyant, G.A., Plovovich, M.E., Yuan, E.D., Jones, T.D., Chantranupong, L., Comb, W., et al. (2015). Metabolism. Lysosomal amino acid transporter SLC38A9 signals arginine sufficiency to mTORC1. *Science* 347, 188–194.
- Wolfson, R.L., Chantranupong, L., Saxton, R.A., Shen, K., Scaria, S.M., Cantor, J.R., and Sabatini, D.M. (2016). Sestrin2 is a leucine sensor for the mTORC1 pathway. *Science* 351, 43–48.
- Wolfson, R.L., Chantranupong, L., Wyant, G.A., Gu, X., Orozoco, J.M., Condon, K.J., Petri, S., Kedir, J., Scaria, S.M., Abu-Remaileh, M., et al. (2017). KICSTOR recruits GATOR1 to the lysosome and is necessary for nutrients to regulate mTORC1. *Nature*. Published online February 15, 2017. <http://dx.doi.org/10.1038/nature21423>.
- Woo, S.Y., Kim, D.H., Jun, C.B., Kim, Y.M., Haar, E.V., Lee, S.I., Hegg, J.W., Bandhakavi, S., Griffin, T.J., and Kim, D.H. (2007). PRR5, a novel component of mTOR complex 2, regulates platelet-derived growth factor receptor beta expression and signaling. *J. Biol. Chem.* 282, 25604–25612.
- Wu, J.J., Liu, J., Chen, E.B., Wang, J.J., Cao, L., Narayan, N., Fergusson, M.M., Rovira, I.I., Allen, M., Springer, D.A., et al. (2013). Increased mammalian lifespan and a segmental and tissue-specific slowing of aging after genetic reduction of mTOR expression. *Cell Rep.* 4, 913–920.
- Yang, Q., Inoki, K., Ikenoue, T., and Guan, K.L. (2006). Identification of Sin1 as an essential TORC2 component required for complex formation and kinase activity. *Genes Dev.* 20, 2820–2832.

- Yang, H., Rudge, D.G., Koos, J.D., Vaidialingam, B., Yang, H.J., and Pavletich, N.P. (2013). mTOR kinase structure, mechanism and regulation. *Nature* **497**, 217–223.
- Yang, G., Murashige, D.S., Humphrey, S.J., and James, D.E. (2015). A Positive Feedback Loop between Akt and mTORC2 via SIN1 Phosphorylation. *Cell Rep.* **12**, 937–943.
- Ye, J., Palm, W., Peng, M., King, B., Lindsten, T., Li, M.O., Koumenis, C., and Thompson, C.B. (2015). GCN2 sustains mTORC1 suppression upon amino acid deprivation by inducing Sestrin2. *Genes Dev.* **29**, 2331–2336.
- Yilmaz, O.H., Katajisto, P., Lamming, D.W., Gültekin, Y., Bauer-Rowe, K.E., Sengupta, S., Birsoy, K., Dursun, A., Yilmaz, V.O., Selig, M., et al. (2012). mTORC1 in the Paneth cell niche couples intestinal stem-cell function to calorie intake. *Nature* **486**, 490–495.
- Yip, C.K., Murata, K., Walz, T., Sabatini, D.M., and Kang, S.A. (2010). Structure of the human mTOR complex 1 and its implications for rapamycin inhibition. *Mol. Cell* **38**, 768–774.
- Yu, Y., Yoon, S.O., Poulogiannis, G., Yang, Q., Ma, X.M., Villén, J., Kubica, N., Hoffman, G.R., Cantley, L.C., Gygi, S.P., and Blenis, J. (2011). Phosphoproteomic analysis identifies Grb10 as an mTORC1 substrate that negatively regulates insulin signaling. *Science* **332**, 1322–1326.
- Yuan, M., Pino, E., Wu, L., Kacergis, M., and Soukas, A.A. (2012). Identification of Akt-independent regulation of hepatic lipogenesis by mammalian target of rapamycin (mTOR) complex 2. *J. Biol. Chem.* **287**, 29579–29588.
- Zeng, L.H., Xu, L., Gutmann, D.H., and Wong, M. (2008). Rapamycin prevents epilepsy in a mouse model of tuberous sclerosis complex. *Ann. Neurol.* **63**, 444–453.
- Zhang, T., Peli-Gulli, M.P., Yang, H., De Virgilio, C., and Ding, J. (2012). Ego3 functions as a homodimer to mediate the interaction between Gtr1-Gtr2 and Ego1 in the ego complex to activate TORC1. *Structure* **20**, 2151–2160.
- Zhang, Y., Nicholatos, J., Dreier, J.R., Ricoult, S.J., Widenmaier, S.B., Hotamisligil, G.S., Kwiatkowski, D.J., and Manning, B.D. (2014). Coordinated regulation of protein synthesis and degradation by mTORC1. *Nature* **513**, 440–443.
- Zhao, J., Zhai, B., Gygi, S.P., and Goldberg, A.L. (2015). mTOR inhibition activates overall protein degradation by the ubiquitin proteasome system as well as by autophagy. *Proc. Natl. Acad. Sci. USA* **112**, 15790–15797.
- Zheng, Y., Collins, S.L., Lutz, M.A., Allen, A.N., Kole, T.P., Zarek, P.E., and Powell, J.D. (2007). A role for mammalian target of rapamycin in regulating T cell activation versus anergy. *J. Immunol.* **178**, 2163–2170.
- Zinzalla, V., Stracka, D., Oppliger, W., and Hall, M.N. (2011). Activation of mTORC2 by association with the ribosome. *Cell* **144**, 757–768.
- Zoncu, R., Bar-Peled, L., Efeyan, A., Wang, S., Sancak, Y., and Sabatini, D.M. (2011). mTORC1 senses lysosomal amino acids through an inside-out mechanism that requires the vacuolar H(+)-ATPase. *Science* **334**, 678–683.



OUR NETWORK IS YOUR NETWORK

With Cell Press Webinars, our network is your network!

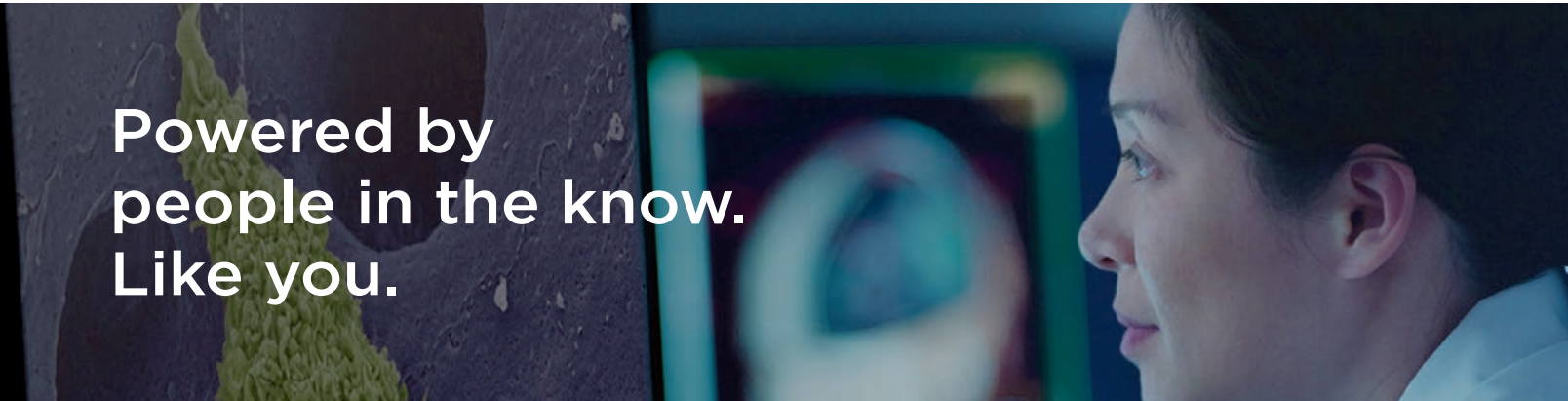
Cell Press Webinars give you access to hot topics in emerging research and the application of new technology.

Watch essential, need-to-know webcasts via live streaming or on demand from the comfort and convenience of your office, lab, or home.

Need-to-know topics, editorially curated

World-class presenters, experts in their field

Moderated by Cell Press editors



Powered by
people in the know.
Like you.

Tap into our network today!
Visit www.cell.com/webinars

CellPress
Webinars

Metabolic Instruction of Immunity

Michael D. Buck,^{1,2} Ryan T. Sowell,³ Susan M. Kaech,^{3,*} and Erika L. Pearce^{1,*}

¹Department of Immunometabolism, Max Planck Institute of Immunobiology and Epigenetics, 79108 Freiburg, Germany

²Division of Biology and Biomedical Sciences Immunology Program, Washington University School of Medicine, St. Louis, MO 63110, USA

³Department of Immunobiology, Yale University School of Medicine, New Haven, CT 06520, USA

*Correspondence: susan.kaech@yale.edu (S.M.K.), pearce@ie-freiburg.mpg.de (E.L.P.)

<http://dx.doi.org/10.1016/j.cell.2017.04.004>

Choices have consequences. Immune cells survey and migrate throughout the body and sometimes take residence in niche environments with distinct communities of cells, extracellular matrix, and nutrients that may differ from those in which they matured. Imbedded in immune cell physiology are metabolic pathways and metabolites that not only provide energy and substrates for growth and survival, but also instruct effector functions, differentiation, and gene expression. This review of immunometabolism will reference the most recent literature to cover the choices that environments impose on the metabolism and function of immune cells and highlight their consequences during homeostasis and disease.

Cells of the immune system possess particular sets of skills—skills that are vital for host defense and tissue homeostasis but also cause disease if not properly controlled—skills that make them altogether fairly peculiar. Unlike other cells in the body, immune cells possess the ability to respond to environmental signals and assume a wide variety of distinct functional fates. Immune cells can morph from dormant sentinels into pathogen killing machines, migrate from one tissue to another, modulate surface receptor expression, clonally expand, secrete copious amounts of effector molecules, or exert controlling effects over neighboring cells. After the burst of activity following an immune response, these specialized cells can die, creating space and limiting tissue damage in a particular environment, or return to resting states that allow them to persist for extended periods of time in readiness for a secondary response.

The activation, growth and proliferation, engagement of effector functions, and return to homeostasis of immune cells are intimately linked and dependent on dynamic changes in cellular metabolism. The utilization of particular metabolic pathways is controlled on one level by growth factors and nutrient availability dictated by competition between other interacting cells and on another level by the exquisite balance of internal metabolites, reactive oxygen species (ROS), and reducing and oxidizing substrates. Studying immune cells, particularly lymphocytes and myeloid cells, has lent deep insight into how cells differentiate and coordinate their behaviors with metabolism under a wide array of settings.

Leukocytes are also nomads and settlers. They migrate from the place where they develop to survey the entire body and sometimes take up residence in tissues in which they did not originate. In doing so, they must adapt to an ecosystem comprised of unique cells, extracellular matrix, growth factors, oxygen, nutrients, and metabolites. How do they do this and what are the genetic, metabolic, and immunological consequences of these adaptations? In this review, we explore the interactions between immune cells and the tissue environments

they inhabit, how these impinge on their metabolism, how their metabolism instructs their function and fate, and how these relationships contribute to tissue homeostasis and disease pathology. The central concepts of immune cell metabolism have been covered extensively in several reviews (Buck et al., 2015; MacIver et al., 2013; O'Neill and Pearce, 2016; O'Neill et al., 2016; Pearce et al., 2013) and thus will not be discussed at length here.

The Tumor Microenvironment

Recent breakthroughs in immunotherapy have shown that eliciting immune responses against multiple types of cancer can lead to considerably longer-lasting remissions, or in some cases, complete regression of metastatic disease (Ribas, 2015). Although it is well known that cancer cells can evade immune recognition through “immunoediting” (the process by which antitumor immune responses, especially those from tumor infiltrating T lymphocytes [TILs], select for cancer cell clones that no longer express detectable tumor antigens) (Vesely and Schreiber, 2013), the advent of effective cancer immunotherapies has shown that additional mechanisms of immunosuppression exist that limit or impair antitumor immunity. Thus, considerable efforts are underway to elucidate other mechanisms that restrain antitumor responses to develop new and more efficacious forms of therapy.

At the forefront of these mechanisms to consider, is how immune cell metabolism, and thus immune cell function, is altered by the tumor microenvironment. Tumors are a major disturbance to tissue homeostasis, creating metabolically demanding environments that encroach on the metabolism and function of the stroma and infiltrating immune cells. The unrestrained cell growth seen in cancer is often supported by aerobic glycolysis, the same metabolic pathway needed to fuel optimal effector functions in many immune cells (Pearce et al., 2013). At minimum, this similarity potentiates a competition for substrates between tumors and immune cells. The demand for nutrients, essential metabolites, and oxygen imposed by proliferative

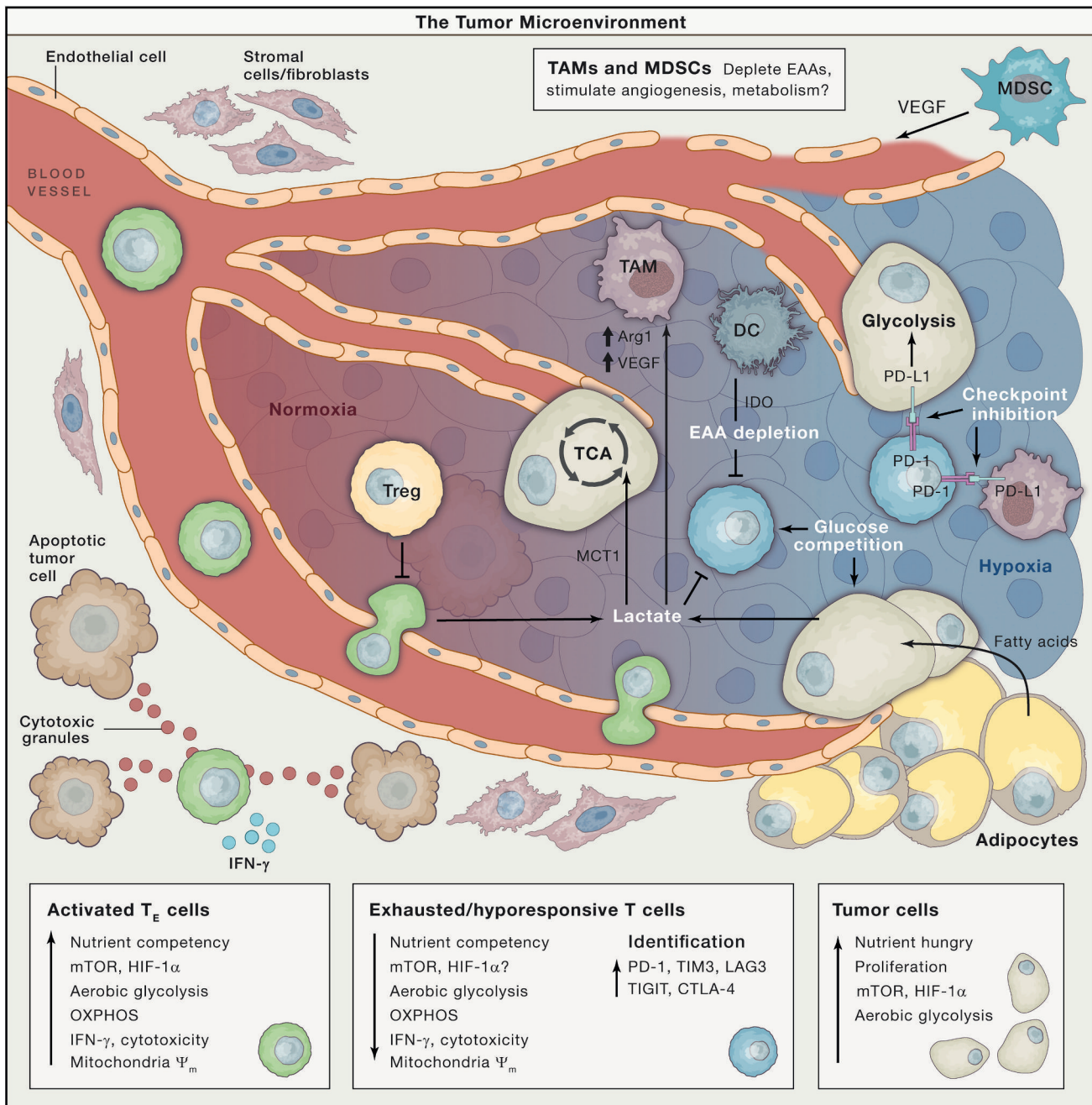


Figure 1. Metabolic Tug-of-War within the Tumor Microenvironment

The balance of nutrients and oxygen within the tumor microenvironment controls immune cell function. Glucose and amino acid consumption by tumor cells can outpace that of infiltrating immune cells, specifically depriving them of nutrients to fuel their effector function. Poorly perfused tumor regions drive hypoxia response programs in tumor cells, macrophages, and T cells. Increased HIF-1 α activity in response to hypoxia or other mechanisms promotes glycolysis and increases concentrations of suppressive metabolites and acidification of the local environment. As a by-product of glycolysis, lactate concentration increases, which is coordinately utilized by tumor cells to fuel their metabolism, promotes macrophage polarization, and directly suppresses T cell function. The ability of T cells to target tumors is further limited by their upregulation of co-inhibitory receptors and engagement with their ligands on neighboring tumor cells and macrophages. As T cells progressively enter a dysfunctional state, their mitochondrial mass and oxidative capacity declines, ultimately leading to their failure to meet bioenergetic demands to sustain effector functions and control tumor cell growth.

cancer cells, in combination with their immunosuppressive by-products, creates harsh environmental conditions in which immune cells must navigate and adapt (Figure 1). How tumor and

immune cells share or compete for resources in this environment, and how such relationships regulate antitumor immunity are important questions to address.

Hypoxia

When tumor growth exceeds the vasculature's ability to fully perfuse the tumor microenvironment with oxygen, regions of hypoxia are established and induction of the hypoxia-responsive transcription factor HIF-1 α intensifies cancer cell glucose utilization and lactate release (Eales et al., 2016). Using ¹³C-labeled glucose, Hensley et al. (2016) traced the fate of glucose within healthy lung tissue and tumors of patients with non-small lung cell carcinoma and found that even within a single tumor, heterogeneity in glucose utilization exists. Lesser-perfused regions of the lung tumors were associated with higher glucose metabolism whereas higher-perfused regions could utilize circulating lactate, transported through monocarboxylate transporter 1 (MCT1), as an alternative TCA cycle substrate (Sonveaux et al., 2008). Lactate metabolism in oxygenated cancer cells also increases glutaminolysis (Pérez-Escuredo et al., 2016). How this metabolic heterogeneity in tumor cells relates to intratumoral immune cell function has not been well elucidated, but exposure of NK and T cells to high concentrations of lactate impairs their activation of the transcription factor NFAT and production of the cytokine interferon gamma (IFN- γ) (Brand et al., 2016). Lactic acid also disrupts T cell motility and causes loss of cytolytic function in CD8 T cells (Haas et al., 2015). Moreover, decreasing conversion of pyruvate to lactate by genetic targeting of lactate dehydrogenase A (LDHA) in tumors helps to restore T cell infiltration and function (Brand et al., 2016), linking lactate production to immunosuppression observed in the tumor microenvironment (Figure 1).

Lactate uptake by tumor-associated macrophages (TAMs) also stimulates tumor progression by inducing vascular endothelial growth factor (VEGF) and arginase I (Arg1) expression through HIF-1 α (Colegio et al., 2014). Moreover, chronic VEGF signaling in hypoxic areas leads to elevated glycolysis in endothelial cells, resulting in excessive endothelial sprouting and abnormal leaky vasculature (Goveia et al., 2014). Interestingly, inhibition of REDD1, a hypoxia-induced inhibitor of mechanistic target of rapamycin (mTOR), in TAMs increases their rates of glycolysis to a level that competes with neighboring endothelial cells for glucose and suppresses their angiogenic activity. This metabolic tug-of-war over glucose helps restore vascular integrity, improve oxygenation within the tumor, and prevent metastases (Wenes et al., 2016), providing an example of an intimate metabolic relationship that exists between cells in tumors.

Hypoxia also has considerable effects on TIL function, proliferation, and migration (Vuillefroy de Silly et al., 2016). Increases in HIF-1 α activity by culturing T cells in physiologic normoxia (~3%–5% O₂), genetic deletion of von Hippel-Lindau (VHL) factor, or inhibiting activity of the oxygen-sensing prolyl-hydroxylase (PHD) family of proteins, enhances CD8 T cell glycolysis and effector functions and promotes antitumor immunity (Clever et al., 2016; Doedens et al., 2013; Finlay et al., 2012; Wang et al., 2011). HIF-1 α is also needed for the production of the metabolite S-2-hydroxyglutarate (S-2HG), which can drive epigenetic remodeling in activated CD8 T cells and enhance interleukin (IL)-2 production and antitumor defenses (Tyrakis et al., 2016).

Thus, one may expect that hypoxia would potentiate HIF-1 α activity and TIL effector functions in tumors, however, this is not what is observed. In addition to signals received from

IFN- γ , HIF-1 α also induces the expression of the suppressive ligand PD-L1 in tumor cells, TAMs, and myeloid-derived suppressor cells (MDSCs) (Noman et al., 2014), and this can lead to TIL suppression via PD-1 (Figure 1). Moreover, recent work in both mouse and human tumors showed that CD8 TILs lose mitochondrial mass, membrane potential, and oxidative capacity, particularly within the most dysfunctional PD-1⁺ CD8 T cells (Scharping et al., 2016). The loss of mitochondrial function in TILs correlated with diminished expression of PPAR-gamma coactivator 1 α (PGC1 α) over time and a block in their proliferation and IFN- γ production. Perhaps severe hypoxia ultimately diminishes TIL effector functions. Indeed, respiratory supplementation of oxygen or treatment with metformin decreased intratumoral hypoxia and relieved several immunosuppressive features in the tumor microenvironment; the latter also served as an adjunct therapy that enhanced the antitumor effects of PD-1 blockade (Hatfield et al., 2015; Scharping et al., 2017). These findings suggest that remodeling the hypoxic tone in tumors may be an essential component to developing more efficacious forms of immunotherapy for patients.

Nutrient Alterations and Competition within the Tumor Microenvironment

Apart from hypoxia, the competition for nutrients and metabolites between tumor cells and infiltrating immune cells can be fierce, consequently influencing signal transduction, gene expression, and the metabolic activities of these neighboring cells. For example, tumor cells manipulate surrounding adipocytes to increase lipolysis to whet their appetite for fatty acids (Nieman et al., 2011). Cancer-associated fibroblasts degrade tryptophan that not only starves immune cells in the local environment of an essential amino acid, but also leads to the production of the immunosuppressive metabolite kynurenine (Hsu et al., 2016). Moreover, glucose is a critical substrate for the antitumor functions of effector T cells and M1 macrophages, which both require engagement of aerobic glycolysis for their activation and full effector functions (Buck et al., 2015; O'Neill and Pearce, 2016). Augmented aerobic glycolysis in cancer cells and endothelial cells places immune cells and their neighbors at odds (Figure 1). Glucose deprivation represses Ca²⁺ signaling, IFN- γ production, cytotoxicity, and motility in T cells and pro-inflammatory functions in macrophages (Cham et al., 2008; Chang et al., 2013, 2015; Macintyre et al., 2014). Several recent studies have demonstrated that the glycolytic activities of cancer cells may restrict glucose utilization by TILs, thereby impairing anti-tumor immunity (Chang et al., 2015; Ho et al., 2015; Zhao et al., 2016). Increasing glycolysis rates of tumor cells through overexpression of the glycolysis enzyme hexokinase 2 (HK2) suppressed glucose-uptake and IFN- γ production in TILs and created more immunoevasive tumors (Chang et al., 2015; Ho et al., 2015). Zhao et al. (2016) found that glucose restriction imposed by ovarian cancer leaves microRNA repression of the methyltransferase EZH2 intact in CD8 T cells, reducing their survival and functional capacity. Thus, tumor cells can selfishly coerce or outcompete neighboring cells for glucose to supply their own metabolic demands in a manner that simultaneously suppresses immune defenses.

Amino acid deprivation in the tumor microenvironment serves as another metabolic checkpoint regulating antitumor immunity.

Glutaminolysis in tumor cells is critical to replenish metabolites through anaplerotic reactions, which could result in competition for glutamine between tumor cells and TILs (Jin et al., 2016; Pérez-Escuredo et al., 2016). Glutamine controls mTOR activation in T cells and macrophages and is also a key substrate for protein O-GlcNAcylation and synthesis of S-2HG that regulate effector T cell function and differentiation (Sinclair et al., 2013; Swamy et al., 2016; Tyrakis et al., 2016). TAMs, MDSCs, and tolerizing dendritic cells (DCs) can suppress TILs through expression of essential amino acid (EAA)-degrading enzymes such as Arg1 and indoleamine-2,3-dioxygenase (IDO) (Figure 1) (Lee et al., 2002; Munn et al., 2002; Rodriguez et al., 2004; Uyttenhove et al., 2003). Indeed, inhibitors of Arg1 and IDO are under investigation as therapeutic targets in clinical trials (Adams et al., 2015). Several recent studies have highlighted the critical roles of other amino acids such as arginine, serine, and glycine in driving T cell expansion and antitumor activity, but how the availability of these fluctuate within the tumor microenvironment is not clear (Geiger et al., 2016; Ma et al., 2017). Currently, a knowledge gap exists on how the availability of various nutrients and metabolites vary across tumor types, genotypes, or even spatially within tumors to affect antitumor immune responses.

Bioactive lipids, modified lipoproteins, and cholesterol metabolism within the tumor are also important mediators of immune cell function. Like macrophages in atherosclerotic plaques, DCs in the tumor can accumulate oxidized lipoproteins through scavenger receptor-mediated internalization and formation of lipid droplets, which can ultimately impair their ability to cross-present tumor antigens and activate T cells (Cubillos-Ruiz et al., 2015; Ramakrishnan et al., 2014). Expression of lectin-type oxidized LDL receptor 1 (LOX-1) selectively marks MDSCs and oxidized lipid uptake and lipoprotein metabolism contributes to their T cell suppressive functions (Condamine et al., 2016). In addition, blocking cholesterol esterification in TILs by targeting ACAT1 pharmacologically or genetically increases intracellular levels of cholesterol and confers superior T cell responses in a model of melanoma (Yang et al., 2016). It is possible that as immune cells adapt to different tumor microenvironments and the limited availability of “immune stimulatory” nutrients, they become more dependent on alternative fuel sources (such as fats or lactate) that are less conducive to supporting antitumor effector functions. In summary, more elaborate knowledge of these forms of metabolic cross talk or competition between cells within tumors is needed before one can begin to think about how to manipulate these relationships in a manner that alters tumor progression.

Metabolic Exhaustion in TILs and Checkpoint Blockade

As TILs adapt to the tumor microenvironment, they progressively lose their ability to respond to T cell receptor (TCR) stimuli, produce effector cytokines, and proliferate—a process termed functional exhaustion or hyporesponsiveness. This is in part due to the upregulation of several inhibitory receptors like PD-1, LAG3, TIGIT, and CTLA-4 that desensitize T cells to tumor antigens (Wherry and Kurachi, 2015) (Figure 1). PD-1, its ligand PD-L1, and CTLA-4 are important checkpoints for T cells in tumors and the targets of a new and powerful class of cancer treatments that elicit effective and durable responses in patients across multiple cancer types (Ribas, 2015). Interestingly, both

chronic exposure to antigen or environmental triggers such as glucose deprivation can upregulate PD-1 (Chang et al., 2013; Wherry and Kurachi, 2015). PD-1 not only suppresses TCR, PI3K, and mTOR signaling in T cells, but also dampens glycolysis and promotes fatty acid oxidation (FAO)—features that may enhance the accumulation of suppressive regulatory CD4 T (Treg) cells in tumors (Bensch et al., 2016; Parry et al., 2005; Patsoukis et al., 2015). Indeed, blockade of PD-1 re-energizes anabolic metabolism and glycolysis in exhausted T cells in an mTORC1-dependent manner (Chang et al., 2015; Staron et al., 2014). This breathes caution into the types of drug combinations one may consider with α -PD-1:PD-L1 blockade or other forms of immunotherapy. Metabolic interventions, such as the use of mTOR inhibitors, must be targeted specifically to avoid unintended compromises of immune cell function. The PD-1:PD-L1 axis may also directly affect the metabolic activity of tumor cells (Figure 1). It was shown that PD-L1 expression correlated with the rates of glycolysis and the expression of glycolytic enzymes in those cells (Chang et al., 2015). Furthermore, checkpoint blockade antibodies including α -PD-L1 led to an increase in extracellular glucose in tumors in vivo that likely contributed to the improved TIL function and subsequent tumor regression observed. On this note, tumor cell-intrinsic PD-1 expression may counterintuitively increase intrinsic mTOR signaling and tumor growth (Kleffel et al., 2015). Collectively, these findings suggest there may be broader role of the PD-1:PD-L1 axis in cellular metabolism that extends beyond T cells.

Balancing Metabolism and Designing Effective Immunotherapies

Improving the proportion of patients that respond to immunotherapy is an intense area of study, ranging from the search for biomarkers of response, target discovery, to testing new combination therapies. Likely, the most effective therapies will coordinately target co-inhibitory receptor-to-ligand interactions and restore a T cells' ability to utilize metabolic substrates necessary to sustain their effector functions. Although not discussed at length here, other factors impinging on immune cell metabolism that one should consider in designing anticancer immunotherapies are the accessibility of growth factor cytokines that modulate nutrient transporter expression on immune cells and the fact that immune cells migrate into tumors to exert their effector functions, a metabolically demanding process. When cells move, their intracellular architecture, controlled in part by the actin cytoskeleton, is continuously remodeled. In an elegant dissection of PI3K-dependent growth factor signaling in epithelial cells, Hu et al. (2016) found cytoskeletal dynamics and glycolysis to be uniquely intertwined. The authors showed that addition of growth factors or insulin activated Rac downstream of PI3K, causing a disruption of the actin cytoskeleton. Loss of this structural integrity released bound aldolase from filamentous F-actin, increasing its catalytic activity. Chemical and genetic inhibition of PI3K, Rac, or actin dynamics modulated glycolysis via mobilization of aldolase (Figure 2). It will be interesting in future studies to explore how other glycolytic enzymes or even the mitochondria in immune cells restructure their metabolic activity through changes in cytoskeletal morphology in response to growth factor or pathogen-derived signals and whether this regulatory circuit can be therapeutically targeted, especially because directed

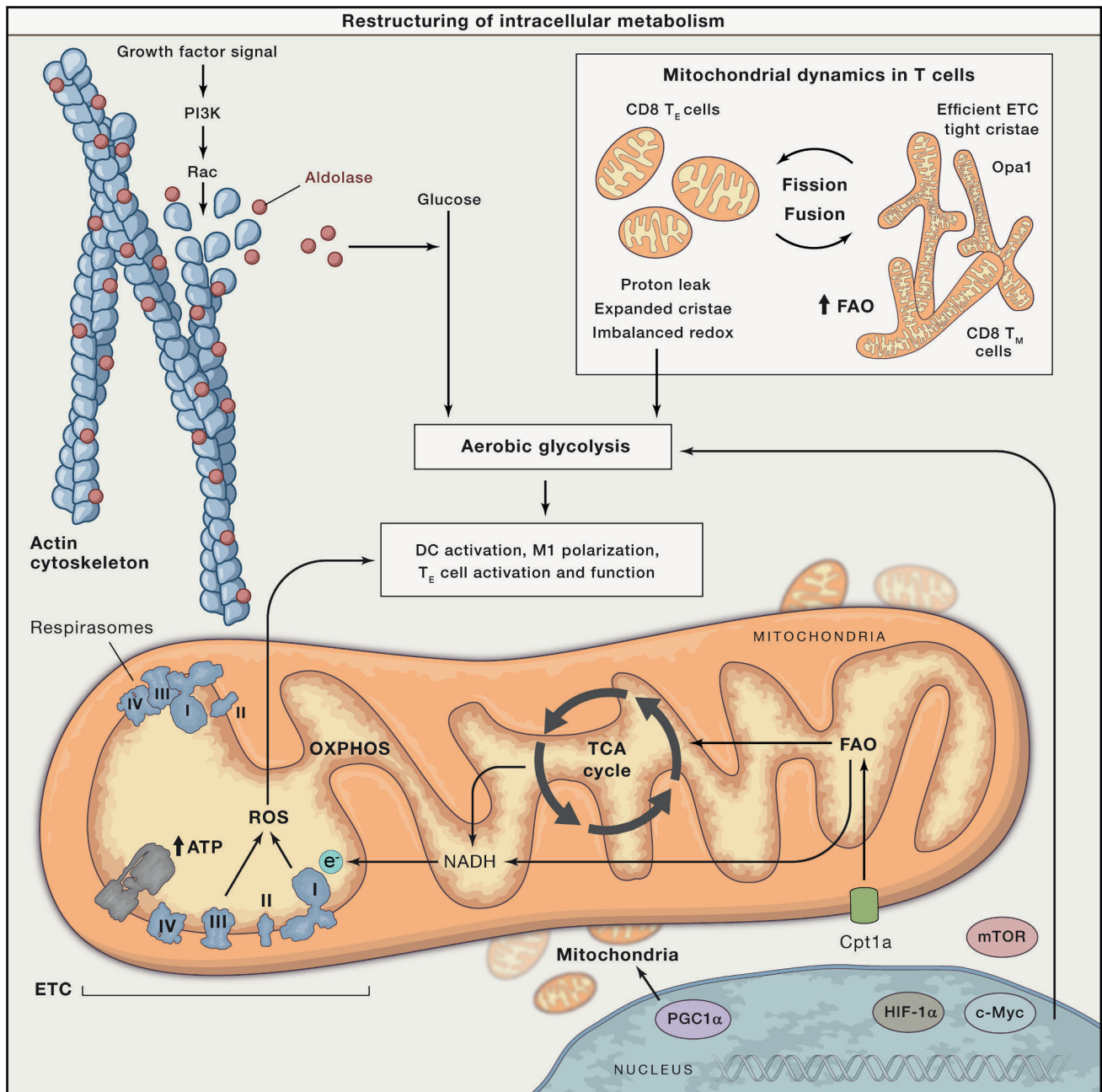


Figure 2. Recent Highlights in the Restructuring of Intracellular Architecture and Metabolism

Immune cell function is a product of their metabolic state. Growth factor signaling, actin rearrangement, and glucose metabolism are closely intertwined. Actin-bound aldolase can be freed from the cytoskeleton downstream of growth factor signaling to mediate glycolysis. Engagement of this pathway is central to the activation and downstream effector functions of DCs, M1 macrophages, and T cells. T cells can dynamically restructure their mitochondria through processes like mitochondrial fission and fusion to signal changes in metabolism and to promote their long-term survival in the transition to memory cells.

cellular migration is such an integral feature of how the disseminated immune system can focus its attention on points of infection or damage.

Additionally, manipulating metabolic enzyme expression to help T cells adapt to metabolic perturbations in the tumor microenvironment may be another viable strategy to improve anti-tumor immunity (Clever et al., 2016; Doedens et al., 2013;

Ho et al., 2015; Scharping et al., 2016), especially for adoptive cell therapy, a personalized form of cancer treatment that allows for the manipulation and expansion of a patient's anti-tumor T cells prior to re-infusion. Seemingly paradoxical is the observation that dampening effector T cell differentiation by impairing glycolysis and boosting mitochondrial FAO and oxidative phosphorylation (OXPHOS), metabolic pathways that favor the

formation of resting memory T cell populations, potentiates effector T cell survival and functional capacity against tumors used in adoptive cell therapy (Buck et al., 2016; Sukumar et al., 2013). On the one hand, the engagement of aerobic glycolysis by activated T cells generates by-products of intermediary metabolism that supply substrates used to build biomass and fuel proliferation, provides an avenue for cells to support the equilibrium of reducing and oxidizing equivalents used to release energy, such as NAD⁺/NADH, and regulates the efficient production of effector cytokines critical for tumor regression (Buck et al., 2015; Chang et al., 2015; Pearce et al., 2013). Activation initiated by TCR ligation and binding with costimulatory molecules also augments OXPHOS in T cells (Chang et al., 2013; Sena et al., 2013). Mitochondria undergo biogenesis and take on a grossly punctate and dispersed morphology with expanded cristae junctions (Buck et al., 2016; Ron-Harel et al., 2016) (Figure 2). During this process, the mitochondrial proteome remodels itself to increase mitochondrial one-carbon metabolism. Knockdown of SHMT2, the first enzyme in this pathway, impairs CD4 T cell survival and proliferation in vivo (Ron-Harel et al., 2016). The generation of mitochondrial-derived ROS is also critical for the activation and expansion of antigen-specific T cells (Sena et al., 2013). As previously discussed, TILs that cannot sustain mitochondrial function have compromised functionality within the tumor microenvironment, and rescuing mitochondrial biogenesis in effector T cells improves antitumor immunity (Bengsch et al., 2016; Scharping et al., 2016).

However, on the other hand, dampening regulators of glycolytic metabolism, such as mTOR or c-Myc, and increasing mitochondrial FAO-dependent OXPHOS favors the formation of long-lived memory T cells (Araki et al., 2009; Cui et al., 2015; O'Sullivan et al., 2014; Pearce et al., 2009; Pollizzi et al., 2016; van der Windt et al., 2012; Verbist et al., 2016) (Figure 2). More recent evidence postulates that while oxidative metabolism and FAO characterizes the generation of long-lived stable central memory T cells (Cui et al., 2015; O'Sullivan et al., 2014; Pearce et al., 2009; van der Windt et al., 2012), augmenting glycolysis genetically via VHL deletion favors the formation of effector memory T cells instead, which have low levels of TCF-1, a transcription factor that is expressed in stable populations of central memory T cells capable of self-renewal (Phan et al., 2016; Zhou et al., 2010). It was also recently shown that activated lymphocytes unequally eliminate aged mitochondria in sibling cells, and this process can determine differentiation versus self-renewal (Adams et al., 2016). Maintenance of mitochondria in some cells was linked to anabolism, PI3K/mTOR activation, glycolysis, and inhibited autophagy while mitochondrial clearance in others was associated with catabolism, FoxO1 transcription factor activity, and self-renewal. Thus, mitochondrial maintenance can drive differentiation over self-renewal, illustrating how these organelles lie at the center of cell fate decisions.

In addition to mitochondrial stasis versus clearance, memory T cells also have distinct mitochondrial morphology from effector T cells. Effector T cells have more “fissed” mitochondria whereas memory T cells have more “fused” mitochondrial networks with tight cristae suggesting a requirement for mitochondrial fusion in memory T cell metabolism and homeostasis. Consistent with this observation, antigen-specific T cells lacking

the inner mitochondrial membrane fusion protein Opa1 fail to generate memory T cells after bacterial infection and have impaired survival in vitro (Buck et al., 2016). The activation, proliferation, and function of Opa1-deficient effector T cells, however, remain intact. Opa1^{-/-} T cells have augmented rates of glycolysis and possess mitochondria with diminished OXPHOS efficiency and malformed cristae compared to controls. It was shown that in quiescent T cells, such as naive and memory T cells, mitochondrial fusion ensured tight cristae associations that allowed for efficient electron transport chain (ETC) function (Figure 2). Tight cristae result in dense packing of ETC complexes, which have been found to associate in specialized configurations termed respiratory supercomplexes or respirasomes. Supercomplexes facilitate efficient transfer of electrons and minimize proton leak during ATP production (Cogliati et al., 2013). CD8 T cells express high levels of methylation-controlled J protein (MCJ), a member of the DnaJ family of chaperones (Champagne et al., 2016). MCJ localizes to the inner membrane of mitochondria and associates with complex I of the ETC. By doing so, it negatively regulates the assembly of complex I into supercomplexes. MCJ deficiency was found to enhance naive and activated CD8 T cell OXPHOS and a unique attribute was its role in the secretion, but not the translation, of effector cytokines. Increased respiration efficiency improved the survival of MCJ^{-/-} effector T cells, which also induced superior protective immunity against viral challenge.

Repurposing the knowledge gained from such studies, boosting oxidative capacity and efficiency through enforcement of mitochondrial fusion or dampening glycolysis with 2-DG, extends the survival and antitumor function of CD8 T cells in models of adoptive cell therapy (Buck et al., 2016; Sukumar et al., 2013). Although aerobic glycolysis initiates and sustains effector functions of activated T cells, augmenting metabolic pathways that support long-lived memory T cells improves T cell responses against tumors, demonstrating a need to strike a balance between these processes, seemingly trading off heightened activation and effector functions of TILs with their sustained functionality and increased survival in the tumor microenvironment. Indeed, modification of the signaling domains within chimeric antigen receptor T cells, used in an alternative form of adoptive cell therapy, with 4-1BB augments mitochondrial biogenesis and oxidative metabolism, enhancing their persistence (Kawalekar et al., 2016). As our capability to selectively reprogram T cell metabolism and reinvigorate tumor-specific T cells improves, there is much promise to provide greater therapeutic benefits to more patients, especially to those with previously incurable cancers.

The Gut Environment

While the tumor microenvironment is often depicted as nutrient restrictive, the mammalian gastrointestinal tract represents a metabolically rich and diverse tissue system. Its primary function is to digest and absorb nutrients with the aid of microbial species contained within the lumen. A single layer of epithelial cells is all that separates these commensal microbes from the rest of the body. The majority of intestinal epithelial cells (IECs) are absorptive enterocytes that digest and transfer nutrients, however, additional specialized epithelial lineages exist with a diverse

array of functions. For example, goblet and Paneth cells secrete mucins and antimicrobial peptides that fortify the barrier against potentially pathogenic microbes, microfold (M) and goblet cells assist in the transferring of luminal antigens across the epithelial barrier for sampling by mucosal DCs, and Tuft cells are important for sensing and responding to protozoa and helminths. Together with intestinal resident immune cells including innate lymphoid cells (ILCs), intraepithelial lymphocytes (IELs), helper T cells and B cells, a balancing act between barrier protection and microbial tolerance with surveillance and inflammation is maintained (Figure 3). While the relationship between gut commensal microbes and immune cell development and function, and also how IECs interface with immune system regulation, has recently been reviewed (Kurashima and Kiyono, 2017), we examine the unique constraints that this environment presents on cellular immunometabolism.

While IECs control the intake of nutrients from the luminal environment of the gut, a recent study provides evidence that the way they are structured and uniquely placed controls their metabolic activity and function (Kaiko et al., 2016). The layer of epithelia in the small intestine are organized into crypts and villi, which form invaginations that serve to optimize surface area whereby nutrients can be absorbed. At the base of the colonic crypt lie epithelial stem/progenitor cells that differentiate into specialized IECs as they migrate up the crypt-villus axis until they are eventually lost from the epithelial layer. This process of self-renewal from the crypt is continuous and therefore is a site of active proliferation (Kurashima and Kiyono, 2017). Kaiko et al. (2016) screened microbiota-derived products for their impact on intestinal epithelial progenitors and identified the short chain fatty acid (SCFA) butyrate as a potent inhibitor of intestinal stem cell proliferation at physiologic concentrations present within the lumen. They further found that differentiated colonocytes located at the forefront of the villi metabolized butyrate to fuel OXPHOS, thereby limiting its access to underlying progenitor cells, which do not readily utilize this substrate. Either removal of the ability to metabolize butyrate via deletion of acyl-CoA dehydrogenase or increased abundance of butyrate prevented the rapid regeneration of epithelial tissue after gut injury. Thus, a combination of physical separation in the crypt and fermentation of butyrate by mature colonocytes protects the proliferating progenitor pool of IECs (Figure 3).

B and T Follicular Helper Cell Metabolism

Another unique structural feature of the gut are the Peyer's patches, aggregates of gut-associated lymphoid tissue (Reboldi and Cyster, 2016). Found in the small intestine, they represent a specialized lymphoid compartment continuously exposed to food- and microbiome-derived antigens. Due to this exposure, Peyer's patches are rich in germinal centers (GCs), which are comprised of B, T, stromal, and follicular DCs. B cells segregate into zones where they undergo cycles of proliferation and differentiation and compete for signals directing class switch recombination (CSR) and survival from T follicular helper (Tfh) cells, allowing further maturation of the antibody repertoire.

Although the literature on B and Tfh cell metabolism is still developing, it has been shown that B cell activation induced by either α -IgM ligation or lipopolysaccharide (LPS) increases Glut1 expression and glucose uptake downstream of PI3K and

mTOR signaling (Caro-Maldonado et al., 2014; Doughty et al., 2006; Jellusova and Rickert, 2016; Lee et al., 2013; Woodland et al., 2008). Glycolysis and OXPHOS are augmented as well as mitochondrial mass (Caro-Maldonado et al., 2014; Doughty et al., 2006; Dufort et al., 2007). Increased glucose acquisition also fuels de novo lipogenesis necessary for B cell proliferation and growth of intracellular membranes. Inhibition of the fatty acid synthesis (FAS) enzyme ATP-citrate lyase in splenic B cells results in reduced expansion and expression of plasma cell differentiation markers (Dufort et al., 2014). Although apoptosis inducing factor (AIF) is required for T cell survival via ETC complex I function and respiration, AIF deficiency in B cells has no impact on their development or survival because of their reliance on glucose metabolism (Milasta et al., 2016). B cells cultured in galactose fail to expand unlike T cells, which can activate and proliferate in the presence of either galactose or glucose (Chang et al., 2013; Milasta et al., 2016). Glycogen synthase 3, which promotes the quiescence and survival of circulating naive B cells, tempers increases in glycolytic metabolism downstream of CD40 costimulatory receptor signaling and sustains the survival of B cells subjected to glucose restriction (Jellusova et al., 2017). On the other hand, the transition to durable humoral immunity by long-lived plasma cells (LLPCs) was shown to be dependent on mitochondrial pyruvate import and metabolism (Figure 3). Glucose supports antibody glycosylation, but LLPCs acquire more glucose than their short-lived counterparts and their long-term survival is dependent on their ability to siphon glucose-derived pyruvate into the mitochondria during times of metabolic stress (Lam et al., 2016).

It is interesting to speculate that with the constant proliferation of GC B cells in the gut and the importance of glucose and glycolysis in activated plasma cells, access to glucose would become limiting for other cells that occupy this microniche. A few studies suggest that Tfh cells have evolved to be uniquely suited to survive under these constraints. It has been shown that Tfh cells have less mTORC1 activation and reduced glycolysis compared to Th1 cells (Ray et al., 2015). In part, this may be due to expression of their lineage defining transcription factor Bcl6, which can suppress glycolysis potentiated by c-Myc and HIF-1 α (Johnston et al., 2009; Nurieva et al., 2009; Oestreich et al., 2014). Consistent with this, overexpression of Bcl6 reduces glycolysis in T cells, and inhibition of mTOR using shRNA favors Tfh cell development over Th1 cells in vivo after viral infection (Ray et al., 2015) (Figure 3). However, a more recent study using mice with conditional deletions of mTORC1 and mTORC2 via OX40 and CD4 cre recombinase observed a requirement of mTOR signaling in Tfh cell development and GC formation within Peyer's patches (Zeng et al., 2016). The former applied retroviral mTOR shRNA, which requires T cells be fully activated prior to knockdown, while this more recent report used mice where mTOR was excised during T cell development or at the moment of T cell activation, which may explain the disparity between the studies.

In addition to possibly limiting quantities of glucose substrate within GCs, these microniches contain areas of hypoxia, resulting in HIF-1 α activation (Abbott et al., 2016; Cho et al., 2016). B cells placed under hypoxic conditions had reduced activation-induced deaminase expression and subsequently underwent less CSR to the pro-inflammatory IgG2c isotype when

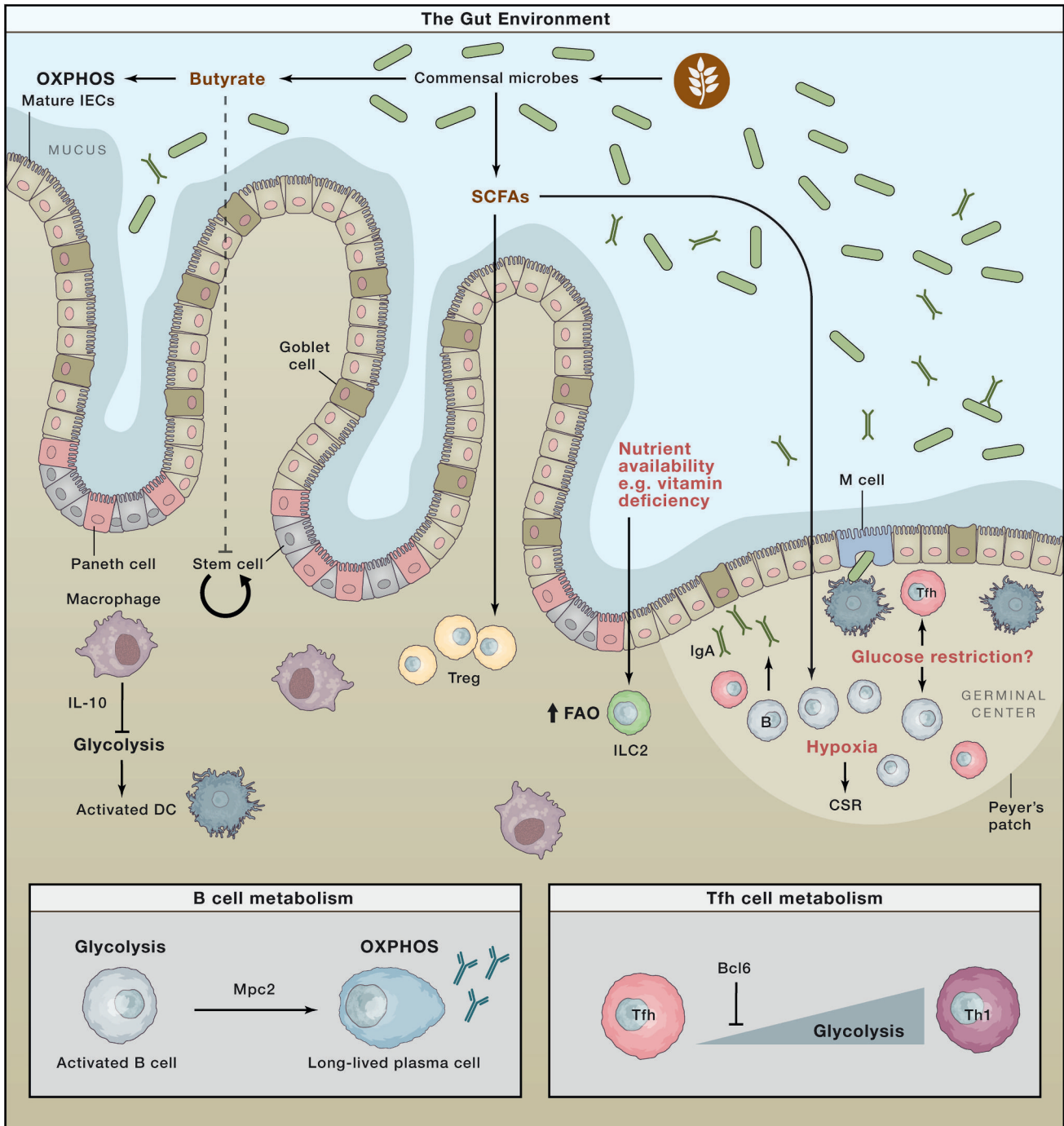


Figure 3. Model of Metabolic Relationships in the Gastrointestinal Tract

The gut serves as a direct interface with the outside world and the foods we consume. A single epithelial cell layer separates the contents of the intestinal lumen from the lamina propria where DCs, macrophages, ILCs, and T cells reside. Peyer's patches are interspersed along the epithelium, which in addition to supporting sampling of luminal antigens by DCs and M cells, house germinal centers that mature IgA-secreting B cells with Tfh cell help. B cells augment glycolysis upon activation and depend on pyruvate import via Mpc2 for longevity as long-lived plasma cells (LLPCs). Plasma cell hunger for glucose may restrict this nutrient from Tfh cells, however, Tfh cells downregulate glycolysis in response to expression of their lineage defining transcription factor Bcl6. In addition, GCs contain areas of hypoxia that impinge on B cell function like class switch recombination (CSR). Commensal bacteria produce metabolites such as short chain fatty acids (SCFAs) from the fermentation of dietary fiber, which influence B cell metabolism and promote IgA secretion. The presence of SCFAs and vitamins support maintenance of barrier function by promoting the development and survival of Tregs and ILCs, respectively. Homeostatic signals secreted by gut resident immune cells (e.g., IL-10) may also modulate metabolism and therefore control their activation state.

cultured in conditions that promote IgG production (Cho et al., 2016). In contrast, B cells cultured in IgA-promoting conditions during hypoxia were unaffected, yielding comparable levels of IgA to cells kept at normoxia and highlighting how lymphocyte function may be fine-tuned to varying oxygen tension in tissues (Figure 3). B cells isolated from mice with constitutive activation of HIF-1 α by deletion of its suppressor VHL had defects in IgG2c production, which was attributed to diminished mTORC1 activation. B cells from Raptor-deficient heterozygotes also yielded fewer IgG antibodies (Cho et al., 2016). A separate study found that the mTOR inhibitor rapamycin dampens CSR, yielding the formation of lower affinity, more cross-reactive B cell antibodies, which offered broad protection against heterosubtypic flu infection (Keating et al., 2013). Both mTORC1 and HIF-1 α promote aerobic glycolysis (O'Neill et al., 2016). However, the metabolic activities of the cells cultured under different isotype conditions while under hypoxia were not explored. A separate study examining mitochondrial function, and specifically mitochondrial ROS, found that B cells with augmented mitochondrial mass, respiration, and ROS stratified cells that underwent CSR marked by IgG1 expression apart from CD138⁺ plasma cells (Jang et al., 2015). The differences seen in mitochondrial function between the B cell populations were in part due to differential regulation of heme synthesis by mitochondrial ROS, however, how the mitochondria affects CSR to other isotypes was not assessed. Cytokines initiate CSR to distinct isotypes and signals derived from these growth factors might be responsible for the differences in metabolic signaling and suggest varying requirements to initiate metabolic programs and CSR in B cells. Secretion of IgA predominates the gut and is critical to maintaining barrier protection and bacterial homeostasis (Kurashima and Kiyono, 2017). The apparent stability of CSR to the IgA isotype under hypoxia and impaired pro-inflammatory IgG2c subtype might have evolved to ensure tolerance with the microbiome, while concurrently providing a stringent method of selection of antibodies produced during inflammatory responses to pathogen-derived antigens.

Nutrients and Immune Signals in the Gut

The metabolic relationship between commensals and immune cells in the gut is further illustrated by the finding that SCFAs derived from the fermentation of dietary fiber by gut microbiota promote B cell metabolism and boost antibody responses in both mouse and human B cells (Kim et al., 2016). Supplementation with dietary fiber or the SCFAs acetate, propionate, and butyrate increases intestinal IgA production, as well as systemic IgG during infection (Figure 3). Culturing B cells with SCFAs was shown to raise acetyl-CoA levels and increase mitochondrial mass, lipid content, and FAS leading to increased plasma cell differentiation and metabolic activity (Kim et al., 2016). Part of this phenotype could be attributed to histone deacetylase (HDAC) inhibition, an established effect of SCFA supplementation.

In addition to their effects on B cells, SCFAs can promote the development and function of colonic Treg cells via induction of Foxp3 in a HDAC-dependent manner (Arpaia et al., 2013; Furusawa et al., 2013; Smith et al., 2013) (Figure 3). Treg cells are critical to maintaining commensal tolerance by the immune system through suppression of aberrant T cell responses. Unlike

other activated T helper subsets, Treg cells have been described to primarily rely on OXPHOS driven by FAO (Newton et al., 2016). However, signals downstream of TLR ligation can augment glycolysis and proliferation of Treg cells and reduce their ability to suppress T cell responses (Gerriets et al., 2016). Retroviral enforced expression of Foxp3 promotes OXPHOS and dampens glucose uptake and glycolysis, whereas Treg cells transduced with Glut1 decreased Foxp3 expression after adoptive transfer in vivo and fail to suppress T cell-mediated colitis in a model of inflammatory bowel disease. These findings suggest that during inflammation and microbial infection, Treg cells may temporarily lose their regulatory function to give way to robust T cell responses and participate as more conventional effector helper T cells. Increases in NaCl either from supplementation in vitro or diet in vivo inhibit the suppressive function of human Treg cells via serum/glucocorticoid-regulated kinase 1 (SGK1), which integrates signals from PI3K and mTORC2 to regulate sodium-controlled signal transduction (Hernandez et al., 2015). However, a study of human Treg cells found that the glycolytic enzyme enolase-1 was required for their suppressive activity through its control of Foxp3-E2 splice variants (De Rosa et al., 2015). Depending on environmental cues and metabolites, it appears that Treg cell metabolism can be modulated, affecting their function.

As discussed, increases in SCFAs either from diet, infection, or exogenous treatment impinge on metabolic processes including HDAC activation (Rooks and Garrett, 2016). A recent study suggests that activation of the HDAC sirtuin 1 (SIRT1) negatively impacts Th9 cell differentiation (Wang et al., 2016b). The exposure of CD4 T cells to distinct cytokine cocktails differentiates them into separate helper lineages. However, perturbing metabolism also modulates CD4 T cell fate. A yin and yang relationship between Th17 and Treg cell differentiation has been established. Th17 cells are particularly glycolytic and depend on engagement of this pathway downstream of mTOR and HIF-1 α activation. Dampening glycolysis through deletion of HIF-1 α or with the inhibitor 2-DG in T cells impairs Th17 development and instead promotes Treg cells, even under Th17-inducing culture conditions (Dang et al., 2011; Shi et al., 2011). Suppression of mTOR with rapamycin or genetic ablation also augments production of Treg cells (Delgoffe et al., 2009; Kopf et al., 2007), and pharmacological inhibition of de novo fatty acid synthesis prevents Th17 differentiation and instead enforces a Treg cell phenotype (Berod et al., 2014).

Although the metabolic characteristics of other CD4 T cell subsets have been compared (Michalek et al., 2011), little was known about Th9 cell metabolism. Th9 cells are characterized by their ability to produce IL-9 and can be generated from naive cells in culture using the cytokines transforming growth factor β (TGF- β) and IL-4. They are implicated in autoimmunity, melanoma, and worm infections (Kaplan et al., 2015). Wang et al. (2016b) found that Th9 cells are highly glycolytic, in part from their active suppression of SIRT1 expression via the kinase TAK1. SIRT1 was previously shown to negatively control HIF-1 α as well as mTOR (Lim et al., 2010; Liu et al., 2014). In line with this, Th9 cell development was augmented in SIRT1-deficient T cells whereas retroviral enforced expression of SIRT1 or dampening of aerobic glycolysis by chemical or genetic

means impaired Th9 cell differentiation (Wang et al., 2016b). Th9, Th17, and Treg cells all share the cytokine TGF- β for their development but then depend on additional cytokine signals for their eventual fates. Given their divergent metabolic phenotypes, as well as HDAC requirements, it would be interesting to explore further whether variances in intracellular levels of SCFA metabolites, for example, might couple with environment signals to influence their eventual metabolic and developmental pathway.

Apart from its effect on CD4 T cells, the SCFA acetate also has been shown to affect secondary recall responses from CD8 memory T cells (Balmer et al., 2016). Germ-free mice reconstituted with commensal microbes, or oral or systemic infection with bacterial species, elevated serum acetate concentrations. Memory T cells generated in vitro or in vivo cultured with acetate levels observed during these infections secreted more IFN- γ and augmented glycolysis after restimulation. Acetate can be quickly converted into acetyl-CoA, which can condense with oxaloacetate into citrate in the mitochondria to fuel the TCA cycle and OXPHOS, can be used as a substrate for FAS, or participate in post translational modification (PTM) of proteins including histones (Pearce et al., 2013). Balmer et al. (2016) mechanistically tied their results to lysine acetylation of the glycolytic enzyme glyceraldehyde 3-phosphate dehydrogenase (GAPDH). GAPDH activity has been shown to regulate T cell production of IFN- γ (Chang et al., 2013; Gubser et al., 2013). Although the study demonstrated that the enzymatic activity of GAPDH was altered by acetylation of K217, whether this PTM was critical to acetate-dependent increases in IFN- γ protein was not explored. In a separate report, CD4 T cells deficient in LDHA expression had defects in IFN- γ production, which stemmed from widespread lack of acetylation of the *Irfng* locus (Peng et al., 2016). LDHA is the critical enzyme that defines aerobic glycolysis, converting pyruvate to lactate. Culturing cells in galactose impairs aerobic glycolysis, as galactose enters glycolysis at a significantly lower rate than glucose via the Leloir pathway (Bustamante and Pedersen, 1977), a result confirmed by tracing galactose metabolism in T cells (Chang et al., 2013). Reducing GAPDH engagement from glycolysis in this fashion permits moonlighting function by this abundantly expressed protein. It was shown that GAPDH binds to the 3'UTR of AU-rich containing cytokine mRNAs, preventing their efficient translation (Chang et al., 2013). Peng et al. (2016) argue against GAPDH posttranscriptional control of T cell function during aerobic glycolysis deficiency via LDHA deletion because modification of the 3'UTR of *Irfng* did not rescue defects in cytokine production in their system. However, as Peng et al. (2016) demonstrated, LDHA-deficient cells have defects in *Irfng* mRNA production, whereas cells forced to respire in galactose remain transcriptionally competent for *Irfng* as those cultured in glucose. Supplementation with the SCFA acetate rescued their epigenetic defect and cytokine production. These studies show that aerobic glycolysis regulates both transcriptional and translational functions in T cells.

While products generated from the microbiome can modulate the metabolism of immune cells and shift the balance between tolerance and inflammation, there are hints that immune-driven signals central to gut homeostasis may also mediate their effects

through metabolic modulation. One such example is the pleiotropic anti-inflammatory cytokine IL-10. Most hematopoietic cells produce and sense IL-10 and its importance for maintaining tolerance with the intestinal microbiota is clearly evident from observations that IL-10- or IL-10R-deficient mice develop spontaneous colitis (Kühn et al., 1993; Spencer et al., 1998). IL-10R deficiency in macrophages is also sufficient to recapitulate onset of severe colitis in mice (Shouval et al., 2014; Zsigmond et al., 2014). Further, mice with a myeloid cell-specific deficiency in STAT3, which is activated downstream of the IL-10R by JAK1, develop chronic enterocolitis as they age (Takeda et al., 1999). In experiments that shed light on the importance of aerobic glycolysis engagement in DC activation, it was found that treatment of DCs with recombinant IL-10 blocked increases in their glycolytic rate after LPS stimulation (Krawczyk et al., 2010). Cells subjected to IL-10R blockade further upregulated glycolysis after activation compared to controls. It is tempting to speculate that one of the ways IL-10 might be anti-inflammatory is through inhibition of metabolic reprogramming to aerobic glycolysis during innate immune cell activation (Figure 3). Coincidentally, STAT3 was found to localize to mitochondria and interact with ETC complexes, which helped maintain efficient OXPHOS in the heart (Wegrzyn et al., 2009). Whether traditional cell surface cytokine-receptor signaling could modulate levels of mitochondrial STAT3 was not explored. Of interest, CD8 T cells with a conditional deletion of the IL-10R fail to form memory T cells (Laidlaw et al., 2015), which depend on FAO-driven OXPHOS for their generation after infection (Cui et al., 2015; Pearce et al., 2009; van der Windt et al., 2012).

The gut is one example of a tissue that presents distinct metabolic challenges for immune cells, which affect their steady state and protective versus inflammatory responses. Other examples, such as skin, provide the potential for commensal organisms to metabolically affect immune cell function, a topic reviewed elsewhere (Hand et al., 2016). The intestinal tract is constantly subjected to fluctuations in diet and sometimes the intake of invasive pathogens can also deprive metabolic substrates from immune cells. The bacterium *Salmonella typhimurium* produces a putative type II asparaginase that depletes available asparagine needed for metabolic reprogramming of activated T cells via c-Myc and mTOR (Torres et al., 2016). The use of asparaginase for acute lymphoblastic leukemia treatment highlights the potential for the depletion of extracellular arginine to significantly affect cellular function (DeBerardinis and Chandel, 2016). Lack of dietary vitamin B1 decreases the number of naive B cells in Peyer's patches due to their dependence on this TCA cycle cofactor, while leaving IgA⁺ plasma cells intact in the lamina propria (Kunisawa et al., 2015). Although ILC metabolism has only recently been explored (Monticelli et al., 2016; Wilhelm et al., 2016), it was found that in settings of vitamin A deficiency, type 2 ILCs sustain their function via increased acquisition and utilization of fatty acids for FAO (Wilhelm et al., 2016) (Figure 3). The internal balance between polyunsaturated fats and saturated fatty acids can also determine the pathogenicity of Th17 cells; cells that help maintain mucosal barrier immunity and contribute to pathogen clearance (Wang et al., 2015). Long chain fatty acids (LCFA) promote Th1 and Th17 cell polarization and mice fed with LCFA have exacerbated T cell-mediated autoimmune responses, whereas

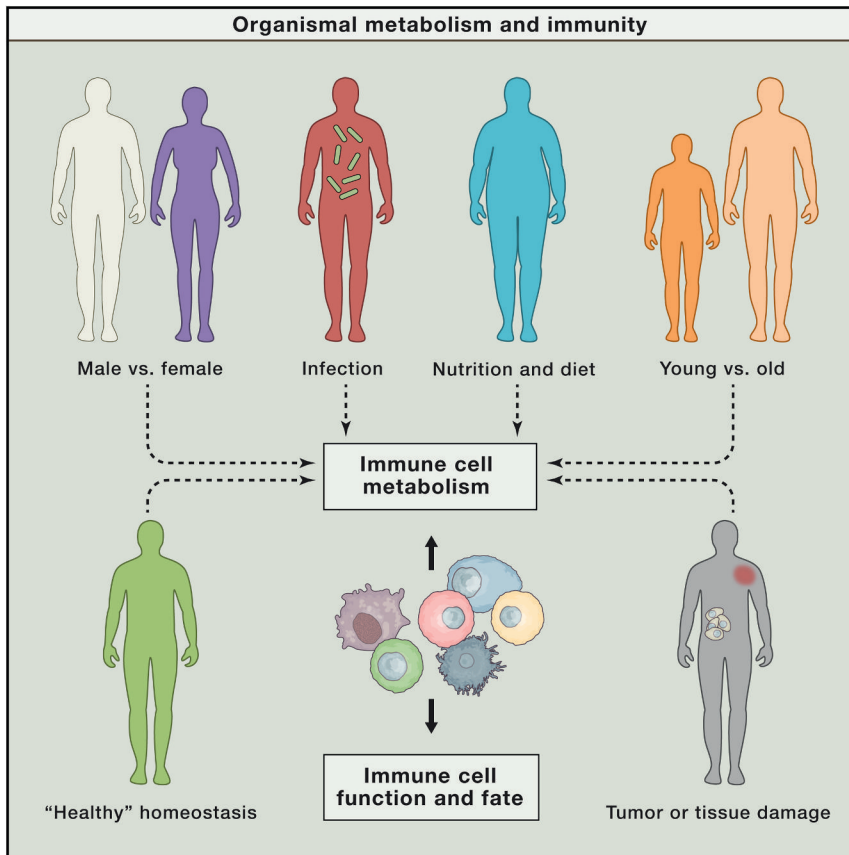


Figure 4. Tying Organismal Metabolism to Cellular Metabolism and Immunity

Throughout the course of life, organisms are exposed to a variety of factors that influence their systemic metabolism, and the relationship between these and immune cell metabolism is only beginning to be explored. As research moves forward, it will be important to understand how these challenges integrate with immune response programs and whether our current paradigms and models regarding immunometabolism match up or must be modified accordingly under these circumstances.

between diet and inflammation with pathological metabolic syndromes such as diabetes and insulin resistance or cardiovascular diseases (Font-Burgada et al., 2016). However, the relationship between changes in whole body metabolism and immunometabolism remains largely an uncharted area waiting to be explored (Man et al., 2017).

Chronic low-grade inflammation is a well-established major risk factor for a plethora of diseases including heart disease, diabetes, metabolic syndromes, and cancer (Hotamisligil, 2017; Park et al., 2010), but our understanding of how inflammation contributes to the pathogenesis of these complex diseases is murky. Part of the complexity is due to the local, regional, and systemic actions

of inflammatory cytokines such as IL-1 β , IL-6, and TNF- α . These are generally considered to be produced in response to local tissue damage or infection, which can regulate not only the metabolic activities of neighboring cells but also act on distal sensors that control host metabolism (Febbraio, 2014). For example, circulating IL-6 levels are elevated in patients with chronic inflammation, which can modulate fatty acid metabolism and cell survival in many tissues including skeletal muscle, hepatocytes, the CNS, and neuroendocrine system (Saltiel and Olefsky, 2017).

mice fed with SCFA are protected (Haghikia et al., 2015). If the internal lipidome of Th17 cells can alter their functional state from protective to inflammatory as does their access to LCFA versus SCFA in the small intestine, it raises the question of how other tissue systems with a rich diversity of fat deposits and cells, such as the adipose tissue, modulate the metabolism and function of resident immune cells. Indeed, a recent study has found that the survival and function of resident memory T cells depends on exogenous lipid uptake and metabolism mediated by fatty acid binding proteins 4 and 5 (Pan et al., 2017).

Organismal Metabolism and Immune Cell Function

Thus far, we have examined the effects of distinct niches in which immune cells come to inhabit that mold their metabolic and functional fates. The tumor microenvironment represents one instance of a pathophysiological situation that immune cells may encounter, whereas the gastrointestinal tract is an example of a physiological tissue system that immune cells come to occupy (Figure 4). During acute or chronic inflammation induced by infection, diet, cancer, or injury, a feed forward loop may exist where effector molecules, released from immune cells responding to these various localized insults to homeostasis, also modulate systemic metabolism, and these changes to organismal metabolism then feed back onto the metabolism of immune cells, altering their subsequent function. Much has been done in the last decades in the regard to associations

In obesity and consumption of a high fat diet (HFD), macrophages accumulate within adipose tissue recruited by dying enlarged adipocytes and produce the inflammatory cytokines IL-6 and TNF- α (Cinti et al., 2005; McLaughlin et al., 2017). Locally, IL-6 can induce lipolysis in neighboring adipocytes and impair lipoprotein lipase, decreasing adipocyte lipid storage. The rise in circulating IL-6 and free fatty acids (FFAs) has broad secondary effects on local and distal tissue microenvironments and can promote local insulin resistance, which can be reversed with therapeutic blockade of IL-6. IL-6 alone can also antagonize insulin receptor signaling and induce insulin resistance (McLaughlin et al., 2017). Interestingly, increased serum triglycerides and LDL is one of the most frequent reported adverse events in patients who receive tocilizumab, an IL-6 receptor blockade antibody, suggesting that IL-6 may play an important role in lipid homeostasis during inflammatory conditions (Schultz et al., 2010).

Increased circulating FFAs have consequences on immune cell function. Accumulation of FFAs in macrophages promotes ROS generation, which in turn augments activation of the NLRP3-ASC inflammasome (Guo et al., 2015). Inflammasome activation increases tissue inflammation through IL-1 β and IL-18 secretion via cleavage activation by caspase-1 and pyroptosis (Rathinam and Fitzgerald, 2016). FFA-induced inflammasome activation promotes insulin resistance, mediated by the secretion of IL-1 β . However, inflammasome activation may exhibit functional specificity for certain FFAs, as not all saturated fatty acids are capable of inflammasome activation. A HFD consisting of mostly monounsaturated fatty acids, while still promoting obesity in mice, does not induce inflammasome activation and the development of insulin resistance (Finucane et al., 2015). Tying into FFA metabolism, NADPH oxidase 4 (NOX4)-deficient mouse and human macrophages stimulated *in vitro* with ATP, nigericin, or silica have impaired caspase-1 activation and subsequent IL-1 β and IL-18 maturation, although TNF- α production remains intact (Moon et al., 2016). Moon et al. (2016) found that inflammasome activation was also diminished in NOX4^{-/-} mice after *Streptococcus pneumoniae* challenge. This defect was identified as an inability of NOX4-deficient cells to augment Cpt1a-dependent FAO during inflammasome activation. Consistent with this observation, Cpt1a-deficient macrophages were unable to activate the NLRP3 inflammasome, but enforced expression of Cpt1a in NOX4-deficient macrophages rescued inflammasome activation and cytokine release. However, exactly how NOX4 regulates Cpt1a protein levels and FAO, and whether extracellular FFAs may contribute to this process, was left unresolved.

Why do inflammatory cytokines exert systemic changes to metabolism on other cells? Perhaps in the case of acute infections, inflammatory cytokines do so to create a temporary period of local and/or systemic insulin resistance, which could allow for redirection of glucose to immune cells, such as T cells, to fuel their rapid division and meet their bioenergetic demands. However, when inflammation persists, like in cancer, obesity, or chronic infection, prolonged disruption of metabolic homeostasis could lead to immune cell dysfunction, dysregulated systemic metabolism, and ultimately cachexia (Porporato, 2016). Cachexia is a multi-organ syndrome of rapid weight loss and loss of appetite, and is one of the most obvious morbidities in cancer patients. The specific etiology of cachexia is debated, and cancer-associated cachexia is not exclusive to tumor burden or therapies suggesting that the state of cancer itself promotes progression of metabolic dysfunction. TNF- α was originally considered the major driver of cachexia as implied by its original name, “cachectin.” However, blockade of TNF- α is insufficient to prevent cachexia, and more recent studies point to the involvement of IL-6 in this process (Porporato, 2016). Chronic inflammation in the tumor microenvironment is a source of IL-6 production that leads to an increase in its systemic levels in cancer patients. IL-6-mediated liberation of fatty acids from systemic lipid stores, in concert with decreases in insulin availability or responsiveness, may instigate a catabolic state that becomes unhinged where lipolysis and also ketosis pillages energy stores within subcutaneous adipose tissue and skeletal muscle culminating in a wasting disorder (Flint et al., 2016; Odegaard

et al., 2007). The extent to which immune cell metabolism is affected by systemic substrate availability *in vivo*, and how cachexia, as well as other situations (e.g., consumption of ketogenic diets) influences nutrient depots and ultimately utilization by immune cells, remains to be investigated.

Feeding behaviors can also affect host immune fitness (Figure 4). The gut-brain axis controls appetite, sensory of luminal contents, and digestion. The hypothalamus also regulates so called “sickness behaviors,” such as sickness-associated anorexia and reduced energy expenditure, but it is still not clear why sickness behaviors occur and more importantly what benefit they might provide to the host response to infection or inflammation. Wang et al. (2016a) asked whether the fed or fasted state was more protective against infection with various pathogens. Bypassing the anorexic response induced by infection with food or glucose supplementation increased lethality during *Listeria monocytogenes* or LPS challenge. Glucose-mediated death was due in part to enhanced neuronal dysfunction, as the mice succumbed to epileptic seizures. Wang et al. (2016a) suggested that increased ROS disrupted neural function, however, whether the enhanced morbidity was dependent on ROS and its cellular source was not identified. Giving mice 2-DG to impair glucose catabolism improved their survival. However, glucose supplementation was protective when mice were challenged with influenza or Poly(I:C). Viral infection promoted endoplasmic reticulum (ER) stress responses that were mitigated by glucose consumption. On the other hand, temporary ketosis was required for survival from LPS-induced sepsis, suggesting that ketones are protective against hypothalamic inflammation and ROS-mediated neuronal damage. Ketogenic diets have been effective to reduce epileptic seizures, and the potential benefits of ketogenic diets have been debated for other conditions such as cancer (Allen et al., 2014). However, pre-fasting or feeding the mice a ketogenic diet for 1–3 days prior to LPS stimulation made them more susceptible to its lethal effects, suggesting that in order to be protective, ketogenic metabolism should be temporally coordinated to the course of infection (Wang et al., 2016a). Interestingly, specific ketone bodies have been shown to minimize inflammation in other instances by blocking NLRP3 inflammasome activation in bone marrow-derived macrophages and human monocytes (Youm et al., 2015).

Some pathogens have evolved strategies to take advantage of modulating feeding behaviors to promote their own fitness. A recent report by Rao et al. (2017) suggests that *Salmonella typhimurium* inhibits infection-induced anorexia upon oral infection by antagonizing caspase-1 activity downstream of inflammasome activation to decrease IL-1 β signaling to the hypothalamus via the vagus nerve. Disrupting this adaptation in *Salmonella* by genetic deletion of its ubiquitin ligase SlrP resulted in modulation of the gut-brain axis. Infection with SlrP-deficient *Salmonella* augmented IL-1 β maturation, resulting in changes to hypothalamic appetite regulation, whereby the mice decreased food consumption and exhibited greater weight loss that ultimately diminished host survival. Severing the gut-CNS connection surgically or force-feeding the mice reversed this anorexic response and increased lethality induced by SlrP-deficient *Salmonella* infection. The studies by Wang et al. (2016a) and Rao et al. (2017) help

give some mechanistic insight into the exciting interconnection between feeding behaviors and disease susceptibility versus tolerance but also show that there is still much to learn about precisely how different pathogens and routes of infection affect this process. We have highlighted only a few examples where, going through the arc of life, many other organismal factors and changes may occur that influence immune cell metabolism, which directly impacts immune cell function and fate (Figure 4). Investigating how these perturbations affect our overall health will not only be challenging, but also interesting for further research.

Outlook

For some time, immunology encompassed a field that sought reductionist approaches to simplify a complex network of cells. Out of necessity, immunologists had to speak a common language or jargon that often excluded scientists in other disciplines. After many decades of hard work, great strides have been made in our understanding of the immune system, and now immunologists are better equipped to cross over into other disciplines. It is this “take a step back and look” approach that has led a number of laboratories to focus on metabolism and how this affects the immune system as well as its greater impact in tissue physiology.

It is obvious to most biologists that metabolism is integrated into every cellular process and fate decision. After all, everything must eat to survive. However, what is perhaps less appreciated is that the immune system is like a liquid organ unto itself. At their inception, immune cells are poised to respond to unknown stimuli, nutrients, and pathogens and are akin to special agents with contingency plans, ready to respond to one disaster scenario after another or relegated to pushing paperwork at the office maintaining the status quo. Throughout this review, we have only highlighted some examples of the complexity of the situations and environments that immune cells face that provide various metabolic instructional cues. This ability to rapidly change and adapt at any given second means that immune cells must intimately integrate their cellular metabolism in a way that most other organ and cell systems in the body do not have to, which we hope this review has shown and inspires research into many questions that remain to be explored. Coupling the unique benefits of studying immunometabolism is the added bonus of the enormous clinical relevance of these cells in human health and disease. First defining and then exploiting their unique metabolism may continue to yield new targets for therapy.

ACKNOWLEDGMENTS

We thank Edward Pearce and members of the Pearce laboratories for their insight and critical reading of the manuscript. This work was supported by grants from the NIH (R01CA181125 and R01AI091965 to E.L.P.; R37AI066232, R01CA195720, R01CA196660, P50CA196530 [PI, Roy S. Herbst] to S.M.K.; Ruth L. Kirschstein National Research Service Award 5T32HL007974 to R.T.S.), the Burroughs Wellcome Fund (Investigator in the Pathogenesis of Infectious Disease Award to E.L.P.), the MRA Team Science Award (to S.M.K.), the Max Planck Society, and the National Science Foundation Graduate Research Fellowship (DGE-1143954 to M.D.B.). We regret that we are unable to cite all relevant studies due to space limitations. E.L.P. is on the scientific advisory board of Immunomet.

REFERENCES

- Abbott, R.K., Thayer, M., Labuda, J., Silva, M., Philbrook, P., Cain, D.W., Kojima, H., Hatfield, S., Sethumadhavan, S., Ohta, A., et al. (2016). Germinal center hypoxia potentiates immunoglobulin class switch recombination. *J. Immunol.* *197*, 4014–4020.
- Adams, J.L., Smothers, J., Srinivasan, R., and Hoos, A. (2015). Big opportunities for small molecules in immuno-oncology. *Nat. Rev. Drug Discov.* *14*, 603–622.
- Adams, W.C., Chen, Y.H., Kratchmarov, R., Yen, B., Nish, S.A., Lin, W.W., Rothman, N.J., Luchsinger, L.L., Klein, U., Busslinger, M., et al. (2016). Anabolism-associated mitochondrial stasis driving lymphocyte differentiation over self-renewal. *Cell Rep.* *17*, 3142–3152.
- Allen, B.G., Bhatia, S.K., Anderson, C.M., Eichenberger-Gilmore, J.M., Sibnaller, Z.A., Mapuskar, K.A., Schoenfeld, J.D., Buatti, J.M., Spitz, D.R., and Fath, M.A. (2014). Ketogenic diets as an adjuvant cancer therapy: History and potential mechanism. *Redox Biol.* *2*, 963–970.
- Araki, K., Turner, A.P., Shaffer, V.O., Gangappa, S., Keller, S.A., Bachmann, M.F., Larsen, C.P., and Ahmed, R. (2009). mTOR regulates memory CD8 T-cell differentiation. *Nature* *460*, 108–112.
- Arpaia, N., Campbell, C., Fan, X., Dikly, S., van der Veeken, J., deRoos, P., Liu, H., Cross, J.R., Pfeffer, K., Coffey, P.J., and Rudensky, A.Y. (2013). Metabolites produced by commensal bacteria promote peripheral regulatory T-cell generation. *Nature* *504*, 451–455.
- Balmer, M.L., Ma, E.H., Bantug, G.R., Grählert, J., Pfister, S., Glatter, T., Jauch, A., Dimeloe, S., Slack, E., Dehio, P., et al. (2016). Memory CD8(+) T cells require increased concentrations of acetate induced by stress for optimal function. *Immunity* *44*, 1312–1324.
- Bensch, B., Johnson, A.L., Kurachi, M., Odorizzi, P.M., Pauken, K.E., Attanasio, J., Stelekati, E., McLane, L.M., Paley, M.A., Delgoffe, G.M., and Wherry, E.J. (2016). Bioenergetic insufficiencies due to metabolic alterations regulated by the inhibitory receptor PD-1 are an early driver of CD8(+) T cell exhaustion. *Immunity* *45*, 358–373.
- Berod, L., Friedrich, C., Nandan, A., Freitag, J., Hagemann, S., Harmrolfs, K., Sandouk, A., Hesse, C., Castro, C.N., Bähre, H., et al. (2014). De novo fatty acid synthesis controls the fate between regulatory T and T helper 17 cells. *Nat. Med.* *20*, 1327–1333.
- Brand, A., Singer, K., Koehl, G.E., Kolitzus, M., Schoenhammer, G., Thiel, A., Matos, C., Bruss, C., Klobuch, S., Peter, K., et al. (2016). LDHA-associated lactic acid production blunts tumor immunosurveillance by T and NK cells. *Cell Metab.* *24*, 657–671.
- Buck, M.D., O’Sullivan, D., and Pearce, E.L. (2015). T cell metabolism drives immunity. *J. Exp. Med.* *212*, 1345–1360.
- Buck, M.D., O’Sullivan, D., Klein Geltink, R.I., Curtis, J.D., Chang, C.H., Sanin, D.E., Qiu, J., Kretz, O., Braas, D., van der Windt, G.J., et al. (2016). Mitochondrial dynamics controls T cell fate through metabolic programming. *Cell* *166*, 63–76.
- Bustamante, E., and Pedersen, P.L. (1977). High aerobic glycolysis of rat hepatoma cells in culture: role of mitochondrial hexokinase. *Proc. Natl. Acad. Sci. USA* *74*, 3735–3739.
- Caro-Maldonado, A., Wang, R., Nichols, A.G., Kuraoka, M., Milasta, S., Sun, L.D., Gavin, A.L., Abel, E.D., Kelsoe, G., Green, D.R., and Rathmell, J.C. (2014). Metabolic reprogramming is required for antibody production that is suppressed in anergic but exaggerated in chronically BAFF-exposed B cells. *J. Immunol.* *192*, 3626–3636.
- Cham, C.M., Driessens, G., O’Keefe, J.P., and Gajewski, T.F. (2008). Glucose deprivation inhibits multiple key gene expression events and effector functions in CD8+ T cells. *Eur. J. Immunol.* *38*, 2438–2450.
- Champagne, D.P., Hatle, K.M., Fortner, K.A., D’Alessandro, A., Thornton, T.M., Yang, R., Torralba, D., Tomás-Cortázar, J., Jun, Y.W., Ahn, K.H., et al. (2016). Fine-tuning of CD8(+) T cell mitochondrial metabolism by the respiratory chain repressor MCJ dictates protection to influenza virus. *Immunity* *44*, 1299–1311.

- Chang, C.H., Curtis, J.D., Maggi, L.B., Jr., Faubert, B., Villarino, A.V., O'Sullivan, D., Huang, S.C., van der Windt, G.J., Blagih, J., Qiu, J., et al. (2013). Posttranscriptional control of T cell effector function by aerobic glycolysis. *Cell* **153**, 1239–1251.
- Chang, C.H., Qiu, J., O'Sullivan, D., Buck, M.D., Noguchi, T., Curtis, J.D., Chen, Q., Gindin, M., Gubin, M.M., van der Windt, G.J., et al. (2015). Metabolic competition in the tumor microenvironment is a driver of cancer progression. *Cell* **162**, 1229–1241.
- Cho, S.H., Raybuck, A.L., Stengel, K., Wei, M., Beck, T.C., Volanakis, E., Thomas, J.W., Hiebert, S., Haase, V.H., and Boothby, M.R. (2016). Germinal centre hypoxia and regulation of antibody qualities by a hypoxia response system. *Nature* **537**, 234–238.
- Cinti, S., Mitchell, G., Barbatelli, G., Murano, I., Ceresi, E., Faloia, E., Wang, S., Fortier, M., Greenberg, A.S., and Obin, M.S. (2005). Adipocyte death defines macrophage localization and function in adipose tissue of obese mice and humans. *J. Lipid Res.* **46**, 2347–2355.
- Clever, D., Roychoudhuri, R., Constantinides, M.G., Askenase, M.H., Sukumar, M., Klebanoff, C.A., Eil, R.L., Hickman, H.D., Yu, Z., Pan, J.H., et al. (2016). Oxygen sensing by T cells establishes an immunologically tolerant metastatic niche. *Cell* **166**, 1117–1131.
- Cogliati, S., Frezza, C., Soriano, M.E., Varanita, T., Quintana-Cabrera, R., Corrado, M., Cipolat, S., Costa, V., Casarin, A., Gomes, L.C., et al. (2013). Mitochondrial cristae shape determines respiratory chain supercomplexes assembly and respiratory efficiency. *Cell* **155**, 160–171.
- Colegio, O.R., Chu, N.Q., Szabo, A.L., Chu, T., Rhebergen, A.M., Jairam, V., Cyrus, N., Brokowski, C.E., Eisenbarth, S.C., Phillips, G.M., et al. (2014). Functional polarization of tumour-associated macrophages by tumour-derived lactic acid. *Nature* **513**, 559–563.
- Condamine, T., Dominguez, G.A., Youn, J.-I., Kossenkov, A.V., Mony, S., Alicea-Torres, K., Tcyganov, E., Hashimoto, A., Nefedova, Y., Lin, C., et al. (2016). Lectin-type oxidized LDL receptor-1 distinguishes population of human polymorphonuclear myeloid-derived suppressor cells in cancer patients. *Sci. Immunol.* **1**, aaf8943.
- Cubillos-Ruiz, J.R., Silberman, P.C., Rutkowski, M.R., Chopra, S., Perales-Puchalt, A., Song, M., Zhang, S., Bettigole, S.E., Gupta, D., Holcomb, K., et al. (2015). ER stress sensor XBP1 controls anti-tumor immunity by disrupting dendritic cell homeostasis. *Cell* **161**, 1527–1538.
- Cui, G., Staron, M.M., Gray, S.M., Ho, P.C., Amezcua, R.A., Wu, J., and Kaech, S.M. (2015). IL-7-induced glycerol transport and TAG synthesis promotes memory CD8⁺ T cell longevity. *Cell* **161**, 750–761.
- Dang, E.V., Barbi, J., Yang, H.Y., Jinasena, D., Yu, H., Zheng, Y., Bordman, Z., Fu, J., Kim, Y., Yen, H.R., et al. (2011). Control of T(H)17/T(reg) balance by hypoxia-inducible factor 1. *Cell* **146**, 772–784.
- De Rosa, V., Galgani, M., Porcellini, A., Colamatteo, A., Santopaolo, M., Zuchegna, C., Romano, A., De Simone, S., Procaccini, C., La Rocca, C., et al. (2015). Glycolysis controls the induction of human regulatory T cells by modulating the expression of FOXP3 exon 2 splicing variants. *Nat. Immunol.* **16**, 1174–1184.
- DeBerardinis, R.J., and Chandel, N.S. (2016). Fundamentals of cancer metabolism. *Sci. Adv.* **2**, e1600200.
- Delgoffe, G.M., Kole, T.P., Zheng, Y., Zarek, P.E., Matthews, K.L., Xiao, B., Worley, P.F., Kozma, S.C., and Powell, J.D. (2009). The mTOR kinase differentially regulates effector and regulatory T cell lineage commitment. *Immunity* **30**, 832–844.
- Doedens, A.L., Phan, A.T., Stradner, M.H., Fujimoto, J.K., Nguyen, J.V., Yang, E., Johnson, R.S., and Goldrath, A.W. (2013). Hypoxia-inducible factors enhance the effector responses of CD8⁺ T cells to persistent antigen. *Nat. Immunol.* **14**, 1173–1182.
- Doughty, C.A., Bleiman, B.F., Wagner, D.J., Dufort, F.J., Mataraza, J.M., Roberts, M.F., and Chiles, T.C. (2006). Antigen receptor-mediated changes in glucose metabolism in B lymphocytes: role of phosphatidylinositol 3-kinase signaling in the glycolytic control of growth. *Blood* **107**, 4458–4465.
- Dufort, F.J., Bleiman, B.F., Gumina, M.R., Blair, D., Wagner, D.J., Roberts, M.F., Abu-Amer, Y., and Chiles, T.C. (2007). Cutting edge: IL-4-mediated protection of primary B lymphocytes from apoptosis via Stat6-dependent regulation of glycolytic metabolism. *J. Immunol.* **179**, 4953–4957.
- Dufort, F.J., Gumina, M.R., Ta, N.L., Tao, Y., Heyse, S.A., Scott, D.A., Richardson, A.D., Seyfried, T.N., and Chiles, T.C. (2014). Glucose-dependent de novo lipogenesis in B lymphocytes: a requirement for atp-citrate lyase in lipopolysaccharide-induced differentiation. *J. Biol. Chem.* **289**, 7011–7024.
- Eales, K.L., Hollinshead, K.E.R., and Tennant, D.A. (2016). Hypoxia and metabolic adaptation of cancer cells. *Oncogenesis* **5**, e190.
- Febbraio, M.A. (2014). Role of interleukins in obesity: implications for metabolic disease. *Trends Endocrinol. Metab.* **25**, 312–319.
- Finlay, D.K., Rosenzweig, E., Sinclair, L.V., Feijoo-Carnero, C., Hukelmann, J.L., Rolf, J., Panteleyev, A.A., Okkenhaug, K., and Cantrell, D.A. (2012). PDK1 regulation of mTOR and hypoxia-inducible factor 1 integrate metabolism and migration of CD8⁺ T cells. *J. Exp. Med.* **209**, 2441–2453.
- Finucane, O.M., Lyons, C.L., Murphy, A.M., Reynolds, C.M., Klinger, R., Healy, N.P., Cooke, A.A., Coll, R.C., McAllan, L., Nilaweera, K.N., et al. (2015). Monounsaturated fatty acid-enriched high-fat diets impede adipose NLRP3 inflammasome-mediated IL-1 β secretion and insulin resistance despite obesity. *Diabetes* **64**, 2116–2128.
- Flint, T.R., Janowitz, T., Connell, C.M., Roberts, E.W., Denton, A.E., Coll, A.P., Jodrell, D.I., and Fearon, D.T. (2016). Tumor-induced IL-6 reprograms host metabolism to suppress anti-tumor immunity. *Cell Metab.* **24**, 672–684.
- Font-Burgada, J., Sun, B., and Karin, M. (2016). Obesity and cancer: the oil that feeds the flame. *Cell Metab.* **23**, 48–62.
- Furusawa, Y., Obata, Y., Fukuda, S., Endo, T.A., Nakato, G., Takahashi, D., Nakanishi, Y., Uetake, C., Kato, K., Kato, T., et al. (2013). Commensal microbe-derived butyrate induces the differentiation of colonic regulatory T cells. *Nature* **504**, 446–450.
- Geiger, R., Rieckmann, J.C., Wolf, T., Basso, C., Feng, Y., Fuhrer, T., Koga-deeva, M., Picotti, P., Meissner, F., Mann, M., et al. (2016). L-arginine modulates T cell metabolism and enhances survival and anti-tumor activity. *Cell* **167**, 829–842.e13.
- Gerriets, V.A., Kishton, R.J., Johnson, M.O., Cohen, S., Siska, P.J., Nichols, A.G., Warmoes, M.O., de Cubas, A.A., MacIver, N.J., Locasale, J.W., et al. (2016). Foxp3 and Toll-like receptor signaling balance Treg cell anabolic metabolism for suppression. *Nat. Immunol.* **17**, 1459–1466.
- Goveia, J., Stapor, P., and Carmeliet, P. (2014). Principles of targeting endothelial cell metabolism to treat angiogenesis and endothelial cell dysfunction in disease. *EMBO Mol. Med.* **6**, 1105–1120.
- Gubser, P.M., Bantug, G.R., Razik, L., Fischer, M., Dimeloe, S., Hoenger, G., Durovic, B., Jauch, A., and Hess, C. (2013). Rapid effector function of memory CD8⁺ T cells requires an immediate-early glycolytic switch. *Nat. Immunol.* **14**, 1064–1072.
- Guo, H., Callaway, J.B., and Ting, J.P. (2015). Inflammasomes: mechanism of action, role in disease, and therapeutics. *Nat. Med.* **21**, 677–687.
- Haas, R., Smith, J., Rocher-Ros, V., Nadkarni, S., Montero-Melendez, T., D'Acquisto, F., Bland, E.J., Bombardieri, M., Pitzalis, C., Perretti, M., et al. (2015). Lactate regulates metabolic and pro-inflammatory circuits in control of T cell migration and effector functions. *PLoS Biol.* **13**, e1002202.
- Haghikia, A., Jörg, S., Duscha, A., Berg, J., Manzel, A., Waschbisch, A., Hammer, A., Lee, D.H., May, C., Wilck, N., et al. (2015). Dietary fatty acids directly impact central nervous system autoimmunity via the small intestine. *Immunity* **43**, 817–829.
- Hand, T.W., Vujkovic-Cvijin, I., Ridaura, V.K., and Belkaid, Y. (2016). Linking the microbiota, chronic disease, and the immune system. *Trends Endocrinol. Metab.* **27**, 831–843.
- Hatfield, S.M., Kjaergaard, J., Lukashev, D., Schreiber, T.H., Belkoff, B., Abbott, R., Sethumadhavan, S., Philbrook, P., Ko, K., Cannici, R., et al. (2015). Immunological mechanisms of the antitumor effects of supplemental oxygenation. *Sci. Transl. Med.* **7**, 277ra230.

- Hensley, C.T., Faubert, B., Yuan, Q., Lev-Cohain, N., Jin, E., Kim, J., Jiang, L., Ko, B., Skelton, R., Loudat, L., et al. (2016). Metabolic heterogeneity in human lung tumors. *Cell* 164, 681–694.
- Hernandez, A.L., Kitz, A., Wu, C., Lowther, D.E., Rodriguez, D.M., Vudattu, N., Deng, S., Herold, K.C., Kuchroo, V.K., Kleinewietfeld, M., and Hafler, D.A. (2015). Sodium chloride inhibits the suppressive function of FOXP3+ regulatory T cells. *J. Clin. Invest.* 125, 4212–4222.
- Ho, P.-C., Bihuniak, J.D., Macintyre, A.N., Staron, M., Liu, X., Amezcua, R., Tsui, Y.C., Cui, G., Micevic, G., Perales, J.C., et al. (2015). Phosphoenolpyruvate is a metabolic checkpoint of anti-tumor T cell responses. *Cell* 162, 1217–1228.
- Hotamisligil, G.S. (2017). Inflammation, metaflammation and immunometabolic disorders. *Nature* 542, 177–185.
- Hsu, Y.-L., Hung, J.-Y., Chiang, S.-Y., Jian, S.-F., Wu, C.-Y., Lin, Y.-S., Tsai, Y.-M., Chou, S.-H., Tsai, M.-J., and Kuo, P.-L. (2016). Lung cancer-derived galectin-1 contributes to cancer associated fibroblast-mediated cancer progression and immune suppression through TDO2/kynurenine axis. *Oncotarget* 7, 27584–27598.
- Hu, H., Juvekar, A., Lyssiotis, C.A., Lien, E.C., Albeck, J.G., Oh, D., Varma, G., Hung, Y.P., Ullas, S., Lauring, J., et al. (2016). Phosphoinositide 3-kinase regulates glycolysis through mobilization of aldolase from the actin cytoskeleton. *Cell* 164, 433–446.
- Jang, K.J., Mano, H., Aoki, K., Hayashi, T., Muto, A., Nambu, Y., Takahashi, K., Itoh, K., Taketani, S., Nutt, S.L., et al. (2015). Mitochondrial function provides instructive signals for activation-induced B-cell fates. *Nat. Commun.* 6, 6750.
- Jellusova, J., and Rickert, R.C. (2016). The PI3K pathway in B cell metabolism. *Crit. Rev. Biochem. Mol. Biol.* 51, 359–378.
- Jellusova, J., Cato, M.H., Apgar, J.R., Ramezani-Rad, P., Leung, C.R., Chen, C., Richardson, A.D., Conner, E.M., Benschop, R.J., Woodgett, J.R., and Rickert, R.C. (2017). Gsk3 is a metabolic checkpoint regulator in B cells. *Nat. Immunol.* 18, 303–312.
- Jin, L., Alesi, G.N., and Kang, S. (2016). Glutaminolysis as a target for cancer therapy. *Oncogene* 35, 3619–3625.
- Johnston, R.J., Poholek, A.C., DiToro, D., Yusuf, I., Eto, D., Barnett, B., Dent, A.L., Craft, J., and Crotty, S. (2009). Bcl6 and Blimp-1 are reciprocal and antagonistic regulators of T follicular helper cell differentiation. *Science* 325, 1006–1010.
- Kaiko, G.E., Ryu, S.H., Koues, O.I., Collins, P.L., Solnica-Krezel, L., Pearce, E.J., Pearce, E.L., Oltz, E.M., and Stappenbeck, T.S. (2016). The colonic crypt protects stem cells from microbiota-derived metabolites. *Cell* 165, 1708–1720.
- Kaplan, M.H., Hufford, M.M., and Olson, M.R. (2015). The development and in vivo function of T helper 9 cells. *Nat. Rev. Immunol.* 15, 295–307.
- Kawalekar, O.U., O'Connor, R.S., Fraietta, J.A., Guo, L., McGettigan, S.E., Posey, A.D., Jr., Patel, P.R., Guedan, S., Scholler, J., Keith, B., et al. (2016). Distinct signaling of coreceptors regulates specific metabolism pathways and impacts memory development in CAR T cells. *Immunity* 44, 380–390.
- Keating, R., Hertz, T., Wehenkel, M., Harris, T.L., Edwards, B.A., McClaren, J.L., Brown, S.A., Surman, S., Wilson, Z.S., Bradley, P., et al. (2013). The kinase mTOR modulates the antibody response to provide cross-protective immunity to lethal infection with influenza virus. *Nat. Immunol.* 14, 1266–1276.
- Kim, M., Qie, Y., Park, J., and Kim, C.H. (2016). Gut microbial metabolites fuel host antibody responses. *Cell Host Microbe* 20, 202–214.
- Kleffel, S., Posch, C., Barthel, S.R., Mueller, H., Schlapbach, C., Guenova, E., Elco, C.P., Lee, N., Juneja, V.R., Zhan, Q., et al. (2015). Melanoma cell-intrinsic PD-1 receptor functions promote tumor growth. *Cell* 162, 1242–1256.
- Kopf, H., de la Rosa, G.M., Howard, O.M., and Chen, X. (2007). Rapamycin inhibits differentiation of Th17 cells and promotes generation of FoxP3+ T regulatory cells. *Int. Immunopharmacol.* 7, 1819–1824.
- Krawczyk, C.M., Holowka, T., Sun, J., Blagih, J., Amiel, E., DeBerardinis, R.J., Cross, J.R., Jung, E., Thompson, C.B., Jones, R.G., and Pearce, E.J. (2010). Toll-like receptor-induced changes in glycolytic metabolism regulate dendritic cell activation. *Blood* 115, 4742–4749.
- Kühn, R., Löhler, J., Rennick, D., Rajewsky, K., and Müller, W. (1993). Interleukin-10-deficient mice develop chronic enterocolitis. *Cell* 75, 263–274.
- Kunisawa, J., Sugiura, Y., Wake, T., Nagatake, T., Suzuki, H., Nagasawa, R., Shikata, S., Honda, K., Hashimoto, E., Suzuki, Y., et al. (2015). Mode of bioenergetic metabolism during B cell differentiation in the intestine determines the distinct requirement for vitamin B1. *Cell Rep.* 13, 122–131.
- Kurashima, Y., and Kiyono, H. (2017). Mucosal ecological network of epithelium and immune cells for gut homeostasis and tissue healing. *Annu. Rev. Immunol.* <http://dx.doi.org/10.1146/annurev-immunol-051116-052424>.
- Laidlaw, B.J., Cui, W., Amezcua, R.A., Gray, S.M., Guan, T., Lu, Y., Kobayashi, Y., Flavell, R.A., Kleinstein, S.H., Craft, J., and Kaech, S.M. (2015). Production of IL-10 by CD4(+) regulatory T cells during the resolution of infection promotes the maturation of memory CD8(+) T cells. *Nat. Immunol.* 16, 871–879.
- Lam, W.Y., Becker, A.M., Kennerly, K.M., Wong, R., Curtis, J.D., Llifrio, E.M., McCommis, K.S., Fahrman, J., Pizzato, H.A., Nunley, R.M., et al. (2016). Mitochondrial pyruvate import promotes long-term survival of antibody-secreting plasma cells. *Immunity* 45, 60–73.
- Lee, G.K., Park, H.J., Macleod, M., Chandler, P., Munn, D.H., and Mellor, A.L. (2002). Tryptophan deprivation sensitizes activated T cells to apoptosis prior to cell division. *Immunology* 107, 452–460.
- Lee, K., Heffington, L., Jellusova, J., Nam, K.T., Raybuck, A., Cho, S.H., Thomas, J.W., Rickert, R.C., and Boothby, M. (2013). Requirement for Rictor in homeostasis and function of mature B lymphoid cells. *Blood* 122, 2369–2379.
- Lim, J.-H., Lee, Y.-M., Chun, Y.-S., Chen, J., Kim, J.-E., and Park, J.-W. (2010). Sirtuin 1 modulates cellular responses to hypoxia by deacetylating hypoxia-inducible factor 1 α . *Mol. Cell* 38, 864–878.
- Liu, G., Bi, Y., Shen, B., Yang, H., Zhang, Y., Wang, X., Liu, H., Lu, Y., Liao, J., Chen, X., and Chu, Y. (2014). SIRT1 limits the function and fate of myeloid-derived suppressor cells in tumors by orchestrating HIF-1 α -dependent glycolysis. *Cancer Res.* 74, 727–737.
- Ma, E.H., Bantug, G., Griss, T., Condotta, S., Johnson, R.M., Samborska, B., Mainolfi, N., Suri, V., Guak, H., Balmer, M.L., et al. (2017). Serine is an essential metabolite for effector T cell expansion. *Cell Metab.* 25, 345–357.
- Macintyre, A.N., Gerriets, V.A., Nichols, A.G., Michalek, R.D., Rudolph, M.C., Deoliveira, D., Anderson, S.M., Abel, E.D., Chen, B.J., Hale, L.P., and Rathmell, J.C. (2014). The glucose transporter Glut1 is selectively essential for CD4 T cell activation and effector function. *Cell Metab.* 20, 61–72.
- MacIver, N.J., Michalek, R.D., and Rathmell, J.C. (2013). Metabolic regulation of T lymphocytes. *Annu. Rev. Immunol.* 31, 259–283.
- Man, K., Kutayin, V.I., and Chawla, A. (2017). Tissue immunometabolism: development, physiology, and pathobiology. *Cell Metab.* 25, 11–26.
- McLaughlin, T., Ackerman, S.E., Shen, L., and Engleman, E. (2017). Role of innate and adaptive immunity in obesity-associated metabolic disease. *J. Clin. Invest.* 127, 5–13.
- Michalek, R.D., Gerriets, V.A., Jacobs, S.R., Macintyre, A.N., MacIver, N.J., Mason, E.F., Sullivan, S.A., Nichols, A.G., and Rathmell, J.C. (2011). Cutting edge: distinct glycolytic and lipid oxidative metabolic programs are essential for effector and regulatory CD4+ T cell subsets. *J. Immunol.* 186, 3299–3303.
- Milasta, S., Dillon, C.P., Sturm, O.E., Verbist, K.C., Brewer, T.L., Quarato, G., Brown, S.A., Frase, S., Janke, L.J., Perry, S.S., et al. (2016). Apoptosis-inducing-factor-dependent mitochondrial function is required for T cell but not B cell function. *Immunity* 44, 88–102.
- Monticelli, L.A., Buck, M.D., Flamar, A.L., Saenz, S.A., Tait Wojno, E.D., Yudanin, N.A., Osborne, L.C., Hepworth, M.R., Tran, S.V., Rodewald, H.R., et al. (2016). Arginase 1 is an innate lymphoid-cell-intrinsic metabolic checkpoint controlling type 2 inflammation. *Nat. Immunol.* 17, 656–665.
- Moon, J.-S., Nakahira, K., Chung, K.-P., DeNicola, G.M., Koo, M.J., Pabón, M.A., Rooney, K.T., Yoon, J.-H., Ryter, S.W., Stout-Delgado, H., and Choi, A.M. (2016). NOX4-dependent fatty acid oxidation promotes NLRP3 inflammasome activation in macrophages. *Nat. Med.* 22, 1002–1012.
- Munn, D.H., Sharma, M.D., Lee, J.R., Jhaver, K.G., Johnson, T.S., Keskin, D.B., Marshall, B., Chandler, P., Antonia, S.J., Burgess, R., et al. (2002).

- Potential regulatory function of human dendritic cells expressing indoleamine 2,3-dioxygenase. *Science* 297, 1867–1870.
- Newton, R., Priyadarshini, B., and Turka, L.A. (2016). Immunometabolism of regulatory T cells. *Nat. Immunol.* 17, 618–625.
- Nieman, K.M., Kenny, H.A., Penicka, C.V., Ladanyi, A., Buell-Gutbrod, R., Zillhardt, M.R., Romero, I.L., Carey, M.S., Mills, G.B., Hotamisligil, G.S., et al. (2011). Adipocytes promote ovarian cancer metastasis and provide energy for rapid tumor growth. *Nat. Med.* 17, 1498–1503.
- Noman, M.Z., Desantis, G., Janji, B., Hasmim, M., Karray, S., Dessen, P., Bronte, V., and Chouaib, S. (2014). PD-L1 is a novel direct target of HIF-1 α , and its blockade under hypoxia enhanced MDSC-mediated T cell activation. *J. Exp. Med.* 211, 781–790.
- Nurieva, R.I., Chung, Y., Martinez, G.J., Yang, X.O., Tanaka, S., Matskevitch, T.D., Wang, Y.H., and Dong, C. (2009). Bcl6 mediates the development of T follicular helper cells. *Science* 325, 1001–1005.
- O'Neill, L.A., and Pearce, E.J. (2016). Immunometabolism governs dendritic cell and macrophage function. *J. Exp. Med.* 213, 15–23.
- O'Neill, L.A.J., Kishton, R.J., and Rathmell, J. (2016). A guide to immunometabolism for immunologists. *Nat. Rev. Immunol.* 16, 553–565.
- O'Sullivan, D., van der Windt, G.J., Huang, S.C., Curtis, J.D., Chang, C.H., Buck, M.D., Qiu, J., Smith, A.M., Lam, W.Y., DiPlato, L.M., et al. (2014). Memory CD8(+) T cells use cell-intrinsic lipolysis to support the metabolic programming necessary for development. *Immunity* 41, 75–88.
- Odegaard, J.I., Ricardo-Gonzalez, R.R., Goforth, M.H., Morel, C.R., Subramanian, V., Mukundan, L., Red Eagle, A., Vats, D., Brombacher, F., Ferrante, A.W., and Chawla, A. (2007). Macrophage-specific PPAR γ controls alternative activation and improves insulin resistance. *Nature* 447, 1116–1120.
- Oestreich, K.J., Read, K.A., Gilbertson, S.E., Hough, K.P., McDonald, P.W., Krishnamoorthy, V., and Weinmann, A.S. (2014). Bcl-6 directly represses the gene program of the glycolysis pathway. *Nat. Immunol.* 15, 957–964.
- Pan, Y., Tian, T., Park, C.O., Lofftus, S.Y., Mei, S., Liu, X., Luo, C., O'Malley, J.T., Gehad, A., Teague, J.E., et al. (2017). Survival of tissue-resident memory T cells requires exogenous lipid uptake and metabolism. *Nature* 543, 252–256.
- Park, E.J., Lee, J.H., Yu, G.Y., He, G., Ali, S.R., Holzer, R.G., Osterreicher, C.H., Takahashi, H., and Karin, M. (2010). Dietary and genetic obesity promote liver inflammation and tumorigenesis by enhancing IL-6 and TNF expression. *Cell* 140, 197–208.
- Parry, R.V., Chemnitz, J.M., Frauwirth, K.A., Lanfranco, A.R., Braunstein, I., Kobayashi, S.V., Linsley, P.S., Thompson, C.B., and Riley, J.L. (2005). CTLA-4 and PD-1 receptors inhibit T-cell activation by distinct mechanisms. *Mol. Cell. Biol.* 25, 9543–9553.
- Patsoukis, N., Bardhan, K., Chatterjee, P., Sari, D., Liu, B., Bell, L.N., Karoly, E.D., Freeman, G.J., Petkova, V., Seth, P., et al. (2015). PD-1 alters T-cell metabolic reprogramming by inhibiting glycolysis and promoting lipolysis and fatty acid oxidation. *Nat. Commun.* 6, 6692.
- Pearce, E.L., Walsh, M.C., Cejas, P.J., Harms, G.M., Shen, H., Wang, L.S., Jones, R.G., and Choi, Y. (2009). Enhancing CD8 T-cell memory by modulating fatty acid metabolism. *Nature* 460, 103–107.
- Pearce, E.L., Poffenberger, M.C., Chang, C.H., and Jones, R.G. (2013). Fueling immunity: insights into metabolism and lymphocyte function. *Science* 342, 1242454.
- Peng, M., Yin, N., Chhangawala, S., Xu, K., Leslie, C.S., and Li, M.O. (2016). Aerobic glycolysis promotes T helper 1 cell differentiation through an epigenetic mechanism. *Science* 354, 481–484.
- Pérez-Escuredo, J., Dadhich, R.K., Dhup, S., Cacace, A., Van Hée, V.F., De Saedeleer, C.J., Sboarina, M., Rodriguez, F., Fontenille, M.-J., Brisson, L., et al. (2016). Lactate promotes glutamine uptake and metabolism in oxidative cancer cells. *Cell Cycle* 15, 72–83.
- Phan, A.T., Doedens, A.L., Palazon, A., Tyrakis, P.A., Cheung, K.P., Johnson, R.S., and Goldrath, A.W. (2016). Constitutive glycolytic metabolism supports CD8(+) T cell effector memory differentiation during viral infection. *Immunity* 45, 1024–1037.
- Pollizzi, K.N., Sun, I.-H., Patel, C.H., Lo, Y.-C., Oh, M.-H., Waickman, A.T., Tam, A.J., Blosser, R.L., Wen, J., Delgoffe, G.M., and Powell, J.D. (2016). Asymmetric inheritance of mTORC1 kinase activity during division dictates CD8(+) T cell differentiation. *Nat. Immunol.* 17, 704–711.
- Porporato, P.E. (2016). Understanding cachexia as a cancer metabolism syndrome. *Oncogenesis* 5, e200.
- Ramakrishnan, R., Tyurin, V.A., Veglia, F., Condamine, T., Amoscato, A., Mohammadyani, D., Johnson, J.J., Zhang, L.M., Klein-Seetharaman, J., Celis, E., et al. (2014). Oxidized lipids block antigen cross-presentation by dendritic cells in cancer. *J. Immunol.* 192, 2920–2931.
- Rao, S., Schieber, A.M., O'Connor, C.P., Leblanc, M., Michel, D., and Ayres, J.S. (2017). Pathogen-mediated inhibition of anorexia promotes host survival and transmission. *Cell* 168, 503–516.
- Rathinam, V.A., and Fitzgerald, K.A. (2016). Inflammasome complexes: emerging mechanisms and effector functions. *Cell* 165, 792–800.
- Ray, J.P., Staron, M.M., Shyer, J.A., Ho, P.C., Marshall, H.D., Gray, S.M., Laidlaw, B.J., Araki, K., Ahmed, R., Kaech, S.M., and Craft, J. (2015). The interleukin-2-mTORC1 kinase axis defines the signaling, differentiation, and metabolism of T helper 1 and follicular B helper T cells. *Immunity* 43, 690–702.
- Reboldi, A., and Cyster, J.G. (2016). Peyer's patches: organizing B-cell responses at the intestinal frontier. *Immunol. Rev.* 271, 230–245.
- Ribas, A. (2015). Releasing the brakes on cancer immunotherapy. *N. Engl. J. Med.* 373, 1490–1492.
- Rodriguez, P.C., Quiceno, D.G., Zabaleta, J., Ortiz, B., Zea, A.H., Piazuelo, M.B., Delgado, A., Correa, P., Brayer, J., Sotomayor, E.M., et al. (2004). Arginase I production in the tumor microenvironment by mature myeloid cells inhibits T-cell receptor expression and antigen-specific T-cell responses. *Cancer Res.* 64, 5839–5849.
- Ron-Harel, N., Santos, D., Ghergurovich, J.M., Sage, P.T., Reddy, A., Lovitch, S.B., Dephoure, N., Satterstrom, F.K., Sheffer, M., Spinelli, J.B., et al. (2016). Mitochondrial biogenesis and proteome remodeling promote one-carbon metabolism for T cell activation. *Cell Metab.* 24, 104–117.
- Rooks, M.G., and Garrett, W.S. (2016). Gut microbiota, metabolites and host immunity. *Nat. Rev. Immunol.* 16, 341–352.
- Sattiel, A.R., and Olefsky, J.M. (2017). Inflammatory mechanisms linking obesity and metabolic disease. *J. Clin. Invest.* 127, 1–4.
- Scharping, N.E., Menk, A.V., Moreci, R.S., Whetstone, R.D., Dadey, R.E., Watkins, S.C., Ferris, R.L., and Delgoffe, G.M. (2016). The tumor microenvironment represses T cell mitochondrial biogenesis to drive intratumoral T cell metabolic insufficiency and dysfunction. *Immunity* 45, 374–388.
- Scharping, N.E., Menk, A.V., Whetstone, R.D., Zeng, X., and Delgoffe, G.M. (2017). Efficacy of PD-1 blockade is potentiated by metformin-induced reduction of tumor hypoxia. *Cancer Immunol. Res.* 5, 9–16.
- Schultz, O., Oberhauser, F., Saech, J., Rubbert-Roth, A., Hahn, M., Krone, W., and Laudes, M. (2010). Effects of inhibition of interleukin-6 signalling on insulin sensitivity and lipoprotein (a) levels in human subjects with rheumatoid diseases. *PLoS ONE* 5, e14328.
- Sena, L.A., Li, S., Jairaman, A., Prakriya, M., Ezponda, T., Hildeman, D.A., Wang, C.R., Schumacker, P.T., Licht, J.D., Perlman, H., et al. (2013). Mitochondria are required for antigen-specific T cell activation through reactive oxygen species signaling. *Immunity* 38, 225–236.
- Shi, L.Z., Wang, R., Huang, G., Vogel, P., Neale, G., Green, D.R., and Chi, H. (2011). HIF1 α -dependent glycolytic pathway orchestrates a metabolic checkpoint for the differentiation of TH17 and Treg cells. *J. Exp. Med.* 208, 1367–1376.
- Shouval, D.S., Biswas, A., Goettel, J.A., McCann, K., Conaway, E., Redhu, N.S., Mascanfroni, I.D., Al Adham, Z., Lavoie, S., Ibourk, M., et al. (2014). Interleukin-10 receptor signaling in innate immune cells regulates mucosal immune tolerance and anti-inflammatory macrophage function. *Immunity* 40, 706–719.
- Sinclair, L.V., Rolf, J., Emslie, E., Shi, Y.B., Taylor, P.M., and Cantrell, D.A. (2013). Control of amino-acid transport by antigen receptors coordinates the metabolic reprogramming essential for T cell differentiation. *Nat. Immunol.* 14, 500–508.

- Smith, P.M., Howitt, M.R., Panikov, N., Michaud, M., Gallini, C.A., Bohlooly-Y, M., Glickman, J.N., and Garrett, W.S. (2013). The microbial metabolites, short-chain fatty acids, regulate colonic Treg cell homeostasis. *Science* *341*, 569–573.
- Sonveaux, P., Végran, F., Schroeder, T., Wergin, M.C., Verrax, J., Rabbani, Z.N., De Saedeleer, C.J., Kennedy, K.M., Diepart, C., Jordan, B.F., et al. (2008). Targeting lactate-fueled respiration selectively kills hypoxic tumor cells in mice. *J. Clin. Invest.* *118*, 3930–3942.
- Spencer, S.D., Di Marco, F., Hooley, J., Pitts-Meek, S., Bauer, M., Ryan, A.M., Sordat, B., Gibbs, V.C., and Aguet, M. (1998). The orphan receptor CRF2-4 is an essential subunit of the interleukin 10 receptor. *J. Exp. Med.* *187*, 571–578.
- Staron, M.M., Gray, S.M., Marshall, H.D., Parish, I.A., Chen, J.H., Perry, C.J., Cui, G., Li, M.O., and Kaech, S.M. (2014). The transcription factor FoxO1 sustains expression of the inhibitory receptor PD-1 and survival of antiviral CD8(+) T cells during chronic infection. *Immunity* *41*, 802–814.
- Sukumar, M., Liu, J., Ji, Y., Subramanian, M., Crompton, J.G., Yu, Z., Roychoudhuri, R., Palmer, D.C., Muranski, P., Karoly, E.D., et al. (2013). Inhibiting glycolytic metabolism enhances CD8+ T cell memory and antitumor function. *J. Clin. Invest.* *123*, 4479–4488.
- Swamy, M., Pathak, S., Grzes, K.M., Damerow, S., Sinclair, L.V., van Aalten, D.M.F., and Cantrell, D.A. (2016). Glucose and glutamine fuel protein O-GlcNAcylation to control T cell self-renewal and malignancy. *Nat. Immunol.* *17*, 712–720.
- Takeda, K., Clausen, B.E., Kaisho, T., Tsujimura, T., Terada, N., Förster, I., and Akira, S. (1999). Enhanced Th1 activity and development of chronic enterocolitis in mice devoid of Stat3 in macrophages and neutrophils. *Immunity* *10*, 39–49.
- Torres, A., Luke, J.D., Kullas, A.L., Kapilashrami, K., Botbol, Y., Koller, A., Tonge, P.J., Chen, E.I., Macian, F., and van der Velden, A.W. (2016). Asparagine deprivation mediated by Salmonella asparaginase causes suppression of activation-induced T cell metabolic reprogramming. *J. Leukoc. Biol.* *99*, 387–398.
- Tyrakis, P.A., Palazon, A., Macias, D., Lee, K.L., Phan, A.T., Veliça, P., You, J., Chia, G.S., Sim, J., Doedens, A., et al. (2016). S-2-hydroxyglutarate regulates CD8(+) T-lymphocyte fate. *Nature* *540*, 236–241.
- Uyttenhove, C., Pilotte, L., Théate, I., Stroobant, V., Colau, D., Parmentier, N., Boon, T., and Van den Eynde, B.J. (2003). Evidence for a tumoral immune resistance mechanism based on tryptophan degradation by indoleamine 2,3-dioxygenase. *Nat. Med.* *9*, 1269–1274.
- van der Windt, G.J., Everts, B., Chang, C.H., Curtis, J.D., Freitas, T.C., Amiel, E., Pearce, E.J., and Pearce, E.L. (2012). Mitochondrial respiratory capacity is a critical regulator of CD8+ T cell memory development. *Immunity* *36*, 68–78.
- Verbist, K.C., Guy, C.S., Milasta, S., Liedmann, S., Kamiński, M.M., Wang, R., and Green, D.R. (2016). Metabolic maintenance of cell asymmetry following division in activated T lymphocytes. *Nature* *532*, 389–393.
- Vesely, M.D., and Schreiber, R.D. (2013). Cancer immunoeediting: antigens, mechanisms, and implications to cancer immunotherapy. *Ann. N Y Acad. Sci.* *1284*, 1–5.
- Vuillefroy de Sully, R., Dietrich, P.-Y., and Walker, P.R. (2016). Hypoxia and antitumor CD8(+) T cells: An incompatible alliance? *Oncolmunology* *5*, e1232236.
- Wang, R., Dillon, C.P., Shi, L.Z., Milasta, S., Carter, R., Finkelstein, D., McCormick, L.L., Fitzgerald, P., Chi, H., Munger, J., and Green, D.R. (2011). The transcription factor Myc controls metabolic reprogramming upon T lymphocyte activation. *Immunity* *35*, 871–882.
- Wang, C., Yosef, N., Gaublot, J., Wu, C., Lee, Y., Clish, C.B., Kaminski, J., Xiao, S., Meyer Zu Horste, G., Pawlak, M., et al. (2015). CD5L/AIM regulates lipid biosynthesis and restrains Th17 cell pathogenicity. *Cell* *163*, 1413–1427.
- Wang, A., Huen, S.C., Luan, H.H., Yu, S., Zhang, C., Gallezot, J.D., Booth, C.J., and Medzhitov, R. (2016a). Opposing effects of fasting metabolism on tissue tolerance in bacterial and viral inflammation. *Cell* *166*, 1512–1525.
- Wang, Y., Bi, Y., Chen, X., Li, C., Li, Y., Zhang, Z., Wang, J., Lu, Y., Yu, Q., Su, H., et al. (2016b). Histone deacetylase SIRT1 negatively regulates the differentiation of interleukin-9-producing CD4(+) T cells. *Immunity* *44*, 1337–1349.
- Wegrzyn, J., Potla, R., Chwae, Y.J., Sepuri, N.B., Zhang, Q., Koeck, T., Derecka, M., Szczepanek, K., Szelag, M., Gornicka, A., et al. (2009). Function of mitochondrial Stat3 in cellular respiration. *Science* *323*, 793–797.
- Wenes, M., Shang, M., Di Matteo, M., Goveia, J., Martín-Pérez, R., Serneels, J., Prenen, H., Ghesquière, B., Carmeliet, P., and Mazzone, M. (2016). Macrophage metabolism controls tumor blood vessel morphogenesis and metastasis. *Cell Metab.* *24*, 701–715.
- Wherry, E.J., and Kurachi, M. (2015). Molecular and cellular insights into T cell exhaustion. *Nat. Rev. Immunol.* *15*, 486–499.
- Wilhelm, C., Harrison, O.J., Schmitt, V., Pelletier, M., Spencer, S.P., Urban, J.F., Jr., Ploch, M., Ramalingam, T.R., Siegel, R.M., and Belkaid, Y. (2016). Critical role of fatty acid metabolism in ILC2-mediated barrier protection during malnutrition and helminth infection. *J. Exp. Med.* *213*, 1409–1418.
- Woodland, R.T., Fox, C.J., Schmidt, M.R., Hammerman, P.S., Opferman, J.T., Korsmeyer, S.J., Hilbert, D.M., and Thompson, C.B. (2008). Multiple signaling pathways promote B lymphocyte stimulator dependent B-cell growth and survival. *Blood* *111*, 750–760.
- Yang, W., Bai, Y., Xiong, Y., Zhang, J., Chen, S., Zheng, X., Meng, X., Li, L., Wang, J., Xu, C., et al. (2016). Potentiating the antitumor response of CD8(+) T cells by modulating cholesterol metabolism. *Nature* *537*, 651–655.
- Youn, Y.H., Nguyen, K.Y., Grant, R.W., Goldberg, E.L., Bodogai, M., Kim, D., D'Agostino, D., Planavsky, N., Lupfer, C., Kanneganti, T.D., et al. (2015). The ketone metabolite β -hydroxybutyrate blocks NLRP3 inflammasome-mediated inflammatory disease. *Nat. Med.* *21*, 263–269.
- Zeng, H., Cohen, S., Guy, C., Shrestha, S., Neale, G., Brown, S.A., Cloer, C., Kishton, R.J., Gao, X., Youngblood, B., et al. (2016). mTORC1 and mTORC2 kinase signaling and glucose metabolism drive follicular helper T cell differentiation. *Immunity* *45*, 540–554.
- Zhao, E., Maj, T., Kryczek, I., Li, W., Wu, K., Zhao, L., Wei, S., Crespo, J., Wan, S., Vatan, L., et al. (2016). Cancer mediates effector T cell dysfunction by targeting microRNAs and EZH2 via glycolysis restriction. *Nat. Immunol.* *17*, 95–103.
- Zhou, X., Yu, S., Zhao, D.M., Harty, J.T., Badovinac, V.P., and Xue, H.H. (2010). Differentiation and persistence of memory CD8(+) T cells depend on T cell factor 1. *Immunity* *33*, 229–240.
- Zigmond, E., Bernshtein, B., Friedlander, G., Walker, C.R., Yona, S., Kim, K.W., Brenner, O., Krauthgamer, R., Varol, C., Müller, W., and Jung, S. (2014). Macrophage-restricted interleukin-10 receptor deficiency, but not IL-10 deficiency, causes severe spontaneous colitis. *Immunity* *40*, 720–733.

Go figure

With author-narrated animations



Introducing Figure360, an author-narrated animation of select figures in Cell Press primary research and review journals.

A short, digestible synopsis puts the figure in context and helps you zoom in on the most important take-home message in a matter of minutes. Why go it alone when the author can help you figure it out in less than half the time?

Check it out at www.cell.com/figure360

Figure360

CellPress

Putting p53 in Context

Edward R. Kasthuber^{1,2} and Scott W. Lowe^{1,3,*}

¹Department of Cancer Biology and Genetics, Sloan Kettering Institute, Memorial Sloan Kettering Cancer Center, New York, NY 10065, USA

²Louis V. Gerstner Jr. Graduate School of Biomedical Sciences, Memorial Sloan Kettering Cancer Center, New York, NY 10065, USA

³Howard Hughes Medical Institute, New York, NY 10065, USA

*Correspondence: lowes@mskcc.org

<http://dx.doi.org/10.1016/j.cell.2017.08.028>

***TP53* is the most frequently mutated gene in human cancer. Functionally, p53 is activated by a host of stress stimuli and, in turn, governs an exquisitely complex anti-proliferative transcriptional program that touches upon a bewildering array of biological responses. Despite the many unveiled facets of the p53 network, a clear appreciation of how and in what contexts p53 exerts its diverse effects remains unclear. How can we interpret p53's disparate activities and the consequences of its dysfunction to understand how cell type, mutation profile, and epigenetic cell state dictate outcomes, and how might we restore its tumor-suppressive activities in cancer?**

p53: The Textbook View

p53 was discovered during the peak of tumor virus research as a 53 kD host protein bound to simian virus 40 large T antigen in virally transformed cells (Lane and Crawford, 1979; Linzer and Levine, 1979). First classified as an oncogene, subsequent work established that wild-type p53, encoded by *TP53*, suppresses growth and oncogenic transformation in cell culture (Finlay et al., 1989) and that inactivating *TP53* mutations are common in human tumors (Baker et al., 1990). In many cancers, *TP53* mutation is linked to poor patient prognosis (Olivier et al., 2010). Consistent with its action as a tumor suppressor, *TP53* mutations are a hallmark of a hereditary cancer predisposition disorder known as Li-Fraumeni syndrome (Malkin et al., 1990), and *Trp53* knockout mice develop tumors at high penetrance (Donehower et al., 1992).

p53 is a sequence-specific DNA binding protein that regulates transcription (reviewed in Laptenko and Prives, 2006). The p53 protein consists of two N-terminal transactivation domains followed by a conserved proline-rich domain, a central DNA binding domain, and a C terminus encoding its nuclear localization signals and an oligomerization domain needed for transcriptional activity. Consistent with the importance of p53-mediated transcription in tumor suppression, the vast majority of tumor-derived *TP53* mutations occur in the region encoding p53's DNA binding domain. In normal cells, p53 protein is maintained at low levels by a series of regulators including *MDM2*, which functions as a p53 ubiquitin ligase to facilitate its degradation (Haupt et al., 1997; Honda et al., 1997; Kubbutat et al., 1997). However, p53 is stabilized in response to various cellular stresses, including DNA damage and replication stress produced by deregulated oncogenes. Mechanisms leading to p53 activation can be stimulus dependent: for example, DNA damage promotes p53 phosphorylation, blocking *MDM2*-mediated degradation (Shieh et al., 1997), whereas oncogenic signaling induces the ARF tumor suppressor to inhibit *MDM2* (Pomerantz et al., 1998; Quelle et al., 1995; Zhang et al., 1998).

The best-understood functions of p53 focus on its ability to promote cell cycle arrest and apoptosis. Indeed, seminal

studies from the early 1990s showed that p53 is crucial for a reversible DNA damage-induced G1 phase checkpoint (Kastan et al., 1991) that is mediated, in part, by its ability to transcriptionally activate the p21 cyclin-dependent kinase inhibitor gene (el-Deiry et al., 1993; Harper et al., 1993), presumably facilitating DNA repair prior to further cell division. In some circumstances, p53 induces cellular senescence, a stable if not permanent cell cycle arrest program that also involves the retinoblastoma (RB) gene product (Serrano et al., 1997; Shay et al., 1991). p53 can also promote apoptosis (Clarke et al., 1993; Lowe et al., 1993; Yonish-Rouach et al., 1991), relying on the induction of pro-apoptotic BCL-2 family members whose action facilitates caspase activation and cell death (Miyashita et al., 1994). Why p53 promotes cell cycle arrest in some cell types and apoptosis in others is incompletely understood (see below).

The settings in which p53 can be activated to arrest or eliminate pre-malignant cells have guided current thinking as to why p53 is such a potent tumor suppressor. On one hand, its ability to arrest or eliminate cells after DNA damage suggests that it might prevent cancer by preventing the *accumulation* of oncogenic mutations (Livingstone et al., 1992; Yin et al., 1992). In this model, p53 loss indirectly promotes cancer by increasing the number of mutations in surviving daughter cells. On the other hand, the ability of p53 to halt the proliferation in response to aberrant oncogene expression suggests a role in limiting the *consequences* of oncogenic mutations. Here, p53 loss directly enables cancer development by allowing oncogene-expressing cells to proliferate unabated, explaining why *TP53* mutations cooperate with oncogenes in transformation (Lowe et al., 1994; Serrano et al., 1997). In both models, p53 acts as the “guardian of the genome” to limit the deleterious consequences of mutation (Lane, 1992). Although this historic view provides a basic conceptual framework as to why *TP53* mutations are so common in human tumors, more recent work paints a much more nuanced picture of p53 action that highlights its context-dependent regulation and the broadly diverse consequences of its activation.

Revisiting the Guardian of the Genome

Upon DNA damage, p53 is activated to promote either the elimination or repair of damaged cells, ultimately reducing their risk of propagating mutations. DNA damage response (DDR) kinases phosphorylate p53, driving cell-cycle arrest, senescence, or apoptosis (reviewed in Williams and Schumacher, 2016). Additionally, p53 stimulates DNA repair by activating target genes that encode components of the DNA repair machinery, and p53-null cells are defective in certain DNA repair activities *in vitro* (Williams and Schumacher, 2016).

While *TP53* mutation can correlate with patterns of single-nucleotide variants and specific co-mutated genes, what is striking is that the association between *TP53* mutation and copy-number variation (CNV) is strong and universal in a pan-cancer analysis (Ciriello et al., 2013). Also, cancers harboring *TP53* mutations are typically aneuploid, with gross changes in numbers of whole chromosomes (Ciriello et al., 2013). Various biological explanations for this association have been proposed, but one mechanism contributing to this relationship is the ability of p53 to regulate processes in G2/M transitions (reviewed in Vitre and Cleveland, 2012). For example, p53 loss dysregulates the spindle assembly checkpoint by derepressing MAD2, leading to an increased rate of chromosome missegregation and tetraploidization (Schvartzman et al., 2011). In the context of tetraploid cells, p53 loss leads to an increased rate of multipolar mitoses and subsequent chromosome missegregation (Vitale et al., 2010).

In an alternative but non-mutually exclusive explanation, p53 can restrict chromosomal instability through its ability to cull cells at risk of aberrant mitoses, particularly following centrosome amplification and/or telomere dysfunction (Eischen, 2016; Lanni and Jacks, 1998). Extra centrosomes lead to Hippo pathway upregulation that, in turn, activates p53 by inhibiting MDM2 (Aylon et al., 2006; Ganem et al., 2014). Accordingly, *TP53* mutations are also associated with whole genome doubling events in human tumors (Dewhurst et al., 2014). Additional studies suggest that p53-deficient cells are better at tolerating proteomic stress produced by aberrant gene dosage (Tang et al., 2011), yet others suggest that p53-mediated culling of aneuploid cells is more efficient against structural aneuploidy than whole chromosome imbalances, implicating the role of DDR in response to chromosome shearing (Soto et al., 2017). Hence, it appears that the absence of p53 both facilitates the accumulation and permits the survival of aneuploid cells.

p53 also appears to suppress a particular type of chromosome shattering and rearrangement event known as chromothripsis. Cells that bypass replicative senescence after p53 and RB inactivation can proliferate despite telomere erosion (Hayashi et al., 2012). Failing this checkpoint, telomere dysfunction initiates chromosome breakage-fusion-bridge cycles that contribute to chromothripsis (Maciejowski et al., 2015). Although the extent to which chromothripsis fosters tumorigenesis remains an open question, the phenomenon is significantly more prevalent in tumors harboring *TP53* mutations (Rausch et al., 2012).

An unanticipated way in which p53 helps maintain genomic integrity is by suppressing the mobilization of retrotranspo-

sons, which are latent virus-derived genetic elements whose aberrant expression can lead to mutagenesis through their mobilization and re-insertion throughout the genome (reviewed in Levine et al., 2016). Experimental activation of mobile elements in *Drosophila* induces DNA double-strand breaks and p53-mediated apoptosis (Wylie et al., 2014) that could, in principle, reduce their mutagenic effects. However, the association between p53 mutation and retrotransposon expression is more than simply a culling effect: indeed, p53 binding to target sites within LINE elements and other transposon sequences are associated with their downregulation (Chang et al., 2007). p53-mediated repression is dependent on epigenetic silencing of retrotransposon loci and not apoptosis, and derepressed retrotransposons are competent for reintegration into the genome (Leonova et al., 2013; Wylie et al., 2016), promoting mutagenesis (Tubio et al., 2014). Genomic analyses have revealed that retrotransposon mobilization is common in human cancers (Ting et al., 2011; Tubio et al., 2014). While the precise impact remains to be determined, there is a significant association between repetitive element expression and p53 status in mouse and human tumors (Wylie et al., 2016).

The immediacy with which p53 cooperates with oncogenes to transform cells indicates that genomic instability is not absolutely required for tumor initiation (Lowe et al., 1994; Serrano et al., 1997). Still, the genomic instability fueled by p53 loss enables acquisition of additional driver events with the potential to accelerate transformation, metastasis, and drug resistance (reviewed in McGranahan and Swanton, 2017). Just as species diversity in an ecosystem is associated with its robustness, subclonal diversity, not the total number of mutations in a tumor, dictates the resilience of a cancer cell population to changing conditions and challenges. In this regard, p53 inactivation may be unique in its ability to both promote genomic instability (by increasing the rate of new variants) and permit the survival of a wider pool of genetic configurations (decreasing the likelihood of extinction of variants). Together, these observations raise the possibility that p53 inactivation contributes to intratumoral heterogeneity.

p53 Controls a Broad and Flexible Network

As if regulating genome integrity, cell cycle arrest, and apoptosis were not enough functions for a single gene, an ever-growing body of work suggests that p53 also controls additional “non-canonical” programs that contribute to its effects (Figure 1). As examples, p53 can modulate autophagy, alter metabolism, repress pluripotency and cellular plasticity, and facilitate an iron-dependent form of cell death known as ferroptosis (reviewed in Aylon and Oren, 2016). Even basal levels of p53 can reinforce multiple other tumor suppressive networks (Pappas et al., 2017). Given extensive past research, it is surprising that there is no clear and simple answer to the question of what exactly p53 does and how. Nevertheless, a take-home message is that the p53 response is remarkably flexible and depends on the cell type, its differentiation state, stress conditions, and collaborating environmental signals.

The varied functions of p53 are anchored in its ability to control distinct sets of its many target genes (Figure 1). For example,

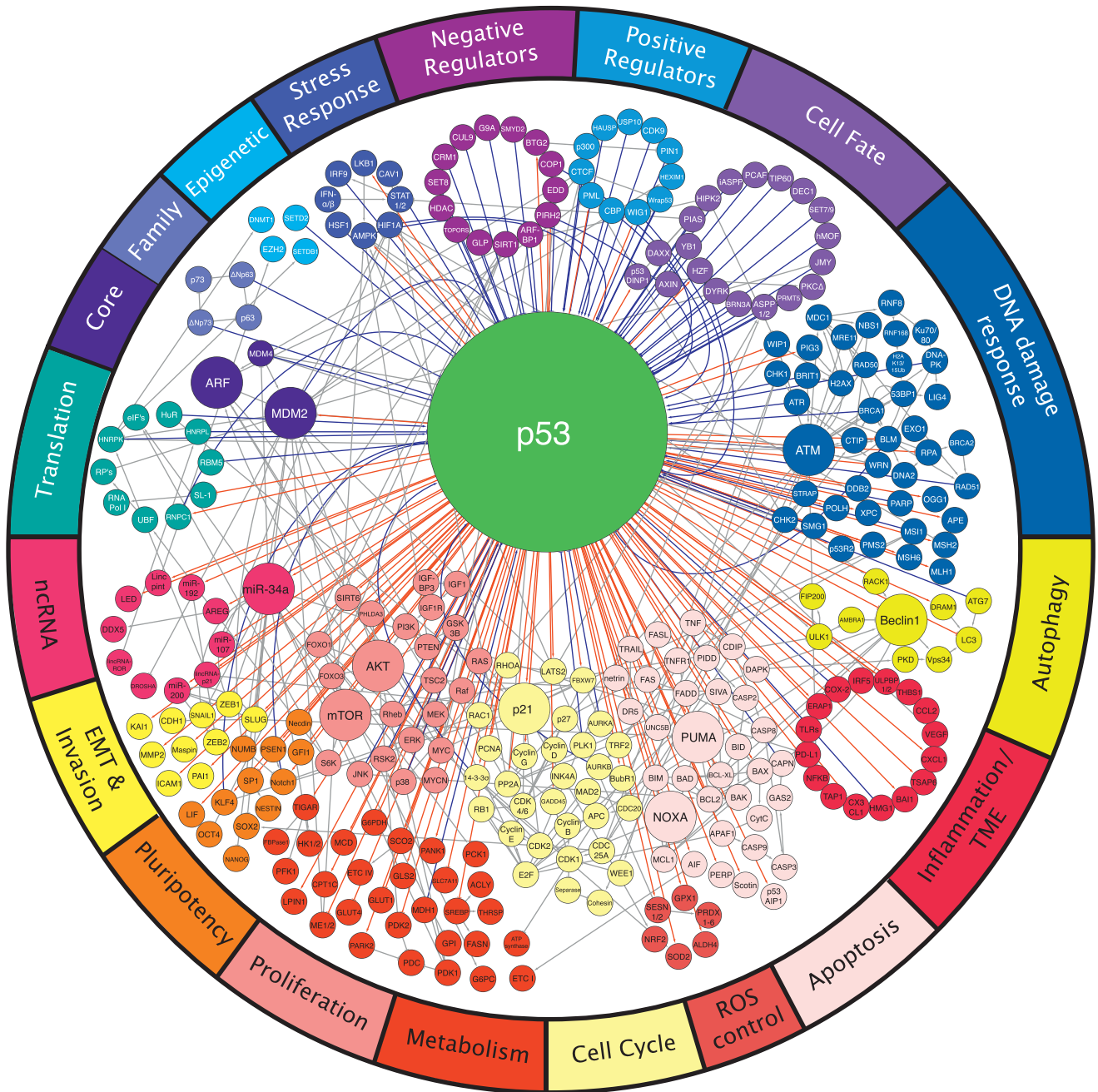


Figure 1. The p53 Network

A wide variety of regulators govern the activity of p53 (top), which, in turn, controls many distinct biological processes (bottom). Each node represents a gene and each line represents an interaction. Direct p53 inputs are indicated as blue lines and direct p53 outputs are indicated as red lines. Noticeably, p53 controls effector processes by activating multiple target genes. Downstream pathways are highly interconnected (gray lines). Interactions are annotated as positive (arrow), negative (T-bar), or modifying (solid circle).

observations that cell cycle arrest and apoptosis are associated with upregulation of p21 or pro-apoptotic Bcl-2 proteins, respectively, obscure the fact that the global transcriptional response to p53 activation includes many other potential modifiers of outcome. Historically, genes have been implicated as p53 targets if p53 binds the locus and the mRNA is induced. More recently,

Global Run-On Sequencing has improved specificity by enabling detection of nascent transcripts induced upon p53 activation (Allen et al., 2014). The nature of p53 targets identified in this analysis provides strong confirmation that non-canonical processes including ROS control, tissue remodeling, autophagy, and metabolism are bona fide processes controlled by p53 (Figure 1).

Efforts to identify a universal set of p53 target genes have invariably failed. Meta-analyses from 16 genome-wide datasets revealed that only about 60 genes were implicated as common targets (Fischer, 2017). It is noteworthy that these surveys involved a restricted number of different cell types and employed distinct methods for p53 induction. However, a central theme is that cellular context and various stimuli incite transcription of qualitatively different sets of genes, not just different levels of the same set of genes. It seems naive to expect that oncogene activation in different tissues (for example, KRAS activation in colon, pancreas, and lung) would precipitate an identical p53 transcriptional response. Moreover, one would not presume *a priori* that the p53 output generated by DNA damage would exactly mirror the gene expression signature elicited by oncogene activation, even in a single cell type. Despite data indicating that p53 can, in principle, control a wide variety of biological processes (reviewed in Olivos and Mayo, 2016), the physiological settings in which one or more processes predominate are incompletely understood and deserve more systematic study.

Cellular metabolism is one non-canonical p53-controlled process that has received much attention (reviewed in Kruiswijk et al., 2015). The collection of metabolic target genes controlled by p53 affect many individual processes: p53 is reported to increase glutamine catabolism, support anti-oxidant activity, downregulate lipid synthesis, increase fatty acid oxidation, and stimulate gluconeogenesis (Kruiswijk et al., 2015). Depending on the cell type, p53 can also have opposing effects on the same metabolic processes. For example, in breast and lung cancer cells, p53 inhibits glycolysis by attenuating glucose uptake (Zhang et al., 2013) or repressing the expression of glycolytic enzymes (Kim et al., 2013). By contrast, in muscle cells, p53 induces glycolytic enzymes (Kruiswijk et al., 2015). Likewise, p53 typically increases (Stambolsky et al., 2006) but can also restrict (Jiang et al., 2013; Wang et al., 2013) flux through the tricarboxylic acid (TCA) cycle. Taken at face value, these results imply that p53 can regulate different aspects of metabolism that produce distinct, or even opposite, biochemical and phenotypic outcomes. Here again, specific contextual factors have yet to be identified.

While it is often assumed that each p53 effector function is a standalone process, there is increasing evidence that cross-talk between separate input and output pathways is more important than previously recognized (Figure 1, gray lines). For example, p53-driven cellular senescence may be supported by activation of autophagy (Young et al., 2009). Alterations in p53 control of metabolism undoubtedly contribute to apoptosis, autophagy, and ferroptosis (Gao et al., 2016). In some settings, p53-mediated processes can apparently be antagonistic: autophagy has the potential to delay apoptosis by reducing levels of PUMA (Thorburn et al., 2014). However, in contexts where p53 fails to repress glycolysis, autophagy is not efficiently engaged and apoptosis is favored (Duan et al., 2015). In these examples, interaction between distinct *biochemical processes* controlled by p53 elicits different *biological outcomes*.

The mechanistic basis underlying the ability of p53 to induce different biological outputs remains unclear. On one hand, p53 can induce *qualitatively* different programs that produce different

biological outcomes depending on cell type and stimulus. One proposed mechanism for qualitatively modulating biological p53's effects involves stimulus-dependent post-translational modifications (PTMs) that can alter p53 affinity for different target genes; for example, phospho-p53 (S46) or acetyl-p53 (K120) stimulates apoptosis, whereas PRMT5-methylated p53 activates p21 more readily than apoptotic genes (reviewed in Kumari et al., 2014). Additionally, PTMs such as SUMOylation, glycosylation, and prolyl isomerization occurring throughout the p53 protein can modify protein stability, and also influence target gene bias (Kumari et al., 2014). Moreover, one post-translational modification may enhance acquisition of another, unlocking additional layers of regulation of protein stability, protein-protein interaction, and biasing DNA binding toward select target genes.

p53 induction can yield either a steady signaling output or one that can oscillate in discrete waves; remarkably, the kinetics of its expression, independent of maximal p53 protein levels, can determine cell fate in response to genotoxic stress (reviewed in Stewart-Ornstein and Lahav, 2017). p53 activation kinetics can be translated into target gene bias owing to differences in p53 binding and dissociation rates at distinct target loci. Here, the p21 promoter is sensitive to short pulses of p53 activity whereas the pro-apoptotic p53 target FAS is not; consequently, a short pulse drives proliferative arrest but a sustained signal induces apoptosis (Espinosa et al., 2003; Gomes and Espinosa, 2010a; Morachis et al., 2010). Perhaps certain p53-driven stress responses instigate a short-term repair and salvage program that, if necessary, reaches a tipping point that progresses to cellular self-destruction.

On the other hand, several factors influence how the cell *interprets* p53 activation. For instance, cell lineage may be a large determinant in the nature of a hypothetical tipping point between alternative cell fates. First, cell-type- and -state-specific chromatin modifications may make particular genes more or less accessible to p53 transactivation (Su et al., 2015). For instance, CTCF insulates the *PUMA* locus from repressive histone modifications under certain conditions, governing whether PUMA is expressed and apoptosis occurs (Gomes and Espinosa, 2010b). In embryonic stem cells (ESCs), p53 can be induced to bind to the p21 promoter, but p21 is not efficiently activated, dependent on cell-type-specific repressive histone H3K27me3 marks at the locus (Itahana et al., 2016). Second, the p53 target spectrum can be altered by cooperation or antagonism with other transcription factors, such as FOXO and NF- κ B, whose levels and occupancy are also context dependent (Cooks et al., 2014; Eijkelenboom and Burgering, 2013). Finally, the same transcriptional output may have different effects depending on the state of the cell. ATM signaling protects cells from p53-mediated apoptosis, not by changing p53-driven transcriptional output but by blocking autophagy, thus maintaining mitochondrial homeostasis and suppressing ROS levels (Sullivan et al., 2015).

Collectively, these observations imply that p53 response is not merely an "on-off" switch; to the contrary, cell fate is a result of a rich palette of p53-driven stress responses. Clearly, p53 is embedded in a densely populated and interconnected network of regulators and effectors (Figure 1) that permit a flexible p53

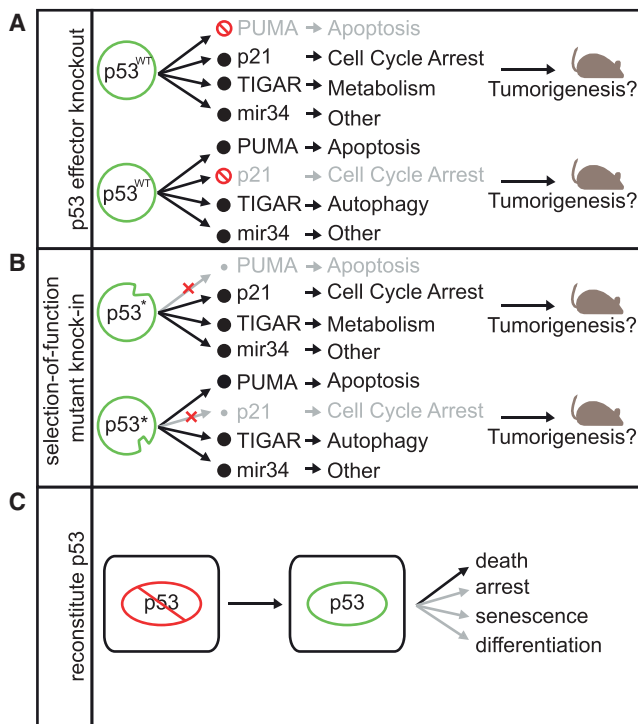


Figure 2. Investigating Mechanisms of Tumor Suppression

Defining the mechanism of p53-mediated tumor suppression has been interrogated in several ways: (A) knocking out p53 target genes and assessing tumor formation, (B) mutating p53 itself, such that it can activate some targets but not others, and (C) reconstituting p53 in p53-deficient cancer and determining the cell fate.

response coordinated to fit cell type and conditions at the time of activation. In short, cellular context (cell type, epigenetic state, tissue microenvironment, activating signal) is central to both the biochemical aspects of p53 activity as well as the biological outcome of a p53 response.

Putting Tumor Suppression in Context

By definition, tumor-suppressor genes regulate processes that limit inappropriate cell expansion and whose inactivation facilitates tumor initiation or progression. Given the many processes that p53 controls, which of its effector functions are critical for tumor suppression has been the topic of much debate. Senescence and apoptosis can clearly be detected in tumors and when these processes are activated, they are certainly tumor suppressive. Still, a recent body of work suggests that apoptosis and senescence can be dispensable for tumor suppression and that, in some settings, other non-canonical p53 functions may be more critical (Valente et al., 2013). There is no consensus view on which p53-dependent process is most important.

The only relevant metric of “tumor suppression” is whether a gene impairs the onset or progression of tumors arising *in vivo*. In this regard, the p53 knockout mouse is a powerful model that develops thymic lymphoma (and sometimes sarcoma) at complete penetrance (Donehower et al., 1992). To address which p53 function(s) is crucial for tumor suppression, mutant strains have been produced in an attempt to isolate specific

p53 functions and the resulting animal cohorts monitored for tumors over time. If the ablation of a p53-driven function allows for tumorigenesis, the underlying process is crucial for the tumor-suppressive activity of p53. If it does not, it is deemed dispensable. However, it bears consideration that thymic lymphoma rarely occurs in people, including Li-Fraumeni patients, so the requirements for suppressing this unusual cancer do not necessarily extend to other systems.

One line of investigation has compared tumor onset and pathology between mice harboring knockouts of p53 target genes versus p53 itself (Figure 2A). For example, mice deficient for p21, Puma, and Noxa do not develop thymic lymphoma, hinting that p53-mediated cell cycle arrest and apoptosis might be dispensable for tumor suppression (Valente et al., 2013). Still, p53 target genes may already be expressed at basal levels so, for example, p53-null cells are by no means p21 null. Consequently, this approach could *overestimate* the contribution of a particular p53 effector to the null phenotype. Conversely, since multiple effectors mediate most p53 outputs, mouse strains deficient for individual p53 effector genes do not fully disable the associated p53 effector program (e.g., p21 loss does not completely disable p53-mediated cell cycle arrest). Hence, this approach may *underestimate* the contribution of the targeted process to tumor suppression. Changes in feedback loops and compensatory mechanisms arising as a consequence of manipulating the pathway may further complicate the interpretation of such studies (Sullivan et al., 2012).

Another approach isolates p53 effects through separation-of-function mutants that selectively retain or lose the ability to regulate certain subsets of p53 target genes and activities (Figure 2B). For example, the tumor-derived $p53^{R175P}$ and $p53^{E180R}$ alleles show defects in apoptosis while retaining the capability to provoke cell cycle arrest, so that mice harboring the equivalent mutations display extended tumor-free survival compared to p53-null animals (Liu et al., 2004). Furthermore, the tumors that do arise in these mice exhibit far less CIN than p53-null tumors, indicating that different p53 mutants may impinge selectively on downstream effector pathways (Liu et al., 2004). Alternatively, engineered structure-function mutants that disrupt p53 transcriptional domains or are defective in being acetylated can separate key p53 functions, at least *in vitro* (Jiang et al., 2015). While these studies reinforce the importance of p53-mediated transcription for tumor suppression (Brady et al., 2011; Jiang et al., 2011), they do not pinpoint a single key process (Jiang et al., 2015).

Although such structure-function approaches are compelling, they also have caveats. Mutant p53 proteins can be more or less stable than the wild-type protein (Brady et al., 2011) and thus differential phenotypes may reflect quantitative as well as qualitative effects. Most structure-function mutants have been characterized in only a limited number of cell types, and given context dependencies, it cannot be assumed that these results extrapolate to tumorigenesis in all tissues. Perhaps these caveats explain why technically sound studies have failed to converge on a common mechanism or theme.

Several studies have circumvented the issues surrounding the manipulation of individual functions peripheral to p53: rather than measuring tumor onset upon p53 loss, they instead take

advantage of mouse strains harboring “switchable” p53 alleles to reawaken endogenous p53 in established tumors (Figure 2C). In all situations examined, p53 restoration produces a marked anti-tumor response, the nature of which depends on the model employed (Martins et al., 2006; Ventura et al., 2007; Xue et al., 2007). In Myc-expressing B cell lymphomas, this response is massive apoptosis; in liver carcinomas and sarcomas, the response is senescence. In other contexts, p53 reactivation can trigger cellular differentiation and a loss of self-renewal (Messina et al., 2012). Although the consequences of p53 reactivation in an established cancer may not reflect the same processes lost during tumorigenesis, these studies reinforce the notion that the p53 response varies depending on context.

So then, what are the most important p53 activities needed for tumor suppression? Certainly, the above caveats preclude generalities without considering context specificity. Indeed, the importance of context is readily observed in mouse studies demonstrating that Puma suppression approaches p53 loss in driving Myc-induced lymphomagenesis but not in promoting thymic lymphoma (Garrison et al., 2008; Hemann et al., 2004). Embracing this notion should enable the identification of tumor-specific modes of tumor suppression and pave the way for restoring the most relevant p53 functions in individual tumors.

The Origins of p53

How and why did the p53 network evolve? Most tumors arise after reproductive age, implying that *TP53* did not evolve to prevent cancer. Moreover, given the diverse outputs of the p53 network, it seems surprising that neonatal p53-null mice seem initially normal. Genes that resemble *TP53* by sequence similarity and induction by DNA damage are found in simple invertebrates (including choanoflagellates, sea anemone, and worms) that are not susceptible to cancer (Lane et al., 2010a, 2010b; Pearson and Sánchez Alvarado, 2010). Like mammalian p53, these genes induce apoptosis in response to stress but, in contrast, are expressed principally in germline stem cells. Perhaps protection of the germline is central and evolved further to suppress tumors in the soma at advanced age (Wylie et al., 2014).

Beyond the germline, a closer look at p53 and the consequences of its disruption indicate that it has important roles in embryonic development. Fundamentally, multicellularity is a compromise among the cells of complex organisms. The most proliferative individuals outcompete populations of single-cell organisms, while multicellular organisms require cellular cooperation, at the expense of competition, to maintain coordinated, specialized functions. The need for cooperation starts in embryonic development, where p53 restricts expansion of individual “cheater” cells, observed in chimeric blastocysts upon p53 knockdown (Dejosez et al., 2013) and following positive selection of spontaneous *TP53* mutations detected in commonly used human ES lines (Merkle et al., 2017). Tight regulation of DNA methylation by DNMT and TET family enzymes requires p53 and it appears that epigenetic disorder contributes to this clonal heterogeneity in p53-deficient ESC colonies (Tovy et al., 2017). Inactivation of p53 rescues cultured cells from apoptosis caused by DNMT1 deficiency and subsequent genomic demethylation,

supporting the notion that p53 can sense and respond to perturbations in the epigenome (Jackson-Grusby et al., 2001).

Other than its familiar role in restricting inappropriate clonal outgrowth, p53 also regulates target genes that fulfill specific biological requirements in development, such as LIF, which is required for efficient mammalian embryo implantation (Feng et al., 2011). *Trp53* knockout mice exhibit a variety of low-penetrance tissue-specific developmental abnormalities in the neural tube, eyes, and testes (Danilova et al., 2008). p53 orthologs in more primitive species can also exhibit conserved non-canonical p53 functions, such as promoting redox control and survival (reviewed in Aylon and Oren, 2016). Moreover, the ortholog Lvp53 is expressed in the soma in shrimp, where cross-talk with NF- κ B eliminates virally infected cells and activates innate immunity (Li et al., 2017). Such observations are consistent with a role for the p53 family in promoting cell survival or fighting infection. Hence, the p53 network evolved diverse physiological roles prior to its implementation for tumor suppression.

TP53 is a member of a broader gene family that includes *TP63* and *TP73* that have diverse and complementary roles. *TP53* of higher eukaryotes diverged from *TP63/TP73* sometime before the appearance of sharks (Lane et al., 2011). Since splitting from its homologs, *TP53* and its network have acquired tumor-suppressive capabilities not shared by *TP63/TP73*, which display even clearer ties to embryonic development (reviewed in Belyi et al., 2010). Triple p53/p63/p73 knockout mice demonstrate that the p53 family is required for mesendodermal differentiation (Wang et al., 2017), exemplifying how p53 can interact with p63/p73 in redundant or cooperative ways. It seems likely that compensation between p53 family members has masked other roles for p53 during development.

Although the p53 protein sequence itself is relatively conserved in higher eukaryotes, domains involved in p53 regulation on the N and C termini (Lane et al., 2011) as well as the downstream p53 response are under continued evolutionary pressure. Indeed, many p53 response elements exhibit surprisingly low conservation with respect to other transcription factor recognition sites (Horvath et al., 2007; Su et al., 2015). Another way in which the p53 network has evolved is by increasing gene dosage. That elephants have acquired up to 20 *TP53* retrogenes may explain, at least in part, how an animal with such a large body size and relative longevity is not subject to high cancer risk (Abeglen et al., 2015; Sulak et al., 2016). A more detailed exploration of the factors selected and counter-selected in p53 biology over evolutionary time has the potential to provide insight into the biological processes critical for tumor suppression.

There is substantial evidence that p53 has additional functions in non-pathological tissue homeostasis. One illustrative example is that p53 function appears to be intertwined with stem cell biology and differentiation in the soma of higher organisms. p53 restricts cellular self-renewal in various stem and progenitor cells, especially those subject to oncogenic stress (Friedmann-Morvinski et al., 2012; Tosoni et al., 2015; Tschaharganeh et al., 2014; Zhao et al., 2010). *Trp53*-null mice consequently have expanded numbers of tissue-specific stem cells, highlighting its importance in maintaining tissue homeostasis (Bondar and Medzhitov, 2010; Liu et al., 2009). p53 limits cellular plasticity (governing transition between cell states) and, at its

extreme, the ability of somatic cells to undergo epigenetic reprogramming into induced pluripotent stem cells (Olivos and Mayo, 2016). The iPS-promoting factors KLF4 and Oct4 repress p53, and conversely, p53 activity antagonizes the efficiency of iPS cell reprogramming (Menendez et al., 2010).

An application of the above principles can be seen in tissue regeneration and the wound-healing response, which is a complex process involving waves of inflammation, angiogenesis, tissue regeneration, extracellular matrix (ECM) remodeling, and fibrosis to prevent infection and resolve tissue damage. During an initial proliferative phase of regeneration, mitogens are activated and p53 must be suppressed to allow tissue remodeling (Charni et al., 2017). By triggering cellular senescence, p53 promotes the release of secretory factors that allow resolution of fibrosis (Krizhanovsky et al., 2008) and coordinate ECM remodeling (Ritschka et al., 2017). Of note, the requirement for p53 to regulate plasticity appears to be evolutionarily conserved, which requires the coordinated suppression and derepression of p53 during salamander limb regeneration (Yun et al., 2013).

It is intriguing that the physiological and developmental functions of p53 are intertwined with the cancer-associated phenotype of p53 loss. Evading terminal differentiation is an essential step in malignant transformation and p53 loss may be one route to weaken this innate barrier to tumorigenesis. Consistent with this notion, an embryonic stem cell-like gene signature is observed in p53 mutant breast cancer (Mizuno et al., 2010). By affecting differentiation, incipient *TP53* mutations facilitate the expansion of hematopoietic stem cell (HSC) clones in otherwise healthy individuals, occasionally overtaking the entire hematopoietic system (Steensma et al., 2015; Xie et al., 2014). The competitive expansion of pre-treatment p53 mutant HSC clones is accentuated by genotoxic chemotherapy, fostering therapy-related AML (t-AML) (Wong et al., 2015). p53 loss can even facilitate lineage switching as a mechanism of resistance to anti-androgen therapy in prostate cancer (Mu et al., 2017). Furthermore, p53 action in wound healing also shapes the tumor microenvironment. For example, the p53-driven senescence-associated secretory phenotype (SASP) in tumor stroma can create a tumor-suppressive immune milieu that influences the incidence of cancer (Lujambio et al., 2013; Xue et al., 2007). In other settings, the SASP can be tumor promoting, by inducing epithelial-mesenchymal transition (EMT) (Laberge et al., 2012; Ritschka et al., 2017).

It appears that evolution has selected for a delicate balance of p53 activity, since too little p53 leads to early-onset cancer and too much p53 exacerbates aging. Regardless, the dangers of excess p53 are evident in pathologies beyond cancer, including aging, ischemic injury, and degeneration (reviewed in Gudkov and Komarova, 2010). As animals age, the cost of eliminating potentially dangerous cells is the attrition of stem cells required for tissue homeostasis. In an accelerated process, patients with the heritable DNA repair deficiency syndrome Fanconi anemia hyperactivate p53 in response to unresolved DNA damage and eventually experience bone marrow failure owing to progressive HSC loss (Ceccaldi et al., 2012). Excessive p53-dependent apoptosis can also drive developmental disorders of the brain (Houlihan and Feng, 2014) and aging-associated neurodegenerative diseases, namely Alzheimer's and Parkinson's dis-

eases (reviewed in Checler and Alves da Costa, 2014). As a regulator of cell death, p53 has been implicated in the pathological response to cerebral and cardiac ischemia; p53 inhibition has been proposed as a protective strategy in the acute phase after injury (Gudkov and Komarova, 2010). Lastly, excessive p53-mediated ferroptosis can trigger lethal kidney ischemia (Friedmann Angeli et al., 2014). Collectively, the characteristics of p53 action in normal physiology and non-cancer pathologies shed light on additional regulatory mechanisms, downstream functions, and possible therapeutic targets.

The Diversity of *TP53* Mutational Events Produces Distinct Functional Consequences

Just as advances in our understanding of p53 biology have complicated, rather than simplified, our views on how *TP53* mutations promote cancer, so has our appreciation of surprising range of ways in which the *TP53* locus is altered in tumors. The most common and well-characterized *TP53* mutations are missense mutations in the DNA binding domain, implying that this feature of p53 is crucial for tumor suppression. Current dogma tends to classify p53 as either wild-type or mutant, but *TP53* mutations occur with different patterns, distinct co-mutations, and in many allelic configurations that produce remarkably interesting functional and phenotypic ramifications.

Genome sequencing of thousands of tumors has confirmed that approximately half of all cancers harbor a *TP53* mutation, though the frequency and the distribution of mutations can vary dramatically between tumor types (Figure 3A). Most of the *TP53* single-nucleotide variants (SNVs) observed across cancers are missense mutations, with 25% of those falling into 5 "hotspot" mutations (Shirole et al., 2016). Unexpectedly, nearly 25% of *TP53* mutations are nonsense or frameshift mutations predicted to encode truncated proteins, whereas the remainder consists of splice site SNVs and in-frame indels of unclear biological significance (Shirole et al., 2016). While several modes to disable the second *TP53* allele are possible, this typically occurs through "loss of heterozygosity" (LOH) by segmental deletion (Figure 3B). These deletions vary widely in size and occur at a frequency that is similar to p53 SNVs (Liu et al., 2016). Nearly all possible allelic combinations are observed such that, in reality, only ~25% of tumors harbor the canonical p53 missense mutation/deletion combination (Liu et al., 2016).

Cancer genome projects have also produced interesting insights into the spectrum of *TP53* mutation and its association with other somatic events. In some cancers, *TP53* mutations often co-occur with activating *KRAS* mutations or *MYC* amplification, an observation reminiscent of age-old functional studies demonstrating the ability of p53 loss to cooperate with oncogenes to transform primary cells. And, as mentioned earlier, *TP53* mutations are frequently associated with high rates of CNV, for example, as occurs in ovarian carcinoma and complex karyotype AML (Ciriello et al., 2013).

The extensive cataloging of *TP53* alterations in different settings allows one to consider whether distinct alterations reflect functional selection or simply different mutagenic processes present during tumorigenesis. Distinct mutational signatures in *TP53* and other genes can be attributed, in part, to the specific source of mutagenesis (Alexandrov et al., 2016). For instance,

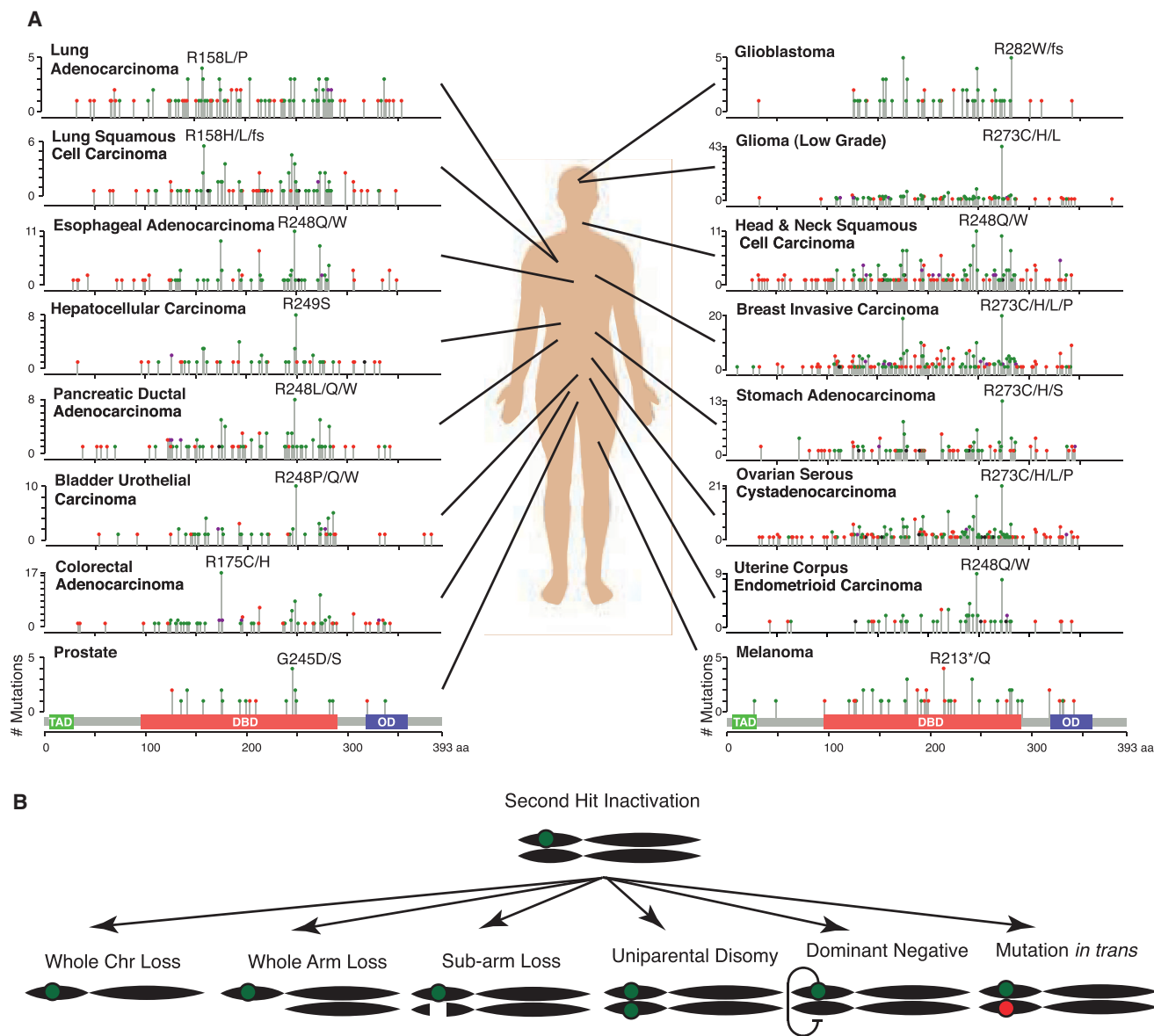


Figure 3. p53 Alteration Spectrum

(A) The *TP53* mutation distribution for 16 cancer types with sufficient available data and frequency of *TP53* alteration. Each histogram depicts the number of mutations found at each position along the p53 protein coding sequence, with the transactivation domain (TAD), DNA-binding domain (DBD), and oligomerization domain (OD) illustrated below. Symbol color indicates mutation type, including missense (green), nonsense (red), in-frame indels (black), or multiple mutation types (purple). Data source: MSKCC cbio portal (Gao et al., 2013).

(B) Multiple avenues to inactivating the second allele of *TP53*.

the R249S mutation prevalent in hepatocellular carcinoma arises from G-to-T transversions linked to aflatoxin exposure and R213* mutations in melanoma are associated with the C-to-T transition signature of UV mutagenesis (Alexandrov et al., 2016). Characterization of mutagenic signatures has revealed recurrent C-to-T mutation patterns attributed to cytidine deaminases, such as AID and APOBEC, which are an intrinsic source of mutagenesis with a physiological role in antibody diversification (Alexandrov et al., 2013). Curiously, the APOBECs can be induced by either wild-type or mutant p53 (Menendez

et al., 2017), though a clear link between p53 status and APOBEC-mediated mutagenesis has not yet been described (Burns et al., 2013; Shinmura et al., 2011). While epidemiology and genome sequencing can implicate environmental or endogenous mutagens as responsible for particular *TP53* mutations, it is difficult, if not impossible, to assess individual alleles without direct functional studies.

In fact, experimental data emerging over the last 25 years have hinted that certain mutant *TP53* alleles have “gain-of-function” properties that produce phenotypes distinct from the null. The

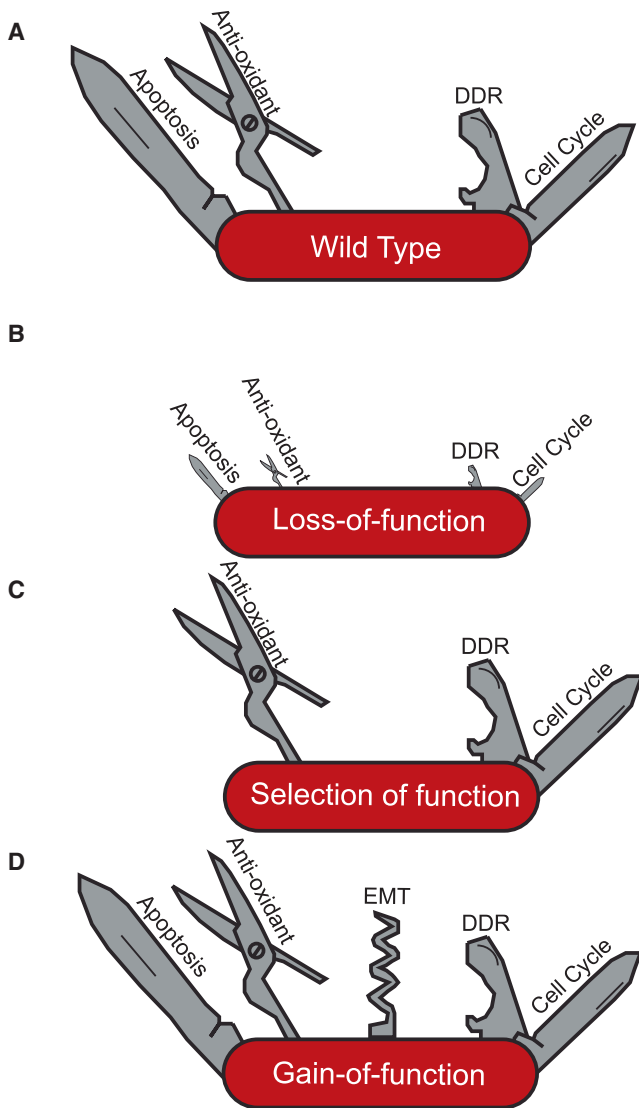


Figure 4. Mutant p53 Gain of Function

Several alternative mechanisms can lead to divergent phenotypes of p53 mutations: (A) wild-type, (B) loss or partial loss of function, (C) selection of function, or (D) neomorphic/gain-of-function.

most prominent phenotype produced by such mutant proteins is their ability to enhance invasion and metastasis, though in some settings particular mutants enhance drug resistance, epigenetic reprogramming, or angiogenesis (reviewed in Aschauer and Muller, 2016). While proposed activities are diverse, an emerging “rule of thumb” is that tumor-derived p53 mutants oppose wild-type p53 functions or, more explicitly, exacerbate the consequences of p53 loss. In any case, the notion that not all p53 mutations are functionally equivalent is further supported by the fact that the onset and pathology of tumors in genetically engineered mouse models and in Li-Fraumeni patients varies by the type of mutant allele (Achatz and Zambetti, 2016; Olive et al., 2004; Xu et al., 2014).

A distinct phenotype of a p53 mutant is not sufficient to define a mutant as “gain-of-function.” Theoretically, p53 mutant alleles

may reflect attenuation of function, separation of function, or neomorphic function. Attenuation of wild-type function (Figure 4A) can produce hypomorphs that can also yield unpredictable and qualitatively different phenotypes depending on the level of p53 suppression (Figure 4B). For instance, p53-targeting shRNAs with varying knockdown efficiency display different abilities to disrupt p53 effector functions and drive lymphomagenesis in mice, with only complete p53 deletion capable of instigating chromosomal instability (Hemann et al., 2003). Loss of function is a common characteristic across all cancer-associated p53 mutants, given the failure of most mutants to induce apoptosis (Freed-Pastor and Prives, 2012). Separation of function—whereby a p53 mutant can retain some but not all interactions (reviewed in Muller and Vousden, 2014)—is also possible (Figure 4C), as exemplified by the aforementioned apoptosis-deficient p53^{R175P} allele (Liu et al., 2004). Finally, a range of neomorphic mutant activities (Figure 4D) has also been described (discussed below). In reality, the mutations encountered in cancer acquire some combination of these independent characteristics. Although p53 mutants are generally classified by their effect on structure—i.e., “contact” mutants that perturb DNA binding and “conformation” mutants that lose proper folding—it is currently not possible to predict precisely how a particular mutation impacts function.

The diversity of proposed mechanisms by which mutant p53 alleles elicit their pro-oncogenic effects are a source of much confusion in the field (Aschauer and Muller, 2016). First, some p53 mutant proteins retain residual transactivation activity and activate novel targets. For instance, mutant p53 is proposed to impact chromatin states by inducing MLL1/2 and MOZ (Zhu et al., 2015). Second, certain unstructured p53 mutants sequester other proteins that, in some settings, enable mutant p53 to bind p63 or p73, leading to changes in transcriptional profiles that alter receptor tyrosine kinase signaling to promote invasion and metastasis (Muller et al., 2013; Weissmueller et al., 2014). Finally, in an instance of gain-of-function protein-protein interaction, mutant p53 can cooperate with the SWI/SNF complex to upregulate the angiogenesis regulator VEGFR2 (Pfister et al., 2015). It remains difficult to reconcile how so many distinct yet selective protein-protein interactions can occur for disparate mutant proteins (reviewed in Freed-Pastor and Prives, 2012).

Although it is generally assumed that *TP53* truncating mutations are null alleles, emerging data suggest that these too can have neomorphic activity. Implying some selective advantage, the frequency of *TP53* nonsense mutations, particularly targeting exon 6, is greater than expected by chance (Shirole et al., 2016). At least some of these are not subject to nonsense-mediated decay, allowing certain truncated p53 mutants to promote invasion and metastasis and sustain tumor maintenance in a manner that mirrors established gain-of-function missense mutants (Shirole et al., 2016). Provocatively, exon 6-truncated proteins mimic the structure and function of a naturally occurring p53 splice variant (p53psi) that promotes cell invasion and is transiently expressed during certain wound-healing responses (Senturk et al., 2014), suggesting that these mutants may represent “separation of function” alleles.

Expression or mimicry of alternative splice variants may contribute to the phenotype of other common mutations as well (Candeias et al., 2016).

Beyond the heterogeneity produced by different p53 SNVs, the variable extent of human chromosome 17p deletions can produce heterogeneity in the nature and number of p53-linked genes subject to reduced dosage during tumorigenesis. Loss of these neighboring genes could well reflect a “passenger” event of no functional consequence; however, 17p deletions observed in human cancer often include other genes now functionally validated as tumor suppressors. Deletions engineered to be syntenic to 17p13 drive more aggressive cancers than simple p53 deficiency in mice by virtue of single copy loss of multiple haploinsufficient tumor suppressors, consistent with the negative prognostic association of 17p deletion independent of p53 mutation that is evident in AML (Liu et al., 2016). These observations and others underscore the unique biology underlying CNVs and highlight the importance of dissecting these understudied events (Tschaharganeh et al., 2016).

Collectively, our emerging understanding of the complexities of the gamut of *TP53* alterations is changing our views on how “the most frequent event in human cancer” promotes tumorigenesis. While there is little doubt that the most substantial biological consequence results from inactivation of p53, it is now clear that both *TP53* mutations and 17p deletions contribute phenotypes to cancer that go beyond p53 loss. Thus, as clinical decision making in the future becomes increasingly based on genomic data, the current classification of tumors as simply “p53 wild-type” or “p53 mutant” must be replaced.

Harnessing the p53 Network

The potency of p53 in tumor suppression and the high rate of p53 alteration in cancers has spurred the development of strategies to target the p53 network in cancer therapy (Figure 5). Indeed, the potential value of engaging p53 in an anticancer response is clear from studies showing that, in some cases, robust responses to conventional chemotherapy can depend on wild-type p53, and studies in mice described above document massive tumor regressions in response to p53 reactivation *in vivo*. For instance, the dramatic cures achieved by retinoic acid and arsenic treatment of acute promyelocytic leukemia is dependent on p53-mediated senescence (Ablain et al., 2014). Since *TP53* mutations inactivate wild-type p53 protein, they are widely considered undruggable and, consequently, efforts to rationally exploit p53 for therapeutic benefit have yet to reach fruition. Nonetheless, some strategies to target mutant p53 proteins, p53 regulators, or vulnerabilities created by *TP53* mutation in cancer and other indications show promise.

One of the most advanced efforts to exploit our understanding of p53 biology for cancer therapy involves efforts to inhibit MDM2 in tumors harboring wild-type p53 (Figure 5A). Led by the development of Nutlin (Vassilev et al., 2004), a panoply of small-molecule and peptide inhibitors of MDM2 and MDMX have been developed aimed at improving the properties of first-generation inhibitors that generally act by targeting the p53 binding site in MDM2 (reviewed in Cheok and Lane, 2017). A number of phase I trials for MDM2 antagonists have been

completed in leukemia and liposarcoma, with neutropenia and thrombocytopenia being prominent dose-limiting toxicities (Andreeff et al., 2016). While these dose-escalation studies preclude conclusions about drug efficacy, induction of p53 target gene expression was observed in most p53 wild-type samples. Moreover, a partial response occurred in 5%–10% of patients, a promising result given that many were heavily pre-treated. Counterintuitively, only some of these MDM2 inhibitor clinical trials stratify patients by *TP53* status (reviewed in Burgess et al., 2016; Wang et al., 2011).

Flipping the situation around, MDM2 inhibitors have also been used in efforts aimed at reducing the toxic side effects of chemotherapy (Figure 5B). In a strategy termed *cyclotherapy*, these drugs are used to stabilize p53 and trigger a transient cell cycle arrest in normal cells, with the intention of having no effect on the cell cycle progression of p53 mutant tumor cells. As many cytotoxic drugs target actively cycling cells, this strategy is predicted to allow use of a higher tolerable dose of chemotherapy, enhancing efficacy against cancer cells that continue to cycle while reducing toxicity to arrested normal cells (Cheok and Lane, 2017). In preclinical studies, cyclotherapy protects mice treated with Polo kinase inhibitor from dose-limiting neutropenia (Sur et al., 2009).

One attractive therapeutic approach involves identifying agents that cause mutant p53 to regain sufficient wild-type p53 activity for tumor suppression (Figure 5C). Although the thermodynamic requirements for achieving this seem daunting, structural studies and *in silico* predictions have propelled multiple strategies that supply proof-of-principle for this approach, including peptides and small molecules that stabilize unstructured mutants (Boeckler et al., 2008; Friedler et al., 2002; Yu et al., 2012). One drug, APR-246, which is purported to reactivate mutant p53 but also has off-target effects, is currently in clinical trials (ClinVar: NCT03072043, NCT02999893) (Deneberg et al., 2016). Other agents that directly stabilize the p53 DNA binding domain show promise in preclinical studies (Cheok and Lane, 2017). Drugs known as metallochaperones can facilitate the reincorporation of zinc into unfolded p53 proteins, leading to a more normal confirmation and an ability to bind DNA (reviewed in Blanden et al., 2015). Yet another approach exploits the unexpected observation that certain p53 mutant proteins have a penchant for aggregation into amyloid-like structures (reviewed in de Oliveira et al., 2015) that, when disrupted, restore p53 function and reportedly trigger tumor regression in xenograft models (Soragni et al., 2016).

While these drugs all aim to coax native wild-type activity out of mutant proteins, strategies to disable or suppress mutant p53 represent an underexplored alternative direction that is justified by the observation that tumors can become “addicted” to mutant p53 (Alexandrova et al., 2015). Several indirect strategies have been proposed to destabilize mutant p53 protein, including HSP90 inhibitors, HDAC inhibitors, and SIRT1 activators (reviewed in Parrales and Iwakuma, 2015). In the absence of readily available tools to directly inhibit mutant p53 function, the opportunity remains to apply existing drugs to target the underlying mechanism whereby mutant p53 promotes invasion, metastasis, and cellular survival (e.g., via HMG CoA reductase, EGFR, or PDGFRβ inhibitors) (Aschauer and Muller, 2016; Weissmueller et al., 2014).

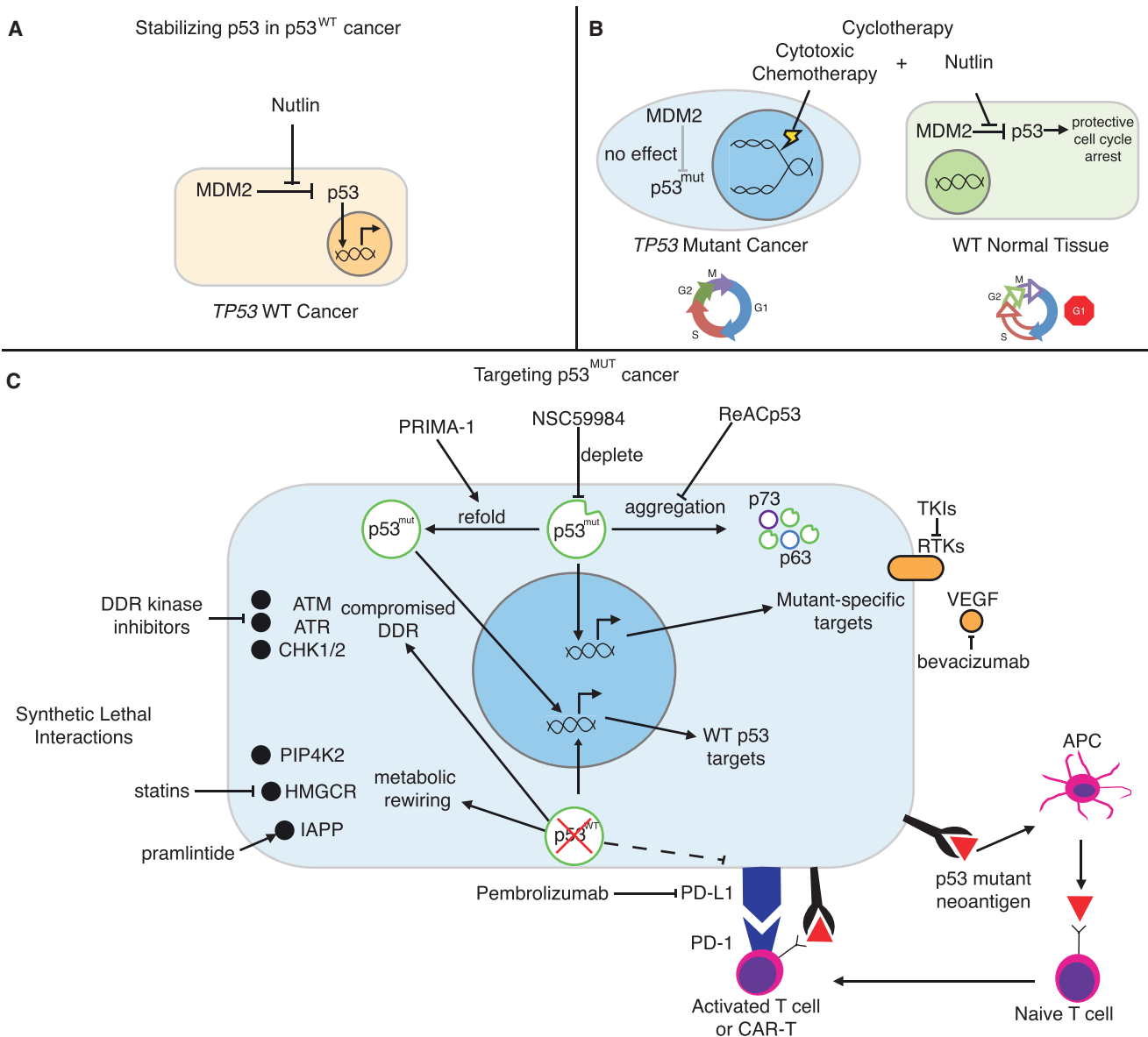


Figure 5. Harnessing p53

(A) Stabilizing p53 in p53^{WT} cancer. Nutlin and other MDM2/MDMX inhibitors (RG7112, RO5503781, SAR405838, HDM201, MK4828, AMG232, and RG7388) allow for the accumulation and activity of p53 in cancer in which it is not mutated.

(B) Cyclotherapy. Nutlin is used to transiently arrest p53^{WT} normal cells, while p53^{MUT} cancer cells continue to cycle and remain vulnerable to genotoxic chemotherapy. Sparing normal tissue allows for increased dosing and reduced toxicity.

(C) Targeting p53^{MUT} cancer. PRIMA-1 and other agents (APR-246, RITA, PK7088, p53R3, and ZMC1) are used to support proper folding of mutant p53 and restore wild-type-like structure and activity. p53 mutant protein is depleted through a number of indirect mechanisms including inhibition of HSP90 (17-AAG), HDAC (SAHA), and SIRT1 (YK-3-237). The aggregation and inactivation of mutant p53 and its family members is inhibited by ReACp53. Synthetic lethal interactions are dependencies in p53 mutant cancer but not in p53^{WT} cells. p53-deficient cells have a compromised DDR, leaving them vulnerable to even further genomic instability by inhibiting DDR-related kinases. Metabolic rewiring introduces druggable dependencies on PIP4K2, cholesterol biosynthesis/HMGCR (statins), and IAPP (pramlintide). Some p53 mutations can result in recognizable neoantigens, which has led to the development of mutant p53-targeted immunotherapy. p53 ablation can also modify antigen presentation efficiency justifying the investigation of immune checkpoint inhibition, especially when combined with other strategies.

Another way in which to attack mutant p53 directly is to harness its potential to serve as a tumor-specific neoantigen (Figure 5C). Mutant p53 proteins are typically expressed at high levels and can be antigenic (Crawford et al., 1982; DeLeo et al., 1979); furthermore, vaccination against mutant p53 can

protect mice from cancer produced by transplanted tumors (Roth et al., 1996). Based on this premise, peptide vaccines (Zeestraten et al., 2013), viral vectors (van der Burg et al., 2002), and dendritic cell vaccines (Ellebaek et al., 2012) have entered phase I/II clinical trials. Regardless of platform,

immunotherapy has been able to induce p53-specific immune reactions in humans, though clinical responses have yet to be observed.

In theory, tumors that have escaped immunoediting are more likely to contain immunogenic neoantigens. Therefore, there is interest in combining p53 immunotherapy with so-called immune checkpoint blockade to enhance T cell reactivity, which may be able to translate previously observed generation of p53-specific T cells into the desired cytotoxicity and clinical responses (Hardwick et al., 2014). Indeed, p53 loss can shield cancer cells from CD8⁺ T cells via PD-L1 derepression, an interaction that accelerates mouse models of cancer and is evident in human lung cancer (Cha et al., 2016; Cortez et al., 2015; Schuster et al., 2011), yet a positive association between p53 alteration and response to immunotherapy by PD-L1 inhibition has not been observed.

An attractive approach to targeting p53 mutant tumors is to exploit *synthetic lethality*, a term describing a situation in which gene mutation creates novel dependencies (Figure 5C). Many previously characterized liabilities imposed by p53 mutation converge around the DNA damage response and metabolism. Although p53-deficient cells can evade apoptosis in the face of DNA-damaging agents, further disabling the DDR leaves p53 mutant tumors hypersensitive to genotoxic damage (Ma et al., 2012). Accordingly, strategies combining DNA-damaging agents with inhibitors of DDR components ATM, CHK2, ATR, and CHK1 have been pursued (reviewed in Morandell and Yaffe, 2012). Supporting the potential of this approach, a WEE1 inhibitor that disables a G2 cell cycle checkpoint enhances the antitumor activity of genotoxic chemotherapy in previously refractory p53 mutant ovarian cancer patients (Leijen et al., 2016). Also, patients with *TP53* mutations have higher response rates to extended cycles of the demethylating agent decitabine (Welch et al., 2016). While the mechanistic basis for this observation is not known, one plausible explanation is that wild-type cells arrest in G2/M upon drug treatment, whereas p53-deficient cells pass through the cell cycle checkpoint, resulting in severe chromosomal damage and death (Nieto et al., 2004). Although exacerbating instability may achieve therapeutic responses, the concern remains that mutagenesis associated with reducing the DDR likely fuels tumor evolution and perhaps even the emergence of treatment-associated cancers.

Additionally, the metabolic rewiring associated with p53 mutation also instills novel dependencies on druggable targets, including PIP4K2A/B, cholesterol biosynthesis, and IAPP (Emerling et al., 2013; Freed-Pastor et al., 2012; Venkatanarayan et al., 2015). Unlike synthetic lethal interactions related to p53 loss of function, a side-effect of single copy chromosome 17p deletions during LOH may be to expose cancers to heightened dependence on linked essential genes such as POLR2A (Liu et al., 2015).

Beyond cancer, pharmacological modulation of p53 is a potentially useful and largely unexplored strategy to aid cell-autonomous defense against infection. Pathogens evolved around mammalian cells, selected to keep the host alive despite the DNA damage, ROS induction, and activation of innate immunity through toll-like receptors that follows infection, all of which can be mediated by p53 (Shatz et al., 2012). Hence, p53 can act as a suppressor of bacterial infection, leading to the concept of

pharmacological p53 activation to mitigate severe infections (Siegl et al., 2014). Some pathogens encode components that inhibit p53, and nutlin-based stabilization of p53 can hinder their propagation (Kaushansky et al., 2013; Siegl et al., 2014). Consequently, it may be worth considering use of MDM2 inhibitors in cases of life-threatening multi-drug-resistant infections with no other treatment options. However, induction of p53 is not universally conducive to combating infection, and defining its disease-specific immune interactions will be a prerequisite for clinical relevance of p53 in infectious diseases. *Trp53*^{-/-} mice are actually more capable of recovering from bacterial pneumonia than wild-type mice (Madenpacher et al., 2013).

Through restoring wild-type function, inhibiting mutant function, or treating a dysregulated immune system, multiple avenues exist to target the p53 network in cancer. Given the obstacles that have been encountered using these strategies to date, further knowledge of basic p53 biology will be required for future successful clinical applications.

Concluding Remarks

p53 has captured the fascination of cancer biologists, and its detailed characterization has produced fundamental insights into mechanisms of gene regulation and nature's safeguards against cancer. While the body of research on p53 is massive and sometimes contradictory, it is now abundantly clear that cellular responses to p53 activation involve a complex interplay between activation triggers, cell lineage, and cell state. While such context-dependent effects on p53 have stymied attempts to generalize the mechanism of p53-mediated tumor suppression, they provide opportunities to exploit the network in cancer cells, while avoiding deleterious consequences of manipulating p53 in all tissues.

Despite decades of intensive research and countless discoveries, there remains much to learn about the roles and regulation of p53. A challenge in the coming era of p53 research will be to distill convergent truths assembled from comprehensive studies and to translate knowledge of p53 into clinical application. Indeed, the difficulties associated with exploiting p53 therapeutically do not mitigate the astounding morbidity associated with *TP53* mutation. In the absence of new therapeutic innovations, *TP53* mutant cancer will lead to the deaths of more than 500 million people alive today. New technologies, together with our ever-increasing understanding of the complexity of p53 action and the diverse consequences of p53 mutation, will hopefully set the stage for more robust clinical advances.

ACKNOWLEDGMENTS

We would like to thank Charles Sherr of HHMI at St. Jude Children's Research Hospital and all members of the Lowe lab for advice and critical discussions, especially Francisco Sanchez-Rivera, Shauna Houlihan, and John P. Morris, IV. E.R.K. is supported by an F31 NRSA predoctoral fellowship from the NCI/National Institutes of Health under award number F31CA192835. S.W.L. is an investigator of the Howard Hughes Medical Institute and the Geoffrey Beene Chair for Cancer Biology. We thank all of the investigators who have contributed to the p53 field and the many ideas presented herein. We apologize to the many investigators whose work could not be cited owing to space constraints.

REFERENCES

- Abegglen, L.M., Caulin, A.F., Chan, A., Lee, K., Robinson, R., Campbell, M.S., Kiso, W.K., Schmitt, D.L., Waddell, P.J., Bhaskara, S., et al. (2015). Potential mechanisms for cancer resistance in elephants and comparative cellular response to DNA damage in humans. *JAMA* *314*, 1850–1860.
- Ablain, J., Rice, K., Soihli, H., de Reynies, A., Minucci, S., and de Thé, H. (2014). Activation of a promyelocytic leukemia-tumor protein 53 axis underlies acute promyelocytic leukemia cure. *Nat. Med.* *20*, 167–174.
- Achatz, M.I., and Zambetti, G.P. (2016). The inherited p53 mutation in the Brazilian population. *Cold Spring Harb. Perspect. Med.* *6*, 6.
- Alexandrov, L.B., Nik-Zainal, S., Wedge, D.C., Aparicio, S.A., Behjati, S., Biankin, A.V., Bignell, G.R., Bolli, N., Borg, A., Børresen-Dale, A.L., et al.; Australian Pancreatic Cancer Genome Initiative; ICGC Breast Cancer Consortium; ICGC MMML-Seq Consortium; ICGC PedBrain (2013). Signatures of mutational processes in human cancer. *Nature* *500*, 415–421.
- Alexandrov, L.B., Ju, Y.S., Haase, K., Van Loo, P., Martincorena, I., Nik-Zainal, S., Totoki, Y., Fujimoto, A., Nakagawa, H., Shibata, T., et al. (2016). Mutational signatures associated with tobacco smoking in human cancer. *Science* *354*, 618–622.
- Alexandrova, E.M., Yallowitz, A.R., Li, D., Xu, S., Schulz, R., Proia, D.A., Lozano, G., Dobbstein, M., and Moll, U.M. (2015). Improving survival by exploiting tumour dependence on stabilized mutant p53 for treatment. *Nature* *523*, 352–356.
- Allen, M.A., Andrysiak, Z., Dengler, V.L., Mellert, H.S., Guarnieri, A., Freeman, J.A., Sullivan, K.D., Galbraith, M.D., Luo, X., Kraus, W.L., et al. (2014). Global analysis of p53-regulated transcription identifies its direct targets and unexpected regulatory mechanisms. *eLife* *3*, e02200.
- Andreoff, M., Kelly, K.R., Yee, K., Assouline, S., Strair, R., Popplewell, L., Bowen, D., Martinelli, G., Drummond, M.W., Vyas, P., et al. (2016). Results of the phase I trial of RG7112, a small-molecule MDM2 antagonist in leukemia. *Clin. Cancer Res.* *22*, 868–876.
- Aschauer, L., and Muller, P.A. (2016). Novel targets and interaction partners of mutant p53 gain-of-function. *Biochem. Soc. Trans.* *44*, 460–466.
- Aylon, Y., and Oren, M. (2016). The paradox of p53: what, how, and why? *Cold Spring Harb. Perspect. Med.* *6*, 6.
- Aylon, Y., Michael, D., Shmueli, A., Yabuta, N., Nojima, H., and Oren, M. (2006). A positive feedback loop between the p53 and Lats2 tumor suppressors prevents tetraploidization. *Genes Dev.* *20*, 2687–2700.
- Baker, S.J., Preisinger, A.C., Jessup, J.M., Paraskeva, C., Markowitz, S., Willson, J.K., Hamilton, S., and Vogelstein, B. (1990). p53 gene mutations occur in combination with 17p allelic deletions as late events in colorectal tumorigenesis. *Cancer Res.* *50*, 7717–7722.
- Belyi, V.A., Ak, P., Markert, E., Wang, H., Hu, W., Puzio-Kuter, A., and Levine, A.J. (2010). The origins and evolution of the p53 family of genes. *Cold Spring Harb. Perspect. Biol.* *2*, a001198.
- Blanden, A.R., Yu, X., Loh, S.N., Levine, A.J., and Carpizo, D.R. (2015). Reactivating mutant p53 using small molecules as zinc metallochaperones: awakening a sleeping giant in cancer. *Drug Discov. Today* *20*, 1391–1397.
- Boeckler, F.M., Joerger, A.C., Jaggi, G., Rutherford, T.J., Veprintsev, D.B., and Fersht, A.R. (2008). Targeted rescue of a destabilized mutant of p53 by an in silico screened drug. *Proc. Natl. Acad. Sci. USA* *105*, 10360–10365.
- Bondar, T., and Medzhitov, R. (2010). p53-mediated hematopoietic stem and progenitor cell competition. *Cell Stem Cell* *6*, 309–322.
- Brady, C.A., Jiang, D., Mello, S.S., Johnson, T.M., Jarvis, L.A., Kozak, M.M., Kenzelmann Broz, D., Basak, S., Park, E.J., McLaughlin, M.E., et al. (2011). Distinct p53 transcriptional programs dictate acute DNA-damage responses and tumor suppression. *Cell* *145*, 571–583.
- Burgess, A., Chia, K.M., Haupt, S., Thomas, D., Haupt, Y., and Lim, E. (2016). Clinical overview of MDM2/X-targeted therapies. *Front. Oncol.* *6*, 7.
- Burns, M.B., Temiz, N.A., and Harris, R.S. (2013). Evidence for APOBEC3B mutagenesis in multiple human cancers. *Nat. Genet.* *45*, 977–983.
- Candeias, M.M., Hagiwara, M., and Matsuda, M. (2016). Cancer-specific mutations in p53 induce the translation of $\Delta 160p53$ promoting tumorigenesis. *EMBO Rep.* *17*, 1542–1551.
- Ceccaldi, R., Parmar, K., Mouly, E., Delord, M., Kim, J.M., Regairaz, M., Pla, M., Vasquez, N., Zhang, Q.S., Pondarre, C., et al. (2012). Bone marrow failure in Fanconi anemia is triggered by an exacerbated p53/p21 DNA damage response that impairs hematopoietic stem and progenitor cells. *Cell Stem Cell* *11*, 36–49.
- Cha, Y.J., Kim, H.R., Lee, C.Y., Cho, B.C., and Shim, H.S. (2016). Clinicopathological and prognostic significance of programmed cell death ligand-1 expression in lung adenocarcinoma and its relationship with p53 status. *Lung Cancer* *97*, 73–80.
- Chang, N.T., Yang, W.K., Huang, H.C., Yeh, K.W., and Wu, C.W. (2007). The transcriptional activity of HERV-I LTR is negatively regulated by its cis-elements and wild type p53 tumor suppressor protein. *J. Biomed. Sci.* *14*, 211–222.
- Charni, M., Aloni-Grinstein, R., Molchadsky, A., and Rotter, V. (2017). p53 on the crossroad between regeneration and cancer. *Cell Death Differ.* *24*, 8–14.
- Checler, F., and Alves da Costa, C. (2014). p53 in neurodegenerative diseases and brain cancers. *Pharmacol. Ther.* *142*, 99–113.
- Cheok, C.F., and Lane, D.P. (2017). Exploiting the p53 pathway for therapy. *Cold Spring Harb. Perspect. Med.* *7*, 7.
- Ciriello, G., Miller, M.L., Aksoy, B.A., Senbabaoglu, Y., Schultz, N., and Sander, C. (2013). Emerging landscape of oncogenic signatures across human cancers. *Nat. Genet.* *45*, 1127–1133.
- Clarke, A.R., Purdie, C.A., Harrison, D.J., Morris, R.G., Bird, C.C., Hooper, M.L., and Wyllie, A.H. (1993). Thymocyte apoptosis induced by p53-dependent and independent pathways. *Nature* *362*, 849–852.
- Cooks, T., Harris, C.C., and Oren, M. (2014). Caught in the cross fire: p53 in inflammation. *Carcinogenesis* *35*, 1680–1690.
- Cortez, M.A., Ivan, C., Valdecanas, D., Wang, X., Peltier, H.J., Ye, Y., Araujo, L., Carbone, D.P., Shilo, K., Giri, D.K., et al. (2015). PDL1 Regulation by p53 via miR-34. *J. Natl. Cancer Inst.* *108*, 108.
- Crawford, L.V., Pim, D.C., and Bulbrook, R.D. (1982). Detection of antibodies against the cellular protein p53 in sera from patients with breast cancer. *Int. J. Cancer* *30*, 403–408.
- Danilova, N., Sakamoto, K.M., and Lin, S. (2008). p53 family in development. *Mech. Dev.* *125*, 919–931.
- de Oliveira, G.A., Rangel, L.P., Costa, D.C., and Silva, J.L. (2015). Misfolding, aggregation, and disordered segments in c-Abl and p53 in human cancer. *Front. Oncol.* *5*, 97.
- Dejosez, M., Ura, H., Brandt, V.L., and Zwaka, T.P. (2013). Safeguards for cell cooperation in mouse embryogenesis shown by genome-wide cheater screen. *Science* *341*, 1511–1514.
- DeLeo, A.B., Jay, G., Appella, E., Dubois, G.C., Law, L.W., and Old, L.J. (1979). Detection of a transformation-related antigen in chemically induced sarcomas and other transformed cells of the mouse. *Proc. Natl. Acad. Sci. USA* *76*, 2420–2424.
- Deneberg, S., Cherif, H., Lazarevic, V., Andersson, P.O., von Euler, M., Juliusson, G., and Lehmann, S. (2016). An open-label phase I dose-finding study of APR-246 in hematological malignancies. *Blood Cancer J.* *6*, e447.
- Dewhurst, S.M., McGranahan, N., Burrell, R.A., Rowan, A.J., Grönroos, E., Endesfelder, D., Joshi, T., Mouradov, D., Gibbs, P., Ward, R.L., et al. (2014). Tolerance of whole-genome doubling propagates chromosomal instability and accelerates cancer genome evolution. *Cancer Discov.* *4*, 175–185.
- Donehower, L.A., Harvey, M., Slagle, B.L., McArthur, M.J., Montgomery, C.A., Jr., Butel, J.S., and Bradley, A. (1992). Mice deficient for p53 are developmentally normal but susceptible to spontaneous tumours. *Nature* *356*, 215–221.
- Duan, L., Perez, R.E., Davaadelger, B., Dedkova, E.N., Blatter, L.A., and Maki, C.G. (2015). p53-regulated autophagy is controlled by glycolysis and determines cell fate. *Oncotarget* *6*, 23135–23156.

- Eijkelenboom, A., and Burgering, B.M. (2013). FOXOs: signalling integrators for homeostasis maintenance. *Nat. Rev. Mol. Cell Biol.* *14*, 83–97.
- Eischen, C.M. (2016). Genome stability requires p53. *Cold Spring Harb. Perspect. Med.* *6*, 6.
- el-Deiry, W.S., Tokino, T., Velculescu, V.E., Levy, D.B., Parsons, R., Trent, J.M., Lin, D., Mercer, W.E., Kinzler, K.W., and Vogelstein, B. (1993). WAF1, a potential mediator of p53 tumor suppression. *Cell* *75*, 817–825.
- Ellebaek, E., Engell-Noerregaard, L., Iversen, T.Z., Froesig, T.M., Munir, S., Hadrup, S.R., Andersen, M.H., and Svane, I.M. (2012). Metastatic melanoma patients treated with dendritic cell vaccination, Interleukin-2 and metronomic cyclophosphamide: results from a phase II trial. *Cancer Immunol. Immunother.* *61*, 1791–1804.
- Emerling, B.M., Hurov, J.B., Poulgiannis, G., Tsukazawa, K.S., Choo-Wing, R., Wulf, G.M., Bell, E.L., Shim, H.S., Lamia, K.A., Rameh, L.E., et al. (2013). Depletion of a putatively druggable class of phosphatidylinositol kinases inhibits growth of p53-null tumors. *Cell* *155*, 844–857.
- Espinosa, J.M., Verdun, R.E., and Emerson, B.M. (2003). p53 functions through stress- and promoter-specific recruitment of transcription initiation components before and after DNA damage. *Mol. Cell* *12*, 1015–1027.
- Feng, Z., Zhang, C., Kang, H.J., Sun, Y., Wang, H., Naqvi, A., Frank, A.K., Rosenwaks, Z., Murphy, M.E., Levine, A.J., and Hu, W. (2011). Regulation of female reproduction by p53 and its family members. *FASEB J.* *25*, 2245–2255.
- Finlay, C.A., Hinds, P.W., and Levine, A.J. (1989). The p53 proto-oncogene can act as a suppressor of transformation. *Cell* *57*, 1083–1093.
- Fischer, M. (2017). Census and evaluation of p53 target genes. *Oncogene* *36*, 3943–3956.
- Freed-Pastor, W.A., and Prives, C. (2012). Mutant p53: one name, many proteins. *Genes Dev.* *26*, 1268–1286.
- Freed-Pastor, W.A., Mizuno, H., Zhao, X., Langerod, A., Moon, S.H., Rodriguez-Barrueco, R., Barsotti, A., Chicas, A., Li, W., Polotskaia, A., et al. (2012). Mutant p53 disrupts mammary tissue architecture via the mevalonate pathway. *Cell* *148*, 244–258.
- Friedler, A., Hansson, L.O., Veprintsev, D.B., Freund, S.M., Rippin, T.M., Nikolaeva, P.V., Proctor, M.R., Rüdiger, S., and Fersht, A.R. (2002). A peptide that binds and stabilizes p53 core domain: chaperone strategy for rescue of oncogenic mutants. *Proc. Natl. Acad. Sci. USA* *99*, 937–942.
- Friedmann Angeli, J.P., Schneider, M., Proneth, B., Tyurina, Y.Y., Tyurin, V.A., Hammond, V.J., Herbach, N., Aichler, M., Walch, A., Eggenhofer, E., et al. (2014). Inactivation of the ferroptosis regulator Gpx4 triggers acute renal failure in mice. *Nat. Cell Biol.* *16*, 1180–1191.
- Friedmann-Morvinski, D., Bushong, E.A., Ke, E., Soda, Y., Marumoto, T., Singer, O., Ellisman, M.H., and Verma, I.M. (2012). Dedifferentiation of neurons and astrocytes by oncogenes can induce gliomas in mice. *Science* *338*, 1080–1084.
- Ganem, N.J., Cornils, H., Chiu, S.Y., O'Rourke, K.P., Arnaud, J., Yimlamai, D., Théry, M., Camargo, F.D., and Pellman, D. (2014). Cytokinesis failure triggers hippo tumor suppressor pathway activation. *Cell* *158*, 833–848.
- Gao, J., Aksoy, B.A., Dogrusoz, U., Dresdner, G., Gross, B., Sumer, S.O., Sun, Y., Jacobsen, A., Sinha, R., Larsson, E., et al. (2013). Integrative analysis of complex cancer genomics and clinical profiles using the cBioPortal. *Sci. Signal.* *6*, pii1.
- Gao, M., Monian, P., Pan, Q., Zhang, W., Xiang, J., and Jiang, X. (2016). Ferroptosis is an autophagic cell death process. *Cell Res.* *26*, 1021–1032.
- Garrison, S.P., Jeffers, J.R., Yang, C., Nilsson, J.A., Hall, M.A., Reh, J.E., Yue, W., Yu, J., Zhang, L., Onciu, M., et al. (2008). Selection against PUMA gene expression in Myc-driven B-cell lymphomagenesis. *Mol. Cell Biol.* *28*, 5391–5402.
- Gomes, N.P., and Espinosa, J.M. (2010a). Disparate chromatin landscapes and kinetics of inactivation impact differential regulation of p53 target genes. *Cell Cycle* *9*, 3428–3437.
- Gomes, N.P., and Espinosa, J.M. (2010b). Gene-specific repression of the p53 target gene PUMA via intragenic CTCF-Cohesin binding. *Genes Dev.* *24*, 1022–1034.
- Gudkov, A.V., and Komarova, E.A. (2010). Pathologies associated with the p53 response. *Cold Spring Harb. Perspect. Biol.* *2*, a001180.
- Hardwick, N., Chung, V., Cristea, M., Ellenhorn, J.D., and Diamond, D.J. (2014). Overcoming immunosuppression to enhance a p53MVA vaccine. *Oncol Immunology* *3*, e958949.
- Harper, J.W., Adami, G.R., Wei, N., Keyomarsi, K., and Elledge, S.J. (1993). The p21 Cdk-interacting protein Cip1 is a potent inhibitor of G1 cyclin-dependent kinases. *Cell* *75*, 805–816.
- Haupt, Y., Maya, R., Kazaz, A., and Oren, M. (1997). Mdm2 promotes the rapid degradation of p53. *Nature* *387*, 296–299.
- Hayashi, M.T., Cesare, A.J., Fitzpatrick, J.A., Lazzarini-Denchi, E., and Karlseder, J. (2012). A telomere-dependent DNA damage checkpoint induced by prolonged mitotic arrest. *Nat. Struct. Mol. Biol.* *19*, 387–394.
- Hemann, M.T., Fridman, J.S., Zilfou, J.T., Hernando, E., Paddison, P.J., Cordon-Cardo, C., Hannon, G.J., and Lowe, S.W. (2003). An epi-allelic series of p53 hypomorphs created by stable RNAi produces distinct tumor phenotypes in vivo. *Nat. Genet.* *33*, 396–400.
- Hemann, M.T., Zilfou, J.T., Zhao, Z., Burgess, D.J., Hannon, G.J., and Lowe, S.W. (2004). Suppression of tumorigenesis by the p53 target PUMA. *Proc. Natl. Acad. Sci. USA* *101*, 9333–9338.
- Honda, R., Tanaka, H., and Yasuda, H. (1997). Oncoprotein MDM2 is a ubiquitin ligase E3 for tumor suppressor p53. *FEBS Lett.* *420*, 25–27.
- Horvath, M.M., Wang, X., Resnick, M.A., and Bell, D.A. (2007). Divergent evolution of human p53 binding sites: cell cycle versus apoptosis. *PLoS Genet.* *3*, e127.
- Houlihan, S.L., and Feng, Y. (2014). The scaffold protein Nde1 safeguards the brain genome during S phase of early neural progenitor differentiation. *eLife* *3*, e03297.
- Itahana, Y., Zhang, J., Göke, J., Vardy, L.A., Han, R., Iwamoto, K., Cukuroglu, E., Robson, P., Pouladi, M.A., Colman, A., and Itahana, K. (2016). Histone modifications and p53 binding poise the p21 promoter for activation in human embryonic stem cells. *Sci. Rep.* *6*, 28112.
- Jackson-Grusby, L., Beard, C., Possemato, R., Tudor, M., Fambrough, D., Csankovszki, G., Dausman, J., Lee, P., Wilson, C., Lander, E., and Jaenisch, R. (2001). Loss of genomic methylation causes p53-dependent apoptosis and epigenetic deregulation. *Nat. Genet.* *27*, 31–39.
- Jiang, D., Brady, C.A., Johnson, T.M., Lee, E.Y., Park, E.J., Scott, M.P., and Attardi, L.D. (2011). Full p53 transcriptional activation potential is dispensable for tumor suppression in diverse lineages. *Proc. Natl. Acad. Sci. USA* *108*, 17123–17128.
- Jiang, P., Du, W., Mancuso, A., Wellen, K.E., and Yang, X. (2013). Reciprocal regulation of p53 and malic enzymes modulates metabolism and senescence. *Nature* *493*, 689–693.
- Jiang, L., Kon, N., Li, T., Wang, S.J., Su, T., Hibshoosh, H., Baer, R., and Gu, W. (2015). Ferroptosis as a p53-mediated activity during tumour suppression. *Nature* *520*, 57–62.
- Kastan, M.B., Onyekwere, O., Sidransky, D., Vogelstein, B., and Craig, R.W. (1991). Participation of p53 protein in the cellular response to DNA damage. *Cancer Res.* *51*, 6304–6311.
- Kaushansky, A., Ye, A.S., Austin, L.S., Mikolajczak, S.A., Vaughan, A.M., Camargo, N., Metzger, P.G., Douglass, A.N., MacBeath, G., and Kappe, S.H. (2013). Suppression of host p53 is critical for *Plasmodium* liver-stage infection. *Cell Rep.* *3*, 630–637.
- Kim, H.R., Roe, J.S., Lee, J.E., Cho, E.J., and Youn, H.D. (2013). p53 regulates glucose metabolism by miR-34a. *Biochem. Biophys. Res. Commun.* *437*, 225–231.
- Krizhanovskiy, V., Yon, M., Dickins, R.A., Hearn, S., Simon, J., Miething, C., Yee, H., Zender, L., and Lowe, S.W. (2008). Senescence of activated stellate cells limits liver fibrosis. *Cell* *134*, 657–667.
- Kruiswijk, F., Labuschagne, C.F., and Vousden, K.H. (2015). p53 in survival, death and metabolic health: a lifeguard with a licence to kill. *Nat. Rev. Mol. Cell Biol.* *16*, 393–405.

- Kubbutat, M.H., Jones, S.N., and Vousden, K.H. (1997). Regulation of p53 stability by Mdm2. *Nature* 387, 299–303.
- Kumari, R., Kohli, S., and Das, S. (2014). p53 regulation upon genotoxic stress: intricacies and complexities. *Mol. Cell. Oncol.* 1, e969653.
- Laberge, R.M., Awad, P., Campisi, J., and Desprez, P.Y. (2012). Epithelial-mesenchymal transition induced by senescent fibroblasts. *Cancer Microenviron.* 5, 39–44.
- Lane, D.P. (1992). Cancer. p53, guardian of the genome. *Nature* 358, 15–16.
- Lane, D.P., and Crawford, L.V. (1979). T antigen is bound to a host protein in SV40-transformed cells. *Nature* 278, 261–263.
- Lane, D.P., Cheok, C.F., Brown, C., Madhumalar, A., Ghadessy, F.J., and Verma, C. (2010a). Mdm2 and p53 are highly conserved from placozoans to man. *Cell Cycle* 9, 540–547.
- Lane, D.P., Cheok, C.F., Brown, C.J., Madhumalar, A., Ghadessy, F.J., and Verma, C. (2010b). The Mdm2 and p53 genes are conserved in the Arachnids. *Cell Cycle* 9, 748–754.
- Lane, D.P., Madhumalar, A., Lee, A.P., Tay, B.H., Verma, C., Brenner, S., and Venkatesh, B. (2011). Conservation of all three p53 family members and Mdm2 and Mdm4 in the cartilaginous fish. *Cell Cycle* 10, 4272–4279.
- Lanni, J.S., and Jacks, T. (1998). Characterization of the p53-dependent post-mitotic checkpoint following spindle disruption. *Mol. Cell. Biol.* 18, 1055–1064.
- Laptenko, O., and Prives, C. (2006). Transcriptional regulation by p53: one protein, many possibilities. *Cell Death Differ.* 13, 951–961.
- Leijen, S., van Geel, R.M., Sonke, G.S., de Jong, D., Rosenberg, E.H., Marchetti, S., Pluim, D., van Werkhoven, E., Rose, S., Lee, M.A., et al. (2016). Phase II Study of WEE1 Inhibitor AZD1775 Plus Carboplatin in Patients With TP53-Mutated Ovarian Cancer Refractory or Resistant to First-Line Therapy Within 3 Months. *J. Clin. Oncol.* 34, 4354–4361.
- Leonova, K.I., Brodsky, L., Lipchick, B., Pal, M., Novototskaya, L., Chenchik, A.A., Sen, G.C., Komarova, E.A., and Gudkov, A.V. (2013). p53 cooperates with DNA methylation and a suicidal interferon response to maintain epigenetic silencing of repeats and noncoding RNAs. *Proc. Natl. Acad. Sci. USA* 110, E89–E98.
- Levine, A.J., Ting, D.T., and Greenbaum, B.D. (2016). P53 and the defenses against genome instability caused by transposons and repetitive elements. *BioEssays* 38, 508–513.
- Li, H., Wang, S., Chen, Y., Lü, K., Yin, B., Li, S., He, J., and Li, C. (2017). Identification of two p53 isoforms from *Litopenaeus vannamei* and their interaction with NF- κ B to induce distinct immune response. *Sci. Rep.* 7, 45821.
- Linzer, D.I., and Levine, A.J. (1979). Characterization of a 54K dalton cellular SV40 tumor antigen present in SV40-transformed cells and uninfected embryonal carcinoma cells. *Cell* 17, 43–52.
- Liu, G., Parant, J.M., Lang, G., Chau, P., Chavez-Reyes, A., El-Naggar, A.K., Multani, A., Chang, S., and Lozano, G. (2004). Chromosome stability, in the absence of apoptosis, is critical for suppression of tumorigenesis in Trp53 mutant mice. *Nat. Genet.* 36, 63–68.
- Liu, Y., Elf, S.E., Miyata, Y., Sashida, G., Liu, Y., Huang, G., Di Giandomenico, S., Lee, J.M., Deblasio, A., Menendez, S., et al. (2009). p53 regulates hematopoietic stem cell quiescence. *Cell Stem Cell* 4, 37–48.
- Liu, Y., Zhang, X., Han, C., Wan, G., Huang, X., Ivan, C., Jiang, D., Rodriguez-Aguayo, C., Lopez-Berestein, G., Rao, P.H., et al. (2015). TP53 loss creates therapeutic vulnerability in colorectal cancer. *Nature* 520, 697–701.
- Liu, Y., Chen, C., Xu, Z., Scuoppo, C., Rillahan, C.D., Gao, J., Spitzer, B., Bosbach, B., Kastenhuber, E.R., Baslan, T., et al. (2016). Deletions linked to TP53 loss drive cancer through p53-independent mechanisms. *Nature* 531, 471–475.
- Livingstone, L.R., White, A., Sprouse, J., Livanos, E., Jacks, T., and Tlsty, T.D. (1992). Altered cell cycle arrest and gene amplification potential accompany loss of wild-type p53. *Cell* 70, 923–935.
- Lowe, S.W., Schmitt, E.M., Smith, S.W., Osborne, B.A., and Jacks, T. (1993). p53 is required for radiation-induced apoptosis in mouse thymocytes. *Nature* 362, 847–849.
- Lowe, S.W., Jacks, T., Housman, D.E., and Ruley, H.E. (1994). Abrogation of oncogene-associated apoptosis allows transformation of p53-deficient cells. *Proc. Natl. Acad. Sci. USA* 91, 2026–2030.
- Lujambio, A., Akkari, L., Simon, J., Grace, D., Tschaharganeh, D.F., Bolden, J.E., Zhao, Z., Thapar, V., Joyce, J.A., Krizhanovsky, V., and Lowe, S.W. (2013). Non-cell-autonomous tumor suppression by p53. *Cell* 153, 449–460.
- Ma, C.X., Cai, S., Li, S., Ryan, C.E., Guo, Z., Schaiff, W.T., Lin, L., Hoog, J., Goiffon, R.J., Prat, A., et al. (2012). Targeting Chk1 in p53-deficient triple-negative breast cancer is therapeutically beneficial in human-in-mouse tumor models. *J. Clin. Invest.* 122, 1541–1552.
- Maciejowski, J., Li, Y., Bosco, N., Campbell, P.J., and de Lange, T. (2015). Chromothripsis and kataegis induced by telomere crisis. *Cell* 163, 1641–1654.
- Madenspacher, J.H., Azzam, K.M., Gowdy, K.M., Malcolm, K.C., Nick, J.A., Dixon, D., Aloor, J.J., Draper, D.W., Guardiola, J.J., Shatz, M., et al. (2013). p53 integrates host defense and cell fate during bacterial pneumonia. *J. Exp. Med.* 210, 891–904.
- Malkin, D., Li, F.P., Strong, L.C., Fraumeni, J.F., Jr., Nelson, C.E., Kim, D.H., Kassel, J., Gryka, M.A., Bischoff, F.Z., Tainsky, M.A., et al. (1990). Germ line p53 mutations in a familial syndrome of breast cancer, sarcomas, and other neoplasms. *Science* 250, 1233–1238.
- Martins, C.P., Brown-Swigart, L., and Evan, G.I. (2006). Modeling the therapeutic efficacy of p53 restoration in tumors. *Cell* 127, 1323–1334.
- McGranahan, N., and Swanton, C. (2017). Clonal heterogeneity and tumor evolution: past, present, and the future. *Cell* 168, 613–628.
- Menendez, S., Camus, S., and Izpisua Belmonte, J.C. (2010). p53: guardian of reprogramming. *Cell Cycle* 9, 3887–3891.
- Menendez, D., Nguyen, T.A., Snipe, J., and Resnick, M.A. (2017). The cytidine deaminase APOBEC3 family is subject to transcriptional regulation by p53. *Mol. Cancer Res.* 15, 735–743.
- Merkle, F.T., Ghosh, S., Kamitaki, N., Mitchell, J., Avior, Y., Mello, C., Kashin, S., Mekhoubad, S., Ilic, D., Charlton, M., et al. (2017). Human pluripotent stem cells recurrently acquire and expand dominant negative P53 mutations. *Nature* 545, 229–233.
- Messina, R.L., Sanfilippo, M., Vella, V., Pandini, G., Vigneri, P., Nicolosi, M.L., Giani, F., Vigneri, R., and Frasca, F. (2012). Reactivation of p53 mutants by prima-1 [corrected] in thyroid cancer cells. *Int. J. Cancer* 130, 2259–2270.
- Miyashita, T., Krajewski, S., Krajewska, M., Wang, H.G., Lin, H.K., Liebermann, D.A., Hoffman, B., and Reed, J.C. (1994). Tumor suppressor p53 is a regulator of bcl-2 and bax gene expression in vitro and in vivo. *Oncogene* 9, 1799–1805.
- Mizuno, H., Spike, B.T., Wahl, G.M., and Levine, A.J. (2010). Inactivation of p53 in breast cancers correlates with stem cell transcriptional signatures. *Proc. Natl. Acad. Sci. USA* 107, 22745–22750.
- Morachis, J.M., Murawsky, C.M., and Emerson, B.M. (2010). Regulation of the p53 transcriptional response by structurally diverse core promoters. *Genes Dev.* 24, 135–147.
- Morandell, S., and Yaffe, M.B. (2012). Exploiting synthetic lethal interactions between DNA damage signaling, checkpoint control, and p53 for targeted cancer therapy. *Prog. Mol. Biol. Transl. Sci.* 110, 289–314.
- Mu, P., Zhang, Z., Benelli, M., Karthaus, W.R., Hoover, E., Chen, C.C., Wongvipat, J., Ku, S.Y., Gao, D., Cao, Z., et al. (2017). SOX2 promotes lineage plasticity and androgen resistance in TP53- and RB1-deficient prostate cancer. *Science* 355, 84–88.
- Muller, P.A., and Vousden, K.H. (2014). Mutant p53 in cancer: new functions and therapeutic opportunities. *Cancer Cell* 25, 304–317.
- Muller, P.A., Trinidad, A.G., Timpson, P., Morton, J.P., Zanivan, S., van den Berghe, P.V., Nixon, C., Karim, S.A., Caswell, P.T., Noll, J.E., et al. (2013). Mutant p53 enhances MET trafficking and signalling to drive cell scattering and invasion. *Oncogene* 32, 1252–1265.
- Nieto, M., Samper, E., Fraga, M.F., González de Buitrago, G., Esteller, M., and Serrano, M. (2004). The absence of p53 is critical for the induction of apoptosis by 5-aza-2'-deoxycytidine. *Oncogene* 23, 735–743.

- Olive, K.P., Tuveson, D.A., Ruhe, Z.C., Yin, B., Willis, N.A., Bronson, R.T., Crowley, D., and Jacks, T. (2004). Mutant p53 gain of function in two mouse models of Li-Fraumeni syndrome. *Cell* 119, 847–860.
- Olivier, M., Hollstein, M., and Hainaut, P. (2010). TP53 mutations in human cancers: origins, consequences, and clinical use. *Cold Spring Harb. Perspect. Biol.* 2, a001008.
- Olivos, D.J., and Mayo, L.D. (2016). Emerging non-canonical functions and regulation by p53: p53 and stemness. *Int. J. Mol. Sci.* 17, 17.
- Pappas, K., Xu, J., Zairis, S., Resnick-Silverman, L., Abate, F., Steinbach, N., Ozturk, S., Saal, L.H., Su, T., Cheung, P., et al. (2017). p53 maintains baseline expression of multiple tumor suppressor genes. *Mol. Cancer Res.* 15, 1051–1062.
- Parrales, A., and Iwakuma, T. (2015). Targeting oncogenic mutant p53 for cancer therapy. *Front. Oncol.* 5, 288.
- Pearson, B.J., and Sánchez Alvarado, A. (2010). A planarian p53 homolog regulates proliferation and self-renewal in adult stem cell lineages. *Development* 137, 213–221.
- Pfister, N.T., Fomin, V., Regunath, K., Zhou, J.Y., Zhou, W., Silwal-Pandit, L., Freed-Pastor, W.A., Laptenko, O., Neo, S.P., Bargonetti, J., et al. (2015). Mutant p53 cooperates with the SWI/SNF chromatin remodeling complex to regulate VEGFR2 in breast cancer cells. *Genes Dev.* 29, 1298–1315.
- Pomerantz, J., Schreiber-Agus, N., Liégeois, N.J., Silverman, A., Alland, L., Chin, L., Potes, J., Chen, K., Orlow, I., Lee, H.W., et al. (1998). The Ink4a tumor suppressor gene product, p19Arf, interacts with MDM2 and neutralizes MDM2's inhibition of p53. *Cell* 92, 713–723.
- Quelle, D.E., Zindy, F., Ashmun, R.A., and Sherr, C.J. (1995). Alternative reading frames of the INK4a tumor suppressor gene encode two unrelated proteins capable of inducing cell cycle arrest. *Cell* 83, 993–1000.
- Rausch, T., Jones, D.T., Zapatka, M., Stütz, A.M., Zichner, T., Weischenfeldt, J., Jäger, N., Remke, M., Shih, D., Northcott, P.A., et al. (2012). Genome sequencing of pediatric medulloblastoma links catastrophic DNA rearrangements with TP53 mutations. *Cell* 148, 59–71.
- Ritschka, B., Storer, M., Mas, A., Heinzmann, F., Ortells, M.C., Morton, J.P., Sansom, O.J., Zender, L., and Keyes, W.M. (2017). The senescence-associated secretory phenotype induces cellular plasticity and tissue regeneration. *Genes Dev.* 31, 172–183.
- Roth, J., Dittmer, D., Rea, D., Tartaglia, J., Paoletti, E., and Levine, A.J. (1996). p53 as a target for cancer vaccines: recombinant canarypox virus vectors expressing p53 protect mice against lethal tumor cell challenge. *Proc. Natl. Acad. Sci. USA* 93, 4781–4786.
- Schuster, C., Berger, A., Hoelzl, M.A., Putz, E.M., Frenzel, A., Simma, O., Moritz, N., Hoelbl, A., Kovacic, B., Freissmuth, M., et al. (2011). The cooperating mutation or “second hit” determines the immunologic visibility toward MYC-induced murine lymphomas. *Blood* 118, 4635–4645.
- Schvartzman, J.M., Duijff, P.H., Sotillo, R., Coker, C., and Benezra, R. (2011). Mad2 is a critical mediator of the chromosome instability observed upon Rb and p53 pathway inhibition. *Cancer Cell* 19, 701–714.
- Senturk, S., Yao, Z., Camiolo, M., Stiles, B., Rathod, T., Walsh, A.M., Nemajerova, A., Lazzara, M.J., Altorki, N.K., Krainer, A., et al. (2014). p53 Ψ is a transcriptionally inactive p53 isoform able to reprogram cells toward a metastatic-like state. *Proc. Natl. Acad. Sci. USA* 111, E3287–E3296.
- Serrano, M., Lin, A.W., McCurrach, M.E., Beach, D., and Lowe, S.W. (1997). Oncogenic ras provokes premature cell senescence associated with accumulation of p53 and p16INK4a. *Cell* 88, 593–602.
- Shatz, M., Menendez, D., and Resnick, M.A. (2012). The human TLR innate immune gene family is differentially influenced by DNA stress and p53 status in cancer cells. *Cancer Res.* 72, 3948–3957.
- Shay, J.W., Pereira-Smith, O.M., and Wright, W.E. (1991). A role for both RB and p53 in the regulation of human cellular senescence. *Exp. Cell Res.* 196, 33–39.
- Shieh, S.Y., Ikeda, M., Taya, Y., and Prives, C. (1997). DNA damage-induced phosphorylation of p53 alleviates inhibition by MDM2. *Cell* 91, 325–334.
- Shimura, K., Igarashi, H., Goto, M., Tao, H., Yamada, H., Matsuura, S., Tajima, M., Matsuda, T., Yamane, A., Funai, K., et al. (2011). Aberrant expression and mutation-inducing activity of AID in human lung cancer. *Ann. Surg. Oncol.* 18, 2084–2092.
- Shirole, N.H., Pal, D., Kastenhuber, E.R., Senturk, S., Boroda, J., Pisterzi, P., Miller, M., Munoz, G., Anderlueh, M., Ladanyi, M., et al. (2016). TP53 exon-6 truncating mutations produce separation of function isoforms with pro-tumorigenic functions. *eLife* 5, 5.
- Siegl, C., Prusty, B.K., Karunakaran, K., Wischhusen, J., and Rudel, T. (2014). Tumor suppressor p53 alters host cell metabolism to limit *Chlamydia trachomatis* infection. *Cell Rep.* 9, 918–929.
- Soragni, A., Janzen, D.M., Johnson, L.M., Lindgren, A.G., Thai-Quynh Nguyen, A., Tiourin, E., Soriaga, A.B., Lu, J., Jiang, L., Faull, K.F., et al. (2016). A designed inhibitor of p53 aggregation rescues p53 tumor suppression in ovarian carcinomas. *Cancer Cell* 29, 90–103.
- Soto, M., Raaijmakers, J.A., Bakker, B., Spierings, D.C.J., Lansdorp, P.M., Foijer, F., and Medema, R.H. (2017). p53 prohibits propagation of chromosome segregation errors that produce structural aneuploidies. *Cell Rep.* 19, 2423–2431.
- Stambolsky, P., Weisz, L., Shats, I., Klein, Y., Goldfinger, N., Oren, M., and Rotter, V. (2006). Regulation of AIF expression by p53. *Cell Death Differ.* 13, 2140–2149.
- Steensma, D.P., Bejar, R., Jaiswal, S., Lindsley, R.C., Sekeres, M.A., Hasserrjan, R.P., and Ebert, B.L. (2015). Clonal hematopoiesis of indeterminate potential and its distinction from myelodysplastic syndromes. *Blood* 126, 9–16.
- Stewart-Ornstein, J., and Lahav, G. (2017). p53 dynamics in response to DNA damage vary across cell lines and are shaped by efficiency of DNA repair and activity of the kinase ATM. *Sci. Signal.* 10, 10.
- Su, D., Wang, X., Campbell, M.R., Song, L., Safi, A., Crawford, G.E., and Bell, D.A. (2015). Interactions of chromatin context, binding site sequence content, and sequence evolution in stress-induced p53 occupancy and transactivation. *PLoS Genet.* 11, e1004885.
- Sulak, M., Fong, L., Mika, K., Chigurupati, S., Yon, L., Mongan, N.P., Emes, R.D., and Lynch, V.J. (2016). TP53 copy number expansion is associated with the evolution of increased body size and an enhanced DNA damage response in elephants. *eLife* 5. <http://dx.doi.org/10.7554/eLife.11994>.
- Sullivan, K.D., Gallant-Behm, C.L., Henry, R.E., Fraikin, J.L., and Espinosa, J.M. (2012). The p53 circuit board. *Biochim. Biophys. Acta* 1825, 229–244.
- Sullivan, K.D., Palaniappan, V.V., and Espinosa, J.M. (2015). ATM regulates cell fate choice upon p53 activation by modulating mitochondrial turnover and ROS levels. *Cell Cycle* 14, 56–63.
- Sur, S., Pagliarini, R., Bunz, F., Rago, C., Diaz, L.A., Jr., Kinzler, K.W., Vogelstein, B., and Papadopoulos, N. (2009). A panel of isogenic human cancer cells suggests a therapeutic approach for cancers with inactivated p53. *Proc. Natl. Acad. Sci. USA* 106, 3964–3969.
- Tang, Y.C., Williams, B.R., Siegel, J.J., and Amon, A. (2011). Identification of aneuploidy-selective antiproliferation compounds. *Cell* 144, 499–512.
- Thorburn, J., Andrysiak, Z., Staskiewicz, L., Gump, J., Maycotte, P., Oberst, A., Green, D.R., Espinosa, J.M., and Thorburn, A. (2014). Autophagy controls the kinetics and extent of mitochondrial apoptosis by regulating PUMA levels. *Cell Rep.* 7, 45–52.
- Ting, D.T., Lipson, D., Paul, S., Brannigan, B.W., Akhavanfard, S., Coffman, E.J., Contino, G., Deshpande, V., Iafrafe, A.J., Letovsky, S., et al. (2011). Aberrant overexpression of satellite repeats in pancreatic and other epithelial cancers. *Science* 331, 593–596.
- Tosoni, D., Zecchini, S., Cozzoli, M., Colaluca, I., Mazzarol, G., Rubio, A., Caccia, M., Villa, E., Zilian, O., Di Fiore, P.P., and Pece, S. (2015). The Numb/p53 circuitry couples replicative self-renewal and tumor suppression in mammary epithelial cells. *J. Cell Biol.* 211, 845–862.
- Tovy, A., Spiro, A., McCarthy, R., Shipony, Z., Aylon, Y., Allton, K., Ainbinder, E., Furth, N., Tanay, A., Barton, M., and Oren, M. (2017). p53 is essential for DNA methylation homeostasis in naïve embryonic stem cells, and its loss promotes clonal heterogeneity. *Genes Dev.* 31, 959–972.

- Tschaharganeh, D.F., Xue, W., Calvisi, D.F., Evert, M., Michurina, T.V., Dow, L.E., Banito, A., Katz, S.F., Kastenhuber, E.R., Weissmueller, S., et al. (2014). p53-dependent Nestin regulation links tumor suppression to cellular plasticity in liver cancer. *Cell* 158, 579–592.
- Tschaharganeh, D.F., Bosbach, B., and Lowe, S.W. (2016). Coordinated tumor suppression by chromosome 8p. *Cancer Cell* 29, 617–619.
- Tubio, J.M.C., Li, Y., Ju, Y.S., Martincorena, I., Cooke, S.L., Tojo, M., Gundem, G., Pipinikas, C.P., Zamora, J., Raine, K., et al.; ICGC Breast Cancer Group; ICGC Bone Cancer Group; ICGC Prostate Cancer Group (2014). Mobile DNA in cancer. Extensive transduction of nonrepetitive DNA mediated by L1 retrotransposition in cancer genomes. *Science* 345, 1251343.
- Valente, L.J., Gray, D.H., Michalak, E.M., Pinon-Hofbauer, J., Egle, A., Scott, C.L., Janic, A., and Strasser, A. (2013). p53 efficiently suppresses tumor development in the complete absence of its cell-cycle inhibitory and proapoptotic effectors p21, Puma, and Noxa. *Cell Rep.* 3, 1339–1345.
- van der Burg, S.H., Menon, A.G., Redeker, A., Bonnet, M.C., Drijfhout, J.W., Tollenaar, R.A., van de Velde, C.J., Moingeon, P., Kuppen, P.J., Offringa, R., and Melief, C.J. (2002). Induction of p53-specific immune responses in colorectal cancer patients receiving a recombinant ALVAC-p53 candidate vaccine. *Clin. Cancer Res.* 8, 1019–1027.
- Vassilev, L.T., Vu, B.T., Graves, B., Carvajal, D., Podlaski, F., Filipovic, Z., Kong, N., Kammlott, U., Lukacs, C., Klein, C., et al. (2004). In vivo activation of the p53 pathway by small-molecule antagonists of MDM2. *Science* 303, 844–848.
- Venkatarayanan, A., Raulji, P., Norton, W., Chakravarti, D., Coarfa, C., Su, X., Sandur, S.K., Ramirez, M.S., Lee, J., Kingsley, C.V., et al. (2015). IAPP-driven metabolic reprogramming induces regression of p53-deficient tumours in vivo. *Nature* 517, 626–630.
- Ventura, A., Kirsch, D.G., McLaughlin, M.E., Tuveson, D.A., Grimm, J., Lintault, L., Newman, J., Reczek, E.E., Weissleder, R., and Jacks, T. (2007). Restoration of p53 function leads to tumour regression in vivo. *Nature* 445, 661–665.
- Vitale, I., Senovilla, L., Jemaà, M., Michaud, M., Galluzzi, L., Kepp, O., Nanty, L., Criollo, A., Rello-Varona, S., Manic, G., et al. (2010). Multipolar mitosis of tetraploid cells: inhibition by p53 and dependency on Mos. *EMBO J.* 29, 1272–1284.
- Vitre, B.D., and Cleveland, D.W. (2012). Centrosomes, chromosome instability (CIN) and aneuploidy. *Curr. Opin. Cell Biol.* 24, 809–815.
- Wang, Y., Suh, Y.A., Fuller, M.Y., Jackson, J.G., Xiong, S., Terzian, T., Quintás-Cardama, A., Bankson, J.A., El-Naggar, A.K., and Lozano, G. (2011). Restoring expression of wild-type p53 suppresses tumor growth but does not cause tumor regression in mice with a p53 missense mutation. *J. Clin. Invest.* 121, 893–904.
- Wang, P.Y., Ma, W., Park, J.Y., Celi, F.S., Arena, R., Choi, J.W., Ali, Q.A., Tripathi, D.J., Zhuang, J., Lago, C.U., et al. (2013). Increased oxidative metabolism in the Li-Fraumeni syndrome. *N. Engl. J. Med.* 368, 1027–1032.
- Wang, Q., Zou, Y., Nowotschin, S., Kim, S.Y., Li, Q.V., Soh, C.L., Su, J., Zhang, C., Shu, W., Xi, Q., et al. (2017). The p53 family coordinates Wnt and nodal inputs in mesendodermal differentiation of embryonic stem cells. *Cell Stem Cell* 20, 70–86.
- Weissmueller, S., Machado, E., Saborowski, M., Morris, J.P., 4th, Wagenblast, E., Davis, C.A., Moon, S.H., Pfister, N.T., Tschaharganeh, D.F., Kitzing, T., et al. (2014). Mutant p53 drives pancreatic cancer metastasis through cell-autonomous PDGF receptor β signaling. *Cell* 157, 382–394.
- Welch, J.S., Petti, A.A., Miller, C.A., Fronick, C.C., O’Laughlin, M., Fulton, R.S., Wilson, R.K., Baty, J.D., Duncavage, E.J., Tandon, B., et al. (2016). TP53 and decitabine in acute myeloid leukemia and myelodysplastic syndromes. *N. Engl. J. Med.* 375, 2023–2036.
- Williams, A.B., and Schumacher, B. (2016). p53 in the DNA-damage-repair process. *Cold Spring Harb. Perspect. Med.* 6, 6.
- Wong, T.N., Ramsingh, G., Young, A.L., Miller, C.A., Touma, W., Welch, J.S., Lamprecht, T.L., Shen, D., Hundal, J., Fulton, R.S., et al. (2015). Role of TP53 mutations in the origin and evolution of therapy-related acute myeloid leukaemia. *Nature* 518, 552–555.
- Wylie, A., Lu, W.J., D’Brot, A., Buszczak, M., and Abrams, J.M. (2014). p53 activity is selectively licensed in the *Drosophila* stem cell compartment. *eLife* 3, e01530.
- Wylie, A., Jones, A.E., D’Brot, A., Lu, W.J., Kurtz, P., Moran, J.V., Rakheja, D., Chen, K.S., Hammer, R.E., Comerford, S.A., et al. (2016). p53 genes function to restrain mobile elements. *Genes Dev.* 30, 64–77.
- Xie, M., Lu, C., Wang, J., McLellan, M.D., Johnson, K.J., Wendl, M.C., McMichael, J.F., Schmidt, H.K., Yellapantula, V., Miller, C.A., et al. (2014). Age-related mutations associated with clonal hematopoietic expansion and malignancies. *Nat. Med.* 20, 1472–1478.
- Xu, J., Qian, J., Hu, Y., Wang, J., Zhou, X., Chen, H., and Fang, J.Y. (2014). Heterogeneity of Li-Fraumeni syndrome links to unequal gain-of-function effects of p53 mutations. *Sci. Rep.* 4, 4223.
- Xue, W., Zender, L., Miething, C., Dickins, R.A., Hernando, E., Krizhanovskiy, V., Cordon-Cardo, C., and Lowe, S.W. (2007). Senescence and tumour clearance is triggered by p53 restoration in murine liver carcinomas. *Nature* 445, 656–660.
- Yin, Y., Tainsky, M.A., Bischoff, F.Z., Strong, L.C., and Wahl, G.M. (1992). Wild-type p53 restores cell cycle control and inhibits gene amplification in cells with mutant p53 alleles. *Cell* 70, 937–948.
- Yonish-Rouach, E., Resnitzky, D., Lotem, J., Sachs, L., Kimchi, A., and Oren, M. (1991). Wild-type p53 induces apoptosis of myeloid leukaemic cells that is inhibited by interleukin-6. *Nature* 352, 345–347.
- Young, A.R., Narita, M., Ferreira, M., Kirschner, K., Sadaie, M., Darot, J.F., Tavaré, S., Arakawa, S., Shimizu, S., Watt, F.M., and Narita, M. (2009). Autophagy mediates the mitotic senescence transition. *Genes Dev.* 23, 798–803.
- Yu, X., Vazquez, A., Levine, A.J., and Carpizo, D.R. (2012). Allele-specific p53 mutant reactivation. *Cancer Cell* 21, 614–625.
- Yun, M.H., Gates, P.B., and Brockes, J.P. (2013). Regulation of p53 is critical for vertebrate limb regeneration. *Proc. Natl. Acad. Sci. USA* 110, 17392–17397.
- Zeebstraten, E.C., Speetjens, F.M., Welters, M.J., Saadatmand, S., Stynenbosch, L.F., Jongen, R., Kapiteijn, E., Gelderblom, H., Nijman, H.W., Valentijn, A.R., et al. (2013). Addition of interferon- α to the p53-SLP® vaccine results in increased production of interferon- γ in vaccinated colorectal cancer patients: a phase I/II clinical trial. *Int. J. Cancer* 132, 1581–1591.
- Zhang, Y., Xiong, Y., and Yarbrough, W.G. (1998). ARF promotes MDM2 degradation and stabilizes p53: ARF-INK4a locus deletion impairs both the Rb and p53 tumor suppression pathways. *Cell* 92, 725–734.
- Zhang, C., Liu, J., Liang, Y., Wu, R., Zhao, Y., Hong, X., Lin, M., Yu, H., Liu, L., Levine, A.J., et al. (2013). Tumour-associated mutant p53 drives the Warburg effect. *Nat. Commun.* 4, 2935.
- Zhao, Z., Zuber, J., Diaz-Flores, E., Lintault, L., Kogan, S.C., Shannon, K., and Lowe, S.W. (2010). p53 loss promotes acute myeloid leukemia by enabling aberrant self-renewal. *Genes Dev.* 24, 1389–1402.
- Zhu, J., Sammons, M.A., Donahue, G., Dou, Z., Vedadi, M., Getlik, M., Barsyte-Lovejoy, D., Al-awar, R., Katona, B.W., Shilatifard, A., et al. (2015). Gain-of-function p53 mutants co-opt chromatin pathways to drive cancer growth. *Nature* 525, 206–211.

Mapping the Neural Substrates of Behavior

Alice A. Robie,¹ Jonathan Hirokawa,^{1,2} Austin W. Edwards,¹ Lowell A. Umayam,¹ Allen Lee,¹ Mary L. Phillips,^{1,4} Gwyneth M. Card,¹ Wyatt Korff,¹ Gerald M. Rubin,¹ Julie H. Simpson,^{1,3} Michael B. Reiser,¹ and Kristin Branson^{1,5,*}

¹Janelia Research Campus, Howard Hughes Medical Institute, Ashburn, VA, USA

²Laboratory of Integrative Brain Function, The Rockefeller University, New York, NY, USA

³Department of Molecular, Cellular, and Developmental Biology, UC Santa Barbara, Santa Barbara, CA, USA

⁴Department of Neurobiology, University of Alabama at Birmingham, Birmingham, AL, USA

⁵Lead Contact

*Correspondence: bransonk@janelia.hhmi.org

<http://dx.doi.org/10.1016/j.cell.2017.06.032>

SUMMARY

Assigning behavioral functions to neural structures has long been a central goal in neuroscience and is a necessary first step toward a circuit-level understanding of how the brain generates behavior. Here, we map the neural substrates of locomotion and social behaviors for *Drosophila melanogaster* using automated machine-vision and machine-learning techniques. From videos of 400,000 flies, we quantified the behavioral effects of activating 2,204 genetically targeted populations of neurons. We combined a novel quantification of anatomy with our behavioral analysis to create brain-behavior correlation maps, which are shared as browsable web pages and interactive software. Based on these maps, we generated hypotheses of regions of the brain causally related to sensory processing, locomotor control, courtship, aggression, and sleep. Our maps directly specify genetic tools to target these regions, which we used to identify a small population of neurons with a role in the control of walking.

INTRODUCTION

To address the fundamental question of how nervous systems generate behavior, we must first identify which neurons constitute the neural circuits generating these behaviors. In model organisms like *Drosophila melanogaster*, if we furthermore obtain genetic access to these neurons, we can leverage powerful genetic tools for manipulating and recording neural activity (Owald et al., 2015; Sivanantharajah and Zhang, 2015) to probe, observe, and ultimately understand the neural computations that give rise to behavior. Comprehensive functional mapping of each neuron to its behavioral roles is difficult, even in model organisms, because of the scales involved: hundreds of thousands of interconnected neurons and approaching-infinite variety of behavior. To create a map of the neural substrates of a single behavior would require the ability to monitor neural activity at the resolution of individual cells across the entire brain in freely behaving animals. Calcium imaging (Ahrens et al., 2013; Seelig and Jayaraman, 2013), calcium integrators (Fosque et al.,

2015), and related approaches (Randlett et al., 2015) have recently been used to measure neural activity in large neuronal populations of behaving animals. As yet, these approaches are limited in at least one of the following ways: the need to restrain the animal or study a single behavior, spatial extent, sensitivity, and spatial and temporal resolution. A complementary method for mapping the neural substrates of behavior, with different strengths and weaknesses, is to manipulate neural activity and observe the behavioral effects. Here, we synthesized whole-brain-behavior maps by combining the results of manipulating activity in thousands of small neural populations across the brain in hundreds of thousands of animals. To make these maps of the neural substrates of behavior, we have taken an approach analogous to early stimulation experiments used to map somatosensory cortex (Penfield, 1950), using modern genetic tools to activate thousands of sparse populations of neurons, and machine-vision and machine-learning methods to extract behavior-anatomy maps from the resulting mass of data. These maps can serve as a guide for future mechanistic and functional studies of the neural substrates of behavior.

We leveraged a powerful resource available in *Drosophila*: a collection of thousands of GAL4 driver lines, each providing control over activity in the same neuronal populations across individuals (Jenett et al., 2012). These neuronal populations consist of tens to hundreds of (often) functionally unrelated cell types across the brain (Pfeiffer et al., 2008). While this feature of GAL4 lines is often viewed as a limitation, it implies that many lines will have overlapping expression, a fact we exploit to accumulate evidence to identify the neural substrates of a behavior. As these driver lines often have expression in multiple regions throughout the brain, we could efficiently test the role of all brain regions by systematically assaying the locomotor and social behavior of flies across a large collection of driver lines. To this end, we quantified the behavioral effects of neuronal activation for over 400,000 flies across 2,204 GAL4 lines, resulting in over 100 billion annotations of behavior. The size of this dataset—over 500 TB of video data—necessitated automation, and we developed computer-vision-based methods to quantitatively profile the behavioral effects of activation. We furthermore mined high-resolution, volumetric images of the GAL4 driver line expression patterns to create a new subdivision of the fly brain into genetically defined subcompartments, then automatically identified which GAL4 lines targeted each neuronal subcompartment. We developed an analytical framework for combining

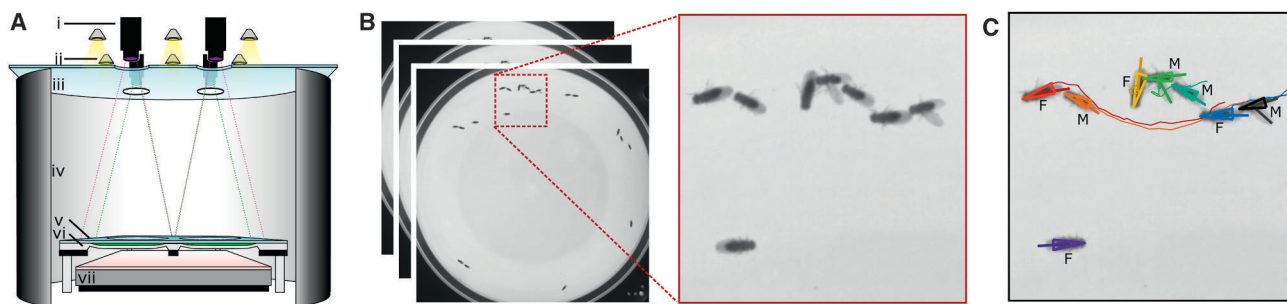


Figure 1. Behavior Video Data Collection and Tracking

(A) Schematic diagram of the Fly Bowl behavior rig. Each of our two rigs consisted of four walking arenas that can be used in parallel; diagram shows a cross-section through the two nearest arenas. *i*: A camera with an IR-pass filter was positioned above each arena. *ii*: Visible light was provided by LED lights and diffused through *iii*, a thin sheet of white acrylic. *iv*: A cylinder with white paper inside and black-out material outside provided a constant visual surround. *v*: A sheet of glass coated with Sigmacote provided a low, slippery ceiling to the arenas. *vi*: The arenas were milled into a sheet of polycarbonate, each with a diameter of 127 mm and a center height of 3.5 mm. To reduce the amount of time spent at the edges, each arena has sloped walls (Simon and Dickinson, 2010). *vii*: A panel of near-IR LEDs provided bright, constant illumination to the camera that was invisible to the flies.

(B) Collected video. Each video consisted of ~30,000 1024 × 1024 pixel frames of ~10 male and ~10 female flies.

(C) Example results of automatic tracking of flies' bodies and wings. We used Ctrax (Branson et al., 2009) to automatically track the flies and fit directed-ellipses to their bodies in each frame (size and orientation indicated by triangles; color indicates identity). The sex of each fly was classified automatically based on fit-ellipse area (M, male; F, female). Thin lines indicate wing angles tracked using custom MATLAB software.

these large, quantitative behavior and anatomy datasets, the results of which were brain-wide maps of the neural substrates for a broad range of behavior phenotypes.

These maps identify distinct neural substrates for the control of at least six behavior features (increased walking, jumping, backing up, wing-grooming, female aggression, and wing angle). They can contain multiple behavior-circuit components, as in the case of the increased walking map, and thus facilitate a circuit-level understanding of behavior control. Additionally, these maps allow immediate identification of genetic tools to further test and investigate the proposed structure-function relationships. We demonstrate how our maps can be used to create sparse, intersectional genetic driver lines targeting specific subpopulations of neurons within the map. To foster the systematic identification and investigation of many more behavior-anatomy relationships throughout the brain, we created searchable websites and interactive software.

RESULTS

Computer-Vision-Based Quantification of the Effects of Neural Activation

2,204 GAL4 lines from the *Janelia* GAL4 collection were selected for behavioral measurement (Table S1) based on their expression patterns, as imaged by the *Janelia* Fly Light project (Jenett et al., 2012), prioritizing lines with sparser expression and providing coverage of the entire brain (Figure S1). To genetically activate subsets of neurons, we used the GAL4-UAS system to target expression of the temperature-sensitive dTRPA1 cation channel. For each of these lines, we recorded approximately eight videos of mixed-sex groups of ~20 flies freely behaving in a Fly Bowl (Simon and Dickinson, 2010), a shallow arena designed to facilitate automatic tracking of groups of walking flies, above the activating temperature for dTRPA1. Parameters of our behavior assay were chosen so that flies from our genetic control

(an empty GAL4 line crossed to the same effector) performed both independent locomotion/foraging behaviors and social behaviors such as courtship, allowing us to see activation-induced increases and decreases in activity and social behavior. Our Fly Bowl apparatus and custom data-capture software were optimized for high-throughput, high-fidelity, consistent behavior data collection (Figures 1A, 1B, and S2A; Method Details). Using this system, we collected data at a rate of up to 116 videos from 25 GAL4 lines per day and recorded and curated in total 20,288 1,000 s videos at 30.3 fps (>500 TB of uncompressed data) over a 1.5-year period. The data collected were sufficiently stereotyped that we could use identical parameters for all analyses, and retests of each GAL4 line produced consistent behavioral measurements.

We used fully automated computer vision methods to measure a broad range of detailed statistics of the flies' locomotion and social behavior at scale. We automatically tracked the body position, orientation, and wing positions and classified the sex of each fly in each video (Figures 1C and S2B–S2D; Method Details) (Branson et al., 2009). From these trajectories, we computed a suite of 128 hand-engineered features, termed per-frame features, that captured behaviorally relevant, continuous properties of the flies' instantaneous poses and movements in each frame, such as the instantaneous speed, the distance to the closest fly, and the angle between the two wings (Figure 2A; Method Details; Table S2) (Kabra et al., 2013).

We created 14 automatic behavior classifiers for locomotion behaviors (walk, stop, back up, crabwalk, pivot-tail, pivot-center, jump, righting, wing grooming) and social behaviors (chase, touch, wing extension, attempted copulation, wing flick) (Figure 2B; Method Details; Movie S1), chosen based on our initial observations of control-line behavior and previously described components of courtship (Yamamoto and Koganezawa, 2013). While this description of fly behavior is not complete, 84% of control-line frames fell into at least one of these categories.

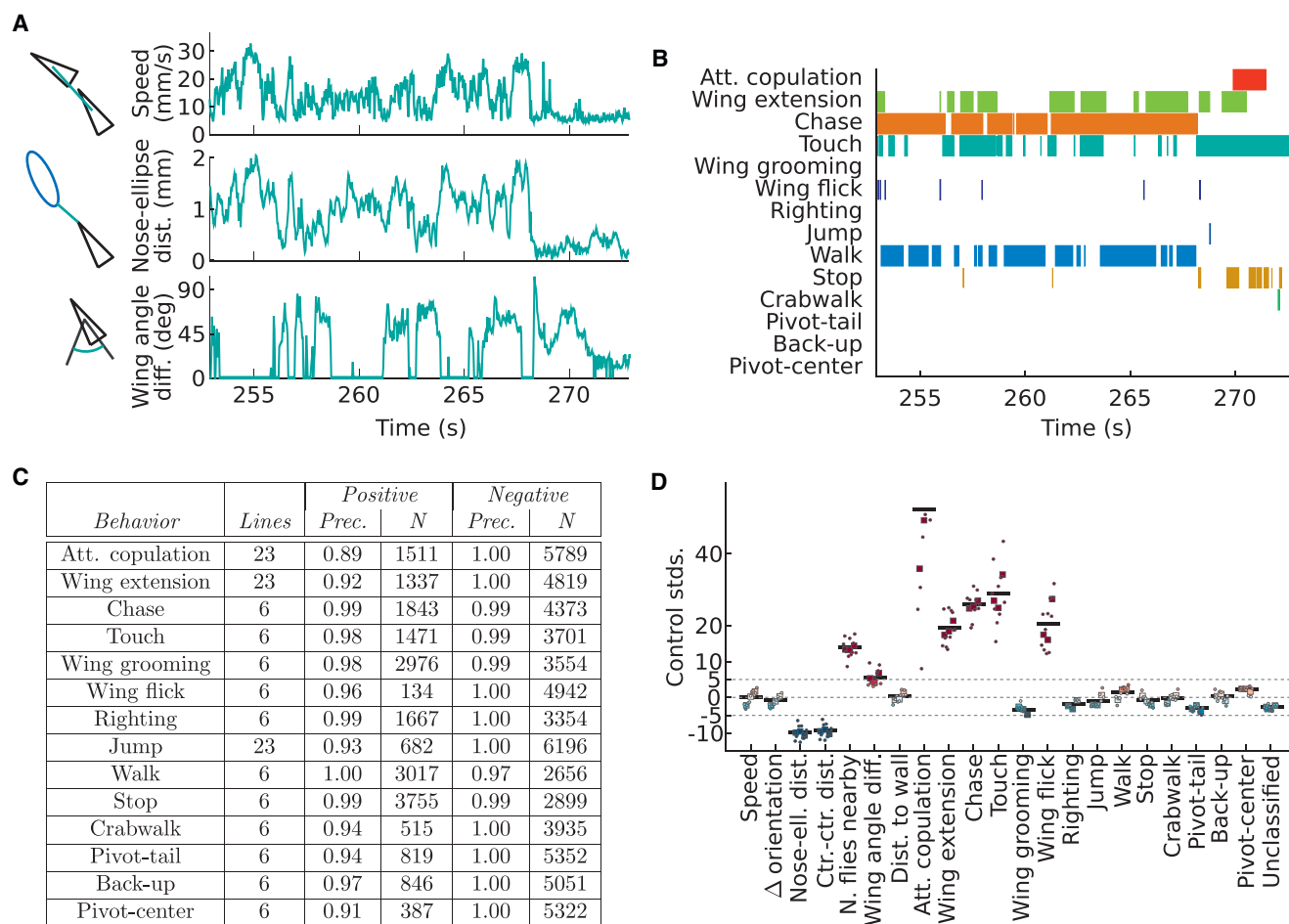


Figure 2. Automated Quantification of Behavior

(A) Example per-frame feature time series for one fly for 20 s. Per-frame features are simple, engineered functions of the trajectories.

(B) Automatic behavior classification results for the same fly and time interval as (A). Each row and color corresponds to a different behavior classifier. Color indicates that the classifier predicted that the behavior was occurring.

(C) Accuracy of automated behavior classifiers. We quantified the classifiers' precision for each behavior classifier—for all frames predicted by the classifier to be of a given class, what fraction were also manually labeled to be of that class? *Positive*, *Negative* class refers to frames for which the behavior is, is not occurring, resp. We report precision (*Prec.*), computed across all frames and lines annotated, and the number of frames predicted as positive and negative (*N*, number of points from which precision is computed). Per-line results are in Table S4.

(D) Example population-level behavior statistics (x axis) for line R82E08, computed from both per-frame features (A) and behavior classifications (B). y axis indicates the signed number of control standard deviations different from control mean. Circles corresponds to videos, squares to retests of the line at different times of year from different crosses, and black horizontal lines to the line-level mean. Across retests, R82E08 spends more time performing social behaviors, e.g., attempted copulation, wing extension, and chase. "Unclassified" is the fraction of time when behavior is not classified as any of our 14 behaviors. Data was clipped at 60 standard deviations.

The automatic classifiers were trained using JAABA, an interactive machine-learning tool (Kabra et al., 2013), to match our behavior definitions. Here, we manually labeled the behaviors the flies were performing in a small set of frames, and the machine-learning algorithm learned classifiers that could automatically reproduce these manual labels. To ensure that the classifiers were accurate across all the behaviorally diverse lines assayed, we used JAABA's interactive training framework to iteratively add training labels for lines selected based on several heuristics (Method Details). On average, to train each classifier, we labeled 9,000 frames from 750 contiguous bouts, nine videos, and eight lines (Table S3). To our knowledge, this is the

largest, most diverse dataset to which machine-vision-based behavior classification has been applied. Averaging across behaviors and GAL4 lines, the classifiers' per-frame average accuracy was 97.6%, measured comparing the automatic classifiers' predictions to human annotations on videos from each of 5–23 representative GAL4 lines (Figures 2C and S3A; Method Details; Table S4).

By combining time series of per-frame features and behavior classifications for a given video, we computed 203 statistics to describe the behavior of the population, such as the fraction of time the flies spent walking, the average speed of the flies, and the average speed of the flies while walking

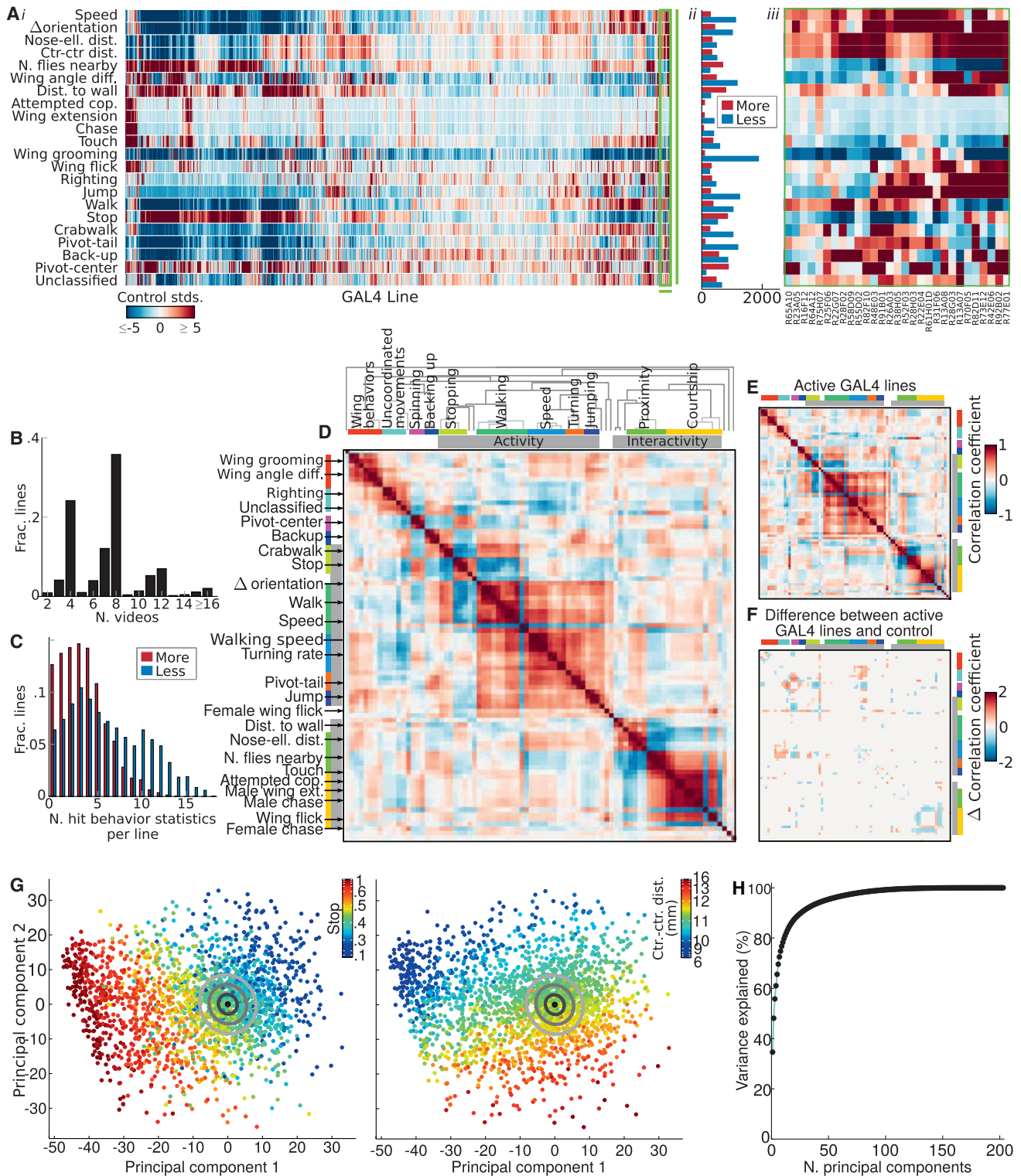


Figure 3. Behavioral Effects of Neural Activation

(A) *i*: Table of behavioral effects of neural activation for all 2,205 GAL4 lines assayed. Rows correspond to line-level behavior statistics (Table S6), columns to GAL4 lines. Color indicates how much higher (red) or lower (blue) the behavior statistic was for the line than control. Lines are sorted to highlight behavioral similarities. *ii*: Number of GAL4 lines that had significantly larger (red) and smaller (blue) values for each of the behavior statistics shown (FDR [false discovery rate] ≤ 0.1). *iii*: Zoom-in of green box in *i*.

(legend continued on next page)

(Figures 2D and 3A; Method Details; Tables S5 and S6). These statistics were hand engineered without looking at the results of the screen and included measures we hypothesized might be independently modulated. We obtained line-level statistics by averaging in a manner chosen to account for the strengths of dependencies: the approximately four videos recorded simultaneously from the same cohort were more similar than the approximately two biological replicates of the same line recorded at different times of the year (Figures 2D and 3B; Method Details). Each line-level behavior statistic was the average of ~ 4 million per-fly, per-frame measurements of behavior and, as measurement noise averaged out, were accurate and consistent across retests (Figures S3B and S3C). This allowed our analyses to be sensitive to smaller changes than were apparent to the human eye; for example, our analyses of walking behavior used increases in walking rates of under 5%.

To measure behavior changes due to neural activation, we compared the measurements for each GAL4 line to those from a genetic control (Figures 3A and 3C; Method Details). For each behavior statistic, we computed both the statistical significance (Method Details) and the magnitude of the effect of activation in terms of the signed number of standard deviations from control. Figure 3A summarizes the effects of neural activation for all 2,205 lines assayed and a subset of the behavior statistics.

As we measured the effects of activation for a large, unbiased sample of neuronal populations, patterns in the observed behavioral effects may be informative about how behavior is modulated by, and thus its representation in, the nervous system. Many of our behavior measurements were strongly correlated or anti-correlated (Figures 3D, 3E, and S4A). Some correlations were a result of our behavior definitions; e.g., fraction of time stopped and average speed are necessarily anti-correlated. Other correlations were a result of the structure of fly behavior; e.g., fraction of time chasing and attempting copulation are highly correlated (Figures 3D, 3E, S4A, and S4B). Both across retests of the control line and across GAL4 lines, behavior appeared to be most commonly modulated on the axes of activity level (e.g., fraction of time stopped) and how much the flies interacted (e.g., average inter-fly distance). Indeed, the first two principal components of the line-versus-behavior matrix (Figure 3A) corresponded to these two properties (Figures 3G, 3H, S4D, and S4E). Furthermore, we observed significant differences in these properties for many lines (60% of lines showed a significant dif-

ference in fraction of time stopped, 40% in inter-fly distance, Figure 3A, ii). For both properties, we observed lines with extreme values (flies that rarely moved and flies that rarely stopped, flies that clustered together and flies that actively avoided each other; Method Details), as well as for every value in between.

Groups of behavior measures that were strongly correlated across control retests (Figure 3D) were usually modulated together by neural activation as well, and the correlation structure across control line retests and across GAL4 lines was remarkably similar (Figures 3D–3F, and S4A–S4C). For example, it was the rare exception to evoke male chasing without also evoking other courtship behaviors such as attempted copulation (though such exceptions did occur; Figure S4B). Similarly, locomotion behaviors were modulated together; e.g., increases in walking were accompanied by increases in turning (Figure S4B).

We were surprised by how common it was to observe behavioral effects of activation, despite the sparsity of the expression patterns of the lines we assayed; based on our sensitive quantitative analyses, we observed a significant difference for at least one behavioral statistic for 98% of the GAL4 lines ($FDR \leq 0.1$; Method Details). We observed a variety of extreme phenotypes, including lines that jumped up to 100 \times more than control and maintained large inter-fly distances (R68C07, R73E12), lines for which males chased up to 20 \times more than control (R82E08, R71G01), lines for which females chased over 20% of the time (R26F09, R26E01), lines that groomed their wings over 5 \times more than control (R29E04, R73E01), a single line that copulated (R34H05), and lines that stopped a large fraction of the time in close proximity to other flies and pivoted around their centers (R61C12, R66A06). The high rate of behavioral phenotypes suggests that the activation of almost any subset of neurons can generate a detectable change in behavior (due to direct as well as indirect effects of activation); thus, our behavior dataset is rich in information about the functional roles of neural structures. However, this also presents a computational challenge for discovering meaningful behavior-anatomy correlations and necessitates analyses that take advantage of automation.

As a resource for the neuroscience community, we have created a website summarizing the measured behavioral effects of activation for each GAL4 line (<http://research.janelia.org/bransonlab/FlyBowl/BehaviorResults>). These webpages can be searched by line name, allowing researchers who have identified anatomically interesting GAL4 lines to find behavioral

(B) Histogram across GAL4 lines of the total number of videos recorded.

(C) Histogram across GAL4 lines of the number of behavior statistics (out of the 22 shown in [A]) that a given GAL4 line has a significantly higher (red) or lower (blue) value for than control ($FDR \leq 0.1$).

(D) Spearman's rank correlation coefficient between line-level behavior statistics across 762 retests of the control line (red indicates positive correlation, e.g., between attempted copulation and male chasing; blue indicates negative correlation, e.g., between stop and walk; and white indicates no correlation). Statistics are sorted according to their hierarchical clustering, shown at the top. We give descriptive names to several clusters (colored bars) and indicate a few representative behavior statistics for each (left). The same ordering is used in (E) and (F) and Figure S4A.

(E) As in (D), but for the 1646 GAL4 lines that are active (stopped less than 55% of the time). The correlation structure between control lines is similar to that of the active lines.

(F) Differences in correlations between active GAL4 lines and control retests. Red indicates that correlation is significantly higher for the GAL4 lines than control retests, blue that it is significantly lower ($FDR \leq 0.1$), white that correlation differences are not significant.

(G) Principal directions of behavioral effects of neural activation. Behavior vectors for all GAL4 lines projected onto their first two principal components. Dots correspond to GAL4 lines, color indicates average fraction of time stopped (left) and inter-fly distance (D center, right). The black dot corresponds to the control line, and gray circles to 1–3 standard deviations. The first component represents activity level, while the second represents how much the flies interacted.

(H) Amount of variance of GAL4-line behavior explained by its principal components.

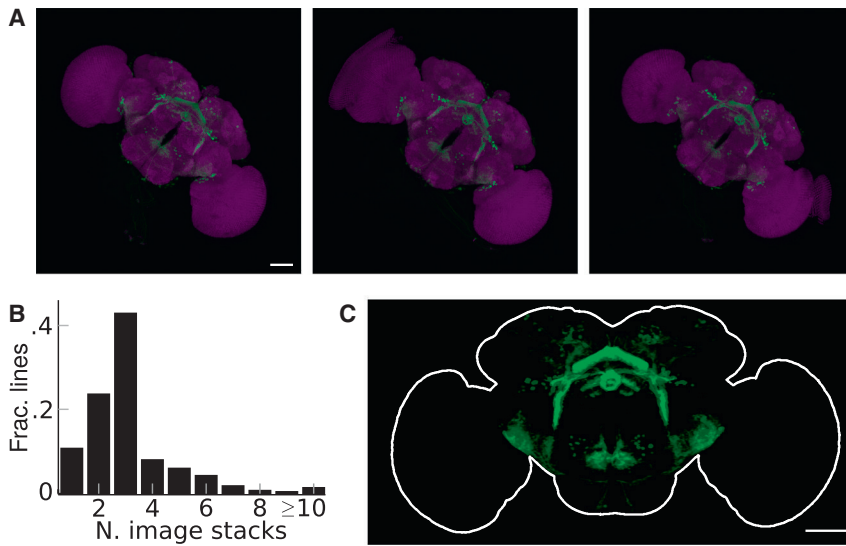


Figure 4. Expression Pattern Image Processing

(A) Maximum intensity projections (MIPs) of raw image stacks of three dissected brain samples for R26C06 (Jenett et al., 2012). GFP expression is in green, and nc82 reference stain is in magenta. All panels: scale bar, 50 μm .

(B) Histogram across GAL4 lines of the number of image stacks combined to create the per-line expression pattern.

(C) Raw image stacks are aligned, normalized, averaged, and blurred to create a single image stack for the GAL4 line.

annotations of the effects of neural activation. Alternatively, they can be indexed by any of our behavior statistics, allowing researchers interested in a particular behavior to find GAL4 lines that exhibit strong phenotypes for those behaviors upon neural activation.

Mapping Behavior to Neural Anatomy

To find regions of the brain correlated with each behavior measure, we combined our behavior dataset with a novel quantification of the neural expression pattern for each GAL4 line. As there is no cell-type annotation of the Janelia GAL4 collection, we developed a method to quantify expression pattern from 3D images of the expression pattern in the brain of each line (Jenett et al., 2012) (Figures 4A and 4B). We aligned (Peng et al., 2011) and normalized the expression pattern images so that, across images and GAL4 lines, each voxel location corresponded to approximately the same location in the brain, and voxel intensity approximated our confidence that there was expression at that location (Figures 4C and S5; Method Details). For each of the 30 million voxels in the brain images, each representing $<1 \mu\text{m}^3$ of the brain, we could test for statistically significant correlation across GAL4 lines between anatomical expression (intensity) at that voxel location and a given behavior measure. However, this amounts to performing 30 million hypothesis tests, and correcting for the effects of this large number of comparisons would require the original correlation hypothesis tests to have extremely high significance. Thus, a subdivision of the brain into larger regions was necessary. The *Drosophila* brain has been partitioned into 68 named structures, such as the mushroom body and the medulla, based on neuroanatomy (Ito et al., 2014). Thus, we could instead perform just 68 correlation hypothesis tests, one for each of these named structures, in which expression for the region is computed by averaging voxel intensities across the region. However, these regions are large and imprecise, and averaging expression across them obscured signal and resulted in incomplete, low-resolution maps.

similar expression across the GAL4 lines. This clustering was based on the assumption that if the expression for a pair of voxels was the same across most GAL4 lines, they might be part of the same neuronal cell type or functional unit (Figures 5A and S7; Method Details). The resulting segmentation shows correspondence to known structures in the fly brain (Figures 5B–5D; Data S1; Movie S2). For example, our segmentation consists of layers in the medulla (Nern et al., 2015) and fan-shaped body (Wolff et al., 2015) and annuli in the ellipsoid body (Wolff et al., 2015). A similar methodology has been employed to discover novel optic glomeruli (Panser et al., 2016) (Method Details).

We used this clustering of the entire fly brain to quantitatively represent the neural expression pattern for each GAL4 line by computing the average pixel intensity within each supervoxel (Figure 6). Then, for a given behavior measure (e.g., walking more than control), we tested whether, for each supervoxel, there was a positive correlation between the behavior measure and the neural expression across the GAL4 lines (Method Details). We visualized the correlated neural regions by mapping the p values of these correlation hypothesis tests back to the supervoxel locations (Figure 7A; Movie S3), creating 3D maps of the neural regions related to the behavior phenotype. Combining information from thousands of lines allowed us to find these correlations despite confounding factors—that multiple regions of the brain are likely involved in a given behavior and that the expression patterns of the majority of GAL4 lines likely contain multiple cell types that interact (Figure 7B).

For each of the behavior statistics we measured, we made such maps for unexpectedly high (e.g., wing grooming more than control) and unexpectedly low values (e.g., wing grooming less than control). In addition, we made behavior-anatomy maps for combined behavior measures (e.g., stopping more but not wing grooming more than control).

We can further analyze these maps by focusing on those lines most important in producing high correlations (lines that both have expression in some of the significantly correlated supervoxels and show the given behavior phenotype; Method Details).

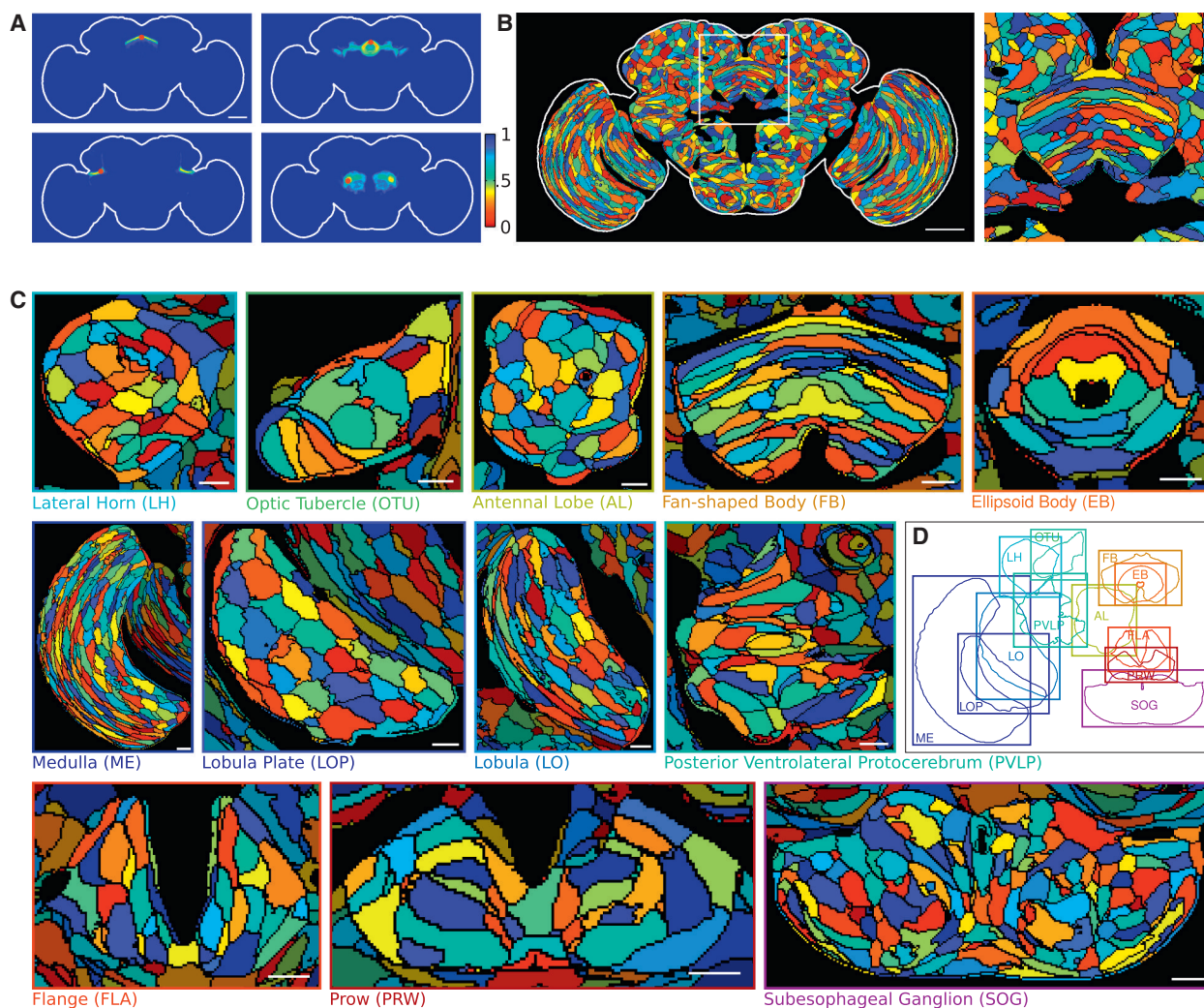


Figure 5. Clustering the Fly Brain

(A) Illustration of voxel clustering distance function. For the voxel indicated by the red dot, we show in pseudocolor the distance to each other voxel (minimum projection over z). Distances to voxels in related regions are smaller. Scale bar, 50 μm .

(B) Resulting clustering of brain into supervoxels. We show cross-sections of supervoxels at $z = 72.5 \mu\text{m}$; each supervoxel has a different, randomly selected color. White box indicates location of zoomed-in region in right panel. Scale bar, 50 μm .

(C) As in (B), clustering for selected z -slices through 12 compartments. Regions outside the given compartment are darkened. Scale bars, 10 μm .

(D) Locations of each of the shown compartments (C) within the brain.

We used these lines to automatically cluster the increased-walking map (Figure 7A) based on expression correlation between supervoxels (Figure S7A). The resulting clustering revealed components of a putative visual information pathway from the optic lobes, through the optic tubercles, to the bulb and ellipsoid body (Figure 7C). Such a visual pathway has been described in other insects (Pfeiffer et al., 2005; Trager et al., 2008), and neurons in the ellipsoid body of *Drosophila* have been shown to have visual response properties (Seelig and Jayaraman, 2013). Our results imply that this visual circuit feeds into the neuronal control of locomotion, and activation of any component of it increases the probability of walking.

The lines most important in producing high correlations for a selected neuronal region also provide direct and immediate ge-

netic access for further investigation of the observed behavior-anatomy correlation. The intersectional split-GAL4 method can be used to refine the expression patterns of these GAL4 lines (Luan et al., 2006; Pfeiffer et al., 2010), creating more precise genetic tools and potentially identifying the specific cell types involved in neural control of the behavior. To demonstrate this, we used the split-GAL4 intersectional strategy with GAL4 lines identified based on our increased-walking map (Figures 7D–7F) to discover a small population of R2/R4 ring neurons in the ellipsoid body that were sufficient to elicit an increase in walking probability (Figures 7D–7F and S7; Method Details; Table S7). A role for these neurons in the control of walking is consistent with earlier studies of structural mutations and inactivation of ellipsoid body neurons, both of which caused

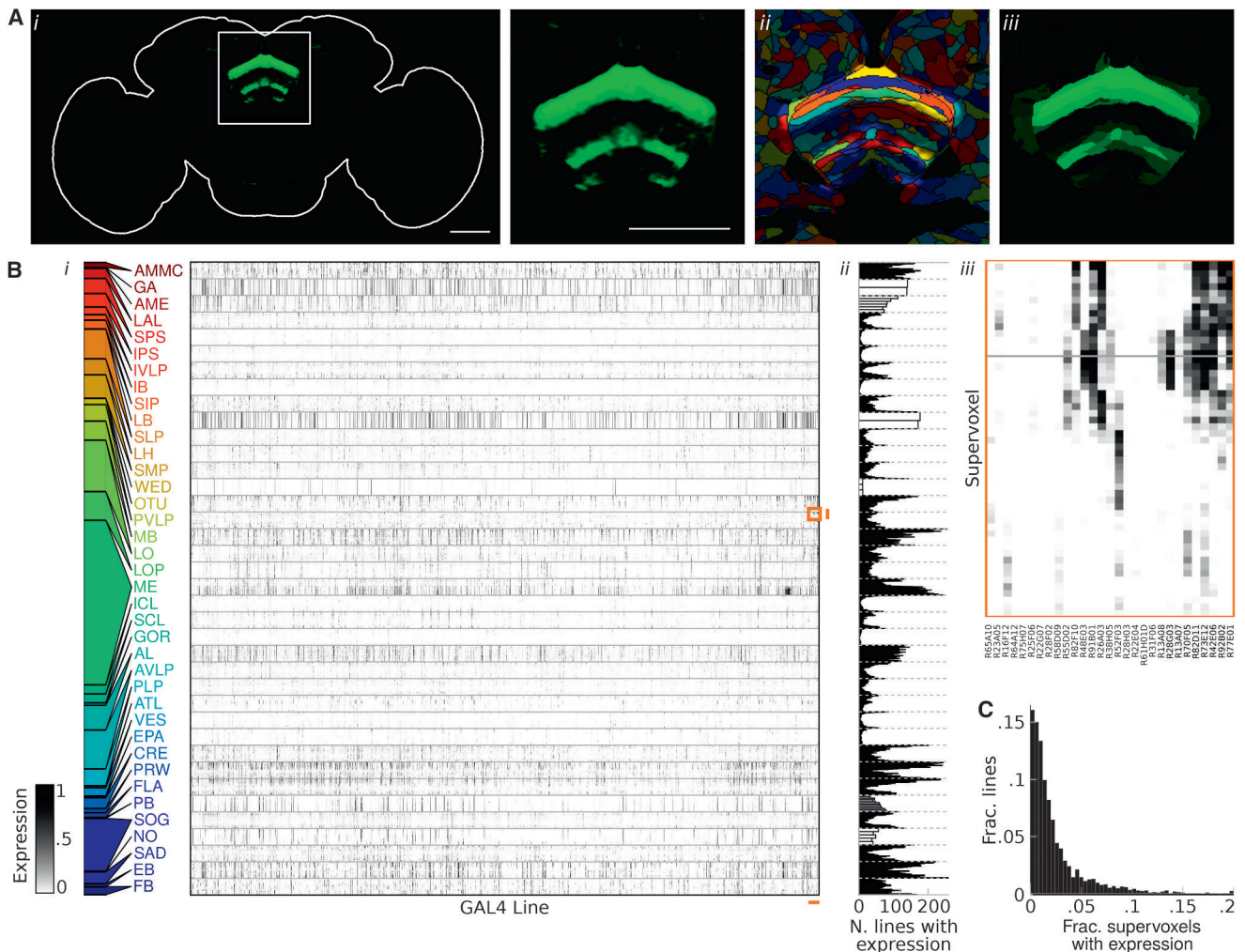


Figure 6. Anatomical Expression Data

(A) Reduced-dimensional representation of the GAL4 expression pattern for R26C06 using the supervoxel clustering. *i*: High-dimensional representation of the expression pattern for R26C06 at $z = 72.5 \mu\text{m}$. *ii*: Expression pattern overlaid on supervoxel clustering, with color indicating supervoxel and brightness indicating expression. Expression appears constant within each supervoxel. Our low-dimensional representation is the average expression within each supervoxel. *iii*: Reconstruction of original 30-million-dimensional expression pattern from 7,065-dimensional supervoxel representation, by setting the expression within an entire supervoxel to its average. Right panel of *i* and *iii* appear similar.

(B) *i*: Table of anatomical expression levels for all GAL4 lines assayed (columns, ordered as in Figure 3A). Rows correspond to supervoxels, which are grouped by compartment (Jenett et al., 2012). Row heights are set so each compartment has the same height. Darkness indicates amount of expression. Colored bar (left) indicates the relative number of supervoxels in each compartment. *ii*: Number of GAL4 lines with expression in each supervoxel. As expression level is a number between 0 and 1, we sum the total expression level values over lines, interpreting non-integer values as probabilities. These counts are mapped to supervoxel location in Figure S1. *iii*: Zoom-in of orange box in *i*.

(C) For each GAL4 line, we computed the fraction of supervoxels with expression, i.e., how dense the expression pattern is (as in [B], interpreting non-integer values as probabilities). We histogram this value across GAL4 lines.

locomotor deficits (Martín-Peña et al., 2014; Strauss and Heisenberg, 1993).

We discovered several other behavior-anatomy correlations by exploring the data collected in our unbiased activation study using our behavior-anatomy maps. We both identified previously known structure-function relationships (Figures 8A and 8B; Movie S3), further confirming the validity of our method, and discovered novel correlations (Figures 8C–8G; Movie S3), demonstrating the potential for identifying novel

neural substrates of behavior. We briefly describe these maps next.

Our map of regions of the brain correlated with increased unilateral wing extension by males (a component of courtship behavior [Yamamoto and Koganezawa, 2013]; Figure 8A; Movie S3) closely resembles the *fruitless* circuit in the protocerebrum (Yu et al., 2010), neuronal regions previously demonstrated to control courtship behavior. Also confirming the validity of our approach, our map of regions of the brain correlated with an

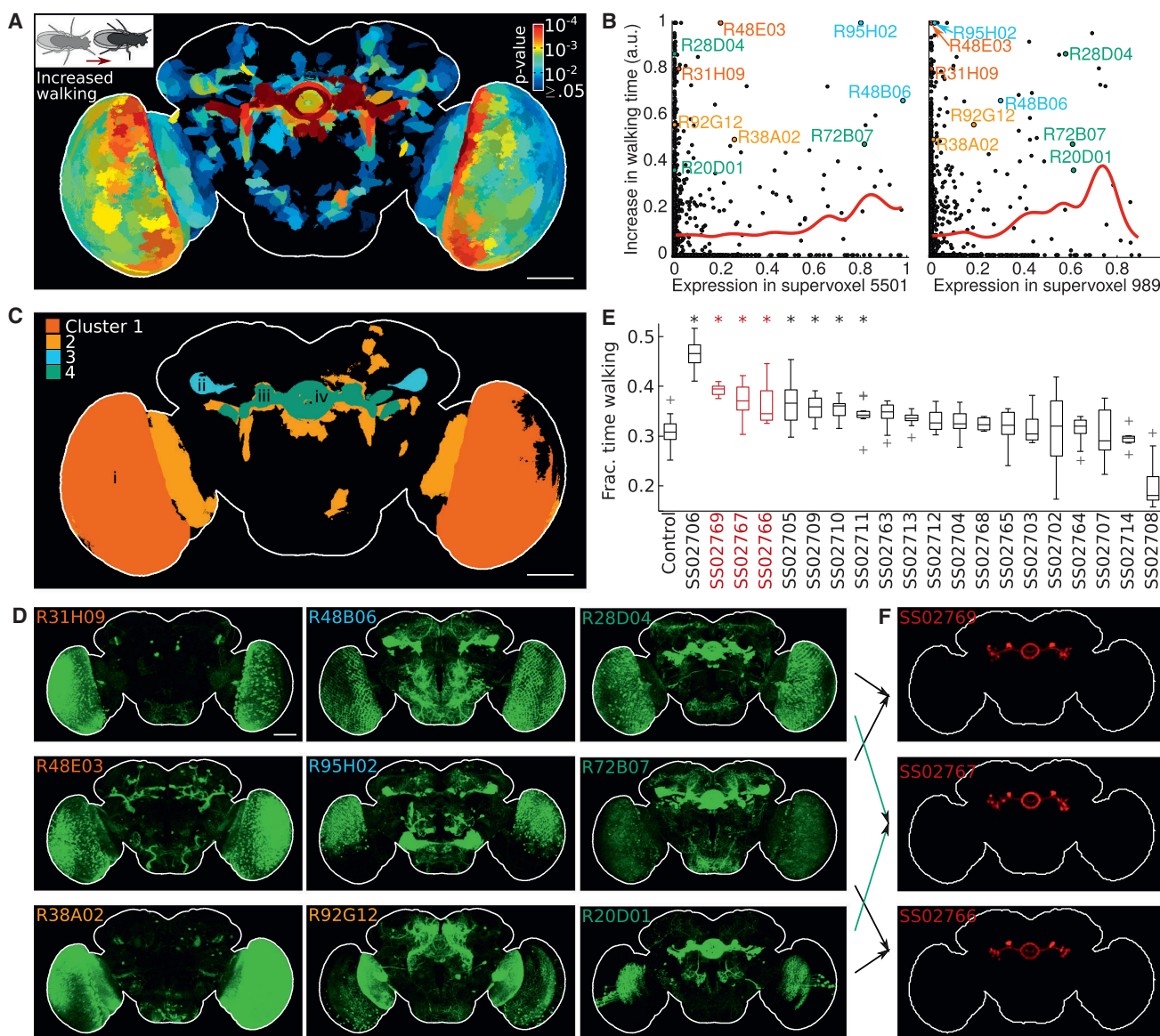


Figure 7. Neural Correlates of Walking

(A) Regions of the brain significantly correlated with an increase in fraction of time spent walking (FDR ≤ 0.25). For each supervoxel, we compute the significance of the observed correlation between expression in the supervoxel and increase in fraction of time spent walking and color by this p value. We show the minimum intensity projection. All panels: Scale bar, 50 μm .

(B) For two significantly correlated supervoxels, relationship between expression and walking behavior across GAL4 lines. Left: Supervoxel within cluster 3; right: cluster 4. We plot expression level versus normalized increased-walking statistic (Method Details) for each GAL4 line (dots). Colored circles indicate lines shown in (D). Red lines indicate average behavior score for GAL4 lines for sliding intervals of supervoxel expression level. While expression level and walking behavior are significantly correlated, we observe both lines in the upper-left of the plots for which other brain regions might be causing the behavior phenotype and lines in the bottom-right for which activation of other brain regions may be masking the behavior phenotype.

(C) Clustering of significantly correlated regions of the increased-walking map ($p \leq 0.005$) into substructures (Method Details). We indicate locations of *i*: optic lobe, *ii*: optic tubercle, *iii*: bulb, and *iv*: ellipsoid body.

(D) For each cluster in (C), we show MIPs of expression patterns for lines important in creating the behavior-anatomy correlation for the cluster (those with the highest product of behavior score and average anatomy score over all supervoxels in the cluster).

(E) Boxplot of fraction of time walking for each of the 20 split-GAL4 lines created from parental lines important in creating the behavior-anatomy correlation for cluster 4. Asterisks indicate significant increases compared to control (Mann-Whitney test, $p < 0.05$ with Bonferroni correction, number of videos ranged from 6 to 22 [Table S7]); boxes indicate 25th and 75th percentiles of data; pluses indicate points outside whiskers. Red indicates split lines shown in (F).

(F) MIPs of expression patterns for split-GAL4 lines with expression in the R2/R4 ring neurons. Arrows indicate parental lines used to create split-half lines.

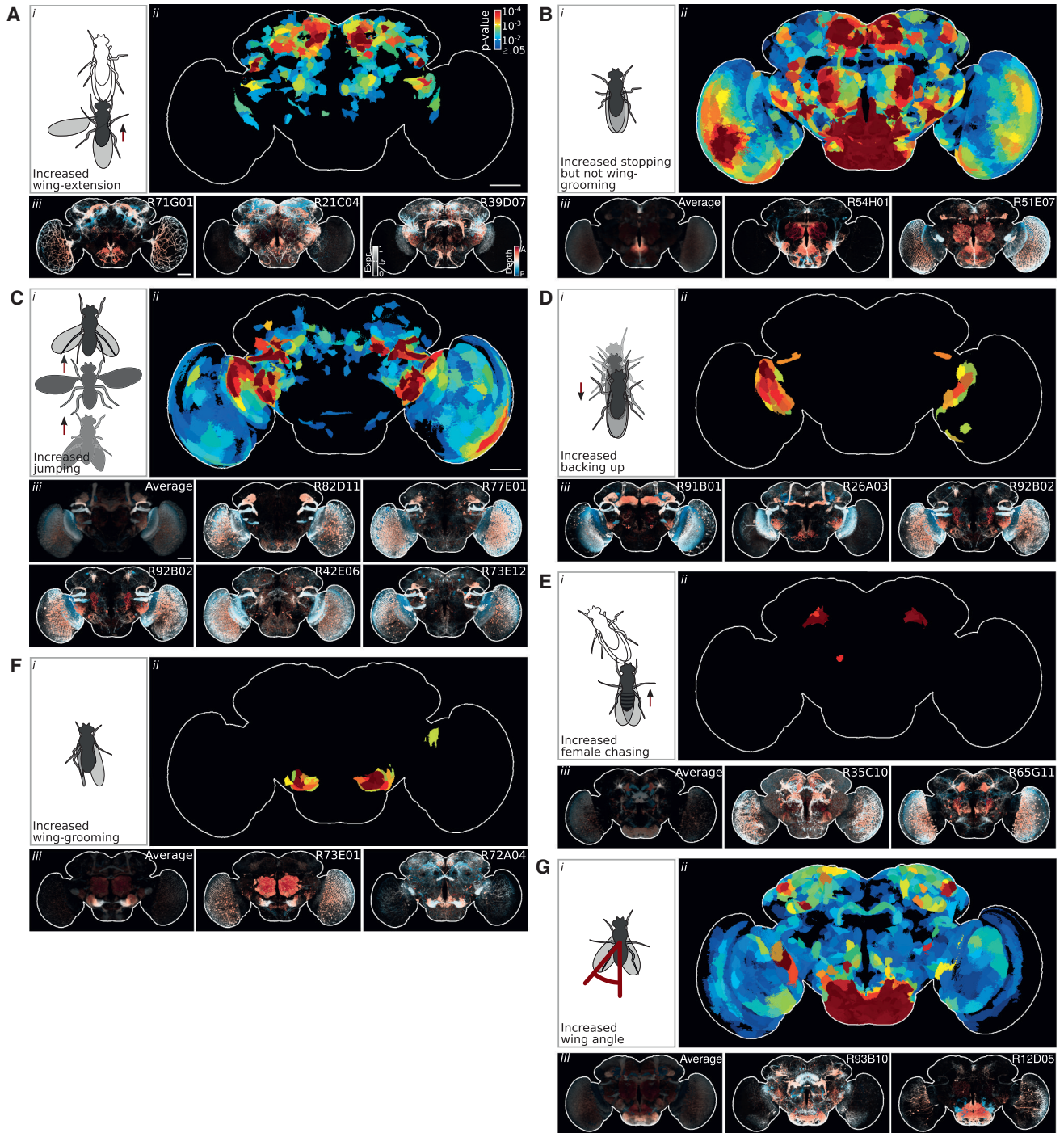


Figure 8. Behavior-Anatomy Correlation Maps

(A–G) Each panel corresponds to a different behavior phenotype. For each, we show:

i: Cartoon illustrating the behavior phenotype.

ii: A map of brain regions significantly correlated with the behavior phenotype ($FDR \leq 0.25$, as in Figure 7A).

iii: Left: Average expression pattern for lines important in creating the significant behavior-anatomy correlations shown in *ii* ($p \leq 0.005$). Right: Selected important lines. All: MIPs for which intensity indicates maximum expression level and hue indicates depth at this maximum (anterior, red; posterior, blue). No average shown in panels (A) and (D). Average shown in (B) corresponds to a selected cluster of supervoxels. Scale bars, 50 μ m.

approximate measure of increased sleep (Figure 8B; Method Details) identified a cell type with morphology similar to a subset of a previously identified heterogeneous population of neuromodulatory neurons involved in sleep, circadian rhythms, and feeding (Cavanaugh et al., 2014; Dus et al., 2015; Foltenyi et al., 2007).

While components of the motor circuits of escape in the fly (jumping) have been well described (Hale et al., 2016), the visual inputs to these circuits are not. Our increased-jumping map (Figure 8C) suggests several such inputs: lobular columnar (LC) neurons with morphologies similar to those of types LC6, LC9, and LC10 (Otsuna and Ito, 2006). Concurrent to our study, using novel split-GAL4 lines targeting each LC type, Wu et al. independently found a jumping activation phenotype for LC6 neurons (Wu et al., 2016), confirming a portion of our increased-jumping map.

The sparse increased-backing-up map (Figure 8D) indicates that there is also a strong correlation between visual projection neurons and the backing-up behavior, which may be an avoidance or lower-intensity escape behavior. These maps contain a previously undescribed LC neuron that projects to a region close to the LC6 glomeruli and enters the ventrolateral protocerebrum (VLPR) from the posterior side. Wu et al. concurrently found a back-up activation phenotype for this cell type, which they termed LC16 (Wu et al., 2016), confirming our increased-backing-up map.

Female aggression has been described in flies (Nilsen et al., 2004), but, unlike male aggression, its neural substrates have not been well characterized. The map corresponding to an increase in chasing (a phenotype of aggression) exclusively in females is very sparse (Figure 8E)—a single bilateral region in the protocerebrum. Besides this increase in female chasing, we also observed that, for lines important for this map, females performed other aggressive behaviors such as low-posture fencing, shoving, and headbutting.

The map corresponding to increased wing grooming (Figure 8F) is similarly sparse and contains a single bilateral brain region within the antennal mechanosensory and motor center (AMMC). There are two plausible alternatives for this observed correlation. The first is causal: connectivity between antennal and wing sensory-motor circuits in the ventral nerve cord (VNC), which cause wing grooming. The second is correlational: activation of a different population of neurons, one for which GAL4 expression is genetically correlated with that in the AMMC, causes wing grooming. This second hypothesis is supported by the fact that the AMMC receives multiple types of mechanosensory input from the antenna, and proteins of mechanosensory transduction are shared across many sensory organs (Walker et al., 2000). To investigate this, we examined VNC images for lines important to the wing-grooming map (Figure S8). While there appears to be expression in the wing sensory neuropil of at least three to five lines, there does not appear to be a common neuronal cell-type throughout. Such images of VNC expression exist for many of the lines we assayed; thus, our methodology could be extended to the VNC, an interesting direction for future research.

The regions of the brain most correlated with the flies' wings being held out are within the subesophageal zone (SEZ) (Fig-

ure 8G). While interactions between feeding and locomotion circuits in the VNC have been described (Mann et al., 2013; Schoofs et al., 2014), this map suggests a novel role for circuits within the SEZ in wing motor control and is congruous with evidence that the SEZ has dense innervation by descending neurons (Hsu and Bhandawat, 2016) that connect the brain and the VNC, where wing motor control circuits are located.

These and other behavior-anatomy correlations suggested by our whole-brain maps will be a source of hypotheses for future research in *Drosophila* neurobiology. As we can create maps not only for the 203 behavior statistics we measured but also for combinations of them, the number of behavior-anatomy maps to explore is practically unlimited. To allow researchers to explore our data, we have created the Browsable Atlas of Behavior-Anatomy Maps (BABAM) software that allows users to select behavior measures and generate behavior-anatomy maps (Data S1; <https://kristinbranson.github.io/BABAM/>; Movie S4). BABAM allows users to explore maps in a variety of ways. Following our analysis of the increased-walking map, they can further cluster the correlated regions of the map (Figure 7C) and explore subregions of a given map. Users can find the GAL4 lines that contribute most to the correlation between a selected behavior and supervoxel or cluster of supervoxels and access the per-line web pages describing their behavior and anatomy. Finally, they can examine the supervoxel clustering of the brain. This software will facilitate testing of our structure-function hypotheses by refining expression using the intersectional split-GAL4 strategy, activating and silencing using other effectors, and/or neural recording.

DISCUSSION

In this work, we used machine-vision and machine-learning methods to quantify the behavioral effects of neural activation for thousands of GAL4 lines with overlapping expression in multiple, often unrelated, cell types. When activating multiple cell types with distinct behavioral roles, it is likely that behavioral effects will combine complexly; for example, behavioral effects of one cell type could mask another's. By using this large dataset to jointly analyze the effects of neural activation across many lines with overlapping expression, we were able to find the same, sometimes subtle, behavioral effects in multiple lines with regions of common expression and thus develop testable hypotheses of the neural substrates of a variety of locomotion and social behaviors across the entire *Drosophila* brain.

These behavior-anatomy maps both recapitulate known and suggest novel structure-function relationships. Novel relationships we discovered include a putative visual information pathway from the optic lobes to the central complex involved in production of walking behavior, visual output neurons involved in escape and avoidance behavior, a subregion of the protocerebrum involved in female aggression, a subregion of the AMMC involved in wing grooming, and a subregion of the SEZ involved in controlling wing position. Our study resulted in thousands such behavior-anatomy maps, which we share with the neuroscience community in the form of our interactive atlas software. This software allows the user to identify GAL4 lines most important in creating a selected region of a map, allowing one to gain

genetic access to sparse neuronal populations within a map. Using these GAL4 lines and lines derived from them via split-intersectional strategies, one can target effectors, markers, and activity indicators to these cells, allowing researchers to manipulate and record activity, test the hypothesized relationship, and further investigate the behavior circuit. Taken together with efforts to find and identify neuronal cell types in these GAL4 lines (Chiang et al., 2011; Costa et al., 2016; Panser et al., 2016), our functional description of the fly brain will enhance the pace of research tackling neural circuit mechanisms.

Our work builds upon a long history of behavior screens in model organisms, from genetic screens elucidating the molecular and genetic bases of behavior to more recent, genetically targeted neural activation and silencing screens in *Drosophila* to identify cellular and circuit mechanisms of behavior control (Owald et al., 2015). Recent behavioral screens of large GAL4 collections have resulted in the identification of behavioral roles for a handful of neurons (Hampel et al., 2015; Hoopfer et al., 2015; Triphan et al., 2016; von Philipsborn et al., 2011). Each of these studies were focused on a single behavior and only provided careful behavior quantification for a few “hits” from their screens. In contrast, we have created a searchable, detailed quantification of the effects of activation for a broad range of behaviors across all 2,204 GAL4 lines assayed. Most similarly, activation phenotypes of 1,054 GAL4 lines were quantified in *Drosophila* larvae but without analysis of the neural anatomy of those lines (Vogelstein et al., 2014). Our work uniquely combines analysis of the behavioral effects of activation and quantification of the anatomical expression patterns to discover correlations between behavior and anatomy: a brain-wide atlas of behavior-anatomy maps.

We collected, to our knowledge, the largest-to-date video behavior dataset as part of this study. It describes the behavioral effects of perturbing the neural activity of thousands of sets of neurons throughout the nervous system. As such, characteristics of the space of behavioral effects may be indicative of the structure and organization of behavior and its neural representation. Despite the sparsity of the expression patterns, we observed significant behavioral effects of activation for a large fraction of GAL4 lines. However, in other ways, for the majority of lines, the behavior statistics we measured were surprisingly normal. We rarely observed abnormal correlations between our measured behavior statistics. Instead, the correlational structure across GAL4 lines was similar to that across retests of our control. This suggests that behavior modules (e.g., courtship, foraging, escape) were more commonly modulated by neural activation, as opposed to individual behavior components within these modules (e.g., chasing and wing extension, walking and turning, jumping and backing up). One explanation is that many of the effects we observed were from sensory or near-sensory neural populations, or neurons that affect the concentrations of neuromodulators, which then affect large downstream populations of neurons—entire behavior modules. Alternatively, one could speculate that the observation that GAL4 line behavior remains within the low-dimensional manifold of normal fly behavior is evidence that neural activity is also regulated to remain within a low-dimensional manifold. By exciting a small population of neurons, we push neural activity away from this

manifold, and one could envision homeostatic mechanisms that pull neural activity back to the closest point on the manifold by compensatory changes in other neurons involved in the behavior module. Low-dimensional neural dynamics during locomotion behaviors have been observed previously in the *C. elegans* (Kato et al., 2015). In the fly, two of the major axes of this manifold, according to our measures of behavior, are activity and interaction levels, the most important features for describing the effects of activation. A potentially fruitful direction of future research is thus to activate sparse neuronal populations suggested by our study and observe the resulting neural dynamics across large populations via calcium imaging. For two lines with seemingly unrelated expression patterns but similar behavior, do we observe similar neural activity patterns upon activation? How does neural activity after activation compare to activity observed in control flies in different environments and states?

An important qualification to the results of this study is that they are based on potentially nonphysiological patterns of neural activity—those induced by several minutes of continuous excitation via the dTrpA effector of multiple, possibly unrelated, neurons. However, as our maps are based on activation effects across many GAL4 lines, they should be less susceptible to irregularities in any single line. Because dTrpA perturbations, in addition to direct effects, will also yield phenotypes due to nonspecific network effects, future experiments will be necessary to establish a causal role for identified brain regions. However, dTrpA activation has been used previously to successfully identify neural substrates of behavior (Hampel et al., 2015; Hoopfer et al., 2015; von Philipsborn et al., 2011). A second qualification of our results is that they are based on correlational analyses, which are not necessarily causal. For example, if there is a strong genetic correlation in expression between region A, which controls a behavior, and one region B, which does not, there will still be a correlation between expression in B and the behavior. However, we rarely observed genetic correlations in expression between regions not known or suspected to be functionally related. For example, in Figure S7A, we observe expression correlation between the selected supervoxel in the crepine and other regions in the central complex. Genetic correlations in expression can be investigated using our interactive software (Movie S4). The structure-function hypotheses suggested by our analyses should be followed up using intersectional genetic techniques, silencing and manipulation with other effectors such as temporally acute optogenetic activators, and/or neural recordings. Our interactive software and web pages will facilitate these follow-up experiments.

Further analyses of our dataset will reveal more about the neural correlates of behavior and its organization, and we make our data publicly available, in the raw video form, at the level of per-fly trajectories and finally at the level of a condensed matrix of per-line behavior statistics. From the videos and trajectories, new behavior classifiers can be trained and applied to our dataset using supervised machine learning (Kabra et al., 2013), and new behavior modes and representations can be discovered using unsupervised clustering or manifold learning techniques (Berman et al., 2014; Schwarz et al., 2015; Vogelstein et al., 2014). We believe that this data will be of interest to

computational ethologists interested in understanding the vocabulary and structure of behavior, neuroanatomists interested in cataloguing cell types, and machine-vision and machine-learning researchers interested in developing behavior analysis techniques that are effective on such large, diverse datasets. From our matrices of per-line behavior statistics and per-line anatomical expression patterns, theorists could develop brain-wide models predicting behavior from neural activity, perhaps in combination with brain-wide electron-microscopy connectomics and whole-brain calcium imaging data currently being collected for *Drosophila*.

STAR★METHODS

Detailed methods are provided in the online version of this paper and include the following:

- KEY RESOURCES TABLE
- CONTACTS FOR REAGENT AND RESOURCE SHARING
- EXPERIMENTAL MODEL AND SUBJECT DETAILS
- METHOD DETAILS
 - Data collection
 - Data curation
 - Tracking
 - Temporal and spatial registration of trajectories
 - Classification of fly sex
 - JAABA behavior classifiers
 - Accuracy of automatic behavior classifiers
 - Computation of per-line behavior statistics
 - Automatic, high-throughput behavior analysis pipeline
 - Testing for significant effects on behavior
 - Behavior statistic correlation analysis
 - Behavioral effects of activation
 - Janelia Fly Light imagery data
 - Processing of neural expression pattern images
 - Clustering the brain into supervoxels
 - Behavior-anatomy correlation
 - Behavior-anatomy maps
 - Identifying ring neurons associated with walking
 - Split-GAL4 line annotation
- QUANTIFICATION AND STATISTICAL ANALYSIS
- DATA AND SOFTWARE AVAILABILITY
 - Software
 - Data

SUPPLEMENTAL INFORMATION

Supplemental Information includes eight figures, seven tables, four movies, and three data files and can be found with this article online at <http://dx.doi.org/10.1016/j.cell.2017.06.032>.

AUTHOR CONTRIBUTIONS

Conceptualization: A.A.R., K.B., M.B.R., G.M.C., W.K., G.M.R., and J.H.S.; Methodology: K.B., A.A.R., W.K., and J.H.; Software: K.B., L.A.U., A.L., and A.A.R.; Formal Analysis: K.B. and A.A.R.; Investigation: A.A.R., J.H., A.W.E., and M.L.P.; Data Curation: A.A.R., J.H., A.W.E., and K.B.; Writing: K.B., A.A.R., and M.B.R.; Visualization: K.B. and A.A.R.; Supervision and Project Administration: A.A.R., K.B., G.M.C., W.K., M.B.R., G.M.R., and J.H.S.

ACKNOWLEDGMENTS

Behavior data was collected as part of the Janelia Fly Olympiad Team Project. We thank A. Nern, A. Jenett, and Y. Aso for selecting GAL4 driver lines based on imagery produced by the Janelia Fly Light team; J. McMahon and the Janelia Fly Core team for fly preparation; S. Roberts for help with data collection; T. Tabachnik and B. Biddle for help with rig design and fabrication; S. Branson and M. Kabra for help with software; the Janelia Fly Light team for access to anatomy images; L. Guignard and P. Keller for help rendering videos; J.-M. Knapp for genetics consulting; J. Jeter for imaging split-GAL4 lines; the Janelia Fly Olympiad Team and Scientific Computing team for support and discussions; Y. Yu, F. Long, and H. Peng for help with anatomy image processing; and P. Keller, V. Jayaraman, U. Heberlein, and A. Hantman for feedback on the manuscript.

Received: December 8, 2016

Revised: May 1, 2017

Accepted: June 19, 2017

Published: July 13, 2017

REFERENCES

- Ahrens, M.B., Orger, M.B., Robson, D.N., Li, J.M., and Keller, P.J. (2013). Whole-brain functional imaging at cellular resolution using light-sheet microscopy. *Nat. Methods* **10**, 413–420.
- Aso, Y., Hattori, D., Yu, Y., Johnston, R.M., Iyer, N.A., Ngo, T.T., Dionne, H., Abbott, L.F., Axel, R., Tanimoto, H., and Rubin, G.M. (2014). The neuronal architecture of the mushroom body provides a logic for associative learning. *eLife* **3**, e04577.
- Benjamini, Y., and Hochberg, Y. (1995). Controlling the false discovery rate - a practical and powerful approach to multiple testing. *J. Roy. Stat. Soc. B* **57**, 289–300.
- Benjamini, Y., and Yekutieli, D. (2001). The control of the false discovery rate in multiple testing under dependency. *Ann. Stat.* **29**, 1165–1188.
- Berman, G.J., Choi, D.M., Bialek, W., and Shaevitz, J.W. (2014). Mapping the stereotyped behaviour of freely moving fruit flies. *J. R. Soc. Interface* **11**, 20140672.
- Branson, K., Robie, A.A., Bender, J., Perona, P., and Dickinson, M.H. (2009). High-throughput ethomics in large groups of *Drosophila*. *Nat. Methods* **6**, 451–457.
- Cavanaugh, D.J., Geratowski, J.D., Wooldorton, J.R., Spaethling, J.M., Hector, C.E., Zheng, X., Johnson, E.C., Eberwine, J.H., and Sehgal, A. (2014). Identification of a circadian output circuit for rest:activity rhythms in *Drosophila*. *Cell* **157**, 689–701.
- Chiang, A.S., Lin, C.Y., Chuang, C.C., Chang, H.M., Hsieh, C.H., Yeh, C.W., Shih, C.T., Wu, J.J., Wang, G.T., Chen, Y.C., et al. (2011). Three-dimensional reconstruction of brain-wide wiring networks in *Drosophila* at single-cell resolution. *Curr. Biol.* **21**, 1–11.
- Costa, M., Manton, J.D., Ostrovsky, A.D., Prohaska, S., and Jefferis, G.S. (2016). NBLAST: rapid, sensitive comparison of neuronal structure and construction of neuron family databases. *Neuron* **91**, 293–311.
- Dasgupta, S., and Long, P.M. (2005). Performance guarantees for hierarchical clustering. *J. Comput. Syst. Sci.* **70**, 555–569.
- Dus, M., Lai, J.S., Gunapala, K.M., Min, S., Tayler, T.D., Hergarden, A.C., Geraud, E., Joseph, C.M., and Suh, G.S. (2015). Nutrient sensor in the brain directs the action of the brain-gut axis in *Drosophila*. *Neuron* **87**, 139–151.
- Foltényi, K., Greenspan, R.J., and Newport, J.W. (2007). Activation of EGFR and ERK by rhomboid signaling regulates the consolidation and maintenance of sleep in *Drosophila*. *Nat. Neurosci.* **10**, 1160–1167.
- Fosque, B.F., Sun, Y., Dana, H., Yang, C.T., Ohyama, T., Tadross, M.R., Patel, R., Zlatić, M., Kim, D.S., Ahrens, M.B., et al. (2015). Neural circuits. Labeling of active neural circuits in vivo with designed calcium integrators. *Science* **347**, 755–760.

- Groppe, D.M., Urbach, T.P., and Kutas, M. (2011). Mass univariate analysis of event-related brain potentials/fields I: a critical tutorial review. *Psychophysiology* 48, 1711–1725.
- Hale, M.E., Katz, H.R., Peek, M.Y., and Fremont, R.T. (2016). Neural circuits that drive startle behavior, with a focus on the Mauthner cells and spiral fiber neurons of fishes. *J. Neurogenet.* 30, 89–100.
- Hampel, S., Franconville, R., Simpson, J.H., and Seeds, A.M. (2015). A neural command circuit for grooming movement control. *eLife* 4, e08758.
- Hanesch, U., Fischbach, K.-F., and Heisenberg, M. (1989). Neuronal architecture of the central complex in *Drosophila melanogaster*. *Cell Tissue Res.* 257, 343–366.
- Hoopfer, E.D., Jung, Y., Inagaki, H.K., Rubin, G.M., and Anderson, D.J. (2015). P1 interneurons promote a persistent internal state that enhances inter-male aggression in *Drosophila*. *eLife* 4, e11346.
- Hsu, C.T., and Bhandawat, V. (2016). Organization of descending neurons in *Drosophila melanogaster*. *Sci. Rep.* 6, 20259.
- Ito, K., Shinomiya, K., Ito, M., Armstrong, J.D., Boyan, G., Hartenstein, V., Harzsch, S., Heisenberg, M., Homberg, U., Jenett, A., et al.; Insect Brain Name Working Group (2014). A systematic nomenclature for the insect brain. *Neuron* 81, 755–765.
- Jenett, A., Rubin, G.M., Ngo, T.T., Shepherd, D., Murphy, C., Dionne, H., Pfeiffer, B.D., Cavallaro, A., Hall, D., Jeter, J., et al. (2012). A GAL4-driver line resource for *Drosophila* neurobiology. *Cell Rep.* 2, 991–1001.
- Kabra, M., Robie, A.A., Rivera-Alba, M., Branson, S., and Branson, K. (2013). JAABA: interactive machine learning for automatic annotation of animal behavior. *Nat. Methods* 10, 64–67.
- Kato, S., Kaplan, H.S., Schrödel, T., Skora, S., Lindsay, T.H., Yemini, E., Lockery, S., and Zimmer, M. (2015). Global brain dynamics embed the motor command sequence of *Caenorhabditis elegans*. *Cell* 163, 656–669.
- Luan, H., Peabody, N.C., Vinson, C.R., and White, B.H. (2006). Refined spatial manipulation of neuronal function by combinatorial restriction of transgene expression. *Neuron* 52, 425–436.
- Mann, K., Gordon, M.D., and Scott, K. (2013). A pair of interneurons influences the choice between feeding and locomotion in *Drosophila*. *Neuron* 79, 754–765.
- Martín-Peña, A., Acebes, A., Rodríguez, J.R., Chevalier, V., Casas-Tinto, S., Triphan, T., Strauss, R., and Ferrús, A. (2014). Cell types and coincident synapses in the ellipsoid body of *Drosophila*. *Eur. J. Neurosci.* 39, 1586–1601.
- Nern, A., Pfeiffer, B.D., and Rubin, G.M. (2015). Optimized tools for multicolor stochastic labeling reveal diverse stereotyped cell arrangements in the fly visual system. *Proc. Natl. Acad. Sci. USA* 112, E2967–E2976.
- Nilsen, S.P., Chan, Y.B., Huber, R., and Kravitz, E.A. (2004). Gender-selective patterns of aggressive behavior in *Drosophila melanogaster*. *Proc. Natl. Acad. Sci. USA* 101, 12342–12347.
- Otsuna, H., and Ito, K. (2006). Systematic analysis of the visual projection neurons of *Drosophila melanogaster*. I. Lobula-specific pathways. *J. Comp. Neurol.* 497, 928–958.
- Owald, D., Lin, S., and Waddell, S. (2015). Light, heat, action: neural control of fruit fly behaviour. *Philos. Trans. R. Soc. Lond. B Biol. Sci.* 370, 20140211.
- Panser, K., Tirian, L., Schulze, F., Villalba, S., Jefferis, G.S., Bühler, K., and Straw, A.D. (2016). Automatic segmentation of *Drosophila* neural compartments using GAL4 expression data reveals novel visual pathways. *Curr. Biol.* 26, 1943–1954.
- Penfield, W. (1950). The supplementary motor area in the cerebral cortex of man. *Arch Psychiatr Nervenkr Z Gesamte Neurol Psychiatr* 185, 670–674.
- Peng, H., Chung, P., Long, F., Qu, L., Jenett, A., Seeds, A.M., Myers, E.W., and Simpson, J.H. (2011). BrainAligner: 3D registration atlases of *Drosophila* brains. *Nat. Methods* 8, 493–500.
- Pfeiffer, B.D., Jenett, A., Hammonds, A.S., Ngo, T.T., Misra, S., Murphy, C., Scully, A., Carlson, J.W., Wan, K.H., Laverty, T.R., et al. (2008). Tools for neuroanatomy and neurogenetics in *Drosophila*. *Proc. Natl. Acad. Sci. USA* 105, 9715–9720.
- Pfeiffer, B.D., Ngo, T.T., Hibbard, K.L., Murphy, C., Jenett, A., Truman, J.W., and Rubin, G.M. (2010). Refinement of tools for targeted gene expression in *Drosophila*. *Genetics* 186, 735–755.
- Pfeiffer, K., Kinoshita, M., and Homberg, U. (2005). Polarization-sensitive and light-sensitive neurons in two parallel pathways passing through the anterior optic tubercle in the locust brain. *J. Neurophysiol.* 94, 3903–3915.
- Randlett, O., Wee, C.L., Naumann, E.A., Nnaemeka, O., Schoppik, D., Fitzgerald, J.E., Portugues, R., Lacoste, A.M., Riegler, C., Engert, F., and Schier, A.F. (2015). Whole-brain activity mapping onto a zebrafish brain atlas. *Nat. Methods* 12, 1039–1046.
- Renn, S.C., Armstrong, J.D., Yang, M., Wang, Z., An, X., Kaiser, K., and Taghert, P.H. (1999). Genetic analysis of the *Drosophila* ellipsoid body neuropil: organization and development of the central complex. *J. Neurobiol.* 41, 189–207.
- Schoofs, A., Hückesfeld, S., Schlegel, P., Miroshnikow, A., Peters, M., Zeymer, M., Spieß, R., Chiang, A.S., and Pankratz, M.J. (2014). Selection of motor programs for suppressing food intake and inducing locomotion in the *Drosophila* brain. *PLoS Biol.* 12, e1001893.
- Schwarz, R.F., Branicky, R., Grundy, L.J., Schafer, W.R., and Brown, A.E. (2015). Changes in postural syntax characterize sensory modulation and natural variation of *C. elegans* locomotion. *PLoS Comput. Biol.* 11, e1004322.
- Seelig, J.D., and Jayaraman, V. (2013). Feature detection and orientation tuning in the *Drosophila* central complex. *Nature* 503, 262–266.
- Simon, J.C., and Dickinson, M.H. (2010). A new chamber for studying the behavior of *Drosophila*. *PLoS ONE* 5, e8793.
- Sivanantharajah, L., and Zhang, B. (2015). Current techniques for high-resolution mapping of behavioral circuits in *Drosophila*. *J. Comp. Physiol. A Neuroethol. Sens. Neural Behav. Physiol.* 201, 895–909.
- Strauss, R., and Heisenberg, M. (1993). A higher control center of locomotor behavior in the *Drosophila* brain. *J. Neurosci.* 13, 1852–1861.
- Träger, U., Wagner, R., Bausenwein, B., and Homberg, U. (2008). A novel type of microglomerular synaptic complex in the polarization vision pathway of the locust brain. *J. Comp. Neurol.* 506, 288–300.
- Triphan, T., Nern, A., Roberts, S.F., Korff, W., Naiman, D.Q., and Strauss, R. (2016). A screen for constituents of motor control and decision making in *Drosophila* reveals visual distance-estimation neurons. *Sci. Rep.* 6, 27000.
- Vogelstein, J.T., Park, Y., Ohyama, T., Kerr, R.A., Truman, J.W., Priebe, C.E., and Zlatic, M. (2014). Discovery of brainwide neural-behavioral maps via multi-scale unsupervised structure learning. *Science* 344, 386–392.
- von Philipsborn, A.C., Liu, T., Yu, J.Y., Masser, C., Bidaye, S.S., and Dickson, B.J. (2011). Neuronal control of *Drosophila* courtship song. *Neuron* 69, 509–522.
- Walker, R.G., Willingham, A.T., and Zuker, C.S. (2000). A *Drosophila* mechanosensory transduction channel. *Science* 287, 2229–2234.
- Wolff, T., Iyer, N.A., and Rubin, G.M. (2015). Neuroarchitecture and neuroanatomy of the *Drosophila* central complex: A GAL4-based dissection of protocerebral bridge neurons and circuits. *J. Comp. Neurol.* 523, 997–1037.
- Wu, M., Nern, A., Williamson, W.R., Morimoto, M.M., Reiser, M.B., Card, G.M., and Rubin, G.M. (2016). Visual projection neurons in the *Drosophila* lobula link feature detection to distinct behavioral programs. *eLife* 5, e21022.
- Yamamoto, D., and Koganezawa, M. (2013). Genes and circuits of courtship behaviour in *Drosophila* males. *Nat. Rev. Neurosci.* 14, 681–692.
- Young, J.M., and Armstrong, J.D. (2010). Structure of the adult central complex in *Drosophila*: organization of distinct neuronal subsets. *J. Comp. Neurol.* 518, 1500–1524.
- Yu, J.Y., Kanai, M.I., Demir, E., Jefferis, G.S., and Dickson, B.J. (2010). Cellular organization of the neural circuit that drives *Drosophila* courtship behavior. *Curr. Biol.* 20, 1602–1614.

Mutation of the Human Circadian Clock Gene *CRY1* in Familial Delayed Sleep Phase Disorder

Alina Patke,^{1,*} Patricia J. Murphy,² Onur Emre Onat,³ Ana C. Krieger,⁴ Tayfun Özçelik,³ Scott S. Campbell,² and Michael W. Young^{1,5,*}

¹Laboratory of Genetics, The Rockefeller University, New York, NY 10065, USA

²Laboratory of Human Chronobiology, Weill Cornell Medical College, White Plains, NY 10605, USA

³Department of Molecular Biology and Genetics, Faculty of Science, Bilkent University, Ankara 06800, Turkey

⁴Department of Medicine, Center for Sleep Medicine, Weill Cornell Medical College, New York, NY 10065, USA

⁵Lead Contact

*Correspondence: patkea@rockefeller.edu (A.P.), young@mail.rockefeller.edu (M.W.Y.)

<http://dx.doi.org/10.1016/j.cell.2017.03.027>

SUMMARY

Patterns of daily human activity are controlled by an intrinsic circadian clock that promotes ~24 hr rhythms in many behavioral and physiological processes. This system is altered in delayed sleep phase disorder (DSPD), a common form of insomnia in which sleep episodes are shifted to later times misaligned with the societal norm. Here, we report a hereditary form of DSPD associated with a dominant coding variation in the core circadian clock gene *CRY1*, which creates a transcriptional inhibitor with enhanced affinity for circadian activator proteins Clock and Bmal1. This gain-of-function *CRY1* variant causes reduced expression of key transcriptional targets and lengthens the period of circadian molecular rhythms, providing a mechanistic link to DSPD symptoms. The allele has a frequency of up to 0.6%, and reverse phenotyping of unrelated families corroborates late and/or fragmented sleep patterns in carriers, suggesting that it affects sleep behavior in a sizeable portion of the human population.

INTRODUCTION

The circadian clock is an internal self-sustained oscillator that operates in organisms' tissues and cells to align recurrent daily changes in physiology and behavior with 24-hr environmental cycles. In humans, dysfunction or misalignment of the circadian clock with environmental cues alters the timing of the sleep-wake cycle, leading to a variety of circadian rhythm sleep disorders (American Academy of Sleep Medicine, 2005). Delayed sleep phase disorder (DSPD), which is characterized by a persistent and intractable delay of sleep onset and offset times relative to the societal norm, represents the most commonly diagnosed type of circadian rhythm sleep disorder, with an estimated prevalence of 0.2%–10% in the general population (Zee et al., 2013). The wide range of prevalence estimates reflects heterogeneity in the manifestation of the disorder as well as variation in the stringency with which clinical diagnosis criteria are applied (Sack

et al., 2007; Weitzman et al., 1981). The pathophysiology of DSPD remains obscure, with suspected causes including a differential susceptibility of an individual's circadian clock to environmental entrainment cues such as the light/dark cycle and altered properties of the oscillator itself that affect its period length (Aoki et al., 2001; Campbell and Murphy, 2007; Chang et al., 2009; Duffy et al., 2001; Micic et al., 2013).

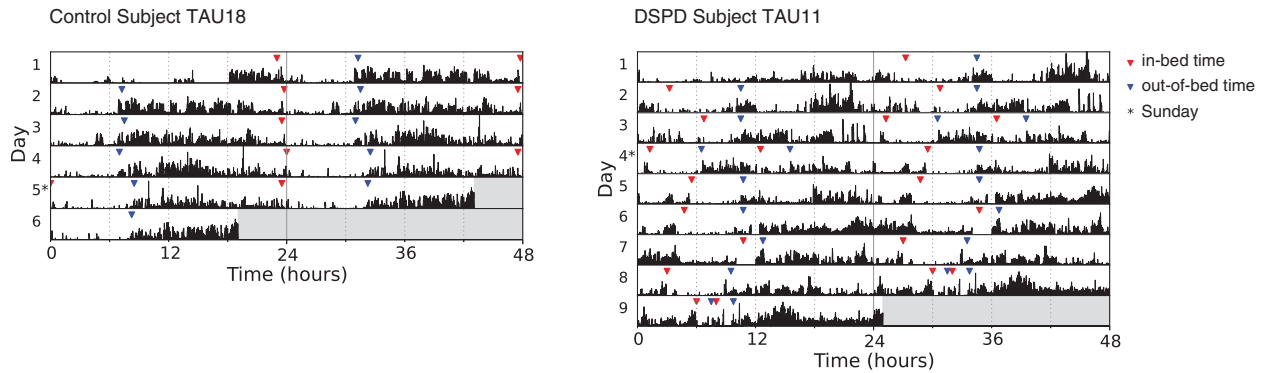
The circadian clock is genetically encoded and susceptible to modification by spontaneous or targeted mutation of the respective factors in animal models (Crane and Young, 2014; Lowrey and Takahashi, 2011). In humans, rare genetic variations that shorten circadian period are linked to familial advanced sleep phase disorder (FASPD), a type of circadian rhythm sleep disorder with habitual sleep times earlier than the societal norm (Hirano et al., 2016; Toh et al., 2001; Xu et al., 2005, 2007). No comparable evidence has yet emerged for DSPD and the association of proposed genetic polymorphisms with late chronotype, and DSPD has remained controversial (Kripke et al., 2014). Yet, many classical twin studies have found a strong hereditary component to chronotype preference in the range of 40%–50%, arguing for an important role of genetic predisposition to DSPD etiology (Barclay et al., 2010; Hur et al., 1998; Koskenvuo et al., 2007; Vink et al., 2001). Here, we report a case of familial DSPD linked to a dominant coding variation in cryptochrome circadian clock 1 (*CRY1*). This association is maintained in unrelated carrier families of the *CRY1* variant. The studied allele encodes a *CRY1* protein with an internal deletion, affecting its function as a transcriptional inhibitor and causing lengthening of the circadian period.

RESULTS

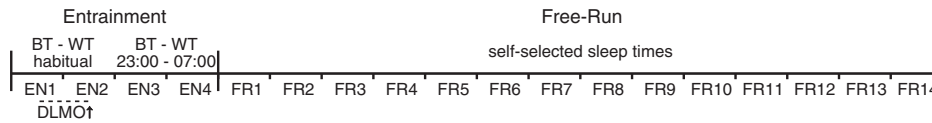
Characterization of Intrinsic Circadian Rhythmicity in the DSPD Proband

The clinical diagnosis of DSPD in the proband, subject "TAU11" (female, aged 46), was based on a sleep history and diagnostic interview, chronotype questionnaires, and actigraphy combined with a sleep log (Figure 1A). To better characterize the intrinsic circadian behavior, the subject completed an in-laboratory study during which sleep and core body temperature were continuously monitored (Figure 1B). The protocol consisted of a 2-day entrainment period with habitual sleep times derived from the sleep log. Entrained phase was determined by salivary dim light

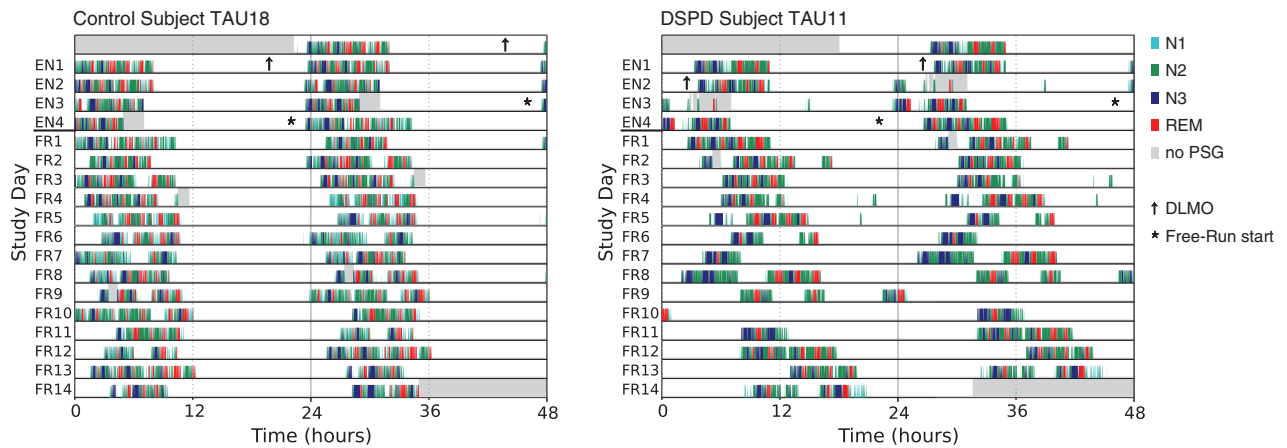
A Home Actigraphy and Sleep Log



B



C Polysomnographic Sleep



D

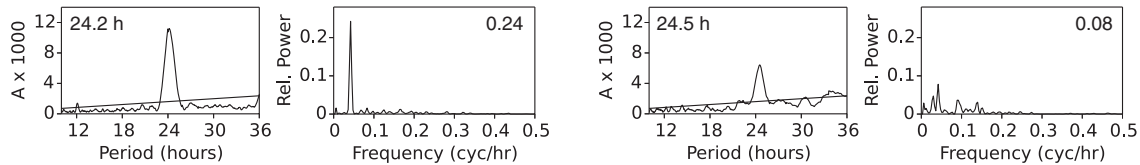


Figure 1. Circadian Behavior of Control Subject “TAU18” and the DSPD proband “TAU11”

(A) Double-plotted home actigraphy records. Red and blue triangles indicate in-bed/out-of-bed times, respectively, according to sleep logs. Asterisks indicate Sundays.

(B) In-laboratory protocol: entrainment conditions on the first 4 days with sleep-log-based, habitual sleep times on entrainment days (EN) 1 and 2 and enforced times in bed from 23:00 to 7:00 on EN3 and 4. Saliva samples for DLMO estimation were collected beginning at 18:00 on EN1 every 30 min until bedtime. From the fifth day on until the end of the study (free-run days FR1–14), subjects were kept under time-isolation conditions with instructions to sleep whenever so inclined. Polysomnographic (PSG) sleep and core body temperature were recorded continuously throughout the study.

(C) Double-plotted sleep/wake behavior during the in-laboratory study. Colors denote sleep stage derived from PSG records (N1, turquoise; N2, green; N3, blue; REM red). Gray areas indicate periods of missing PSG data during log-based time in bed. On the first and last study days, gray shading marks the beginning and end of data acquisition. Arrow denotes DLMO. Asterisk denotes the beginning of the free-run.

(D) Analysis of sleep rhythmicity. Circadian rhythm parameters during the free-run were analyzed by X^2 periodogram and fast Fourier transform (FFT) analysis, which yielded period and amplitude, respectively.

melatonin onset (DLMO) on the second entrainment night. This was followed by 2 days of enforced time in bed from 23:00 to 7:00. At the end of the 4-day entrainment interval, the subject entered a 14-day period of time isolation during which sleep was permitted whenever so inclined (free-run).

Compared to a control subject of normal chronotype undergoing the same protocol, several circadian abnormalities were apparent in the proband: consistent with a phase delay, entrained DLMO occurred at 2:32, well after the time expected in a subject of normal chronotype (typically between 20:00 and 22:00) and closer to the time of habitual sleep onset (Figure 1C) (Chang et al., 2009; Molina and Burgess, 2011). Sleep during the free-run was highly variable both in the timing and the duration of major sleep periods, consistent with at-home actigraphy and sleep-log records (Figures 1A and 1C). The resulting gross sleep/wake rhythm had a period of 24.5 hr with noticeably dampened amplitude (Figure 1D). By contrast, the 24.2-hr period length of a control subject undergoing the same protocol matches the intrinsic period length reported for normal human subjects (Czeisler et al., 1999). Aberrant rhythmicity in the sleep behavior of TAU11 was mirrored by the pattern of core body temperature oscillations in which a long-period rhythm of 24.8 hr and diminished amplitude were even more pronounced (Figures 2A–2C and S1). The phenotypic concordance of the different circadian measures strongly argues for the presence of an intrinsic circadian rhythm disorder in the proband.

Identification of *CRY1* c.1657+3A>C as a Candidate DSPD Allele

To identify the cause of circadian dysfunction in the proband, we performed candidate sequencing of genes that form the circadian clock in mammals. The core molecular clock consists of a negative-feedback loop in which the activity of the transcription factors Clock and Bmal1 (called ARNTL in humans) is repressed by the products of its target genes of the Per and Cry family, creating a cycle that takes ~24 hr to complete (Figure 3A). In this complex process also involving regulation of post-translational modification and nuclear translocation, Cry1 is commonly recognized as the main transcriptional repressor of Clock and Bmal1 (Anand et al., 2013; Griffin et al., 1999; Kume et al., 1999; Oster et al., 2002; van der Horst et al., 1999; Vitaterna et al., 1999; Ye et al., 2014). By contrast, the mechanism of action of the Per proteins appears to be more variable, ranging from indirect repression through recruitment of generic chromatin modifiers to in fact promoting transcriptional de-repression (Chiou et al., 2016; Duong et al., 2011; Duong and Weitz, 2014). Our candidate gene sequencing identified an adenine-to-cytosine transversion within the 5' splice site following exon 11 in one allele of the proband's *CRY1* gene (Figures 3B and 3C). Given usual conservation of the +3 position as a purine, this change is expected to cause splice site disruption and exon skipping (King et al., 1997). To test for a resulting coding change, we amplified part of the *CRY1* cDNA encompassing exon 11 from a primary dermal fibroblast cell line derived from the proband. Indeed, an additional product corresponding to the expected $\Delta 11$ size was present in the proband's sample, but not in those derived from 18 other unrelated subjects (Figure 3D). With a size of 72 base pairs, exon 11 skipping is

predicted to cause an in-frame deletion of 24 residues in the C-terminal region of the *CRY1* protein, and a matching, higher-mobility band was specifically detected in protein extracts from the proband cell line (Figure 3E).

Given the prominent role of *CRY1* in the mammalian clock, we postulated that the circadian abnormalities in the proband were related to the observed modification of *CRY1*. To test this hypothesis, we obtained information on sleep patterns from members of the proband's family and genotyped them for presence or absence of the candidate allele. Delayed sleep behavior was found to be common among male and female family members and across several generations, consistent with an autosomal-dominant inheritance pattern (Figures 4A and S2; Table S1). Presence of the *CRY1* c.1657+3A>C allele segregated with delayed sleep timing, with the exception of one carrier (TAUX08), who reported a history of persistent sleep problems but was complaint free at the time of study, on an occupationally required very early routine that was purposely maintained on free days (see Table S1 for details).

In a complementary approach, we also performed an unbiased search for genetic variants co-segregating with aberrant sleep behavior in the proband kindred through whole exome sequencing of additional family members (three affected, one unaffected). Among variants with minor allele frequencies below 1%, which are common to all affected subjects, but not the unaffected, and which are predicted to affect protein coding, the candidate *CRY1* allele was the only variant affecting a gene with a known or implicated role in the regulation of sleep or circadian rhythmicity (Table S2). Also, although some additional more common clock-gene variants were also present in the original proband TAU11, none of these segregated with sleep behavior in the family (see Methods Details). These results point to the *CRY1* c.1657+3A>C allele as a strong candidate-genetic variant for familial DSPD.

Reverse Phenotyping of Sleep Behavior in Heterozygous and Homozygous Carriers of the *CRY1* c.1657+3A>C Allele from an Unrelated Population

In databases of human genetic variation, the candidate *CRY1* allele has a frequency of up to 0.6% (rs184039278: minor allele frequency 0.0012 in 1000 Genomes, 0.004335 in ExAC total with 0.006537 in non-Finnish Europeans). This frequency lies within the reported range of DSPD prevalence (Zee et al., 2013) and is high enough to attempt the identification of additional carriers consenting to a characterization of their sleep behavior through a reverse-phenotyping approach (Özçelik and Onat, 2016). In genomic databases of the Turkish population, we identified 28 carriers of the *CRY1* c.1657+3A>C allele, including one homozygous individual. Of these, investigation of sleep behavior through questionnaires and personal interview was possible in six unrelated families (DSPD-1, -2, -4, -6, -7, -9, and -14) totaling 70 subjects (8 homozygous carriers, 31 heterozygous carriers, 31 non-carriers) (Figure 5 and Table S1). Subjects also provided a DNA sample to determine the *CRY1* allele status. Aberrant sleep behavior was reported by 38 carriers, but not by their non-carrier relatives or spouses, indicating a very high penetrance of *CRY1*-related sleep disturbance consistent with the original proband family. In addition to late sleep times, a subset of carriers reported a pattern of fragmented

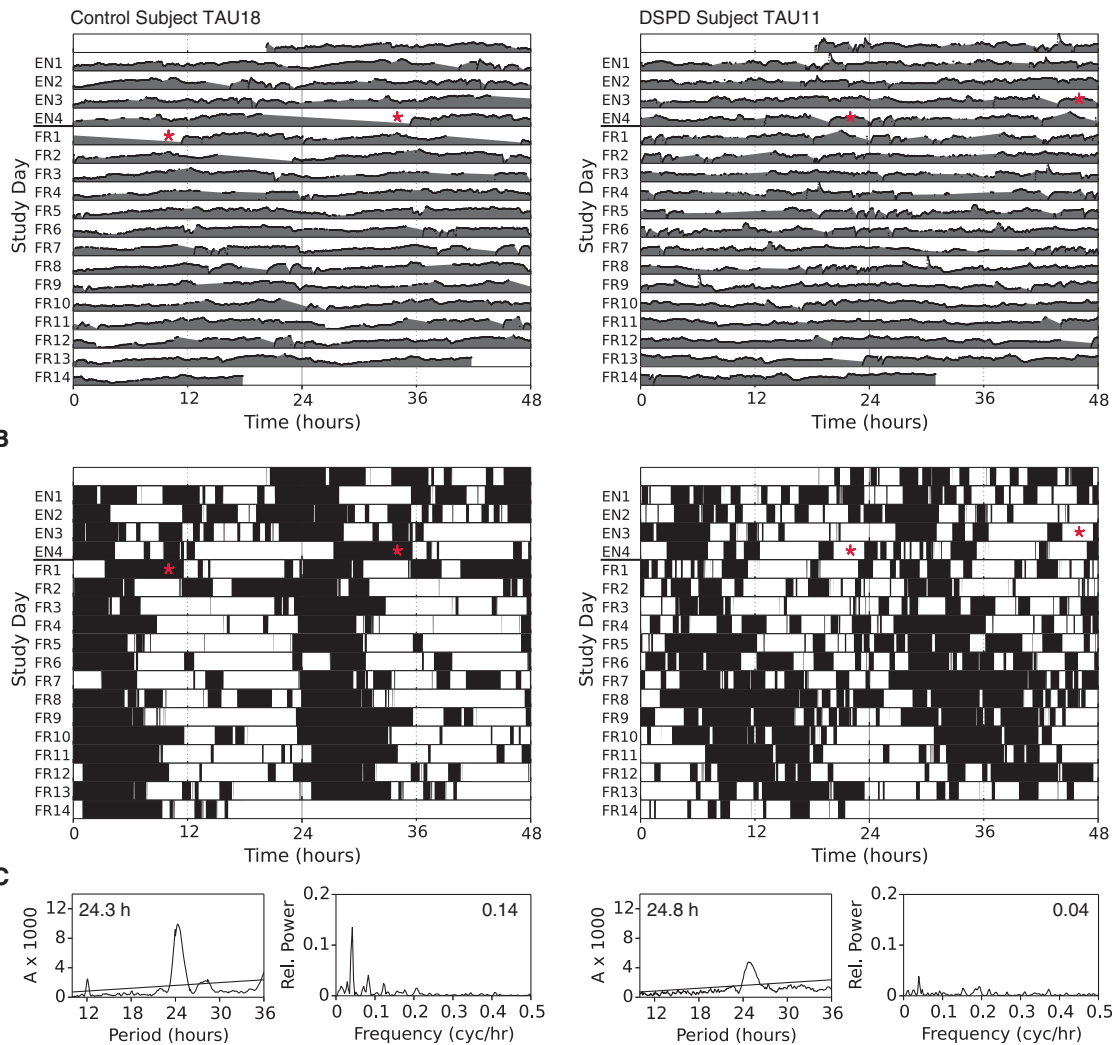
A Core Body Temperature

Figure 2. Core Body Temperature of Control Subject “TAU18” and the DSPD proband “TAU11”

(A) Double-plotted core body temperature during the in-laboratory study. The scale of the y axis for each individual study day is 2.3°C. Data shown as gray fill are interpolated from raw data shown as black dot overlay (see STAR Methods for details). Red asterisk in the DSPD proband denotes the beginning of the free-run. In the control subject, the indicated free-run start time corresponds to the time used for analysis of rhythmicity and differs from the actual free-run start time due to a preceding ~12-hr gap in the temperature record.

(B) Double-plotted sub-mean core body temperature. The mean temperature of the entire data series was calculated from outlier-corrected, interpolated data for each subject, and data points below the mean are plotted as black fill.

(C) Analysis of core body temperature rhythmicity. Circadian rhythmicity during the free-run was analyzed by X^2 periodogram and FFT analysis to measure period and amplitude, respectively.

See also Figure S1.

sleep consisting of a brief sleep period early in the night and extended naps during the day. Fragmented sleep was particularly prevalent among those carriers for whom early rising was a necessity due to cultural or social obligations. Of note, no difference in sleep behavior was observed between heterozygous and homozygous carriers of the *CRY1* allele, consistent with an autosomal-dominant mode of inheritance. The one carrier with reported conventional sleep times (DSPD-6 16-068) was subject to work-imposed strong light exposure, raising the possibility that the *CRY1*-mediated disposition can be modifiable given

adequate environmental conditions. Nevertheless, there was a very strong association between *CRY1* allele status and sleep behavior in the reverse-phenotyped families and the original proband kindred (Fisher’s exact $p < 0.0001$, odds ratio = 1,928, 95% confidence interval 76–48,904).

***CRY1* Exon 11 Deletion Affects Circadian Clock Cycling and *CRY1* Molecular Function**

To directly test whether the deletion of exon 11 of *CRY1* affects the circadian clock, we created cell lines differing only in the

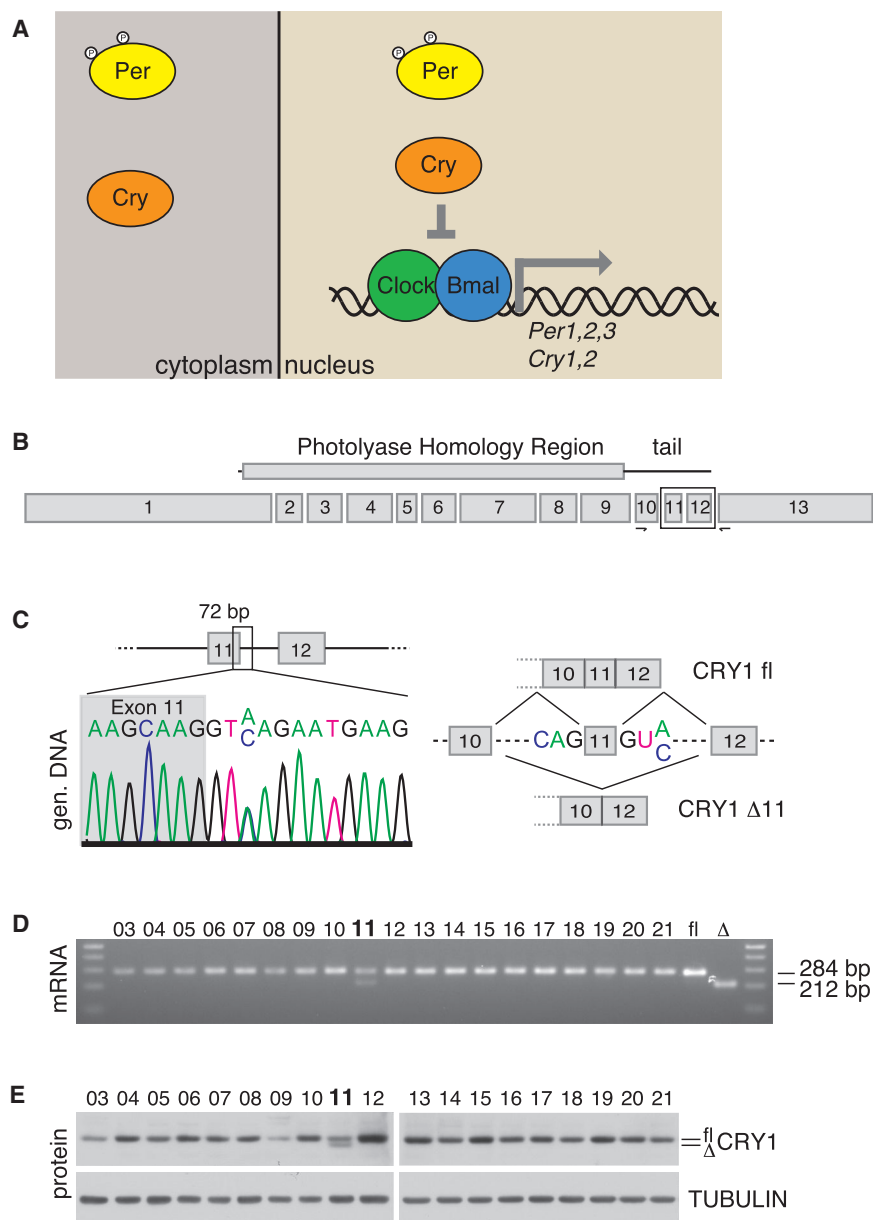


Figure 3. Mutation of *CRY1*

(A) The core molecular circadian clock in mammals. Transcriptional activity of Clock and Bmal1 leads to expression of Per and Cry family genes, whose products undergo posttranslational modification, translocate to the nucleus, and inhibit Clock/Bmal1-mediated transcription with Cry1 acting as the main repressor.

(B) Exon organization of the human *CRY1* gene with the encoded protein regions shown above. Box represents the region enlarged in (C). Arrows indicate primer binding sites used in (D).

(C) Primary sequencing trace of the region immediately following exon 11 in the proband's genomic DNA (left) and schematic diagram depicting the expected consequences of the A-to-C transversion on *CRY1* mRNA splicing (right).

(D) RT-PCR analysis of the *CRY1* mRNA between exons 10 and 13. Samples 03 to 21 are amplified from primary fibroblast cell lines from 19 different subjects, with number 11 belonging to the proband. Controls on the right are amplified from cloned *CRY1* full-length and Δ 11 cDNA. Expected product sizes are indicated.

(E) *CRY1* protein expression in the 19 subject-derived fibroblast cell lines. TUBULIN levels are shown as a loading control.

rhythmicity, consistent with previous reports (Khan et al., 2012), and the differential period length between the two *CRY1* forms was still observed in its presence (Figure S3A). These results demonstrate a direct effect of *CRY1* exon 11 deletion on circadian period length, which matches DSPD symptoms.

The Cry1 protein consists of a conserved photolyase homology region, which mediates transcriptional repression of Clock/Bmal1, a C-terminal helix previously described as a predicted coiled coil, which interacts with Per2 and Fbx13 in a mutually exclusive manner and a C-terminal extension also referred to as the "tail" (Figures 3B and S3B)

expressed *CRY1* form. Human full-length or *CRY1* Δ 11 variants were expressed in *CRY1/2* double-deficient mouse embryonic fibroblasts (DKO MEFs) using regulatory elements previously characterized to recapitulate endogenous *CRY1* oscillation (Ukai-Tadenuma et al., 2011). As expected, *CRY1* expression restored circadian cycling of a Bmal1-luciferase reporter in previously arrhythmic DKO MEFs, albeit with a long period, as previously described for this experimental system (Khan et al., 2012) (Figure 4B). Compared to full-length *CRY1*, expression of the Δ 11 form increased circadian period by approximately half an hour, similar to the phenotype observed in the proband. The effect was not due to differences in the amounts of the ectopically expressed *CRY1* forms (Figure 4B). In contrast to *CRY1*, expression of *CRY2* in *CRY1* DKO MEFs did not restore their circadian

(Chaves et al., 2011; Merbitz-Zahradnik and Wolf, 2015). The Cry1 tail region represents the most poorly conserved and least functionally and structurally characterized region of the protein. It has been shown to affect Cry1 nuclear translocation, to interact with the Bmal1 transactivation domain possibly in an acetylation-dependent fashion, and to be phosphorylated in a manner that involves regulation by DNA-PK (Chaves et al., 2006; Czarna et al., 2011; Gao et al., 2013; Hirayama et al., 2007; Xu et al., 2015). Interestingly, the tail is not essential to Cry1's ability to restore circadian cycling to arrhythmic DKO MEFs but does modulate the period length and amplitude of the resulting oscillation (Khan et al., 2012; Li et al., 2016). Overall, current evidence points to a regulatory role of the Cry1 tail in the transcriptional repression complex involving Clock, Bmal1, and possibly other factors at

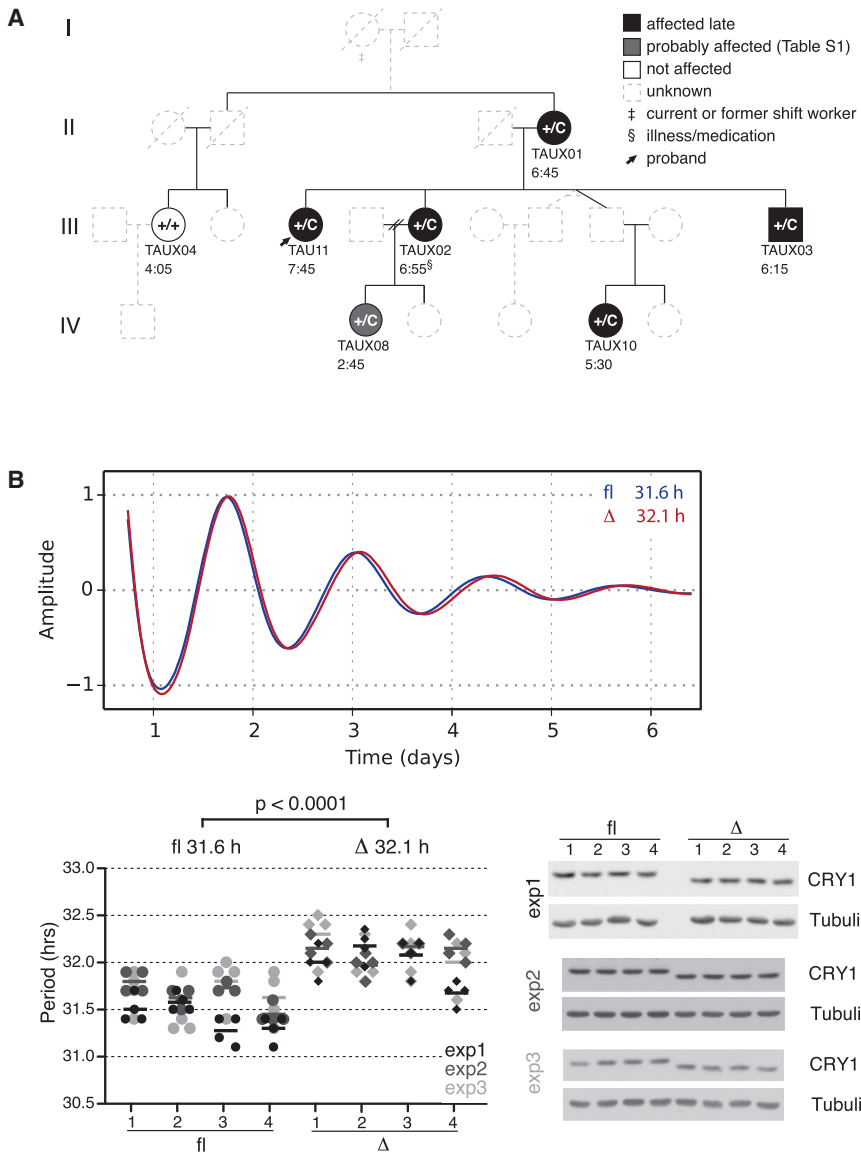


Figure 4. Effect of the *CRY1* Mutation on Human Sleep Timing and Clock Oscillation

(A) Segregation of the *CRY1* c.1657+3A>C allele with delayed sleep in the proband's family. Genotype is shown inside symbols. Color code and symbols are explained in the legend. Numbers represent midsleep point on free days (MSF) (Roenneberg et al., 2003). See also Table S1 for details.

(B) Deletion of *CRY1* exon 11 affects circadian period length. *CRY1* fl or Δ11 cDNAs were expressed in Bmal1-luc DKO MEFs using a lentiviral expression system that preserved the regulatory elements necessary to recapitulate endogenous *CRY1* expression. Cells were synchronized with 20 μM forskolin, and bioluminescence output was recorded for ~7 days. Traces show average detrended bioluminescence counts normalized to the first peak for each genotype (*CRY1* fl blue, *CRY1* Δ11 red). Period was calculated from bioluminescence recordings of quadruplicate samples from quadruplicate *CRY1* infections (circles, fl 1–4; diamonds, Δ 1–4). Data from three independent experiments are shown (gray shading). Mean periods from each infection (indicated by horizontal lines) were used to assess statistical significance between genotypes. The overall mean period was 31.6 hr for full-length *CRY1* and 32.1 hr for Δ11 *CRY1*. Steady-state *CRY1* levels for infections 1–4 from each experiment were measured by western blot with Tubulin shown as loading control.

See also Figures S2 and S3 and Table S1.

various stages of the circadian cycle. Deletion of exon 11 results in the removal of 24 residues from the *CRY1* C-terminal tail. In accordance with previous functional characterizations of the *Cry1* protein regions, we did not observe a difference in the capacity of *CRY1* Δ11 to inhibit Clock/Bmal1-dependent transcription of an E-box-driven luciferase reporter plasmid in heterologous cell-based assays, which do not require the *Cry1* tail (Chaves et al., 2006; Khan et al., 2012) (Figures S3C and S3D). Further, although some modifications within the tail region can affect the half-life of the *Cry1* protein under certain conditions (Gao et al., 2013), we did not observe gross differences in the stability of *CRY1* Δ11 versus the full-length form in the subject's primary fibroblasts (Figure S3E), and luciferase fusion proteins with the respective *CRY1* forms decayed at a similar rate (Figure S3F).

The existence of a nuclear localization signal in the *Cry1* tail, albeit C-terminal to the exon 11 region, prompted us to assess

the subcellular distribution of the different *CRY1* forms. Unexpectedly, deletion of exon 11 increased *CRY1* abundance in the nuclear fraction of the proband's fibroblasts throughout the circadian cycle (Figures 6A and S4A). This increased abundance was not caused by potential additional variations in the proband's cells but represents an intrinsic property of the modified *CRY1* protein, as enhanced *CRY1* Δ11 nuclear localization was also observed in DKO MEFs engineered to express both *CRY1* forms (*CRY1* fl/Δ MEFs) (Figures 6B and S4B).

***CRY1* Δ11 Shows Enhanced Interactions with Clock and Bmal1 Proteins**

Preferential nuclear localization of *CRY1* Δ11 led us to assess its binding to its target transcription factors Clock and Bmal1. Although both *CRY1* forms present in the subject's fibroblasts were found to be capable of interaction, the fraction of *CRY1* immunoprecipitating with ARNTL or Clock was enriched for the Δ11 form (Figures 6C and S4C). This is not solely a reflection of differential subcellular distribution as ARNTL or Clock immunoprecipitated from purified nuclear extracts still bound more Δ11 than full-length *CRY1*. Enhanced interaction with the *CRY1* Δ11 form was replicated in *CRY1* fl/Δ MEFs independent

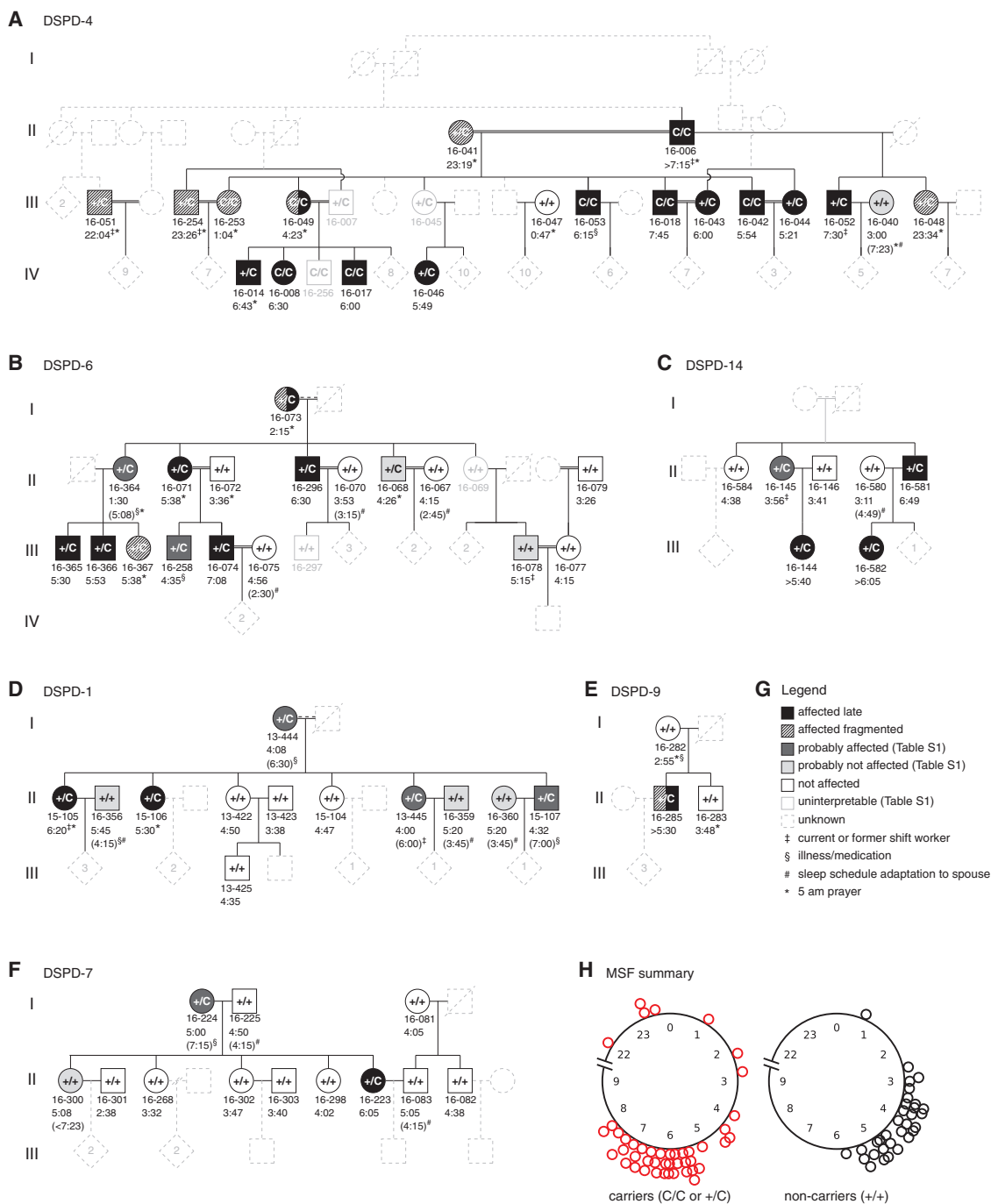


Figure 5. Sleep Behavior in *CRY1* c.1657+3A>C Carrier Families of Turkish Descent

(A–F) Sleep behavior in families DSPD-4, -6, -14, -1, -9, and -7 assessed through sleep and chronotype questionnaires and personal interview. Genotype is shown inside symbols. Numbers represent mid-sleep point on free days (MSF) (Roenneberg et al., 2003). See also Table S1 for details.

(G) Legend for colors and symbols used in (A–F).

(H) MSF from subjects in (A–F) as well as Figure 4A are plotted on a discontinuous clock face from 22:00 to 9:00 for carriers (left, red) and non-carriers (right, black). No subject data fell within the gap time (9:00 to 22:00) not represented in the plot.

of circadian phase (Figures 6D and S4D). Interestingly, although exon 11 partially overlaps with a region in the *Cry1* tail that has been identified as a binding site for the Bmal1 transactivation

domain acetylated at lysine 538, we still observed preferential binding of *CRY1* Δ11 to acetylated Bmal1. We also consistently detected higher overall levels of acetyl-Bmal1 in control DKO

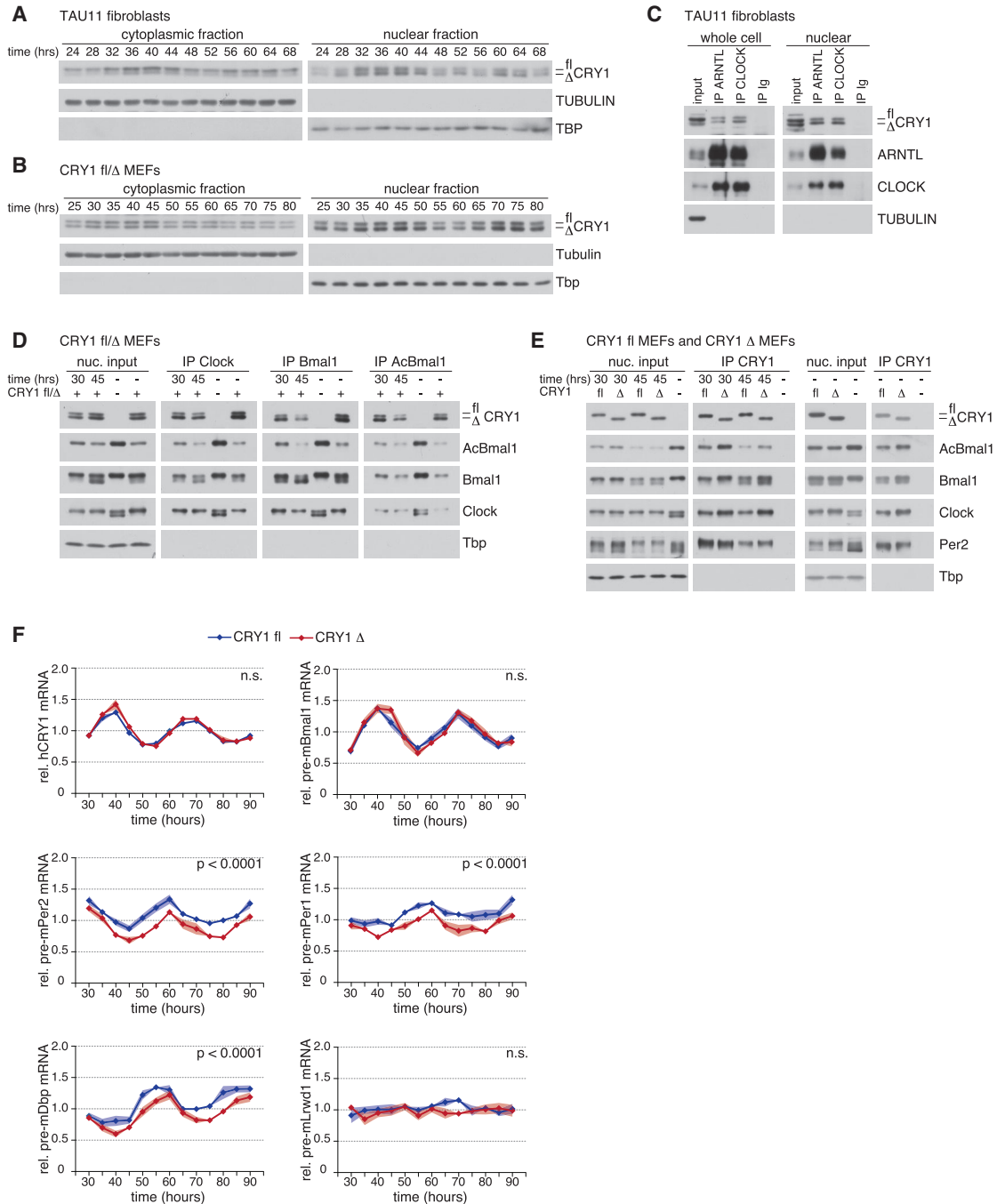


Figure 6. Exon 11 Deletion Enhances CRY1 Function in the Molecular Circadian Clock

(A) CRY1 expression was assessed in fractionated extracts prepared from the proband's fibroblasts at the indicated times following synchronization. TUBULIN and TBP were used as loading controls for cytoplasmic and nuclear extracts, respectively, and to assess fractionation purity.

(B) Same as (A) except proband fibroblasts were replaced with CRY1 fl/Δ MEFs, and the sampling interval was adjusted to account for the longer circadian period in this cell type.

(C) Co-immunoprecipitation of CRY1 with ARNTL and CLOCK in unsynchronized whole-cell (left) and nuclear (right) extracts from the proband's fibroblasts.

(D) Co-immunoprecipitation of CRY1 with Clock, Bmal1, and K538 Acetyl-Bmal1 in nuclear extracts from CRY1 fl/Δ MEFs at 30 or 45 hr post-synchronization as well as from unsynchronized CRY1 fl/Δ and empty vector control DKO MEFs.

(E) Co-immunoprecipitation of Clock, Bmal1, K538 Acetyl-Bmal1, and Per2 with CRY1 from nuclear extracts of CRY1 fl or Δ11 MEFs at 30 or 45 hr post-synchronization as well as from unsynchronized CRY1 fl or Δ11 MEFs and the empty vector control.

(legend continued on next page)

MEFs, which only received empty vector and remained devoid of cryptochromes, potentially indicating a more complex role of Bmal1 acetylation than currently suggested. Selective expression of either the full-length or the CRY1 $\Delta 11$ form in DKO MEFs allowed us to assess CRY1 binding to its interaction partners in reciprocal immunoprecipitations of the respective CRY1 form. Consistent with our other findings, more Clock, acetyl-Bmal1, and total Bmal1 immunoprecipitated with CRY1 $\Delta 11$ than with the full-length protein (Figures 6E and S4E). At the same time, the levels of CRY1-associated Per2 remained similar between the two CRY1 forms, suggesting the presence of separate CRY1-containing protein complexes with differential susceptibility to exon 11 deletion. Together, these results demonstrate that, rather than disabling CRY1, deletion of exon 11 enhances its presence in the nucleus and the binding to its target transcription factors, properties that are expected to promote its function as a transcriptional inhibitor.

CRY1 $\Delta 11$ Strengthens Transcriptional Inhibition

To directly test whether CRY1 $\Delta 11$ acts as a more potent transcriptional inhibitor during the intact clock cycle, we compared the expression of selected target genes in our engineered cell lines expressing either full length or CRY1 $\Delta 11$. As expected, cyclic CRY1 expression restored the circadian oscillation of *pre-Bmal1*, *pre-Per2*, *pre-Per1*, and *pre-Dbp* mRNAs with a long-period rhythm, although the sampling interval impeded an accurate determination of period length, as previously achieved by the high-resolution luciferase assay (Figure 6F). Compared to CRY1 full-length cells, the levels of *pre-Per2*, *pre-Per1*, and *pre-Dbp* mRNAs were reduced in CRY1 $\Delta 11$ cells, demonstrating stronger repression of Clock/Bmal1-mediated transcription by CRY1 $\Delta 11$ consistent with its other properties. In contrast, expression of *pre-Bmal1*, which is controlled by a different set of regulatory elements (Preitner et al., 2002; Ueda et al., 2002), remained unaffected by the CRY1 modification, as did the levels of a non-circadian control gene.

Given enhanced association with the target transcription factors as well as reduced expression of the relevant transcripts, we wondered whether exon 11 deletion affected CRY1 occupancy at its target gene promoters. In the circadian transcriptional feedback loop, repression can occur by blocking of the DNA-bound transcription factors or by their displacement and sequestration away from DNA (Menet et al., 2010). Cry1-dependent inhibition of gene expression has been shown to involve both of these modes (Ye et al., 2014). Using our cell lines engineered to selectively express full length or CRY1 $\Delta 11$, we measured the binding of CRY1, Bmal1, and Clock to target regions in the *Per2* and *Dbp* promoters by chromatin immunoprecipitation (Figures 7A–B). At the time of high Bmal1/low Per2 expression, reduced promoter association of CRY1, Bmal1, and Clock was observed in cells expressing CRY1 $\Delta 11$ compared to the full-length form, while the association of the control histone 3 trimethylated at lysine 4 (H3K4me3) remained

unaltered. As expected, in control reactions measuring a non-circadian promoter, only H3K4me3 binding was observed while the amounts of CRY1, Bmal1, and Clock were at or near the background levels of the assay (Figure 7C). These results demonstrate that CRY1 exon 11 deletion specifically reduces the presence of clock gene proteins at target gene promoters, consistent with Cry1-mediated transcriptional regulation through displacement of Clock and Bmal1.

DISCUSSION

As the major transcriptional inhibitor in the negative feedback loop that constitutes the core molecular clock, Cry1 represents a critical regulator of circadian period length. In general, there is a positive correlation between the amount of Cry1 and period length, although exceptions to this rule can occur upon manipulation of selected protein regions (Busino et al., 2007; Godinho et al., 2007; Hirota et al., 2012; Ode et al., 2016; Oshima et al., 2015; Siepkka et al., 2007; van der Horst et al., 1999; Vitaterna et al., 1999; Zhang et al., 2009). Moreover, period length has been shown to correlate with the affinity of Cry1 to Bmal1 (Xu et al., 2015).

Our results show that the CRY1 DSPD allele represents a gain-of-function mutation with deletion of exon 11 leading to increased CRY1 nuclear localization, enhanced interaction with the transcription factors Clock and Bmal1, their displacement from chromatin, and heightened inhibition of their target genes (Figure S5). Expression of this more potent CRY1 form (CRY1 $\Delta 11$) is associated with a lengthened period of molecular circadian rhythms in cells. A human carrier of CRY1 $\Delta 11$ studied in temporal isolation displayed corresponding, long-period behavioral and body-temperature rhythms with diminished amplitudes. These phenotypic changes are consistent with the established positive correlation of period length with CRY1 availability and affinity to its target transcription factors, thus providing a mechanistic explanation for the development of DSPD in carriers of the CRY1 $\Delta 11$ allele.

The stronger inhibitory function of the CRY1 $\Delta 11$ variant is only observed in the context of an intact clock cycle, raising interesting questions regarding the mechanism by which the CRY1 protein tail influences Clock/Bmal1 transcriptional activity. While currently available structural characterizations of the mammalian cryptochrome proteins have been insightful regarding their binding to Per2 and Fbxl3, the interaction with their target transcription factors has yet to be visualized, and none of the structures includes the Cry1 tail region (Merbitz-Zahradnik and Wolf, 2015). It is conceivable that the tail could affect transcription factor/repressor interaction through regulated binding to the CRY1 photolyase homology region or Clock/Bmal1, causing conformational changes to the complex. Such an event could be temporally controlled through recruitment or loss of additional complex components, through inducible post-translational modification of any of the proteins, or through changes to the CRY1 protein such as its redox state or the presence of cofactors, including flavin adenine dinucleotide or zinc ions. While

(F) Levels of CRY1, *pre-Bmal1*, *pre-Per2*, *pre-Per1*, *pre-Dbp*, and *pre-Lrwd1* were assessed by real-time quantitative RT-PCR in synchronized CRY1 fl (blue) or $\Delta 11$ (red) MEFs. Graphs show mean expression levels from five independent experiments, with the shaded area indicating the standard error. Statistically significant differences in gene expression between genotypes are indicated. n.s., not significant. See also Figure S4.

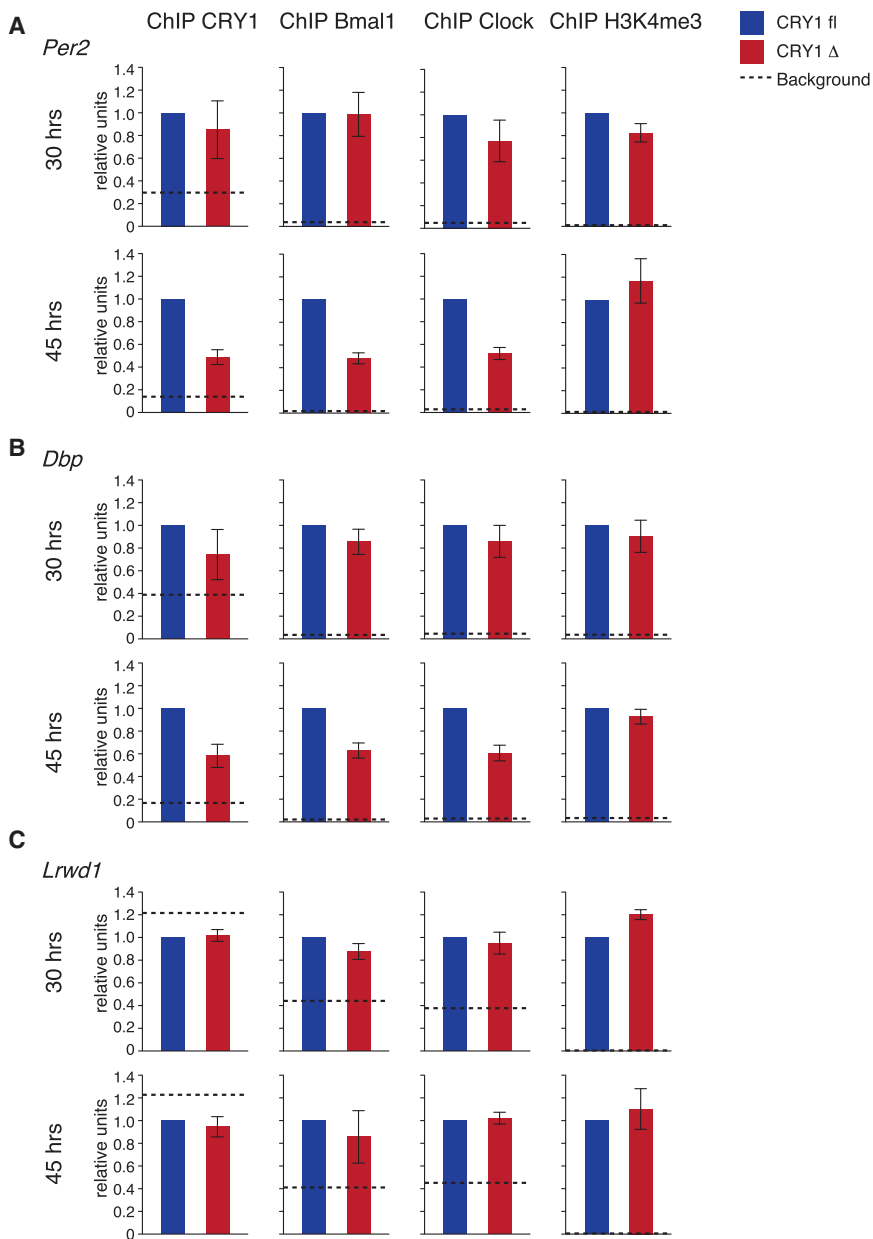


Figure 7. CRY1 Δ 11 Affects the Occupancy of CRY1, Bmal1, and Clock at Target Gene Promoters

(A–C) CRY1, Bmal1, Clock, and H3K4me3 were immunoprecipitated from CRY1 fl (blue) or Δ 11 (red) MEFs at 30 or 45 hr post-synchronization following chromatin crosslinking. The amount of *Per2*- (A), *Dbp*- (B), and *Lrwd1*-promoter DNA (C) in the immunoprecipitates was assessed by real-time quantitative PCR. The background signal (dashed line) corresponds to the respective real-time quantitative PCR values of a control reaction using a CRY1 chromatin-immunoprecipitate from Cry-deficient cells as template. Data in each experiment were normalized to the amount in the CRY1 fl sample, which was set to 1. Error bars represent the standard error from three independent experiments.

melatonin onset (DLMO) by \sim 2–2.5 hr. These predictions agree well with the behavioral and physiological findings we have presented.

Databases of human genetic variation report a frequency between 0.1% and 0.6% for the CRY1 c.1657+3A>C allele, such that up to 1 in 75 members of certain populations could carry the dominant CRY1 variant. Our analyses of the original proband family as well as a large number of subjects from unrelated families of completely different ethnicity show that both homo- and heterozygous CRY1 c.1657+3A>C carrier status is strongly associated with late sleep times and sleep fragmentation. Possibly, the latter behavior may be a manifestation of carrier allele status under environmental conditions that do not accommodate late sleep times, as can often be the case due to cultural, social, or professional obligations. Alternatively, inter-individual differences in genetic background or exposure to environmental entrainment signals may affect the nature and penetrance of sleep

disturbances in CRY1 Δ 11 allele carriers, and similar phenomena have been observed in both human and animal studies of circadian rhythmicity (Azzi et al., 2014; Pittendigh and Daan, 1976; Shimomura et al., 2013; Toh et al., 2001). The CRY1 Δ 11 variant may thus lead to a broader range of sleep-disorder phenotypes with delay being the most common manifestation.

dispensable for basic repression, the CRY1 tail could thus exert the capacity to modulate transcriptional inhibition at defined stages of the circadian cycle. In our analyses of cellular circadian rhythms, the CRY1 Δ 11 allele consistently lengthened the period of molecular oscillations by approximately half an hour. Earlier work has demonstrated a strong relationship between circadian period, entrained phase, and sleep timing in humans, such that moderate changes in period are associated with much larger shifts in the relative phases of bedtime and the evening increase in serum melatonin (Gronfier et al., 2007; Wright et al., 2005). Accordingly, a half-hour change in the period of the human circadian clock is expected to change the relationship of sleep timing and evening

disturbances in CRY1 Δ 11 allele carriers, and similar phenomena have been observed in both human and animal studies of circadian rhythmicity (Azzi et al., 2014; Pittendigh and Daan, 1976; Shimomura et al., 2013; Toh et al., 2001). The CRY1 Δ 11 variant may thus lead to a broader range of sleep-disorder phenotypes with delay being the most common manifestation.

STAR METHODS

Detailed methods are provided in the online version of this paper and include the following:

- KEY RESOURCES TABLE

- CONTACT FOR REAGENT AND RESOURCE SHARING
- EXPERIMENTAL MODEL AND SUBJECT DETAILS
 - Human Studies
 - Subject Screening for Human In-Laboratory Study
 - Data Collection for Human In-Laboratory Study
 - Proband Family Study
 - Reverse Phenotyping of additional CRY1 c.1657+3A>C Carrier Families
 - Derivation of Human Dermal Fibroblast Cell Lines
 - Cell Lines and Tissue Culture
- METHOD DETAILS
 - Candidate Gene Sequencing
 - Whole Exome Sequencing
 - CRY1 c.1657+3A>C Genotyping
 - Cloning of CRY1 Constructs
 - Real-Time Circadian Reporter Assay
 - Preparation of Protein Extracts, Immunoprecipitation, and Western Blot
 - Clock Gene Expression Analysis
 - Chromatin Immunoprecipitation
 - Luciferase Repression Assay
 - Luciferase Stability Assay
- QUANTIFICATION AND STATISTICAL ANALYSIS
 - Data Analysis for Human In-Laboratory Study
 - Data Analysis for Whole Exome Sequencing
 - Cellular Period Analysis
 - Association between CRY1 c.1657+3A>C Genotype and Sleep Behavior
 - Analysis of Western Blot Data
 - Analysis of Clock Gene Expression Data
 - Analysis of ChIP Data
- DATA AND SOFTWARE AVAILABILITY

SUPPLEMENTAL INFORMATION

Supplemental Information includes five figures and three tables and can be found with this article online at <http://dx.doi.org/10.1016/j.cell.2017.03.027>.

AUTHOR CONTRIBUTIONS

A.P., P.J.M., S.S.C., and M.W.Y. conceived of the project. P.J.M. and S.S.C. designed experiments and collected data for Figures 1, 2, 4A, S1, and S2. A.P. and M.W.Y. analyzed data for Figures 1, 2, 4A, S1, and S2 with input from P.J.M., A.C.K. and S.S.C. A.P. designed and performed experiments in Figures 3, 4B, 6, 7, S3, and S4. O.E.O. and T.Ö. collected data for Figure 5. A.P., O.E.O., T.Ö., and M.W.Y. analyzed data for Figure 5. A.P. prepared all figures and wrote the manuscript with input from all authors. A.P., T.Ö., S.S.C., and M.W.Y. secured funding.

ACKNOWLEDGMENTS

We thank the human study participants; the technical staff of the Laboratory of Human Chronobiology; Adam Savitz for conducting physical exams; Mary Morton for obtaining skin biopsies; Melanie Roberts for recruiting and obtaining data from the proband's family; Boris Dubrovsky for scoring polysomnography records; Nazlı Başak, Ali Dursun, Uğur Özbek, Köksal Özgül, and Bülent Yıldız for establishing initial contact to Turkish DSPD families; Hiroki Ueda, Steve Kay, and Steven Reppert for reagents; Avinash Abhyankar and the New York Genome Center for help with whole exome sequencing; Jeffrey Friedman for discussion and help with subject identification; Philip Kidd for help with processing of raw core body temperature data; the Friedman and Tarakhovskiy laboratories for generously sharing equipment; and Cori Barg-

mann, Joseph Gleeson, André Hoelz, and Leslie Vosshall for comments on the manuscript. This work was supported by NIH grant RO1 NS052495 (S.S.C.), a sub-award #12081164 of NS052495 provided by Weill Cornell Medical College (M.W.Y.), Calico Life Sciences LLC (M.W.Y.), The Rockefeller University Center for Clinical and Translational Science grants UL1 TR000043 and UL1 TR001866 (A.P.), the Turkish Academy of Sciences-TÜBA (T.Ö.), The Rockefeller University Women & Science Postdoctoral Fellowship program (A.P.), and a NARSAD Young Investigator Grant #21131 from the Brain & Behavior Research Foundation (A.P.). P.J.M. is currently employed by Eisai Inc.

Received: January 14, 2017

Revised: February 18, 2017

Accepted: March 20, 2017

Published: April 6, 2017

REFERENCES

- American Academy of Sleep Medicine (2005). International Classification of Sleep Disorders: Diagnostic and Coding Manual, Second Edition (Westchester, Illinois: American Academy of Sleep Medicine).
- Anand, S.N., Maywood, E.S., Chesham, J.E., Joynson, G., Banks, G.T., Hastings, M.H., and Nolan, P.M. (2013). Distinct and separable roles for endogenous CRY1 and CRY2 within the circadian molecular clockwork of the suprachiasmatic nucleus, as revealed by the *Fbxl3*(*Afh*) mutation. *J. Neurosci.* 33, 7145–7153.
- Aoki, H., Ozeki, Y., and Yamada, N. (2001). Hypersensitivity of melatonin suppression in response to light in patients with delayed sleep phase syndrome. *Chronobiol. Int.* 18, 263–271.
- Archer, S.N., Robilliard, D.L., Skene, D.J., Smits, M., Williams, A., Arendt, J., and von Schantz, M. (2003). A length polymorphism in the circadian clock gene *Per3* is linked to delayed sleep phase syndrome and extreme diurnal preference. *Sleep* 26, 413–415.
- Azzi, A., Dallmann, R., Casserly, A., Rehrauer, H., Patrignani, A., Maier, B., Kramer, A., and Brown, S.A. (2014). Circadian behavior is light-reprogrammed by plastic DNA methylation. *Nat. Neurosci.* 17, 377–382.
- Barclay, N.L., Eley, T.C., Buysse, D.J., Archer, S.N., and Gregory, A.M. (2010). Diurnal preference and sleep quality: same genes? A study of young adult twins. *Chronobiol. Int.* 27, 278–296.
- Benloucif, S., Burgess, H.J., Klerman, E.B., Lewy, A.J., Middleton, B., Murphy, P.J., Parry, B.L., and Revell, V.L. (2008). Measuring melatonin in humans. *J. Clin. Sleep Med.* 4, 66–69.
- Brown, S.A., Fleury-Olela, F., Nagoshi, E., Hauser, C., Juge, C., Meier, C.A., Chicheportiche, R., Dayer, J.M., Albrecht, U., and Schibler, U. (2005). The period length of fibroblast circadian gene expression varies widely among human individuals. *PLoS Biol.* 3, e338.
- Busino, L., Bassermann, F., Maiolica, A., Lee, C., Nolan, P.M., Godinho, S.I., Draetta, G.F., and Pagano, M. (2007). SCFF^{bxl3} controls the oscillation of the circadian clock by directing the degradation of cryptochrome proteins. *Science* 316, 900–904.
- Campbell, S.S., and Murphy, P.J. (2007). Delayed sleep phase disorder in temporal isolation. *Sleep* 30, 1225–1228.
- Chang, A.M., Reid, K.J., Gourineni, R., and Zee, P.C. (2009). Sleep timing and circadian phase in delayed sleep phase syndrome. *J. Biol. Rhythms* 24, 313–321.
- Chaves, I., Pokorny, R., Byrdin, M., Hoang, N., Ritz, T., Brettel, K., Essen, L.O., van der Horst, G.T., Batschauer, A., and Ahmad, M. (2011). The cryptochromes: blue light photoreceptors in plants and animals. *Annu. Rev. Plant Biol.* 62, 335–364.
- Chaves, I., Yagita, K., Barnhoorn, S., Okamura, H., van der Horst, G.T., and Tamanini, F. (2006). Functional evolution of the photolyase/cryptochrome protein family: importance of the C terminus of mammalian CRY1 for circadian core oscillator performance. *Mol. Cell. Biol.* 26, 1743–1753.
- Chiou, Y.Y., Yang, Y., Rashid, N., Ye, R., Selby, C.P., and Sancar, A. (2016). Mammalian Period represses and de-represses transcription by displacing

- CLOCK-BMAL1 from promoters in a Cryptochrome-dependent manner. *Proc. Natl. Acad. Sci. USA* 113, E6072–E6079.
- Ciarleglio, C.M., Ryckman, K.K., Servick, S.V., Hida, A., Robbins, S., Wells, N., Hicks, J., Larson, S.A., Wiedermann, J.P., Carver, K., et al. (2008). Genetic differences in human circadian clock genes among worldwide populations. *J. Biol. Rhythms* 23, 330–340.
- Cingolani, P., Platts, A., Wang, L., Coon, M., Nguyen, T., Wang, L., Land, S.J., Lu, X., and Ruden, D.M. (2012). A program for annotating and predicting the effects of single nucleotide polymorphisms, SnpEff: SNPs in the genome of *Drosophila melanogaster* strain w1118; iso-2; iso-3. *Fly (Austin)* 6, 80–92.
- Crane, B.R., and Young, M.W. (2014). Interactive features of proteins composing eukaryotic circadian clocks. *Annu. Rev. Biochem.* 83, 191–219.
- Czarna, A., Breitkreuz, H., Mahrenholz, C.C., Arens, J., Strauss, H.M., and Wolf, E. (2011). Quantitative analyses of cryptochrome-mBMAL1 interactions: mechanistic insights into the transcriptional regulation of the mammalian circadian clock. *J. Biol. Chem.* 286, 22414–22425.
- Czeisler, C.A., Duffy, J.F., Shanahan, T.L., Brown, E.N., Mitchell, J.F., Rimmer, D.W., Ronda, J.M., Silva, E.J., Allan, J.S., Emens, J.S., et al. (1999). Stability, precision, and near-24-hour period of the human circadian pacemaker. *Science* 284, 2177–2181.
- Danecek, P., Auton, A., Abecasis, G., Albers, C.A., Banks, E., DePristo, M.A., Handsaker, R.E., Lunter, G., Marth, G.T., Sherry, S.T., et al.; 1000 Genomes Project Analysis Group (2011). The variant call format and VCFtools. *Bioinformatics* 27, 2156–2158.
- DePristo, M.A., Banks, E., Poplin, R., Garimella, K.V., Maguire, J.R., Hartl, C., Philippakis, A.A., del Angel, G., Rivas, M.A., Hanna, M., et al. (2011). A framework for variation discovery and genotyping using next-generation DNA sequencing data. *Nat. Genet.* 43, 491–498.
- Duffy, J.F., Rimmer, D.W., and Czeisler, C.A. (2001). Association of intrinsic circadian period with morningness-eveningness, usual wake time, and circadian phase. *Behav. Neurosci.* 115, 895–899.
- Duong, H.A., Robles, M.S., Knutti, D., and Weitz, C.J. (2011). A molecular mechanism for circadian clock negative feedback. *Science* 332, 1436–1439.
- Duong, H.A., and Weitz, C.J. (2014). Temporal orchestration of repressive chromatin modifiers by circadian clock period complexes. *Nat. Struct. Mol. Biol.* 21, 126–132.
- Ebisawa, T., Uchiyama, M., Kajimura, N., Mishima, K., Kamei, Y., Katoh, M., Watanabe, T., Sekimoto, M., Shibui, K., Kim, K., et al. (2001). Association of structural polymorphisms in the human period3 gene with delayed sleep phase syndrome. *EMBO Rep.* 2, 342–346.
- Gao, P., Yoo, S.H., Lee, K.J., Rosensweig, C., Takahashi, J.S., Chen, B.P., and Green, C.B. (2013). Phosphorylation of the cryptochrome 1 C-terminal tail regulates circadian period length. *J. Biol. Chem.* 288, 35277–35286.
- Godinho, S.I., Maywood, E.S., Shaw, L., Tucci, V., Barnard, A.R., Busino, L., Pagano, M., Kendall, R., Quwillid, M.M., Romero, M.R., et al. (2007). The after-hours mutant reveals a role for Fbxl3 in determining mammalian circadian period. *Science* 316, 897–900.
- Griffin, E.A., Jr., Staknis, D., and Weitz, C.J. (1999). Light-independent role of CRY1 and CRY2 in the mammalian circadian clock. *Science* 286, 768–771.
- Gronfier, C., Wright, K.P., Jr., Kronauer, R.E., and Czeisler, C.A. (2007). Entrainment of the human circadian pacemaker to longer-than-24-h days. *Proc. Natl. Acad. Sci. USA* 104, 9081–9086.
- Hawkins, G.A., Meyers, D.A., Bleeker, E.R., and Pack, A.I. (2008). Identification of coding polymorphisms in human circadian rhythm genes PER1, PER2, PER3, CLOCK, ARNTL, CRY1, CRY2 and TIMELESS in a multi-ethnic screening panel. *DNA Seq.* 19, 44–49.
- Hida, A., Kitamura, S., Katayose, Y., Kato, M., Ono, H., Kadotani, H., Uchiyama, M., Ebisawa, T., Inoue, Y., Kamei, Y., et al. (2014). Screening of clock gene polymorphisms demonstrates association of a PER3 polymorphism with morningness-eveningness preference and circadian rhythm sleep disorder. *Sci. Rep.* 4, 6309.
- Hirano, A., Shi, G., Jones, C.R., Lipzen, A., Pennacchio, L.A., Xu, Y., Hallows, W.C., McMahon, T., Yamazaki, M., Ptáček, L.J., and Fu, Y.H. (2016). A Cryptochrome 2 mutation yields advanced sleep phase in humans. *eLife* 5, e16695.
- Hirayama, J., Sahar, S., Grimaldi, B., Tamaru, T., Takamatsu, K., Nakahata, Y., and Sassone-Corsi, P. (2007). CLOCK-mediated acetylation of BMAL1 controls circadian function. *Nature* 450, 1086–1090.
- Hirota, T., Lee, J.W., St John, P.C., Sawa, M., Iwaisako, K., Noguchi, T., Pong-sawakul, P.Y., Sonntag, T., Welsh, D.K., Brenner, D.A., et al. (2012). Identification of small molecule activators of cryptochrome. *Science* 337, 1094–1097.
- Hur, Y.M., Bouchard, T.J., and Lykken, D.T. (1998). Genetic and environmental influence on morningness–eveningness. *Pers. Individ. Dif.* 25, 917–925.
- Khan, S.K., Xu, H., Ukai-Tadenuma, M., Burton, B., Wang, Y., Ueda, H.R., and Liu, A.C. (2012). Identification of a novel cryptochrome differentiating domain required for feedback repression in circadian clock function. *J. Biol. Chem.* 287, 25917–25926.
- King, D.P., Zhao, Y., Sangoram, A.M., Wilsbacher, L.D., Tanaka, M., Antoch, M.P., Steeves, T.D., Vitaterna, M.H., Kornhauser, J.M., Lowrey, P.L., et al. (1997). Positional cloning of the mouse circadian clock gene. *Cell* 89, 641–653.
- Koskenvuo, M., Hublin, C., Partinen, M., Heikkilä, K., and Kaprio, J. (2007). Heritability of diurnal type: a nationwide study of 8753 adult twin pairs. *J. Sleep Res.* 16, 156–162.
- Kripke, D.F., Klimecki, W.T., Nievergelt, C.M., Rex, K.M., Murray, S.S., Shekhtman, T., Tranah, G.J., Loving, R.T., Lee, H.J., Rhee, M.K., et al. (2014). Circadian polymorphisms in night owls, in bipolars, and in non-24-hour sleep cycles. *Psychiatry Investig.* 11, 345–362.
- Kume, K., Zylka, M.J., Sriram, S., Shearman, L.P., Weaver, D.R., Jin, X., Maywood, E.S., Hastings, M.H., and Reppert, S.M. (1999). mCRY1 and mCRY2 are essential components of the negative limb of the circadian clock feedback loop. *Cell* 98, 193–205.
- Lek, M., Karczewski, K.J., Minikel, E.V., Samocha, K.E., Banks, E., Fennell, T., O'Donnell-Luria, A.H., Ware, J.S., Hill, A.J., Cummings, B.B., et al.; Exome Aggregation Consortium (2016). Analysis of protein-coding genetic variation in 60,706 humans. *Nature* 536, 285–291.
- Li, H., and Durbin, R. (2009). Fast and accurate short read alignment with Burrows-Wheeler transform. *Bioinformatics* 25, 1754–1760.
- Li, Y., Xiong, W., and Zhang, E.E. (2016). The ratio of intracellular CRY proteins determines the clock period length. *Biochem. Biophys. Res. Commun.* 472, 531–538.
- Liu, A.C., Tran, H.G., Zhang, E.E., Priest, A.A., Welsh, D.K., and Kay, S.A. (2008). Redundant function of REV-ERB α and β and non-essential role for Bmal1 cycling in transcriptional regulation of intracellular circadian rhythms. *PLoS Genet.* 4, e1000023.
- Lowrey, P.L., and Takahashi, J.S. (2011). Genetics of circadian rhythms in Mammalian model organisms. *Adv. Genet.* 74, 175–230.
- McLaren, W., Gil, L., Hunt, S.E., Riat, H.S., Ritchie, G.R., Thormann, A., Flicek, P., and Cunningham, F. (2016). The Ensembl Variant Effect Predictor. *Genome Biol.* 17, 122.
- Menet, J.S., Abruzy, K.C., Desrochers, J., Rodriguez, J., and Rosbash, M. (2010). Dynamic PER repression mechanisms in the *Drosophila* circadian clock: from on-DNA to off-DNA. *Genes Dev.* 24, 358–367.
- Merbitz-Zahradnik, T., and Wolf, E. (2015). How is the inner circadian clock controlled by interactive clock proteins?: Structural analysis of clock proteins elucidates their physiological role. *FEBS Lett.* 589, 1516–1529.
- Micic, G., de Bruyn, A., Lovato, N., Wright, H., Grdisar, M., Ferguson, S., Burgess, H.J., and Lack, L. (2013). The endogenous circadian temperature period length (τ) in delayed sleep phase disorder compared to good sleepers. *J. Sleep Res.* 22, 617–624.
- Molina, T.A., and Burgess, H.J. (2011). Calculating the dim light melatonin onset: the impact of threshold and sampling rate. *Chronobiol. Int.* 28, 714–718.
- Ode, K.L., Ukai, H., Susaki, E.A., Narumi, R., Matsumoto, K., Hara, J., Koide, N., Abe, T., Kanemaki, M.T., Kiyonari, H., et al. (2016). Knockout-rescue embryonic stem cell-derived mouse reveals circadian-period control by quality and quantity of CRY1. *Mol. Cell* 65, 176–190.

- Oshima, T., Yamanaka, I., Kumar, A., Yamaguchi, J., Nishiwaki-Ohkawa, T., Muto, K., Kawamura, R., Hirota, T., Yagita, K., Irle, S., et al. (2015). C-H activation generates period-shortening molecules that target cryptochrome in the mammalian circadian clock. *Angew. Chem. Int. Ed. Engl.* *54*, 7193–7197.
- Osland, T.M., Bjorvatn, B.R., Steen, V.M., and Pallesen, S.I. (2011). Association study of a variable-number tandem repeat polymorphism in the clock gene PERIOD3 and chronotype in Norwegian university students. *Chronobiol. Int.* *28*, 764–770.
- Oster, H., Yasui, A., van der Horst, G.T., and Albrecht, U. (2002). Disruption of mCry2 restores circadian rhythmicity in mPer2 mutant mice. *Genes Dev.* *16*, 2633–2638.
- Özçelik, T., and Onat, O.E. (2016). Genomic landscape of the Greater Middle East. *Nat. Genet.* *48*, 978–979.
- Pereira, D.S., Tufik, S., Louzada, F.M., Benedito-Silva, A.A., Lopez, A.R., Lemos, N.A., Korczak, A.L., D’Almeida, V., and Pedrazzoli, M. (2005). Association of the length polymorphism in the human Per3 gene with the delayed sleep-phase syndrome: does latitude have an influence upon it? *Sleep* *28*, 29–32.
- Pittendrigh, C.S., and Daan, S. (1976). Functional-Analysis of Circadian Pacemakers in Nocturnal Rodents 0.1. Stability and Lability of Spontaneous Frequency. *J. Comp. Physiol.* *106*, 223–252.
- Preitner, N., Damiola, F., Lopez-Molina, L., Zakany, J., Duboule, D., Albrecht, U., and Schibler, U. (2002). The orphan nuclear receptor REV-ERB α controls circadian transcription within the positive limb of the mammalian circadian oscillator. *Cell* *110*, 251–260.
- Roenneberg, T., Wirz-Justice, A., and Mrosovsky, M. (2003). Life between clocks: daily temporal patterns of human chronotypes. *J. Biol. Rhythms* *18*, 80–90.
- Sack, R.L., Auckley, D., Auger, R.R., Carskadon, M.A., Wright, K.P., Jr., Vitiello, M.V., and Zhdanova, I.V.; American Academy of Sleep Medicine (2007). Circadian rhythm sleep disorders: part II, advanced sleep phase disorder, delayed sleep phase disorder, free-running disorder, and irregular sleep-wake rhythm. An American Academy of Sleep Medicine review. *Sleep* *30*, 1484–1501.
- Shimomura, K., Kumar, V., Koike, N., Kim, T.K., Chong, J., Buhr, E.D., Whiteley, A.R., Low, S.S., Omura, C., Fenner, D., et al. (2013). Usf1, a suppressor of the circadian Clock mutant, reveals the nature of the DNA-binding of the CLOCK:BMAL1 complex in mice. *eLife* *2*, e00426.
- Siepkka, S.M., Yoo, S.H., Park, J., Song, W., Kumar, V., Hu, Y., Lee, C., and Takahashi, J.S. (2007). Circadian mutant Overtime reveals F-box protein FBXL3 regulation of cryptochrome and period gene expression. *Cell* *129*, 1011–1023.
- Toh, K.L., Jones, C.R., He, Y., Eide, E.J., Hinz, W.A., Virshup, D.M., Ptáček, L.J., and Fu, Y.H. (2001). An hPer2 phosphorylation site mutation in familial advanced sleep phase syndrome. *Science* *291*, 1040–1043.
- Ueda, H.R., Chen, W., Adachi, A., Wakamatsu, H., Hayashi, S., Takasugi, T., Nagano, M., Nakahama, K., Suzuki, Y., Sugano, S., et al. (2002). A transcription factor response element for gene expression during circadian night. *Nature* *418*, 534–539.
- Ukai-Tadenuma, M., Yamada, R.G., Xu, H., Ripperger, J.A., Liu, A.C., and Ueda, H.R. (2011). Delay in feedback repression by cryptochrome 1 is required for circadian clock function. *Cell* *144*, 268–281.
- van der Horst, G.T., Muijtjens, M., Kobayashi, K., Takano, R., Kanno, S., Takao, M., de Wit, J., Verkerk, A., Eker, A.P., van Leenen, D., et al. (1999). Mammalian Cry1 and Cry2 are essential for maintenance of circadian rhythms. *Nature* *398*, 627–630.
- Vink, J.M., Groot, A.S., Kerkhof, G.A., and Boomsma, D.I. (2001). Genetic analysis of morningness and eveningness. *Chronobiol. Int.* *18*, 809–822.
- Vitaterna, M.H., Selby, C.P., Todo, T., Niwa, H., Thompson, C., Fruechte, E.M., Hitomi, K., Thresher, R.J., Ishikawa, T., Miyazaki, J., et al. (1999). Differential regulation of mammalian period genes and circadian rhythmicity by cryptochromes 1 and 2. *Proc. Natl. Acad. Sci. USA* *96*, 12114–12119.
- Weitzman, E.D., Czeisler, C.A., Coleman, R.M., Spielman, A.J., Zimmerman, J.C., Dement, W., Richardson, G., and Pollak, C.P. (1981). Delayed sleep phase syndrome. A chronobiological disorder with sleep-onset insomnia. *Arch. Gen. Psychiatry* *38*, 737–746.
- Wright, K.P., Jr., Gronfier, C., Duffy, J.F., and Czeisler, C.A. (2005). Intrinsic period and light intensity determine the phase relationship between melatonin and sleep in humans. *J. Biol. Rhythms* *20*, 168–177.
- Xu, H., Gustafson, C.L., Sammons, P.J., Khan, S.K., Parsley, N.C., Ramathan, C., Lee, H.W., Liu, A.C., and Partch, C.L. (2015). Cryptochrome 1 regulates the circadian clock through dynamic interactions with the BMAL1 C terminus. *Nat. Struct. Mol. Biol.* *22*, 476–484.
- Xu, Y., Padiath, Q.S., Shapiro, R.E., Jones, C.R., Wu, S.C., Saigoh, N., Saigoh, K., Ptáček, L.J., and Fu, Y.H. (2005). Functional consequences of a CK1delta mutation causing familial advanced sleep phase syndrome. *Nature* *434*, 640–644.
- Xu, Y., Toh, K.L., Jones, C.R., Shin, J.Y., Fu, Y.H., and Ptáček, L.J. (2007). Modeling of a human circadian mutation yields insights into clock regulation by PER2. *Cell* *128*, 59–70.
- Ye, R., Selby, C.P., Chiou, Y.Y., Ozkan-Dagliyan, I., Gaddameedhi, S., and Sancar, A. (2014). Dual modes of CLOCK:BMAL1 inhibition mediated by Cryptochrome and Period proteins in the mammalian circadian clock. *Genes Dev.* *28*, 1989–1998.
- Zee, P.C., Attarian, H., and Videnovic, A. (2013). Circadian rhythm abnormalities. *Continuum (Minneapolis, Minn.)* *19*(1 Sleep Disorders), 132–147.
- Zhang, E.E., Liu, A.C., Hirota, T., Miraglia, L.J., Welch, G., Pongsawakul, P.Y., Liu, X., Atwood, A., Huss, J.W., 3rd, Janes, J., et al. (2009). A genome-wide RNAi screen for modifiers of the circadian clock in human cells. *Cell* *139*, 199–210.

Innate Immune Landscape in Early Lung Adenocarcinoma by Paired Single-Cell Analyses

Yonit Lavin,^{1,2,3} Soma Kobayashi,^{1,2,3,14} Andrew Leader,^{1,2,3,14} El-ad David Amir,^{2,3,9} Naama Elefant,¹⁰ Camille Bigenwald,^{1,2,3} Romain Remark,^{1,2,3,13} Robert Sweeney,^{6,7} Christian D. Becker,⁴ Jacob H. Levine,¹¹ Klaus Meinhof,⁴ Andrew Chow,^{1,2,3} Seunghye Kim-Shulze,^{2,3,9} Andrea Wolf,⁶ Chiara Medaglia,¹⁰ Hanjie Li,¹⁰ Julie A. Rytlewski,¹² Ryan O. Emerson,¹² Alexander Solovyov,^{1,3,5,8} Benjamin D. Greenbaum,^{1,3,5,8} Catherine Sanders,¹² Marissa Vignali,¹² Mary Beth Beasley,⁸ Raja Flores,⁶ Sacha Gnjatic,^{2,3,5,9} Dana Pe'er,¹¹ Adeeb Rahman,^{2,3,7,9} Ido Amit,¹⁰ and Miriam Merad^{1,2,3,9,15,*}

¹Department of Oncological Sciences

²The Precision Immunology Institute

³Tisch Cancer Institute

⁴Division of Pulmonology

⁵Division of Hematology/Oncology

⁶Department of Thoracic Surgery

⁷Department of Genetics and Genomic Sciences

⁸Department of Pathology

⁹Human Immune Monitoring Center

Icahn School of Medicine at Mount Sinai, New York, NY 10029, USA

¹⁰Department of Immunology, Weizmann Institute, Rehovot 76100, Israel

¹¹Computational and Systems Biology Program, Sloan Kettering Institute, New York, NY 10065, USA

¹²Adaptive Biotechnologies Inc., Seattle, WA 98102, USA

¹³Present address: Innate Pharma, 117 Avenue de Luminy, 13009 Marseille, France

¹⁴These authors contributed equally

¹⁵Lead Contact

*Correspondence: miriam.merad@mssm.edu

<http://dx.doi.org/10.1016/j.cell.2017.04.014>

SUMMARY

To guide the design of immunotherapy strategies for patients with early stage lung tumors, we developed a multiscale immune profiling strategy to map the immune landscape of early lung adenocarcinoma lesions to search for tumor-driven immune changes. Utilizing a barcoding method that allows a simultaneous single-cell analysis of the tumor, non-involved lung, and blood cells, we provide a detailed immune cell atlas of early lung tumors. We show that stage I lung adenocarcinoma lesions already harbor significantly altered T cell and NK cell compartments. Moreover, we identified changes in tumor-infiltrating myeloid cell (TIM) subsets that likely compromise anti-tumor T cell immunity. Paired single-cell analyses thus offer valuable knowledge of tumor-driven immune changes, providing a powerful tool for the rational design of immune therapies.

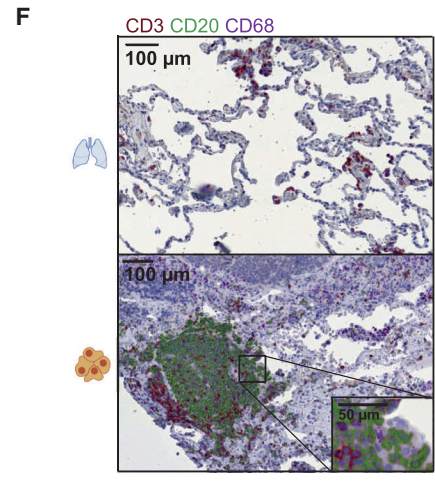
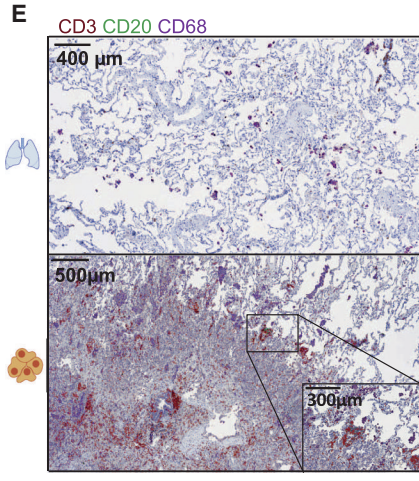
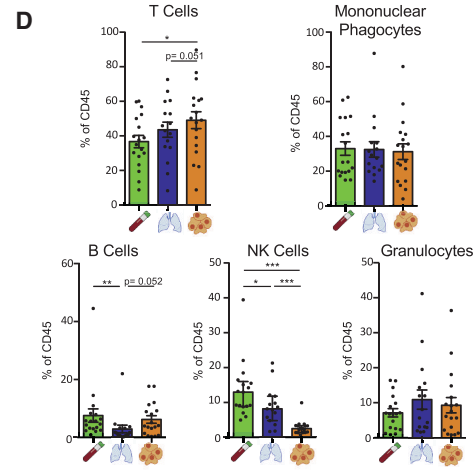
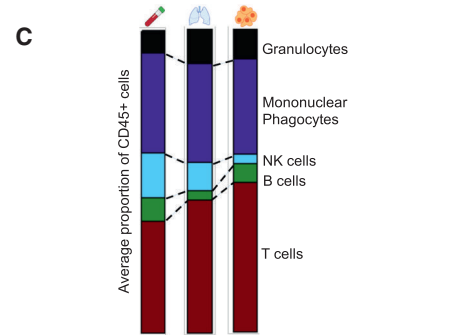
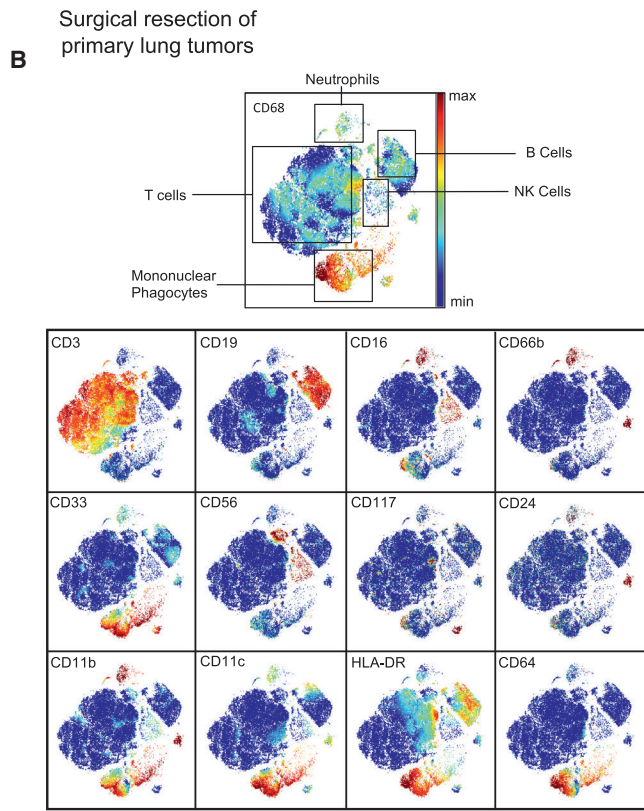
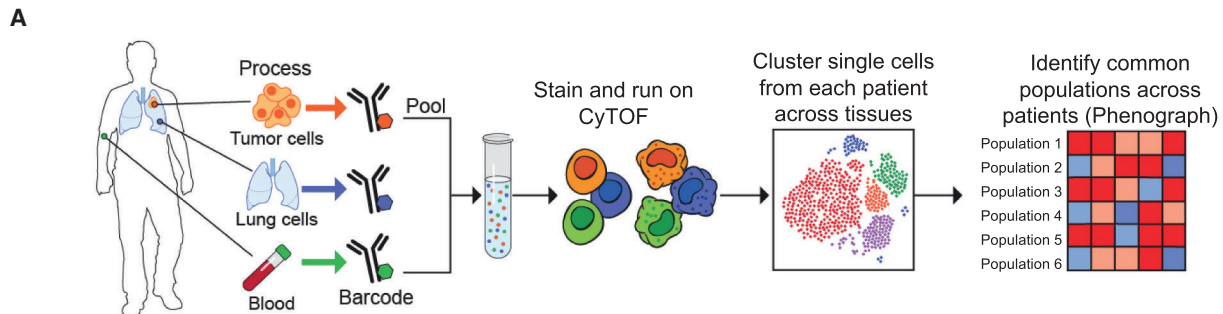
INTRODUCTION

Current checkpoint blockade therapies mainly function to rescue T cells from exhaustion or deplete T regulatory cells (Treg). Studies have begun to dissect the details of T cell function and distribution in advanced tumor lesions to identify novel strategies

to further strengthen anti-tumor T cell immunity. Myeloid cells, through their ability to present tumor-associated antigens to T cells and to produce critical T cell differentiation cytokines, have a unique ability to control T cell function at the tumor site. Yet, much less is known about the diversity of the myeloid compartment at the tumor site.

Myeloid cells are a diverse population of immune cells that share the ability to sense and respond to tissue injuries by clearing damaged cells and by promoting the recruitment of immune effector cells that will help restore tissue integrity (Lavin and Merad, 2013; Pham, 2006). Tumor-infiltrating myeloid cells (TIM) consist of granulocytes and mononuclear phagocytes at varying stages of differentiation and have been shown to contribute to shaping tumor progression and response to treatment (Engblom et al., 2016; Gabrilovich et al., 2012). Of these, mononuclear phagocytes refer to monocytes, macrophages, and dendritic cells (DC), which, in addition to their innate immune function, share the ability to present tumor-associated antigens to T cells (Ginhoux and Jung, 2014). Among TIM, DC are the best equipped to drive T cell activation (Merad et al., 2013), and a subset of DC, named CD103+ DC, was shown to control local CD8+ T cell activation (Broz et al., 2014; Hildner et al., 2008; Salmon et al., 2016; Sánchez-Paulete et al., 2016). Thus, TIM composition appears to control tumor-infiltrating lymphocyte (TIL) composition, activation, and anti-tumor function, and harnessing the TIM compartment may provide a powerful synergistic strategy to potentiate T cell targeting immunotherapies.

Currently, the majority of lung cancer cases are diagnosed at advanced stage. However, this is likely to change, as low-dose



(legend on next page)

CT screening programs in populations at risk have shown benefits and are being widely implemented (Aberle et al., 2011; Black et al., 2015). Five-year survival rates for patients with pathologic stage IA and IB non-small cell lung cancer (NSCLC) are only 83% and 71%, respectively, and these numbers drop to 50% for stage II disease (Goldstraw et al., 2016) with minimal improvement from adjuvant chemotherapy (Pignon et al., 2008). Preliminary data suggest impressive activity of neoadjuvant immunotherapy in a small number of early stage resectable lung NSCLC lesions treated with anti-PD-1 mAb blockade (Forde et al., 2016). Although these studies need to be confirmed in a larger cohort, these results are consistent with the notion that immunotherapy agents are most efficient at low tumor burden and in patients naïve of immunomodulatory chemotherapy agents. The design of immunomodulatory strategies for the treatment of NSCLC will, however, tremendously benefit from a detailed understanding of the immune cell landscape that develops specifically in response to tumor cues.

To this end, we developed a multiscale immune profiling strategy to map the immune microenvironment of early lung adenocarcinoma lesions. As tissue cues significantly impact the biology of tissue-resident immune cells and specifically innate cells (Lavin et al., 2014), we designed a barcoding strategy that allowed the simultaneous single-cell analysis of the distinct immune cell compartments that reside in the tumor site, non-involved lung tissue (nLung), and blood of each patient to distinguish tumor-driven immune signatures from those caused by normal tissue-imprinting cues. Using mass cytometry by time-of-flight (CyTOF) combined with single-cell transcriptomics and multiplex tissue imaging of the lung tumor, we identify NK and myeloid cell responses that are unique to tumor lesions and absent from nLung or blood from the same patients. We show that these changes are present as early as in stage I tumors and likely compromise anti-tumor immunity. These data suggest that neoadjuvant immunotherapy strategies targeting innate immune cells in early lung adenocarcinoma lesions have the potential to reactivate the TIL microenvironment and transform tumor response to checkpoint blockade.

RESULTS

High-Dimensional Single-Cell Profiling of Lung Tumors

To map the immune microenvironment of lung adenocarcinoma lesions, we designed a clinical multiscale immune profiling study of freshly resected tumors. Patients selected were treatment naïve at the time of surgery. For each patient, we obtained

NSCLC tumor tissues including invasive margins, nLung tissue, and blood cells (Figure 1A; STAR Methods). Of 32 patients, 28 were diagnosed with lung adenocarcinoma. Patients were representative of the lung adenocarcinoma distribution across age, gender, mutational status, and predominant histological subtype (Table S1).

To distinguish tumor-specific immune changes from the lung tissue immune environment, we sought to simultaneously map the immune compartment of the lung tumor lesion, the nLung tissue, and the peripheral blood. To this end, we developed a novel barcoding method that allows a simultaneous analysis of cells from all three sample types. In the first 18-patient cohort, immune cells isolated from the tumor lesion, nLung, and blood were barcoded with anti-CD45 antibodies (Ab) conjugated to unique metal isotopes before samples were pooled. Pooled samples were then stained with two panels of more than 30 antibodies each and analyzed by CyTOF, thus allowing the measurement of single-cell expression on immune cells residing in each tissue type of each patient (Figure 1A). The mass cytometry panels were subsequently extended to include cytokine measurement in a cohort of ten additional lung adenocarcinoma patients, as described in the STAR Methods.

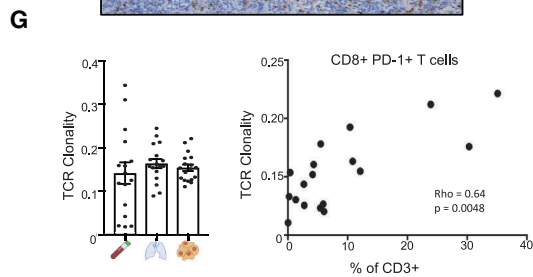
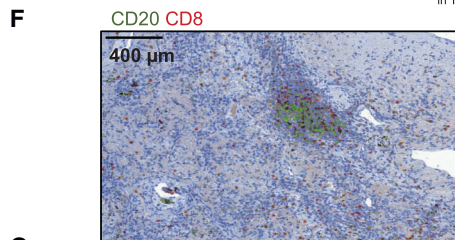
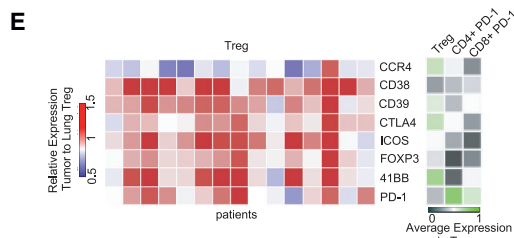
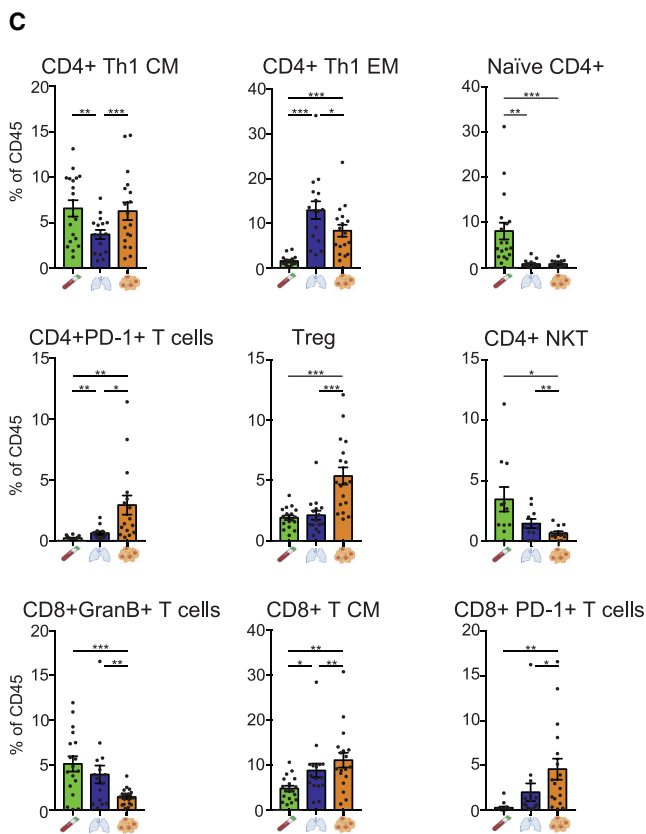
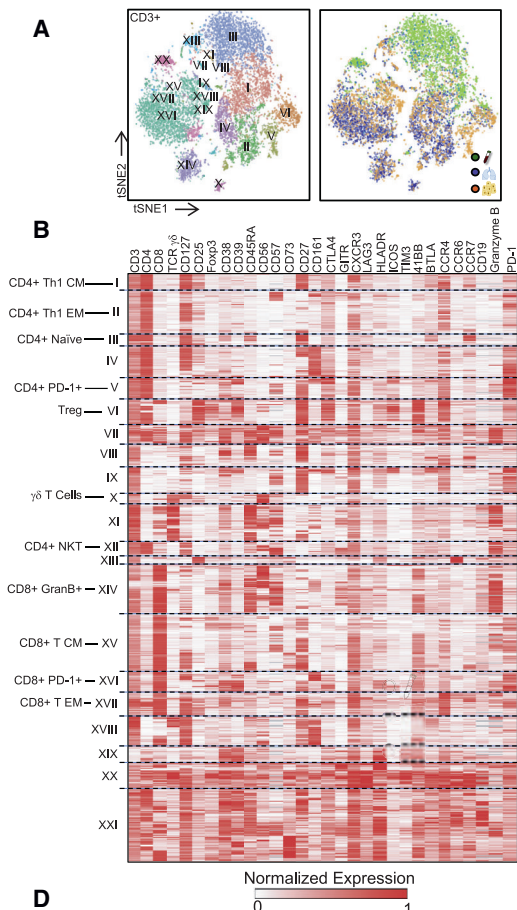
T Cells and Mononuclear Phagocytes Dominate the Early Lung Adenocarcinoma Microenvironment

Using viSNE to visualize high-dimensional data in two dimensions while preserving single-cell resolution (Amir et al., 2013), we analyzed the distribution of the different immune cell lineages that accumulated in lung tumor lesions, nLung, and blood circulation across patients (Table S1 and Data S1). A higher number of immune cells accumulated in the tumor tissues compared to nLung (Figure S1A). The tumor-resident immune cell compartment comprised all major immune lineages, and the most abundant were the T lymphocytes and mononuclear phagocytes (Figures 1B–1D, and S1B). Mononuclear phagocytes and granulocytes were equally represented in tumor lesions compared to nLung. In contrast, T and B lymphocytes were present at a higher frequency in the tumor microenvironment compared to the nLung, whereas the frequency of NK cells was significantly reduced across all lung adenocarcinoma patients examined (Figures 1C, 1D, and S1C).

We also analyzed the cytokines and chemokines produced in the tumor milieu. Whereas many chemokines and cytokines were expressed at much higher levels in the tumors compared to the blood, similar chemokine levels were often detected in tumors and adjacent nLung, which could potentially reflect the

Figure 1. Robust Immune Response to Early Lung Adenocarcinoma Tumor Lesions

(A) Schematic for defining the immune composition of lung tumors. Blood, non-involved lung (nLung), and tumor tissue were collected from patients undergoing surgical resection of primary tumors, processed, barcoded, pooled, and stained with antibodies conjugated to metal isotopes. Mass cytometry (CyTOF) single-cell data was clustered using Phenograph to identify common populations across patients. Artwork printed with the permission of Mount Sinai Health System. (B) viSNE analysis of immune cells from tumor colored by relative expression of CyTOF markers, with populations indicated (top). (C and D) Frequency of immune lineages based on summation of Phenograph metaclusters (STAR Methods; $n = 18$). Composition of the CD45+ compartment showing average frequencies of major immune lineages for each tissue ([C]; $n = 18$) across patients and bar plots showing frequencies for each patient ([D]; * $p < 0.05$, ** $p < 0.01$, and *** $p < 0.001$ by paired t-test). Bar plots show mean \pm SEM. (E and F) MICSSS for CD3, CD68, and CD20 of immune infiltrate (E) and a tertiary lymphoid structure (TLS; [F]) at the tumor invasive margin and non-involved lung from representative patients. See also Figure S1.



(legend on next page)

local diffusion of tumor-produced soluble molecules to the adjacent lung tissue (Figures S1D and S1E). Interestingly, CX3CL1 (fractalkine) was expressed at slightly higher levels in tumors compared to nLung and correlated with the frequency of the mononuclear phagocyte infiltrate (Figure S1F).

Recent studies have shown that, in addition to cell composition, the spatial distribution of immune cells at the tumor site may affect tumor outcome (Germain et al., 2014). Using a new tissue-profiling method named “multiplexed immunohistochemical consecutive staining on a single slide” (MICSSS) that we recently developed in the laboratory (Remark et al., 2016), we assessed the distribution of immune cells in the tumor and nLung sections. Immune cells accumulated mainly in the stroma and invasive margin surrounding the tumor islets as previously described (Salmon et al., 2012; Turley et al., 2015), although some macrophages and T cells were able to infiltrate into the tumors (Figures 1E and S1I). We also observed an abundance of mononuclear phagocytes and T cells at the tumor site across patients supporting the CyTOF results (Figures 1D, 1E, and S1B). Importantly, many patients had tertiary lymphoid structures (TLS), which accumulated near the tumor invasive margin and were absent from nLung (Figures 1F and S1I). Tumor lesions enriched in TLS had significantly more T lymphocytes and fewer mononuclear phagocytes as measured by CyTOF at the tumor site (Figure S1H).

To further probe the nature of the immune response induced at the tumor site in an unbiased manner, we analyzed the CyTOF data using the Phenograph algorithm to systematically identify common cellular communities across the three tissues and across all patients (Levine et al., 2015). We first clustered single cells based on shared protein expression across tumor lesions, nLung, and peripheral blood mononuclear cells (PBMCs) within each patient then merged clusters from each patient using a secondary clustering analysis to identify metaclusters common across patients and tissues (Figure 1A).

Tumor Lesions Are Enriched in Treg and Non-functional T Cells

Phenograph clustering across tissues and across all patients revealed distinct T lymphoid metaclusters (Figures 2A, 2B, and S2A) that corresponded to known immune cell populations and had a unique distribution across tissue sites (Figures 2C and S2B).

Paired mass cytometry analysis revealed a distinct composition and phenotype of T cell subsets (Figures 2C and S2B). Spe-

cifically, Treg were significantly increased in the tumor lesion across all patients even at early stages (Figure 2C). Importantly, Treg at the tumor sites expressed high levels of CTLA4, CD39, ICOS, and 41BB compared to other T cells (Figures 2D and S2D). They were also clearly distinguishable from Treg that resided in nLung based on higher expression of Foxp3, CTLA4, PD-1, CD39, ICOS, CD38, and 41BB, whereas CCR4 was decreased (Figures 2E, S2E, and S2F). In contrast, cytolytic CD8⁺ T cells were significantly reduced in frequency in the tumor compared to nLung and blood from the same patients (Figure 2C). Moreover, total CD8⁺ T cells present in tumors expressed significantly less granzyme B and IFN γ upon stimulation compared to their nLung counterparts (Figure S2G). A reduced T-effector/Treg ratio was thus a strong signature of the lung tumor lesion (Figure S2C).

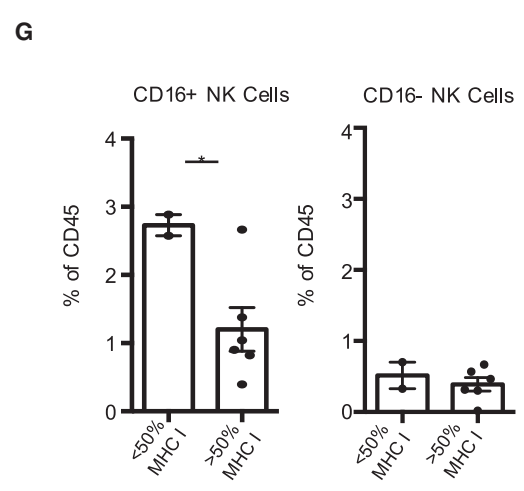
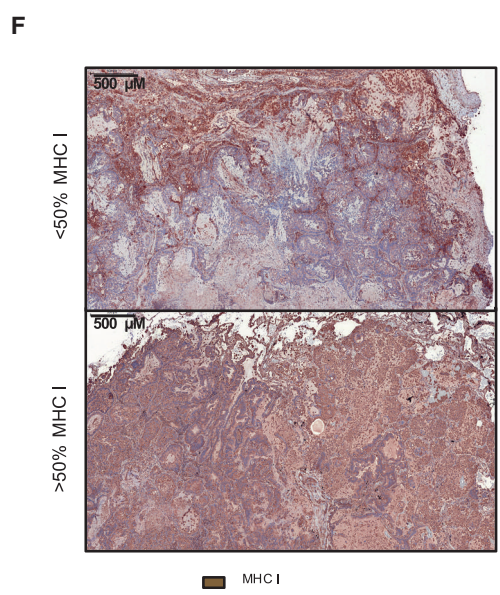
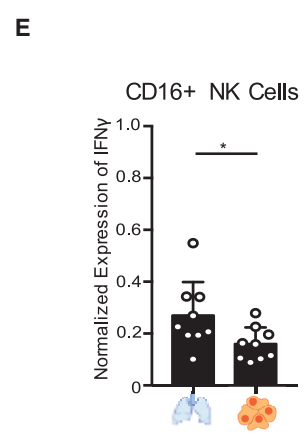
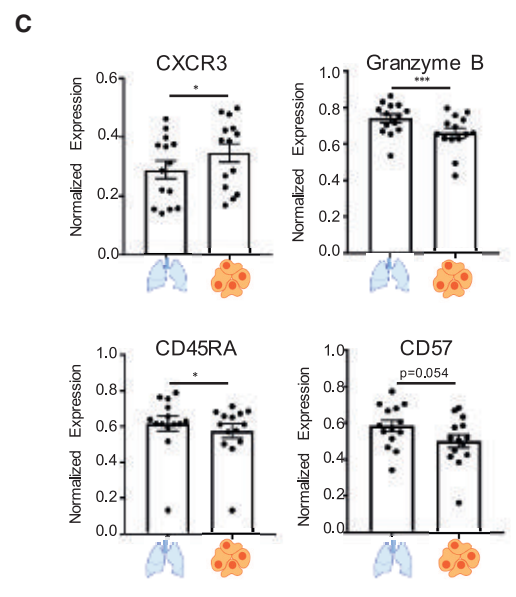
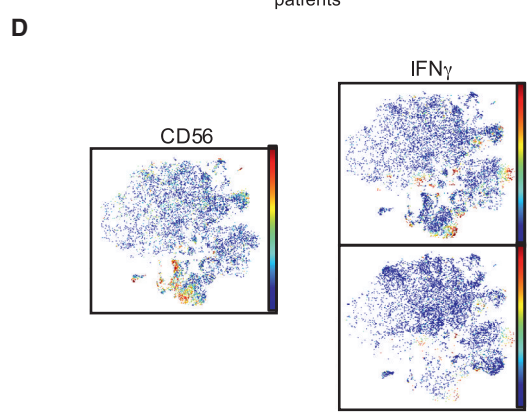
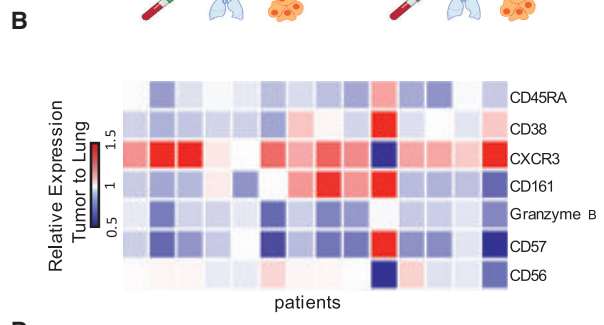
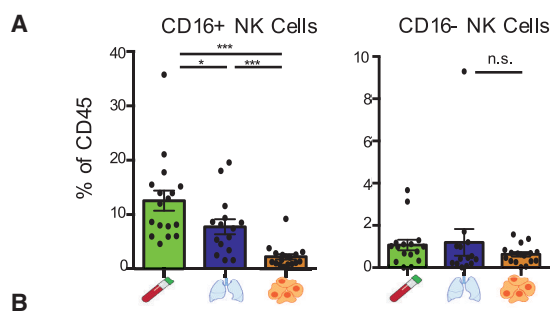
Given the success of anti-PD-1 checkpoint blockade in lung cancer patients, we examined the expression of the checkpoint molecule PD-1 on all T cell metaclusters identified across tissues. PD-1 was distinctly expressed on a small subset of CD4⁺ and CD8⁺ T cells that were a unique feature of the tumor (Figures 2C and S2H) and at a lower level on Treg at the tumor site (Figure 2D). CD8⁺ T cells accumulate at the tumor site and in TLS, where they preferentially expand (Figures 2F and S2I; Goc et al., 2014; Joshi et al., 2015), and clonality of the T cell receptor (TCR) repertoire has been associated with TLS density (Zhu et al., 2015). Consistent with these findings, T cells were significantly increased in TLS-enriched tumors (Figure S1H). Moreover, while there was no enrichment in TCR clonality in tumors compared to nLung, the CD8⁺PD-1⁺ T cell subset uniquely and significantly correlated with increased TCR clonality at the tumor site but not in nLung (Figures 2G and S2J). These results suggest that CD8⁺ T cells expressing PD-1 are clonally expanded at the tumor site and that this expansion may preferentially occur in TLS-enriched tumor lesions.

Cytolytic NK Cells Are Excluded from Lung Adenocarcinoma Lesions

In addition to measuring adaptive lymphocyte responses to tumors, we also analyzed the distribution of innate lymphocytes and in particular NK cells in lung tumor lesions. Strikingly, NK cells were the least abundant immune cell lineage in lung adenocarcinoma lesions compared to nLung (Figures 1C and 1D). Importantly, the NK cell subset expressing CD16 was most dramatically reduced in the tumor compared to nLung (Figures 3A and S3A). NK cells that infiltrated the tumor lesion expressed

Figure 2. Lymphoid Function Is Dysregulated at the Tumor Site

- (A) viSNE analysis of CD3⁺ immune cells colored and labeled by Phenograph metacluster (left) and tissue (right) for a representative patient.
 (B) Heatmap of Phenograph clusters of CD3⁺ cells. Rows represent clusters of single cells within individual patients grouped by metacluster across patients.
 (C) Bar plots of frequencies of metaclusters from (B) across tissue for 18 lung adenocarcinoma patients (*p < 0.05, **p < 0.01, and ***p < 0.001 by paired t-test).
 (D) Normalized expression of PD-1, CTLA-4, and CD39 on tumor CD3⁺ cells shown by viSNE plot for a representative patient (left) and bar plots of normalized expression across patients for indicated metaclusters (n = 18; right).
 (E) Heatmap showing relative normalized protein expression on tumor Tregs as ratio to nLung Tregs for 15 patients (left) and average expression of indicated markers across patients on tumor Tregs, PD-1⁺ CD4⁺ and CD8⁺ T cells (right).
 (F) MICSSS for CD8 and CD20 showing a TLS in tumor of a representative patient.
 (G) Clonality of T cell receptor (TCR) repertoire across tissues (n = 16; left), and frequency of CD8⁺ PD-1⁺ T cells in tumor correlated to overall TCR clonality (Spearman's rank-based correlation; right).
 Bar plots show mean \pm SEM.
 See also Figure S2.



(legend on next page)

higher CXCR3 levels, a molecule shown to be required for NK infiltration of tumors (Figures 3B and 3C; Wendel et al., 2008). Moreover, NK cells that remained at the tumor site were less cytolytic, as they expressed lower levels of granzyme B and CD57 as well as less IFN γ (Figures 3C–3E and S3C). Conversely, since NK cells function to eliminate MHC class-I-deficient cells, we assessed the distribution of MHC class I throughout the tumor cells using MICSSS (Figure 3F). Tumor lesions with reduced frequency of MHC class-I-expressing tumor cells had higher numbers of tumor-infiltrating CD16+ NK cells, suggesting that the presence of cytolytic NK cells may have led to MHC class I immuno-editing (Figures 3G and S3D).

Deciphering the Diversity of TIM in Lung Adenocarcinoma Lesions

To fully capture the heterogeneity of the TIM compartment, we first performed an unbiased single-cell transcriptomic analysis of non-lymphocyte cells that accumulated in the tumor lesion and in the nLung of a stage I patient using massively parallel single-cell RNA-sequencing (MARS-seq; Figure 4A; Data S2B; STAR Methods; Jaitin et al., 2014). Single-cell RNA-seq analysis of TIM-enriched cells, using an unbiased expectation-maximization algorithm previously described (STAR Methods; Paul et al., 2015), revealed several immune cell types distinguished based on characteristic gene expression profiles identified according to highly expressed and differential genes (Figure 4A; Table S3). Specifically, we identified three distinct clusters expressing high levels of MHC class II molecules, *CD1C*, *CCL22*, and *CD207* (Figure 4A, clusters 2–4) and slightly higher *BATF3* and *CSF2RA* expression levels (Figures 4E and S4A), which we inferred to be DC. Other clusters were identified as macrophages (Figure 4A, clusters 5–8) and monocytes (clusters 9–10) based on the differential expression of *CD68*, *MAFB*, and *CSF1R* (Figures 4E and S4A). A macrophage cluster comprised predominantly of cells from tumor lesions (cluster 7) was distinct from those comprised predominantly of cells from nLung (clusters 5–6), indicating that tumor-associated macrophages were distinct from their nLung-resident macrophage counterparts.

To detail the TIM compartment across patients, we systematically defined myeloid cell populations across patients using simultaneous CyTOF analysis of PBMC, nLung, and tumor immune cells. Phenograph clustering of all tissues in all patients confirmed the diversity of myeloid cells in the tumor, and macrophages, DC subsets, and monocytes subsets were identified based on expression of protein markers, including CD68, CSF1-R, CSF2-R, CD11C, CD1C, CD141, and HLA-DR among others (Figures 4B, 4C, 4E, and S4B). TIM were distinct from

their lung and PBMC counterparts (Figures 4D and S4C). Indeed, paired CyTOF analysis revealed unique distributions and functions of CD14+ and CD16+ monocyte subsets in the tumor site (Figures 4D and S4D). While CD14+ monocytes were robust cytokine producers compared to other mononuclear phagocytes (Figures 4F, S4E, and S4F), they produced less IL-8 and less IL-1 β at the tumor site compared to the nLung (Figures 4G and S4G). In contrast to the CD14+ monocytes that equally infiltrated tumor and lung tissues, CD16+ monocytes were significantly reduced in tumor tissues and highly correlated with NK cell infiltration at the tumor site (Figures 4D, S4D, and S3B).

Finally, while tumor lesions were equally enriched in neutrophils and eosinophils compared to nLung, they contained significantly fewer basophils and were strongly depleted of mast cells (Figure 4D).

Paired Immune Cell Mapping Reveals a Distinct Macrophage Signature in Lung Adenocarcinoma

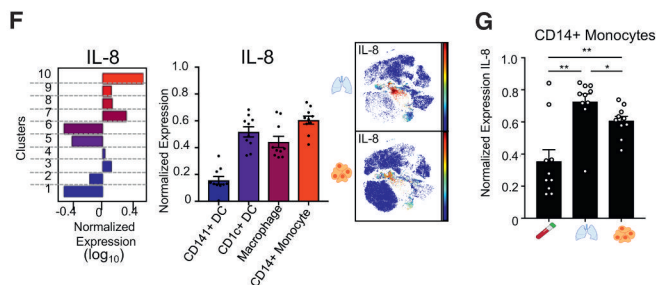
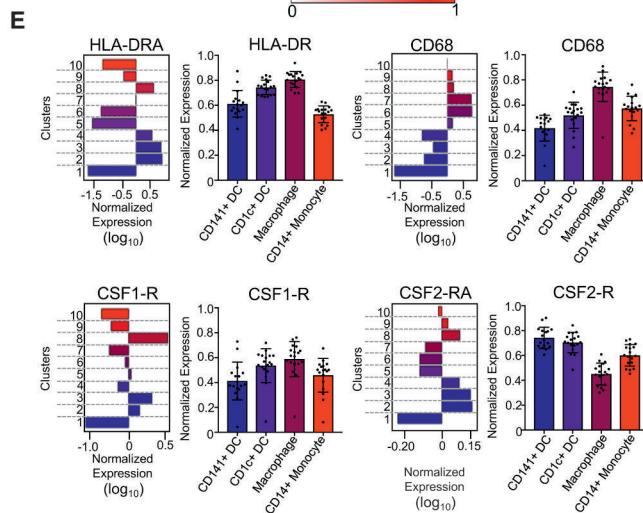
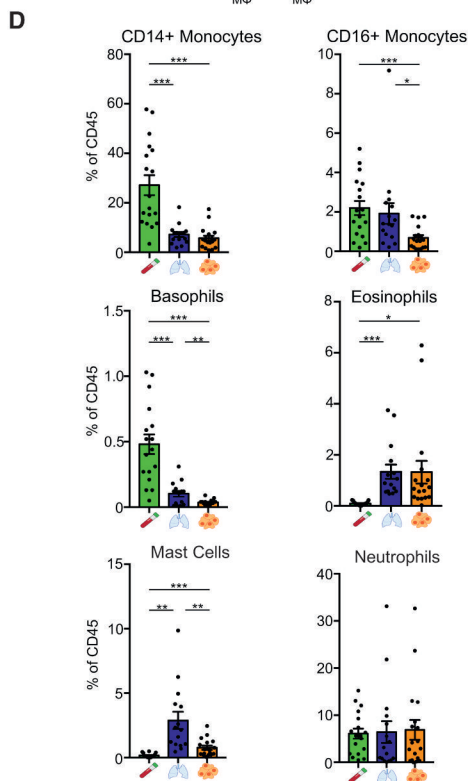
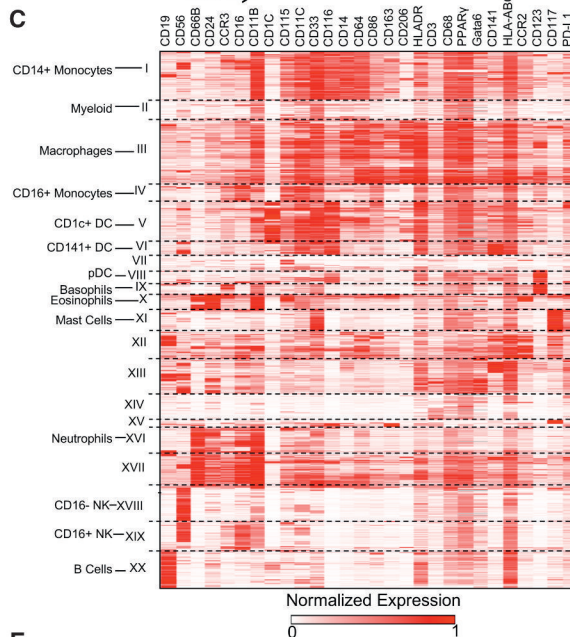
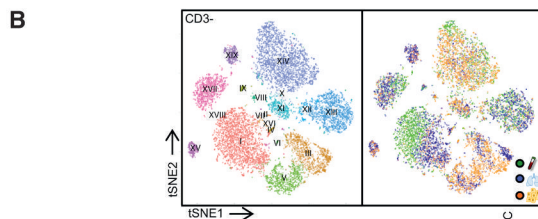
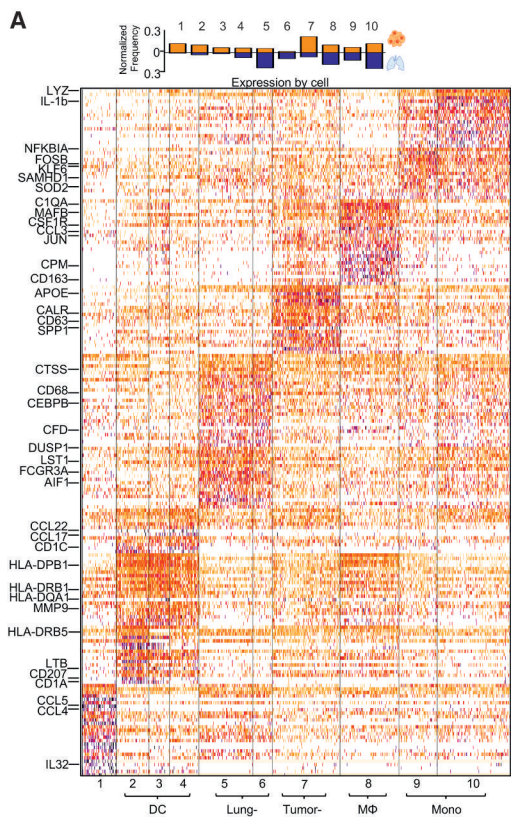
Single-cell transcriptomic analysis revealed distinct macrophage clusters that were differentially distributed in the tumor and nLung (Figure 4A, clusters 5–8). Comparing the macrophage cluster enriched in tumors (cluster 7) to those comprised primarily of nLung cells (clusters 5 and 6) revealed many differentially expressed genes, suggesting that tumor-associated macrophages have a distinct transcriptional signature (Figure 5B).

Using paired CyTOF analyses, we found that, while macrophages were not enriched in frequency in the tumor site compared to nLung (Figures 5A and S5A), tumor macrophages exhibited a distinct signature compared to their lung-resident counterparts across all patients (Figures 5C and 5D). CyTOF analysis validated several of single-cell transcriptomics findings, thereby confirming that tumor macrophages expressed higher levels of the immunomodulatory transcription factor PPAR γ ; higher CD64, CD14, and CD11c levels; and lower CD86 and CD206 levels compared to macrophages that resided in nLung (Figure 5D).

Single-cell transcriptional analysis identified additional transcripts up-regulated on the tumor macrophage cluster compared to their nLung counterparts (cluster 7), including triggering receptor expressed on myeloid cells-2 (*TREM2*), tetraspanin *CD81*, macrophage receptor with collagenous structure (*MARCO*), and apolipoprotein E (*APOE*; Figure 5B). To understand whether this differential transcriptional signature extends to other patients, we stratified 515 lung adenocarcinoma patients from the TCGA database according to the differential transcriptional profile. A significant survival disadvantage was observed in patients

Figure 3. Cytolytic NK Cells Are Excluded from Tumor and Produce Less Granzyme B and IFN γ

(A) Bar plots of frequencies of CD16+ and CD16- NK cell metaclusters across tissue for 17 lung adenocarcinoma patients (see Figure 4C).
 (B) Heatmap showing relative normalized protein expression on tumor NK cell as ratio to those from nLung for 14 patients (see STAR Methods).
 (C) Bar plots of normalized expression of indicated proteins on NK cells from nLung and tumor (n = 14).
 (D) viSNE plots showing CD56 expression (left) and IFN γ expression in tumor and nLung upon stimulation in a representative patient.
 (E) Bar plot showing normalized IFN γ expression upon stimulation (n = 9).
 (F) Immunohistochemical staining from representative patients depicting greater (>50%) or less than 50% (<50%) of tumor cells staining for MHC I in the tumor.
 (G) Bar plot stratifying the frequency of CD16+ NK cells and CD16- NK cells in patients by tumor cells staining for MHC I (n = 8; *p < 0.05, by unpaired t-test). Bar plots show mean \pm SEM; *p < 0.05, **p < 0.01, and ***p < 0.001 by paired t-test.
 See also Figure S3.



(legend on next page)

with a high ratio of tumor macrophages to lung macrophage gene expression profile (Figure S5G), suggesting that the macrophage signature identified in this study may include novel myeloid targets for lung cancer treatment.

Given the clinical success of anti-PD-L1 in lung cancer (Besse et al., 2015; Fehrenbacher et al., 2016), we examined the distribution of PD-L1 in lung tumor lesions using paired mass cytometry analysis. Strikingly, PD-L1 was most highly expressed on macrophages and mast cells both in tumor and nLung (Figures 5E, S5B, and S5C). These results are consistent with our data in mice (data not shown) and suggest a potential role for PD-L1 in the physiological regulation of lung-immune homeostasis, which could explain the increased rate of pneumonitis in patients treated with PD-L1 inhibitors (Naidoo et al., 2017; Nishino et al., 2016). Given the impact of PD-L1+ cells on tumor outcome, we analyzed the spatial distribution of PD-L1+ macrophages and found that they accumulated in tight clusters at the tumor invasive margin (Figures 5E and S5D) and negatively correlated with T cell infiltration in tumor lesions but not in nLung (Figure S5E).

Tumor macrophages also spontaneously produced significantly more IL-6 than macrophages in nLung (Figures 5F and S5F). Given the potential role for IL-6 in tumor invasiveness (Chang et al., 2013; Yu et al., 2014) and the negative correlation between the presence of macrophages and T cells at the tumor site, these data emphasize the immunosuppressive role of tissue-resident macrophages in early lung adenocarcinoma lesions.

CD141+ DC Have a Distinct Phenotype and Are Excluded from Lung Tumor Lesions

DC excel at antigen presentation and play a key role in the induction of anti-tumor T cell immunity. Single-cell transcriptional analysis of the tumor and nLung revealed the presence of two DC clusters (Figure 4A, clusters 2 and 4), one of which expressed high *CD207*, *CLEC9A*, and *XCR1* levels and likely represent CD141+ DC (Dutertre et al., 2014; Haniffa et al., 2013). We also detected a second DC cluster expressing higher levels of *CD1c*, *CX3CR1* and *IRF4*, which we inferred to be CD1c+ DC (Figures 6A, 6B, and S6B). The CD1c+ DC cluster also expressed higher levels of *CCL22* and *CCL17*, ligands for CCR4, a molecule expressed mainly by CD4+ T cells (Yoshie and Matsushima, 2015), and higher lysozyme transcripts compared to the CD141+ DC (Figure 6B). These findings are in line with the increased

potency to interact with CD4+ T cells and increased degradative potential of CD1c+ DC, in contrast to CD141+ DC that interact preferentially with CD8+ T cells (Dutertre et al., 2014; Haniffa et al., 2013; Merad et al., 2013). Lymphotoxin beta (LTB) transcript, encoding a membrane-bound protein important for the formation of secondary lymphoid organs and potentially TLS (Pitzalis et al., 2014), was highly expressed by DC and at slightly higher levels by the CD141+ DC cluster (Figure 6E).

Paired CyTOF analyses identified the presence of two DC subsets at the tumor site across patients. Strikingly, CD141+ DC, but not CD1c+ DC, were significantly reduced in tumors compared to nLung, and the CD1c+ DC/CD141+ DC ratio was thus increased in tumor lesions (Figures 6C, S6A and S6C). Importantly, CD1c+ DC expressed a very similar cytokine profile to CD14+ monocytes and produced IL-6, IL-8, and IL-1 β cytokines in the tumor and nLung (Figure S4E). Using MICSSS, we found that, in lesions infiltrated with TLS, DC localized in TLS and close to T cells (Figures 6D and S6D), in line with their role in T cell activation and clonal expansion (Dieu-Nosjean et al., 2008).

Lung Adenocarcinomas Have a Unique Immune Signature that Is Independent of TNM Stage

Altogether, our results establish an immune cell atlas of early untreated lung adenocarcinoma lesions. We show that these lesions are enriched in PPAR γ ^{hi}CD64^{hi}CD14^{hi}PPAR γ ^{hi}IL-6^{hi} macrophages, CD1c+ DC, Treg, and exhausted T cells and depleted of CD141+ DC, CD16+ monocytes, NK cells, and Granzyme B+ effector cells (Figures 6F and S6E). These differences compared to nLung likely work in concert to promote an immunosuppressive microenvironment.

As TNM staging is used to determine both prognosis and treatment options, we examined whether the immune contexture of the tumor lesions significantly differed between early stage (stage I) and later stage tumors (stages II and III). With the exception of increased neutrophils and TNF α production in stage II and stage III patients (Figure 6G), all immune changes detected in later stage tumor lesions were already present in stage I tumors. The distribution of immune cell subsets including macrophages, monocytes, NK cells, and DC as well as B and T cell subsets did not significantly differ in frequency across stages (Figures 6F and S6F). In addition, expression levels of PD-1 and PD-L1 on macrophages and T cells, respectively, were stable across TNM stages (Figures S6G and S6H),

Figure 4. Unbiased Characterization of the Mononuclear Phagocyte Compartment

(A) MARS-seq of 1,473 cells pooled from tumor and nLung of a stage IA adenocarcinoma patient. Cells were gated in silico and clustering on 770 mononuclear phagocytes is shown (see STAR methods). Columns represent single cells, with most variable genes from low (white) to high (purple). Normalized frequency of each cluster in tumor or nLung (top). Macrophages, M Φ ; monocytes, Mono.

(B) viSNE analysis of CD3⁻ immune cells colored and labeled by Phenograph metaclusters (left) and tissue (right) for a representative patient.

(C) Heatmap of Phenograph clusters of CD3⁻ cells; rows represent clusters of single cells within individual patients grouped by metacluster across multiple patients.

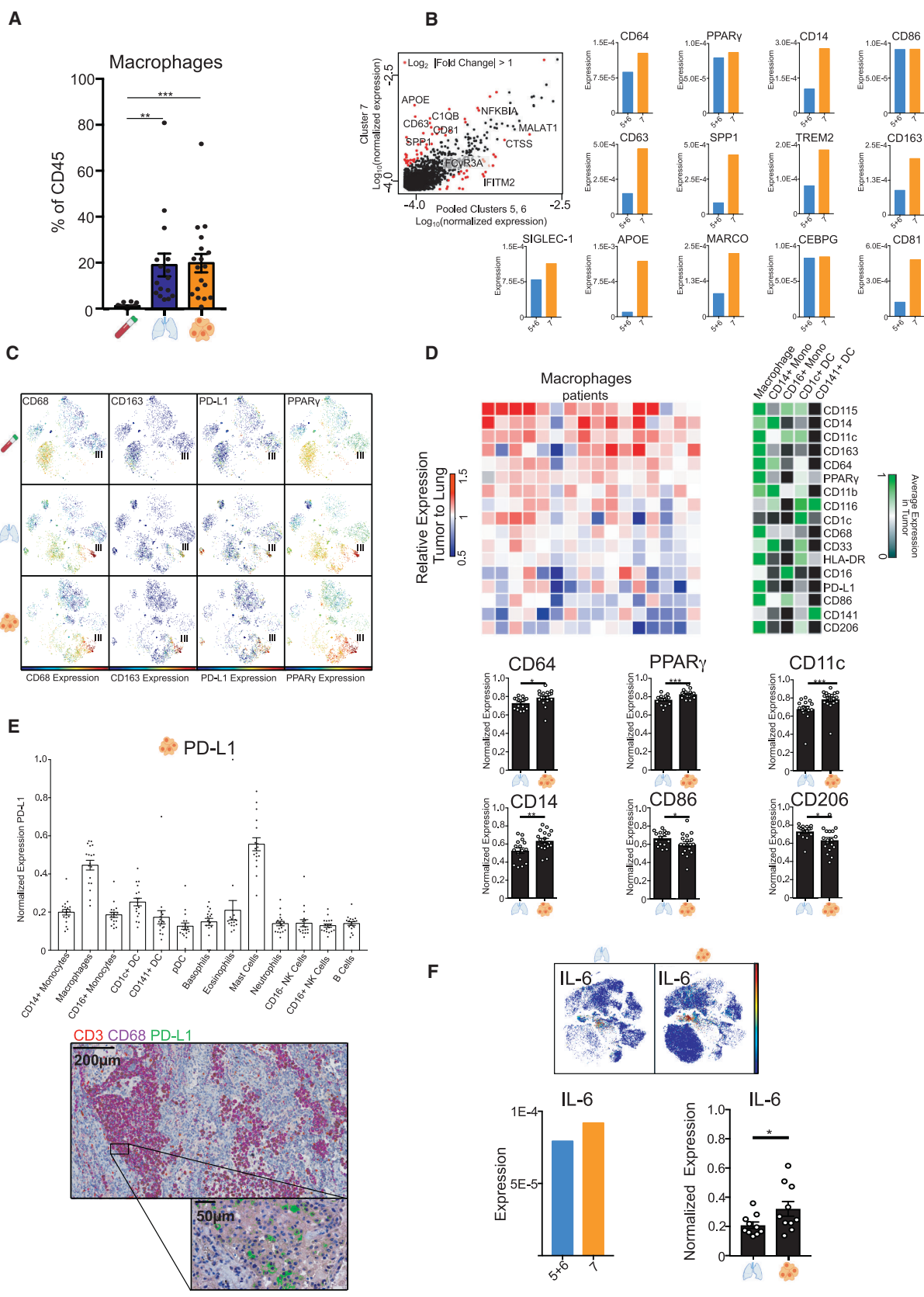
(D) Bar plots of metacluster frequencies from 18 lung adenocarcinoma patients across tissue (*p < 0.05, **p < 0.01, and ***p < 0.001 by paired t-test).

(E and F) Expression of corresponding transcript and protein by MARS-seq and CyTOF, respectively. Normalized transcript expression of MARS-seq clusters (left) and normalized protein expression of select Phenograph metaclusters in the tumor (right) for phenotypic markers ([E]; n = 18), and cytokines ([F]; n = 10) with corresponding viSNE plots.

(G) Bar plot of normalized IL-8 expression by CD14+ monocytes across tissue (n = 10; *p < 0.05, **p < 0.01, and ***p < 0.001 by paired t-test).

Bar plots show mean \pm SEM.

See also Figure S4.



(legend on next page)

suggesting that immunomodulatory strategies could benefit early stage tumors.

DISCUSSION

Driven by the premise that the myeloid cell compartment and most specifically the tumor-infiltrating antigen-presenting cells critically shape the composition of anti-tumor T cells, the objective of this study was to provide an innate immune cell atlas of early lung adenocarcinoma lesions. Using paired single-cell analyses of the immune cells that reside in the tumor, nLung, and peripheral blood, we distinguished the immune changes driven by the tumor lesion from those driven by the lung tissue, emphasizing the relevance of this type of analysis for the study of the tumor microenvironment.

Strikingly, as early as in stage I disease, lung adenocarcinoma lesions had a strongly reduced CD8⁺ T effector/Treg ratio compared to nLung. This altered T cell ratio resulted from a significant reduction of CD8⁺ T cells expressing granzyme B and IFN γ and also from a significant expansion of CD39^{hi}CD38^{hi}PD-1^{hi}CTLA4^{hi}Foxp3^{hi} Tregs at the tumor site. In line with previous results showing that Foxp3/CD3 ratio is a strong predictor of recurrence in early stage tumors (Suzuki et al., 2013), reduced CD8⁺ granzyme B+/CD39^{hi}CD38^{hi}PD-1^{hi}CTLA4^{hi}Foxp3^{hi} Treg ratio may be useful as a refined biomarker of disease course or response to treatment.

The distinct TIL tumor signature was accompanied by significant alterations of tumor CD16⁺ NK cells, as they were strongly reduced in tumors and the few remaining NK cells expressed lower levels of granzyme B and less IFN γ compared to lung NK cells. Tumor-infiltrating NK cells were thus poorly cytolytic, and expansion or activation of NK cells could provide a strategy to restore anti-tumor immunity in early lung tumors.

Strikingly, we also identified distinct changes in all antigen-presenting cell subsets that resided in lung adenocarcinoma tumor lesions across TNM stages. Specifically, as early as stage I, lung adenocarcinoma lesions were significantly depleted in CD141⁺ DC and enriched in PPAR γ ^{hi} macrophages. Monocytes included two main subsets, the CD16⁺ and CD14⁺ monocyte subsets, shown to have different fates and functions in tissues (Yona and Jung, 2010). CD16⁺ monocytes, but not CD14⁺ monocytes, were strongly reduced at the tumor site and significantly correlated with reduced CD16⁺ NK cells in tumors. Interestingly, CD16⁺ monocytes have been shown to promote NK

cell recruitment to tumors (Hanna et al., 2015), and thus, reduced CD16⁺ monocytes in lung tumors might have contributed to NK cell paucity in tumor lesions. CD14⁺ monocytes in the tumor produced high levels of the cytokine IL-8, but those in nLung produced even more. IL-8 can promote lung cancer growth and metastasis (Chen et al., 2003; Zhu et al., 2004), and in smokers, IL-8 expression in non-tumor lung tissue is part of a lung cancer biomarker signature (Spira et al., 2007). Given the potential role of monocytes in lung metastasis (Qian et al., 2011), monocyte-derived IL-8 in nLung may have contributed to tumor cell engraftment. Interestingly, while we identified a drastic increase in cytokine production in the tumor tissue compared to the blood, many cytokines were equally expressed in the tumor and nLung. CX3CL1, however, tended to be expressed at higher levels at the tumor site and significantly correlated with mononuclear phagocytes, particularly CD14⁺ monocytes in the tumor lesion. CX3CL1 was found to be increased in patients that failed to respond to PD-1 (Herbst et al., 2014). Therefore, it will be important to further assess CX3CL1 and CD14⁺ monocytes as biomarkers of treatment response.

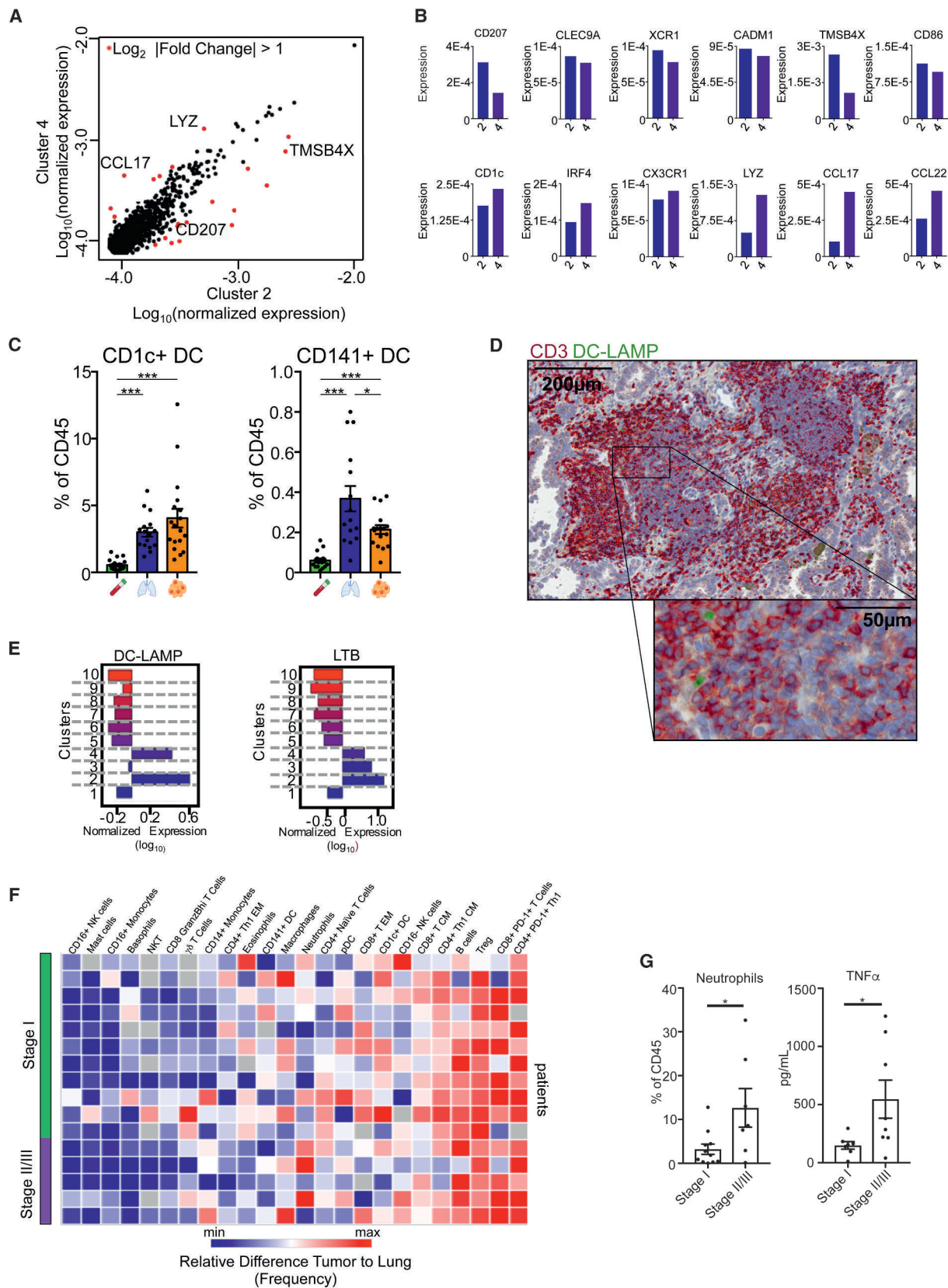
Tissue-resident DC consist of two main subsets that are transcriptionally and functionally distinct. In mice tissues, these include the CD103⁺ DC subset, which derives from DC-restricted precursors and excels in the cross-presentation and priming of CD8⁺ T cells, and the CD11b⁺ DC subset, which has a higher degradative potential than CD103⁺ DC and mainly interacts with CD4⁺ T cells (Merad et al., 2013). Human CD141⁺ DC and CD1c⁺ DC share similar transcriptional profiles with murine CD103⁺ DC and CD11b⁺ DC, respectively, and are thought to represent their human counterparts (Dutertre et al., 2014; Haniffa et al., 2013).

We and others found that the absence of CD103⁺ DC abolishes tumor response to checkpoint blockade in experimental tumor models, while expansion and activation of CD103⁺ DC dramatically increased T cell recruitment to the tumor site and transformed response to checkpoint blockade (Broz et al., 2014; Hildner et al., 2008; Roberts et al., 2016; Salmon et al., 2016; Sánchez-Paulete et al., 2016). Here, we found that early lung adenocarcinoma tumors were significantly depleted in CD141⁺ DC compared to nLung, while CD1c⁺ DC were slightly increased in tumors, resulting in an increased CD1c⁺/CD141⁺ DC ratio at the tumor site.

We also found that tumor CD1c⁺ DC shared the same innate cytokine profile with monocytes, consistent with the notion that

Figure 5. The TME Contains Macrophages with a Distinct Phenotype

(A) Bar plot of macrophage metacluster frequency from 18 lung adenocarcinoma patients across tissue (see Figure 4C).
 (B) Comparison of average transcript expression between macrophage clusters enriched in tumor (cluster 7) or lung (weighted average of clusters 5 and 6; Figure 4A), showing highly expressed transcripts, genes with FC > 2 colored red (left), bar plots of indicated transcript expression (right).
 (C) viSNE plots showing single-cell expression of CD68, CD163, PD-L1, and PPAR γ across tissues in a representative patient.
 (D) Heatmap showing relative normalized protein expression of tumor macrophages as ratio to those from nLung for 16 patients (left) and average expression across patients of indicated markers on mononuclear phagocyte metaclusters in tumor (right). Bar plots of normalized expression of indicated proteins by macrophages in tumor and nLung (n = 18).
 (E) Bar plot of normalized PD-L1 expression across metaclusters in tumor (n = 18; top). MICSSS for CD3, CD68, and PD-L1 showing a macrophage-dense region at the tumor invasive margin (bottom).
 (F) IL-6 expression in nLung and tumor macrophages. viSNE plots showing IL-6 expression of a representative patient (top). Bar plot showing expression of IL-6 transcripts (left) and normalized protein expression across macrophages in nLung and tumor (right; n = 10).
 Bar plots show mean \pm SEM; *p < 0.05, **p < 0.01 and ***p < 0.001 by paired t-test. Fold-change, FC.
 See also Figure S5.



(legend on next page)

CD1c+ DC likely represent monocyte-derived cells generated upon entry at the tumor site, whereas CD141+ DC are thought to arise from DC-restricted precursors (Dutertre et al., 2014; Haniffa et al., 2013). Interestingly, DC localized close to T cells in TLS, in line with their potential key role in T cell activation and clonal expansion (Dieu-Nosjean et al., 2008). DC-derived LT has recently been shown to directly act on high endothelial venules (HEV) to promote lymphocyte homing to peripheral lymph nodes in vivo (Moussion and Girard, 2011). Our finding that DC and especially the CD141+ DC subset expressed lymphotoxin beta (LTB) transcripts in lung tumor tissues likely reflects that CD141+ DC contribute to TLS formation, potentially through HEV-mediated recruitment of lymphocytes. This hypothesis is consistent with our finding that TLS-enriched tumors have increased T cells, and it strengthens the mechanistic understanding of the positive prognostic value conferred by TLS when identified by DC-LAMP immunostaining (Dieu-Nosjean et al., 2008; Germain et al., 2014; Pitzalis et al., 2014). Altogether, these results suggest that expansion of intra-tumoral CD141+ DC may provide a key strategy for the induction of potent anti-tumor immunity.

Importantly, while macrophages were not enriched in the tumor lesion compared to nLung, tumor macrophages expressed a unique phenotype compared to macrophages in nLung. In particular, tumor macrophages expressed higher levels of PPAR γ , a transcription factor known to drive an immunosuppressive program (Reddy, 2008; Ricote et al., 1998), and lower levels of the co-stimulatory molecule CD86. They also produced higher levels of IL-6, indicating that these tumor macrophages are pro-tumorigenic. CD206, thought to represent a marker of alternatively activated macrophages and tumor macrophages, was expressed at lower or similar levels on tumor macrophages compared to lung macrophages, consistent with recent data showing that CD206 is a marker of lung alveolar macrophages (Desch et al., 2016; Yu et al., 2016). This emphasizes the importance of paired analyses to distinguish tumor-driven immune changes from normal tissue-imprinting. Single-cell transcriptomic analysis of myeloid cells further extended these results and identified a unique gene signature of tumor macrophages that included, among other genes, *TREM2*, recently shown to promote chronic lung diseases through inhibition of macrophage apoptosis after acute viral infection (Wu et al., 2015). Finally, using multiplex tissue imaging, we identified clusters of PD-L1+ macrophages at the tumor-invasive margin, suggesting their potential contribution to modulating T cell entry in the tumor lesion. Accordingly, increased macrophages correlated with reduced T cells at the tumor site and, in contrast to TLS-enriched tumors, lesions devoid of TLS were mostly enriched in macrophages. Thus, lung tumors enriched in

macrophages and reduced in TLS may specifically benefit from immunotherapy strategies to deplete macrophages while expanding DC prior to treatment with checkpoint blockade.

By combining multiplex tissue imaging and paired single-cell analysis of the tumor, nLung, and blood, this study provides a detailed immune cell atlas of early lung adenocarcinoma and identifies, along with specific T cell alterations, innate immune cell changes that are unique to the tumor lesion and absent from nLung. Our identification of significant innate immune cell changes in early stage lung adenocarcinoma lesions suggests that neo-adjuvant or adjuvant immunotherapy strategies tailored to restore innate immune changes might be uniquely poised to shape the tumor T cell microenvironment and transform tumor response to checkpoint blockade.

STAR★METHODS

Detailed methods are provided in the online version of this paper and include the following:

- KEY RESOURCES TABLE
- CONTACT FOR REAGENT AND RESOURCE SHARING
- EXPERIMENTAL MODEL AND SUBJECT DETAILS
 - Human Specimens
 - Patient Clinical Characteristics
- METHOD DETAILS
 - Sample Collection
 - Collection of Histological Sections
 - Multiplexed Immunohistochemical Consecutive Staining on a Single Slide
 - Histological Quantification
 - TCR Variable Beta Chain Sequencing
 - Statistical Analyses of TCR- β Sequencing
 - Tissue Digestion
 - PBMC Isolation
 - Secreted Soluble Factor Profiling
 - Measurement of Multiplex Biomarkers
 - CyTOF Sample Preparation
 - CyTOF Data Acquisition
 - CyTOF Clustering: viSNE and Phenograph
 - CyTOF Statistical Analysis
 - Single-Cell Sorting
 - Massively Parallel Single Cell RNA-Seq
 - Single-Cell RNA-seq Clustering Analysis
 - RNA Isolation for Bulk RNA-seq
 - Bulk RNA-seq
 - TCGA Analysis

Figure 6. CD141+ DC Are Excluded from Lung Tumors and Immune Signature of Lung Adenocarcinoma Tumors

(A and B) Comparison of the average transcript expression between DC clusters (Figure 4A, clusters 2 and 4), showing highly expressed transcripts in these clusters, genes with FC > 2 colored red (A), and bar plots showing expression of indicated transcripts (B).

(C) Bar plots of DC metacluster frequencies across tissue (Figure 4C; n = 18; *p < 0.05, **p < 0.01, and ***p < 0.001 by paired t-test).

(D) MICSSS for CD3 and DC-LAMP showing a TLS at the tumor margin in a representative patient.

(E) MARS-seq transcript levels normalized across mononuclear phagocyte clusters (Figure 4A).

(F) Heatmap showing the relative differences in metacluster frequency between tumor and nLung across 16 patients, grouped by stage.

(G) Bar plots showing neutrophil metacluster frequency and secreted soluble TNF α (pg/ml) at the tumor, stratified by stage (*p < 0.05 by unpaired t-test).

Bar plots show mean \pm SEM.

See also Figure S6.

- QUANTIFICATION AND STATISTICAL ANALYSIS
- DATA AND SOFTWARE AVAILABILITY

SUPPLEMENTAL INFORMATION

Supplemental Information includes six figures, three tables, and two data files and can be found with this article online at <http://dx.doi.org/10.1016/j.cell.2017.04.014>.

A video abstract is available at <http://dx.doi.org/10.1016/j.cell.2017.04.014#mmc6>.

AUTHOR CONTRIBUTIONS

Conceptualization: M.M., Y.L., and C.D.B.; Methodology: M.M., Y.L., A.R., I.A., E.D.A., and J.H.L.; Software: E.D.A., A.L.; Formal Analysis: Y.L., A.L., E.D.A., N.E., S.K., A.S., B.D.G., J.A.R., R.O.E., C.S., M.V.; Investigation: Y.L., S.K., C.B., R.S., C.M., R.R., K.M., and A.R.; Resources: R.F. and A.W.; Data Curation: S.K., C.B., R.S., and C.D.B.; Writing – Original: M.M., Y.L., A.L., and S.K.; Writing – Review & Editing: M.M., Y.L., A.L., and S.K.; Visualization: Y.L., S.K., and A.L.; Supervision: M.M., A.R., I.A., D.P., C.D.B., S.K.-S., M.B.B., S.G., and A.C.; Project Administration: M.M.; Funding Acquisition: M.M.

ACKNOWLEDGEMENTS

We thank the Merad laboratory for helpful discussions and input. We would like to thank H el ene Salmon for critical review of the manuscript. We would like to thank the Human Immune Monitoring Core (HIMC) for their excellent technical support and assistance throughout the project, in particular Adeeb Rahman and the members of the CyTOF core, Oksana Mayovska and Victor Guo, and Manishkumar Patel. We would like to thank the Biorepository & Pathology Core and the Flow Cytometry facility. We would like to thank Jill Gregory for her assistance with the artwork. C.B. is funded by Foundation pour la Recherche Medicale DEA20150633125. M.M. is funded by NIH grants R01, R01 CA173861, U19AI128949, U24 AI 118644, and U19 AI 117873-01.

Received: January 10, 2017

Revised: February 26, 2017

Accepted: April 11, 2017

Published: May 4, 2017

REFERENCES

Aberle, D.R., Adams, A.M., Berg, C.D., Black, W.C., Clapp, J.D., Fagerstrom, R.M., Gareen, I.F., Gatsonis, C., Marcus, P.M., and Sicks, J.D.; National Lung Screening Trial Research Team (2011). Reduced lung-cancer mortality with low-dose computed tomographic screening. *N. Engl. J. Med.* **365**, 395–409.

Amir, A.D., Davis, K.L., Tadmor, M.D., Simonds, E.F., Levine, J.H., Bendall, S.C., Shenfeld, D.K., Krishnaswamy, S., Nolan, G.P., and Pe'er, D. (2013). viSNE enables visualization of high dimensional single-cell data and reveals phenotypic heterogeneity of leukemia. *Nat. Biotechnol.* **31**, 545–552.

Besse, B., Johnson, M., Janne, P.A., Janne, P.A., Garassino, M.C., Eberhardt, W.E., Peters, S., Toh, C.K., Kurata, T., Li, Z., et al. (2015). 16LBA Phase II, single-arm trial (BIRCH) of atezolizumab as first-line or subsequent therapy for locally advanced or metastatic PD-L1-selected non-small cell lung cancer (NSCLC). *Eur. J. Cancer* **51**, S717–S718.

Black, W.C., Keeler, E.B., and Soneji, S.S. (2015). Cost-effectiveness of CT screening in the National Lung Screening Trial. *N. Engl. J. Med.* **372**, 388.

Blondel, V.D., Guillaume, J.-L., Lambiotte, R., and Lefebvre, E. (2008). Fast unfolding of communities in large networks. *J. Stat. Mech.* **2008**, P10008.

Broz, M.L., Binnewies, M., Boldajipour, B., Nelson, A.E., Pollack, J.L., Erle, D.J., Barczak, A., Rosenblum, M.D., Daud, A., Barber, D.L., et al. (2014). Dis-

secting the tumor myeloid compartment reveals rare activating antigen-presenting cells critical for T cell immunity. *Cancer Cell* **26**, 638–652.

Carlson, C.S., Emerson, R.O., Sherwood, A.M., Desmarais, C., Chung, M.-W., Parsons, J.M., Steen, M.S., LaMadrid-Herrmannsfeldt, M.A., Williamson, D.W., Livingston, R.J., et al. (2013). Using synthetic templates to design an unbiased multiplex PCR assay. *Nat. Commun.* **4**, 2680.

Chang, Q., Bournazou, E., Sansone, P., Berishaj, M., Gao, S.P., Daly, L., Wels, J., Theilen, T., Granitto, S., Zhang, X., et al. (2013). The IL-6/JAK/Stat3 feed-forward loop drives tumorigenesis and metastasis. *Neoplasia* **15**, 848–862.

Chen, J.J., Yao, P.L., Yuan, A., Hong, T.M., Shun, C.T., Kuo, M.L., Lee, Y.C., and Yang, P.C. (2003). Up-regulation of tumor interleukin-8 expression by infiltrating macrophages: its correlation with tumor angiogenesis and patient survival in non-small cell lung cancer. *Clin. Cancer Res.* **9**, 729–737.

Chen, T.J., and Kotecha, N. (2014). Cytobank: providing an analytics platform for community cytometry data analysis and collaboration. In *High-Dimensional Single Cell Analysis*, H.G. Fienberg and G.P. Nolan, eds. (Springer), pp. 127–157.

Csardi, G., and Nepusz, T. (2006). The igraph software package for complex network research. *InterJournal. Complex Syst.* **1695**, 1–9.

Desch, A.N., Gibbings, S.L., Goyal, R., Kolde, R., Bednarek, J., Bruno, T., Slansky, J.E., Jacobelli, J., Mason, R., Ito, Y., et al. (2016). Flow cytometric analysis of mononuclear phagocytes in nondiseased human lung and lung-draining lymph nodes. *Am. J. Respir. Crit. Care Med.* **193**, 614–626.

Dieu-Nosjean, M.C., Antoine, M., Danel, C., Heudes, D., Wislez, M., Poulot, V., Rabbe, N., Laurans, L., Tartour, E., de Chaisemartin, L., et al. (2008). Long-term survival for patients with non-small-cell lung cancer with intratumoral lymphoid structures. *J. Clin. Oncol.* **26**, 4410–4417.

Dutertre, C.A., Wang, L.F., and Ginhoux, F. (2014). Aligning bona fide dendritic cell populations across species. *Cell. Immunol.* **291**, 3–10.

Edgar, R., Domrachev, M., and Lash, A.E. (2002). Gene Expression Omnibus: NCBI gene expression and hybridization array data repository. *Nucleic Acids Res* **30**, 207–210.

Engblom, C., Pfirschke, C., and Pittet, M.J. (2016). The role of myeloid cells in cancer therapies. *Nat. Rev. Cancer* **16**, 447–462.

Fehrenbacher, L., Spira, A., Ballinger, M., Kowanzet, M., Vansteenkiste, J., Mazieres, J., Park, K., Smith, D., Artal-Cortes, A., Lewanski, C., et al.; POPLAR Study Group (2016). Atezolizumab versus docetaxel for patients with previously treated non-small-cell lung cancer (POPLAR): a multicentre, open-label, phase 2 randomised controlled trial. *Lancet* **387**, 1837–1846.

Forde, P.M., Smith, K.N., Chaff, J.E., Hellmann, M., Merghoub, T., Wolchok, J.D., Yang, S.C., Battafarano, R.J., Gabrielson, E., Georgiades, C.S., et al. (2016). Neoadjuvant anti-PD1, nivolumab, in early stage resectable non-small-cell lung cancer. *ESMO 2016 Congress* **27**, 1–36.

Gabrilovich, D.I., Ostrand-Rosenberg, S., and Bronte, V. (2012). Coordinated regulation of myeloid cells by tumours. *Nat. Rev. Immunol.* **12**, 253–268.

Germain, C., Gnjatich, S., Tamzalit, F., Knockaert, S., Remark, R., Goc, J., Lepelletier, A., Becht, E., Katsahian, S., Bizouard, G., et al. (2014). Presence of B cells in tertiary lymphoid structures is associated with a protective immunity in patients with lung cancer. *Am. J. Respir. Crit. Care Med.* **189**, 832–844.

Ginhoux, F., and Jung, S. (2014). Monocytes and macrophages: developmental pathways and tissue homeostasis. *Nat. Rev. Immunol.* **14**, 392–404.

Goc, J., Germain, C., Vo-Bourgais, T.K., Lupo, A., Klein, C., Knockaert, S., de Chaisemartin, L., Ouakrim, H., Becht, E., Alifano, M., et al. (2014). Dendritic cells in tumor-associated tertiary lymphoid structures signal a Th1 cytotoxic immune contexture and license the positive prognostic value of infiltrating CD8+ T cells. *Cancer Res.* **74**, 705–715.

Goldstraw, P., Chansky, K., Crowley, J., Rami-Porta, R., Asamura, H., Eberhardt, W.E.E., Nicholson, A.G., Groome, P., Mitchell, A., and Bolejack, V.; International Association for the Study of Lung Cancer Staging and Prognostic Factors Committee, Advisory Boards, and Participating Institutions; International Association for the Study of Lung Cancer Staging and Prognostic Factors Committee Advisory Boards and Participating Institutions (2016). The IASLC Lung Cancer Staging Project: Proposals for revision of the TNM stage

- groupings in the forthcoming (eighth) edition of the TNM classification for lung cancer. *J. Thorac. Oncol.* **11**, 39–51.
- Haniffa, M., Collin, M., and Ginhoux, F. (2013). Ontogeny and functional specialization of dendritic cells in human and mouse. *Adv. Immunol.* **120**, 1–49.
- Hanna, R.N., Cekic, C., Sag, D., Tacke, R., Thomas, G.D., Nowyhed, H., Herrley, E., Rasquinha, N., McArdle, S., Wu, R., et al. (2015). Patrolling monocytes control tumor metastasis to the lung. *Science* **350**, 985–990.
- Herbst, R.S., Soria, J.C., Kowanetz, M., Fine, G.D., Hamid, O., Gordon, M.S., Sosman, J.A., McDermott, D.F., Powderly, J.D., Gettinger, S.N., et al. (2014). Predictive correlates of response to the anti-PD-L1 antibody MPDL3280A in cancer patients. *Nature* **515**, 563–567.
- Hildner, K., Edelson, B.T., Purtha, W.E., Diamond, M., Matsushita, H., Kohyama, M., Calderon, B., Schraml, B.U., Unanue, E.R., Diamond, M.S., et al. (2008). *Batf3* deficiency reveals a critical role for CD8 α^+ dendritic cells in cytotoxic T cell immunity. *Science* **322**, 1097–1100.
- Jaitin, D.A., Kenigsberg, E., Keren-Shaul, H., Elefant, N., Paul, F., Zaretsky, I., Mildner, A., Cohen, N., Jung, S., Tanay, A., and Amit, I. (2014). Massively parallel single-cell RNA-seq for marker-free decomposition of tissues into cell types. *Science* **343**, 776–779.
- Joshi, N.S., Akama-Garren, E.H., Lu, Y., Lee, D.Y., Chang, G.P., Li, A., DuPage, M., Tammela, T., Kerper, N.R., Farago, A.F., et al. (2015). Regulatory T cells in tumor-associated tertiary lymphoid structures suppress anti-tumor T cell responses. *Immunity* **43**, 579–590.
- Kirsch, I., Vignali, M., and Robins, H. (2015). T-cell receptor profiling in cancer. *Mol. Oncol.* **9**, 2063–2070.
- Krijthe, J. (2015). Rtsne: T-Distributed stochastic neighbor embedding using Barnes-Hut implementation. R package version 010, URL <http://CRAN.R-project.org/package=Rtsne>.
- Lavin, Y., and Merad, M. (2013). Macrophages: gatekeepers of tissue integrity. *Cancer Immunol. Res.* **1**, 201–209.
- Lavin, Y., Winter, D., Blecher-Gonen, R., David, E., Keren-Shaul, H., Merad, M., Jung, S., and Amit, I. (2014). Tissue-resident macrophage enhancer landscapes are shaped by the local microenvironment. *Cell* **159**, 1312–1326.
- Levine, J.H., Simonds, E.F., Bendall, S.C., Davis, K.L., Amir, A.D., Tadmor, M.D., Litvin, O., Fienberg, H.G., Jager, A., Zunder, E.R., et al. (2015). Data-driven phenotypic dissection of AML reveals progenitor-like cells that correlate with prognosis. *Cell* **162**, 184–197.
- Merad, M., Sathe, P., Helft, J., Miller, J., and Mortha, A. (2013). The dendritic cell lineage: ontogeny and function of dendritic cells and their subsets in the steady state and the inflamed setting. *Annu. Rev. Immunol.* **31**, 563–604.
- Moussion, C., and Girard, J.P. (2011). Dendritic cells control lymphocyte entry to lymph nodes through high endothelial venules. *Nature* **479**, 542–546.
- Naidoo, J., Wang, X., Woo, K.M., Iyriboz, T., Halpenny, D., Cunningham, J., Chaft, J.E., Segal, N.H., Callahan, M.K., Lesokhin, A.M., et al. (2017). Pneumonitis in patients treated with anti-programmed death-1/programmed death ligand 1 therapy. *J. Clin. Oncol.* **35**, 709–717.
- Nishino, M., Giobbie-Hurder, A., Hatabu, H., Ramaiya, N.H., and Hodi, F.S. (2016). Incidence of programmed cell death 1 inhibitor-related pneumonitis in patients with advanced cancer: A systematic review and meta-analysis. *JAMA Oncol.* **2**, 1607–1616.
- Paul, F., Arkin, Y., Giladi, A., Jaitin, D.A., Kenigsberg, E., Keren-Shaul, H., Winter, D., Lara-Astiaso, D., Gury, M., Weiner, A., et al. (2015). Transcriptional heterogeneity and lineage commitment in myeloid progenitors. *Cell* **163**, 1663–1677.
- Pham, C.T. (2006). Neutrophil serine proteases: specific regulators of inflammation. *Nat. Rev. Immunol.* **6**, 541–550.
- Pignon, J.P., Tribodet, H., Scagliotti, G.V., Douillard, J.Y., Shepherd, F.A., Stephens, R.J., Dunant, A., Torri, V., Rosell, R., Seymour, L., et al.; LACE Collaborative Group (2008). Lung adjuvant cisplatin evaluation: a pooled analysis by the LACE Collaborative Group. *J. Clin. Oncol.* **26**, 3552–3559.
- Pitzalis, C., Jones, G.W., Bombardieri, M., and Jones, S.A. (2014). Ectopic lymphoid-like structures in infection, cancer and autoimmunity. *Nat. Rev. Immunol.* **14**, 447–462.
- Qian, B.-Z., Li, J., Zhang, H., Kitamura, T., Zhang, J., Campion, L.R., Kaiser, E.A., Snyder, L.A., and Pollard, J.W. (2011). CCL2 recruits inflammatory monocytes to facilitate breast-tumour metastasis. *Nature* **475**, 222–225.
- R Core Team (2016). R: A language and environment for statistical computing (R Foundation for Statistical Computing).
- Reddy, R.C. (2008). Immunomodulatory role of PPAR- γ in alveolar macrophages. *J. Investig. Med.* **56**, 522–527.
- Remark, R., Merghoub, T., Grabe, N., Litjens, G., Damotte, D., Wolchok, J.D., Merad, M., and Gnjatic, S. (2016). In-depth tissue profiling using multiplexed immunohistochemical consecutive staining on single slide. *Science Immunology* **1**, aaf6925.
- Ricote, M., Li, A.C., Willson, T.M., Kelly, C.J., and Glass, C.K. (1998). The peroxisome proliferator-activated receptor-gamma is a negative regulator of macrophage activation. *Nature* **391**, 79–82.
- Ritchie, M.E., Phipson, B., Wu, D., Hu, Y., Law, C.W., Shi, W., and Smyth, G.K. (2015). limma powers differential expression analyses for RNA-sequencing and microarray studies. *Nucleic Acids Res.* **43**, e47.
- Roberts, E.W., Broz, M.L., Binnewies, M., Headley, M.B., Nelson, A.E., Wolf, D.M., Kaisho, T., Bogunovic, D., Bhardwaj, N., and Krummel, M.F. (2016). Critical role for CD103(+)/CD141(+) dendritic cells bearing CCR7 for tumor antigen trafficking and priming of T cell immunity in melanoma. *Cancer Cell* **30**, 324–336.
- Robins, H., Desmarais, C., Matthis, J., Livingston, R., Andriesen, J., Reijonen, H., Carlson, C., Nepom, G., Yee, C., and Cerosaletti, K. (2012). Ultra-sensitive detection of rare T cell clones. *J. Immunol. Methods* **375**, 14–19.
- Robins, H.S., Campregher, P.V., Srivastava, S.K., Wacher, A., Turtle, C.J., Kahsai, O., Riddell, S.R., Warren, E.H., and Carlson, C.S. (2009). Comprehensive assessment of T-cell receptor beta-chain diversity in alphabeta T cells. *Blood* **114**, 4099–4107.
- Robinson, M.D., and Oshlack, A. (2010). A scaling normalization method for differential expression analysis of RNA-seq data. *Genome Biol.* **11**, R25.
- Salmon, H., Franciszkiewicz, K., Damotte, D., Dieu-Nosjean, M.C., Validire, P., Trautmann, A., Mami-Chouaib, F., and Donnadieu, E. (2012). Matrix architecture defines the preferential localization and migration of T cells into the stroma of human lung tumors. *J. Clin. Invest.* **122**, 899–910.
- Salmon, H., Idoyaga, J., Rahman, A., Leboeuf, M., Remark, R., Jordan, S., Casanova-Acebes, M., Khudoynazarova, M., Agudo, J., Tung, N., et al. (2016). Expansion and activation of CD103(+) dendritic cell progenitors at the tumor site enhances tumor responses to therapeutic PD-L1 and BRAF inhibition. *Immunity* **44**, 924–938.
- Sánchez-Paulete, A.R., Cueto, F.J., Martínez-López, M., Labiano, S., Morales-Kastresana, A., Rodríguez-Ruiz, M.E., Jure-Kunkel, M., Azpilikueta, A., Aznar, M.A., Quejgas, J.I., et al. (2016). Cancer immunotherapy with immunomodulatory anti-CD137 and anti-PD-1 monoclonal antibodies requires BATF3-dependent dendritic cells. *Cancer Discov.* **6**, 71–79.
- Spira, A., Beane, J.E., Shah, V., Steiling, K., Liu, G., Schembri, F., Gilman, S., Dumas, Y.M., Calner, P., Sebastiani, P., et al. (2007). Airway epithelial gene expression in the diagnostic evaluation of smokers with suspect lung cancer. *Nat. Med.* **13**, 361–366.
- Suzuki, K., Kadota, K., Sima, C.S., Nitadori, J., Rusch, V.W., Travis, W.D., Sadelain, M., and Adusumilli, P.S. (2013). Clinical impact of immune microenvironment in stage I lung adenocarcinoma: tumor interleukin-12 receptor $\beta 2$ (IL-12R $\beta 2$), IL-7R, and stromal FoxP3/CD3 ratio are independent predictors of recurrence. *J. Clin. Oncol.* **31**, 490–498.
- Turley, S.J., Cremasco, V., and Astarita, J.L. (2015). Immunological hallmarks of stromal cells in the tumour microenvironment. *Nat. Rev. Immunol.* **15**, 669–682.
- van der Maaten, L. (2014). Accelerating t-SNE using tree-based algorithms. *J. Mach. Learn. Res.* **15**, 3221–3245.
- van der Maaten, L., and Hinton, G. (2008). Visualizing data using t-SNE. *J. Mach. Learn. Res.* **9**, 2579–2605.

- Wendel, M., Galani, I.E., Suri-Payer, E., and Cerwenka, A. (2008). Natural killer cell accumulation in tumors is dependent on IFN-gamma and CXCR3 ligands. *Cancer Res.* *68*, 8437–8445.
- Wickham, H. (2009). *ggplot2: Elegant Graphics for Data Analysis* (Springer-Verlag New York).
- Wickham, H. (2016). *tidyverse: Easily Install and Load 'Tidyverse' Packages*. R package version 1.0.0.
- Wu, K., Byers, D.E., Jin, X., Agapov, E., Alexander-Brett, J., Patel, A.C., Cella, M., Gilfilan, S., Colonna, M., Kober, D.L., et al. (2015). TREM-2 promotes macrophage survival and lung disease after respiratory viral infection. *J. Exp. Med.* *212*, 681–697.
- Yona, S., and Jung, S. (2010). Monocytes: subsets, origins, fates and functions. *Curr. Opin. Hematol.* *17*, 53–59.
- Yoshie, O., and Matsushima, K. (2015). CCR4 and its ligands: from bench to bedside. *Int. Immunol.* *27*, 11–20.
- Yu, H., Lee, H., Herrmann, A., Buettner, R., and Jove, R. (2014). Revisiting STAT3 signalling in cancer: new and unexpected biological functions. *Nat. Rev. Cancer* *14*, 736–746.
- Yu, Y.R., Hotten, D.F., Malakhau, Y., Volker, E., Ghio, A.J., Noble, P.W., Kraft, M., Hollingsworth, J.W., Gunn, M.D., and Tighe, R.M. (2016). Flow cytometric analysis of myeloid cells in human blood, bronchoalveolar lavage, and lung tissues. *Am. J. Respir. Cell Mol. Biol.* *54*, 13–24.
- Zhu, W., Germain, C., Liu, Z., Sebastian, Y., Devi, P., Knockaert, S., Brohawn, P., Lehmann, K., Damotte, D., Validire, P., et al. (2015). A high density of tertiary lymphoid structure B cells in lung tumors is associated with increased CD4(+) T cell receptor repertoire clonality. *Oncolmmunology* *4*, e1051922.
- Zhu, Y.M., Webster, S.J., Flower, D., and Woll, P.J. (2004). Interleukin-8/CXCL8 is a growth factor for human lung cancer cells. *Br. J. Cancer* *91*, 1970–1976.

Crystal Structure of the Human Cannabinoid Receptor CB₁

Tian Hua,^{1,2} Kiran Vemuri,³ Mengchen Pu,² Lu Qu,^{1,2} Gye Won Han,⁴ Yiran Wu,¹ Suwen Zhao,¹ Wenqing Shui,¹ Shanshan Li,¹ Anisha Korde,³ Robert B. Laprairie,⁵ Edward L. Stahl,⁵ Jo-Hao Ho,⁵ Nikolai Zvonok,³ Han Zhou,³ Irina Kufareva,⁶ Beili Wu,⁷ Qiang Zhao,⁷ Michael A. Hanson,⁸ Laura M. Bohn,^{5,*} Alexandros Makriyannis,^{3,*} Raymond C. Stevens,^{1,4,9,*} and Zhi-Jie Liu^{1,2,*}

¹Human Institute, ShanghaiTech University, Shanghai 201210, China

²National Laboratory of Biomacromolecules, Institute of Biophysics, Chinese Academy of Sciences, Beijing 100101, China

³Center for Drug Discovery, Department of Pharmaceutical Sciences and Department of Chemistry and Chemical Biology, Northeastern University, Boston, MA 02115, USA

⁴Departments of Biological Sciences and Chemistry, Bridge Institute, University of Southern California, Los Angeles, CA 90089, USA

⁵Departments of Molecular Therapeutics and Neuroscience, The Scripps Research Institute, Jupiter, FL 33458, USA

⁶University of California, San Diego, La Jolla, CA 92093, USA

⁷CAS Key Laboratory of Receptor Research, Shanghai Institute of Materia Medica, Chinese Academy of Sciences, Shanghai 201203, China

⁸GPCR Consortium, San Marcos, CA 92078, USA

⁹Lead Contact

*Correspondence: lbohn@scripps.edu (L.M.B.), a.makriyannis@northeastern.edu (A.M.), stevens@shanghaitech.edu.cn (R.C.S.), liuzhj@shanghaitech.edu.cn (Z.-J.L.)

http://dx.doi.org/10.1016/j.cell.2016.10.004

SUMMARY

Cannabinoid receptor 1 (CB₁) is the principal target of Δ^9 -tetrahydrocannabinol (THC), a psychoactive chemical from *Cannabis sativa* with a wide range of therapeutic applications and a long history of recreational use. CB₁ is activated by endocannabinoids and is a promising therapeutic target for pain management, inflammation, obesity, and substance abuse disorders. Here, we present the 2.8 Å crystal structure of human CB₁ in complex with AM6538, a stabilizing antagonist, synthesized and characterized for this structural study. The structure of the CB₁-AM6538 complex reveals key features of the receptor and critical interactions for antagonist binding. In combination with functional studies and molecular modeling, the structure provides insight into the binding mode of naturally occurring CB₁ ligands, such as THC, and synthetic cannabinoids. This enhances our understanding of the molecular basis for the physiological functions of CB₁ and provides new opportunities for the design of next-generation CB₁-targeting pharmaceuticals.

INTRODUCTION

Marijuana from *Cannabis sativa* L. has been used for both therapeutic and recreational purposes for many centuries (Lemberger, 1980; Li, 1973). In the 1940s, chemistry based on compounds isolated from the plant (Wollner et al., 1942) produced novel biologically active molecules (Adams et al., 1948; Ghosh et al., 1940); however, it was not until the 1960s that the active constituent of marijuana, Δ^9 -tetrahydrocannabinol (THC), a

terpenoid molecule, was isolated and characterized (Gaoni and Mechoulam, 1964). This provided an early molecular foundation for medicinal chemists to develop related structural analogs and new synthetic ligands (Makriyannis and Rapaka, 1990; Razdan, 1986). Initially, due to their lipophilic nature, it was assumed that cannabinoids exerted their effects by perturbing the physical properties of biological membranes (Makriyannis, 2014; Mavromoustakos et al., 1995). This assumption was challenged with the discovery, cloning, and expression of the first cannabinoid-specific membrane receptor, then designated as the cannabinoid receptor (CB) (Devane et al., 1988; Matsuda et al., 1990). With the subsequent identification of a second receptor, the designation evolved to CB₁ and CB₂ (Munro et al., 1993). The discovery of the endogenous agonists to the receptors, the endocannabinoids, anandamide (Devane et al., 1992), and 2-arachidonoyl glycerol (2-AG) (Mechoulam et al., 1995) soon followed.

Cannabinoid receptors belong to the class A G protein-coupled receptor (GPCR) family, signal through inhibitory G $\alpha_{i/o}$ heterotrimeric G proteins (Howlett, 1985), and interact with β -arrestins (Jin et al., 1999). CB₁ is the most highly expressed GPCR in the human brain and is expressed throughout the body, with the highest levels found in the central nervous system (Herkenham et al., 1990).

Cannabis has been used for centuries in many cultures to treat a wide range of medical conditions. More recently, therapeutic considerations have moved beyond the plant extract to explore and produce more pharmacologically refined compounds. CB₁-selective small-molecule agonists have shown therapeutic promise in a wide range of disorders, including pain and inflammation (Cravatt and Lichtman, 2004), multiple sclerosis (Pertwee, 2002; Pryce and Baker, 2015), and neurodegenerative disorders (Fernández-Ruiz et al., 2015). The first CB₁-selective antagonist/inverse agonist, rimonabant (SR141716, Acomplia [Sanofi-Aventis]) (Rinaldi-Carmona

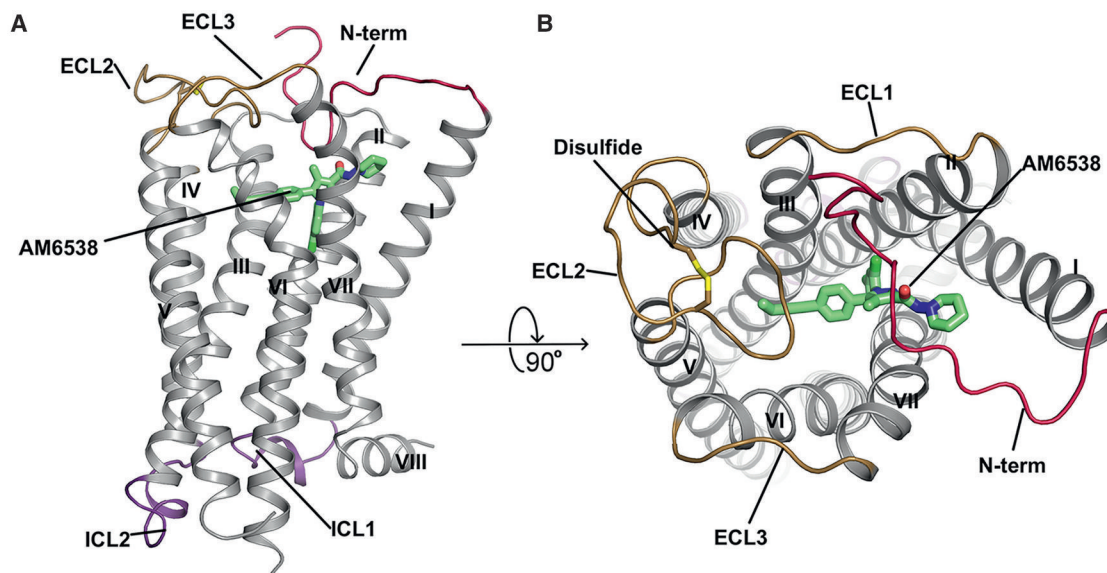


Figure 1. Overall Structure of CB₁-AM6538 Complex

(A) Side view of the CB₁-AM6538 complex. The receptor is shown in gray cartoon representation. The ligand AM6538, shown with green sticks, demarcates the binding pocket, which is partially occluded by the N-terminal loop (red). The nitrate group is not modeled in the experimental crystal structure, as the electron density was not observed. The extracellular loops (ECLs) are shown in brown and the intracellular loops (ICLs) are shown in purple.

(B) Top view of the extracellular side. The disulfide bond in ECL2 is shown as yellow sticks.

See also Figures S2 and S3.

et al., 1994), received approval from the European Medical Agency as an adjunct to diet and exercise for treating obesity (Janero and Makriyannis, 2009). Antagonists of CB₁ have been explored as potential therapeutics for obesity-related metabolic disorders (Mazier et al., 2015), mental illness (Black et al., 2011; Rubino et al., 2015), liver fibrosis (Mallat et al., 2013), and nicotine addiction (Schindler et al., 2016). However, rimonabant and other ligands in its class were not approved in the United States due to concerns about adverse events, such as increased anxiety, depression, and suicidal ideation.

Numerous studies have investigated how ligands binding CB₁ can mediate downstream signaling. While the variety of compounds exhibiting different pharmacological profiles have provided clues regarding CB₁ activation, the molecular details defining the binding modes of both endogenous and exogenous ligands are still largely unknown (Guo et al., 1994; Makriyannis, 2014; Picone et al., 2005). In order to address this deficit in understanding, we have determined the crystal structure of CB₁ in complex with a tight binding antagonist AM6538. In conjunction with molecular docking, the structure was used to elucidate the binding modes of a diverse set of antagonists/inverse agonists and agonists of CB₁. The structural details of the cannabinoid receptor reported herein improve our understanding of how ligands engage to modulate the cannabinoid system and provide a useful model to facilitate the design of next-generation pharmaceuticals to avoid unwanted side effects. The findings provide insight into mechanisms of slow dissociation of antagonists, which may potentially translate into long acting pharmacological effects.

RESULTS

Synthesis of CB₁ Stabilizing Antagonist AM6538 for Structural Studies

One of the key factors facilitating the structure determination of CB₁ (Figure 1) is utilization of the antagonist AM6538, the synthesis of which resulted from the strategic modification of rimonabant to enhance its ability to stabilize the ligand-receptor complex and promote CB₁ crystal formation. In contrast with rimonabant, the 5-phenyl ring substituent was modified so as to introduce motifs (ex. alkyne unit) that could favor increased affinity for the CB₁ receptor (Tam et al., 2010). The rimonabant analog, AM251, (1, Figure 2A) (Lan et al., 1999), a compound that has been used extensively as a pharmacological standard CB₁-selective antagonist, was used as the precursor in the AM6538 synthetic process. Synthesis of AM6538 involves the functionalization of the iodo substituent at the para position of the 5-phenyl ring in AM251 with an acetylenic chain system consisting of four carbons and substituted at the omega carbon. To this end, we initially focused on targeting cysteine residues within CB₁ by introducing suitable electrophilic groups (Janero et al., 2015; Li et al., 2005; Mercier et al., 2010; Picone et al., 2005; Szymanski et al., 2011) at the fourth carbon of the alkyne unit, capable of forming a covalent bond with the cysteine thiol group. For AM6538, we introduced at this position a nitrate group (ONO₂) whose role was to serve as a polar group, which may be displaced by a suitable nucleophile (e.g., thiol) (Pattison and Brown, 1956; Yeates et al., 1985) at or near the binding domain or alternatively bind as an intact group so as to obtain a non-covalent, near-irreversible attachment by interacting with hydrogen bonding amino acid residues, as well as

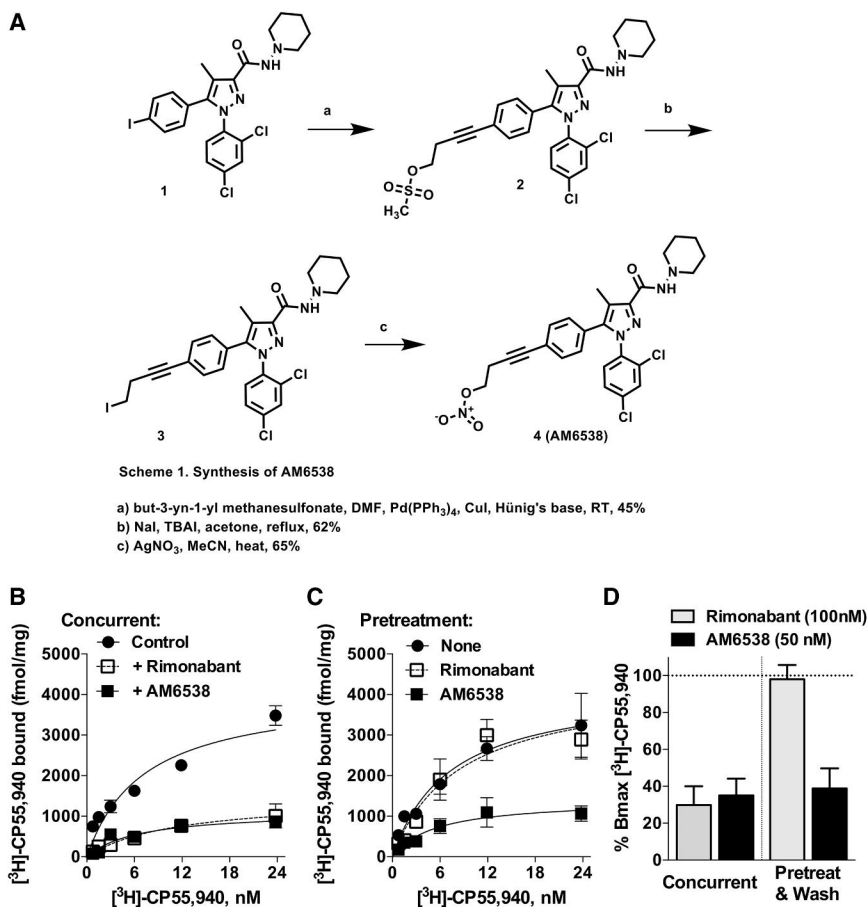


Figure 2. Synthesis and Characterization of AM6538

(A) Synthetic procedures for compound AM6538. (B) Saturation [³H]-CP55,940 binding assays in the absence (control) or presence of rimonabant (100 nM) or AM6538 (50 nM) demonstrates that both antagonists cause displacement of specific binding of the radioligand when present concurrently in the 1 hr binding assay.

(C) Following pretreatment of membranes (37°C, 6 hr) with buffer only (none), rimonabant (100 nM), or AM6538 (50 nM); membranes were washed with buffer 3× prior to [³H]-CP55,940 binding as described for (B).

(D) Percentage of remaining binding (B_{max}) detected following the conditions described in (B) (concurrent) and (C) (pretreat and wash). Both antagonists decrease the binding of [³H]-CP55,940 to ~30% when incubated concurrently during the 1 hr binding assay. Under pretreatment and washout conditions, rimonabant does not affect subsequent radioligand binding, while AM6538 continues to compete despite washing of the membranes.

See also Figure S1 and Table S1.

residues capable of π - π interactions. In the present study, affinity mass spectrometry analysis suggests that AM6538 reacts with CB₁ as an intact molecule with no evidence of covalent modification of relevant cysteine residues.

AM6538 was a strong candidate for crystallographic studies of the receptor based on its high affinity and wash-resistant binding to CB₁ as determined by radioligand competition assays against the tritiated agonist, [³H]-CP55,940 ($K_i = 3.4 \pm 1.0$ nM) (Figures 2B–2D). This is in contrast to rimonabant, which can be readily washed out of membranes, permitting subsequent radioligand binding (Figures 2B–2D). Importantly, the crystallized CB₁ construct (described below) has comparable affinity for AM6538 as the wild-type receptor ($K_i = 5.1 \pm 0.9$ nM).

In functional assays, AM6538 is a competitive antagonist of the effects of CP55,940 and THC on CB₁-mediated inhibition of adenylyl cyclase activity and β -arrestin2 recruitment in overexpression systems (Figures S1A and S1B and Table S1). Competitive antagonism was confirmed by the [³⁵S]-GTP γ S binding assays performed in mouse cerebellum (Figure S1C). For comparison purposes, competitive antagonism was demonstrated for rimonabant in the same systems (Figure S1 and Table S1).

Structure Determination of CB₁-AM6538 Complex

To facilitate crystallization, it was necessary to modify the wild-type (WT) CB₁ sequence. Construct optimization proced-

ures (Lv et al., 2016) identified Flavodoxin (Chun et al., 2012) as a stabilizing fusion partner when inserted within the receptor's third intracellular loop (ICL3) at Val306 and Pro332. Additionally, the WT receptor was truncated on both the N and C termini by 98 and 58 residues, respectively. Finally, in order to

improve the expression and thermostability of the receptor, four computationally predicted mutations (Thr210^{3,46}Ala [D'Antona et al., 2006], Glu273^{5,37}Lys, Thr283^{5,47}Val, and Arg340^{6,32}Glu) were introduced to the CB₁ sequence (Figures S2A–S2C) (superscripts denote amino acid position as described by Ballesteros and Weinstein [1995]). The modified CB₁ construct was inserted into a pTT5 vector for expression in HEK293F cells to generate protein (Figure S2D) that formed crystals in lipidic cubic phase supplemented with cholesterol (Figure S3E); the crystals diffracted to 2.8 Å (Table 1).

Based on affinity mass spectrometry analysis, intact AM6538 is associated with the CB₁ protein (Figure S3F). Electron density with three branches was observed near the orthosteric binding site and modeled as core AM6538 atoms with the terminal nitrate group omitted (Figures 3D and S3). A molecular dynamics (MD) simulation was performed on the CB₁-AM6538 complex with the nitrate group intact and modeled through docking analysis, and the results revealed that the root mean square fluctuation (RMSF) values for the nitrate group and the hinge carbon atom are higher, suggesting that the nitrate group is more mobile than other atoms in AM6538 (Figure S4B). As a modeled ligand with other possibilities to fit the electron density, further studies on ligand binding are under investigation.

Table 1. Crystallographic Data Collection and Refinement Statistics

Data Collection and Refinement Statistics	
Ligand	AM6538
Number of crystals	29
Data Collection	
Space group	C2
Cell dimensions	
a,b,c (Å)	116.56, 52.63, 143.63
β (°)	111.14
Number of reflections measured	160,794
Number of unique reflections	19,837
Resolution (Å)	47.30 - 2.80 (2.90-2.80)
R_{merge}^a	0.126 (0.520)
Mean $I/\sigma(I)$	10.1 (2.1)
Completeness (%)	97.4 (94.1)
Redundancy	8.1 (4.6)
$CC_{1/2}$	0.999 (0.44)
Refinement	
Resolution (Å)	47.05 - 2.80
Number of reflections (test set)	19,827 (985)
$R_{\text{work}}/R_{\text{free}}$	0.207/0.238
Number of Atoms	
CB ₁	2,312
Flavodoxin	1,103
AM6538 ^b	33
Lipid and other	102
Average B Factor (Å ²)	
Wilson	73.6
Overall	87.4
CB ₁	110.6
Flavodoxin	66.6
AM6538	119.5
Lipid and other	79.7
rmsds	
Bond lengths (Å)	0.004
Bond angles (°)	0.638
Ramachandran Plot Statistics (%) ^c	
Favored regions	97.7
Allowed regions	2.3
Disallowed regions	0

^aData for high-resolution shells are shown in parenthesis.
^bNitrate group is excluded due to the absence of electron density.
^cAs defined in MolProbity.

Structural Features of CB₁ in Complex with AM6538

The overall CB₁ structural fold shares a similar architecture with previously solved class A GPCR structures, containing seven transmembrane (7TM) α -helices (I to VII) connected by three extracellular loops (ECL1–3), three intracellular loops (ICL1–3), and an amphipathic helix VIII (Figures 1A and S3A). The non-truncated

part of the N terminus of CB₁, residues 99–112, forms a V-shaped loop, which inserts into the ligand-binding pocket and functions as a plug, restricting access to the pocket from the extracellular side (Figures 1A and 1B). While the influence of crystal packing interactions on the conformation of the N terminus (Figure S3B) cannot be ruled out, it is interesting to note that the N terminus has been consistently observed in an ordered form in the structures of the related lipid receptors LPA₁ (lysophosphatidic acid receptor 1) (Chrencik et al., 2015) and S1P₁ (sphingosine 1-phosphate receptor 1) (Hanson et al., 2012) and that the function of CB₁ is very sensitive to the presence of the ordered portion of the N terminus (Andersson et al., 2003; Fay and Farrens, 2013). ECL2 in CB₁ consists of 21 residues folding into an intricate structure that projects four residues (268–271) into the binding pocket. Previous work has shown that the four residues are important for mediating interactions with certain classes of ligands (Ahn et al., 2009; Bertalovitz et al., 2010) and that the two cysteines (Cys257 and Cys264) in ECL2 are critical to the function of CB₁ (Fay et al., 2005). In the structure, the conformation of ECL2 is constrained by the presence of an intraloop disulfide bond (Cys257-Cys264) (Figure 1B) previously found in the structures of the closely related LPA₁ and S1P₁ receptors. The highly conserved disulfide bond between ECL2 and helix III (Cys^{3,25}) in most class A GPCRs is lacking in all three lipid receptor structures.

AM6538 Interactions in CB₁ Ligand-Binding Pocket

The position of the ligand-binding pocket of CB₁ is different from the previously described orthosteric binding sites of other class A GPCRs. AM6538 lies quite low in the binding pocket of CB₁, immediately above the conserved Trp356^{6,48} (Figures 3A and 3B). The ligand adopts an extended conformation with the ligand strain close to its local minimum as determined by quantum mechanical calculations (Figure S3D).

AM6538 forms mainly hydrophobic interactions with ECL2 and the N terminus, as well as with all CB₁ helices except helix IV (Figures 3A and 3B). As described above, the ligand has a pyrazole ring core with three functional groups. For clarity, we have termed the 2,4-dichlorophenyl ring “arm 1,” the 4-aliphatic chain substituted phenyl ring “arm 2,” and the piperidin-1-ylcarbonyl “arm 3” (Figure 3C). The pyrazole ring core (including the 4-methyl group) is situated between helices II and VII, forming hydrophobic interactions with the side chains of Phe170^{2,57}, Phe379^{7,35}, and Ser383^{7,39} (Figure 3C) and is capped by the N-terminal loop interactions (Met103^{N-term}). Arm 1 is located in a narrow side pocket (Figure 3B) formed by helices II, III, VI, and VII and forms edge-face π - π interactions with the side chain of Phe170^{2,57} and with the backbone amide bond between Gly166^{2,53} and Ser167^{2,54}. This substituted ring moiety forms hydrophobic interactions with Val196^{3,32}, Trp356^{6,48}, Cys386^{7,42}, Leu387^{7,43}, and Met103^{N-term} (Figure 3C). The 2,4-dichlorophenyl ring in arm 1 fits well into the shape of the narrow side pocket (Figure S3C), which explains why 2,4-dichloro or 2-chloro substitutions result in optimal binding (Lange and Kruse, 2005).

Arm 2 of the ligand extends toward a long, narrow channel (Figure 3B) formed by helices III, V, VI, and ECL2. The phenyl group in arm 2 establishes π - π interactions with Phe102^{N-term}, Phe268^{ECL2}, and Trp356^{6,48}; hydrophobic interactions with

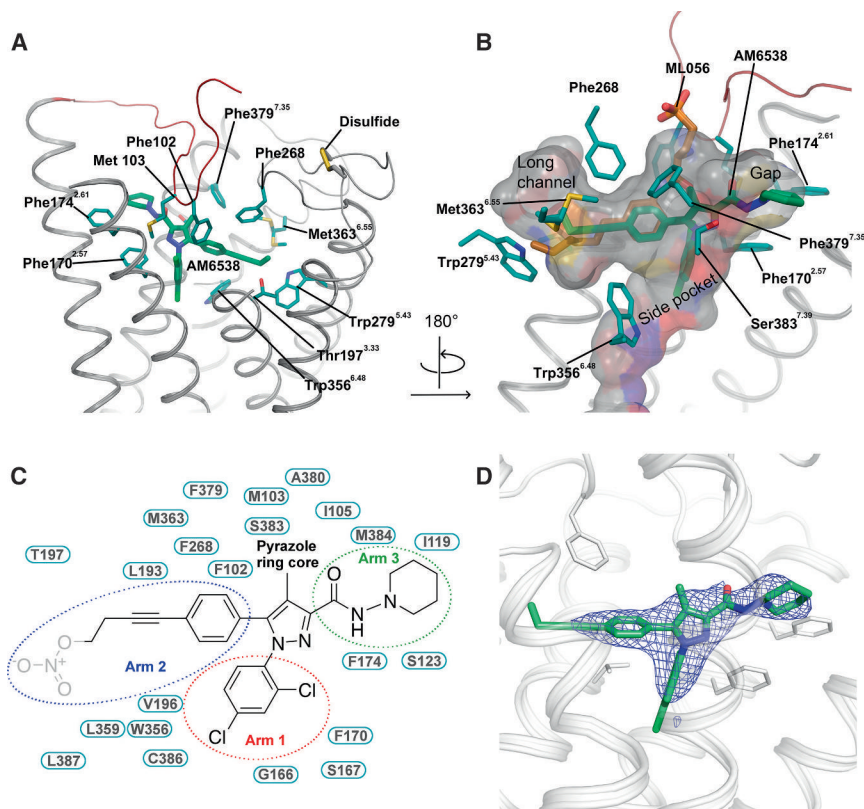


Figure 3. Analysis of the Ligand Binding Pocket of CB₁

(A) Key residues in CB₁ for AM6538 binding. AM6538 (green carbons) and CB₁ residues (teal carbons) involved in ligand binding are shown in stick representation. The receptor is shown in gray cartoon representation.

(B) The shape of the ligand binding pocket. AM6538 (green carbons) and ML056 (brown carbons) are shown in stick representation.

(C) Schematic representation of interactions between CB₁ and AM6538. The 2,4-dichlorophenyl ring in the red circle is termed as arm 1; the 4-aliphatic chain substituted phenyl ring in the blue circle is termed as arm 2; the piperidin-1-ylcarbamoyl in the green circle is termed as arm 3. The nitrate group, which was not observed in the electron density, is shown in gray.

(D) Electron density maps calculated from the refined structure of the CB₁-AM6538 complex. [Fo]-|Fc| omit map (blue mesh) of the ligand AM6538 is shown (contoured at 3 σ).

See also Figure S3.

Leu193^{3,29}, Val196^{3,32}, and Leu359^{6,51} are observed. A triple bond within the long aliphatic chain in arm 2 forms π - π interactions with Phe268^{ECL2} and Trp356^{6,48} and forms hydrophobic interactions with several residues, including Leu193^{3,29}, Val196^{3,32}, Thr197^{3,33}, Leu359^{6,51}, and Met363^{6,55} (Figure 3C). Interestingly, the binding mode of the long hydrophobic chain is similar to that of ML056 with the S1P₁ receptor (Figure 3B), implying that this could be a conserved binding pocket for long aliphatic chains in lipid-binding receptors. In regards to the nitrate group that has not been observed in the crystallographic structure, our docking experiments define a domain in which the nitrate group is interacting with residues Thr197^{3,33}, Tyr275^{5,39}, and Trp279^{5,43} through hydrogen bonding and π - π interactions (Figure S4A).

Finally, arm 3 extends toward a gap constituted by helices I, II, VII capped by the N-terminal loop (Figure 3B). It forms interactions with hydrophobic residues, Met103^{N-term}, Ile105^{N-term}, Ile119^{1,35}, Ser123^{1,39}, Phe170^{2,57}, Phe174^{2,61}, Ala380^{7,36}, Ser383^{7,39}, and Met384^{7,40} (Figure 3C). Unlike the π - π interactions formed by the other two arms, the interactions between arm 3 and the receptor are non-specific.

Among the interactions between AM6538 and CB₁, Phe170^{2,57} plays an important role by interacting with the pyrazole ring core, as well as rings in arm 1 and arm 3. Moreover, Phe170^{2,57} is pushed by the ligand to move toward helix I, resulting in a tilt of the last two turns (residues 170–177) of helix II toward helix I, compared to S1P₁ and LPA₁, the two closest homologs (Figures 4A and 4B). This tilted helix II, in turn, pushes

helix I by about 7 Å, mainly due to interactions with the two bulky residues Phe170^{2,57} and Phe174^{2,61}.

The role of Lys192^{3,28} in CB₁ has been intensively researched. It was reported that Lys192Ala/Lys192Gln/Lys192Glu mutants decreased the affinities of several agonists such as CP55,940, HU-210, and anandamide (Chin et al., 1998; Hurst et al., 2002; Pan et al., 1998; Song and Bonner, 1996). Previously, it was suggested that Lys192^{3,28} has direct interactions with CB₁ ligands. However, in our CB₁ structure, Lys192^{3,28} does not interact directly with AM6538. Instead, it forms a salt bridge/hydrogen bond network that stabilizes the conformation of ECL1, the N terminus, and the extracellular parts of helices II and III. The side chain of Lys192^{3,28} points away from the binding pocket and forms salt bridges with Asp176^{2,63} and Asp184^{ECL1}, while Asp184^{ECL1} further stabilizes the N terminus by forming a hydrogen bond with the backbone of Phe102^{N-term} (Figure 4C).

Structural Comparison of the CB₁, LPA₁, and S1P₁ Receptors

CB₁, LPA₁, and S1P₁ receptors all bind lipid-derived endogenous ligands (anandamide/sn-2-arachidonoylglycerol, sphingosine-1-phosphate, lysophosphatidic acid) (Shimizu, 2009). Early sequence analysis revealed that CB₁ has a moderate sequence identity with LPA₁ (13% overall, 28% in TM regions) and S1P₁ (14% overall, 27% in TM regions) (Bramblett et al., 1995; Isberg et al., 2016) (Figure S5). Crystal structures of LPA₁ (Chrencik et al., 2015) and S1P₁ (Hanson et al., 2012) have been recently determined. The main structural difference between the three lipid receptors occurs in the extracellular portion, with the most striking being the unique conformation of the N-terminal loop of CB₁ (Figures 4A and 4B). For all three receptors, the N terminus has a role in ligand recognition. Comparing the ligand binding

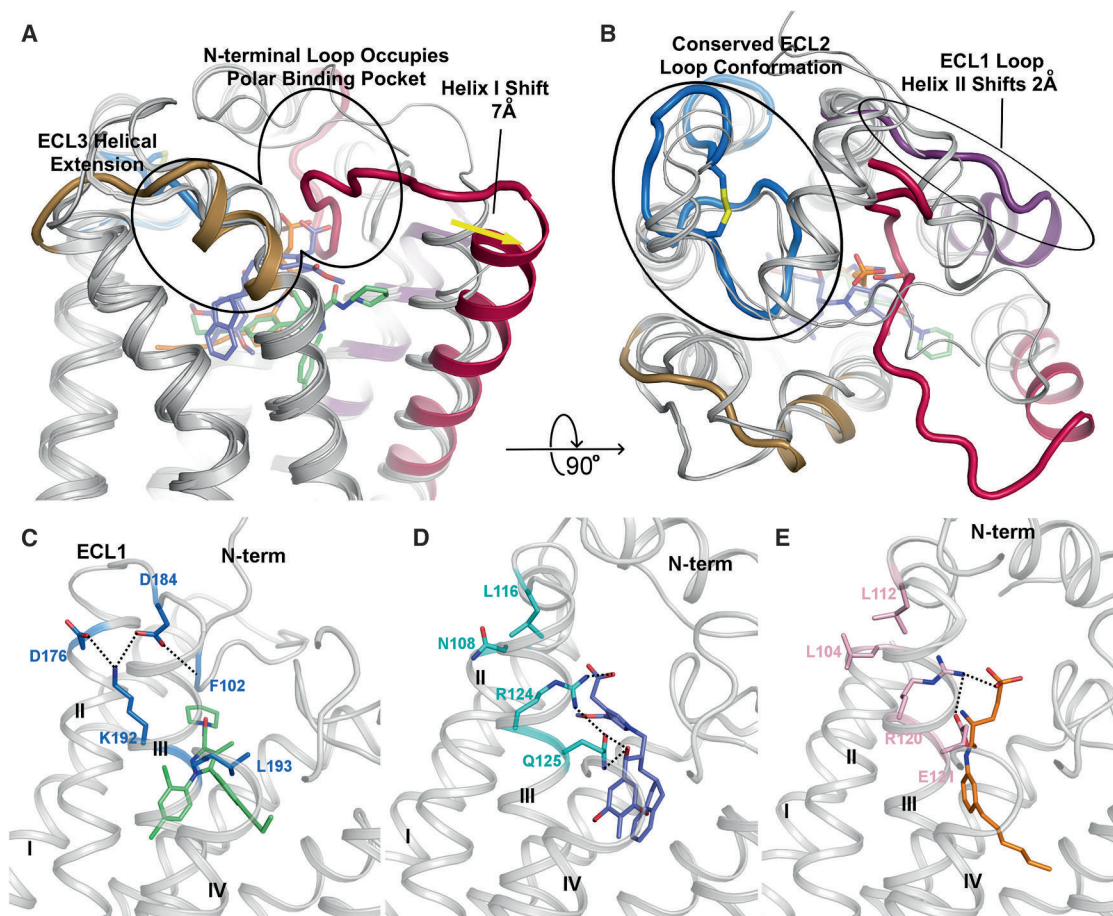


Figure 4. Comparison of CB₁, LPA₁, and S1P₁ Structural Features

(A) Side view of CB₁ with structurally divergent regions of LPA₁ (PDB: 4Z34) and S1P₁ (PDB: 3V2Y) overlaid. LPA₁ and S1P₁ receptors are shown in gray cartoons. The CB₁ N-terminal loop (red) occupies the polar binding pocket, helix I (red helix) is shifted out 7 Å compared with the other two receptors. ECL3 of CB₁ shows a three helical turn extension of helix VII (brown helix).

(B) 90° rotation of (A) for a top view of CB₁ with structurally divergent regions of LPA₁ (4Z34) and S1P₁ (3V2Y) overlaid. CB₁ shows a conserved conformation of ECL2 (blue) with the other two receptors, helix II is shifted out 2 Å (purple helix).

(C–E) The interaction network of position 3.28 of CB₁ (K192), LPA₁ (R124), and S1P₁ (R120). Polar interactions are represented by black dashed lines. (C) CB₁ is shown in gray cartoon, AM6538 is shown in green sticks and the key residues are shown in blue sticks; (D) LPA₁ is shown in gray cartoon, ONO-9780307 is shown in purple-blue sticks and the key residues are shown in cyan sticks; (E) S1P₁ is shown in gray cartoon, ML056 is shown in orange sticks and the key residues are shown in pink sticks.

See also Figure S5.

positions of the three receptors, AM6538 lies more horizontally than the ligands in LPA₁ and S1P₁, with arm 1 inserted deeper into the side pocket (Figure 4A). Consistently, the N-terminal loop in CB₁ is positioned deeper into the binding pocket compared to the N-terminal helices of LPA₁ and S1P₁, which are both positioned as a cap on their respective ligand binding pockets. As a consequence, helix I of CB₁ is pushed outward ~7 Å relative to LPA₁ and S1P₁ by arm 2, opening a wider gap between helices I and VII than what was observed in LPA₁ and S1P₁ (Figure 4A). Moreover, helix II and ECL1 change their conformation in CB₁, with helix II shifting 2 Å further from the binding pocket compared with LPA₁ and S1P₁, and ECL1 changing from a short helical region in LPA₁ and S1P₁ to a loop in CB₁ (Figure 4B). These conformational changes effectively enlarge the binding pocket of

CB₁, allowing access to the re-entrant N-terminal loop, and contribute to the extensive surface area and multiple sub-pockets associated with CB₁. Finally, the ECL3 region of CB₁ differs from that of its related receptors by a three helical turn extension of helix VII, which increases the rigidity and presumably decreases the flexibility of this loop region in CB₁ (Figure 4A).

The arrangement of Lys192^{3.28} in CB₁ is unique when compared with its equivalent residue Arg^{3.28} in LPA₁ and S1P₁. In LPA₁ and S1P₁, Arg^{3.28} points into the binding pocket forming a strong interaction with the phosphate head group of the ligands (Figures 4D and 4E); it is stabilized by the negatively charged or polar residue 3.29 (Gln125 in LPA₁ and Glu121 in S1P₁). However, in CB₁ the environment near Leu193^{3.29} and the ligand is hydrophobic, thus, it is energetically favorable for the positively

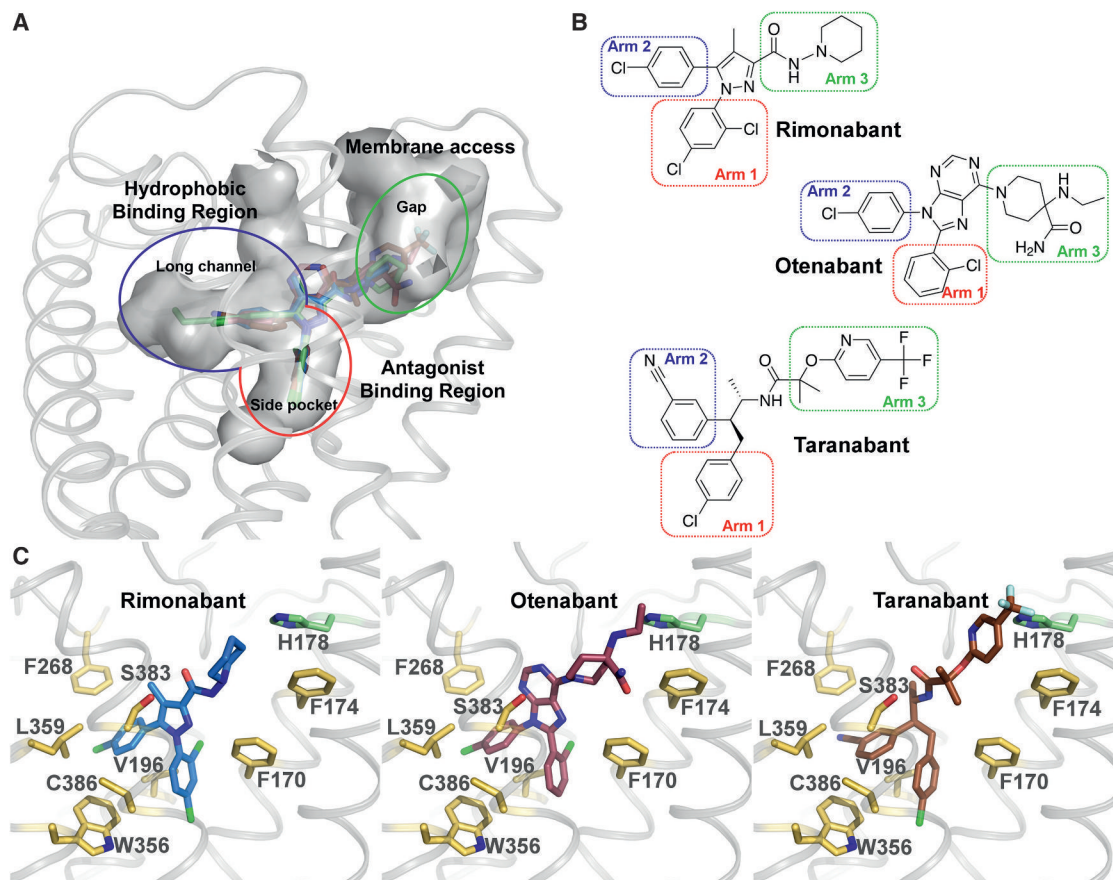


Figure 5. Docking of Different Antagonists in the CB₁ Crystal Structure

(A) CB₁ binding pocket with rimonabant (blue sticks), otenabant (raspberry sticks), and taranabant (brown sticks) are shown in gray surface representation. (B) Chemical structures of rimonabant, otenabant, and taranabant. The red/blue/green rectangles highlight previously described “arms” of the molecule termed arm 1/arm 2/arm 3 (see Figure 3C). (C) Predicted binding modes of rimonabant (blue sticks), otenabant (raspberry sticks), and taranabant (brown sticks) with CB₁. The interacting residues are shown in yellow sticks, and H178 is shown in green sticks. See also Figure S4 and Table S2.

charged Lys192^{3,28} to point away from the binding pocket (Figure 4C). In fact, Lys192^{3,28} functions as a stabilization anchor by forming a salt bridge/hydrogen bond network instead of directly interacting with the ligand as Arg^{3,28} in LPA₁ and S1P₁. Another major difference of the endogenous ligands of CB₁ (anandamide, 2-AG), LPA₁ (LPA) and S1P₁ (S1P) is the head group. The heads of LPA₁ and S1P₁ ligands are negatively charged phosphate groups, while the heads of CB₁ ligands are neutral. In fact, phosphorylation of the head group of CB₁ ligands anandamide and 2-AG would transform them into ligands of LPA₁ (Chrencik et al., 2015).

Binding Modes of Representative Antagonists to CB₁

We performed docking of AM6538 and three CB₁ antagonists: rimonabant, otenabant, and taranabant (Figure 5, Table S2), which represent diverse scaffolds of CB₁ antagonists used in clinical trials. For each compound, the top one ranked pose was used for analysis. The docking pose of AM6538 reproduces the crystallographic pose (Figure S4A), with a root mean

square deviation (RMSD) of 0.55 Å. For the three antagonists, their first-ranked docking poses resemble that of AM6538 in the crystal structure, with three arms that fit into the three branches of the binding pocket, as described in the AM6538 binding mode (Figure 5A). As denoted for AM6538, the arms in the side pocket, long channel, and gap are termed arm 1, arm 2, and arm 3 (Figure 5B). The scaffolds of arm 1 and arm 2 of the three antagonists are very similar to each other, and so are the docking poses. The biggest difference is from arm 3, yet they are all quite bulky, which we speculate is the signature for CB₁ antagonists. Taranabant has the highest affinity with CB₁ among the three ligands (Table S2). It does not have a rigid aromatic ring at the core, allowing its arm 2 and arm 3 to have more freedom to form stronger interactions with surrounding residues (Figure 5C). Mutagenesis of Phe170^{2,57}Ala or Phe174^{2,61}Ala results in dramatically reduced functional affinity for rimonabant and AM6538, while neither mutation alters the potency of the agonist, CP55,940. More conservative mutations to tryptophan (Phe170^{2,57}Trp or Phe174^{2,61}Trp) at either site have no

appreciable effect on antagonist binding, further supporting the importance of the hydrophobic interactions at this site (Figures S4G and S4H). In addition, we performed 50 ns MD simulations to visually assess the predicted ligand-receptor interactions, starting from the docking poses. The RMSD values of AM6538, rimonabant, and otenabant are about 1.4 Å. For taranabant, the value is larger (about 3 Å), in accordance with its lack of the core aromatic ring (Figures S4C–S4F). The predicted interactions of the ligands are conserved during the short MD simulations. The central structure of AM6538 in MD simulation is closest to the docking pose.

Docking Poses of Representative Agonists of CB₁

Although the crystal structure we present is in the inactive state, we are able to investigate how representative agonists likely bind to the orthosteric pocket of CB₁ by integrating molecular docking, mutagenesis, and SAR data (Ahn et al., 2009; Aung et al., 2000; Bertalovitz et al., 2010). Six CB₁ agonists (Table S2)—the classical cannabinoids, THC and CP55,940; the endogenous agonists, anandamide and 2-AG; and indole derivatives, JWH-018 and WIN 55,212-2—were selected for docking studies. These agonists mainly interact with ECL2, N-terminal loop, helices III, VI, and VII, and they do not interact with helices I and II. Their predicted binding modes are shown in Figure 6. For THC and CP55,940, the rings reside between the N-terminal loop and ECL2, forming π - π interactions with Phe268^{ECL2} (Figures 6A and 6B), and the carbon chains extend into the long channel and interact with residues from helices III, VI, and VII. CP55,940 does not interact with helices I and II, which is supported by our mutagenesis studies: mutations on Phe170 and Phe174 (Phe170^{2,57}Ala/Trp or Phe174^{2,61}Ala/Trp) do not alter the potency of CP55,940 (Figure S4G). Anandamide and 2-AG were predicted to adopt a C-shaped conformation and occupy a similar space as THC (Figures 6C and 6D). Their hydrophilic heads are sandwiched between the N-terminal loop and ECL2, and their long aliphatic tails extend deeper into the long channel. JWH-018 and WIN 55,212-2, however, are predicted to bind deeper in the pocket than THC (Figures 6E and 6F). Both the indole rings and naphthalene rings form π - π interactions with Phe268^{ECL2}. The *N*-substituents reach the end of the long channel and interact with helix V. The binding mode of JWH-018 and WIN 55,212-2 is supported by mutations on helix V (McAllister et al., 2003; Song et al., 1999) and SAR study of *N*-alkyl chain length (Aung et al., 2000). Notably, all of the agonists interact with Phe268^{ECL2} and Phe379^{7,35} in our docking poses, which is consistent with mutagenesis studies on ECL2 (Ahn et al., 2009) and Phe379^{7,35} (Figure S4I). Any of the following individual mutations—Phe268^{ECL2}Trp, Pro269^{ECL2}Ala, His270^{ECL2}Ala, Ile271^{ECL2}Ala, or breaking of the disulfide bond Cys257-Cys264 on ECL2—dramatically decreased the binding of all three different types of agonists, yet had little impact on antagonist binding (Ahn et al., 2009). The prominent role of Phe379^{7,35} to facilitate CP55,940 functional affinity is supported by the loss of CP55,940 potency with the Phe379^{7,35} Trp mutation and an even greater loss of agonist activity with the Phe379^{7,35}Ala mutation (Figure S4I). While these mutations dramatically affected CP55,940 agonism, they had no impact on antagonist/inverse agonist (AM6538 or rimonabant) displacement of agonist (Fig-

ure S4J), further supporting the predicted binding pose of CP55,940 (Figure 6G).

DISCUSSION

The ligand used in this study, AM6538, was designed with the aim of stabilizing the ligand-CB₁ receptor complex and promoting CB₁ crystal formation. For this purpose, our approach focused on the use of the substituted biarylpyrazole chemotype based on the structure of rimonabant for obtaining highly utilized proprietary probes. Within this class of compounds, a slight modification of the chemotype led to AM251, a commonly used CB₁ inverse agonist/antagonist (Lan et al., 1999), and AM281, a CB₁ antagonist whose radiolabeling produced the first in vivo imaging agent for labeling CB₁ in nonhuman primates and humans (Berding et al., 2004; Gatley et al., 1998). AM6538 acts as a CB₁ stabilizing antagonist, and the ligand was effective in allowing structural determination of CB₁. AM6538 reacts as an intact molecule with no crystallographic evidence of covalent binding while at the same time not revealing the location of the terminal nitrate group in the X-ray structure. While radioligand binding studies demonstrate that AM6538 binds tightly to the receptor, the precise mode of action for stabilizing the receptor remains to be determined.

To date, there remains considerable controversy with regards to CB₁ ligands and their diverse medical applications. This is likely due in part to the wide availability and illicit nature of the most famous CB₁ pharmaceutical, marijuana. Marijuana has been widely used across many cultures to treat multiple conditions, with most of the results relayed via oral tradition, anecdote, political position, or with economic interest preventing an objective interpretation of therapeutic efficacy in any particular disease state (Whiting et al., 2015). The medicinal marijuana movement continues to gain support, and clinical trials with well-defined endpoints will continue to educate the medical and pharmaceutical communities regarding the relative benefits and drawbacks of targeting this physiological system. The crystal structure of CB₁ in complex with AM6538 reveals an expansive and complicated binding pocket network consisting of multiple sub-pockets and channels to various regions of the receptor. The three-arm ligand structure is common to CB₁ antagonists and inverse agonists and may be critical for stabilizing the inherent flexibility of the native receptor in a non-signaling conformation. Combining the 3D structure of CB₁ and molecular docking of the three representative antagonists, which act as inverse agonists, rimonabant, otenabant, and taranabant, the role of each arm is clearly illustrated. Arm 1 is crucial for high affinity binding, while arm 2 extends into the long channel. An aliphatic or aromatic ring on arm 3 pushes on helices I and II, causing them to bend outward, and potentially modulating the pharmacological signaling state of the receptor. Together with structure and modeling data, we speculate that a bulky ring on arm 3 is essential for CB₁ antagonism. This observation provides direction for designing more diverse compounds as we have learned that variable chemical groups are tolerated at the core of arm 3, a long carbon chain can be added at the *para*-position of the phenyl ring in arm 2. For example, introduction of a 4-cyanobut-1-ynyl at arm 2

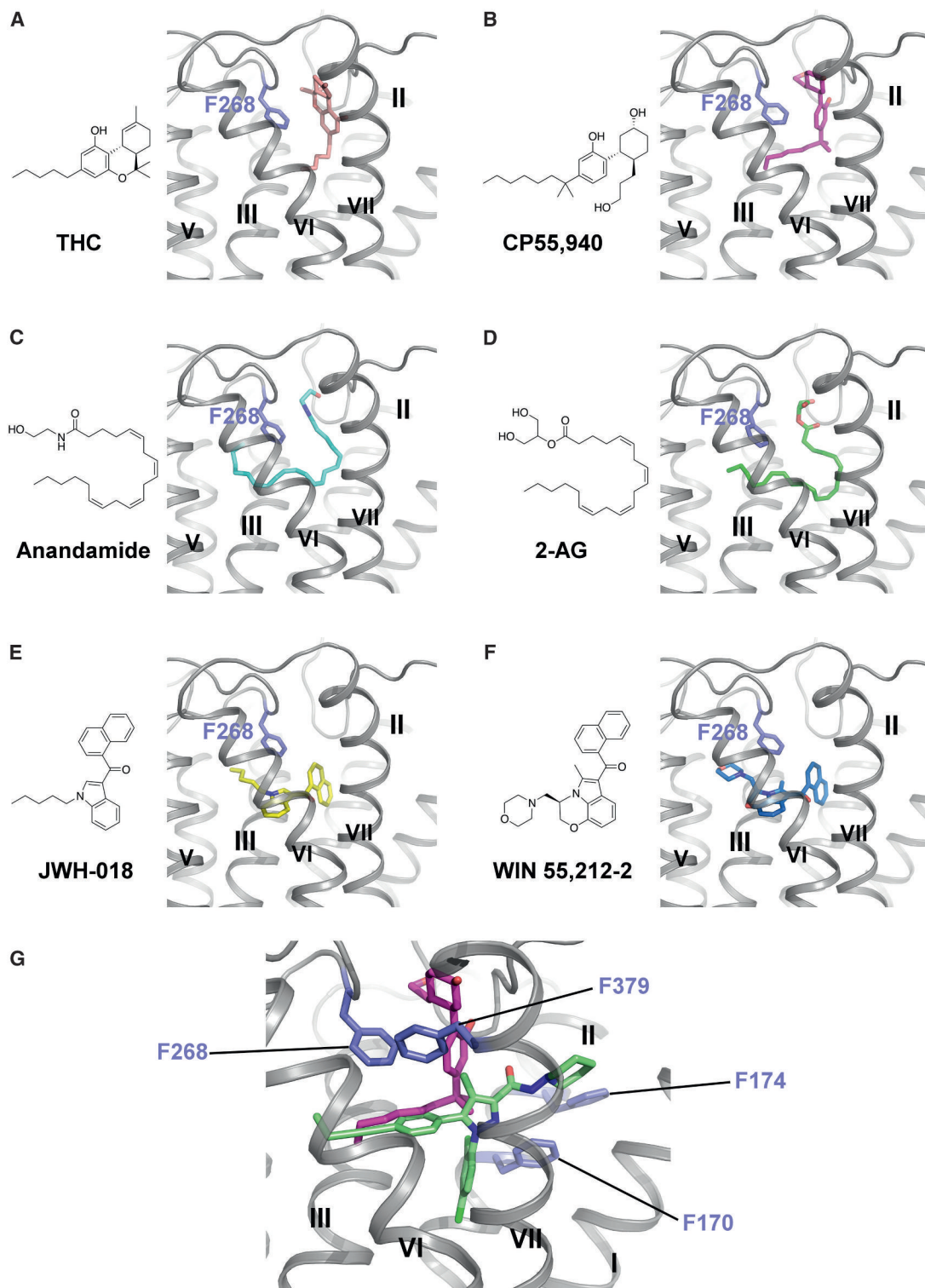


Figure 6. Docking Poses of Different Cannabinoid Receptor Agonists

(A–F) Chemical structures and predicted binding poses of THC (pink sticks) (A), CP55,940 (magenta sticks) (B), Anandamide (cyan sticks) (C), 2-AG (green sticks) (D), JWH-018 (yellow sticks) (E), and WIN 55,212-2 (blue sticks) (F).

(G) Zoom-in view of predicted CP55,940 binding pose. CP55,940 is shown in magenta sticks, AM6538 is shown in green sticks, and the key residues are shown in slate sticks.

See also Figure S4 and Table S2.

produces AM6545 (Table S2), a high-affinity CB₁ neutral antagonist (Tam et al., 2010).

Understanding the nuances of CB₁ binding and activation is important, as human use has noted differences between the phytocannabinoid agonist THC and the synthetic cannabinoid constituents of “Spice” or “K-2” such as JWH-018. In general, cannabinoid agonists are routinely abused substances; yet, while overdose of THC/marijuana has not been documented, there have been cases of severe and even deadly responses to the ingestion of such synthetic mixtures resulting in federal restrictions by many countries, including the US. It remains unclear as to why THC can have such a high safety margin, while the synthetic cannabinoid constituents can prove toxic with varying severities of serious side effects (Hermanns-Clausen et al., 2013). Going forward, the study of cannabinoids present in *Cannabis sativa* will provide clues to its high efficacy and safety margins and may continue to inspire a rich source of pharmacologically refined compounds and novel therapeutics; the utility of the crystal structure may provide inspiration for drug design toward refining efficacy and avoiding adverse events.

STAR★METHODS

Detailed methods are provided in the online version of this paper and include the following:

- KEY RESOURCES TABLE
- CONTACT FOR REAGENT AND RESOURCE SHARING
- EXPERIMENTAL MODEL AND SUBJECT DETAILS
 - Mice
- METHOD DETAILS
 - Synthesis and Characterization of AM6538
 - Rational Design of Thermostabilizing Mutations of CB₁
 - Protein Engineering for Structure Determination
 - Protein Expression in Mammalian Expression System
 - Protein Purification
 - Lipidic Cubic Phase Crystallization of CB₁-AM6538 Complex
 - Data Collection and Structure Determination
 - Quantum Mechanical Optimization of AM6538
 - Docking Simulations of CB₁ Ligands
 - Molecular Dynamics Simulation of CB₁ in Complex with AM6538 and Representative Antagonists
 - Radioligand Binding Assay
 - WT and Mutant hCB₁-CHO Cell Line Generation for Functional Studies
 - Functional Analysis Studies
 - Protein Stability Assays
 - Affinity Mass Spectrometry Analysis of AM6538
- QUANTIFICATION AND STATISTICAL ANALYSIS
- DATA AND SOFTWARE AVAILABILITY
 - Data Resources

SUPPLEMENTAL INFORMATION

Supplemental Information includes five figures and two tables and can be found with this article online at <http://dx.doi.org/10.1016/j.cell.2016.10.004>.

AUTHOR CONTRIBUTIONS

Conceptualization, L.M.B., A.M., R.C.S., Z.-J.L.; Methodology, K.V., A.M. J.-H.H., R.B.L., E.L.S., B.W., Q.Z.; Validation, G.W.H.; Formal Analysis, T.H., M.P., L.Q., G.W.H., Y.W., S.Z., W.S., S.L., R.B.L., E.L.S., N.Z., B.W., Q.Z., M.A.H., L.M.B., A.M., Z.-J.L.; Investigation, T.H., K.V., L.Q., G.W.H., W.S., S.L., A.K., R.B.L., E.L.S., J.-H.H., N.Z., H.Z., I.K.; Writing – Original Draft, T.H.; Writing, Reviewing & Editing, T.H., K.V., Y.W., S.Z., W.S., I.K., M.A.H., L.M.B., A.M., R.C.S., Z.-J.L.; Visualization, T.H., M.P., M.A.H.; Supervision, L.M.B., A.M., R.C.S., Z.-J.L.

ACKNOWLEDGMENTS

This work was supported by the Ministry of Science and Technology of China grants 2014CB910400 and 2015CB910104 and The National Nature Science Foundation of China grant 31330019 to (Z.-J.L.); National Institutes of Health grants P01DA009158 (A.M. and L.M.B.), R37DA023142 (A.M.), and R01AI118985 (I.K.); and NSF grants. We thank the Shanghai Municipal Government, ShanghaiTech University, and GPCR Consortium for financial support. The synchrotron radiation experiments were performed at the BL41XU of Spring-8 with approval of the Japan Synchrotron Radiation Research Institute (JASRI) (proposal numbers 2015B1031 and 2016A2731), GM/CA@APS of Argonne National Lab, which is supported by the U.S. Department of Energy, Office of Science, Office of Basic Energy Sciences under contract number DE-AC02-06CH11357, and beamline BL17U1 (Shanghai Synchrotron Radiation Facility [SSRF]). We thank the Cloning, Cell Expression, and Protein Purification Core Facilities of iHuman Institute for their support. We thank A. Walker for assistance with the manuscript; we also thank F. Xu, V. Cherezov, V. Katritch, A. Ishchenko, H. Tao, J. Cheng, D. Liu, W. Zhong, and W. Liu for helpful discussions. The NIDA Drug supply program provided standards used in this study. A.M. is a founder of MAKScientific, LLC, a research company engaged in discovering medications for metabolic disorders with an interest in CB₁. R.C.S. is a board member and shareholder with Birdrock Bio, an antibody therapeutic company with an interest in CB₁.

Received: July 15, 2016

Revised: September 6, 2016

Accepted: October 3, 2016

Published: October 20, 2016

SUPPORTING CITATIONS

The following references appear in the Supplemental Information: Ben-Shabat et al., 1998; Felder et al., 1995; Fong et al., 2007; Griffith et al., 2009; Kuster et al., 1993; Showalter et al., 1996; Wiley et al., 1998.

REFERENCES

- Abagyan, R., and Totrov, M. (1994). Biased probability Monte Carlo conformational searches and electrostatic calculations for peptides and proteins. *J. Mol. Biol.* 235, 983–1002.
- Abraham, M.J., Murtola, T., Schulz, R., Páll, S., Smith, J.C., Hess, B., and Lindahl, E. (2015). GROMACS: High performance molecular simulations through multi-level parallelism from laptops to supercomputers. *SoftwareX* 1–2, 19–25.
- Adams, R., MacKenzie, S., Jr., and Loewe, S. (1948). Tetrahydrocannabinol homologs with double branched alkyl groups in the 3-position. *J. Am. Chem. Soc.* 70, 664–668.
- Adams, P.D., Afonine, P.V., Bunkóczi, G., Chen, V.B., Davis, I.W., Echols, N., Headd, J.J., Hung, L.W., Kapral, G.J., Grosse-Kunstleve, R.W., et al. (2010). PHENIX: a comprehensive Python-based system for macromolecular structure solution. *Acta Crystallogr. D Biol. Crystallogr.* 66, 213–221.
- Ahn, K.H., Bertalovitz, A.C., Mierke, D.F., and Kendall, D.A. (2009). Dual role of the second extracellular loop of the cannabinoid receptor 1: ligand binding and receptor localization. *Mol. Pharmacol.* 76, 833–842.

- Alexandrov, A.I., Mileni, M., Chien, E.Y., Hanson, M.A., and Stevens, R.C. (2008). Microscale fluorescent thermal stability assay for membrane proteins. *Structure* 16, 351–359.
- Andersson, H., D'Antona, A.M., Kendall, D.A., Von Heijne, G., and Chin, C.N. (2003). Membrane assembly of the cannabinoid receptor 1: impact of a long N-terminal tail. *Mol. Pharmacol.* 64, 570–577.
- Aung, M.M., Griffin, G., Huffman, J.W., Wu, M., Keel, C., Yang, B., Showalter, V.M., Abood, M.E., and Martin, B.R. (2000). Influence of the N-1 alkyl chain length of cannabimimetic indoles upon CB(1) and CB(2) receptor binding. *Drug Alcohol Depend.* 60, 133–140.
- Ballesteros, J.A., and Weinstein, H. (1995). Integrated methods for the construction of three-dimensional models and computational probing of structure-function relations in G protein-coupled receptors. In *Methods in Neurosciences*, C.S. Stuart, ed. (Academic Press), pp. 366–428.
- Ben-Shabat, S., Fride, E., Sheskin, T., Tamiri, T., Rhee, M.H., Vogel, Z., Bisogno, T., De Petrocellis, L., Di Marzo, V., and Mechoulam, R. (1998). An entourage effect: inactive endogenous fatty acid glycerol esters enhance 2-arachidonoyl-glycerol cannabinoid activity. *Eur. J. Pharmacol.* 353, 23–31.
- Berding, G., Müller-Vahl, K., Schneider, U., Gielow, P., Fitschen, J., Stuhmann, M., Harke, H., Buchert, R., Donnerstag, F., Hofmann, M., et al. (2004). [123I]AM281 single-photon emission computed tomography imaging of central cannabinoid CB1 receptors before and after Delta9-tetrahydrocannabinol therapy and whole-body scanning for assessment of radiation dose in tourette patients. *Biol. Psychiatry* 55, 904–915.
- Bertalovitz, A.C., Ahn, K.H., and Kendall, D.A. (2010). Ligand Binding Sensitivity of the Extracellular Loop Two of the Cannabinoid Receptor 1. *Drug Dev. Res.* 71, 404–411.
- Black, M.D., Stevens, R.J., Rogacki, N., Featherstone, R.E., Senyah, Y., Giardino, O., Borowsky, B., Stemmelin, J., Cohen, C., Pichat, P., et al. (2011). AVE1625, a cannabinoid CB1 receptor antagonist, as a co-treatment with antipsychotics for schizophrenia: improvement in cognitive function and reduction of antipsychotic-side effects in rodents. *Psychopharmacology (Berl.)* 215, 149–163.
- Bohn, L.M., Zhou, L., and Ho, J.H. (2015). Approaches to Assess Functional Selectivity in GPCRs: Evaluating G Protein Signaling in an Endogenous Environment. *Methods Mol. Biol.* 1335, 177–189.
- Bramblett, R.D., Panu, A.M., Ballesteros, J.A., and Reggio, P.H. (1995). Construction of a 3D model of the cannabinoid CB1 receptor: determination of helix ends and helix orientation. *Life Sci.* 56, 1971–1982.
- Caffrey, M., and Cherezov, V. (2009). Crystallizing membrane proteins using lipidic mesophases. *Nat. Protoc.* 4, 706–731.
- Cherezov, V., Hanson, M.A., Griffith, M.T., Hilgart, M.C., Sanishvili, R., Nagarajan, V., Stepanov, S., Fischetti, R.F., Kuhn, P., and Stevens, R.C. (2009). Rastering strategy for screening and centring of microcrystal samples of human membrane proteins with a sub-10 microm size X-ray synchrotron beam. *J. R. Soc. Interface* 6 (Suppl 5), S587–S597.
- Chin, C.N., Lucas-Lenard, J., Abadji, V., and Kendall, D.A. (1998). Ligand binding and modulation of cyclic AMP levels depend on the chemical nature of residue 192 of the human cannabinoid receptor 1. *J. Neurochem.* 70, 366–373.
- Chrencik, J.E., Roth, C.B., Terakado, M., Kurata, H., Omi, R., Kihara, Y., Warshaviak, D., Nakade, S., Asmar-Rovira, G., Mileni, M., et al. (2015). Crystal Structure of Antagonist Bound Human Lysophosphatidic Acid Receptor 1. *Cell* 161, 1633–1643.
- Chun, E., Thompson, A.A., Liu, W., Roth, C.B., Griffith, M.T., Katritch, V., Kunken, J., Xu, F., Cherezov, V., Hanson, M.A., and Stevens, R.C. (2012). Fusion partner toolchest for the stabilization and crystallization of G protein-coupled receptors. *Structure* 20, 967–976.
- Collaborative Computational Project, Number 4 (1994). The CCP4 suite: programs for protein crystallography. *Acta Crystallogr. D Biol. Crystallogr.* 50, 760–763.
- Cravatt, B.F., and Lichtman, A.H. (2004). The endogenous cannabinoid system and its role in nociceptive behavior. *J. Neurobiol.* 61, 149–160.
- D'Antona, A.M., Ahn, K.H., and Kendall, D.A. (2006). Mutations of CB1 T210 produce active and inactive receptor forms: correlations with ligand affinity, receptor stability, and cellular localization. *Biochemistry* 45, 5606–5617.
- Devane, W.A., Dysarz, F.A., 3rd, Johnson, M.R., Melvin, L.S., and Howlett, A.C. (1988). Determination and characterization of a cannabinoid receptor in rat brain. *Mol. Pharmacol.* 34, 605–613.
- Devane, W.A., Hanus, L., Breuer, A., Pertwee, R.G., Stevenson, L.A., Griffin, G., Gibson, D., Mandelbaum, A., Etinger, A., and Mechoulam, R. (1992). Isolation and structure of a brain constituent that binds to the cannabinoid receptor. *Science* 258, 1946–1949.
- Emsley, P., Lohkamp, B., Scott, W.G., and Cowtan, K. (2010). Features and development of Coot. *Acta Crystallogr. D Biol. Crystallogr.* 66, 486–501.
- Fay, J.F., and Farrens, D.L. (2013). The membrane proximal region of the cannabinoid receptor CB1 N-terminus can allosterically modulate ligand affinity. *Biochemistry* 52, 8286–8294.
- Fay, J.F., Dunham, T.D., and Farrens, D.L. (2005). Cysteine residues in the human cannabinoid receptor: only C257 and C264 are required for a functional receptor, and steric bulk at C386 impairs antagonist SR141716A binding. *Biochemistry* 44, 8757–8769.
- Felder, E., and Schrott-Fischer, A. (1995). Quantitative evaluation of myelinated nerve fibres and hair cells in cochleae of humans with age-related high-tone hearing loss. *Hear. Res.* 91, 19–32.
- Felder, C.C., Joyce, K.E., Briley, E.M., Mansouri, J., Mackie, K., Blond, O., Lai, Y., Ma, A.L., and Mitchell, R.L. (1995). Comparison of the pharmacology and signal transduction of the human cannabinoid CB1 and CB2 receptors. *Mol. Pharmacol.* 48, 443–450.
- Feller, S.E., and MacKerell, A.D. (2000). An improved empirical potential energy function for molecular simulations of phospholipids. *J. Phys. Chem. B* 104, 7510–7515.
- Fernández-Ruiz, J., Romero, J., and Ramos, J.A. (2015). Endocannabinoids and Neurodegenerative Disorders: Parkinson's Disease, Huntington's Chorea, Alzheimer's Disease, and Others. *Handbook Exp. Pharmacol.* 231, 233–259.
- Fong, T.M., Guan, X.M., Marsh, D.J., Shen, C.P., Stribling, D.S., Rosko, K.M., Lao, J., Yu, H., Feng, Y., Xiao, J.C., et al. (2007). Antiobesity efficacy of a novel cannabinoid-1 receptor inverse agonist, N-[[1S,2S]-3-(4-chlorophenyl)-2-(3-cyanophenyl)-1-methylpropyl]-2-methyl-2-[[5-(trifluoromethyl)pyridin-2-yl]oxy]propanamide (MK-0364), in rodents. *J. Pharmacol. Exp. Ther.* 321, 1013–1022.
- Friesner, R.A., Banks, J.L., Murphy, R.B., Halgren, T.A., Klicic, J.J., Mainz, D.T., Repasky, M.P., Knoll, E.H., Shelley, M., Perry, J.K., et al. (2004). Glide: a new approach for rapid, accurate docking and scoring. 1. Method and assessment of docking accuracy. *J. Med. Chem.* 47, 1739–1749.
- Friesner, R.A., Murphy, R.B., Repasky, M.P., Frye, L.L., Greenwood, J.R., Halgren, T.A., Sanschagrin, P.C., and Mainz, D.T. (2006). Extra precision glide: docking and scoring incorporating a model of hydrophobic enclosure for protein-ligand complexes. *J. Med. Chem.* 49, 6177–6196.
- Gaoni, Y., and Mechoulam, R. (1964). Isolation, Structure, and Partial Synthesis of an Active Constituent of Hashish. *J. Am. Chem. Soc.* 86, 1646–1647.
- Gatley, S.J., Lan, R., Volkow, N.D., Pappas, N., King, P., Wong, C.T., Gifford, A.N., Pyatt, B., Dewey, S.L., and Makriyannis, A. (1998). Imaging the brain marijuana receptor: development of a radioligand that binds to cannabinoid CB1 receptors in vivo. *J. Neurochem.* 70, 417–423.
- Ghosh, R., Todd, A.R., and Wilkinson, S. (1940). 206. Cannabis indica. Part IV. The synthesis of some tetrahydrodibenzopyran derivatives. *J. Am. Chem. Soc.*, 1121–1125.
- Griffith, D.A., Hadcock, J.R., Black, S.C., Iredale, P.A., Carpino, P.A., DaSilva-Jardine, P., Day, R., DiBrino, J., Dow, R.L., Landis, M.S., et al. (2009). Discovery of 1-[9-(4-chlorophenyl)-8-(2-chlorophenyl)-9H-purin-6-yl]-4-ethylaminopiperidine-4-carboxylic acid amide hydrochloride (CP-945,598), a novel, potent, and selective cannabinoid type 1 receptor antagonist. *J. Med. Chem.* 52, 234–237.
- Guo, Y., Abadji, V., Morse, K.L., Fournier, D.J., Li, X., and Makriyannis, A. (1994). (-)-11-Hydroxy-7'-isothiocyanato-1',1'-dimethylheptyl-delta 8-THC: a

- novel, high-affinity irreversible probe for the cannabinoid receptor in the brain. *J. Med. Chem.* **37**, 3867–3870.
- Halgren, T.A., Murphy, R.B., Friesner, R.A., Beard, H.S., Frye, L.L., Pollard, W.T., and Banks, J.L. (2004). Glide: a new approach for rapid, accurate docking and scoring. 2. Enrichment factors in database screening. *J. Med. Chem.* **47**, 1750–1759.
- Hanson, M.A., Roth, C.B., Jo, E., Griffith, M.T., Scott, F.L., Reinhart, G., Desale, H., Clemons, B., Cahalan, S.M., Schuerer, S.C., et al. (2012). Crystal structure of a lipid G protein-coupled receptor. *Science* **335**, 851–855.
- Herkenham, M., Lynn, A.B., Little, M.D., Johnson, M.R., Melvin, L.S., de Costa, B.R., and Rice, K.C. (1990). Cannabinoid receptor localization in brain. *Proc. Natl. Acad. Sci. USA* **87**, 1932–1936.
- Hermanns-Clausen, M., Kneisel, S., Szabo, B., and Auwärter, V. (2013). Acute toxicity due to the confirmed consumption of synthetic cannabinoids: clinical and laboratory findings. *Addiction* **108**, 534–544.
- Howlett, A.C. (1985). Cannabinoid inhibition of adenylate cyclase. *Biochemistry of the response in neuroblastoma cell membranes.* *Mol. Pharmacol.* **27**, 429–436.
- Hurst, D.P., Lynch, D.L., Barnett-Norris, J., Hyatt, S.M., Seltzman, H.H., Zhong, M., Song, Z.H., Nie, J., Lewis, D., and Reggio, P.H. (2002). N-(piperidin-1-yl)-5-(4-chlorophenyl)-1-(2,4-dichlorophenyl)-4-methyl-1H-pyrazole-3-carboxamide (SR141716A) interaction with LYS 3.28(192) is crucial for its inverse agonism at the cannabinoid CB1 receptor. *Mol. Pharmacol.* **62**, 1274–1287.
- Isberg, V., Mordalski, S., Munk, C., Rataj, K., Harpsøe, K., Hauser, A.S., Vroiling, B., Bojarski, A.J., Vriend, G., and Gloriam, D.E. (2016). GPCRdb: an information system for G protein-coupled receptors. *Nucleic Acids Res.* **44** (D1), D356–D364.
- Janero, D.R., and Makriyannis, A. (2009). Cannabinoid receptor antagonists: pharmacological opportunities, clinical experience, and translational prognosis. *Expert Opin. Emerg. Drugs* **14**, 43–65.
- Janero, D.R., Yaddanapudi, S., Zvonok, N., Subramanian, K.V., Shukla, V.G., Stahl, E., Zhou, L., Hurst, D., Wager-Miller, J., Bohn, L.M., et al. (2015). Molecular-interaction and signaling profiles of AM3677, a novel covalent agonist selective for the cannabinoid 1 receptor. *ACS Chem. Neurosci.* **6**, 1400–1410.
- Jin, W., Brown, S., Roche, J.P., Hsieh, C., Celver, J.P., Kovoor, A., Chavkin, C., and Mackie, K. (1999). Distinct domains of the CB1 cannabinoid receptor mediate desensitization and internalization. *J. Neurosci.* **19**, 3773–3780.
- Kabsch, W. (2010). Xds. *Acta Crystallogr. D Biol. Crystallogr.* **66**, 125–132.
- Kandasamy, S.K., and Larson, R.G. (2006). Molecular dynamics simulations of model trans-membrane peptides in lipid bilayers: a systematic investigation of hydrophobic mismatch. *Biophys. J.* **90**, 2326–2343.
- Katoh, K., and Standley, D.M. (2013). MAFFT multiple sequence alignment software version 7: improvements in performance and usability. *Mol. Biol. Evol.* **30**, 772–780.
- Kuster, J.E., Stevenson, J.I., Ward, S.J., D'Ambra, T.E., and Haycock, D.A. (1993). Aminoalkylindole binding in rat cerebellum: selective displacement by natural and synthetic cannabinoids. *J. Pharmacol. Exp. Ther.* **264**, 1352–1363.
- Lan, R., Liu, Q., Fan, P., Lin, S., Fernando, S.R., McCallion, D., Pertwee, R., and Makriyannis, A. (1999). Structure-activity relationships of pyrazole derivatives as cannabinoid receptor antagonists. *J. Med. Chem.* **42**, 769–776.
- Lange, J.H., and Kruse, C.G. (2005). Keynote review: Medicinal chemistry strategies to CB1 cannabinoid receptor antagonists. *Drug Discov. Today* **10**, 693–702.
- Lemberger, L. (1980). Potential therapeutic usefulness of marijuana. *Annu. Rev. Pharmacol. Toxicol.* **20**, 151–172.
- Li, H.-L. (1973). An archaeological and historical account of cannabis in China. *Econ. Bot.* **28**, 437–448.
- Li, C., Xu, W., Vadivel, S.K., Fan, P., and Makriyannis, A. (2005). High affinity electrophilic and photoactivatable covalent endocannabinoid probes for the CB1 receptor. *J. Med. Chem.* **48**, 6423–6429.
- Lv, X., Liu, J., Shi, Q., Tan, Q., Wu, D., Skinner, J.J., Walker, A.L., Zhao, L., Gu, X., Chen, N., et al. (2016). In vitro expression and analysis of the 826 human G protein-coupled receptors. *Protein Cell* **7**, 325–337.
- MacKerell, A.D., Bashford, D., Bellott, M., Dunbrack, R.L., Evanseck, J.D., Field, M.J., Fischer, S., Gao, J., Guo, H., Ha, S., et al. (1998). All-atom empirical potential for molecular modeling and dynamics studies of proteins. *J. Phys. Chem. B* **102**, 3586–3616.
- Mackereell, A.D., Jr., Feig, M., and Brooks, C.L., 3rd. (2004). Extending the treatment of backbone energetics in protein force fields: limitations of gas-phase quantum mechanics in reproducing protein conformational distributions in molecular dynamics simulations. *J. Comput. Chem.* **25**, 1400–1415.
- Makriyannis, A. (2014). 2012 Division of medicinal chemistry award address. Trekking the cannabinoid road: a personal perspective. *J. Med. Chem.* **57**, 3891–3911.
- Makriyannis, A., and Rapaka, R.S. (1990). The molecular basis of cannabinoid activity. *Life Sci.* **47**, 2173–2184.
- Makriyannis, A., and Vemuri, V.K. (April, 2016). Cannabinergic nitrate esters and related analogs. Patent Application US 2016/0096822 A1.
- Mallat, A., Teixeira-Clerc, F., and Lotersztajn, S. (2013). Cannabinoid signaling and liver therapeutics. *J. Hepatol.* **59**, 891–896.
- Matsuda, L.A., Lolait, S.J., Brownstein, M.J., Young, A.C., and Bonner, T.I. (1990). Structure of a cannabinoid receptor and functional expression of the cloned cDNA. *Nature* **346**, 561–564.
- Mavromoustakos, T., Yang, D.P., and Makriyannis, A. (1995). Small angle X-ray diffraction and differential scanning calorimetric studies on O-methyl-(δ)-8-tetrahydrocannabinol and its 5' iodinated derivative in membrane bilayers. *Biochim. Biophys. Acta* **1237**, 183–188.
- Mazier, W., Saucisse, N., Gatta-Cherifi, B., and Cota, D. (2015). The Endocannabinoid System: Pivotal Orchestrator of Obesity and Metabolic Disease. *Trends Endocrinol. Metab.* **26**, 524–537.
- McAllister, S.D., Rizvi, G., Anavi-Goffer, S., Hurst, D.P., Barnett-Norris, J., Lynch, D.L., Reggio, P.H., and Abood, M.E. (2003). An aromatic microdomain at the cannabinoid CB(1) receptor constitutes an agonist/inverse agonist binding region. *J. Med. Chem.* **46**, 5139–5152.
- McCoy, A.J., Grosse-Kunstleve, R.W., Adams, P.D., Winn, M.D., Storoni, L.C., and Read, R.J. (2007). Phaser crystallographic software. *J. Appl. Cryst.* **40**, 658–674.
- Mechoulam, R., Ben-Shabat, S., Hanus, L., Ligumsky, M., Kaminski, N.E., Schatz, A.R., Gopher, A., Almog, S., Martin, B.R., Compton, D.R., et al. (1995). Identification of an endogenous 2-monoglyceride, present in canine gut, that binds to cannabinoid receptors. *Biochem. Pharmacol.* **50**, 83–90.
- Mercier, R.W., Pei, Y., Pandarinathan, L., Janero, D.R., Zhang, J., and Makriyannis, A. (2010). hCB2 ligand-interaction landscape: cysteine residues critical to biarylpyrazole antagonist binding motif and receptor modulation. *Chem. Biol.* **17**, 1132–1142.
- Munro, S., Thomas, K.L., and Abu-Shaar, M. (1993). Molecular characterization of a peripheral receptor for cannabinoids. *Nature* **365**, 61–65.
- Pan, X., Ikeda, S.R., and Lewis, D.L. (1998). SR 141716A acts as an inverse agonist to increase neuronal voltage-dependent Ca²⁺ currents by reversal of tonic CB1 cannabinoid receptor activity. *Mol. Pharmacol.* **54**, 1064–1072.
- Pattison, F.L.M., and Brown, G.M. (1956). Organic Nitrates As Synthetic Intermediates: Preparations Of Nitrates And Some Representative Reactions. *Can. J. Chem.* **34**, 879–884.
- Pertwee, R.G. (2002). Cannabinoids and multiple sclerosis. *Pharmacol. Ther.* **95**, 165–174.
- Picone, R.P., Khanolkar, A.D., Xu, W., Ayotte, L.A., Thakur, G.A., Hurst, D.P., Abood, M.E., Reggio, P.H., Fournier, D.J., and Makriyannis, A. (2005). (δ)-7'-isothiocyanato-11-hydroxy-1',1'-dimethylheptylhexahydrocannabinol (AM841), a high-affinity electrophilic ligand, interacts covalently with a cysteine in helix six and activates the CB1 cannabinoid receptor. *Mol. Pharmacol.* **68**, 1623–1635.
- Pryce, G., and Baker, D. (2015). Endocannabinoids in Multiple Sclerosis and Amyotrophic Lateral Sclerosis. *Handbook Exp. Pharmacol.* **231**, 213–231.

- Razdan, R.K. (1986). Structure-activity relationships in cannabinoids. *Pharmacol. Rev.* **38**, 75–149.
- Rinaldi-Carmona, M., Barth, F., Héaulme, M., Shire, D., Calandra, B., Congy, C., Martinez, S., Maruani, J., Néliat, G., Caput, D., et al. (1994). SR141716A, a potent and selective antagonist of the brain cannabinoid receptor. *FEBS Lett.* **350**, 240–244.
- Robert, X., and Gouet, P. (2014). Deciphering key features in protein structures with the new ENDscript server. *Nucleic Acids Res.* **42**, W320–W324.
- Rubino, T., Zamberletti, E., and Parolaro, D. (2015). Endocannabinoids and Mental Disorders. *Handbook Exp. Pharmacol.* **231**, 261–283.
- Schindler, C.W., Redhi, G.H., Vemuri, K., Makriyannis, A., Le Foll, B., Bergman, J., Goldberg, S.R., and Justinova, Z. (2016). Blockade of Nicotine and Cannabinoid Reinforcement and Relapse by a Cannabinoid CB1-Receptor Neutral Antagonist AM4113 and Inverse Agonist Rimonabant in Squirrel Monkeys. *Neuropsychopharmacology* **41**, 2283–2293.
- Schrödinger (2015a). Glide, version 6.9 (Schrödinger, LLC).
- Schrödinger (2015b). Induced Fit Docking Protocol 2015-4, Glide version 6.4, Prime version 3.7 (Schrödinger, LLC).
- Sherman, W., Day, T., Jacobson, M.P., Friesner, R.A., and Farid, R. (2006). Novel procedure for modeling ligand/receptor induced fit effects. *J. Med. Chem.* **49**, 534–553.
- Shimizu, T. (2009). Lipid mediators in health and disease: enzymes and receptors as therapeutic targets for the regulation of immunity and inflammation. *Annu. Rev. Pharmacol. Toxicol.* **49**, 123–150.
- Showalter, V.M., Compton, D.R., Martin, B.R., and Abood, M.E. (1996). Evaluation of binding in a transfected cell line expressing a peripheral cannabinoid receptor (CB2): identification of cannabinoid receptor subtype selective ligands. *J. Pharmacol. Exp. Ther.* **278**, 989–999.
- Smart, O.S., Womack, T.O., Flensburg, C., Keller, P., Paciorek, W., Sharff, A., Vonrhein, C., and Bricogne, G. (2012). Exploiting structure similarity in refinement: automated NCS and target-structure restraints in BUSTER. *Acta Crystallogr. D Biol. Crystallogr.* **68**, 368–380.
- Song, Z.H., and Bonner, T.I. (1996). A lysine residue of the cannabinoid receptor is critical for receptor recognition by several agonists but not WIN55212-2. *Mol. Pharmacol.* **49**, 891–896.
- Song, Z.H., Slowey, C.A., Hurst, D.P., and Reggio, P.H. (1999). The difference between the CB(1) and CB(2) cannabinoid receptors at position 5.46 is crucial for the selectivity of WIN55212-2 for CB(2). *Mol. Pharmacol.* **56**, 834–840.
- Szymanski, D.W., Papanastasiou, M., Melchior, K., Zvonok, N., Mercier, R.W., Janero, D.R., Thakur, G.A., Cha, S., Wu, B., Karger, B., and Makriyannis, A. (2011). Mass spectrometry-based proteomics of human cannabinoid receptor 2: covalent cysteine 6.47(257)-ligand interaction affording megagonist receptor activation. *J. Proteome Res.* **10**, 4789–4798.
- Tam, J., Vemuri, V.K., Liu, J., Bátkai, S., Mukhopadhyay, B., Godlewski, G., Osei-Hyiaman, D., Ohnuma, S., Ambudkar, S.V., Pickel, J., et al. (2010). Peripheral CB1 cannabinoid receptor blockade improves cardiometabolic risk in mouse models of obesity. *J. Clin. Invest.* **120**, 2953–2966.
- Tang, W., and Prusov, E.V. (2012). Total synthesis of RNA-polymerase inhibitor ripostatin B and 15-deoxyripostatin A. *Angew. Chem. Int. Ed. Engl.* **51**, 3401–3404.
- Whiting, P.F., Wolff, R.F., Deshpande, S., Di Nisio, M., Duffy, S., Hernandez, A.V., Keurentjes, J.C., Lang, S., Misso, K., Ryder, S., et al. (2015). Cannabinoids for Medical Use: A Systematic Review and Meta-analysis. *JAMA* **313**, 2456–2473.
- Wiley, J.L., Compton, D.R., Dai, D., Lainton, J.A., Phillips, M., Huffman, J.W., and Martin, B.R. (1998). Structure-activity relationships of indole- and pyrrole-derived cannabinoids. *J. Pharmacol. Exp. Ther.* **285**, 995–1004.
- Wollner, H.J., Matchett, J.R., Levine, J., and Loewe, S. (1942). Isolation of a Physiologically Active Tetrahydrocannabinol from Cannabis Sativa Resin. *J. Am. Chem. Soc.* **64**, 26–29.
- Yeates, R.A., Laufen, H., and Leitold, M. (1985). The reaction between organic nitrates and sulfhydryl compounds. A possible model system for the activation of organic nitrates. *Mol. Pharmacol.* **28**, 555–559.
- Zoete, V., Cuendet, M.A., Grosdidier, A., and Michielin, O. (2011). Swiss-Param: a fast force field generation tool for small organic molecules. *J. Comput. Chem.* **32**, 2359–2368.

Interspecies Chimerism with Mammalian Pluripotent Stem Cells

Jun Wu,¹ Aida Platero-Luengo,¹ Masahiro Sakurai,¹ Atsushi Sugawara,¹ Maria Antonia Gil,² Takayoshi Yamauchi,¹ Keiichiro Suzuki,¹ Yanina Soledad Bogliotti,³ Cristina Cuello,² Mariana Morales Valencia,¹ Daiji Okumura,^{1,7} Jingping Luo,¹ Marcela Vilariño,³ Inmaculada Parrilla,² Delia Alba Soto,³ Cristina A. Martinez,² Tomoaki Hishida,¹ Sonia Sánchez-Bautista,⁴ M. Llanos Martínez-Martínez,⁴ Huili Wang,³ Alicia Nohalez,² Emi Aizawa,¹ Paloma Martínez-Redondo,¹ Alejandro Ocampo,¹ Pradeep Reddy,¹ Jordi Roca,² Elizabeth A. Maga,³ Concepcion Rodriguez Esteban,¹ W. Travis Berggren,¹ Estrella Nuñez Delicado,⁴ Jeronimo Lajara,⁴ Isabel Guillen,⁵ Pedro Guillen,^{4,5} Josep M. Campistol,⁶ Emilio A. Martínez,² Pablo Juan Ross,³ and Juan Carlos Izpisua Belmonte^{1,8,*}

¹Salk Institute for Biological Studies, 10010 N. Torrey Pines Road, La Jolla, CA 92037, USA

²Department of Animal Medicine and Surgery, University of Murcia Campus de Espinardo, 30100 Murcia, Spain

³Department of Animal Science, University of California Davis, One Shields Avenue, Davis, CA 95616, USA

⁴Universidad Católica San Antonio de Murcia (UCAM) Campus de los Jerónimos, N° 135 Guadalupe 30107 Murcia, Spain

⁵Clinica Centro Fundación Pedro Guillén, Clínica CEMTRO, Avenida Ventisquero de la Condesa 42, 28035 Madrid, Spain

⁶Hospital Clínico de Barcelona-IDIBAPS, Universitat de Barcelona, 08007 Barcelona, Spain

⁷Present address: Graduate School of Agriculture, Department of Advanced Bioscience, Kinki University, 3327-204 Nakamachi, Nara 631-8505, Japan

⁸Lead Contact

*Correspondence: belmonte@salk.edu

<http://dx.doi.org/10.1016/j.cell.2016.12.036>

SUMMARY

Interspecies blastocyst complementation enables organ-specific enrichment of xenogenic pluripotent stem cell (PSC) derivatives. Here, we establish a versatile blastocyst complementation platform based on CRISPR-Cas9-mediated zygote genome editing and show enrichment of rat PSC-derivatives in several tissues of gene-edited organogenesis-disabled mice. Besides gaining insights into species evolution, embryogenesis, and human disease, interspecies blastocyst complementation might allow human organ generation in animals whose organ size, anatomy, and physiology are closer to humans. To date, however, whether human PSCs (hPSCs) can contribute to chimera formation in non-rodent species remains unknown. We systematically evaluate the chimeric competency of several types of hPSCs using a more diversified clade of mammals, the ungulates. We find that naïve hPSCs robustly engraft in both pig and cattle pre-implantation blastocysts but show limited contribution to post-implantation pig embryos. Instead, an intermediate hPSC type exhibits higher degree of chimerism and is able to generate differentiated progenies in post-implantation pig embryos.

INTRODUCTION

Embryonic pluripotency has been captured in vitro at a spectrum of different states, ranging from the naïve state, which reflects

unbiased developmental potential, to the primed state, in which cells are poised for lineage differentiation (Weinberger et al., 2016; Wu and Izpisua Belmonte, 2016). When attempting to introduce cultured pluripotent stem cells (PSCs) into a developing embryo of the same species, recent studies demonstrated that matching developmental timing is critical for successful chimera formation. For example, naïve mouse embryonic stem cells (mESCs) contribute to chimera formation when injected into a blastocyst, whereas primed mouse epiblast stem cells (mEpiSCs) efficiently engraft into mouse gastrula-stage embryos, but not vice versa (Huang et al., 2012; Wu et al., 2015). Live rodent interspecies chimeras have also been generated using naïve PSCs (Isotani et al., 2011; Kobayashi et al., 2010; Xiang et al., 2008). However, it remains unclear whether naïve PSCs can be used to generate chimeras between more distantly related species.

The successful derivation of human PSCs (hPSCs), including ESCs from pre-implantation human embryos (Reubinoff et al., 2000; Thomson et al., 1998), as well as the generation of induced pluripotent stem cells (iPSCs) from somatic cells through cellular reprogramming (Takahashi et al., 2007; Park et al., 2008; Wernig et al., 2007; Yu et al., 2007; Aasen et al., 2008), has revolutionized the way we study human development and is heralding a new age of regenerative medicine. Several lines of evidence indicate that conventional hPSCs are in the primed pluripotent state, similar to mEpiSCs (Tesar et al., 2007; Wu et al., 2015). A number of recent studies have also reported the generation of putative naïve hPSCs that molecularly resemble mESCs (Gafni et al., 2013; Takashima et al., 2014; Theunissen et al., 2014). These naïve hPSCs have already provided practical and experimental advantages, including high single-cell cloning efficiency and facile genome editing (Gafni et al., 2013). Despite these advances, it remains unclear how the putative higher developmental potential of naïve hPSCs can be used to better

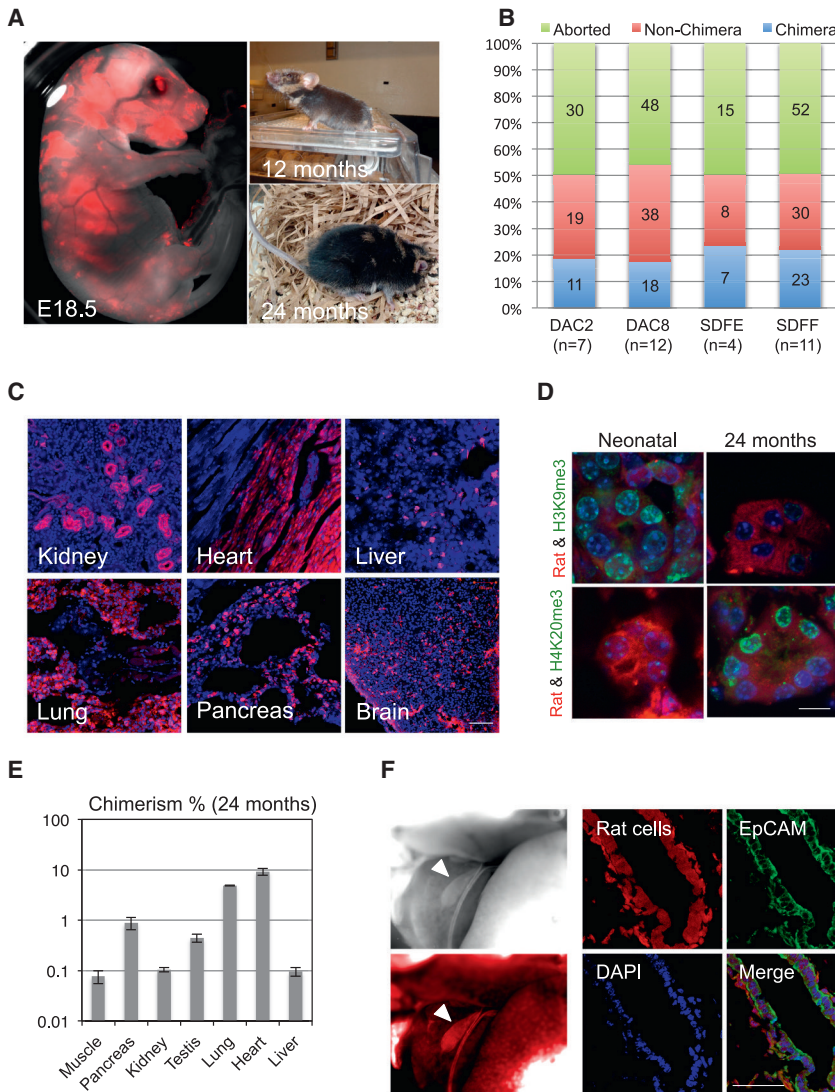


Figure 1. Interspecies Rat-Mouse Chimeras Derived from Rat PSCs

(A) Rat-mouse chimeras generated by rat ESCs (DAC2). Left, an E18.5 rat-mouse chimeric fetus. Red, hKO-labeled rat cells. Right, a 12-month-old (top) and 24-month-old (bottom) rat-mouse chimera.

(B) Chimera forming efficiencies with rat ESC lines (DAC2 and DAC8) and rat iPSC lines (SDFE and SDF). n, number of embryo transfers.

(C) Representative fluorescence images showing hKO-labeled rat ESCs (DAC2) contributed to different tissues in the 24-month-old rat-mouse chimera. Red, hKO-labeled rat cells. Blue, DAPI. Scale bar, 100 μ m.

(D) Representative immunofluorescence images showing the expression of aging-related histone marks, including H3K9me3 and H4K20me3, in the kidney tissue of neonatal and 24-month-old chimeras. Scale bar, 10 μ m.

(E) Levels of chimerism of rat ESCs (DAC2) in different tissues of the 24-month-old rat-mouse chimera. Error bars indicate SD.

(F) Rat iPSCs (SDFE) contributed to the neonatal mouse gall bladder. Left, bright-field (top) and fluorescence (bottom) images showing a neonatal mouse gallbladder contained cells derived from rat iPSCs. White arrowheads indicate the gallbladder. Right, representative immunofluorescence images showing the expression of a gallbladder epithelium marker (EpCAM) by rat cells. Red, hKO-labeled rat cells; blue, DAPI. Scale bar, 50 μ m. See also Figure S1 and Table S2.

understand human embryogenesis and to develop regenerative therapies for treating patients.

Like naive rodent PSCs, naive hPSCs can potentially be used to generate interspecies chimeras for studying human development and disease, and producing functional human tissues via interspecies blastocyst complementation. To date, however, all reported attempts on generating hPSC-derived interspecies chimeras have used the mouse as the host animal, and the results obtained suggest that this process is rather inefficient (Gafni et al., 2013; Theunissen et al., 2014, 2016). Although the mouse is one of the most important experimental models for stem cell research, there are considerable differences between humans and mice (e.g., early post-implantation development, embryo size, gestational length, and developmental speed), which may hinder not only the efficiency but also the usefulness of human-mouse chimeric studies. Thus, expanding the repertoire of host species may complement this incipient but promising area of research in the field of regenerative medicine. In particular, interspecies chimera research of

chimeric contribution of various types of hPSCs in the ungulates are thus imperative, but currently lacking. To start filling this void, we tested different types of hPSCs for their chimeric contribution potential in two ungulate species, pigs and cattle.

RESULTS

Naive Rat PSCs Robustly Contribute to Rat-Mouse Interspecies Chimera Formation

We first used rodent models to gain a better understanding of the factors and caveats underlying interspecies chimerism with PSCs. To this end, we used two chimeric-competent rat ESC lines, DAC2 and DAC8 (Li et al., 2008). We labeled both lines with a fluorescent marker, humanized kusabira orange (hKO), for cell tracking and injected them into mouse blastocysts. Following embryo transfer (ET) into surrogate mouse mothers, both DAC2 and DAC8 lines gave rise to live rat-mouse chimeras (Figures 1A and S1A). Many of the chimeras developed into

adulthood, and one chimera reached 2 years of age (Figure 1A), indicating that the xenogeneic rat cells sustained the physiological requirements of the mouse host without compromising its life span. We also generated two rat iPSC lines (SDFE and SDFE) from tail tip fibroblasts (TTFs) isolated from a neonatal Sprague-Dawley rat and used them to generate rat-mouse chimeras. Similar to rat ESCs, rat iPSCs could also robustly contribute to chimera formation in mice (Figure S1B). Overall, the chimera forming efficiencies of all rat PSC lines tested were ~20%, consistent with a previous report (Figure 1B) (Kobayashi et al., 2010).

We observed contribution of rat cells to a wide range of tissues and organs in both neonatal and aged rat-mouse chimeras (Figures 1C, S1A, and S1B). We examined aging-related histone marks in both neonatal and aged chimeras and found that the 2-year-old chimera exhibited histone signatures characteristic of aging (Figure 1D). We quantified the degree of chimerism in different organs of the aged chimera via quantitative qPCR analysis of genomic DNA using a rat-specific primer (Table S2). We found that different tissues contained different percentages of rat cells, with the highest contribution observed in the heart (~10%) (Figure 1E).

One anatomical difference between mice and rats is that rats lack a gallbladder. In agreement with a previous report (Kobayashi et al., 2010), we also observed the presence of gallbladders in rat-mouse chimeras (chimeras derived from injecting rat PSCs into a mouse blastocyst). Interestingly, rat cells contributed to the chimeric gallbladder and expressed the gallbladder epithelium marker EpCAM (Figures 1F and S1C), which suggests that the mouse embryonic microenvironment was able to unlock a gallbladder developmental program in rat PSCs that is normally suppressed during rat development.

A Versatile CRISPR-Cas9-Mediated Interspecies Blastocyst Complementation System

Chimeric contribution of PSCs is random and varies among different host blastocysts and donor cell lines used. To selectively enrich chimerism in a specific organ, a strategy called blastocyst complementation has been developed where the host blastocysts are obtained from a mutant mouse strain in which a gene critical for the development of a particular lineage is disabled (Chen et al., 1993; Kobayashi et al., 2010; Wu and Izpisua Belmonte, 2015). Mutant blastocysts used for complementation experiments were previously obtained from existing lines of knockout mice, which were generated by gene targeting in germ-line-competent mouse ESCs—a time-consuming process. To relieve the dependence on existing mutant strains, we developed a blastocyst complementation platform based on targeted genome editing in zygotes. We chose to use the CRISPR-Cas9 system, which has been harnessed for the efficient generation of knockout mouse models (Wang et al., 2013) (Figure 2A).

For proof-of-concept, we knocked out the *Pdx1* gene in mouse by co-injecting Cas9 mRNA and *Pdx1* single-guide RNA (sgRNA) into mouse zygotes. During mouse development, *Pdx1* expression is restricted to the developing pancreatic anlagen and is a key player in pancreatic development. Mice homozygous for a targeted mutation in *Pdx1* lack a pancreas and

die within a few days after birth (Jonsson et al., 1994; Offield et al., 1996). Similarly, *Pdx1*^{-/-} mice generated by the zygotic co-injection of Cas9 mRNA and *Pdx1* sgRNA were apancreatic, whereas other internal organs appeared normal (Figure S2A). These mice survived only a few days after birth. We observed the efficiency for obtaining *Pdx1*^{-/-} mouse via CRISPR-Cas9 zygote genome editing was ~60% (Figure S2F). Next, we combined zygotic co-injection of Cas9/sgRNA with blastocyst injection of rat PSCs, and found that rat PSC-derivatives were enriched in the neonatal pancreas of *Pdx1*^{-/-} mice and expressed α -AMYLASE, a pancreatic enzyme that helps digest carbohydrates (Figures 2B and S2B). Of note is that in these animals the pancreatic endothelial cells were still mostly of mouse origin, as revealed by staining with an anti-CD31 antibody (Figure 2B). Importantly, pancreas enriched with rat cells supported the successful development of *Pdx1*^{-/-} mouse host into adulthood (>7 months), and maintained normal serum glucose levels in response to glucose loading, as determined using the glucose tolerance test (GTT) (Figure S2C).

Taking advantage of the flexibility of the CRISPR-Cas9 zygotic genome editing, we next sought to enrich xenogenic rat cells toward other lineages. *Nkx2.5* plays a critical role in early stages of cardiogenesis, and its deficiency leads to severe growth retardation with abnormal cardiac looping morphogenesis, an important process that leads to chamber and valve formation (Lyons et al., 1995; Tanaka et al., 1999). Mice lacking *Nkx2.5* typically die around E10.5 (Lyons et al., 1995; Tanaka et al., 1999). Consistent with previous observations, CRISPR-Cas9 mediated inactivation of *Nkx2.5* resulted in marked growth-retardation and severe malformation of the heart at E10.5 (Figure S2D). In contrast, when complemented with rat PSCs, the resultant *Nkx2.5*^{-/-} mouse hearts were enriched with rat cells and displayed a normal morphology, and the embryo size was restored to normal (Figures 2C and S2D). Of note is that although rat PSCs rescued embryo growth and cardiac formation in E10.5 *Nkx2.5*^{-/-} mouse embryos, to date we still have not obtained a live rescued chimera (n = 12, where n is the number of ETs). *Pax6* is a transcription factor that plays key roles in development of the eye, nose and brain. Mice homozygous for a *Pax6* loss-of-function mutation lack eyes, nasal cavities, and olfactory bulbs, and exhibit abnormal cortical plate formation, among other phenotypes (Gehring and Ikeo, 1999). *Pax6* is best known for its conserved function in eye development across all species examined (Gehring and Ikeo, 1999). In agreement with the published work, CRISPR-Cas9 mediated *Pax6* inactivation disrupted eye formation in the E15.5 mouse embryo (Figure S2E). When complemented with rat PSCs, we observed the formation of chimeric eyes enriched with rat cells in *Pax6*^{-/-} mouse neonate (Figures 2D and S2E). Similar to *Pdx1*^{-/-}, we observed efficient generation of homozygous *Nkx2.5*^{-/-} and *Pax6*^{-/-} mouse embryos via zygotic co-injection of Cas9 mRNA and sgRNAs (Figure S2F). All DNA sequencing results of CRISPR-Cas9 mediated gene knockouts and gRNA sequences are summarized in Tables S1 and S2, respectively.

In sum, for the pancreas, heart, and eye, as well as several other organs (data not shown), we successfully generated chimerized organs that were enriched with rat cells, demonstrating

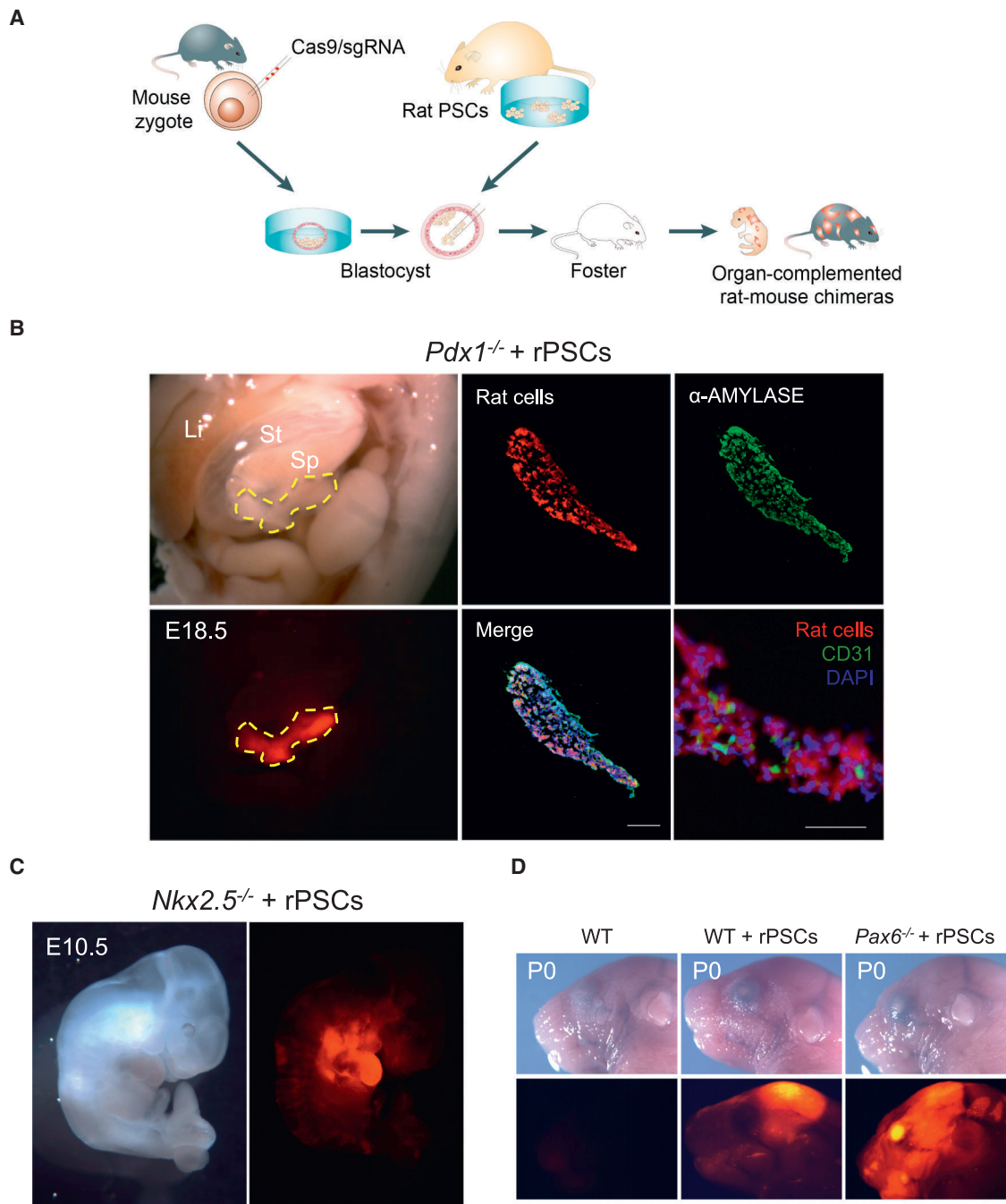


Figure 2. Interspecies Blastocyst Complementation via CRISPR-Cas9-Mediated Zygote Genome Editing

(A) Schematic of the CRISPR-Cas9 mediated rat-mouse blastocyst complementation strategy.

(B) Left, bright-field (top) and fluorescence (bottom) images showing the enrichment of rat cells in the pancreas of an E18.5 *Pdx1*^{-/-} mouse. Li, liver; St, stomach; Sp, spleen. Yellow-dotted line encircles the pancreas. Red, hKO-labeled rat cells. Middle and right (top), representative immunofluorescence images showing rat cells expressed α -amylase in the *Pdx1*^{-/-} mouse pancreas. Blue, DAPI. Right (bottom), a representative immunofluorescence image showing that some pancreatic endothelial cells, as marked by a CD31 antibody, were not derived from rat PSCs. Scale bar, 100 μ m.

(C) Bright field (left) and fluorescence (right) images showing the enrichment of rat cells in the heart of an E10.5 *Nkx2.5*^{-/-} mouse. Red, hKO-labeled rat cells.

(D) Bright field (top) and fluorescence (bottom) images showing the enrichment of rat cells in the eye of a neonatal *Pax6*^{-/-} mouse. Red, hKO-labeled rat cells. WT, mouse control; WT+rPSCs, control rat-mouse chimera without Cas9/sgRNA injection.

See also Figure S2 and Tables S1 and S2.

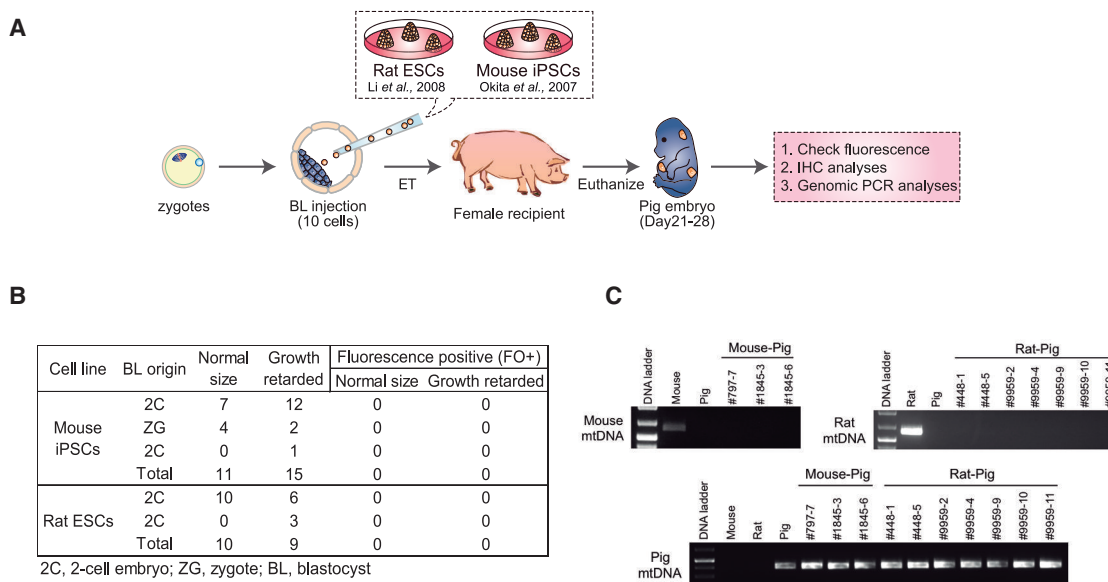


Figure 3. Naive Rodent PSCs Fail to Contribute to Chimera Formation in Pigs

(A) Schematic of the generation and analyses of post-implantation pig embryos derived from blastocyst injection of naive rodent PSCs.

(B) Summary of the pig embryos recovered between day 21–28 of pregnancy.

(C) Genomic PCR analyses of pig embryos derived from blastocyst injection of mouse iPSCs or rat ESCs. Mouse- and rat- specific mtDNA primers were used for the detection of chimeric contribution from mouse iPSCs and rat ESCs, respectively. Pig-specific mtDNA primers were used for the control.

See also Tables S2 and S3.

the efficacy and versatility of the CRISPR-Cas9 mediated interspecies blastocyst complementation platform.

Naive Rodent PSCs Do Not Contribute to Chimera Formation in Pigs

It is commonly accepted that the key functional feature of naive PSCs is their ability to generate intraspecies germline chimeras (Nichols and Smith, 2009). Studies in rodents also support the notion that attaining the naive pluripotent state is the key step in enabling chimera formation across species boundaries (Xiang et al., 2008; Isotani et al., 2011; Kobayashi et al., 2010). However, it has not yet been tested whether naive rodent PSCs can contribute to chimera formation when using a non-rodent host. To further examine the relationship between naive PSCs and interspecies chimerism, we injected rat ESCs into pig blastocysts followed by ET to recipient sows. In addition to rat ESCs, we also used a germline competent mouse iPSC line (Okita et al., 2007). Several criteria were used to determine the chimeric contribution of rodent cells in pig embryos, namely, (1) detection of fluorescence (hKO) signal, (2) immunohistochemical (IHC) labeling of embryo sections with an anti-hKO antibody, and (3) genomic PCR with mouse- or rat-specific primers targeting mitochondrial DNA (mtDNA) (Figure 3A). We terminated the pregnancy between day 21–28 of pig development and collected embryos derived from the injection of mouse iPSCs or rat ESCs into pig blastocyst (26 and 19 embryos, respectively) (Figure 3B; Table S3). We failed to detect any hKO signal in both normal size and growth retarded embryos (Figure 3B). We next sectioned the pig embryos and stained them with an antibody against hKO. Similarly, we did not detect any hKO-positive cells

in the embryonic sections examined (data not shown). Finally, we employed a more sensitive test, using genomic PCR to amplify rat- or mouse-specific mtDNA sequences (pig-specific mtDNA primers served as the loading control) (Table S2). Consistently, genomic PCR analyses did not detect any rodent contribution to the pig embryos (Figure 3C). Taken together, although naive rodent PSCs can robustly contribute to rodent-specific interspecies chimeras, our results show that these cells are incapable of contributing to normal embryonic development in pigs.

Generation of Naive, Intermediate, and Primed hiPSCs

Next, we sought to systematically evaluate the chimeric competency of hPSCs in ungulate embryos. We generated hiPSCs using several reported naive PSC culture methods, a culture protocol supporting a putative intermediate pluripotent state between naive mESCs and primed mEpiSCs (Tsukiyama and Ohinata, 2014), and a primed culture condition (Figure 4A). Mouse ground state culture condition (2iL) induces the differentiation of primed hPSCs. However, when combined with the forced expression of NANOG and KLF2 (NK2), transcription factors that help to maintain murine naive pluripotency, 2iL culture can stabilize hPSCs in an immature state (Takashima et al., 2014; Theunissen et al., 2014). We generated doxycycline (DOX)-inducible NK2-expressing naive hiPSCs cultured in 2iL medium from primed hiPSCs (2iLD-hiPSCs). Transgene-free primed hiPSCs were reprogramed from human foreskin fibroblasts (HFFs) using episomal vectors (Okita et al., 2011). For comparison, we also generated naive hiPSCs from HFFs using the NHSM culture condition (Gafni et al., 2013) (NHSM-hiPSCs). It has been shown that cells grown in 4i medium, a

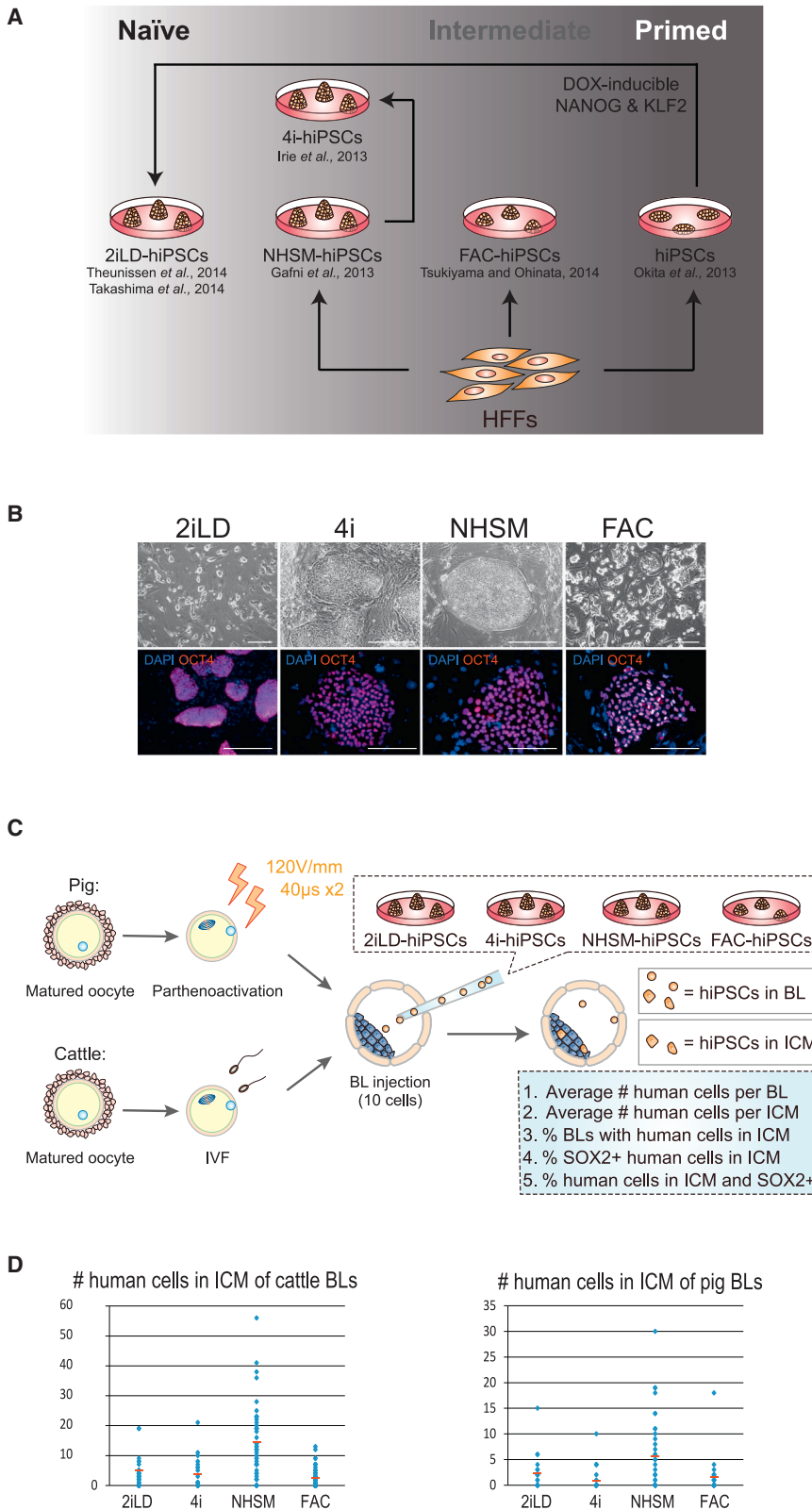


Figure 4. Generation and Interspecies ICM Incorporation of Different Types of hiPSCs

(A) Schematic of the strategy for generating naïve, intermediate, and primed hiPSCs.

(B) (Top) Representative bright-field images showing the colony morphologies of naïve (2iLD-, 4i-, and NHSM-hiPSCs) and intermediate (FAC-hiPSCs) hiPSCs. Bottom, representative immunofluorescence images of naïve and intermediate hiPSCs stained with an anti-OCT4 antibody. Red, OCT4; blue, DAPI. Scale bar, 100 μ m.

(C) Schematic of the experimental procedures for producing cattle and pig blastocysts obtained from in vitro fertilization (IVF) and parthenoactivation, respectively. Blastocysts were subsequently used for laser-assisted blastocyst injection of hiPSCs. After hiPSC injection, blastocysts were cultured in vitro for 2 days before fixation and analyzed by immunostaining with an anti-HuNu and an anti-SOX2 antibodies. Criteria to evaluate the survival of human cells, as well as the degree and efficiency of ICM incorporation are shown in the blue box.

(D) Number of hiPSCs that integrated into the cattle (left) and pig (right) ICMs after ten hiPSCs were injected into the blastocyst followed by 2 days of in vitro culture. Red line, the average number of ICM-incorporated hiPSCs. Blue dot, the number of ICM-incorporated hiPSCs in each blastocyst.

See also Figure S3 and Table S4.

simplified version of NHSM, have a significant potential for germ cell induction, a distinguishing feature between naive mESCs and primed mEpiSCs (Irie et al., 2015). Thus, we also culture-adapted NHSM-hiPSCs in 4i medium (4i-hiPSCs), resulting in stable 4i-hiPSCs with similar morphological and molecular characteristics to parental NHSM-hiPSCs (Figure 4B). In addition, we generated another type of hiPSC by direct reprogramming of HFFs in a modified mEpiSC medium containing bFGF, Activin-A, and CHIR99021 (FAC; Figure 4A). mEpiSCs cultured in FAC medium exhibited features characteristic of both naive mESCs and primed mEpiSCs, supporting an intermediate pluripotent state (Tsukiyama and Ohinata, 2014). hiPSCs generated and cultured in FAC medium (FAC-hiPSCs) displayed a colony morphology intermediate between that of 2iLD- and primed hiPSCs, with less defined borders (Figure 4B). 2iLD-hiPSCs, NHSM-hiPSCs, 4i-hiPSCs, and FAC-hiPSCs could all be stably maintained long term in culture, preserving normal karyotypes and the homogeneous, nuclear localization of OCT4 protein (Figure 4B; data not shown). Notably, similar to hiPSCs grown in naive cultures (2iLD-hiPSCs, NHSM-hiPSCs, 4i-hiPSCs), FAC-hiPSCs could also be efficiently propagated by single-cell dissociation without using a ROCK kinase inhibitor. After injecting cells into the kidney capsule of immunodeficient NSG mice, all of these hiPSCs formed teratomas that consisted of tissues from all three germ layers: endoderm, mesoderm, and ectoderm (Figure S3A). To facilitate the identification of human cells in subsequent chimera experiments, we labeled hiPSCs with either green fluorescence protein (GFP) or hKO fluorescence markers.

Chimeric Contribution of hiPSCs to Pig and Cattle Blastocysts

The ability to integrate into the inner cell mass (ICM) of a blastocyst is informative for evaluating whether hiPSCs are compatible with pre-implantation epiblasts of the ungulate species. This is also one of the earliest indicators of chimeric capability. We therefore evaluated interspecies chimeric ICM formation by injecting hiPSCs into blastocysts from two ungulate species, pig and cattle.

Cattle-assisted reproductive technologies, such as in vitro embryo production, are well established given the commercial benefits of improving the genetics of these animals. Cattle also serve as a research model because of several similarities to human pre-implantation development (Hansen, 2014; Hasler, 2014). Using techniques for producing cattle embryos in vitro, we developed a system for testing the ability and efficiency of hiPSCs to survive in the blastocyst environment and to integrate into the cattle ICM (Figure 4C). Cattle embryos were obtained by in vitro fertilization (IVF) using in vitro matured oocytes collected from ovaries obtained from a local slaughterhouse. The tightly connected cells of the blastocyst trophectoderm from large livestock species, such as pig and cattle, form a barrier that complicates cell microinjection into the blastocoel. Thus, microinjection often results in embryo collapse and the inability to deposit the cells into the embryo. To facilitate cell injection we employed a laser-assisted approach, using the laser to perforate the zona pellucida and to induce damage to a limited number of trophectoderm cells. This allowed for easy access into the blastocyst cavity for transferring the human cells (Figure S3B). Furthermore,

the zona ablation and trophectoderm access allowed use a blunt-end pipette for cell transfer, thus minimizing further embryo damage. This method resulted in a nearly 100% injection effectiveness and >90% embryo survival.

To determine whether hiPSCs could engraft into the cattle ICM, we injected ten cells from each condition into cattle blastocysts collected 7 days after fertilization. After injection, we cultured these blastocysts for additional 2 days before analysis. We used several criteria to evaluate the chimeric contribution of hiPSCs to cattle blastocysts: (1) average number of human cells in each blastocyst, (2) average number of human cells in each ICM, (3) percentage of blastocysts with the presence of human cells in the ICM, (4) percentage of SOX2⁺ human cells in the ICM, and (5) percentage of human cells in the ICM that are SOX2⁺ (Figure 4C). Our results indicated that both naive and intermediate (but not primed) hiPSCs could survive and integrate into cattle ICMs, albeit with variable efficiencies (Figures 4D and S3C–S3E; Table S4). Compared with other cell types, 4i-hiPSCs exhibited the best survival (22/23 blastocysts contained human cells), but the majority of these cells lost SOX2 expression (only 13.6% of human cells remained SOX2⁺). On average, 3.64 4i-hiPSCs were incorporated into the ICM. NHSM-hiPSCs were detected in 46 of 59 injected blastocysts, with 14.41 cells per ICM. Of these, 89.7% remained SOX2⁺. For 2iLD-hiPSCs, 40 of 52 injected blastocysts contained human cells, with 5.11 cells per ICM, and 69.9% of the ICM-incorporated human cells remained SOX2⁺. FAC-hiPSCs exhibited moderate survival rate (65/101) and ICM incorporation efficiency (39/101), with an average of 2.31 cells incorporated into the ICM, and 89.3% remaining SOX2⁺.

We also performed ICM incorporation assays by injecting hiPSCs into pig blastocysts. Because certain complications are frequently associated with pig IVF (Abeydeera, 2002; Grupen, 2014) (e.g., high levels of polyspermic fertilization), we used a parthenogenetic activation model, which enabled us to efficiently produce embryos that developed into blastocysts (King et al., 2002). Pig oocytes were obtained from ovaries collected at a local slaughterhouse. Once the oocytes were matured in vitro, we removed the cumulus cells and artificially activated the oocytes using electrical stimulation. They were then cultured to blastocyst stage (Figure 4C). We injected ten hiPSCs into each pig parthenogenetic blastocyst and evaluated their chimeric contribution after 2 days of in vitro culture (Figures 4C and S3C–S3E; Table S4). Similar to the results in cattle, we found that hiPSCs cultured in 4i and NHSM media survived better and yielded a higher percentage of blastocysts harboring human cells (28/35 and 37/44, respectively). Also, among all blastocysts containing human cells, we observed an average of 9.5 cells per blastocyst for 4i-hiPSCs and 9.97 cells for NHSM-hiPSCs. For NHSM-hiPSCs, 19/44 blastocysts had human cells incorporated into the ICM. In contrast, only 6/35 blastocysts had 4i-hiPSCs localized to the ICM. For 2iLD-hiPSCs, we observed an average of 5.7 cells per blastocyst, with 2.25 human cells localized to the ICM. For FAC-hiPSCs, an average of 3.96 and 1.62 human cells were found in the blastocyst and ICM, respectively. Once incorporated into the ICM, 82.2%, 72%, 60.9%, and 40% of 2iLD-, 4i-, NHSM-, and FAC-hiPSCs, respectively, stained positive for the pluripotency

marker SOX2. These results indicate that both naive and intermediate hiPSCs seem to perform better when injected into cattle than pig blastocysts. This suggests a different *in vivo* blastocyst environment in pig and cattle, with the cattle blastocysts providing an environment that is more permissive for hiPSC integration and survival.

Chimeric Contribution of hiPSCs to Post-implantation Pig Embryos

Although ICM incorporation of hiPSCs is the necessary first step to contribute to the embryo proper of host animals, it has limited predictive value for post-implantation chimera formation, as other factors are involved. Next, we investigated if any of the naive and intermediate hiPSCs that we generated, which showed robust ICM incorporation in pre-implantation blastocysts, could contribute to post-implantation development following ET. The pig has certain advantages over cattle for experiments involving post-implantation embryos, as they are a polytocus species, and are commonly used as a translational model given their similarities to humans concerning organ physiology, size, and anatomy. We thus chose the pig for these experiments. Since there was little to no contribution of primed hiPSCs, even at the pre-implantation blastocyst stage, we excluded these cells from the ET experiments. Pig embryos were derived *in vivo* or through parthenogenesis. A total of 167 embryo donors were used in this study, from which we collected 1,298 zygotes, 1,004 two-cell embryos and 91 morulae (Table S5). Embryos were cultured *in vitro* until they reached the blastocyst stage (Figures S4AA and S4B). Overall, 2,181 good quality blastocysts with a well-defined ICM were selected for subsequent blastocyst injections, of which 1,052 were derived from zygotes, 897 from two-cell embryos, 91 from morulae, and 141 from parthenogenetic activation (Table S5). We injected 3–10 hiPSCs into the blastocoel of each of these blastocysts (Figures 5A, S4A, and S4C; Table S6). After *in vitro* embryo culture, a total of 2,075 embryos (1,466 for hiPSCs; Table S6; 477 for rodent PSCs; Table S3) that retained good quality were transferred to surrogate sows. A total of 41 surrogate sows received 30–50 embryos each, resulting in 18 pregnancies (Table S6). Collection of embryos between day 21–28 of development resulted in the harvesting of 186 embryos: 43 from 2iLD-hiPSCs, 64 from FAC-hiPSCs, 39 from 4i-hiPSCs, and 40 from NHSM-hiPSCs (Figures 5B, S4A, S4D, and S4F). In addition, 17 control embryos were collected from an artificially inseminated sow (Figure 5B).

Following evaluating the developmental status of the obtained embryos, more than half showed retarded growth and were smaller than control embryos (Figures 5B and S4B), as was seen when pig blastocysts were injected with rodent PSCs (Figure 3B). Among different hiPSCs, embryos injected with FAC-hiPSCs were more frequently found to be normal size (Figure 5C). From the recovered embryos, and based on fluorescence imaging (GFP for 2iLD-hiPSCs and FAC-hiPSCs; hKO for 4i-hiPSCs and NHSM-hiPSCs), we observed positive fluorescence signal (FO+) in 67 embryos among which 17 showed a normal size and morphology, whereas the rest were morphologically underdeveloped (Figures 5B). In contrast, among fluorescence negative embryos we found the majority (82/119) appeared normal size (Figure 5E), suggesting contribution of hiPSCs might have

interfered with normal pig development. Closer examination of the underdeveloped embryos revealed that 50 out of 87 were FO+ (Figures 5B). Among all the FO+ embryos the distribution of normal size versus growth retarded embryos for each cell lines was: 3:19 for 2iLD-hiPSCs, 7:14 for FAC-hiPSCs, 2:12 for 4i-hiPSCs, and 5:5 for NHSM-hiPSCs (Figure 5D). Among normal size embryos we found 3/13 from 2iLD-hiPSCs, 7/47 from FAC-hiPSCs, 2/14 from 4i-hiPSCs, and 5/25 from NHSM-hiPSCs that were FO+ (Figure 5B). All normal size FO+ embryos derived from 2iLD-hiPSCs, 4i-hiPSCs, or NHSM-hiPSCs showed a very limited fluorescence signal (Figure S5A). In contrast, normal size FO+ FAC-hiPSC-derived embryos typically exhibited a more robust fluorescence signal (Figures 6A and S5A).

Detecting fluorescence signal alone is insufficient to claim chimeric contribution of donor hiPSCs to these embryos, as auto-fluorescence from certain tissues and apoptotic cells can yield false positives, especially when chimerism is low. We thus sectioned all normal size embryos deemed positive based on the presence of fluorescence signal and subjected them to IHC analyses with antibodies detecting GFP or hKO. For 2iLD-hiPSC-, 4i-hiPSC-, and NHSM-hiPSC-derived embryos, in agreement with fluorescence signals observed in whole-embryo analysis, we detected only a few hKO- or GFP-positive cells in limited number of sections (Figure S5A). This precluded us from conducting further IHC analysis using lineage markers. For FAC-hiPSC-derived embryos, we confirmed via IHC analysis (using an anti-GFP antibody) that they contained more human cells (Figures 6A, S5A, and S5B). We then stained additional sections using antibodies against TUJ1, EPCAM, SMA, CK8, and HNF3 β (Figures 6B and S5C) and observed differentiation of FAC-hiPSCs into different cell lineages. In addition, these cells were found negative for OCT4, a pluripotency marker (data not shown). Moreover, the presence of human cells was further verified with a human-specific HuNu antibody staining (Figure 6B) and a sensitive genomic PCR assay using a human specific *Alu* sequence primer (Figure 6C; Table S2). Together, these results indicate that naive hiPSCs injected into pig blastocysts inefficiently contribute to chimera formation, and are only rarely detected in post-implantation pig embryos. An intermediate hPSC type (FAC-hiPSCs) showed better chimeric contribution and differentiated to several cell types in post-implantation human-pig chimeric embryos. It should be noted that the levels of chimerism from all hiPSCs, including the FAC-hiPSCs, in pig embryos were much lower when compare to rat-mouse chimeras (Figures 1C, 1E, S1A, and 1B), which may reflect the larger evolutionary distance between human-pig than between rat-mouse.

DISCUSSION

Our study confirms that live rat-mouse chimeras with extensive contribution from naive rat PSCs can be generated. This is in contrast to earlier work in which rat ICMs were injected into mouse blastocysts (Gardner and Johnson, 1973). One possible explanation for this discrepancy is that cultured PSCs acquire artificial features that make them more proliferative and/or better able to survive than embryonic ICM cells, which in turn leads to their more robust xeno-engraftment capability in a mouse host.

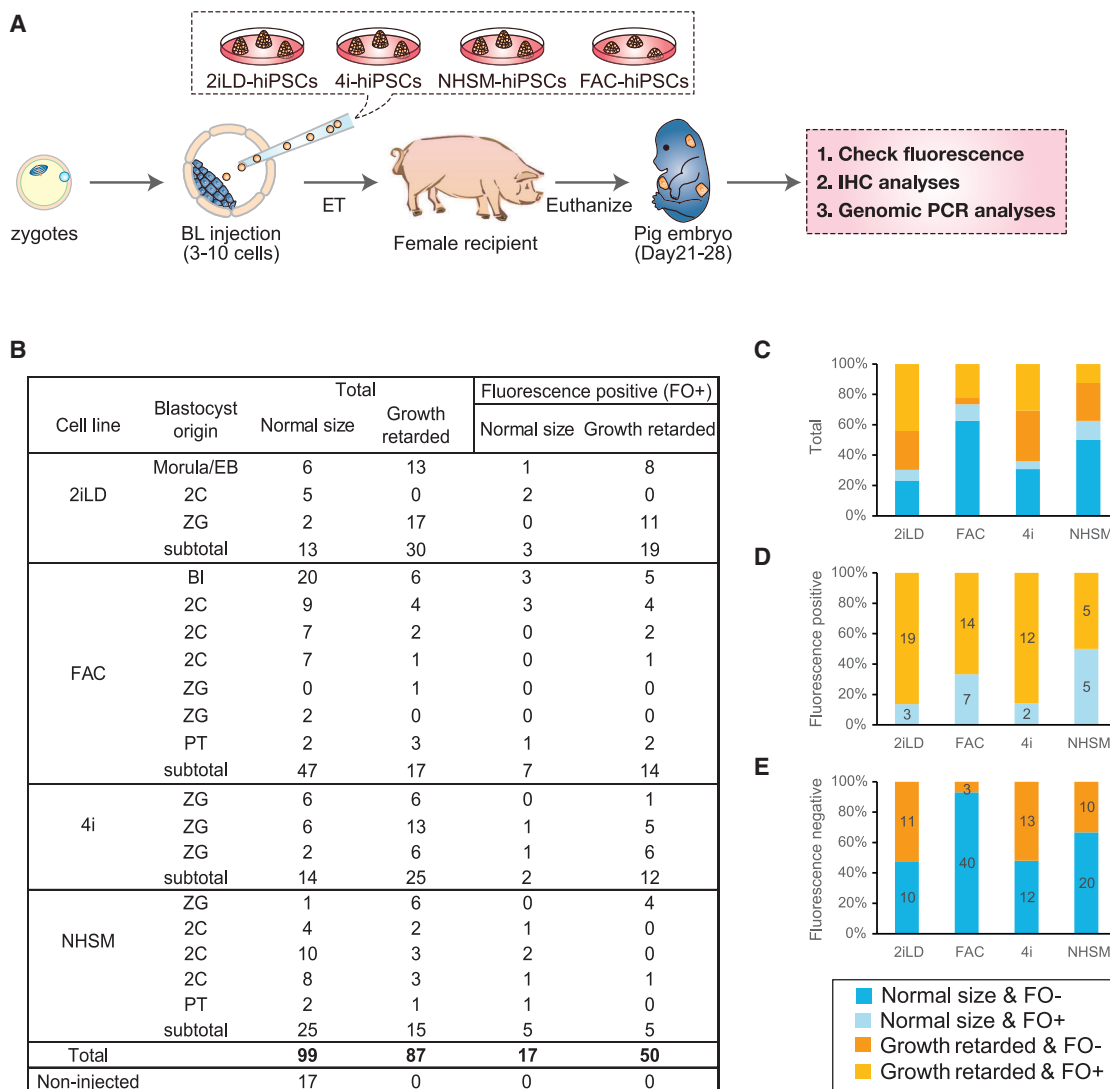


Figure 5. Generation of Post-implantation Human-Pig Chimeric Embryos

(A) Schematic of the experimental procedures for the generation and analyses of post-implantation pig embryos derived from blastocyst injection of naive and intermediate hiPSCs.

(B) Summary of the pig embryos recovered between day 21–28 of pregnancy.

(C) Bar graph showing proportions of normal size and growth retarded embryos, as well as the proportion of fluorescence-positive and -negative embryos, generated from different types of hiPSCs.

(D) Bar graph showing the proportion of normal size and growth-retarded embryos (among those exhibiting a fluorescence signal) generated from different types of hiPSCs.

(E) Bar graph showing the proportion of normal-sized and growth-retarded embryos (among those without exhibiting a fluorescence signal) generated from different types of hiPSCs.

See also Figure S4 and Tables S5 and S6.

Rat-mouse chimeras generated by injecting donor rat PSCs into a mouse host were mouse-sized and developed into adulthood with apparently normal appearance and physiology. We further show in this study that a rat-mouse chimera could live a full mouse lifespan (about 2 years) and exhibit molecular signatures characteristic of aged cells. This demonstrates that cells from two different species, which diverged ~18 million years ago, can live in a symbiotic environment and are able to support normal organismal aging. The fact that rat PSCs were able to

contribute to the mouse gallbladder, an organ that is absent in the rat, highlights the importance of embryonic niches in orchestrating the specification, proliferation, and morphogenesis of tissues and organs during organismal development and evolutionary speciation (Izpisua-Belmonte et al., 1992).

Previous interspecies blastocyst complementation experiments generated host embryos by crossing heterozygous mutant mouse strains, which were themselves generated through targeted gene disruption in germline competent ESCs.

These experiments are labor intensive and time consuming. Moreover, only ~25% of blastocysts derived from genetic crosses are homozygous mutants, posing a limitation for efficient complementation. CRISPR-Cas9 mediated zygote genome editing offers a faster and more efficient one-step process for generating mice carrying homozygous mutations, thereby providing a robust interspecies blastocyst complementation platform. Additionally, the multiplexing capability of CRISPR-Cas9 (Cong et al., 2013; Yang et al., 2015) could potentially be harnessed for multi-lineage complementation. For example, in the case of the pancreas, one might hope to eliminate both the pancreatic parenchyma and vasculature of the host to generate a more complete xenogeneic pancreas. Despite the advantages, there are several technical limitations of the CRISPR-Cas9 blastocyst complementation system that need to be overcome before unlocking its full potential. First, gene inactivation relies on the error-prone, non-homologous end joining (NHEJ) pathway, which is often unpredictable. In-frame mutations and mosaicism are among the factors that may affect outcomes. A more predictable targeted gene inactivation strategy that utilizes homologous recombination (HR) is still inefficient in the zygote. Second, each embryo must be injected twice when using this system and embryos must be cultured *in vitro* for several days before ET, thereby compromising embryo quality. Technical advancements that include a more robust gene-disruption strategy (e.g., targeted generation of frameshift mutations via homology independent targeted integration [Suzuki et al., 2016]), alternative CRISPR/Cas9 delivery methods, and improved culture conditions for manipulated embryos will likely help improve and optimize the generation of organogenesis-disabled hosts.

We observed a slower clearance of an intraperitoneally injected glucose load for *Pdx1*^{-/-} than *Pdx1*^{+/-} rat-mouse chimeras, while both were slower than wild-type mouse controls (Figure S2C). While this result may seem to contradict a previous report (Kobayashi et al., 2010), the discrepancy is likely due to the development of autoimmune type inflammation that is often observed in adult rat-mouse (chimeras made by injection of rat PSCs into mouse blastocyst, data not shown) (>7 months, this study) and mouse-rat chimeras (chimeras made by injection of mouse PSCs into rat blastocyst; H. Nakachi, personal communication), which is less evident in young chimeras (~8 weeks; Kobayashi et al. 2010). Interestingly though, we did observe a similarly slower clearance of glucose load in wild-type rats, although the initial spike was much lower in rats compared to mice or chimeras (Figure S2C). Thus, the rat cellular origin might also have played a role in the different GTT responses observed.

Rodent ESCs/iPSCs, considered as the gold standard cells for defining naive pluripotency, can robustly contribute to intra- and inter-species chimeras within rodent species. These and other results have led to the assumption that naive PSCs are the cells of choice when attempting to generate interspecies chimeras involving more disparate species. Here, we show that rodent PSCs fail to contribute to chimera formation when injected into pig blastocysts. This highlights the importance of other contributing factors underlying interspecies chimerism that may include, but not limited to, species-specific differences in epiblast and trophectoderm development, developmental kinetics, and maternal microenvironment.

To date, and taking into consideration all published studies that have used the mouse as the host species, it is probably appropriate to conclude that interspecies chimera formation involving hPSCs is inefficient (De Los Angeles et al., 2015). It has been argued that this apparent inefficiency results from species-specific differences between human and mouse embryogenesis. Therefore, studies utilizing other animal hosts would help address this important question. Here we focused on two species, pig and cattle, from a more diverse clade of mammals and found that naive and intermediate, but not primed, hiPSCs could robustly incorporate into pre-implantation host ICMs. Following ET, we observed, in general and similar to the mouse studies, low chimera forming efficiencies for all hiPSCs tested. Interestingly, injected hiPSCs seemed to negatively affect normal pig development as evidenced by the high proportion of growth retarded embryos. Nonetheless, we observed that FAC-hiPSCs, a putative intermediate PSC type between naive and primed pluripotent states, displayed a higher level of chimerism in post-implantation pig embryos. IHC analyses revealed that FAC-hiPSCs integrated and subsequently differentiated in host pig embryos (as shown by the expression of different lineage markers, and the lack of expression of the pluripotency marker OCT4). Whether the degree of chimerism conferred by FAC-hiPSCs could be sufficient for eliciting a successful interspecies human-pig blastocyst complementation, as demonstrated herein between rats and mice, remains to be demonstrated. Studies and approaches to improve the efficiency and level of hPSC interspecies chimerism (Wu et al., 2016), such as matching developmental timing, providing a selective advantage for donor hPSCs, generating diverse hPSCs with a higher chimeric potential and selecting a species evolutionarily closer to humans, among others parameters, will be needed.

The procedures and observations reported here on the capability of human pluripotent stem cells to integrate and differentiate in a ungulate embryo, albeit at a low level and efficiency, when

Figure 6. Chimeric Contribution of hiPSCs to Post-implantation Pig Embryos

(A) Representative bright field (left top) fluorescence (left bottom and middle) and immunofluorescence (right) images of GFP-labeled FAC-hiPSCs derivatives in a normal size day 28 pig embryo (FAC #1). Scale bar, 100 μ m.

(B) Representative immunofluorescence images showing chimeric contribution and differentiation of FAC-hiPSCs in a normal size, day 28 pig embryo (FAC #1). FAC-hiPSC derivatives are visualized by antibodies against GFP (top), TUJ1, SMA, CK8 and HuNu (middle). (Bottom) Merged images with DAPI. Insets are higher magnification images of boxed regions. Scale bar, 100 μ m.

(C) Representative gel images showing genomic PCR analyses of pig embryos derived from blastocyst injection of 2iLD-iPSCs (surrogates #8164 and #20749) and FAC-hiPSCs (surrogates #9159 and #18771) using a human specific Alu primer. A pig specific primer Cyt b was used for loading control. nc, negative control with no genomic DNA loaded. pc, positive controls with human cells. Pig 1D, 1G, and 1I, pig controls. ID, surrogate and pig embryos.

See also Figure S5 and Table S2.

optimized, may constitute a first step towards realizing the potential of interspecies blastocyst complementation with hPSCs. In particular, they may provide a better understanding of human embryogenesis, facilitate the development and implementation of humanized animal drug test platforms, as well as offer new insights on the onset and progression of human diseases in an in vivo setting. Ultimately, these observations also raise the possibility of xeno-generating transplantable human tissues and organs towards addressing the worldwide shortage of organ donors.

STAR★METHODS

Detailed methods are provided in the online version of this paper and include the following:

- KEY RESOURCES TABLE
- CONTACT FOR REAGENT AND RESOURCE SHARING
- EXPERIMENTAL MODEL AND SUBJECT DETAILS
 - Rodents
 - Pigs
 - Human iPSC Culture Media
 - Culture and maintenance of rat ESCs/iPSCs and mouse iPSCs
- METHOD DETAILS
 - Chemicals Unless Otherwise Indicated, Chemicals Were Obtained from Sigma-Aldrich
 - Rat iPSC Generation
 - Human iPSC Generation
 - Generation of Fluorescently Labeled Rat PSCs and hiPSCs
 - Mouse Embryo Collection
 - sgRNA Design and In Vitro Transcription
 - Microinjection of Cas9 mRNA and sgRNAs to Mouse Zygotes
 - Microinjection of Rat PSCs to Mouse Blastocysts
 - Mouse Embryo Transfer
 - Genomic PCR
 - Quantitative Genomic PCR
 - Genotyping and DNA Sequencing
 - Glucose Tolerance Test
 - Cattle In Vitro Embryo Production
 - Pig Parthenogenetic Embryo Production
 - Microinjection of PSCs to Cattle and Pig Blastocysts and Embryo Culture
 - Pig and Cattle Blastocyst Immunostaining
 - Pig In Vivo Embryo Recovery and Transfer
 - Pig Parthenogenetic Embryo Transfer
 - Immunocytochemistry
- QUANTIFICATION AND STATISTICAL ANALYSIS

SUPPLEMENTAL INFORMATION

Supplemental Information includes five figures and six tables and can be found with this article online at <http://dx.doi.org/10.1016/j.cell.2016.12.036>.

AUTHOR CONTRIBUTIONS

J.W. and J.C.I.B. conceived the study. J.W. generated and characterized all naive and intermediate hiPSC lines. K.S. generated and characterized primed

hiPSCs. J.W. and T.H. generated rat iPSCs. J.W., A.P.-L., T.Y., M.M.V., D.O., A.O., P.R., C.R.E., J.W., and P.M.R. performed immunohistochemistry analyses of mouse and pig embryos. K.S., T.Y., E.S., A.P.-L., and M.M.V. performed genotyping, genomic PCR, and genomic qPCR analyses. A.S., M.S., and J.P.L. performed mouse Cas9/sgRNA injection, blastocyst injection, and embryo transfer. Y.S.B., M.S., and M.V. prepared hiPSCs, performed morulae and blastocyst injections, and analyzed hiPSC contribution to cattle and pig ICMS. H.W. produced parthenogenetic pig embryos. D.A.S., Y.S.B., and M.V. produced cattle embryos. Work at UC Davis and University of Murcia was performed under the supervision of P.J.R. and E.A.M., respectively. E.A.M., M.A.G., C.C., I.P., C.A.M., S.S.B., A.N., and J.R. designed, coordinated, performed, and analyzed data related to pig embryo collection, embryo culture, blastocyst injection, embryo transfer, and embryo recover. E.N.D., J.L., I.G., P.G., T.B., M.L.M.-M., and J.M.C. coordinated work between Salk, and University of Murcia. J.W., P.J.R., and J.C.I.B. wrote the manuscript.

ACKNOWLEDGMENTS

J.C.I.B. dedicates this paper to Dr. Rafael Matesanz, Director of the Spain's National Organ Transplant Organization. Rafael's work has helped save thousands of patients in need of an organ. He constitutes a relentless inspiration for those of us trying to understand and alleviate human disease. The authors are grateful to Xiomara Lucas, Maria Dolores Ortega, Moises Gonzalez, Jose Antonio Godinez, and Jesus Gomis for their assistance throughout this work. We thank the staff of the Agropor S.A. and Porcisan S.A. piggeries (Murcia, Spain) for the help and excellent management of animals. We thank Joan Rowe, Bret McNabb, Aaron Prinz, and Kent Parker and their crews for excellent assistance with embryo transfers and pig care at UC Davis. We thank Mako Yamamoto for help with mouse embryo dissection. We would like to thank Uri Manor of the Salk Waitt Advanced Biophotonics Core for technical advice on imaging analysis. We would like to thank the Salk Stem Cell Core for providing cell culture reagents. We would like to thank May Schwarz and Peter Schwarz for administrative help. We thank David O'Keefe for critical reading and editing of the manuscript. This experimental study was supported by The Fundación Séneca (GERM 19892/GERM/15), Murcia, Spain. The MINECO is acknowledged for their grant-based support (BES-2013-064087 and BES-2013-064069) (to C.A.M. and A.N.). P.J.R. was supported by a UC Davis Academic Senate New Research grant. Work in the laboratory of J.C.I.B. was supported by the UCAM, Fundacion Dr. Pedro Guillen, G. Harold and Leila Y. Mathers Charitable Foundation, and The Moxie Foundation.

Received: February 2, 2016

Revised: October 30, 2016

Accepted: December 22, 2016

Published: January 26, 2017

REFERENCES

- Aasen, T., Raya, A., Barrero, M.J., Garreta, E., Consiglio, A., González, F., Vasena, R., Bilić, J., Pekarik, V., Tiscornia, G., et al. (2008). Efficient and rapid generation of induced pluripotent stem cells from human keratinocytes. *Nat. Biotechnol.* 26, 1276–1284.
- Abeydeera, L.R. (2002). In vitro production of embryos in swine. *Theriogenology* 57, 256–273.
- Chen, J., Lansford, R., Stewart, V., Young, F., and Alt, F.W. (1993). RAG-2-deficient blastocyst complementation: an assay of gene function in lymphocyte development. *Proc. Natl. Acad. Sci. USA* 90, 4528–4532.
- Cong, L., Ran, F.A., Cox, D., Lin, S., Barretto, R., Habib, N., Hsu, P.D., Wu, X., Jiang, W., Marraffini, L.A., and Zhang, F. (2013). Multiplex genome engineering using CRISPR/Cas systems. *Science* 339, 819–823.
- De Los Angeles, A., Ferrari, F., Xi, R., Fujiwara, Y., Benvenisty, N., Deng, H., Hochedlinger, K., Jaenisch, R., Lee, S., Leitch, H.G., et al. (2015). Hallmarks of pluripotency. *Nature* 525, 469–478.

- Dull, T., Zufferey, R., Kelly, M., Mandel, R.J., Nguyen, M., Trono, D., and Naldini, L. (1998). A third-generation lentivirus vector with a conditional packaging system. *J. Virol.* **72**, 8463–8471.
- Funahashi, H., Ekwall, H., and Rodriguez-Martinez, H. (2000). Zona reaction in porcine oocytes fertilized in vivo and in vitro as seen with scanning electron microscopy. *Biol. Reprod.* **63**, 1437–1442.
- Gafni, O., Weinberger, L., Mansour, A.A., Manor, Y.S., Chomsky, E., Ben-Yosef, D., Kalma, Y., Viukov, S., Maza, I., Zviran, A., et al. (2013). Derivation of novel human ground state naive pluripotent stem cells. *Nature* **504**, 282–286.
- Gardner, R.L., and Johnson, M.H. (1973). Investigation of early mammalian development using interspecific chimaeras between rat and mouse. *Nat. New Biol.* **246**, 86–89.
- Gehring, W.J., and Ikeo, K. (1999). Pax 6: mastering eye morphogenesis and eye evolution. *Trends Genet.* **15**, 371–377.
- Gruppen, C.G. (2014). The evolution of porcine embryo in vitro production. *Theriogenology* **81**, 24–37.
- Hansen, P.J. (2014). Current and future assisted reproductive technologies for mammalian farm animals. In *Current and Future Reproductive Technologies and World Food Production*, G. Cliff Lamb and N. DiLorenzo, eds. (Springer New York), pp. 1–22.
- Hasler, J.F. (2014). Forty years of embryo transfer in cattle: a review focusing on the journal *Theriogenology*, the growth of the industry in North America, and personal reminiscences. *Theriogenology* **81**, 152–169.
- Hishida, T., Nozaki, Y., Nakachi, Y., Mizuno, Y., Okazaki, Y., Ema, M., Takahashi, S., Nishimoto, M., and Okuda, A. (2011). Indefinite self-renewal of ESCs through Myc/Max transcriptional complex-independent mechanisms. *Cell Stem Cell* **9**, 37–49.
- Hockemeyer, D., Soldner, F., Cook, E.G., Gao, Q., Mitalipova, M., and Jaenisch, R. (2008). A drug-inducible system for direct reprogramming of human somatic cells to pluripotency. *Cell Stem Cell* **3**, 346–353.
- Holm, P., Booth, P.J., Schmidt, M.H., Greve, T., and Callesen, H. (1999). High bovine blastocyst development in a static in vitro production system using SOFaa medium supplemented with sodium citrate and myo-inositol with or without serum-proteins. *Theriogenology* **52**, 683–700.
- Huang, Y., Osorno, R., Tsakiridis, A., and Wilson, V. (2012). In vivo differentiation potential of epiblast stem cells revealed by chimeric embryo formation. *Cell Rep.* **2**, 1571–1578.
- Irie, N., Weinberger, L., Tang, W.W.C., Kobayashi, T., Viukov, S., Manor, Y.S., Dietmann, S., Hanna, J.H., and Surani, M.A. (2015). SOX17 is a critical specifier of human primordial germ cell fate. *Cell* **160**, 253–268.
- Isotani, A., Hatayama, H., Kaseda, K., Ikawa, M., and Okabe, M. (2011). Formation of a thymus from rat ES cells in xenogeneic nude mouse \leftrightarrow rat ES chimeras. *Genes Cells* **16**, 397–405.
- Izpisua-Belmonte, J.C., Brown, J.M., Crawley, A., Duboule, D., and Tickle, C. (1992). Hox-4 gene expression in mouse/chicken heterospecific grafts of signalling regions to limb buds reveals similarities in patterning mechanisms. *Development* **115**, 553–560.
- Jonsson, J., Carlsson, L., Edlund, T., and Edlund, H. (1994). Insulin-promoter factor 1 is required for pancreas development in mice. *Nature* **371**, 606–609.
- King, T.J., Dobrinsky, J.R., Zhu, J., Finlayson, H.A., Bosma, W., Harkness, L., Ritchie, W.A., Travers, A., McCorquodale, C., Day, B.N., et al. (2002). Embryo development and establishment of pregnancy after embryo transfer in pigs: coping with limitations in the availability of viable embryos. *Reproduction* **123**, 507–515.
- Kobayashi, T., Yamaguchi, T., Hamanaka, S., Kato-Itoh, M., Yamazaki, Y., Ibata, M., Sato, H., Lee, Y.-S., Usui, J., Knisely, A.S., et al. (2010). Generation of rat pancreas in mouse by interspecific blastocyst injection of pluripotent stem cells. *Cell* **142**, 787–799.
- Kutner, R.H., Zhang, X.-Y., and Reiser, J. (2009). Production, concentration and titration of pseudotyped HIV-1-based lentiviral vectors. *Nat. Protoc.* **4**, 495–505.
- Li, P., Tong, C., Mehrian-Shai, R., Jia, L., Wu, N., Yan, Y., Maxson, R.E., Schulze, E.N., Song, H., Hsieh, C.-L., et al. (2008). Germline competent embryonic stem cells derived from rat blastocysts. *Cell* **135**, 1299–1310.
- Lyons, I., Parsons, L.M., Hartley, L., Li, R., Andrews, J.E., Robb, L., and Harvey, R.P. (1995). Myogenic and morphogenetic defects in the heart tubes of murine embryos lacking the homeo box gene Nkx2-5. *Genes Dev.* **9**, 1654–1666.
- Martinez, E.A., Angel, M.A., Cuello, C., Sanchez-Osorio, J., Gomis, J., Parrilla, I., Vila, J., Colina, I., Diaz, M., Reixach, J., et al. (2014). Successful non-surgical deep uterine transfer of porcine morulae after 24 hour culture in a chemically defined medium. *PLoS ONE* **9**, e104696.
- Nichols, J., and Smith, A. (2009). Naive and primed pluripotent states. *Cell Stem Cell* **4**, 487–492.
- Offield, M.F., Jettton, T.L., Labosky, P.A., Ray, M., Stein, R.W., Magnuson, M.A., Hogan, B.L., and Wright, C.V. (1996). PDX-1 is required for pancreatic outgrowth and differentiation of the rostral duodenum. *Development* **122**, 983–995.
- Okita, K., Ichisaka, T., and Yamanaka, S. (2007). Generation of germline-competent induced pluripotent stem cells. *Nature* **448**, 313–317.
- Okita, K., Matsumura, Y., Sato, Y., Okada, A., Morizane, A., Okamoto, S., Hong, H., Nakagawa, M., Tanabe, K., Tezuka, K., et al. (2011). A more efficient method to generate integration-free human iPS cells. *Nat. Methods* **8**, 409–412.
- Park, I.H., Zhao, R., West, J.A., Yabuuchi, A., Huo, H., Ince, T.A., Lerou, P.H., Lensch, M.W., and Daley, G.Q. (2008). Reprogramming of human somatic cells to pluripotency with defined factors. *Nature* **451**, 141–146.
- Parrish, J.J., Susko-Parrish, J.L., Leibfried-Rutledge, M.L., Critser, E.S., Eye-stone, W.H., and First, N.L. (1986). Bovine in vitro fertilization with frozen-thawed semen. *Theriogenology* **25**, 591–600.
- Parrish, J.J., Susko-Parrish, J., Winer, M.A., and First, N.L. (1988). Capacitation of bovine sperm by heparin. *Biol. Reprod.* **38**, 1171–1180.
- Petters, R.M., and Wells, K.D. (1993). Culture of pig embryos. *J. Reprod. Fertil. Suppl.* **48**, 61–73.
- Pursel, V.G., and Johnson, L.A. (1975). Freezing of boar spermatozoa: fertilizing capacity with concentrated semen and a new thawing procedure. *J. Anim. Sci.* **40**, 99–102.
- Reubinoff, B.E., Pera, M.F., Fong, C.Y., Trounson, A., and Bongso, A. (2000). Embryonic stem cell lines from human blastocysts: somatic differentiation in vitro. *Nat. Biotechnol.* **18**, 399–404.
- Ross, P.J., Ragina, N.P., Rodriguez, R.M., Lager, A.E., Siripattaraprat, K., Lopez-Corrales, N., and Cibelli, J.B. (2008). Polycomb gene expression and histone H3 lysine 27 trimethylation changes during bovine preimplantation development. *Reproduction* **136**, 777–785.
- Suzuki, K., Tsunekawa, Y., Hernandez-Benitez, R., Wu, J., Zhu, J., Kim, E.J., Hatanaka, F., Yamamoto, M., Araoka, T., Li, Z., et al. (2016). In vivo genome editing via CRISPR/Cas9 mediated homology-independent targeted integration. *Nature* **540**, 144–149.
- Takahashi, K., Tanabe, K., Ohnuki, M., Narita, M., Ichisaka, T., Tomoda, K., and Yamanaka, S. (2007). Induction of pluripotent stem cells from adult human fibroblasts by defined factors. *Cell* **131**, 861–872.
- Takashima, Y., Guo, G., Loos, R., Nichols, J., Ficiz, G., Krueger, F., Oxley, D., Santos, F., Clarke, J., Mansfield, W., et al. (2014). Resetting transcription factor control circuitry toward ground-state pluripotency in human. *Cell* **158**, 1254–1269.
- Tanaka, M., Chen, Z., Bartunkova, S., Yamasaki, N., and Izumo, S. (1999). The cardiac homeobox gene Csx/Nkx2.5 lies genetically upstream of multiple genes essential for heart development. *Development* **126**, 1269–1280.
- Tesar, P.J., Chenoweth, J.G., Brook, F.A., Davies, T.J., Evans, E.P., Mack, D.L., Gardner, R.L., and McKay, R.D.G. (2007). New cell lines from mouse epiblast share defining features with human embryonic stem cells. *Nature* **448**, 196–199.
- Theunissen, T.W., Powell, B.E., Wang, H., Mitalipova, M., Faddah, D.A., Reddy, J., Fan, Z.P., Maetzel, D., Ganz, K., Shi, L., et al. (2014). Systematic

- identification of culture conditions for induction and maintenance of naive human pluripotency. *Cell Stem Cell* 15, 471–487.
- Theunissen, T.W., Friedli, M., He, Y., Planet, E., O'Neil, R.C., Markoulaki, S., Pontis, J., Wang, H., Iouranova, A., Imbeault, M., et al. (2016). Molecular criteria for defining the naive human pluripotent state. *Cell Stem Cell* 19, 502–515.
- Thomson, J.A., Itskovitz-Eldor, J., Shapiro, S.S., Waknitz, M.A., Swiergiel, J.J., Marshall, V.S., and Jones, J.M. (1998). Embryonic stem cell lines derived from human blastocysts. *Science* 282, 1145–1147.
- Tsukiyama, T., and Ohinata, Y. (2014). A modified EpiSC culture condition containing a GSK3 inhibitor can support germline-competent pluripotency in mice. *PLoS ONE* 9, e95329.
- Wang, H., Yang, H., Shivalila, C.S., Dawlaty, M.M., Cheng, A.W., Zhang, F., and Jaenisch, R. (2013). One-step generation of mice carrying mutations in multiple genes by CRISPR/Cas-mediated genome engineering. *Cell* 153, 910–918.
- Weinberger, L., Ayyash, M., Novershtern, N., and Hanna, J.H. (2016). Dynamic stem cell states: naive to primed pluripotency in rodents and humans. *Nat. Rev. Mol. Cell Biol.* 17, 155–169.
- Wernig, M., Meissner, A., Foreman, R., Brambrink, T., Ku, M., Hochedlinger, K., Bernstein, B.E., and Jaenisch, R. (2007). In vitro reprogramming of fibroblasts into a pluripotent ES-cell-like state. *Nature* 448, 318–324.
- Wu, J., and Izpisua Belmonte, J.C. (2015). Dynamic pluripotent stem cell states and their applications. *Cell Stem Cell* 17, 509–525.
- Wu, J., and Izpisua Belmonte, J.C. (2016). Stem cells: a renaissance in human biology research. *Cell* 165, 1572–1585.
- Wu, J., Okamura, D., Li, M., Suzuki, K., Luo, C., Ma, L., He, Y., Li, Z., Benner, C., Tamura, I., et al. (2015). An alternative pluripotent state confers interspecies chimaeric competency. *Nature* 521, 316–321.
- Wu, J., Greely, H.T., Jaenisch, R., Nakauchi, H., Rossant, J., and Belmonte, J.C. (2016). Stem cells and interspecies chimaeras. *Nature* 540, 51–59.
- Xiang, A.P., Mao, F.F., Li, W.-Q., Park, D., Ma, B.-F., Wang, T., Vallender, T.W., Vallender, E.J., Zhang, L., Lee, J., et al. (2008). Extensive contribution of embryonic stem cells to the development of an evolutionarily divergent host. *Hum. Mol. Genet.* 17, 27–37.
- Yang, L., Güell, M., Niu, D., George, H., Lesho, E., Grishin, D., Aach, J., Shrock, E., Xu, W., Poci, J., et al. (2015). Genome-wide inactivation of porcine endogenous retroviruses (PERVs). *Science* 350, 1101–1104.
- Yoshioka, K., Noguchi, M., and Suzuki, C. (2012). Production of piglets from in vitro-produced embryos following non-surgical transfer. *Anim. Reprod. Sci.* 131, 23–29.
- Yu, J., Vodyanik, M.A., Smuga-Otto, K., Antosiewicz-Bourget, J., Frane, J.L., Tian, S., Nie, J., Jonsdottir, G.A., Ruotti, V., Stewart, R., et al. (2007). Induced pluripotent stem cell lines derived from human somatic cells. *Science* 318, 1917–1920.
- Zou, J., Maeder, M.L., Mali, P., Pruett-Miller, S.M., Thibodeau-Beganny, S., Chou, B.-K., Chen, G., Ye, Z., Park, I.H., Daley, G.Q., et al. (2009). Gene targeting of a disease-related gene in human induced pluripotent stem and embryonic stem cells. *Cell Stem Cell* 5, 97–110.

Oncolytic Virotherapy Promotes Intratumoral T Cell Infiltration and Improves Anti-PD-1 Immunotherapy

Antoni Ribas,^{1,18,*} Reinhard Dummer,² Igor Puzanov,³ Ari VanderWalde,⁴ Robert H.I. Andtbacka,⁵ Olivier Michielin,⁶ Anthony J. Olszanski,⁷ Josep Malvehy,⁸ Jonathan Cebon,⁹ Eugenio Fernandez,¹⁰ John M. Kirkwood,¹¹ Thomas F. Gajewski,¹² Lisa Chen,¹³ Kevin S. Gorski,¹⁴ Abraham A. Anderson,¹³ Scott J. Diede,¹⁵ Michael E. Lassman,¹⁵ Jennifer Gansert,¹³ F. Stephen Hodi,¹⁶ and Georgina V. Long¹⁷

¹University of California at Los Angeles, Jonsson Comprehensive Cancer Center, Los Angeles, CA, USA

²University Hospital of Zurich, Zurich, Switzerland

³Roswell Park Cancer Institute, Buffalo, NY, USA

⁴The West Clinic, Memphis, TN, USA

⁵University of Utah Huntsman Cancer Institute, Salt Lake City, UT, USA

⁶Centre Hospitalier Universitaire Vaudois, Lausanne, Switzerland

⁷Fox Chase Cancer Center, Philadelphia, PA, USA

⁸Hospital Clinic i Provincial de Barcelona, Barcelona, Spain

⁹Olivia Newton-John Cancer Research Institute, Austin Health, School of Cancer Medicine, LaTrobe University, Heidelberg, VIC, Australia

¹⁰Hopitaux Universitaires de Genève, Geneva, Switzerland

¹¹University of Pittsburgh Cancer Institute and Hillman UPMC Cancer Center, Pittsburgh, PA, USA

¹²The University of Chicago School of Medicine, Chicago, IL, USA

¹³Amgen Inc., Thousand Oaks, CA, USA

¹⁴Amgen Inc., South San Francisco, CA, USA

¹⁵Merck & Co., Inc., Kenilworth, NJ, USA

¹⁶Dana-Farber Cancer Institute, Boston, MA, USA

¹⁷Melanoma Institute Australia, The University of Sydney and Royal North Shore and Mater Hospitals, Sydney, NSW, Australia

¹⁸Lead Contact

*Correspondence: aribas@mednet.ucla.edu

<http://dx.doi.org/10.1016/j.cell.2017.08.027>

SUMMARY

Here we report a phase 1b clinical trial testing the impact of oncolytic virotherapy with talimogene laherparepvec on cytotoxic T cell infiltration and therapeutic efficacy of the anti-PD-1 antibody pembrolizumab. Twenty-one patients with advanced melanoma were treated with talimogene laherparepvec followed by combination therapy with pembrolizumab. Therapy was generally well tolerated, with fatigue, fevers, and chills as the most common adverse events. No dose-limiting toxicities occurred. Confirmed objective response rate was 62%, with a complete response rate of 33% per immune-related response criteria. Patients who responded to combination therapy had increased CD8⁺ T cells, elevated PD-L1 protein expression, as well as IFN- γ gene expression on several cell subsets in tumors after talimogene laherparepvec treatment. Response to combination therapy did not appear to be associated with baseline CD8⁺ T cell infiltration or baseline IFN- γ signature. These findings suggest that oncolytic virotherapy may improve the efficacy of anti-PD-1 therapy by changing the tumor microenvironment.

INTRODUCTION

Treatment with anti-programmed death protein 1 (PD-1) or anti-PD ligand 1 (PD-L1) antibodies results in long-lasting antitumor responses in patients with a variety of cancers, and it is becoming standard of care treatment for patients with metastatic melanoma, carcinomas of the head and neck, lung, kidney, and bladder, Merkel cell carcinoma, and Hodgkin disease (Sharma and Allison, 2015). However, in all of these indications, only a subset of patients respond to therapy, with the majority of patients being primarily resistant to PD-1 blockade. By analyzing baseline biopsies of patients treated with anti-PD-1 antibodies, it was previously observed that patients who did not respond were more likely to lack CD8⁺ T cells inside the tumor lesions (Herbst et al., 2014; Tumeo et al., 2014). If there are no CD8⁺ T cells within a tumor that are inhibited by the PD-1:PD-L1 interaction, then PD-1 blockade therapy is unlikely to work (Pardoll, 2012; Ribas, 2015; Spranger et al., 2013). In this setting, combination immunotherapy designed to attract CD8⁺ T cells into tumors by altering the immune-suppressive tumor microenvironment may improve the antitumor activity of PD-1 blockade therapy.

We hypothesized that the intratumoral administration of an oncolytic virus optimized to attract immune cells might favorably change the tumor microenvironment in the injected lesions and increase CD8⁺ T cell infiltration. Furthermore, reactive expression of PD-L1 in the tumor microenvironment could be a mechanism of resistance to oncolysis, which would be obviated by

concurrent PD-1 blockade. After combined therapy, tumor antigen-specific CD8⁺ T cells that were fully stimulated in the injected lesion would be able to traffic to and infiltrate distant metastatic lesions to exert systemic antitumor activity, thereby reversing primary resistance to PD-1 blockade therapy.

Talimogene laherparepvec is a genetically modified herpes simplex virus type 1 designed to selectively replicate in tumors and produce granulocyte-macrophage colony-stimulating factor (GM-CSF) to enhance antigen release, presentation, and systemic antitumor immune response (Liu et al., 2003). In a prior phase 3 clinical trial, the intratumoral injection of talimogene laherparepvec into melanoma metastases improved the durable response rate compared with subcutaneous GM-CSF in patients with advanced melanoma (Andtbacka et al., 2015). Promising antitumor activity was demonstrated in a phase 1 study of talimogene laherparepvec combined with the checkpoint inhibitor ipilimumab, which blocks the cytotoxic T cell-associated antigen 4 (CTLA-4) (Chesney et al., 2016; Puzanov et al., 2016), and was confirmed in a phase 2 randomized trial comparing the same combination with ipilimumab alone (Chesney et al., 2017). There was a significant increase in the confirmed objective response rate by immune-related response criteria (irRC) with the combination compared with ipilimumab alone (39% versus 18%, respectively, $p = 0.002$).

We designed a phase 1b trial in patients with advanced melanoma combining the intratumoral injection of talimogene laherparepvec with the systemic administration of the anti-PD-1 antibody pembrolizumab, with baseline and repeated on-therapy biopsies; the primary objective was to test the safety of this combination and to explore its ability to boost inflammatory status of tumors. Specifically, we evaluated the ability of talimogene laherparepvec to reverse the low baseline presence of intratumoral CD8⁺ T cells in some of the metastatic lesions and then mediate increased objective tumor responses systemically.

RESULTS

A Phase 1b Clinical Trial Combining Talimogene Laherparepvec with Pembrolizumab

The phase 1b trial included a baseline biopsy before initiation of intratumoral talimogene laherparepvec injections, with a first injection of up to 4 mL \times 10⁶ plaque-forming units (pfu) per mL with the goal of inducing seroconversion and a protective immune response to the oncolytic viral vector, followed 3 weeks later with repeated injections of the full dose of up to 4 mL \times 10⁸ pfu/mL of talimogene laherparepvec every 2 weeks (Figure 1A). A second tumor biopsy was performed before administration of the second full dose of talimogene laherparepvec and before commencing treatment with pembrolizumab 200 mg intravenously every 2 weeks coinciding with subsequent doses of talimogene laherparepvec. The run-in period with single-agent talimogene laherparepvec administration was designed to analyze how intratumoral injection of this agent alters the tumor microenvironment before combination therapy began. A third tumor biopsy was planned, if feasible, during the combination therapy part of the study (Figures 1A and S1). The clinical trial enrolled 21 patients with advanced melanoma and dermal, subcutaneous, or nodal melanoma lesions amenable to intratumoral injection between December 2014 and March 2015 (see Table S1 for full patient

characteristics); seven (33%) had received prior anticancer therapy (including adjuvant therapy) and four (19%) had received prior radiotherapy. Patients had a median (range) potential follow-up time of 18.6 (17.7–20.8) months at the time of reporting.

Combined Talimogene Laherparepvec and Pembrolizumab Did Not Increase the Toxicities from Single-Agent Therapy

With the combined therapy, there were no novel or dose-limiting toxicities in any of the 21 patients (see Table S2 for full details on toxicities). The most common treatment-related toxicities were fatigue (62%), chills (48%), and fever (43%), which are anticipated with the intratumoral injection of talimogene laherparepvec (Andtbacka et al., 2015). Frequently occurring and partially overlapping pembrolizumab-related adverse events were fatigue (62%), rash (33%), arthralgia (33%), fever (29%), and chills (29%), which are anticipated with this agent (Ribas et al., 2016). One event of grade 1 cytokine-release syndrome resulted in hospitalization and was described as possibly related to the combination. The only other serious adverse events were attributed solely to pembrolizumab and included grade 3 autoimmune hepatitis, grade 3 aseptic meningitis, and grade 4 pneumonitis (one patient each). In the patient with treatment-related aseptic meningitis, no herpes simplex virus was detected in the cerebrospinal fluid; the patient had stopped therapy with talimogene laherparepvec and pembrolizumab 1 month earlier and had already switched therapy to dabrafenib and trametinib at the time of first presentation of this adverse event.

Antitumor Activity with Combined Talimogene Laherparepvec and Pembrolizumab

The confirmed objective response rate as evaluated by investigators per irRC (Wolchok et al., 2009) was 61.9% (95% CI, 38.4%–81.9%), with a confirmed complete response rate of 33.3% (95% CI, 14.6%–57.0%) (Table 1). Responses occurred across all substages of melanoma (Figures 1B and 1C). Nine patients presented a transient increase in overall tumor size during the administration of talimogene laherparepvec, in particular after the first dose (10⁶ pfu/mL) and before receiving the 10⁸-pfu/mL dose in combination with pembrolizumab; however, these lesions later responded to combined therapy (Figure 1D). Median progression-free survival (PFS) and overall survival (OS) were not reached at the time of last follow up (Figures 1E and 1F). The combination treatment resulted in a >50% reduction in 82% of injected, 43% of noninjected nonvisceral, and 33% of noninjected visceral lesions (Figure S2). Interestingly, among the seven patients with stage IIIB/IIIC disease, four patients had noninjected nonvisceral lesions. In these patients, there were a total of 16 injected and 10 noninjected nonvisceral lesions (baseline and new) that were evaluable for assessment of percentage change in tumor area from baseline. Fifteen injected lesions (93.7%) showed any reduction; 6 noninjected lesions (60%) showed any reduction (Table S3).

Tumor Responses Independent of Baseline CD8⁺ Infiltration, PD-L1 Status, and Interferon- γ Signature

PD-L1 is induced by interferon gamma (IFN- γ) produced by tumor-infiltrating, antigen-specific T cells, in what is termed

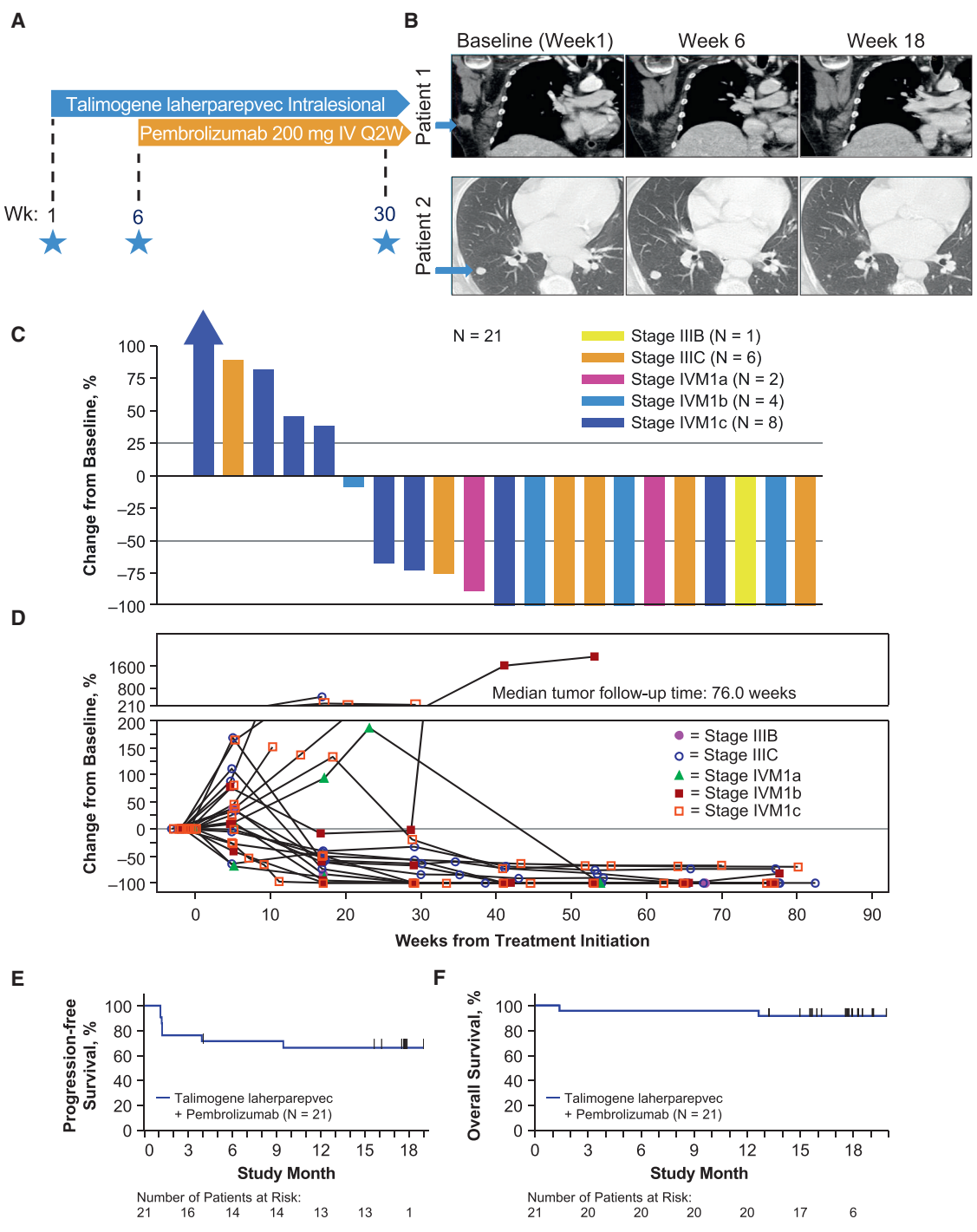


Figure 1. Melanoma Study Design and Clinical Response to Combination of Talimogene Laherparepvec and Pembrolizumab
 (A) Phase 1b study design schema. Stars indicate the time of scheduled tumor biopsies.
 (B) Computed tomography scans of two patients with response to the combination therapy. Melanoma metastases are marked with a blue arrow at baseline.
 (C) Waterfall plot of best response change in tumor burden from baseline. Patients were required to have baseline and ≥ 1 postbaseline tumor assessments to be included.
 (D) Change in tumor burden over time.
 (E) Kaplan-Meier analysis of progression-free survival.
 (F) Kaplan-Meier analysis of overall survival.
 See also Figures S1 and S2.

Table 1. Best Overall Response^a

	Talimogene Laherparepvec Plus Pembrolizumab (N = 21)	
	Total ^b	Confirmed ^b
Patients with a response	15	13
Response rate, % (95% CI)	71 (48–89)	62 (38–82)
Best overall response, n (%)		
Complete response	8 (38)	7 (33)
Partial response	7 (33)	6 (29)
Stable disease ^c	1 (5)	3 (14)
Progressive disease	5 (24)	5 (24)
Disease control rate, n (%)	16 (76)	16 (76)

^aResponse was evaluated per immune-related response criteria by investigators; data cutoff was August 31, 2016.

^bResponses were confirmed by a subsequent assessment at least 4 weeks later.

^cA best overall response of stable disease required an evaluation of stable disease no earlier than 77 days after enrollment.

adaptive immune resistance allowing cancer cells to avoid the cytotoxic activity of T cells (Pardoll, 2012; Ribas, 2015). Because these T cells are then blocked by PD-1:PD-L1 interactions, it is not surprising that patients who respond to single-agent PD-1 blockade therapy have higher densities of baseline CD8⁺ infiltration, IFN- γ gene expression signatures, and PD-L1 expression (Herbst et al., 2014; Ribas et al., 2015; Tumei et al., 2014). We analyzed baseline biopsies of patients in this study for CD8⁺ T cell density, PD-L1 positivity, and IFN- γ gene signature. As opposed to prior experience with single-agent pembrolizumab therapy (Ribas et al., 2015; Tumei et al., 2014), responses in this clinical trial were evident in patients whose baseline biopsies had very low CD8⁺ T cell infiltrates or negative IFN- γ gene signature. Among 13 patients in whom biopsies revealed a CD8⁺ density < 1,000 cells/mm², 9 patients went on to respond to therapy and 4 patients had disease progression (Figure 2A). Out of the five patients with baseline biopsies with a low IFN- γ signature, three patients went on to have a complete response and two had disease progression (Figure 2B). There was only one baseline biopsy that was scored as PD-L1 negative, but that patient went on to have a complete response to the combined therapy (Figure 2B).

Talimogene Laherparepvec Intratumoral Injections Increase CD8⁺ T Cell Infiltration in Patients Who Respond to Combined Therapy

Because some patients whose baseline biopsies had relatively low CD8⁺ cell density and were not positive for an IFN- γ gene signature went on to have an objective response, we analyzed whether the run-in period with single-agent talimogene laherparepvec had changed the tumor microenvironment by bringing T cells into metastatic melanoma lesions in patients who responded to therapy. Indeed, immunohistochemical (IHC) analysis comparing baseline biopsies with biopsies performed after talimogene laherparepvec alone showed an increase in the density of infiltrating CD8⁺ T cells in 8 out of 12 injected lesions available for analysis, which further increased in several of the

biopsies obtained at the time of combined therapy (Figures 3A and 3B). In three patients with a response to therapy, the CD8⁺ density decreased in the on-therapy biopsy, and one additional patient had no change in CD8⁺ density. The three patients without a response all had a decrease in CD8⁺ density in the on-therapy biopsies. Overall, the increase in CD8⁺ density was most evident in the injected lesions of the patients who went on to respond to therapy (Figure 3B), a relationship supported by logistic regression analysis ($p = 0.0048$; Figure S3A; logistic regression described in STAR Methods). The change in CD8⁺ infiltration density was variable in the noninjected lesions at week 6 even in patients who later responded to therapy, with the caveat that there are only three such biopsies available for interpretation (Figures 3B and S3B). Some posttreatment tumor-depleted samples were not initially analyzed because of histologic absence of tumor in the sample, but upon reevaluation were found to have evidence of prior tumor content (indicated by open symbols in Figures 3B and 3C). In the five patients with tumor-depleted samples at week 6, the CD8⁺ cell density was much higher in the injected lesions from the four responding patients as compared with the single nonresponder. We also performed IHC for the cytotoxic granule component granzyme B (associated with the cytotoxic subset of CD8⁺ T cells and natural killer cells), which has been shown to increase in tumors after PD-1 blockade (Tumei et al., 2014). A trend suggesting increased granzyme B in tumors after talimogene laherparepvec and combination treatment was also observed, in particular for the biopsies with low residual tumor content (Figure 3C). Furthermore, on analysis of tumor gene expression data, we found that CD8 α and IFN- γ mRNAs were elevated after treatment, providing additional supporting evidence for treatment-related change in the tumor microenvironment increasing the number of IFN- γ -producing cytotoxic T cells (Figures 3D and 3E). CD8 α increased 1.7-fold ($p = 0.01$) in injected lesions at week 6 compared with baseline and 1.44-fold ($p = 0.0012$) in noninjected lesions. Similarly, the IFN- γ fold increases for injected and noninjected lesions were 1.63 ($p = 0.0004$) and 1.41 ($p = 0.17$), respectively.

Characterization of Changes in Immune Cell Infiltrates in Talimogene Laherparepvec Injected and Noninjected Lesions

To further characterize changes in tumors, we performed multiplexed immunofluorescence staining of paired biopsies at different time points from 13 patients. We observed broad changes in tumor inflammation after talimogene laherparepvec at week 6, including increased infiltration by immune cells and a clear increase in cells expressing PD-L1 in eight out of ten injected tumors and in two out of four noninjected tumors (Figure 4A). Changes in immune infiltrates in the on-treatment biopsies from some patients included an influx of a large proportion of CD4⁺ and CD8⁺ T cells, many coexpressing PD-1, as well as CD56⁺-expressing cells and CD20⁺ B cells (the full set of immunofluorescence analyses in biopsies is reported in Table S4). Increases were also observed in the density of cells expressing the memory T cell marker CD45RO and in cells expressing the regulatory T cell (Treg) marker Foxp3 (Figure 4A). The magnitude of effector T cell (Teff) increases, however, was

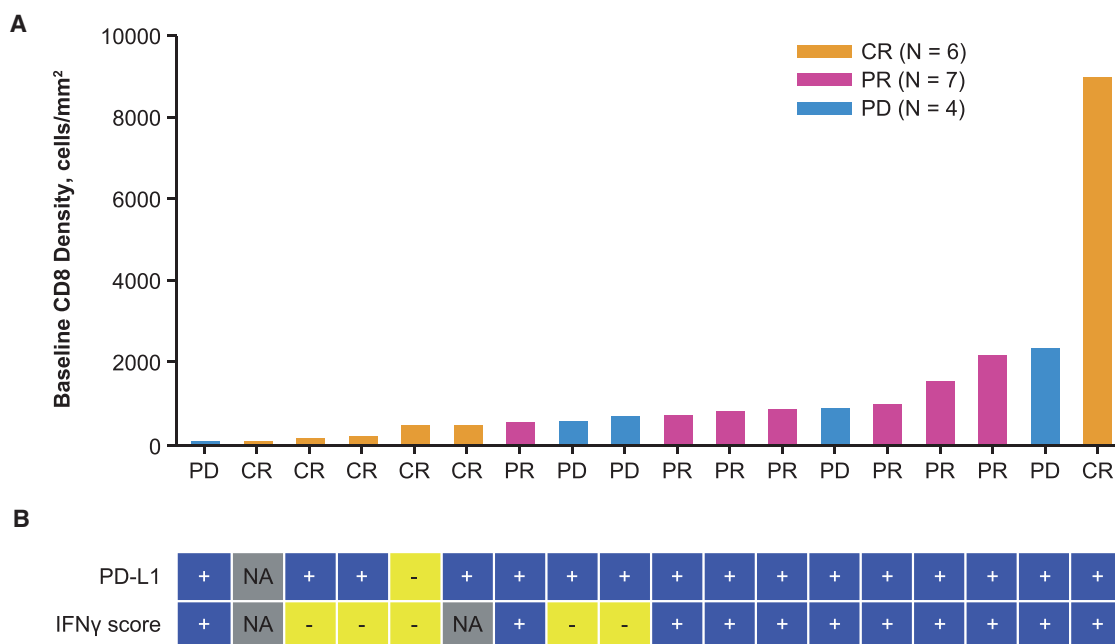


Figure 2. Combination of Talimogene Laherparepvec and Pembrolizumab Is Effective in Patients with Low Tumor CD8⁺ Density

(A) Baseline CD8⁺ density in tumor biopsies according to response rate. Magnitude of bars indicates baseline tumor CD8⁺ density in each patient's baseline biopsy, and best overall response is indicated on x axis and by bar color. Gold, CR; pink, PR; blue, PD.

(B) Baseline PD-L1 by IHC status (1% cutoff) and IFN- γ signature score by NanoString analysis is shown under each patient's CD8 result. Best overall response per investigator is shown as of cutoff date of August 2016. Abbreviations: CR, complete response; IFN- γ , interferon γ ; IHC, immunohistochemistry; NA, result not available; PD, progressive disease; PR, partial response.

much larger relative to Treg cells, resulting in an overall decrease in the Treg to Teff ratio in tumors after talimogene laherparepvec (Figure S4) consistent with previous reports (Kaufman et al., 2010). Table S4 additionally shows that there was no apparent change in the density of macrophages based on CD68 staining. An example of increased CD8⁺ and PD-L1 density by immunofluorescence at weeks 6 and 30 relative to baseline is shown in Figure 4B. At weeks 6 and 30, tumor cells costaining for S100 (blue) and PD-L1 (red) are evident along with CD8⁺ T cells (green), showing coexpression of PD-L1. The biopsy taken during combined therapy in a responding patient was nearly completely infiltrated by CD8⁺ T cells. Additional representative images are shown in Figure S5. Finally, to address potential changes in dendritic cell subsets, we assessed *CD141* (marker of Batf3 cross-priming dendritic cells) and *CD123* (a marker of plasmacytoid dendritic cells) mRNA levels. We did not observe significant changes in either marker in biopsies from talimogene laherparepvec-injected and -noninjected lesions from week 1 to 6 (Figure S6).

Changes in the Functional Phenotype of Circulating T Cells with Combined Therapy

We also analyzed changes in immune cells in peripheral blood as a potential pharmacodynamic effect of single-agent and combined therapy. After talimogene laherparepvec single-agent therapy, the majority of patients had an increase in the number of circulating CD8⁺ and CD4⁺ T cells in peripheral blood, which did not increase further when pembrolizumab

was added (Figures 5A and 5B). However, the addition of pembrolizumab tended to increase the number of dividing CD8⁺ T cells in circulation as indicated by increases in Ki67⁺CD3⁺CD8⁺ T cells (Figure 5C). Analysis of the expression of different immune checkpoint receptors in circulating CD3⁺CD8⁺ T cells revealed an increase in PD-1 and TIM-3 (a molecule expressed on IFN- γ -producing CD8⁺ and CD4⁺ T cells) with single-agent talimogene laherparepvec therapy (Figures 5D and 5E), whereas there was no change in B- and T-lymphocyte attenuator protein (BTLA; Figure 5F). No associations of response with baseline cell levels or changes over time passed our false discovery controls.

DISCUSSION

This first-in-human combination immunotherapy clinical trial demonstrates a high overall and complete response rate in patients with advanced melanoma, which was associated with changes in tumor biopsies that were mechanistically correlated with the hypothesis that the injection of the oncolytic virus talimogene laherparepvec would change the tumor microenvironment by attracting T cells that may induce a systemic response in distant metastases after subsequent blockade of PD-1 with pembrolizumab. Indeed, during the run-in period of the study with single-agent talimogene laherparepvec intratumoral administration, there was evidence of a systemic increase in circulating CD4⁺ and CD8⁺ T cells and increased CD8⁺ T cell infiltration into tumors. These T cells expressed PD-1 and the tumor cells expressed PD-L1, likely limiting

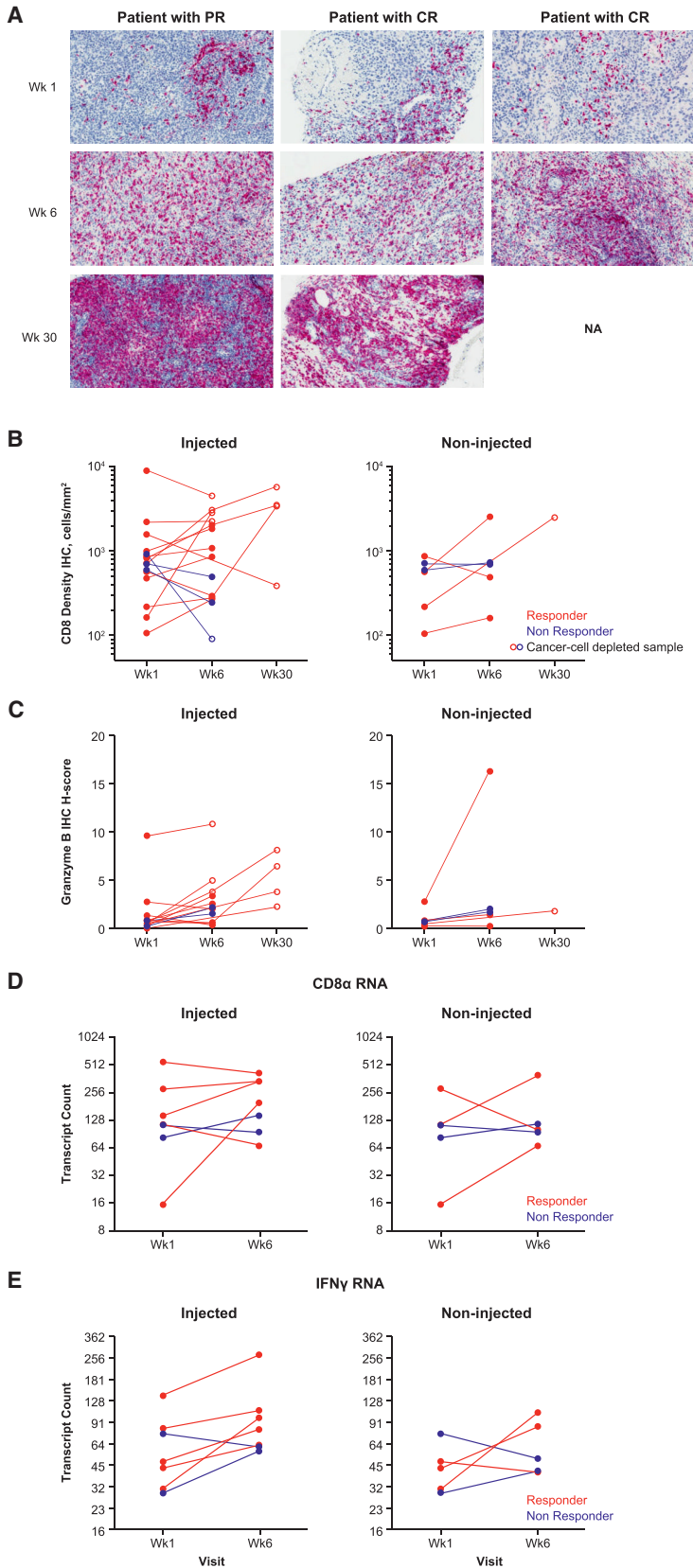


Figure 3. Talimogene Laherparepvec Increases Tumor CD8⁺ Density in Patients Responding to Combination of Talimogene Laherparepvec and Pembrolizumab

(A) Examples of pre (week 1) and post (week 6) talimogene laherparepvec and talimogene laherparepvec plus pembrolizumab (week 30) CD8⁺ density in tumor biopsies: visualization of cells stained with CD8 antibody with red chromogen. Staining was quantified for tissue regions of interest including CD8⁺ density in the tumor as shown for talimogene laherparepvec-injected tumors. (B and C) CD8⁺ density (B) and granzyme B H-score (C) is shown for baseline and postbaseline biopsies. The left side in each panel shows postbaseline results from injected lesions, and the right side in each panel shows results from noninjected lesions. Open circles indicate results from tumor biopsies that were depleted of melanoma cells but had pathologic features of having previously been infiltrated by melanoma cells such as melanin deposits. Response is color coded for best overall response per investigator (complete or partial response in red and nonresponse in blue). (D and E) CD8α (D) and IFN-γ normalized (E) mRNA transcript count were measured in the NanoString Pan Cancer Immune Profiling Panel. IFN-γ = interferon γ. See also Figure S3.

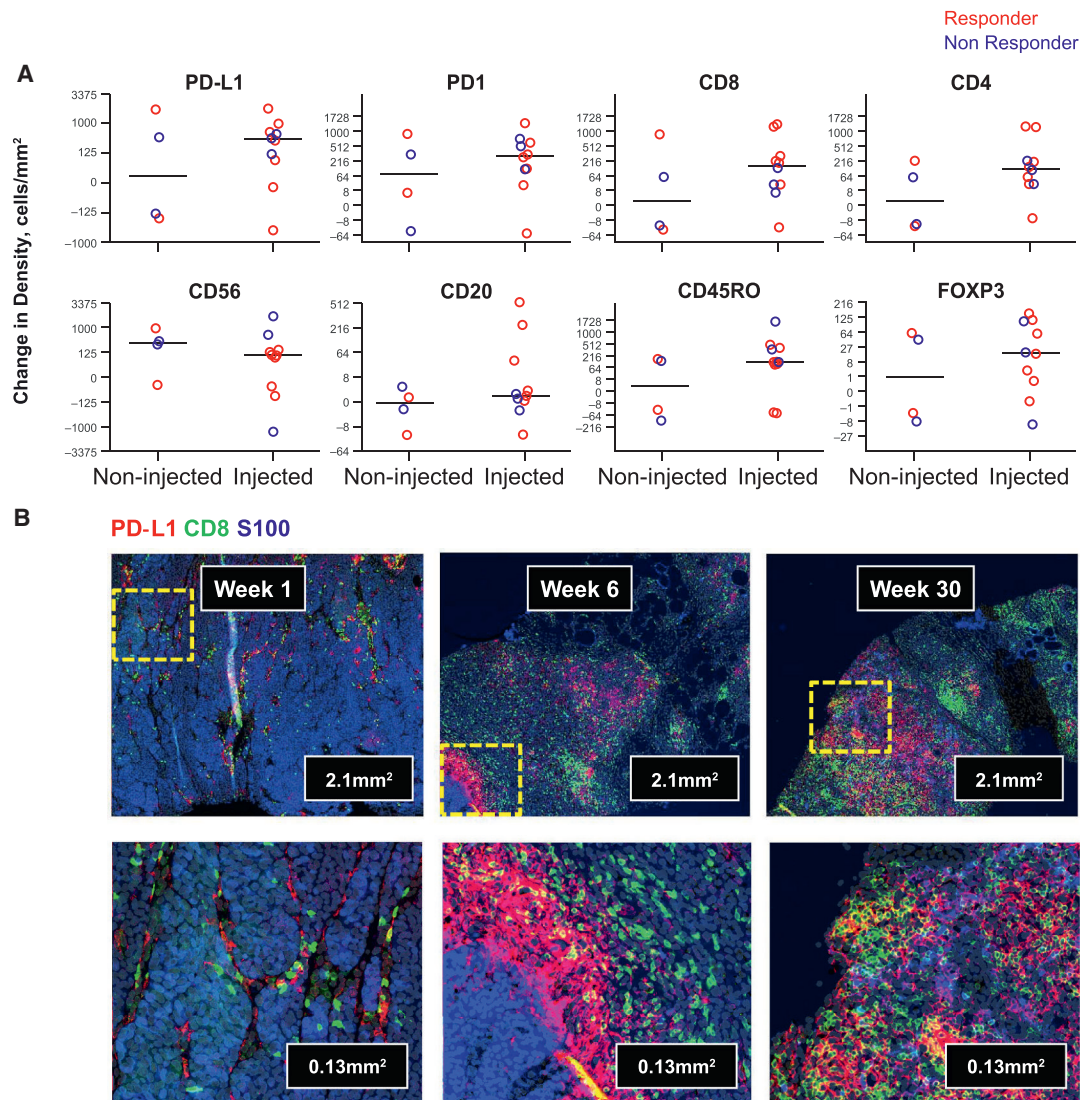


Figure 4. Talimogene Laherparepvec Increases Tumor-Infiltrating Lymphocyte Density and PD-L1 Expression in Tumors

Twelve-color immunofluorescence staining was performed on a single slide from paired pre- and post-talimogene laherparepvec tumor biopsies from each of 13 patients. Markers evaluated included S100 (as melanoma segmentation marker), CD3, CD4, CD8, PD-1, PD-L1, CTLA-4, CD45RO, Foxp3, CD56, CD68, and CD20.

(A) A subset of changes at week 6 from baseline in marker cell positive cell density for results with statistical significance (PD-L1, PD-1, CD8, CD4, CD56, CD20, CD45RO, and Foxp3) are graphed for noninjected (left) and injected (right) samples. Median change for each subset is shown with a horizontal line. Response is color coded for best overall response per investigator: complete or partial response in red and nonresponse in blue.

(B) Example of the combination of S100 (blue), CD8 (green), and PD-L1 (red) staining is shown at low (top) and high (bottom) magnification for a baseline biopsy from a patient who went on to have a partial response (week 1), week 6 after injection of talimogene laherparepvec, and at week 30 after long-term treatment with the combination of talimogene laherparepvec and pembrolizumab. Abbreviations: CTLA-4, cytotoxic T cell-associated antigen 4; I, biopsy of an injected metastasis; PD-1, programmed death protein 1; PD-L1, programmed death ligand 1; NI, biopsy of a noninjected metastasis.

See also Figures S4–S6.

the antitumor activity of single-agent talimogene laherparepvec, which benefitted from PD-1 blockade, thereby resulting in clinical activity beyond what would be expected with either therapy alone. The benefit of increased responses was achieved with a low rate of toxicities, most of which were expected with the single-agent use of talimogene laherparepvec or pembrolizumab (Andtbacka et al., 2015; Ribas et al., 2016).

PD-1 blockade therapy with pembrolizumab or nivolumab leads to an objective response of approximately 35% to 40% for treatment-naïve patients with metastatic melanoma (Ribas et al., 2016; Robert et al., 2015a, 2015b). Although the need to select patients who had injectable lesions may have skewed the population toward those with a good prognosis, an overall response rate of 62% and a CR rate of 33% is unlikely to be a

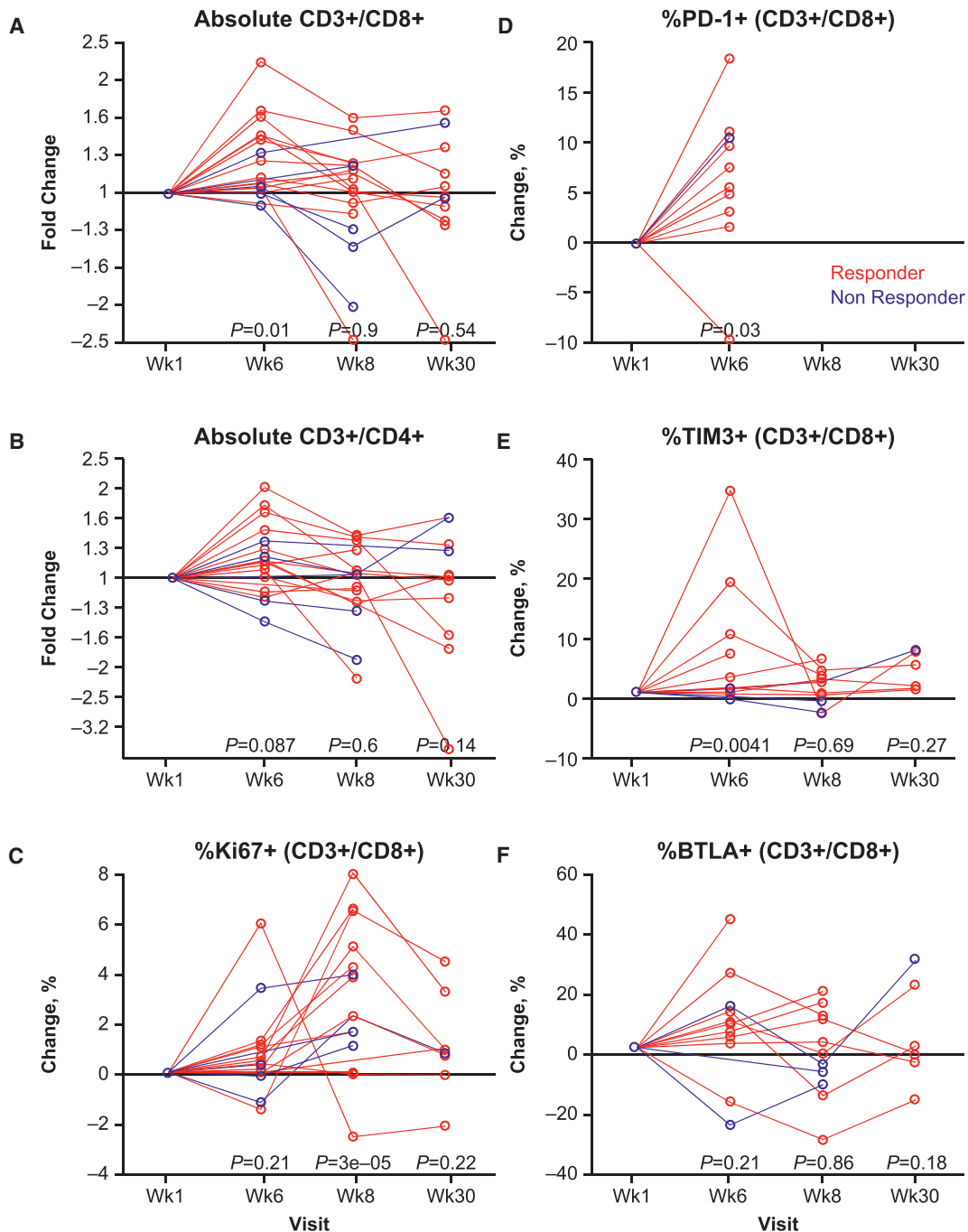


Figure 5. Circulating T Cell Subsets and Expression of Activation Markers

Peripheral blood cells obtained from baseline, week 1, week 6, week 8, and week 30 were analyzed by flow cytometry.

(A) Fold change in absolute CD3⁺CD8⁺ cells.

(B) Fold change in absolute CD3⁺CD4⁺ cells.

(C) Percentage change in Ki67⁺ (CD3⁺CD8⁺) cells.

(D) Percentage change in PD-1⁺ (CD3⁺CD8⁺) cells at week 1 and week 6 only; after starting on pembrolizumab, the staining antibody competed for the same epitope.

(E) Percentage change in TIM3⁺ (CD3⁺CD8⁺) cells.

(F) Percentage change in BTLA⁺ (CD3⁺CD8⁺) cells.

p values for comparison with baseline are shown below data for each postbaseline visit, based on contrasts from linear mixed-effects modeling. Response is color-coded for best overall response per investigator (complete or partial response in red and nonresponse in blue). Abbreviations: BTLA, B- and T-lymphocyte attenuator; PD-1, programmed death protein 1.

result of anti-PD-1 therapy alone. In a study of 655 patients treated with pembrolizumab, there were 34 patients who had only skin and nodal metastases (stage M1a), and the overall response rate in this group of patients was 38% (Ribas et al., 2016). When evaluating the efficacy outcomes of the current study, it is important to note that the primary objective of this study was to evaluate the safety of the combination of talimogene laherparepvec and pembrolizumab in patients with advanced melanoma. Therefore, we acknowledge that the interpretation of the efficacy outcomes is limited by the small size of the study population ($n = 21$) and the limited number of enrolled patients with stage IV M1c disease. Only a randomized trial would be able to definitively demonstrate that the combination is better than either single-agent pembrolizumab or talimogene laherparepvec. An ongoing phase 3 clinical trial is currently comparing systemic administration of pembrolizumab with intralesional injection of talimogene laherparepvec or placebo in patients with stage IIIB-IV melanoma (ClinicalTrials.gov: NCT02263508).

To significantly increase the response rate to single-agent anti-PD-1, a new combination therapy should address the major mechanism for primary resistance. Patients whose baseline biopsies had low densities of CD8⁺ T cells, lack of significant IFN- γ expression, and resulting low PD-L1 expression would be unlikely to respond (Postow et al., 2015; Ribas et al., 2015; Topalian et al., 2012; Tumei et al., 2014). Therefore, the combination therapy should increase the intratumoral infiltration by CD8⁺ T cells, which may attract enough T cells with tumor specificity to reverse the primary resistance to PD-1 blockade therapy (Chen et al., 2016; Ribas, 2015). Our data suggest that talimogene laherparepvec may provide this combinatorial effect. In this study, the number of patients with tumors with low baseline CD8⁺ density and a low IFN- γ signature who had an objective response to combined therapy was high compared with prior trials of single-agent pembrolizumab (Ribas et al., 2015; Tumei et al., 2014).

Evidence that local administration of talimogene laherparepvec contributed to a systemic antitumor effect was provided by the increase in circulating CD8⁺ and CD4⁺ T cells and the increase in inflammation observed in tumors not injected with talimogene laherparepvec before the introduction of pembrolizumab. In the pivotal single-agent study of talimogene laherparepvec, a decrease in tumor size was observed in 15% of evaluable, noninjected, measurable visceral lesions (Andtbacka et al., 2015, 2016). We also observed reductions in dimensions of noninjected lesions, including both visceral and nonvisceral lesions (including in patients with stage IIIB/IIIC disease). Approximately two out of the four week 6 noninjected lesions showed increased CD8⁺ density and PD-L1 (by immunofluorescence), and three out of five for IFN- γ mRNA. Alternatively, talimogene laherparepvec's unique properties (incorporating local GM-CSF for dendritic cell recruitment together with its own innate immune stimulation via toll-like receptors and cytoplasmic sensing pathways to promote adaptive immune responses) may provide a unique set of signals, making it ideal for immunotherapy combinations, including checkpoint inhibitors. Although we did not detect any differences in dendritic cell subset markers from week 1 to week 6 in the either injected or noninjected lesions (Figure S6), it is possible that the late timing of the biopsies (with week 6 occurring 2 weeks after the previous talimogene laherparepvec

injection) was not optimal to address this question. Another possibility is that the selected marker, *CD141* (mRNA), was not specific enough to accurately represent Batf3 DC abundance. Therefore, we also evaluated additional Batf3 DC markers, *IRF8* and *XCR1*, but significant changes were not observed for these markers either. Future studies evaluating biopsies soon after talimogene laherparepvec injection will be needed to determine the timing of dendritic cell recruitment and to address the role of local GM-CSF. Further information on events leading to CD8⁺ infiltration is provided by preclinical studies. Administration of OncoVEXmGM-CSF (talimogene laherparepvec with the mouse GM-CSF transgene) alone or in combination with checkpoint blockade in an A20 contralateral murine tumor model resulted in increased tumor-specific CD8⁺ T cells and also anti-AH1 T cells and systemic efficacy (Moesta et al., 2017).

We will seek confirmation of the conclusions from this 21-patient phase 1b study (e.g., lack of requirement for baseline tumor infiltration) in the ongoing phase 3 study of the combination of talimogene laherparepvec plus pembrolizumab, which is currently accruing 660 patients, half receiving combination therapy and half receiving pembrolizumab with intratumoral placebo in the control arm (ClinicalTrials.gov: NCT02263508). Also, to further evaluate systemic effects of talimogene laherparepvec, a separate biomarker study is ongoing to evaluate baseline and post-talimogene laherparepvec noninjected tumors from more than 100 patients (ClinicalTrials.gov: NCT02366195). This will help provide follow-up data on findings from the small set of tumor biopsies not injected with talimogene laherparepvec in this series, many of which showed increased tumor inflammation.

In conclusion, the high response rate in this phase 1 clinical trial and the mechanistic changes documented in patient biopsies suggest that the combination of talimogene laherparepvec and pembrolizumab may be able to overcome some limitations of either single-agent therapy and provide responses beyond what would be expected with either talimogene laherparepvec or pembrolizumab administered alone.

STAR★METHODS

Detailed methods are provided in the online version of this paper and include the following:

- KEY RESOURCES TABLE
- CONTACT FOR REAGENT AND RESOURCE SHARING
- EXPERIMENTAL MODEL AND PATIENT DETAILS
- METHOD DETAILS
 - Study Design
 - Study Clinical Assessments
 - Biomarker Analysis
- QUANTIFICATION AND STATISTICAL ANALYSIS
- DATA AND SOFTWARE AVAILABILITY
- ADDITIONAL RESOURCES

SUPPLEMENTAL INFORMATION

Supplemental Information includes six figures and four tables and can be found with this article online at <http://dx.doi.org/10.1016/j.cell.2017.08.027>.

A video abstract is available at <http://dx.doi.org/10.1016/j.cell.2017.08.027#mmc2>.

AUTHOR CONTRIBUTIONS

A.R., R.D., I.P., O.M., A.J.O., J.M., J.C., E.F., and G.V.L. participated in patient data collection, data acquisition, analysis and interpretation of data, and the writing and editing of the manuscript. A.V.W. and R.H.I.A. participated in the conception and design of the study, patient data collection, data acquisition, analysis and interpretation of data, and the writing and editing of the manuscript. J.M.K., T.F.G., and A.A.A. assisted with the analysis and interpretation of the data and the writing and editing of the manuscript. L.C., K.S.G., and F.S.H. participated in the conception and design of the study, assisted with the analysis and interpretation of the data, and contributed to the writing and editing of the manuscript. S.J.D., M.L., and J.G. assisted with the analysis and interpretation of the data and contributed to the writing and editing of the manuscript.

ACKNOWLEDGMENTS

The authors thank the following individuals: Richard Scolyer, Robyn Saw, Andrew Spillane, Kenneth Lee, and Omgo Neiwig of the Melanoma Institute Australia for tumor excision biopsies to maximize tissue acquisition; Hajime Hiraragi (Amgen Inc.) for peer review of tumor biopsy analyses. Jessica Stern (Amgen Inc.) for flow cytometry peer review and organization of IHC image galleries for preparation of figures, David Kaufman and Christine Gause from Merck & Co for many hours of designing the study and the statistical plan for both the phase 1b and 3 portions, and with special acknowledgment to Jeffrey Chou, MD, PhD, for his medical and scientific contributions to the design and execution of this study during his tenure as the Amgen medical monitor. A.R. is supported by the NIH grant R35 CA197633. I.P. is supported by NIH grant P20CA016056 to Roswell Park Cancer Institute. G.V.L. is supported by an Australian NHMRC fellowship (APP1119059) and the Medical Foundation K8625, University of Sydney. Lastly, we wish to thank Meghan Johnson, PhD (Complete Healthcare Communications, LLC, West Chester, PA), whose work was funded by Amgen Inc., Emily Plummer, PhD (Amgen Inc.), and Mee Rhan Kim, PhD (Amgen Inc.) for assistance in the preparation of this manuscript. The study was funded by Amgen Inc.

A.R. has received consulting fees from Amgen Inc. and Merck. R.D. has intermittent, project-focused consulting and/or advisory relationships with Novartis, Merck Sharp & Dohme, Bristol-Myers Squibb, Roche, Amgen Inc., Takeda, and Pierre Fabre outside the submitted work. I.P. has received consulting fees and honoraria from Amgen Inc. A.V.W. has received research grants from Amgen Inc. and consulting fees from Bristol-Myers Squibb, AstraZeneca, and Amgen Inc. R.H.I.A. has received consulting fees from Amgen Inc., Merck, Takara, and Provectus. O.M. has previously served on advisory boards for Bristol-Myers Squibb, Merck Sharp & Dohme, Roche, Novartis, and Amgen Inc. and has received travel assistance from Bristol-Myers Squibb, Merck Sharp & Dohme, and Amgen Inc. A.J.O. has received research grants from Takeda, Bristol-Myers Squibb, Kyowa, Immunocore, EMD Serono, Amgen Inc., Incyte, Eli Lilly, Advaxis, Mirati, Ignyta, Novartis, Pfizer, and Kura and has received consulting fees from Merck, Takeda, Bristol-Myers Squibb, G1 therapeutics, and Kyowa Hakko Kirin. J.M. has received research grants from Almirall, Amgen Inc., Roche, GlaxoSmithKline, and Bristol-Myers Squibb; has received consulting fees from Almirall, Amgen Inc., Pierre Fabre, and Leo Pharma; and has served on speakers' bureaus for Amgen Inc., Almirall, Novartis, and Isdin. J.C. has received honoraria from GlaxoSmithKline, Bristol-Myers Squibb, Novartis, Merck Sharp & Dohme, and Amgen Inc.; has served in a non-remunerative position of influence for Austin Health Oncology Information System project Control Group, Olivia Newton-John Cancer & Wellness Centre Executive Committee, and Olivia Newton-John Cancer and Wellness Centre MRI Advisory Committee; has served as a consultant/advisor for Amgen Inc., Biogen, Bristol-Myers Squibb, Merck Sharp & Dohme, and Novartis; has received research funding to his institution from GlaxoSmithKline and CSL; has patents/intellectual property at GlaxoSmithKline, Bristol-Myers Squibb, and Novartis; and is an employee of the Olivia Newton-John Cancer Research Institute. E.F. has received consulting fees from Amgen, Inc. J.M.K. has received research grants from Merck and Prometheus and has received consulting fees from Bristol-Myers Squibb, Green Peptide, Roche, Solaran RX, Checkmate Pharmaceuticals, and Novartis. T.F.G. has received research

funding from Amgen Inc., Bristol-Myers Squibb, Merck, Roche/Genentech, Ono, Incyte, and Seattle Genetics; has served on advisory board or as a consultant for Merck, Roche/Genentech, Bayer, Abbvie, Aduro, and Jounce; and owns stock in Jounce. L.C., K.S.G., A.A.A., and J.G. are employees of, and own stock in, Amgen Inc. S.J.D. and M.L. are employees of, and own stock in, Merck. F.S.H. has received research funding from Bristol-Myers Squibb; has received consulting fees from Amgen Inc., Merck, Bristol-Myers Squibb, Novartis, EMD Serono, Celldex, and Genentech; and has received royalties to his institution (per institutional policy) from MICA; related disorders patent pending. G.V.L. has received consulting fees from Amgen Inc., Array, Bristol-Myers Squibb, Merck Sharp & Dohme, Novartis, Roche, and Pierre Fabre.

Received: April 10, 2017

Revised: July 11, 2017

Accepted: August 15, 2017

Published: September 7, 2017

REFERENCES

- Andtbacka, R.H., Kaufman, H.L., Collichio, F., Amatruda, T., Senzer, N., Chesney, J., Delman, K.A., Spittle, L.E., Puzanov, I., Agarwala, S.S., et al. (2015). Talimogene laherparepvec improves durable response rate in patients with advanced melanoma. *J. Clin. Oncol.* **33**, 2780–2788.
- Andtbacka, R.H., Ross, M., Puzanov, I., Milhem, M., Collichio, F., Delman, K.A., Amatruda, T., Zager, J.S., Cranmer, L., Hsueh, E., et al. (2016). Patterns of clinical response with talimogene laherparepvec (T-VEC) in patients with melanoma treated in the OPTiM phase III clinical trial. *Ann. Surg. Oncol.* **23**, 4169–4177.
- Chen, P.L., Roh, W., Reuben, A., Cooper, Z.A., Spencer, C.N., Prieto, P.A., Miller, J.P., Bassett, R.L., Gopalakrishnan, V., Wani, K., et al. (2016). Analysis of immune signatures in longitudinal tumor samples yields insight into biomarkers of response and mechanisms of resistance to immune checkpoint blockade. *Cancer Discov.* **6**, 827–837.
- Chesney, J., Collichio, F., Andtbacka, R.H., Puzanov, I., Glaspy, J.A., Milhem, M., Hamid, O., Cranmer, L., Saenger, Y., Ross, M., et al. (2016). Interim safety and efficacy of a randomized (1:1), open-label phase 2 study of talimogene laherparepvec (T) and ipilimumab (I) vs I alone in unresected, stage IIIB–IV melanoma. *Ann. Oncol.* **27**, <http://dx.doi.org/10.1093/annonc/mdw379.04>.
- Chesney, J., Puzanov, I., Ross, M., Collichio, F., Milhem, M., Chen, L., Kim, J.H., Garbe, C., Hauschild, A., and Andtbacka, R.H.I. (2017). Primary results from a randomized (1:1), open-label phase II study of talimogene laherparepvec (T) and ipilimumab (I) vs I alone in unresected stage IIIB–IV melanoma. *J. Clin. Oncol.* **35**, 9509–9509.
- Daud, A.I., Wolchok, J.D., Robert, C., Hwu, W.J., Weber, J.S., Ribas, A., Hodi, F.S., Joshua, A.M., Kefford, R., Hersey, P., et al. (2016). Programmed death-ligand 1 expression and response to the anti-programmed death 1 antibody pembrolizumab in melanoma. *J. Clin. Oncol.* **34**, 4102–4109.
- Gerdes, M.J., Sevinsky, C.J., Sood, A., Adak, S., Bello, M.O., Bordwell, A., Can, A., Corwin, A., Dinn, S., Filkins, R.J., et al. (2013). Highly multiplexed single-cell analysis of formalin-fixed, paraffin-embedded cancer tissue. *Proc. Natl. Acad. Sci. USA* **110**, 11982–11987.
- Herbst, R.S., Soria, J.C., Kowanetz, M., Fine, G.D., Hamid, O., Gordon, M.S., Sosman, J.A., McDermott, D.F., Powderly, J.D., Gettinger, S.N., et al. (2014). Predictive correlates of response to the anti-PD-L1 antibody MPDL3280A in cancer patients. *Nature* **515**, 563–567.
- Hoffner, B., Iodice, G.M., and Gasal, E. (2016). Administration and handling of talimogene laherparepvec: an intralesional oncolytic immunotherapy for melanoma. *Oncol. Nurs. Forum* **43**, 219–226.
- Kaufman, H.L., Kim, D.W., DeRaffele, G., Mitcham, J., Coffin, R.S., and Kim-Schulze, S. (2010). Local and distant immunity induced by intralesional vaccination with an oncolytic herpes virus encoding GM-CSF in patients with stage IIIc and IV melanoma. *Ann. Surg. Oncol.* **17**, 718–730.
- Liu, B.L., Robinson, M., Han, Z.Q., Branston, R.H., English, C., Reay, P., McGrath, Y., Thomas, S.K., Thornton, M., Bullock, P., et al. (2003). ICP34.5

- deleted herpes simplex virus with enhanced oncolytic, immune stimulating, and anti-tumour properties. *Gene Ther.* 10, 292–303.
- Moesta, A.K., Cooke, K., Piasecki, J., Mitchell, P., Rottman, J.B., Fitzgerald, K., Zhan, J., Yang, B., Le, T., Belmontes, B., et al. (2017). Local delivery of OncoVEX(^{mGM-CSF}) generates systemic anti-tumor immune responses enhanced by cytotoxic T-lymphocyte-associated protein blockade. *Clin. Cancer Res.* Published online July 13, 2017. <http://dx.doi.org/10.1158/1078-0432.CCR-17-0681>.
- Pardoll, D.M. (2012). The blockade of immune checkpoints in cancer immunotherapy. *Nat. Rev. Cancer* 12, 252–264.
- Postow, M.A., Callahan, M.K., and Wolchok, J.D. (2015). Immune checkpoint blockade in cancer therapy. *J. Clin. Oncol.* 33, 1974–1982.
- Puzanov, I., Milhem, M.M., Minor, D., Hamid, O., Li, A., Chen, L., Chastain, M., Gorski, K.S., Anderson, A., Chou, J., et al. (2016). Talimogene laherparepvec in combination with ipilimumab in previously untreated, unresectable stage IIIB-IV melanoma. *J. Clin. Oncol.* 34, 2619–2626.
- Ribas, A. (2015). Adaptive immune resistance: how cancer protects from immune attack. *Cancer Discov.* 5, 915–919.
- Ribas, A., Robert, C., Hodi, F.S., Wolchok, J.D., Joshua, A.M., Hwu, W.J., Weber, J.S., Zarour, H.M., Kefford, R., Loboda, A., et al. (2015). Association of response to programmed death receptor 1 (PD-1) blockade with pembrolizumab (MK-3475) with an interferon-inflammatory immune gene signature. *J. Clin. Oncol.* 33, 3001.
- Ribas, A., Hamid, O., Daud, A., Hodi, F.S., Wolchok, J.D., Kefford, R., Joshua, A.M., Patnaik, A., Hwu, W.J., Weber, J.S., et al. (2016). Association of pembrolizumab with tumor response and survival among patients with advanced melanoma. *JAMA* 315, 1600–1609.
- Robert, C., Long, G.V., Brady, B., Dutriaux, C., Maio, M., Mortier, L., Hassel, J.C., Rutkowski, P., McNeil, C., Kalinka-Warzocho, E., et al. (2015a). Nivolumab in previously untreated melanoma without BRAF mutation. *N. Engl. J. Med.* 372, 320–330.
- Robert, C., Schachter, J., Long, G.V., Arance, A., Grob, J.J., Mortier, L., Daud, A., Carlino, M.S., McNeil, C., Lotem, M., et al.; KEYNOTE-006 investigators (2015b). Pembrolizumab versus ipilimumab in advanced melanoma. *N. Engl. J. Med.* 372, 2521–2532.
- Sharma, P., and Allison, J.P. (2015). The future of immune checkpoint therapy. *Science* 348, 56–61.
- Spranger, S., Spaepen, R.M., Zha, Y., Williams, J., Meng, Y., Ha, T.T., and Gajewski, T.F. (2013). Up-regulation of PD-L1, IDO, and T(regs) in the melanoma tumor microenvironment is driven by CD8(+) T cells. *Sci. Transl. Med.* 5, 200ra116.
- Topalian, S.L., Hodi, F.S., Brahmer, J.R., Gettinger, S.N., Smith, D.C., McDermott, D.F., Powderly, J.D., Carvajal, R.D., Sosman, J.A., Atkins, M.B., et al. (2012). Safety, activity, and immune correlates of anti-PD-1 antibody in cancer. *N. Engl. J. Med.* 366, 2443–2454.
- Tumeh, P.C., Harview, C.L., Yearley, J.H., Shintaku, I.P., Taylor, E.J., Robert, L., Chmielowski, B., Spasic, M., Henry, G., Ciobanu, V., et al. (2014). PD-1 blockade induces responses by inhibiting adaptive immune resistance. *Nature* 515, 568–571.
- Wolchok, J.D., Hoos, A., O'Day, S., Weber, J.S., Hamid, O., Lebbé, C., Maio, M., Binder, M., Bohnsack, O., Nichol, G., et al. (2009). Guidelines for the evaluation of immune therapy activity in solid tumors: immune-related response criteria. *Clin. Cancer Res.* 15, 7412–7420.

Modified mRNA Vaccines Protect against Zika Virus Infection

Justin M. Richner,^{1,9} Sunny Himansu,^{2,9} Kimberly A. Dowd,³ Scott L. Butler,² Vanessa Salazar,¹ Julie M. Fox,¹ Justin G. Julander,⁴ William W. Tang,⁵ Sujan Shrestha,⁵ Theodore C. Pierson,³ Giuseppe Ciaramella,^{2,*} and Michael S. Diamond^{1,6,7,8,10,*}

¹Department of Medicine, Washington University School of Medicine, St. Louis, MO 63110, USA

²Valera LLC, a Moderna Venture, 500 Technology Square, Cambridge, MA, 02139, USA

³Viral Pathogenesis Section, National Institutes of Health, Bethesda, MD 20892 USA

⁴Institute for Antiviral Research, Utah State University, Logan, UT, 84335 USA

⁵Division of Inflammation Biology, La Jolla Institute for Allergy and Immunology, La Jolla, CA 92037, USA

⁶Department of Pathology and Immunology, Washington University School of Medicine, St. Louis, MO 63110, USA

⁷Department of Molecular Microbiology, Washington University School of Medicine, St. Louis, MO 63110, USA

⁸The Andrew M. and Jane M. Bursky Center for Human Immunology and Immunotherapy Programs, Washington University School of Medicine, St. Louis, MO 63110, USA

⁹Co-first authors

¹⁰Lead Contact: Michael S. Diamond

*Correspondence: diamond@wusm.wustl.edu (M.S.D.), Giuseppe.Ciaramella@Valeratx.com (G.C.)

<http://dx.doi.org/10.1016/j.cell.2017.02.017>

SUMMARY

The emergence of ZIKV infection has prompted a global effort to develop safe and effective vaccines. We engineered a lipid nanoparticle (LNP) encapsulated modified mRNA vaccine encoding wild-type or variant ZIKV structural genes and tested immunogenicity and protection in mice. Two doses of modified mRNA LNPs encoding prM-E genes that produced virus-like particles resulted in high neutralizing antibody titers (~1/100,000) that protected against ZIKV infection and conferred sterilizing immunity. To offset a theoretical concern of ZIKV vaccines inducing antibodies that cross-react with the related dengue virus (DENV), we designed modified prM-E RNA encoding mutations destroying the conserved fusion-loop epitope in the E protein. This variant protected against ZIKV and diminished production of antibodies enhancing DENV infection in cells or mice. A modified mRNA vaccine can prevent ZIKV disease and be adapted to reduce the risk of sensitizing individuals to subsequent exposure to DENV, should this become a clinically relevant concern.

INTRODUCTION

Zika virus (ZIKV) was identified in 1947 from a Rhesus monkey in the Zika Forest of Uganda (Dick, 1952; Dick et al., 1952). Historically, ZIKV circulated between *Aedes* species mosquitoes and non-human primates and episodically spilled into human populations in parts of Africa and Asia. Prior to 2010, ZIKV infection was described as a self-limiting febrile illness with headache, rash, conjunctivitis, and myalgia. More recently, and especially

in the context of its spread in the Western Hemisphere, more severe clinical consequences have been observed (Lazear and Diamond, 2016). Infection of fetuses during pregnancy has been associated with placental insufficiency and congenital malformations including cerebral calcifications, microcephaly, and miscarriage (Brasil et al., 2016; Rasmussen et al., 2016; van der Eijk et al., 2016). In adults, ZIKV infection is linked to Guillain-Barré syndrome (GBS), an autoimmune disease characterized by paralysis and polyneuropathy (Cao-Lormeau et al., 2016; Oehler et al., 2014). Sexual transmission of ZIKV also has been described from men-to-women (Foy et al., 2011), men-to-men (Deckard et al., 2016), and women-to-men (Davidson et al., 2016). Persistent ZIKV has been detected in semen, sperm, and vaginal secretions up to 6 months following infection (Mansuy et al., 2016; Murray et al., 2017). ZIKV is now a global disease of the Americas, Africa, and Asia.

ZIKV is a member of the *Flavivirus* genus of the *Flaviviridae* family of enveloped RNA viruses. ZIKV has an ~11 kb positive sense RNA genome. Translation of viral RNA in the cytoplasm generates a polyprotein that is cleaved into three structural proteins (capsid [C], pre-membrane/membrane [prM/M], and envelope [E]) and seven non-structural proteins (NS1, NS2A, NS2B, NS3, NS4A, NS4B, and NS5). ZIKV buds into the lumen of the endoplasmic reticulum as an immature virion composed of 60 icosahedrally arranged prM-E heterotrimers (Prasad et al., 2017). As the virus transits through the secretory pathway, the acidic environment of the Golgi network triggers exposure of a furin protease cleavage site within prM. Cleavage of prM and release of the pr peptide in the extracellular space produces mature, infectious virions that display 90 antiparallel E homodimers on their surface. The ZIKV E protein is composed of three ectodomains (DI, DII, and DIII) and is the primary target of neutralizing antibodies. Potently inhibitory monoclonal antibodies (mAbs) against ZIKV target epitopes in all three E protein domains as well as quaternary structures composed of multiple domains within or across E dimers (Barba-Spaeth et al., 2016;

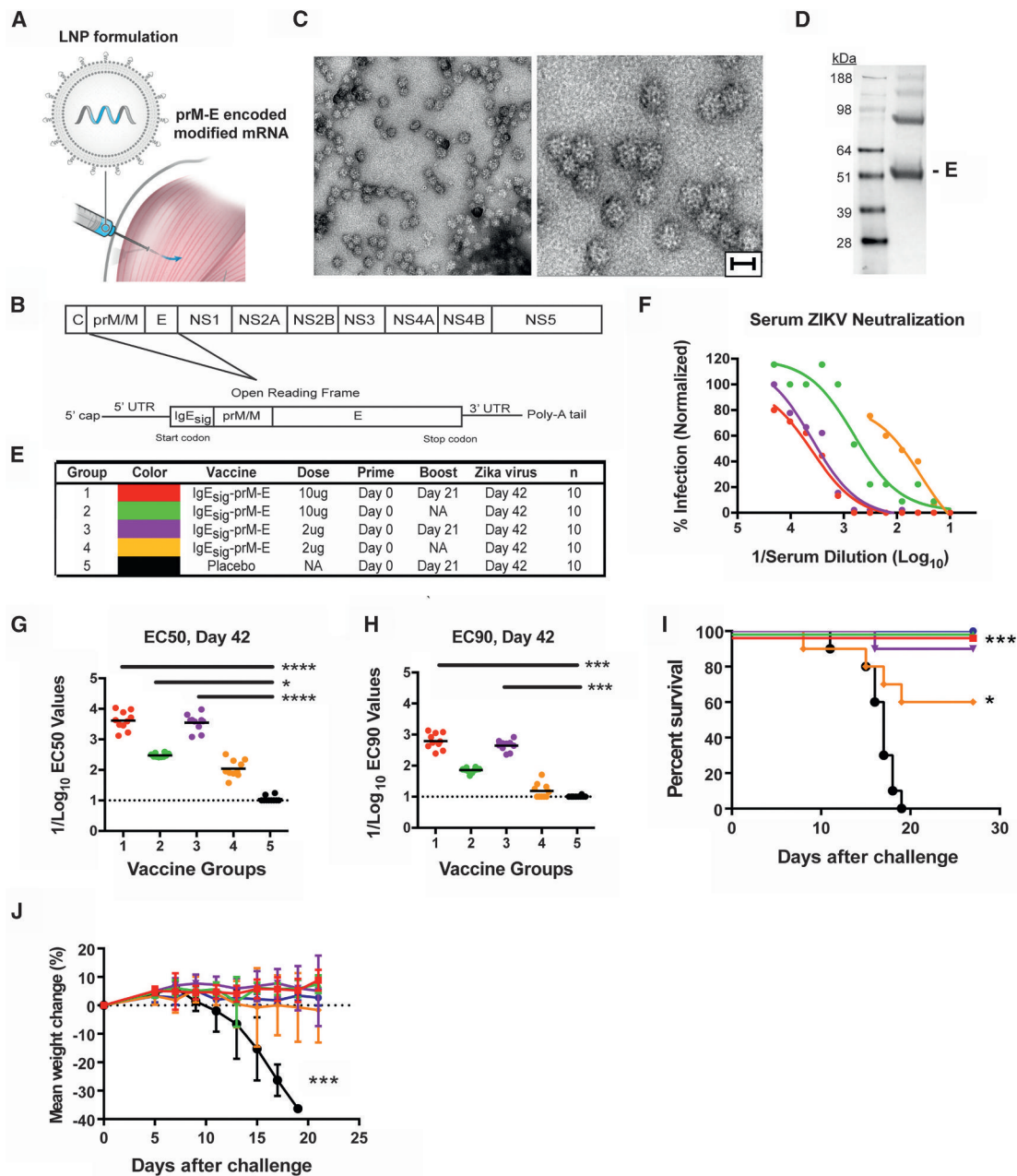


Figure 1. ZIKV mRNA LNP Vaccine Testing in AG129 Mice

(A) ZIKV prM-E modified mRNA is packaged into LNPs for intramuscular delivery.

(B) Schematic of ZIKV genome (top). An mRNA encoding the ZIKV prM/M and E structural genes was engineered (bottom). In this construct, prM is directed into the ER using a heterologous IgE signal sequence (IgE_{sig}) at the amino-terminus.

(C) HeLa cells were transfected with prM-E mRNA, and SVPs in the supernatant were purified and concentrated by ultracentrifugation and then subjected to electron microscopy and negative staining. Low- and high-power images of purified SVPs are shown. Scale bar, 30 nm. One representative experiment of several is shown.

(D) HeLa cell supernatants were collected for western blotting under non-reducing conditions with a mAb against the ZIKV E protein.

(E) Scheme of immunization of AG129 mice with one (prime) or two (prime-boost) doses of 2 or 10 μ g with IgE_{sig} prM-E or placebo mRNA LNP vaccines.

(F–H) Serum was collected at 6 weeks after vaccination and analyzed for neutralization of ZIKV by PRNT assay. Representative curves are shown (F), and EC50 (G) and EC90 (H) values were calculated for individual animals in each group. Each point represents the mean of two independent experiments per animal. Data are a composite of two independent experiments with sera from each of the ten animals per group. EC50 and EC90 data were analyzed by a Kruskal-Wallis test with a multiple comparisons correction and compared to the placebo LNP vaccine (* $p < 0.05$; *** $p < 0.001$; **** $p < 0.0001$). The dashed lines indicate the limit of detection of the assay.

(legend continued on next page)

Sapparapu et al., 2016; Stettler et al., 2016; Swanstrom et al., 2016; Wang et al., 2016; Zhao et al., 2016). In addition to induction by infectious or inactivated virus particles, neutralizing antibodies against ZIKV can be produced after immunization with DNA plasmids encoding M-E protein (Larocca et al., 2016) or prM-E, which in some cases generates secreted virus-like subviral particles (SVPs) (Dowd et al., 2016b; Muthumani et al., 2016).

The existence of two ZIKV lineages, African and Asian/American (Haddow et al., 2012) does not impact antibody neutralization substantively and thus, ZIKV is classified as a single serotype (Dowd et al., 2016a). ZIKV is related to several pathogens that cause disease globally including dengue (DENV), yellow fever (YFV), West Nile (WNV), Japanese encephalitis (JEV), and tick-borne encephalitis (TBEV) viruses. Of these viruses, ZIKV is most closely related to the four serotypes of DENV as it shares 54 to 59% amino acid identity in the viral E protein (Dejnirattisai et al., 2016).

Because of its potential to infect and cause harm to developing fetuses and neonates (Huang et al., 2016), there is an urgent call to develop countermeasures (Marston et al., 2016). Several groups have developed subunit (prM-E or M-E DNA plasmid or adenovirus-vectored) or inactivated virus vaccine platforms capable of eliciting neutralizing antibodies that protect against ZIKV viremia in mice and non-human primates (Abblink et al., 2016; Dowd et al., 2016b; Larocca et al., 2016; Muthumani et al., 2016). Some of these vaccine candidates have initiated or are scheduled to begin recruitment of subjects for evaluation in humans (NCT02840487, NCT02887482, NCT02809443, NCT02937233, NCT02952833, and NCT02963909).

The sequence similarity between ZIKV and DENV poses issues for vaccine development due to cross-reactivity of the human anti-ZIKV antibody response (Dejnirattisai et al., 2016; Sapparapu et al., 2016; Stettler et al., 2016). Cross-reactive antibody responses may contribute minimally to protection, consistent with the limited neutralizing activity of many broadly-reactive anti-flavivirus mAbs in cell culture. Whereas primary infection with DENV generates an antibody response that protects against the homologous serotype, secondary infection with a heterologous DENV serotype can result in a potentially lethal shock syndrome. This disease is attributed in part to antibody-dependent enhancement of infection (ADE), whereby cross-reactive antibodies elicited by the first DENV serotype augment infection of the second DENV serotype in cells expressing Fc- γ receptors (Morens, 1994). This phenomenon could be relevant to ZIKV vaccination because DENV and ZIKV are related closely, and vaccinated subjects in or travelers to endemic areas could become exposed secondarily to DENV, which infects ~390 million people per year (Bhatt et al., 2013). Indeed, cross-reactive antibodies targeting the highly conserved fusion loop in DII of E (E-DII-FL) derived during natural ZIKV infection can augment infectivity of DENV in cell culture (Dejnirattisai et al., 2016; Ka-

wiecki and Christofferson, 2016; Stettler et al., 2016) and in vivo in mice (Stettler et al., 2016). These laboratory-based data are not conclusive, as epidemiological studies, which may take years to perform, are required to establish the impact of ZIKV humoral immunity on DENV pathogenesis. Vaccine strategies that reduce induction of cross-reactive antibodies (Crill et al., 2012) might minimize the risk of sensitizing recipients to severe DENV infections, should the clinical relevance of ZIKV immunity on DENV pathogenesis be established.

We generated a versatile ZIKV vaccine platform in which lipid nanoparticles encapsulate modified mRNA encoding wild-type (WT) or variant ZIKV structural genes. Unlike DNA plasmid based vaccines, mRNA does not integrate into chromosomes, which can lead to insertional mutagenesis and potential oncogenesis (Pardi and Weissman, 2017). Non-amplifying or self-amplifying mRNA-based vaccines were used recently to generate humoral responses against influenza A virus in mice (Hekele et al., 2013; Petsch et al., 2012) or HIV in non-human primates (Bogers et al., 2015). Our modified non self-amplifying mRNA vaccines have an optimized mRNA containing an open reading frame that encodes the antigen of interest, 5' and 3' untranslated regions that optimize translation efficiency and intracellular stability, and a proprietary nucleoside modification to minimize the indiscriminate activation of innate immunity. mRNA can stimulate innate immunity through Toll-like and RIG-I-like receptors (Desmet and Ishii, 2012; Karikó et al., 2004). Although the adjuvant effect of stimulating innate immunity might be advantageous for protein vaccines, indiscriminate immune activation can inhibit mRNA translation, thus reducing antigen expression and immunogenicity of an mRNA vaccine (Cláudio et al., 2013; Coffman et al., 2010). This can be overcome by replacing uridine nucleosides with naturally-occurring base modifications, such as pseudouridine and 5-methylcytidine (Anderson et al., 2011). Here, a two-dose immunization of modified mRNA encoding ZIKV prM-E induced high levels of neutralizing antibodies that protected mice with genetic or acquired innate immune deficiencies against severe infection. Because mRNA vaccines can be synthesized with virtually any sequence, we created modified mRNA immunogens encoding mutations that abolished an immunodominant cross-reactive epitope in E-DII-FL. These mRNA induced protective antibody responses against ZIKV in mice and minimized the generation of cross-reactive antibodies that enhanced DENV infection in cell culture and pathogenicity in mice.

RESULTS

An mRNA Vaccine Platform for ZIKV

We developed a vaccine platform for generating optimized lipid nanoparticles that encapsulate modified mRNA for intramuscular delivery to induce high levels of protein expression in vivo (Figure 1A and Figure S1). As a proof-of-principle, we designed a modified mRNA encoding a type 1 (N7^mGpppG^m) cap,

(I–J) AG129 Mice were challenged at 6 weeks post-vaccination with 10^4 PFU of ZIKV P6-740. Animals were monitored for survival (I) and weight loss (J). Error bars indicate standard error the mean (SEM). Survival data were analyzed by the log rank test (* $p < 0.05$; *** $p < 0.001$). Weight loss was analyzed by two-way ANOVA (** $p < 0.001$).

See also related Figures S1 and S2.

optimized 5' and 3' untranslated sequences (see STAR Methods), the signal sequence from human IgE, and the full-length prM and E genes from an Asian (Mirconesia 2007) ZIKV strain (Lanciotti et al., 2008), which has >99% amino acid sequence identity relative to strains from the Americas (Figure 1B). The modified mRNA was synthesized enzymatically and packaged into lipid nanoparticles (LNPs). Incubation of LNPs containing IgE signal-prM-E mRNA (IgE_{sig}-prM-E) with 293T or HeLa cells resulted in efficient expression and secretion of ~30 nm SVPs, as judged by electron microscopy (Figure 1C), western blotting (Figure 1D) and mass spectrometry for ZIKV structural proteins in the cell supernatants (data not shown).

Vaccine Efficacy in AG129 Mice

We first assessed the immunogenicity and protective activity of IgE_{sig}-prM-E LNPs in immunocompromised mice lacking type I and II interferon (IFN) signaling responses. Eight-week-old *Ifnar1*^{-/-} *Ifngr*^{-/-} AG129 male and female mice were divided into five groups, which received an intramuscular inoculation of 2 or 10 μg of IgE_{sig}-prM-E LNPs or 10 μg of a non-translating RNA LNP. Groups 1, 3, and 5 were boosted with the same dose at 21 days after vaccination whereas Groups 2 and 4 were not boosted (Figure 1E). At day 42 after immunization, mice were phlebotomized for serum neutralizing antibody analysis (Figures 1F–1H and Figure S2). Mice receiving the IgE_{sig}-prM-E LNPs with a boost had the strongest serum neutralizing response against ZIKV, with reciprocal dilution EC50 (half-maximal inhibition of virus infection) and EC90 values of up to 1/10,000 and 1/1,000, respectively. Mice receiving only a single immunization had lower neutralizing titers.

At 42 days after vaccination, AG129 mice were challenged with the ZIKV strain P6-740 (Malaysia, 1966). As expected (Aliota et al., 2016), AG129 mice receiving the negative control LNP vaccine succumbed to ZIKV infection (Figure 1I). With the exception of a single animal, recipients of the 2 or 10 μg IgE_{sig}-prM-E LNP vaccine with a boost as well as those receiving a single 10 μg dose all survived infection. In comparison, mice receiving a single 2 μg dose of the vaccine displayed an intermediate phenotype with a 60% survival rate. Weight measurements correlated with lethality, as mice receiving the IgE_{sig}-prM-E LNP vaccine were protected, whereas the negative controls lost weight beginning at approximately day 10 after challenge (Figure 1J).

Vaccine Efficacy in C57BL/6 Mice

To test the immunogenicity and efficacy of the IgE_{sig}-prM-E LNP vaccine efficacy in an immunocompetent mouse strain, we inoculated via intramuscular injection 8-week-old male C57BL/6 WT mice with 10 μg of IgE_{sig}-prM-E LNPs. These animals were phlebotomized prior to a single boost at day 28 (4 weeks) and before challenge at either day 56 (8 weeks) or day 126 (18 weeks). As expected, serum neutralization titers were relatively low prior to boosting; however, titers peaked at 4 weeks after boosting (EC50 of 1/10,000) and remained elevated 18 weeks post-initial vaccination (Figures 2A–2C and Figure S3). To create a lethal challenge model, we passively transferred 2 mg of a blocking anti-*ifnar1* antibody 1 day prior to infection with 10⁶ focus-forming units (FFU) of a mouse-adapted African ZIKV strain (Dakar 41519) (Sapparapu et al., 2016; Zhao et al., 2016). All mice immu-

nized with IgE_{sig}-prM-E LNPs were protected against lethal ZIKV infection compared to the control group, which had a 30% survival rate (Figure 2D). Mice vaccinated with IgE_{sig}-prM-E mRNA LNPs did not display any loss in weight (Figure 2E) nor had measurable viremia in serum at 5 days after challenge (Figure 2F).

Modified Vaccines Lacking the Immunodominant E-DII-FL Epitope Generate a Protective Anti-ZIKV Response

The highly conserved FL epitope in DII of the flavivirus E protein is immunodominant in humans (Beltramello et al., 2010; Crill et al., 2007; Dejnirattisai et al., 2010; Oliphant et al., 2007; Sapparapu et al., 2016; Stettler et al., 2016). As such, infection with ZIKV or vaccination with ZIKV structural proteins could induce cross-reactive antibodies, which might enhance DENV infection and disease through ADE (Morens, 1994; Stettler et al., 2016). To minimize this possibility, we generated modified mRNA vaccines by engineering four mutations (T76R, Q77E, W101R, and L107R) in or near the E-DII-FL (prM-E-FL) that abolish antibody reactivity of FL-specific antibodies (Chabierski et al., 2014; Crill et al., 2012; Oliphant et al., 2007). We also generated a separate series of mRNA LNPs by replacing the IgE leader sequence with one from Japanese encephalitis virus (JEV_{sig}), a feature included in other flavivirus prM-E DNA vaccines to increase the efficiency of host signalase cleavage (Davis et al., 2001; Dowd et al., 2016b), and by further optimizing codon usage (Figure 3A). Western blotting analysis showed similar levels of SVP expression in HeLa cell supernatants after transfection of WT and FL mutant mRNA, and a loss of FL reactivity was confirmed for the prM-E-FL mRNA by an absence of binding of a mAb (WNV E60) that recognizes this epitope (Oliphant et al., 2006) (Figure 3B).

Immunocompetent 8-week-old female BALB/c mice were immunized with 2 μg or 10 μg of IgE_{sig}-prM-E or JEV_{sig}-prM-E (WT or FL mutant) LNPs and boosted with the same LNPs 4 weeks later. At 8 weeks after initial vaccination, serum was analyzed for neutralizing activity using ZIKV reporter virus particles (RVPs) (Dowd et al., 2016a) (Figure 3 and Figure S4). Mice receiving 2 or 10 μg doses of the IgE_{sig}-prM-E WT and FL mutant LNPs showed similar neutralization titers (Figure 3C), with EC50 values of ~1/5,000 (Figure 3E). The 2 and 10 μg dose of the WT JEV_{sig}-prM-E LNPs induced stronger inhibitory responses with EC50 values of ~1/100,000 (Figures 3D and 3E) and EC90 values of ~1/10,000 (Figure 3F). The mutant JEV_{sig}-prM-E-FL LNPs, however, induced antibody responses with lower EC50 and EC90 values, which still approached 1/10,000 and 1/500, respectively.

At ~13 weeks after initial vaccination, mice were challenged with ZIKV Dakar 41519 after pre-administration of anti-*ifnar1* blocking antibody. At day 3 after infection, serum was analyzed for viremia. Consistent with their high neutralizing titers, all mice immunized with 2 or 10 μg doses of JEV_{sig}-prM-E LNPs lacked measurable viremia (Figure 3G). All other vaccine groups (IgE_{sig}-prM-E LNPs (WT or FL) or JEV_{sig}-prM-E FL LNPs) had breakthrough viremia in some animals, although levels were 10- to 100-fold lower than observed with placebo LNPs. Mice were euthanized at day 7 after infection and spleen, uterus, and brain were analyzed for ZIKV RNA levels (Figures 3H–3J). Most mice

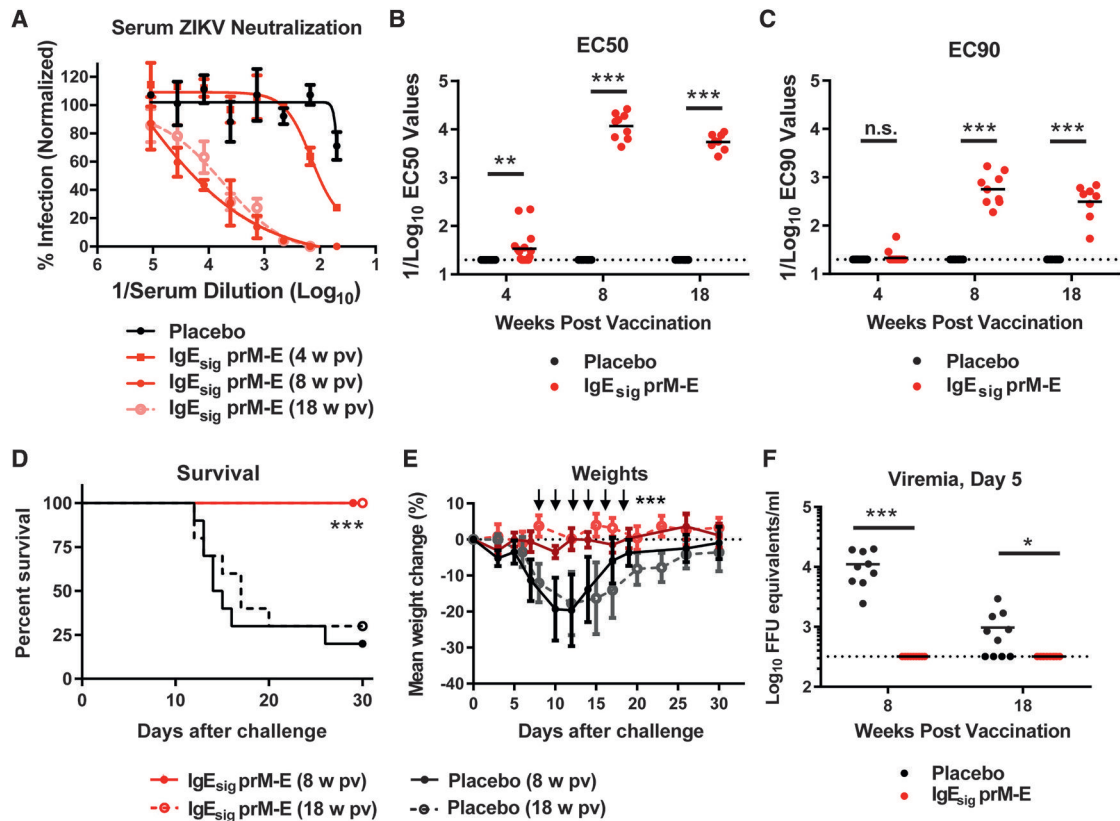


Figure 2. ZIKV mRNA LNP Vaccine Protects C57BL/6 Mice

WT C57BL/6 mice ($n = 10$, pooled from two independent experiments) were immunized with $10 \mu\text{g}$ of placebo or IgE_{sig} prM-E mRNA LNPs and boosted with an equivalent dose four weeks later.

(A) Serum was collected at 4, 8, and 18 weeks post-initial vaccination and analyzed for ZIKV neutralization activity by FRNT assay. Representative neutralization curves are shown for each group. Error bars denote SD of triplicate technical replicates.

(B and C) EC50 (B) and EC90 (C) values were calculated for individual animals in each group. The dashed lines indicate the limit of detection of the assay. Data were analyzed using the Mann-Whitney test and compared to the placebo LNP vaccine at each time point (** $p < 0.01$; *** $p < 0.001$; n.s. indicates not significant).

(D–F) At week 8 or 18, vaccinated C57BL/6 mice were administered 2 mg of anti-ifnar1 blocking antibody and 1 day later challenged with 10^5 FFU of mouse adapted ZIKV Dakar 41519. Animals were monitored for survival (D) and weight loss (E). At day 5 after viral challenge, serum was analyzed for levels of ZIKV RNA (F). The dashed line indicates the limit of detection of the assay. Survival data were analyzed by the log rank test (** $p < 0.001$). Weight loss was analyzed by two-way ANOVA (** $p < 0.001$) for surviving animals; arrows indicate days having statistically significant differences from placebo vaccine. Viremia data were analyzed by a Mann-Whitney test (* $p < 0.05$; *** $p < 0.001$). See also related Figure S3.

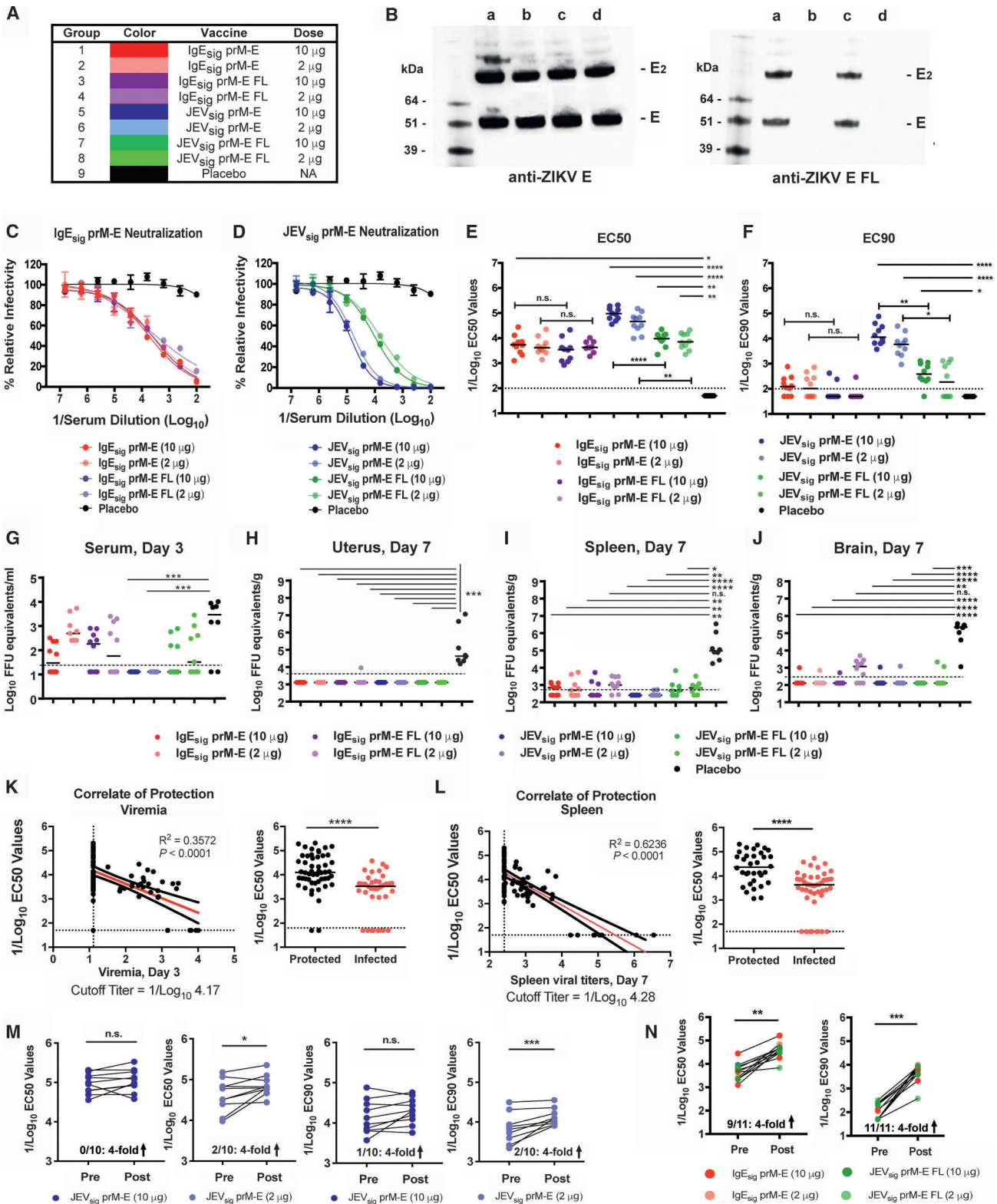
vaccinated with prM-E LNPs showed markedly reduced levels of viral RNA in the spleen (>100 -fold) and virtually no detectable viral RNA in the uterus or brain, whereas the placebo immunized animals had mean levels of 10^5 to 10^6 FFU equivalents per gram of tissue. Mice vaccinated with the $2 \mu\text{g}$ dose of IgE_{sig} -prM-E FL or JEV_{sig} -prM-E FL LNPs showed slightly less protection, as viral RNA was detectable in some animals in the spleen and brain, albeit at much lower levels than those immunized with placebo LNPs.

To establish an immune correlate of complete protection against ZIKV in this model, we compared the EC50 values from all mRNA LNP vaccines with the levels of viral RNA recovered in the serum and spleen from individual mice. This analysis revealed an expected inverse relationship between neutralizing titers and levels of ZIKV RNA in serum and tissues and defined a cut-off EC50 value of $\sim 1/10,000$ to completely prevent viremia and tissue dissemination (Figures 3K and 3L). We next evaluated

whether the JEV_{sig} -prM-E mRNA LNP vaccines, which protected almost completely against viremia or infection in tissues, conferred sterilizing immunity. The vast majority of animals (80% to 90%) receiving 2 or $10 \mu\text{g}$ doses of the JEV_{sig} -prM-E mRNA vaccines failed to boost neutralizing titers one week after challenge with infectious ZIKV, consistent with sterilizing immunity (Figure 3M). In comparison, most animals (82%–100%) showing breakthrough viremia or tissue burden with the IgE_{sig} -prM-E or JEV_{sig} -prM-E FL mRNA vaccines sustained marked increases in EC50 and EC90 values after challenge (Figure 3N), consistent with the induction of an anamnestic response.

Mutation of the DII-Fusion Loop Epitope Diminishes ADE in Cells and Mice

To evaluate whether the FL mutant vaccines diminished induction of cross-reactive enhancing antibodies, we incubated dilutions of serum obtained at 8 weeks after immunization with



(legend on next page)

DENV serotype 1 (DENV-1) RVPs (Dowd et al., 2015) and assessed infection in K562 cells, which express the activating human Fc- γ receptor IIA (CD32A). Whereas sera from mice vaccinated with WT IgE_{sig}-prM-E or JEV_{sig}-prM-E mRNA LNPs all showed bell-shaped, canonical antibody enhancement curves, many of the sera from mice immunized with serum from IgE_{sig}-prM-E-FL or JEV_{sig}-prM-E-FL LNPs supported enhancement at only high concentrations and with considerably reduced efficiency (Figures 4A–4C and Figure S5). Indeed, the peak serum enhancement titer (PET [Boonnak et al., 2008]) was \sim 100-fold lower in mice immunized with mutant forms of the fusion loop (Figure 4D). A similar reduction in enhancing power, or the fraction of infected cells at the PET was observed (Figures 4A, B, and 4E). Thus, introduction of mutations in the FL of ZIKV E reduced the production of enhancing antibodies against DENV, as judged by cell culture assays.

To determine the physiological significance of these results, we used an established passive transfer model of ADE for DENV in AG129 mice (Balsitis et al., 2010; Zellweger et al., 2010) with serum from the IgE_{sig}-prM-E and IgE_{sig}-prM-E-FL or JEV_{sig}-prM-E and JEV_{sig}-prM-E-FL vaccinated mice. We first evaluated the relative neutralizing activity of DENV-2 of pooled ZIKV serum using an established RVP assay in Raji-DCSIGNR cells (Dowd et al., 2015). Consistent with studies using FL-specific mAbs (Williams et al., 2013), the pooled sera from IgE_{sig}-prM-E or JEV_{sig}-prM-E but not IgE_{sig}-prM-E-FL or JEV_{sig}-prM-E-FL vaccinated animals inhibited DENV-2 infection in cell culture (Figure 4F and Figure S6A), indicating a cross-reactive antibody (likely FL-specific) was produced only in mice receiving the WT but not FL mutant vaccines, and this antibody could neutralize infection in Raji-DCSIGNR cells lacking activating Fc- γ receptors. We next transferred pooled sera to AG129 mice 1 day prior to challenge with a non-lethal dose of DENV-2. Whereas administration of 1 or 10 μ L of serum from mice vaccinated with WT IgE_{sig}-prM-E

or JEV_{sig}-prM-E LNPs or a positive control anti-prM mAb (2H2) resulted in uniformly lethal infection and severe disease due to antibody enhancement, transfer of equivalent amounts of sera from mice vaccinated with IgE_{sig}-prM-E FL or JEV_{sig}-prM-E-FL mutant LNPs resulted in significantly less morbidity and mortality (Figure 4G and 4H and Figure S6B).

DISCUSSION

As ZIKV emerges, the urgency for development and deployment of counter-measures to control infection increases (Marston et al., 2016). Here, we developed a ZIKV vaccine platform with modified mRNA encoding the prM-E proteins that was packaged into LNPs. Although mRNA-based vaccines were used recently to generate humoral responses against influenza A virus in mice (Hekele et al., 2013; Petsch et al., 2012) or HIV in non-human primates (Bogers et al., 2015), these platforms differed from ours in their use of self-replicating RNA or protamine complexed mRNA. We selected LNPs for delivery of the modified mRNA as they have been validated in clinical trials for siRNA delivery and are well tolerated compared to other non-viral delivery systems (Coelho et al., 2013). In proof-of-principle studies, we showed that LNP-delivered modified mRNA induced neutralizing antibodies that protected several strains (129 Sv, BALB/c, or C57BL/6) of susceptible mice with genetic or acquired deficiencies in IFN signaling against lethal ZIKV challenge. The neutralization titers induced by the IgE_{sig}-prM-E mRNA LNPs were uniformly high (50% neutralization titer of \sim 1/10,000) in all three mouse models. The protective responses conferred by mRNA LNP vaccines were durable; even 14 weeks after boosting, challenged mice showed no morbidity or mortality. Furthermore, by further optimizing the prM signal sequence and codon usage (JEV_{sig}-prM-E), we induced even more potent responses (EC50 of \sim 1/100,000 and EC90 of

Figure 3. ZIKV mRNA LNP Vaccines Containing WT or Mutant FL Sequences Induce Neutralizing Antibody Responses and Protect BALB/c Mice

(A) Immunization scheme. Female WT BALB/c mice ($n = 10$, pooled from two independent experiments) were immunized with 2 or 10 μ g of prM-E mRNA LNP vaccines containing either IgE or JEV signal sequences at the N terminus of prM and WT or mutant FL sequences in the E gene. Animals were boosted with the equivalent dose of the same vaccine 28 days later.

(B) HeLa cells were transfected with different modified mRNA (Lane a, IgE_{sig}-prM-E; Lane b, IgE_{sig}-prM-E FL mutant; Lane c, JEV_{sig}-prM-E; and Lane d, JEV_{sig}-prM-E FL mutant), and ZIKV E protein in the supernatant was detected by western blotting with a type-specific anti-ZIKV E antibody (left) or a cross-reactive anti-ZIKV E antibody that binds the FL (right). Results are the representative of two independent experiments. E, monomer; E₂, dimer.

(C–F) At week 8, serum was harvested from IgE_{sig}-prM-E (C) or JEV_{sig}-prM-E (D) mRNA LNP vaccinated mice and analyzed for neutralization capacity using ZIKV RVPs. Representative curves for each group (with EC50 values at or near the group median) are shown in (C) and (D). Error bars indicate the range of duplicate technical replicates. EC50 (E) and EC90 (F) values were calculated for individual animals in each group. Each point represents the results from a single experiment or the mean of two independent experiments. The dotted line indicates the limit of detection of the assay.

(G–J) At week 8, vaccinated BALB/c mice were administered 2 mg of anti-ifnar1 blocking antibody and 1 day later challenged with 10⁵ FFU of mouse adapted ZIKV Dakar 41519. At 3 (G) and 7 (H–J) days after viral challenge, serum (G), uterus (H), spleen (I), and brain (J) tissues were harvested and analyzed for ZIKV RNA. EC50, EC90, and viral titer data were analyzed by a Kruskal-Wallis test with a multiple comparisons correction and compared to the placebo LNP vaccine (* $p < 0.05$; ** $p < 0.01$; *** $p < 0.001$; **** $p < 0.0001$; n.s., not significant).

(K and L) Correlates of day 3 viral load (K, left), day 7 spleen titers (L, left) and protective efficacy (K and L, right) are shown. Data from all JEV_{sig}-prM-E and IgE_{sig}-prM-E mRNA LNP vaccines was included in this analysis. p values and R^2 values reflect Spearman rank-correlation tests. For correlate data, values at which the line would cross the limit of detection of the y axis are indicated below the graphs. Red line represents the best fit linear regression. For protective efficacy data, bars indicate median values (**** $p < 0.0001$; Mann-Whitney test).

(M and N) Anamnestic neutralizing antibody response. Paired sera were collected from vaccinated animals (JEV_{sig}-prM-E [M] or IgE_{sig}-prM-E and JEV_{sig}-prM-E FL [N]) immediately before (Pre) or 7 days after (Post) ZIKV challenge and analyzed for neutralizing activity using ZIKV RVPs. EC50 and EC90 values were analyzed for differences by a paired t test (n.s., not significant; * $p < 0.05$; ** $p < 0.01$; *** $p < 0.001$). Indicated at the bottom of the graphs are the number of animals showing a 4-fold increase in neutralization titer (positive anamnestic response) at 7 days after ZIKV challenge.

See also related Figure S4.

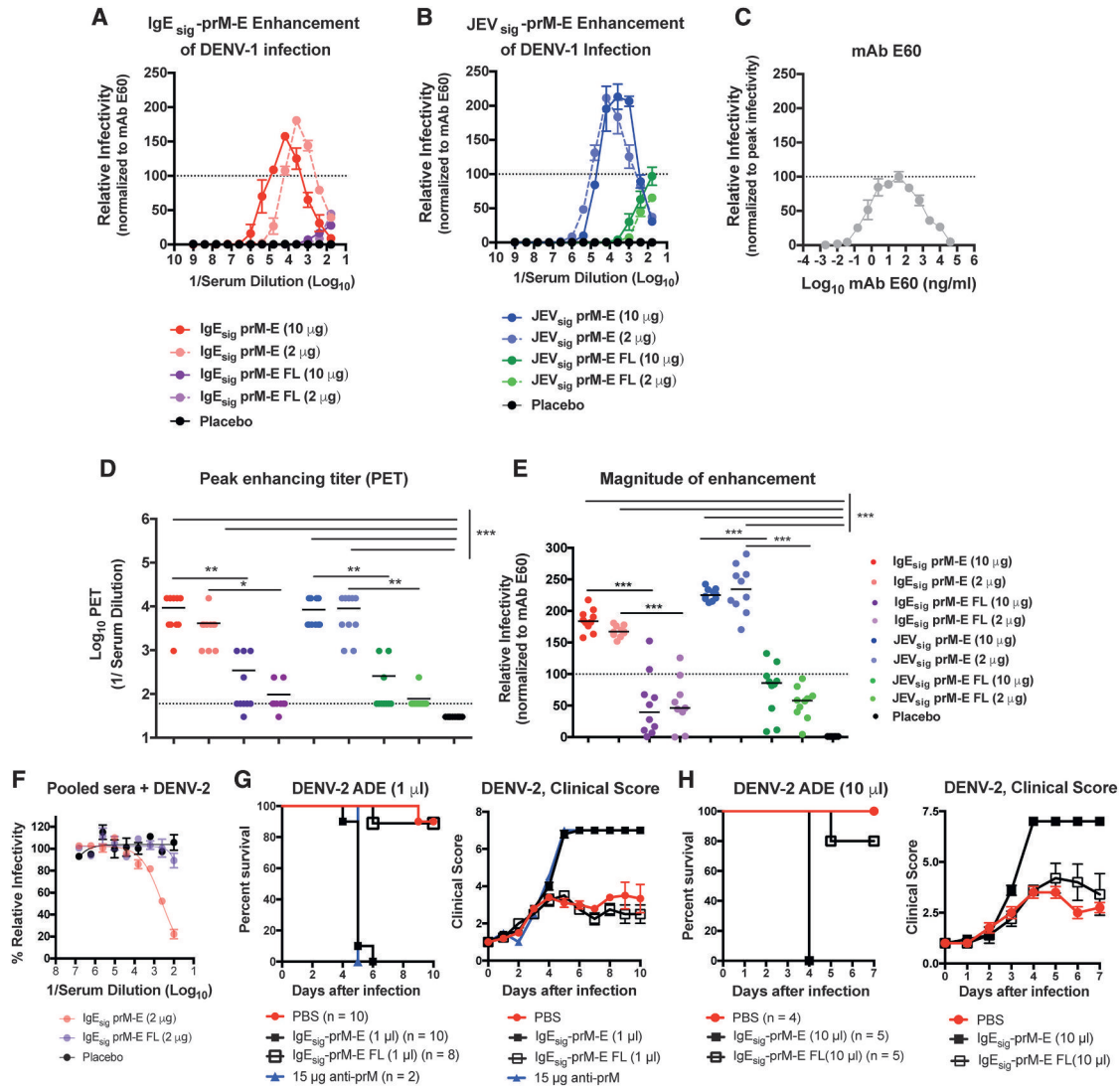


Figure 4. ZIKV mRNA LNP Vaccines Containing Mutant FL Sequences Showed Reduced ADE against DENV in Cell Culture and in AG129 Mice

(A and B) Serial dilutions of serum obtained at week 8 (see Figure 3) from BALB/c mice immunized with 2 or 10 μg of IgE_{sig}-prM-E (A) or JEV_{sig}-prM-E (B) mRNA LNPs with WT or mutant FL sequences were mixed with DENV-1 RVPs and incubated with Fc-γ receptor expressing K562 cells. Infected cells were quantified by flow cytometry. Representative curves for each group (with peak enhancement titers (PET) at or near the group median) are shown in (A) and (B). (C) Results are displayed relative to the maximum infectivity observed with the control cross-reactive WNV mAb E60 (FL-specific) run in parallel (C). The dotted line is provided as a reference for mAb E60 normalization. Error bars indicate the range of duplicate technical replicates.

(D) Peak enhancement titer (PET) for each mouse per group. Data were analyzed by a Kruskal-Wallis one-way ANOVA with a multiple comparisons correction and compared to the control LNP vaccine (**p < 0.01; ***p < 0.001).

(E) Magnitude of enhancement (extent of infection at the PET) for each mouse per group.

(F) Neutralization of DENV-2 RVPs by sera pooled from placebo or IgE_{sig}-prM-E (2 μg dose of WT or FL mutant) vaccinated mice. Error bars indicate the range of duplicate technical replicates.

(G and H) Enhancing effects of ZIKV immune serum on DENV-2 infection in AG129 mice. Recipient AG129 mice were passively transferred PBS, 1 μl (G) or 10 μl (H) of pooled serum from BALB/c mice vaccinated with WT or FL mutant IgE_{sig}-prM-E LNPs, or 15 μg of anti-prM mAb (2H2, positive control). One day later, animals were challenged with 10⁵ FFU of DENV-2 (strain S221) and followed for mortality (left) and clinical score (right) (1 (healthy) to 7 (deceased) scale; see STAR Methods). Results are pooled from two to three independent challenge experiments (numbers of animals indicated beneath graph) with the exception of the anti-prM mAb, which was administered in only one of the two experiments as a positive control. Survival curves between serum transfers from IgE_{sig}-prM-E (WT and FL mutant LNPs) vaccinated mice were statistically different (****p < 0.0001, log-rank test).

See also related Figures S5 and S6.

1/10,000) that resulted in sterilizing immunity in the majority of mice. The basis for the enhanced immunogenicity of the JEV_{sig}-prM-E versus IgE_{sig}-prM-E mRNA remains uncertain at this time.

While other candidate ZIKV vaccines have demonstrated protection in mice against ZIKV viremia with IgG titers of ~1/2,000 (Larocca et al., 2016), some of these studies used

immunocompetent strains for challenge, which do not support as efficient ZIKV infection due to a species-specific lack of antagonism of IFN signaling (Grant et al., 2016; Kumar et al., 2016; Lazear et al., 2016). Passive transfer and challenge studies in non-human primates with DNA plasmid or inactivated vaccines suggested that a neutralization titer of 1/100 (measured by micro-neutralization assay) or 1/1,000 (measured by RVP assay) is required to prevent viremia in the majority of ZIKV-infected animals (Abbink et al., 2016; Dowd et al., 2016b). However, no prior study assessed sterilizing immunity, as judged by the combined absence of virus in target tissues and lack of evidence of an anamnestic humoral response. For vaccine development, a key question remains as to correlates of vaccine protection in pregnancy and whether sterilizing immunity will be required to prevent seeding of the placenta and fetal infection and injury. In anti-*ifnar1*-treated susceptible mice, the level of neutralizing antibodies required for conferring sterilizing immunity was substantially higher (> 100 to 1,000-fold) than required to reduce viral burden or confer survival protection. Vaccination studies in pregnant animals are planned to establish the correlate of immune protection that completely prevents maternal-fetal transmission.

Because of the versatility of the platform, we engineered additional mRNA LNP vaccines with mutations in the conserved E-DII-FL, which abolish reactivity of monoclonal and polyclonal antibodies targeting this region (Chabierski et al., 2014; Crill et al., 2012; Hughes et al., 2012; Vogt et al., 2011). The FL mutant mRNA vaccines induced neutralizing antibody responses in non-pregnant female BALB/c mice that protected against virus dissemination to the uterus and brain. Moreover, the FL mutant ZIKV vaccines induced serum antibody responses that resulted in less ADE of DENV-1 infection in cell culture and immune enhancement of DENV-2 infection in AG129 mice. Our results are analogous to a prior study with a DENV-1 DNA plasmid vaccine in which the FL epitope was altered by introducing G106R and L107D mutations (Crill et al., 2012); in that study, mice immunized with cross-reactivity-reduced monovalent DENV-1 DNA vaccines had diminished immune enhancement of DENV-2 infection in mice. Although our FL mutant mRNA LNP vaccines minimized ADE, we did observe a reduction in neutralizing titer (~7-fold decrease in EC50) for JEV_{sig}-prM-E FL LNPs compared to the respective WT LNPs; however, no significant difference in neutralization was observed between IgE_{sig}-prM-E WT and FL mutant vaccines. Although further studies are warranted, mRNA LNPs with FL mutations may induce lower neutralizing responses because (a) they produce SVPs that are less stable; (b) the absence of the FL results in a change in the display of neutralizing epitopes; or (c) the mutation of the FL in ZIKV SVPs prevents induction of neutralizing antibodies that bind epitopes proximal to the FL, as observed with EDE antibodies (Barba-Spaeth et al., 2016; Dejnirattisai et al., 2016). Thus, there is a trade-off for using the FL mutant LNPs; although cross-reactivity and ADE of DENV infection is reduced, neutralizing activity and the likelihood of conferring sterilizing immunity also are reduced. Second generation cross-reactivity reduced constructs with a different array of mutations in conserved regions may prove even more immunogenic.

Our mRNA LNP ZIKV vaccine platform adds to a burgeoning pipeline that focuses on subunit-based or inactivated virion approaches. Three groups reported DNA plasmid vaccines encod-

ing ZIKV M-E or prM-E genes that induced neutralizing antibodies in mice and non-human primates and protected against viremia or lethal virus challenge (Abbink et al., 2016; Dowd et al., 2016b; Larocca et al., 2016; Muthumani et al., 2016). A rhesus adenovirus-vectored vaccine encoding ZIKV M-E genes induced neutralizing antibodies after a single dose in four rhesus macaques (Abbink et al., 2016). Immunization of BALB/c mice or rhesus macaques with an alum-adjuvanted chemically inactivated ZIKV vaccine induced neutralizing antibodies and cellular immunity after two doses (Larocca et al., 2016) and protected against plasma viremia, or viral RNA in urine, cerebrospinal fluid, colorectal, and cervicovaginal secretions (Abbink et al., 2016). A human adenovirus vectored vaccine producing soluble E protein trimers induced neutralizing antibodies and protected 1-week-old mice from ZIKV challenge (Kim et al., 2016). Although all of these vaccine platforms show promise, none have been evaluated for induction of cross-reactive antibodies that in theory, could enhance DENV infection and disease. Nonetheless, it remains to be established whether the enhancement of DENV infection and disease, which can be demonstrated *in vitro* and in mice, becomes a clinically relevant concern for ZIKV vaccines. In the absence of epidemiological proof, it may be difficult to justify the evaluation of cross-reactivity reduced variant vaccines in humans, in view of the decreased immunogenicity, especially when compared to the extraordinarily strong response generated with our WT JEV_{sig}-prM-E construct. Nonetheless, the modified mRNA platform is well-positioned to respond rapidly to emerging epidemiology data.

In summary, we describe the generation of a ZIKV vaccine, utilizing modified mRNA encapsulated into LNPs that can be easily manipulated to optimize neutralization capacity and limit potentially undesired cross-reactivity. Our JEV_{sig}-prM-E mRNA LNPs induced remarkable neutralizing titers that in most animals conferred sterilizing immunity. Consistent with our results, a recent study also reported the utility of LNP-encapsulated mRNA encoding the prM and E genes as a candidate vaccine for ZIKV infection (Pardi et al., 2017). The flexibility of this platform allows for the future inclusion of additional mRNA encoding other flavivirus proteins (e.g., NS1) that could augment protective responses (Costa et al., 2007; Costa et al., 2006) or immunodominant helper CD4 T cell epitopes (Hung et al., 2007). Future studies will be directed on evaluating the immunogenicity and protective efficacy of these mRNA vaccines in pregnant mice, non-human primates, and ultimately, humans.

STAR★METHODS

Detailed methods are provided in the online version of this paper and include the following:

- KEY RESOURCES TABLE
- CONTACT FOR REAGENT AND RESOURCE SHARING
- EXPERIMENTAL MODEL AND SUBJECT DETAILS
 - Ethics statement
 - Mouse experiments
- METHOD DETAILS
 - Viruses and cells
 - Generation of modified mRNA and LNP

- Viral protein analysis
- Electron microscopy of SVPs
- Measurement of viral burden
- Neutralization assays
- ADE assays
- QUANTIFICATION AND STATISTICAL ANALYSIS
- DATA AND SOFTWARE AVAILABILITY
- ADDITIONAL RESOURCES

AUTHOR CONTRIBUTION

J.M.R., S.H., K.A.D., S.L.B., J.G.J., S.S., T.C.P., G.C., and M.S.D. designed the experiments. J.M.R., S.H., K.A.D., J.M.F., V.S., and W.W.T. performed the experiments. J.M.R., S.H., K.A.D., S.S., T.C.P., G.C., and M.S.D. analyzed the data. J.M.R. and M.S.D. wrote the first draft of the paper; all authors edited the manuscript.

ACKNOWLEDGMENTS

This work was supported by grants from the NIH-NIAID (R01 AI073755, R01 AI104972, and P01 AI106695 to M.S.D.; R01 AI116813 to S.S.), the intramural program of NIH-NIAID (T.C.P.), a research grant from DARPA (agreement #W911NF-13-1-0417), and by a research grant from Moderna. We thank W. H. Hui (University of California, Los Angeles) for performing the negative stain imaging of the SVPs. M.S.D. is a consultant for Inbios, Visterra, and Takeda Pharmaceuticals and on the Scientific Advisory Boards of Moderna and OvaGene. S.H., S.L.B., and G.C. are employees of Valera LLC, a Moderna Venture focusing on the development of therapeutic approaches for infectious diseases, including ZIKV mRNA vaccines.

Received: January 27, 2017

Revised: February 8, 2017

Accepted: February 8, 2017

Published: February 17, 2017; corrected online: March 9, 2017

REFERENCES

Abbink, P., Larocca, R.A., De La Barrera, R.A., Bricault, C.A., Moseley, E.T., Boyd, M., Kirilova, M., Li, Z., Ng'ang'a, D., Nanayakkara, O., et al. (2016). Protective efficacy of multiple vaccine platforms against Zika virus challenge in rhesus monkeys. *Science* 353, 1129–1132.

Aliota, M.T., Caine, E.A., Walker, E.C., Larkin, K.E., Camacho, E., and Osorio, J.E. (2016). Characterization of Lethal Zika Virus Infection in AG129 Mice. *PLoS Negl. Trop. Dis.* 10, e0004682.

Anderson, B.R., Muramatsu, H., Jha, B.K., Silverman, R.H., Weissman, D., and Karikó, K. (2011). Nucleoside modifications in RNA limit activation of 2'-5'-oligoadenylate synthetase and increase resistance to cleavage by RNase L. *Nucleic Acids Res.* 39, 9329–9338.

Balsitis, S.J., Williams, K.L., Lachica, R., Flores, D., Kyle, J.L., Mehlhop, E., Johnson, S., Diamond, M.S., Beatty, P.R., and Harris, E. (2010). Lethal antibody enhancement of dengue disease in mice is prevented by Fc modification. *PLoS Pathog.* 6, e1000790.

Barba-Spaeth, G., Dejnirattisai, W., Rouvinski, A., Vaney, M.C., Medits, I., Sharma, A., Simon-Lorière, E., Sakuntabhai, A., Cao-Lormeau, V.M., Haouz, A., et al. (2016). Structural basis of potent Zika-dengue virus antibody cross-neutralization. *Nature* 536, 48–53.

Beltramello, M., Williams, K.L., Simmons, C.P., Macagno, A., Simonelli, L., Quyen, N.T., Sukupolvi-Petty, S., Navarro-Sanchez, E., Young, P.R., de Silva, A.M., et al. (2010). The human immune response to Dengue virus is dominated by highly cross-reactive antibodies endowed with neutralizing and enhancing activity. *Cell Host Microbe* 8, 271–283.

Bhatt, S., Gething, P.W., Brady, O.J., Messina, J.P., Farlow, A.W., Moyes, C.L., Drake, J.M., Brownstein, J.S., Hoen, A.G., Sankoh, O., et al. (2013). The global distribution and burden of dengue. *Nature* 496, 504–507.

Bogers, W.M., Oostermeijer, H., Mooij, P., Koopman, G., Verschoor, E.J., Davis, D., Ulmer, J.B., Brito, L.A., Cu, Y., Banerjee, K., et al. (2015). Potent immune responses in rhesus macaques induced by nonviral delivery of a self-amplifying RNA vaccine expressing HIV type 1 envelope with a cationic nanoemulsion. *J. Infect. Dis.* 211, 947–955.

Boonnak, K., Slike, B.M., Burgess, T.H., Mason, R.M., Wu, S.J., Sun, P., Porter, K., Rudiman, I.F., Yuwono, D., Puthavathana, P., and Marovich, M.A. (2008). Role of dendritic cells in antibody-dependent enhancement of dengue virus infection. *J. Virol.* 82, 3939–3951.

Brasil, P., Pereira, J.P., Jr., Moreira, M.E., Ribeiro Nogueira, R.M., Damasceno, L., Wakimoto, M., Rabello, R.S., Valderramos, S.G., Halai, U.A., Salles, T.S., et al. (2016). Zika Virus Infection in Pregnant Women in Rio de Janeiro. *N. Engl. J. Med.* 375, 2321–2334.

Brien, J.D., Lazear, H.M., and Diamond, M.S. (2013). Propagation, quantification, detection, and storage of West Nile virus. *Curr Protoc Microbiol* 37, 15D 13 11–15D 13 18.

Cao-Lormeau, V.M., Blake, A., Mons, S., Lastère, S., Roche, C., Vanhomwegen, J., Dub, T., Baudouin, L., Teissier, A., Larre, P., et al. (2016). Guillain-Barré Syndrome outbreak associated with Zika virus infection in French Polynesia: a case-control study. *Lancet* 387, 1531–1539.

Chabierski, S., Barzon, L., Papa, A., Niedrig, M., Bramson, J.L., Richner, J.M., Palù, G., Diamond, M.S., and Ulbert, S. (2014). Distinguishing West Nile virus infection using a recombinant envelope protein with mutations in the conserved fusion-loop. *BMC Infect. Dis.* 14, 246.

Chen, S., Tam, Y.Y., Lin, P.J., Sung, M.M., Tam, Y.K., and Cullis, P.R. (2016). Influence of particle size on the in vivo potency of lipid nanoparticle formulations of siRNA. *J. Control. Release* 235, 236–244.

Cláudio, N., Dalet, A., Gatti, E., and Pierre, P. (2013). Mapping the crossroads of immune activation and cellular stress response pathways. *EMBO J.* 32, 1214–1224.

Coelho, T., Adams, D., Silva, A., Lozeron, P., Hawkins, P.N., Mant, T., Perez, J., Chiesa, J., Warrington, S., Tranter, E., et al. (2013). Safety and efficacy of RNAi therapy for transthyretin amyloidosis. *N. Engl. J. Med.* 369, 819–829.

Coffman, R.L., Sher, A., and Seder, R.A. (2010). Vaccine adjuvants: putting innate immunity to work. *Immunity* 33, 492–503.

Costa, S.M., Freire, M.S., and Alves, A.M. (2006). DNA vaccine against the non-structural 1 protein (NS1) of dengue 2 virus. *Vaccine* 24, 4562–4564.

Costa, S.M., Azevedo, A.S., Paes, M.V., Sarges, F.S., Freire, M.S., and Alves, A.M. (2007). DNA vaccines against dengue virus based on the ns1 gene: the influence of different signal sequences on the protein expression and its correlation to the immune response elicited in mice. *Virology* 358, 413–423.

Crill, W.D., Trainor, N.B., and Chang, G.J. (2007). A detailed mutagenesis study of flavivirus cross-reactive epitopes using West Nile virus-like particles. *J. Gen. Virol.* 88, 1169–1174.

Crill, W.D., Hughes, H.R., Trainor, N.B., Davis, B.S., Whitney, M.T., and Chang, G.J. (2012). Sculpting humoral immunity through dengue vaccination to enhance protective immunity. *Front. Immunol.* 3, 334.

Davidson, A., Slavinski, S., Komoto, K., Rakeman, J., and Weiss, D. (2016). Suspected Female-to-Male Sexual Transmission of Zika Virus - New York City, 2016. *MMWR Morb. Mortal. wkly. Rep.* 65, 716–717.

Davis, B.S., Chang, G.J., Cropp, B., Roehrig, J.T., Martin, D.A., Mitchell, C.J., Bowen, R., and Bunning, M.L. (2001). West Nile virus recombinant DNA vaccine protects mouse and horse from virus challenge and expresses in vitro a noninfectious recombinant antigen that can be used in enzyme-linked immunosorbent assays. *J. Virol.* 75, 4040–4047.

Deckard, D.T., Chung, W.M., Brooks, J.T., Smith, J.C., Woldai, S., Hennessey, M., Kwit, N., and Mead, P. (2016). Male-to-Male Sexual Transmission of Zika Virus-Texas, January 2016. *MMWR Morb. Mortal. wkly. Rep.* 65, 372–374.

Dejnirattisai, W., Jumnainsong, A., Onsirakul, N., Fitton, P., Vasanawathana, S., Limpitikul, W., Puttikhunt, C., Edwards, C., Duangchinda, T., Supasa, S., et al. (2010). Cross-reacting antibodies enhance dengue virus infection in humans. *Science* 328, 745–748.

- Dejnirattisai, W., Supasa, P., Wongwiwat, W., Rouvinski, A., Barba-Spaeth, G., Duangchinda, T., Sakuntabhai, A., Cao-Lorreau, V.M., Malasit, P., Rey, F.A., et al. (2016). Dengue virus sero-cross-reactivity drives antibody-dependent enhancement of infection with Zika virus. *Nat. Immunol.* **17**, 1102–1108.
- Desmet, C.J., and Ishii, K.J. (2012). Nucleic acid sensing at the interface between innate and adaptive immunity in vaccination. *Nat. Rev. Immunol.* **12**, 479–491.
- Dick, G.W. (1952). Zika virus. II. Pathogenicity and physical properties. *Trans. R. Soc. Trop. Med. Hyg.* **46**, 521–534.
- Dick, G.W., Kitchen, S.F., and Haddock, A.J. (1952). Zika virus. I. Isolations and serological specificity. *Trans. R. Soc. Trop. Med. Hyg.* **46**, 509–520.
- Dowd, K.A., DeMaso, C.R., and Pierson, T.C. (2015). Genotypic Differences in Dengue Virus Neutralization Are Explained by a Single Amino Acid Mutation That Modulates Virus Breathing. *MBio* **6**, e01559–e15.
- Dowd, K.A., DeMaso, C.R., Pelc, R.S., Speer, S.D., Smith, A.R., Goo, L., Platt, D.J., Mascola, J.R., Graham, B.S., Mulligan, M.J., et al. (2016a). Broadly Neutralizing Activity of Zika Virus-Immune Sera Identifies a Single Viral Serotype. *Cell Rep.* **16**, 1485–1491.
- Dowd, K.A., Ko, S.Y., Morabito, K.M., Yang, E.S., Pelc, R.S., DeMaso, C.R., Castilho, L.R., Abbink, P., Boyd, M., Nityanandam, R., et al. (2016b). Rapid development of a DNA vaccine for Zika virus. *Science* **354**, 237–240.
- Foy, B.D., Kobylinski, K.C., Chilson Foy, J.L., Blitvich, B.J., Travassos da Rosa, A., Haddock, A.D., Lanciotti, R.S., and Tesh, R.B. (2011). Probable non-vector-borne transmission of Zika virus, Colorado, USA. *Emerg. Infect. Dis.* **17**, 880–882.
- Grant, A., Ponia, S.S., Tripathi, S., Balasubramaniam, V., Miorin, L., Sourisseau, M., Schwarz, M.C., Sánchez-Seco, M.P., Evans, M.J., Best, S.M., and García-Sastre, A. (2016). Zika Virus Targets Human STAT2 to Inhibit Type I Interferon Signaling. *Cell Host Microbe* **19**, 882–890.
- Haddock, A.D., Schuh, A.J., Yasuda, C.Y., Kasper, M.R., Heang, V., Huy, R., Guzman, H., Tesh, R.B., and Weaver, S.C. (2012). Genetic characterization of Zika virus strains: geographic expansion of the Asian lineage. *PLoS Negl. Trop. Dis.* **6**, e1477.
- Hekele, A., Bertholet, S., Archer, J., Gibson, D.G., Palladino, G., Brito, L.A., Otten, G.R., Brazzoli, M., Buccato, S., Bonci, A., et al. (2013). Rapidly produced SAM(®) vaccine against H7N9 influenza is immunogenic in mice. *Emerg. Microbes Infect.* **2**, e52.
- Huang, W.C., Abraham, R., Shim, B.S., Choe, H., and Page, D.T. (2016). Zika virus infection during the period of maximal brain growth causes microcephaly and corticospinal neuron apoptosis in wild type mice. *Sci. Rep.* **6**, 34793.
- Hughes, H.R., Crill, W.D., and Chang, G.J. (2012). Manipulation of immunodominant dengue virus E protein epitopes reduces potential antibody-dependent enhancement. *Virology* **439**, 115–125.
- Hung, C.F., Tsai, Y.C., He, L., and Wu, T.C. (2007). DNA vaccines encoding li-PADRE generates potent PADRE-specific CD4+ T-cell immune responses and enhances vaccine potency. *Mol. Ther.* **15**, 1211–1219.
- Karikó, K., Ni, H., Capodici, J., Lamphier, M., and Weissman, D. (2004). mRNA is an endogenous ligand for Toll-like receptor 3. *J. Biol. Chem.* **279**, 12542–12550.
- Kawiecki, A.B., and Christofferson, R.C. (2016). Zika Virus-Induced Antibody Response Enhances Dengue Virus Serotype 2 Replication In Vitro. *J. Infect. Dis.* **214**, 1357–1360.
- Kim, E., Erdos, G., Huang, S., Kenniston, T., Faló, L.D., Jr., and Gambotto, A. (2016). Preventative Vaccines for Zika Virus Outbreak: Preliminary Evaluation. *EBioMedicine* **13**, 315–320.
- Kumar, A., Hou, S., Airo, A.M., Limonta, D., Mancinelli, V., Branton, W., Power, C., and Hobman, T.C. (2016). Zika virus inhibits type-I interferon production and downstream signaling. *EMBO Rep.* **17**, 1766–1775.
- Lanciotti, R.S., Kosoy, O.L., Laven, J.J., Velez, J.O., Lambert, A.J., Johnson, A.J., Stanfield, S.M., and Duffy, M.R. (2008). Genetic and serological properties of Zika virus associated with an epidemic, Yap State, Micronesia, 2007. *Emerg. Infect. Dis.* **14**, 1232–1239.
- Larocca, R.A., Abbink, P., Peron, J.P., Zanutto, P.M., Iampietro, M.J., Badamchi-Zadeh, A., Boyd, M., Ng'ang'a, D., Kirilova, M., Nityanandam, R., et al. (2016). Vaccine protection against Zika virus from Brazil. *Nature* **536**, 474–478.
- Lazear, H.M., and Diamond, M.S. (2016). Zika Virus: New Clinical Syndromes and Its Emergence in the Western Hemisphere. *J. Virol.* **90**, 4864–4875.
- Lazear, H.M., Govero, J., Smith, A.M., Platt, D.J., Fernandez, E., Miner, J.J., and Diamond, M.S. (2016). A Mouse Model of Zika Virus Pathogenesis. *Cell Host Microbe* **19**, 720–730.
- Mansuy, J.M., Suberbielle, E., Chapuy-Regaud, S., Mengelle, C., Bujan, L., Marchou, B., Delobel, P., Gonzalez-Dunia, D., Malnou, C.E., Izopet, J., and Martin-Blondel, G. (2016). Zika virus in semen and spermatozoa. *Lancet Infect. Dis.* **16**, 1106–1107.
- Marston, H.D., Lurie, N., Borio, L.L., and Fauci, A.S. (2016). Considerations for Developing a Zika Virus Vaccine. *N. Engl. J. Med.* **375**, 1209–1212.
- Morens, D.M. (1994). Antibody-dependent enhancement of infection and the pathogenesis of viral disease. *Clin. Infect. Dis.* **19**, 500–512.
- Murray, K.O., Gorchakov, R., Carlson, A.R., Berry, R., Lai, L., Natrajan, M., Garcia, M.N., Correa, A., Patel, S.M., Aagaard, K., and Mulligan, M.J. (2017). Prolonged Detection of Zika Virus in Vaginal Secretions and Whole Blood. *Emerg. Infect. Dis.* **23**, 99–101.
- Muthumani, K., Griffin, B.D., Agarwal, S., Kudchodkar, S.B., Reuschel, E.L., Choi, H., Krainyak, K.A., Duperret, E.K., Keaton, A.A., Chung, C., et al. (2016). In vivo protection against ZIKV infection and pathogenesis through passive antibody transfer and active immunisation with a prMEnv DNA vaccine. *NPJ Vaccines*. Published online November 10, 2016. <http://dx.doi.org/10.1038/npjvaccines.2016.1021>.
- Oehler, E., Watrin, L., Larre, P., Leparc-Goffart, I., Lastere, S., Valour, F., Baudouin, L., Mallet, H., Musso, D., and Ghawche, F. (2014). Zika virus infection complicated by Guillain-Barre syndrome—case report, French Polynesia, December 2013. *Euro Surveill.* **19**, 20720.
- Oliphant, T., Nybakken, G.E., Engle, M., Xu, Q., Nelson, C.A., Sukupolvi-Petty, S., Marri, A., Lachmi, B.E., Olshefsky, U., Fremont, D.H., et al. (2006). Antibody recognition and neutralization determinants on domains I and II of West Nile Virus envelope protein. *J. Virol.* **80**, 12149–12159.
- Oliphant, T., Nybakken, G.E., Austin, S.K., Xu, Q., Bramson, J., Loeb, M., Throsby, M., Fremont, D.H., Pierson, T.C., and Diamond, M.S. (2007). Induction of epitope-specific neutralizing antibodies against West Nile virus. *J. Virol.* **81**, 11828–11839.
- Pardi, N., and Weissman, D. (2017). Nucleoside Modified mRNA Vaccines for Infectious Diseases. *Methods Mol. Biol.* **1499**, 109–121.
- Pardi, N., Hogan, M.J., Pelc, R.S., Muramatsu, H., Andersen, H., DeMaso, C.R., Dowd, K.A., Sutherland, L.L., Scearce, R.M., Parks, R., et al. (2017). Zika virus protection by a single low-dose nucleoside-modified mRNA vaccination. *Nature*. Published online February 2, 2017. <http://dx.doi.org/10.1038/nature21428>.
- Petsch, B., Schnee, M., Vogel, A.B., Lange, E., Hoffmann, B., Voss, D., Schlake, T., Thess, A., Kallen, K.J., Stitz, L., and Kramps, T. (2012). Protective efficacy of in vitro synthesized, specific mRNA vaccines against influenza A virus infection. *Nat. Biotechnol.* **30**, 1210–1216.
- Prasad, V.M., Miller, A.S., Klose, T., Sirohi, D., Buda, G., Jiang, W., Kuhn, R.J., and Rossmann, M.G. (2017). Structure of the immature Zika virus at 9 Å resolution. *Nat. Struct. Mol. Biol.* **24**, 184–186.
- Rasmussen, S.A., Jamieson, D.J., Honein, M.A., and Petersen, L.R. (2016). Zika Virus and Birth Defects—Reviewing the Evidence for Causality. *N. Engl. J. Med.* **374**, 1981–1987.
- Sapparapu, G., Fernandez, E., Kose, N., Bin, Cao, Fox, J.M., Bombardi, R.G., Zhao, H., Nelson, C.A., Bryan, A.L., Barnes, T., et al. (2016). Neutralizing human antibodies prevent Zika virus replication and fetal disease in mice. *Nature* **540**, 443–447.
- Sheehan, K.C., Lai, K.S., Dunn, G.P., Bruce, A.T., Diamond, M.S., Heutel, J.D., Dongo-Arthur, C., Carrero, J.A., White, J.M., Hertzog, P.J., and Schreiber, R.D. (2006). Blocking monoclonal antibodies specific for mouse IFN-alpha/beta

- receptor subunit 1 (IFNAR-1) from mice immunized by in vivo hydrodynamic transfection. *J. Interferon Cytokine Res.* 26, 804–819.
- Stettler, K., Beltramello, M., Espinosa, D.A., Graham, V., Cassotta, A., Bianchi, S., Vanzetta, F., Minola, A., Jaconi, S., Mele, F., et al. (2016). Specificity, cross-reactivity, and function of antibodies elicited by Zika virus infection. *Science* 353, 823–826.
- Swanstrom, J.A., Plante, J.A., Plante, K.S., Young, E.F., McGowan, E., Gallichotte, E.N., Widman, D.G., Heise, M.T., de Silva, A.M., and Baric, R.S. (2016). Dengue Virus Envelope Dimer Epitope Monoclonal Antibodies Isolated from Dengue Patients Are Protective against Zika Virus. *MBio* 7, 7.
- Tang, W.W., Young, M.P., Mamidi, A., Regla-Nava, J.A., Kim, K., and Shresta, S. (2016). A Mouse Model of Zika Virus Sexual Transmission and Vaginal Viral Replication. *Cell Rep.* 17, 3091–3098.
- Tsetsarkin, K.A., Kenney, H., Chen, R., Liu, G., Manukyan, H., Whitehead, S.S., Laassri, M., Chumakov, K., and Pletnev, A.G. (2016). A Full-Length Infectious cDNA Clone of Zika Virus from the 2015 Epidemic in Brazil as a Genetic Platform for Studies of Virus-Host Interactions and Vaccine Development. *MBio* 7, e01114–e01116.
- van der Eijk, A.A., van Genderen, P.J., Verdijk, R.M., Reusken, C.B., Mögling, R., van Kampen, J.J., Widagdo, W., Aron, G.I., GeurtsvanKessel, C.H., Pas, S.D., et al. (2016). Miscarriage Associated with Zika Virus Infection. *N. Engl. J. Med.* 375, 1002–1004.
- Vogt, M.R., Dowd, K.A., Engle, M., Tesh, R.B., Johnson, S., Pierson, T.C., and Diamond, M.S. (2011). Poorly neutralizing cross-reactive antibodies against the fusion loop of West Nile virus envelope protein protect in vivo via Fcγ receptor and complement-dependent effector mechanisms. *J. Virol.* 85, 11567–11580.
- Wang, Q., Yang, H., Liu, X., Dai, L., Ma, T., Qi, J., Wong, G., Peng, R., Liu, S., Li, J., et al. (2016). Molecular determinants of human neutralizing antibodies isolated from a patient infected with Zika virus. *Sci. Transl. Med.* 8, 369ra179.
- Williams, K.L., Sukupolvi-Petty, S., Beltramello, M., Johnson, S., Sallusto, F., Lanzavecchia, A., Diamond, M.S., and Harris, E. (2013). Therapeutic efficacy of antibodies lacking Fcγ receptor binding against lethal dengue virus infection is due to neutralizing potency and blocking of enhancing antibodies [corrected]. *PLoS Pathog.* 9, e1003157.
- Yauch, L.E., Zellweger, R.M., Kotturi, M.F., Qutubuddin, A., Sidney, J., Peters, B., Prestwood, T.R., Sette, A., and Shresta, S. (2009). A protective role for dengue virus-specific CD8+ T cells. *J. Immunol.* 182, 4865–4873.
- Zellweger, R.M., Prestwood, T.R., and Shresta, S. (2010). Enhanced infection of liver sinusoidal endothelial cells in a mouse model of antibody-induced severe dengue disease. *Cell Host Microbe* 7, 128–139.
- Zhao, H., Fernandez, E., Dowd, K.A., Speer, S.D., Platt, D.J., Gorman, M.J., Govero, J., Nelson, C.A., Pierson, T.C., Diamond, M.S., and Fremont, D.H. (2016). Structural Basis of Zika Virus-Specific Antibody Protection. *Cell* 166, 1016–1027.



JOIN THE DEBATE

With Cell Press Reviews

Insight and perspective is a powerful combination. That's why we offer readers a critical examination of the evidence that provokes thought and facilitates discussion within scientific communities.

To propel your research forward, faster, turn to Cell Press Reviews. Our insightful, authoritative reviews—published across the life sciences in our primary research and *Trends* journals—go beyond synthesis and offer a point of view.

**Find your way
with Cell Press Reviews**

www.cell.com/reviews

CellPress
Your work is our life

Gut Microbiota Regulate Motor Deficits and Neuroinflammation in a Model of Parkinson's Disease

Timothy R. Sampson,^{1,*} Justine W. Debelius,² Taren Thron,¹ Stefan Janssen,² Gauri G. Shastri,¹ Zehra Esra Ilhan,³ Collin Challis,¹ Catherine E. Schretter,¹ Sandra Rocha,⁴ Viviana Gradinaru,¹ Marie-Francoise Chesselet,⁵ Ali Keshavarzian,⁶ Kathleen M. Shannon,^{7,9} Rosa Krajmalnik-Brown,³ Pernilla Wittung-Stafshede,⁴ Rob Knight,^{2,8} and Sarkis K. Mazmanian^{1,10,*}

¹Division of Biology & Biological Engineering, California Institute of Technology, Pasadena, CA 91125, USA

²Department of Pediatrics, University of California, San Diego, San Diego, CA 92110, USA

³Swette Center for Environmental Biotechnology, Biodesign Institute, Arizona State University, Tempe, AZ 85287, USA

⁴Biology and Biological Engineering Department, Chalmers University of Technology, Gothenburg 41296, Sweden

⁵Department of Neurology, The David Geffen School of Medicine at UCLA, Los Angeles, CA 90095, USA

⁶Department of Internal Medicine, Division of Gastroenterology, Rush University Medical Center, Chicago, IL 60612, USA

⁷Department of Neurological Sciences, Section of Movement Disorders, Rush University Medical Center, Chicago, IL 60612, USA

⁸Department of Computer Science and Engineering, University of California, San Diego, San Diego, CA 92093, USA

⁹Present address: Department of Neurology, University of Wisconsin-Madison, Madison, WI 53705, USA

¹⁰Lead Contact

*Correspondence: trsamps@caltech.edu (T.R.S.), sarkis@caltech.edu (S.K.M.)

<http://dx.doi.org/10.1016/j.cell.2016.11.018>

SUMMARY

The intestinal microbiota influence neurodevelopment, modulate behavior, and contribute to neurological disorders. However, a functional link between gut bacteria and neurodegenerative diseases remains unexplored. Synucleinopathies are characterized by aggregation of the protein α -synuclein (α Syn), often resulting in motor dysfunction as exemplified by Parkinson's disease (PD). Using mice that overexpress α Syn, we report herein that gut microbiota are required for motor deficits, microglia activation, and α Syn pathology. Antibiotic treatment ameliorates, while microbial re-colonization promotes, pathophysiology in adult animals, suggesting that postnatal signaling between the gut and the brain modulates disease. Indeed, oral administration of specific microbial metabolites to germ-free mice promotes neuroinflammation and motor symptoms. Remarkably, colonization of α Syn-overexpressing mice with microbiota from PD-affected patients enhances physical impairments compared to microbiota transplants from healthy human donors. These findings reveal that gut bacteria regulate movement disorders in mice and suggest that alterations in the human microbiome represent a risk factor for PD.

INTRODUCTION

Neurological dysfunction is the basis of numerous human diseases. Behavioral, psychiatric, and neurodegenerative disorders

often display hallmark neuropathologies within the central nervous system (CNS). One neuropathology, amyloidosis, results from aberrant aggregation of specific neuronal proteins that disrupt many cellular functions. Affected tissues often contain insoluble aggregates of proteins that display altered conformations, a feature believed to contribute to an estimated 50 distinct human diseases (Sacchetti and Kelly, 2002). Neurodegenerative amyloid disorders, including Alzheimer's, Huntington's, and Parkinson's diseases (PD), are each associated with a distinct amyloid protein (Brettschneider et al., 2015). PD is the second most common neurodegenerative disease in the United States, affecting an estimated 1 million people and 1% of the US population over 60 years of age (Nalls et al., 2014). Worldwide, about 3 million patients and caregivers suffer from the often-debilitating symptoms of PD, which involve motor deficits including tremors, muscle rigidity, bradykinesia, and impaired gait. It is a multifactorial disorder that has a strong environmental component, as less than 10% of cases are hereditary (Nalls et al., 2014). Aggregation of α -synuclein (α Syn) is thought to be pathogenic in a family of diseases termed synucleinopathies, which includes PD, multiple system atrophy, and Lewy body disease (Brettschneider et al., 2015; Luk et al., 2012; Prusiner et al., 2015). α Syn aggregation is a stepwise process, leading to oligomeric species and intransient fibrils that accumulate within neurons. Dopaminergic neurons of the substantia nigra pars compacta (SNpc) appear particularly vulnerable to effects of α Syn aggregates. Dopamine modulators are a first-line therapeutic in PD; however, treatments can carry serious side effects and often lose effectiveness (Jenner, 2008). Discovery of safe and effective therapeutics are needed to address the increasing burden of PD in an ever-aging population, a paradoxical consequence of mankind's achievements in increased lifespan.

Although neurological diseases have been historically studied within the CNS, peripheral influences have been implicated in the

onset and/or progression of diseases that impact the brain (Dinan and Cryan, 2015). Indeed, emerging data suggest bidirectional communication between the gut and the brain in anxiety, depression, nociception, and autism spectrum disorder (ASD), among others (Mayer et al., 2014; Schroeder and Bäckhed, 2016; Sharon et al., 2016). Gastrointestinal (GI) physiology and motility are influenced by signals arising both locally within the gut and from the CNS. Neurotransmitters, immune signaling, hormones, and neuropeptides produced within the gut may, in turn, impact the brain (Selkrig et al., 2014; Wall et al., 2014). Research into how the gut-brain axis influences neurological conditions may reveal insights into disease etiology.

The human body is permanently colonized by microbes on virtually all environmentally exposed surfaces, the majority of which reside within the GI tract (Ley et al., 2006). Increasingly, research is beginning to uncover the profound impacts that the microbiota can have on neurodevelopment and the CNS (Sharon et al., 2016). Germ-free (GF) mice and antibiotic-treated specific-pathogen-free (SPF) mice are altered in hippocampal neurogenesis, resulting in impaired spatial and object recognition (Möhle et al., 2016). The microbiota regulate expression of the 5-hydroxytryptamine receptor (5-HT_{1A}), brain-derived neurotrophic factor (BDNF), and NMDA receptor subunit 2 (NR2A) (Bercik et al., 2011; Diaz Heijtz et al., 2011; Sudo et al., 2004). GF mice have altered cortical myelination and impaired blood-brain barrier function (Braniste et al., 2014; Hoban et al., 2016). Additionally, the microbiota promotes enteric and circulating serotonin production in mice (Yano et al., 2015) and affects anxiety, hyperactivity, and cognition (Clarke et al., 2013; Diaz Heijtz et al., 2011; Neufeld et al., 2011; Selkrig et al., 2014). To augment mouse models, dysbiosis (alterations to the microbial composition) of the human microbiome has been reported in subjects diagnosed with several neurological diseases (Schroeder and Bäckhed, 2016). For example, fecal and mucosa-associated gut microbes are different between individuals with PD and healthy controls (Hasegawa et al., 2015; Keshavarzian et al., 2015; Scheperjans et al., 2015; Unger et al., 2016). Yet, how dysbiosis arises and whether this feature contributes to PD pathogenesis remains unknown.

Gut bacteria control the differentiation and function of immune cells in the intestine, periphery, and brain (Ery et al., 2015; Matcovitch-Natan et al., 2016; Rooks and Garrett, 2016). Intriguingly, subjects with PD exhibit intestinal inflammation (Devos et al., 2013), and GI abnormalities such as constipation often precede motor defects by many years (Braak et al., 2003; Verbaan et al., 2007). Braak's hypothesis posits that aberrant α Syn accumulation initiates in the gut and propagates via the vagus nerve to the brain in a prion-like fashion (Del Tredici and Braak, 2008). This notion is supported by pathophysiologic evidence: α Syn inclusions appear early in the enteric nervous system (ENS) and the glossopharyngeal and vagal nerves (Braak et al., 2003; Shannon et al., 2012), and vagotomized individuals are at reduced risk for PD (Svensson et al., 2015). Further, injection of α Syn fibrils into the gut tissue of healthy rodents is sufficient to induce pathology within the vagus nerve and brainstem (Holmqvist et al., 2014). However, the notion that α Syn aggregation initiates in the ENS and spreads to the CNS via retrograde transmission remains controversial (Burke et al., 2008), and

experimental support for a gut microbial connection to PD is lacking.

Based on the common occurrence of GI symptoms in PD, dysbiosis among PD patients, and evidence that the microbiota impacts CNS function, we tested the hypothesis that gut bacteria regulate the hallmark motor deficits and pathophysiology of synucleinopathies. Herein, we report that the microbiota is necessary to promote α Syn pathology, neuroinflammation, and characteristic motor features in a validated mouse model. We identify specific microbial metabolites that are sufficient to promote disease symptoms. Remarkably, fecal microbes from PD patients impair motor function significantly more than microbiota from healthy controls when transplanted into mice. Together, these results suggest that gut microbes may play a critical and functional role in the pathogenesis of synucleinopathies such as PD.

RESULTS

Gut Microbes Promote Motor and GI Dysfunction

The Thy1- α Syn (alpha-synuclein-overexpressing [ASO]) mouse displays progressive deficits in fine and gross motor function, as well as gut motility defects (Chesselet et al., 2012; Rockenstein et al., 2002). Recent evidence has linked unregulated α Syn expression in humans to a higher risk of PD (Soldner et al., 2016), providing an epidemiological foundation for the Thy1- α Syn mouse model. Defects in coordinated motor tasks become evident at 12 weeks of age (Fleming et al., 2004). Motor function was measured via four tests: beam traversal, pole descent, nasal adhesive removal, and hindlimb clasping reflexes, as previously validated in this model (Fleming et al., 2004). 12- to 13-week-old ASO animals harboring a complex microbiota (SPF-ASO) require significantly more time to cross a challenging beam compared to wild-type littermates (SPF-WT) and also exhibit increased time to descend a pole, two measures of gross motor function (Figures 1A and 1B). Removal of an adhesive from the nasal bridge, a test of fine motor control, is impaired in SPF-ASO mice compared to SPF-WT mice (Figure 1C). Finally, the hindlimb clasping reflex, a measure of striatal dysfunction (Zhang et al., 2014), is defective in SPF-ASO mice (Figure 1D). To assess the contribution of gut bacteria, we re-derived ASO mice (GF-ASO) and wild-type mice (GF-WT) under germ-free conditions. Remarkably, 12- to 13-week-old GF-ASO animals exhibit reduced deficits in beam traversal, pole descent, adhesive removal, and hindlimb clasping (Figures 1A–1D). In fact, the execution of motor function tasks by GF-ASO mice resembles performance levels of WT animals in many cases. GF-ASO mice do not exhibit differences in weight compared to SPF-ASO animals (Figure S1A), while both SPF-ASO and GF-ASO animals display defects in the inverted grid assay, a measure of limb strength (Figure S1B)—thus, outcomes in motor tests are not due to weight or physical strength. At a later age (24–25 weeks old), SPF-ASO animals exhibit a progressive decline in motor function (Figures S1C–S1G), which is significantly delayed in GF-ASO animals (Figures S1C–S1G). We do not observe consistent differences in motor tasks between GF-WT and SPF-WT animals, providing evidence for gene-microbiome interactions.

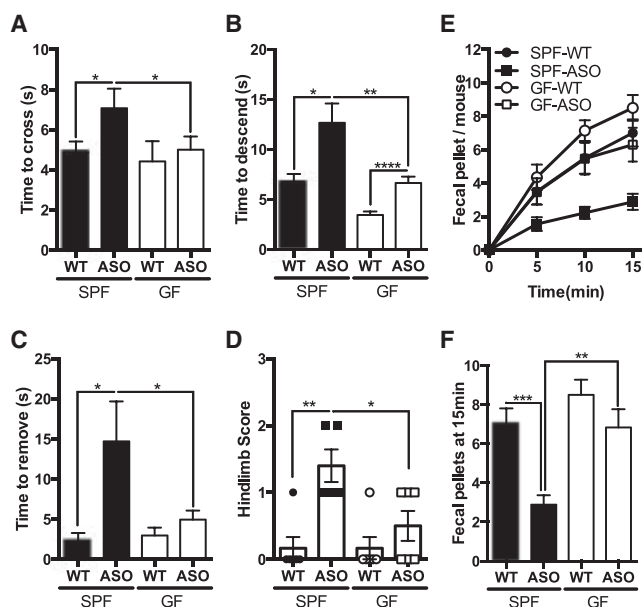


Figure 1. Gut Microbes Promote Motor and Gastrointestinal Dysfunction

- (A) Time to traverse beam apparatus.
 (B) Time to descend pole.
 (C) Time to remove adhesive from nasal bridge.
 (D) Hind-limb clasp score.
 (E) Time course of fecal output in a novel environment over 15 min.
 (F) Total fecal pellets produced in 15 min.

Animals were tested at 12–13 weeks of age. $n = 4–6$, error bars represent the mean and standard error from three trials per animal. Data are representative of two experiments. * $p \leq 0.05$; ** $p \leq 0.01$; *** $p \leq 0.001$; **** $p \leq 0.0001$. Abbreviations: SPF, specific-pathogen-free; GF, germ-free; WT, wild-type; ASO, Thy1- α -synuclein genotype. See also Figure S1.

As in PD, motor dysfunction in this mouse model co-occurs with decreased GI function and constipation (Verbaan et al., 2007; Wang et al., 2012). In SPF-ASO animals, we observe a marked decrease in the total output of fecal pellets, at both 12–13 weeks and 24–25 weeks of age, while fecal output is unaltered in GF-ASO animals (Figures 1E, 1F, S1H, and S1I). Further, fecal pellets produced by SPF-ASO mice contain reduced water content compared to GF-ASO mice (Figure S1J), together revealing reduced GI defects in GF animals. Indeed, compilation of all motor phenotypes into a principal-component analysis (PCoA) displays a striking segregation by the SPF-ASO group, while GF-ASO animals cluster more similarly to WT mice (Figure S1K). Together, these data demonstrate that the presence of gut microbes promote the hallmark motor and intestinal dysfunction in a preclinical model of PD.

The Gut Microbiota Is Required for α Syn Pathology

Motor deficits in PD coincide with the aggregation of α Syn. Utilizing an antibody that recognizes only conformation-specific α Syn aggregates and fibrils, we performed immunofluorescence microscopy to visualize α Syn inclusions in the brains of mice. Under SPF conditions, we observe notable aggregation of α Syn in the caudoputamen (CP) and substantia nigra

(SN) of ASO animals (Figures 2A and 2B), brain regions of the nigrostriatal pathway affected in both mouse models and human PD (Brettschneider et al., 2015). Surprisingly, GF-ASO mice display appreciably fewer α Syn aggregates (Figures 2A and 2B). To quantify α Syn aggregation, we performed western blots of brain extracts (Figure 2C). We reveal significantly less insoluble α Syn in brains of GF-ASO animals (Figures 2C–2E). To further confirm these findings, we performed dot blot analysis for aggregated α Syn in the CP and inferior midbrain, where the SN is located, and observe similarly decreased α Syn aggregation in GF-ASO animals (Figures S2A–S2C). Interestingly, we observe regional specificity of α Syn aggregation: in the frontal cortex (FC), GF-ASO animals harbor fewer α Syn aggregation than SPF animals, while in the cerebellum (CB), we observe nearly equal quantities of α Syn in SPF and GF mice (Figures S2D–S2H). To ensure that these findings do not reflect differences in transgene expression, we report similar levels of α Syn transcript and protein in the inferior midbrain and the CP between SPF- and GF-ASO animals (Figures 2F and 2G). These data suggest that the microbiota regulates pathways that promote α Syn aggregation and/or prevent the clearance of insoluble protein aggregates.

α Syn-Dependent Microglia Activation by the Microbiota

The microbiota modulates immune development in the CNS (Erny et al., 2015; Matcovitch-Natan et al., 2016), and α Syn aggregates activate immune cells, including brain-resident microglia (Kim et al., 2013; Sanchez-Guajardo et al., 2013). Microglia undergo significant morphological changes upon activation, transitioning from thin cell bodies with numerous branched extensions to round, amoeboid cells with fewer branches (Erny et al., 2015). In situ 3D reconstructions of individual microglia cells from confocal fluorescence microscopy reveals that wild-type GF animals harbor microglia that are distinct from SPF animals. Within the CP and SN, microglia in GF-WT mice display increased numbers and total lengths of microglia branches compared to SPF-WT animals (Figures 3A–3C). These morphological features are indicative of an arrest in microglia maturation and/or a reduced activation state in GF animals, corroborating a recent report that gut bacteria affect immune cells in the brain (Erny et al., 2015).

Extending these observations to a disease model, microglia from SPF-ASO mice display significant increases in cell body diameter, along with fewer processes of shorter length compared to GF-ASO mice (Figures 3A–3C). Tissue homogenates from the CP and inferior midbrain of SPF-ASO mice contain a marked increase in the pro-inflammatory cytokines tumor necrosis factor- α (TNF- α) and interleukin-6 (IL-6) compared to GF-ASO mice (Figures 3D and 3E). Both cytokines are elevated in the brains of PD patients (Mogi et al., 1994a, 1994b). Gene expression analysis of RNA from enriched CD11b⁺ cells (primarily microglia) reveals increased *Tnfa* and *Il6* expression in SPF-ASO animals, which is nearly absent in GF animals (Figure 3F). Neuroprotective *Bdnf* and the cell cycle marker *Ddit4* levels are upregulated in GF animals (Figure S2I), as observed in previous studies (Erny et al., 2015; Matcovitch-Natan et al., 2016). Neuroinflammatory responses are region specific with increased in microglia diameter and TNF- α

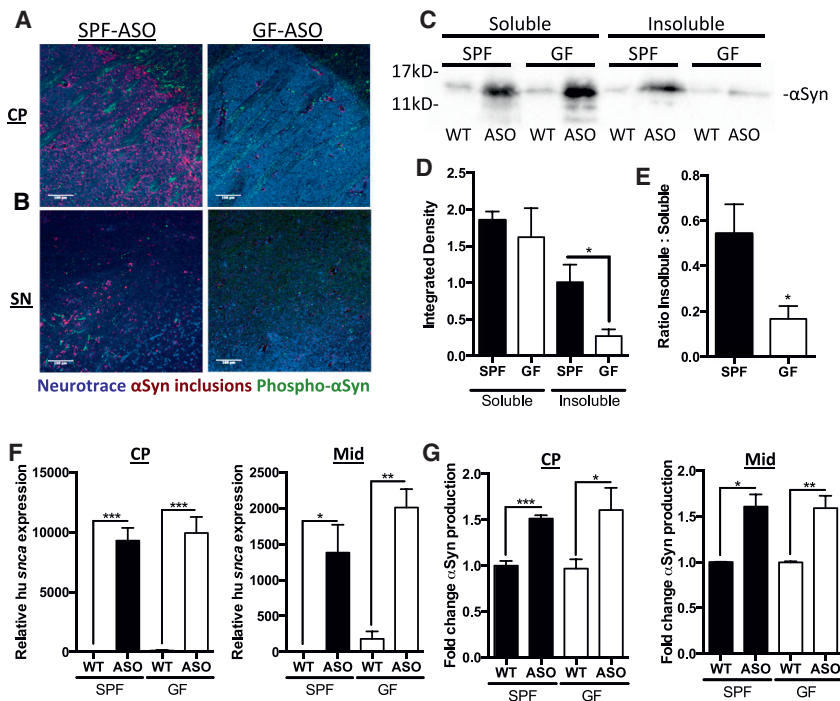


Figure 2. α Syn Pathology Is Increased in Mice Harboring a Gut Microbiota

(A) Representative images of the caudoputamen (CP) from SPF-ASO or GF-ASO animals stained with aggregation-specific α Syn antibody (red), Phospho-Ser129- α Syn antibody (green), and Neurotrace/Nissl (blue).

(B) Representative images of the substantia nigra (SN) from SPF-ASO or GF-ASO animals, stained as above.

(C) Representative western blot of triton soluble and insoluble brain homogenates, immunostained with anti- α Syn antibody.

(D and E) Densitometry quantification of anti- α Syn western blots for (D) all α Syn and (E) ratio of insoluble to soluble α Syn staining.

(F) qRT-PCR analysis of human α Syn in the CP or inferior midbrain (Mid).

(G) ELISA analysis of total α Syn present in homogenates from the CP or inferior midbrain (Mid).

Tissues collected from mice at 12–13 weeks of age. $n = 3–4$, error bars represent the mean and standard error. * $p \leq 0.05$; ** $p \leq 0.01$; *** $p \leq 0.001$. Abbreviations: SPF, specific-pathogen-free; GF, germ-free; WT, wild-type; ASO, Thy1- α -synuclein genotype. See also Figure S2.

production in the FC but not the CB (Figures 3G and 3H). Overall, these findings support the hypothesis that gut microbes promote α Syn-dependent activation of microglia within specific brain regions involved in disease.

Postnatal Microbial Signals Modulate α Syn-Dependent Pathophysiology

The microbiota influence neurological outcomes during gestation, as well as via active gut-to-brain signaling in adulthood. In order to differentiate between these mechanisms, we treated SPF animals with an antibiotic cocktail to postnatally deplete the microbiota (Figure 4A). Conversely, we colonized groups of 5- to 6-week-old GF mice with a complex microbiota from SPF-WT animals (Figure 4A). Remarkably, antibiotic-treated (Abx) animals display little α Syn-dependent motor dysfunction, closely resembling mice born under GF conditions (Figures 4B–4E). Postnatal colonization of previously GF animals (Ex-GF) recapitulates the genotype effect observed in SPF mice, with mice that overexpress α Syn displaying significant motor dysfunction (Figures 4B–4E). GI function, as measured by fecal output, is also significantly improved in Abx-treated animals, while Ex-GF mice exhibit an α Syn-dependent decrease in total fecal output (Figures 4F and 4G). Furthermore, in the transgenic ASO line, microglia from Ex-GF animals have increased cell body diameters comparable to those in SPF mice (Figures 4H and 4I). Abx-ASO animals, however, harbor microglia with diameters similar to GF animals (Figures 4H and 4I). While not excluding a role for the microbiota during prenatal neurodevelopment, modulation of microglia activation during adulthood contributes to α Syn-mediated motor dysfunction and neuroinflammation, suggesting active gut-brain signaling by the microbiota.

SCFAs Are Sufficient to Promote α Syn-Mediated Neuroinflammation

Recently, it was revealed that gut bacteria modulate microglia activation during viral infection through production of microbial metabolites, namely short-chain fatty acids (SCFAs) (Erny et al., 2015). Indeed, we observe lower fecal SCFA concentrations in GF and Abx-treated animals, compared to SPF mice (Figure S3A; Smith et al., 2013). To address whether SCFAs impact neuroimmune responses in a mouse model of PD, we treated GF-ASO and GF-WT animals with a mixture of the SCFAs acetate, propionate, and butyrate (while the animals remained microbiologically sterile) and significantly restored fecal SCFA concentrations (Figure S3A). Within affected brain regions (i.e., CP and SN), microglia in SCFA-administered animals display morphology indicative of increased activation compared to untreated mice, and similar to cells from Ex-GF and SPF mice (Figures 5A, 5B, S3B, and S3C; see also Figures 3 and 4). Microglia from GF-ASO mice fed SCFAs (SCFA-ASO) are significantly larger in diameter than those of GF-WT animals treated with SCFAs (SCFA-WT), with a concomitant decrease in the length and total number of branches. Abx-treated animals, however, display microglia morphology similar to GF animals (Figures 5B, S3B, and S3C; see also Figures 3 and 4). Changes in microglia diameter are also observed in the FC, but not the CB, demonstrating region-specific responses (Figures S3D and S3E).

Corresponding to microglia morphology, we reveal α Syn aggregates in mice administered SCFAs compared to untreated and Abx-treated mice, and similar to Ex-GF animals (Figures S3F–S3I). Strikingly, we observe that postnatal signaling by microbes induces increased α Syn aggregation in the CP and SN (Figures S3F and S3G), with no observable difference in the FC and CB (Figures S3H and S3I), confirmed by quantification and

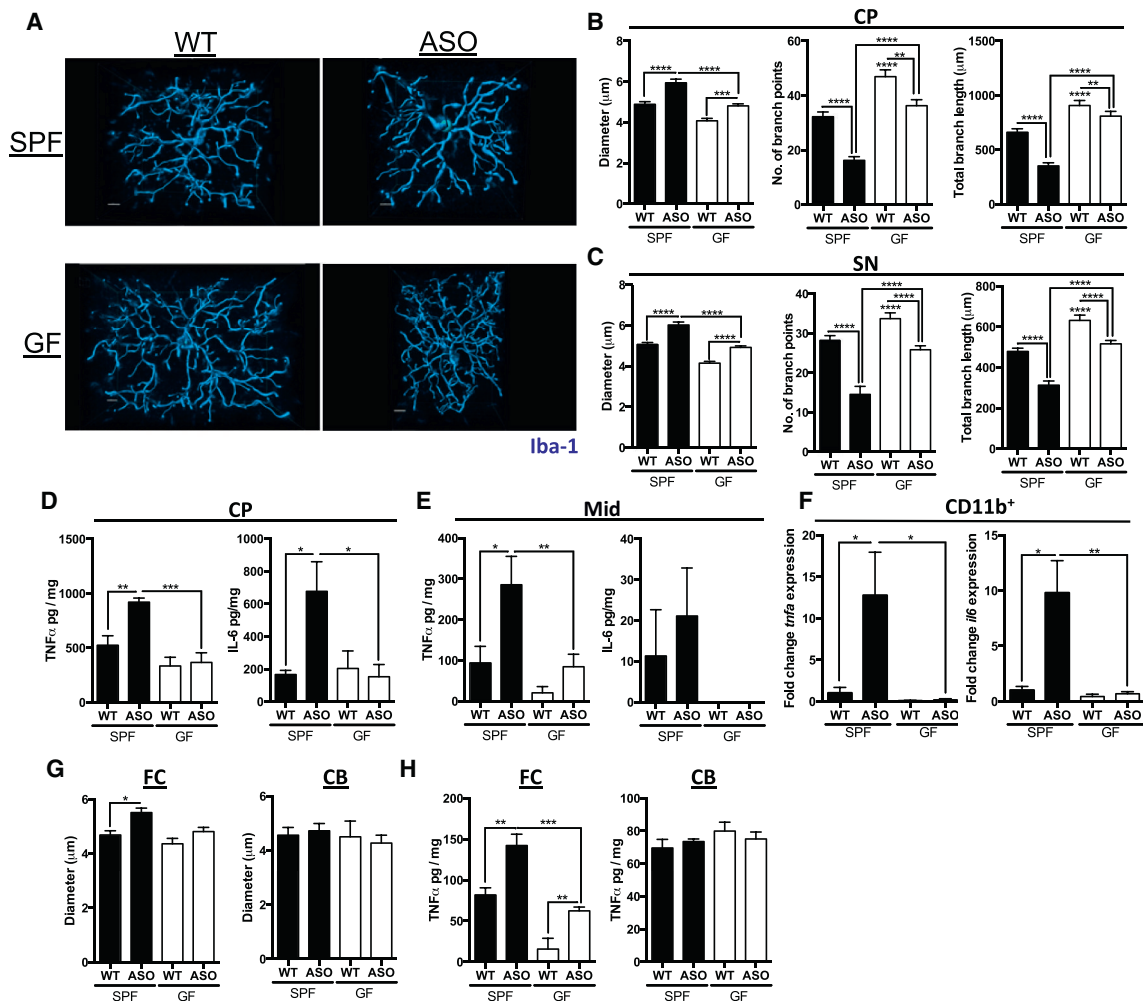


Figure 3. α Syn-Dependent Microglia Activation by the Microbiota

(A) Representative 3D reconstructions of Iba1-stained microglia residing in the caudoputamen (CP) of SPF-WT, SPF-ASO, GF-WT, and GF-ASO animals.

(B) CP-resident microglia parameters diameter, number of branch points, and total branch length.

(C) Substantia nigra (SN)-resident microglia parameters diameter, number of branch points, and total branch length.

(D) ELISA analysis for TNF- α and IL-6 present in homogenates from the CP.

(E) ELISA analysis for TNF- α and IL-6 present in homogenates from the inferior midbrain (Mid).

(F) qPCR analysis of CD11b⁺ cells derived from brain homogenate for *tnfa* and *il6*.

(G) Diameter of microglia residing in the frontal cortex (FC) or cerebellum (CB).

(H) ELISA analysis for TNF- α present in homogenates from the FC or CB.

Tissues collected from mice at 12–13 weeks of age. n = 3–4 (with 20–60 cells per region per animal analyzed); error bars represent the mean and standard error.

*p \leq 0.05; **p \leq 0.01; ***p \leq 0.001; ****p \leq 0.0001. Abbreviations: SPF, specific-pathogen-free; GF, germ-free; WT, wild-type; ASO, Thy1- α -synuclein genotype. See also Figure S2.

western blot (Figures S3J–S3O). SCFAs either singly or in a mixture, over a range of concentrations, do not expedite the aggregation of human α Syn in vitro (Figures S4A–S4G), nor do they alter the overall structure of α Syn amyloid fibrils (Figures S4H and S4I). Though additional studies are needed, it appears that SCFAs accelerate in vivo α Syn aggregation, albeit independently of direct molecular interactions.

SCFAs Are Sufficient to Promote Motor Deficits

To explore a link between microbial metabolites and motor symptoms in the Thy1- α Syn model, GF animals were treated

with the SCFA mixture beginning at 5–6 weeks of age, and motor function was assessed at 12–13 weeks of age. SCFA-ASO mice display significantly impaired performance in several motor tasks compared to untreated GF-ASO animals (Figures 5C–5F), including impairment in beam traversal, pole descent, and hindlimb reflex (compare GF-ASO to SCFA-ASO mice). All effects by SCFAs are genotype specific to the Thy1- α Syn mice. GI deficits are also observed in the SCFA-treated transgenic animals (Figures 5G and 5H). Oral treatment of GF animals with heat-killed bacteria does not induce motor deficits (Figures S4J–S4M), suggesting that bacteria need to be metabolically

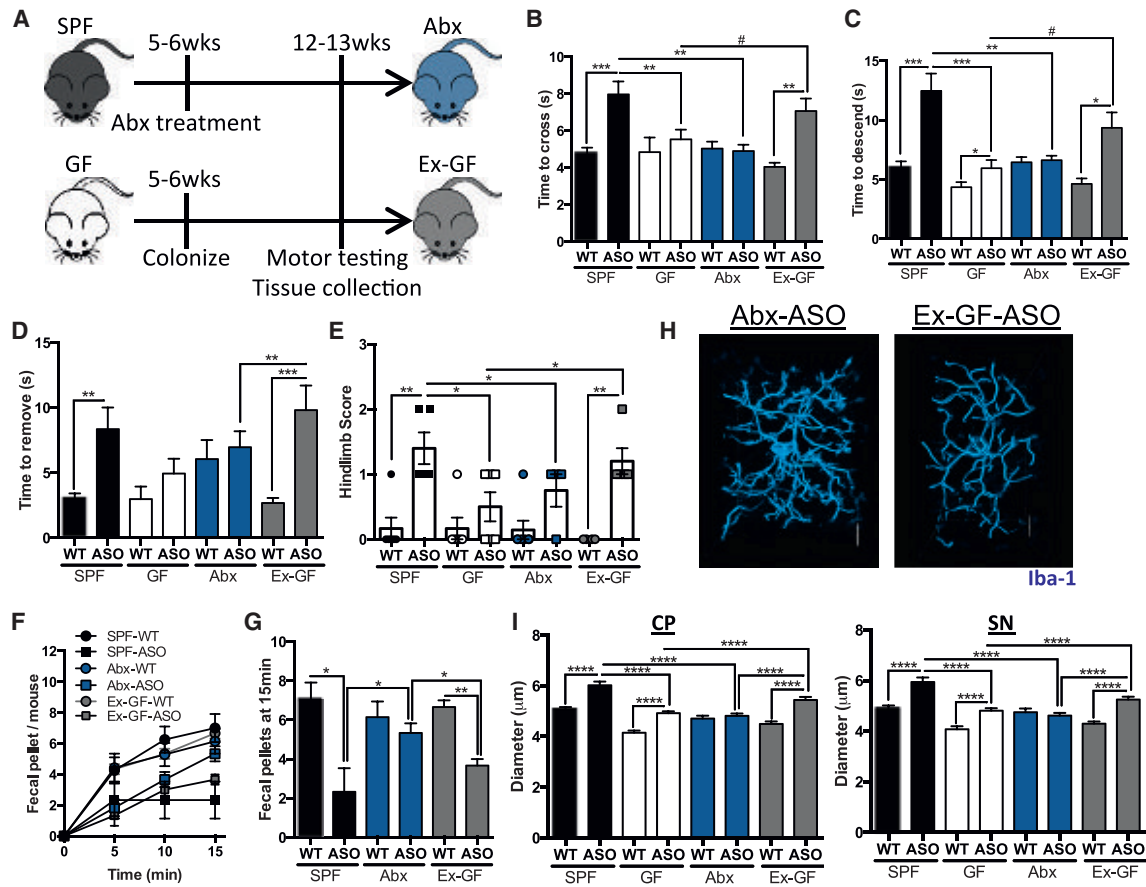


Figure 4. Postnatal Microbial Signals Promote Motor and Gastrointestinal Dysfunction

(A) Time course schema for animal treatment and testing. (B) Time to traverse beam apparatus. (C) Time to descend pole. (D) Time to remove nasal adhesive. (E) Hindlimb clasping reflex score. (F) Time course of fecal output in a novel environment over 15 min. (G) Total fecal pellets produced in 15 min. (H) Representative 3D reconstructions of Iba1-stained microglia residing in the caudoputamen (CP) of Abx-ASO or Ex-GF-ASO animals. (I) Diameter of microglia residing in the CP or substantia nigra (SN). Animals were tested at 12–13 weeks of age. n = 6–12; error bars represent the mean and standard error from 3 trials per animal, and compiled from 2 independent cohorts or 20–60 microglia per region analyzed. #0.05 < p < 0.1; *p ≤ 0.05; **p ≤ 0.01; ***p ≤ 0.001; ****p ≤ 0.0001. Abbreviations: SPF, specific-pathogen-free; GF, germ-free; Abx, antibiotic-treated; Ex-GF, recolonized germ-free animals; WT, wild-type; ASO, Thy1- α -synuclein genotype. See also Figure S3.

active. Additionally, oral treatment of SCFA-fed animals with the anti-inflammatory compound minocycline is sufficient to reduce TNF- α production, reduce α Syn aggregation, and improve motor function, without altering transgene expression (Figures S5A–S5H). We propose that the microbiota actively produce metabolites, such as SCFAs, that are required for microglia activation and α Syn aggregation, contributing to motor dysfunction in a preclinical model of PD.

Dysbiosis of the PD Microbiome

Given recent evidence that PD patients display altered microbiomes (Hasegawa et al., 2015; Keshavarzian et al., 2015; Scheperjans et al., 2015), we sought to determine whether human gut microbes affect disease outcomes when transferred into GF

mice. We collected fecal samples from six human subjects diagnosed with PD as well as six matched healthy controls (Table S1). To limit confounding effects, only new-onset, treatment-naive PD patients with healthy intestinal histology were chosen, among other relevant inclusion and exclusion criteria (see STAR Methods and Table S1).

Fecal microbiota from PD patients or controls were transplanted into individual groups of GF recipient animals via oral gavage. Fecal pellets were collected from “humanized” mice, bacterial DNA was extracted, and 16S rRNA sequencing was performed. Sequences were annotated into operational taxonomic units (OTUs), using closed reference picking against the Greengenes database and metagenome function was predicted by PICRUSt. Recipient animal groups were most similar to their

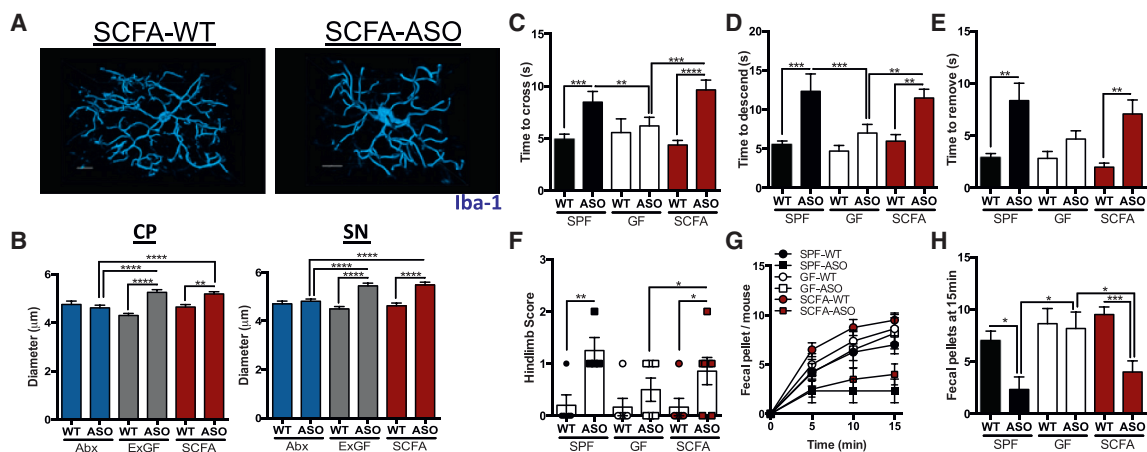


Figure 5. SCFAs Promote α Syn-Stimulated Microglia Activation and Motor Dysfunction

(A) Representative 3D reconstructions of Iba1-stained microglia residing in the caudoputamen (CP) of wild-type or ASO SCFA-treated animals. (B) Diameter of microglia residing in the CP or substantia nigra (SN). (C) Time to traverse beam apparatus. (D) Time to descend pole. (E) Time to remove nasal adhesive. (F) Hindlimb clasp reflex score. (G) Time course of fecal output in a novel environment over 15 min. (H) Total fecal pellets produced in 15 min.

Animals were tested at 12–13 weeks of age. $n = 6$ –12, error bars represent the mean and standard error from 3 trials per animal, and compiled from 2 independent cohorts or 20–60 microglia per region analyzed. Data are plotted with controls from Figure 4 for clarity. * $p \leq 0.05$; ** $p \leq 0.01$; *** $p \leq 0.001$; **** $p \leq 0.0001$. Abbreviations: SPF, specific-pathogen-free; GF, germ-free; SCFA, short-chain fatty acid-treated; WT, wild-type; ASO, Thy1- α -synuclein genotype. See also Figures S3, S4, and S5.

respective human donor's profile in unweighted UniFrac (Lozupone and Knight, 2005), based on PCoA (Figures 6A and 6B). Strikingly, the disease status of the donor had a strong effect on the microbial communities within recipient mice. Humanized mouse groups from PD donors are significantly more similar to each other than to communities transplanted from healthy donors, with this trend persisting when stratified by genetic background (Figures 6C and 6D). Furthermore, there are significant differences between the healthy and PD donors in the ASO background compared to WT recipients, suggesting genotype effects on microbial community configuration (Figures 6C and 6D).

We identified a number of genera that are altered in animals colonized with microbiota derived from PD donors, compared to healthy controls (Figure 6E), as well as altered KEGG pathways between these groups as indicated by Bray-Curtis distances (Figures S6A–S6C). OTUs increased in abundance in mice with PD microbiomes include *Proteus* sp., *Bilophila* sp., and *Roseburia* sp., with a concomitant loss of members of families Lachnospiraceae, Rikenellaceae, and Peptostreptococcaceae, as well as *Butyricicoccus* sp. (Figure 6E). Interestingly, some taxa are altered only in ASO animals (e.g., *Proteus* sp., *Bilophila* sp., and Lachnospiraceae), while others display significant changes independent of mouse genotype (e.g., *Roseburia* sp., Rikenellaceae, and *Enterococcus* sp.) (Figure 6E). Intriguingly, the abundance of three SCFA-producing KEGG families (K00929, butyrate kinase, and K01034 and K01035, acetate CoA/acetate CoA transferase alpha and beta) are increased in mice that received fecal microbes derived from PD donors (Figure S6D). Further, we observe that animals

receiving PD donor-derived microbiota display a significantly altered SCFA profile, with a lower concentration of acetate and higher relative abundances of propionate and butyrate, compared to animals colonized with microbes from healthy controls (Figure S6E). Together, these data indicate that differences in fecal microbial communities between PD patients and controls can be maintained after transfer into mice. Further, α Syn overexpression engenders distinct alterations to the gut microbiome profile after transplantation.

PD-Derived Gut Microbiota Promotes Motor Dysfunction

To assess microbiota function, groups of humanized animals from each of the donor pairs were tested for motor function. Consistent among four of the six pairs (pairs #1, 3, 4, and 5), microbiota derived from individuals with PD promote increased α Syn-mediated motor dysfunction (Figures 7A–7F). Beam traversal, pole descent, and nasal adhesive removal are significantly impaired in ASO animals colonized with PD microbiota compared to genotype-matched recipient mice harboring gut bacteria from healthy controls. Hindlimb reflex scores, on the other hand, are generally not different between individual donors. Interestingly, microbiota from one pair of samples did not induce significant genotype effects in the beam traversal and pole descent tasks (pair #2, Figure 7B), reflecting potential heterogeneity in the population that needs to be addressed through well-powered cohort studies. We observed no notable effects in motor function by WT recipient animals colonized with microbiota from either donor group (Figures 7A–7F). This finding in a

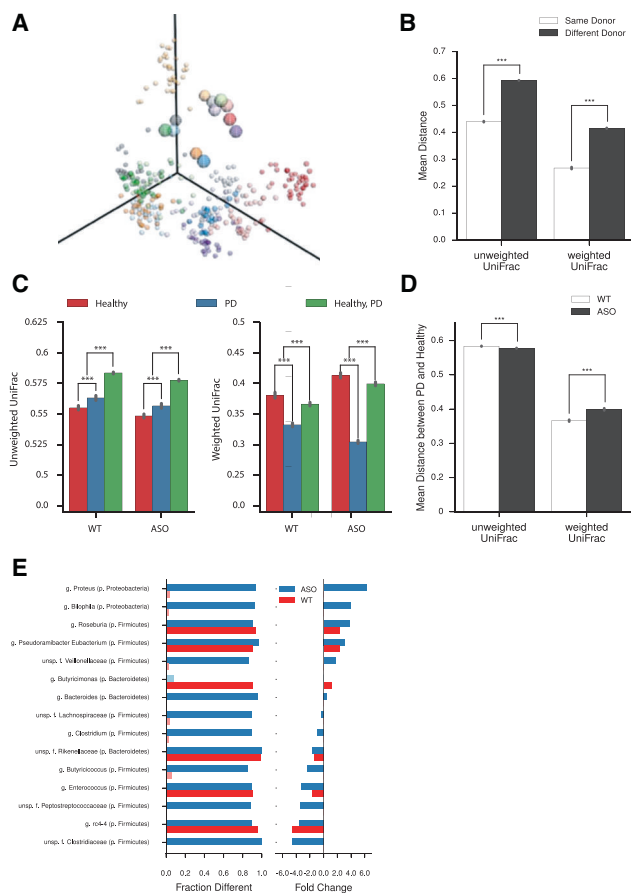


Figure 6. Microbiome Dysbiosis of PD Patient Samples after Transplant into Germ-free Mice

(A) Unweighted UniFrac Principle Coordinate Analysis of microbial communities of human donors (large circles) and recipient mice (small circles). Each donor and recipient sample are matched by color.

(B) Unweighted and weighted UniFrac analysis of microbial communities in recipient animals based on donor identity.

(C) Unweighted and weighted UniFrac analysis of microbial communities in recipient animals based on mouse genotype.

(D) Comparison of unweighted and weighted UniFrac analysis of microbial communities in recipient animals.

(E) Taxa-level analysis of individual genera altered between PD and healthy donors as a function of recipient mouse genotype. Left column indicates percentage with significant differences observed; right column indicates fold change between PD and healthy donors. Light colors indicate non-statistically significant differences.

$n = 3-6$, over 3 time points post-colonization. Error bars represent the mean and standard error. $***p \leq 0.001$, 999 permutations. Abbreviations: HC, germ-free mice colonized with fecal microbes from healthy controls; PD, germ-free mice colonized with fecal microbes from Parkinson's disease patients; WT, wild-type; ASO, Thy1- α -synuclein genotype. See also Figure S6.

preclinical mouse model supports the notion the PD microbiota contributes to disease symptoms in genetically susceptible hosts. Notably, recipient animals display little alteration to weight and GI function as measured by fecal output (Figures S7A–S7F). Compilation of performance data from all groups reveals that microbiota from PD patients induce increased motor impairment in ASO animals compared to microbes from healthy controls in

three of four tests used in this study (Figure 7G). In fact, depicting all motor function by PCoA displays striking global differences between animals colonized with microbiota from PD donors, compared to those colonized with gut bacteria derived from healthy individuals (Figure S7G). The observation that gut bacteria from PD patients compared to healthy controls enhance motor deficits in a mouse model provides evidence for a functional contribution by the microbiota to synuclenopathies.

DISCUSSION

Parkinson's disease represents a growing health concern for an ever-aging population. While genetic risks have been identified, environmental factors and gene-environment interactions probably account for most PD cases (Nalls et al., 2014; Ritz et al., 2016). We provide evidence that the gut microbiota are required for postnatal events that promote hallmark motor deficits in an animal model. Under GF conditions, or when bacteria are depleted with antibiotics, transgenic animals overexpressing human α Syn display reduced microglia activation, α Syn inclusions, and motor deficits compared to animals with a complex microbiota. Treatment with microbially produced SCFAs restores all major features of disease in GF mice, identifying potential molecular mediators involved in gut-brain signaling. Exacerbated motor symptoms in humanized mice transplanted with a PD microbiota compared to healthy controls suggest that α Syn overexpression (genetics) and dysbiosis (environment) combine to influence disease outcomes in mice. Extrapolation of these preclinical findings to humans may embolden the concept that gene-microbiome interactions represent a previously unrecognized etiology for PD.

Mechanisms by which gut bacteria promote α Syn-mediated pathophysiology are likely complex; herein, we have identified one potential pathway requiring microbiota-dependent effects on microglia. Recent studies have demonstrated an active role for the gut microbiota in promoting full maturation and inflammatory capabilities of microglia through the production of SCFAs (Erny et al., 2015). Despite a requirement for the SCFA receptor FFAR2 for microglia maturation, these cells are not known to express FFAR2, but do express other SCFA-responsive genes such as the histone deacetylases that modulate gene expression (Erny et al., 2015). SCFAs may cross the BBB and impact the physiology of cells in the CNS (Mitchell et al., 2011), or they may have peripheral effects, which indirectly activate and mature microglia by currently unknown mechanisms (Erny et al., 2015). Further, insoluble aggregates and oligomeric forms of α Syn activate microglia (Kim et al., 2013; Sanchez-Guajardo et al., 2013). Increases in the activation state of microglia and the production of pro-inflammatory cytokines alter neuronal function and increase cell death in models of PD and other neurodegenerative diseases (Kannarkat et al., 2013; Sanchez-Guajardo et al., 2013). Intriguingly, an inflammatory environment is known to enhance α Syn aggregation, which may further activate microglia upon contact and promote a feed-forward cascade that leads to additional α Syn aggregation and propagation and progression of disease (Gao et al., 2011). If true, possible future treatment options may include targeting immune activation by the microbiota, a notion consistent with research

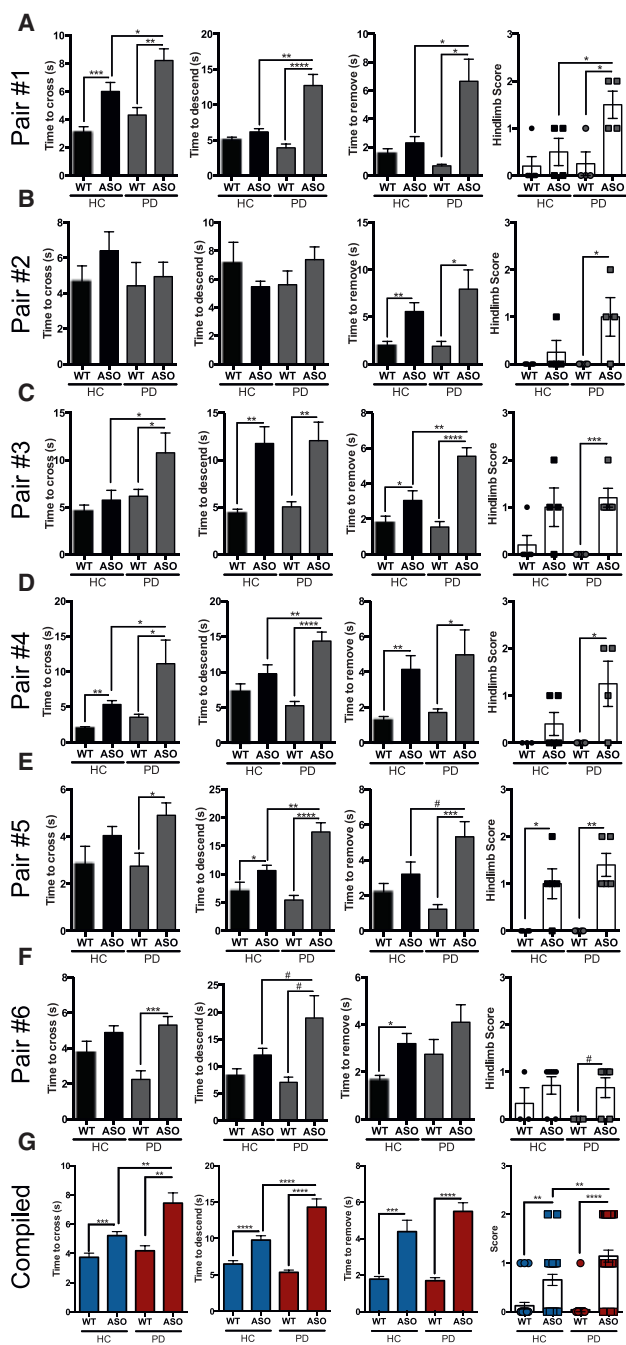


Figure 7. Microbiota from PD Patients Induce Increased α Syn-Mediated Motor Deficits

(A–F) Time to cross a beam, time to descend the pole, time to remove nasal adhesive, and hindlimb clasping reflex scores of mice humanized with microbiota from either PD patients or matched healthy controls.

(G) Compilation of all independent cohorts in each motor task: beam traversal, pole descent, adhesive removal, and hindlimb clasping reflex score, grouped by health status of fecal donor.

Animals were tested at 12–13 weeks of age. $n = 3–6$, error bars represent the mean and standard error from 3 trials per animal. # $0.05 < p < 0.1$; * $p \leq 0.05$; ** $p \leq 0.01$; *** $p \leq 0.001$; **** $p \leq 0.0001$. Abbreviations: HC, germ-free mice colonized with fecal microbes from healthy controls; PD, germ-

free mice colonized with fecal microbes from Parkinson's disease patients; WT, wild-type; ASO, Thy1- α -synuclein genotype. See also Figure S7 and Table S1.

into anti-inflammatory therapeutic modalities for PD (Valera and Masliah, 2016). While the microbiota promote microglia maturation, there are likely other disease-modifying processes that remain undiscovered. These include effects by the microbiota on autophagy (Lin et al., 2014), a cellular recycling process that is genetically linked to PD risk and when impaired may lead to reduced clearance of α Syn aggregates (Beilina and Cookson, 2015; Nalls et al., 2014). Additionally, intestinal bacteria have been shown to modulate proteasome function (Cleyne et al., 2014), which may also aid in the clearance of α Syn inclusions. The protective effects of autophagy and the proteasome are not specific to synucleinopathies, and the ability of the microbiota to modulate these critical cellular functions suggests that other amyloid disorders, such as Alzheimer's and Huntington's diseases, may be impacted by gut bacteria. In fact, recent studies have implicated the gut microbiota in promoting amyloid beta pathology in a model of Alzheimer's disease (Minter et al., 2016). Though we have explored postnatal effects of the microbiota in a model of neurodegenerative disease, our findings do not address the likely important role of microbial signals during prenatal neurodevelopment. Whether gut microbes alter the development of the dopaminergic system, perhaps by modulating neurogenesis or neural differentiation in utero or early life, remains unexplored. Furthermore, gut microbes can produce dopamine and its precursors from dietary substrates, with almost half of the body's dopamine generated in the GI tract (Eisenhofer et al., 1997; Wall et al., 2014). Deciphering microbiota effects on microglia activation, cellular protein clearance pathways, neurotransmitter production, and/or other mechanisms may offer an integrated approach to understand the pathogenesis of a complex and enigmatic disorder such as PD.

We reveal that gut bacteria from PD patients promote enhanced motor impairment compared to microbiota from healthy controls when transplanted into genetically susceptible ASO mice. This surprising finding suggests that distinct microbes associated with PD, rather than general microbial stimulation, manifest disease symptoms. Several bacterial taxa are altered in mice receiving fecal transplants from PD patients compared to healthy controls. Additionally, a number of bacterial genera are changed specifically in ASO animals, but not WT mice, receiving microbes from the same donor. These include depletions in members of family Lachnospiraceae and Ruminococceae in recipient mice, a notable finding as these same genera are significantly reduced in fecal samples directly from PD patients (Keshavarzian et al., 2015). Conversely, the gut microbiomes in human subjects with PD contain an increased abundance of Proteobacteria (Hasegawa et al., 2015; Keshavarzian et al., 2015; Scheperjans et al., 2015; Unger et al., 2016), remarkably similar to our results in mice. Whether these specific microbes play a role in disease processes remains unknown. Intriguingly, a recent study demonstrated alterations in fecal SCFA ratios between patients and healthy controls, including an elevated relative concentration of butyrate, possibly

free mice colonized with fecal microbes from Parkinson's disease patients; WT, wild-type; ASO, Thy1- α -synuclein genotype. See also Figure S7 and Table S1.

implicating a role for SCFAs in PD (Unger et al., 2016). Accordingly, we observe altered SCFA abundances in animals colonized with PD donor-derived microbiota, and the discovery that SCFAs are sufficient to generate α Syn-reactive microglia in the brain is consistent with expansive literature showing that altered microbial communities impact immune responses in the gut and periphery (Hooper et al., 2012).

What causes dysbiosis in PD? Physiological functions in affected individuals, such as altered intestinal absorption, reduced gastric motility, or dietary habits, represent factors that may change the microbiome. Epidemiological evidence has linked specific pesticide exposure to the incidence of PD (Ritz et al., 2016), with some pesticides known to impact microbiome configuration (Gao et al., 2016). Given the structure of α Syn and its ability to associate with membranes (Jo et al., 2000), it is tempting to speculate that extracellular α Syn may act as an antimicrobial, similar to recent observations with amyloid beta (Kumar et al., 2016), and shape the PD microbiome. Whether microbial community alterations are caused by extrinsic or intrinsic factors, the PD microbiota may be missing or reduced in protective microbes, harbor increased pathogenic resident microbes, or both. In turn, dysbiosis will result in differential production of microbial molecules in the gut. Metabolites produced by a deranged microbiota may enter the circulation (or even the brain) and impact neurological function. Identification of bacterial taxa or microbial metabolites that are altered in PD may serve as disease biomarkers or even drug targets, and interventions that correct dysbiosis may provide safe and effective treatments to slow or halt the progression of often debilitating motor symptoms.

Our findings establish that the microbiota are required for the hallmark motor and GI dysfunction in a mouse model of PD, via postnatal gut-brain signaling by microbial molecules that impact neuroinflammation and α Syn aggregation. Coupled with emerging research that has linked gut bacteria to disorders such as anxiety, depression, and autism, we propose the provocative hypothesis that certain neurologic conditions that have classically been studied as disorders of the brain may also have etiologies in the gut.

STAR★METHODS

Detailed methods are provided in the online version of this paper and include the following:

- KEY RESOURCES TABLE
- CONTACT FOR REAGENT AND RESOURCE SHARING
- EXPERIMENTAL MODEL AND SUBJECT DETAILS
 - Mice
 - Human Donor and Criteria
- METHOD DETAILS
 - Motor Function and Gastrointestinal Testing
 - Immunostaining and Microglia Reconstructions
 - CD11b Enrichment and qPCR Analysis
 - Cytokine and α Syn ELISAs and Western Blots
 - α Syn Aggregation Assays
 - SCFA Extraction and Analysis
 - Microbiome Profiling

- QUANTIFICATION AND STATISTICAL ANALYSIS
- DATA AND SOFTWARE AVAILABILITY

SUPPLEMENTAL INFORMATION

Supplemental Information includes seven figures and one table and can be found with this article online at <http://dx.doi.org/10.1016/j.cell.2016.11.018>.

AUTHOR CONTRIBUTIONS

Conceptualization, T.R.S., C.E.S., M.-F.C., and S.K.M.; Formal Analysis, J.W.D., S.J., and C.C.; Investigation, T.R.S., T.T., G.G.S., Z.E.L., and S.R.; Resources, A.K. and K.M.S.; Writing - Original Draft, T.R.S. and S.K.M.; Writing - Review and Editing, all authors; Supervision, V.G., R.K.-B., P.W.-S., R.K., and S.K.M.; Funding Acquisition, T.R.S., V.G., M.-F.C., A.K., P.W.-S., R.K., and S.K.M.

ACKNOWLEDGMENTS

We thank E. Hsiao, M. Sampson, and the S.K.M. laboratory for helpful critiques. We are grateful to K. Ly, A. Maskell, and M. Quintos for animal husbandry and Y. Garcia-Flores, G. Ackermann, G. Humphrey, and H. Derderian for technical support. Imaging and analysis was performed in the Caltech Biological Imaging Facility, with the support of the Caltech Beckman Institute and the Arnold and Mabel Beckman Foundation. T.R.S. is a Larry L. Hillblom Foundation postdoctoral fellow. This project was supported by funds from the Knut and Alice Wallenberg Foundation and Swedish Research Council to P.W.-S.; a gift from Mrs. and Mr. Larry Field to A.K.; the Heritage Medical Research Institute to V.G. and S.K.M.; and NIH grant NS085910 to S.K.M.

Received: June 29, 2016

Revised: October 12, 2016

Accepted: November 10, 2016

Published: December 1, 2016

REFERENCES

- Beilina, A., and Cookson, M.R. (2015). Genes associated with Parkinson's disease: regulation of autophagy and beyond. *J. Neurochem.* *139* (Suppl 1), 91–107.
- Bercik, P., Denou, E., Collins, J., Jackson, W., Lu, J., Jury, J., Deng, Y., Blennerhassett, P., Macri, J., McCoy, K.D., et al. (2011). The intestinal microbiota affect central levels of brain-derived neurotrophic factor and behavior in mice. *Gastroenterology* *141*, 599–609, 609.e1–609.e3.
- Braak, H., Rüb, U., Gai, W.P., and Del Tredici, K. (2003). Idiopathic Parkinson's disease: possible routes by which vulnerable neuronal types may be subject to neuroinvasion by an unknown pathogen. *J. Neural Transm. (Vienna)* *110*, 517–536.
- Braniste, V., Al-Asmakh, M., Kowal, C., Anuar, F., Abbaspour, A., Tóth, M., Korecka, A., Bakocevic, N., Ng, L.G., Kundu, P., et al. (2014). The gut microbiota influences blood-brain barrier permeability in mice. *Sci. Transl. Med.* *6*, 263ra158.
- Brettschneider, J., Del Tredici, K., Lee, V.M., and Trojanowski, J.Q. (2015). Spreading of pathology in neurodegenerative diseases: a focus on human studies. *Nat. Rev. Neurosci.* *16*, 109–120.
- Burke, R.E., Dauer, W.T., and Vonsattel, J.P. (2008). A critical evaluation of the Braak staging scheme for Parkinson's disease. *Ann. Neurol.* *64*, 485–491.
- Caporaso, J.G., Kuczynski, J., Stombaugh, J., Bittinger, K., Bushman, F.D., Costello, E.K., Fierer, N., Peña, A.G., Goodrich, J.K., Gordon, J.I., et al. (2010). QIIME allows analysis of high-throughput community sequencing data. *Nat. Methods* *7*, 335–336.
- Chesselet, M.F., Richter, F., Zhu, C., Magen, I., Watson, M.B., and Subramaniam, S.R. (2012). A progressive mouse model of Parkinson's disease: the Thy1- α Syn ("Line 61") mice. *Neurotherapeutics* *9*, 297–314.

- Chorell, E., Andersson, E., Evans, M.L., Jain, N., Götheson, A., Åden, J., Chapman, M.R., Almqvist, F., and Wittung-Stafshede, P. (2015). Bacterial chaperones CsgE and CsgG differentially modulate human α -synuclein amyloid formation via transient contacts. *PLoS ONE* *10*, e0140194.
- Clarke, G., Grenham, S., Scully, P., Fitzgerald, P., Moloney, R.D., Shanahan, F., Dinan, T.G., and Cryan, J.F. (2013). The microbiome-gut-brain axis during early life regulates the hippocampal serotonergic system in a sex-dependent manner. *Mol. Psychiatry* *18*, 666–673.
- Cleynen, I., Vazeille, E., Artieda, M., Verspaget, H.W., Szczypiorska, M., Bringer, M.A., Lakatos, P.L., Seibold, F., Parnell, K., Weersma, R.K., et al. (2014). Genetic and microbial factors modulating the ubiquitin proteasome system in inflammatory bowel disease. *Gut* *63*, 1265–1274.
- Del Tredici, K., and Braak, H. (2008). A not entirely benign procedure: progression of Parkinson's disease. *Acta Neuropathol.* *115*, 379–384.
- Devos, D., Lebouvier, T., Lardeux, B., Biraud, M., Rouaud, T., Pouclet, H., Coron, E., Bruley des Varannes, S., Naveilhan, P., Nguyen, J.M., et al. (2013). Colonic inflammation in Parkinson's disease. *Neurobiol. Dis.* *50*, 42–48.
- Diaz Heijtz, R., Wang, S., Anuar, F., Qian, Y., Björkholm, B., Samuelsson, A., Hibberd, M.L., Forsberg, H., and Pettersson, S. (2011). Normal gut microbiota modulates brain development and behavior. *Proc. Natl. Acad. Sci. USA* *108*, 3047–3052.
- Dinan, T.G., and Cryan, J.F. (2015). The impact of gut microbiota on brain and behaviour: implications for psychiatry. *Curr. Opin. Clin. Nutr. Metab. Care* *18*, 552–558.
- Eisenhofer, G., Aneman, A., Friberg, P., Hooper, D., Fändriks, L., Lonroth, H., Hunyady, B., and Mezey, E. (1997). Substantial production of dopamine in the human gastrointestinal tract. *J. Clin. Endocrinol. Metab.* *82*, 3864–3871.
- Erny, D., Hrabě de Angelis, A.L., Jaitin, D., Wieghofer, P., Staszewski, O., David, E., Keren-Shaul, H., Mhlahkoiv, T., Jakobshagen, K., Buch, T., et al. (2015). Host microbiota constantly control maturation and function of microglia in the CNS. *Nat. Neurosci.* *18*, 965–977.
- Fleming, S.M., Salcedo, J., Fernagut, P.O., Rockenstein, E., Masliah, E., Levine, M.S., and Chesselet, M.F. (2004). Early and progressive sensorimotor anomalies in mice overexpressing wild-type human alpha-synuclein. *J. Neurosci.* *24*, 9434–9440.
- Gao, H.M., Zhang, F., Zhou, H., Kam, W., Wilson, B., and Hong, J.S. (2011). Neuroinflammation and α -synuclein dysfunction potentiate each other, driving chronic progression of neurodegeneration in a mouse model of Parkinson's disease. *Environ. Health Perspect.* *119*, 807–814.
- Gao, B., Bian, X., Mahbub, R., and Lu, K. (2016). Gender-specific effects of organophosphate diazinon on the gut microbiome and its metabolic functions. *Environ. Health Perspect.* Published online May 20, 2016. <http://dx.doi.org/10.1289/EHP202>.
- Gilbert, J.A., Jansson, J.K., and Knight, R. (2014). The Earth Microbiome project: successes and aspirations. *BMC Biol.* *12*, 69.
- Hasegawa, S., Goto, S., Tsuji, H., Okuno, T., Asahara, T., Nomoto, K., Shibata, A., Fujisawa, Y., Minato, T., Okamoto, A., et al. (2015). Intestinal dysbiosis and lowered serum lipopolysaccharide-binding protein in Parkinson's disease. *PLoS ONE* *10*, e0142164.
- Hoban, A.E., Stilling, R.M., Ryan, F.J., Shanahan, F., Dinan, T.G., Claesson, M.J., Clarke, G., and Cryan, J.F. (2016). Regulation of prefrontal cortex myelination by the microbiota. *Transl. Psychiatry* *6*, e774.
- Holmqvist, S., Chutna, O., Bousset, L., Aldrin-Kirk, P., Li, W., Björklund, T., Wang, Z.Y., Roybon, L., Melki, R., and Li, J.Y. (2014). Direct evidence of Parkinson pathology spread from the gastrointestinal tract to the brain in rats. *Acta Neuropathol.* *128*, 805–820.
- Hooper, L.V., Littman, D.R., and Macpherson, A.J. (2012). Interactions between the microbiota and the immune system. *Science* *336*, 1268–1273.
- Jenner, P. (2008). Molecular mechanisms of L-DOPA-induced dyskinesia. *Nat. Rev. Neurosci.* *9*, 665–677.
- Jo, E., McLaurin, J., Yip, C.M., St George-Hyslop, P., and Fraser, P.E. (2000). alpha-Synuclein membrane interactions and lipid specificity. *J. Biol. Chem.* *275*, 34328–34334.
- Kannarkat, G.T., Boss, J.M., and Tansey, M.G. (2013). The role of innate and adaptive immunity in Parkinson's disease. *J. Parkinsons Dis.* *3*, 493–514.
- Keshavarzian, A., Green, S.J., Engen, P.A., Voigt, R.M., Naqib, A., Forsyth, C.B., Mutlu, E., and Shannon, K.M. (2015). Colonic bacterial composition in Parkinson's disease. *Mov. Disord.* *30*, 1351–1360.
- Kim, C., Ho, D.H., Suk, J.E., You, S., Michael, S., Kang, J., Joong Lee, S., Masliah, E., Hwang, D., Lee, H.J., and Lee, S.J. (2013). Neuron-released oligomeric α -synuclein is an endogenous agonist of TLR2 for paracrine activation of microglia. *Nat. Commun.* *4*, 1562.
- Klucken, J., Ingelsson, M., Shin, Y., Irizarry, M.C., Hedley-Whyte, E.T., Frosch, M., Growdon, J., McLean, P., and Hyman, B.T. (2006). Clinical and biochemical correlates of insoluble alpha-synuclein in dementia with Lewy bodies. *Acta Neuropathol.* *111*, 101–108.
- Kohman, R.A., Bhattacharya, T.K., Kilby, C., Bucko, P., and Rhodes, J.S. (2013). Effects of minocycline on spatial learning, hippocampal neurogenesis and microglia in aged and adult mice. *Behav. Brain Res.* *242*, 17–24.
- Kopylova, E., Noé, L., and Touzet, H. (2012). SortMeRNA: fast and accurate filtering of ribosomal RNAs in metatranscriptomic data. *Bioinformatics* *28*, 3211–3217.
- Kumar, D.K., Choi, S.H., Washicosky, K.J., Eimer, W.A., Tucker, S., Ghofrani, J., Lefkowitz, A., McColl, G., Goldstein, L.E., Tanzi, R.E., and Moir, R.D. (2016). Amyloid- β peptide protects against microbial infection in mouse and worm models of Alzheimer's disease. *Sci. Transl. Med.* *8*, 340ra72.
- Langille, M.G., Zaneveld, J., Caporaso, J.G., McDonald, D., Knights, D., Reyes, J.A., Clemente, J.C., Burkepile, D.E., Vega Thurber, R.L., Knight, R., et al. (2013). Predictive functional profiling of microbial communities using 16S rRNA marker gene sequences. *Nat. Biotechnol.* *31*, 814–821.
- Ley, R.E., Peterson, D.A., and Gordon, J.I. (2006). Ecological and evolutionary forces shaping microbial diversity in the human intestine. *Cell* *124*, 837–848.
- Lin, R., Jiang, Y., Zhao, X.Y., Guan, Y., Qian, W., Fu, X.C., Ren, H.Y., and Hou, X.H. (2014). Four types of Bifidobacteria trigger autophagy response in intestinal epithelial cells. *J. Dig. Dis.* *15*, 597–605.
- Lozupone, C., and Knight, R. (2005). UniFrac: a new phylogenetic method for comparing microbial communities. *Appl. Environ. Microbiol.* *71*, 8228–8235.
- Luk, K.C., Kehm, V., Carroll, J., Zhang, B., O'Brien, P., Trojanowski, J.Q., and Lee, V.M. (2012). Pathological α -synuclein transmission initiates Parkinson-like neurodegeneration in nontransgenic mice. *Science* *338*, 949–953.
- Mandal, S., Van Treuren, W., White, R.A., Eggesbø, M., Knight, R., and Pedada, S.D. (2015). Analysis of composition of microbiomes: a novel method for studying microbial composition. *Microb. Ecol. Health Dis.* *26*, 27663.
- Matcovitch-Natan, O., Winter, D.R., Giladi, A., Vargas Aguilar, S., Spinrad, A., Sarrazin, S., Ben-Yehuda, H., David, E., Zelada González, F., Perrin, P., et al. (2016). Microglia development follows a stepwise program to regulate brain homeostasis. *Science* *353*, aad8670.
- Mayer, E.A., Padua, D., and Tillisch, K. (2014). Altered brain-gut axis in autism: comorbidity or causative mechanisms? *BioEssays* *36*, 933–939.
- McDonald, D., Price, M.N., Goodrich, J., Nawrocki, E.P., DeSantis, T.Z., Probst, A., Andersen, G.L., Knight, R., and Hugenholtz, P. (2012). An improved Greengenes taxonomy with explicit ranks for ecological and evolutionary analyses of bacteria and archaea. *ISME J.* *6*, 610–618.
- Minter, M.R., Zhang, C., Leone, V., Ringus, D.L., Zhang, X., Oyler-Castrillo, P., Musch, M.W., Liao, F., Ward, J.F., Holtzman, D.M., et al. (2016). Antibiotic-induced perturbations in gut microbial diversity influences neuro-inflammation and amyloidosis in a murine model of Alzheimer's disease. *Sci. Rep.* *6*, 30028.
- Mitchell, R.W., On, N.H., Del Bigio, M.R., Miller, D.W., and Hatch, G.M. (2011). Fatty acid transport protein expression in human brain and potential role in fatty acid transport across human brain microvessel endothelial cells. *J. Neurochem.* *117*, 735–746.
- Mogi, M., Harada, M., Kondo, T., Riederer, P., Inagaki, H., Minami, M., and Nagatsu, T. (1994a). Interleukin-1 beta, interleukin-6, epidermal growth factor and transforming growth factor-alpha are elevated in the brain from parkinsonian patients. *Neurosci. Lett.* *180*, 147–150.

- Mogi, M., Harada, M., Riederer, P., Narabayashi, H., Fujita, K., and Nagatsu, T. (1994b). Tumor necrosis factor- α (TNF- α) increases both in the brain and in the cerebrospinal fluid from parkinsonian patients. *Neurosci. Lett.* **165**, 208–210.
- Möhle, L., Mattei, D., Heimesaat, M.M., Bereswill, S., Fischer, A., Alutis, M., French, T., Hambardzumyan, D., Matzinger, P., Dunay, I.R., and Wolf, S.A. (2016). Ly6C(hi) monocytes provide a link between antibiotic-induced changes in gut microbiota and adult hippocampal neurogenesis. *Cell Rep.* **15**, 1945–1956.
- Nalls, M.A., Pankratz, N., Lill, C.M., Do, C.B., Hernandez, D.G., Saad, M., DeStefano, A.L., Kara, E., Bras, J., Sharma, M., et al.; International Parkinson's Disease Genomics Consortium (IPDGC); Parkinson's Study Group (PSG) Parkinson's Research: The Organized GENetics Initiative (PROGENI); 23andMe; GenePD; NeuroGenetics Research Consortium (NGRC); Hussman Institute of Human Genomics (HIHG); Ashkenazi Jewish Dataset Investigator; Cohorts for Health and Aging Research in Genetic Epidemiology (CHARGE); North American Brain Expression Consortium (NABEC); United Kingdom Brain Expression Consortium (UKBEC); Greek Parkinson's Disease Consortium; Alzheimer Genetic Analysis Group (2014). Large-scale meta-analysis of genome-wide association data identifies six new risk loci for Parkinson's disease. *Nat. Genet.* **46**, 989–993.
- Neufeld, K.M., Kang, N., Bienenstock, J., and Foster, J.A. (2011). Reduced anxiety-like behavior and central neurochemical change in germ-free mice. *Neurogastroenterol. Motil.* **23**, 255–264, e119.
- Prusiner, S.B., Woerman, A.L., Mordes, D.A., Watts, J.C., Rampersaud, R., Berry, D.B., Patel, S., Oehler, A., Lowe, J.K., Kravitz, S.N., et al. (2015). Evidence for α -synuclein prions causing multiple system atrophy in humans with parkinsonism. *Proc. Natl. Acad. Sci. USA* **112**, E5308–E5317.
- Ritz, B.R., Paul, K.C., and Bronstein, J.M. (2016). Of pesticides and men: a California story of genes and environment in Parkinson's disease. *Curr. Environ. Health Rep.* **3**, 40–52.
- Rockenstein, E., Mallory, M., Hashimoto, M., Song, D., Shults, C.W., Lang, I., and Masliah, E. (2002). Differential neuropathological alterations in transgenic mice expressing alpha-synuclein from the platelet-derived growth factor and Thy-1 promoters. *J. Neurosci. Res.* **68**, 568–578.
- Rooks, M.G., and Garrett, W.S. (2016). Gut microbiota, metabolites and host immunity. *Nat. Rev. Immunol.* **16**, 341–352.
- Sacchettini, J.C., and Kelly, J.W. (2002). Therapeutic strategies for human amyloid diseases. *Nat. Rev. Drug Discov.* **1**, 267–275.
- Sanchez-Guajardo, V., Barnum, C.J., Tansey, M.G., and Romero-Ramos, M. (2013). Neuroimmunological processes in Parkinson's disease and their relation to α -synuclein: microglia as the referee between neuronal processes and peripheral immunity. *ASN Neuro* **5**, 113–139.
- Scheperjans, F., Aho, V., Pereira, P.A., Koskinen, K., Paulin, L., Pekkonen, E., Haapaniemi, E., Kaakkola, S., Eerola-Rautio, J., Pohja, M., et al. (2015). Gut microbiota are related to Parkinson's disease and clinical phenotype. *Mov. Disord.* **30**, 350–358.
- Schroeder, B.O., and Bäckhed, F. (2016). Signals from the gut microbiota to distant organs in physiology and disease. *Nat. Med.* **22**, 1079–1089.
- Selkrig, J., Wong, P., Zhang, X., and Pettersson, S. (2014). Metabolic tinkering by the gut microbiome: Implications for brain development and function. *Gut Microbes* **5**, 369–380.
- Shannon, K.M., Keshavarzian, A., Dodiya, H.B., Jakate, S., and Kordower, J.H. (2012). Is alpha-synuclein in the colon a biomarker for premotor Parkinson's disease? Evidence from 3 cases. *Mov. Disord.* **27**, 716–719.
- Sharon, G., Sampson, T.R., Geschwind, D.H., and Mazmanian, S.K. (2016). The central nervous system and the gut microbiome. *Cell* **167**, 915–932.
- Smith, P.M., Howitt, M.R., Panikov, N., Michaud, M., Gallini, C.A., Bohlooly-Y, M., Glickman, J.N., and Garrett, W.S. (2013). The microbial metabolites, short-chain fatty acids, regulate colonic Treg cell homeostasis. *Science* **341**, 569–573.
- Soldner, F., Stelzer, Y., Shivalila, C.S., Abraham, B.J., Latourelle, J.C., Barasa, M.I., Goldmann, J., Myers, R.H., Young, R.A., and Jaenisch, R. (2016). Parkinson-associated risk variant in distal enhancer of α -synuclein modulates target gene expression. *Nature* **533**, 95–99.
- Sudo, N., Chida, Y., Aiba, Y., Sonoda, J., Oyama, N., Yu, X.N., Kubo, C., and Koga, Y. (2004). Postnatal microbial colonization programs the hypothalamic-pituitary-adrenal system for stress response in mice. *J. Physiol.* **558**, 263–275.
- Svensson, E., Horváth-Puhó, E., Thomsen, R.W., Djurhuus, J.C., Pedersen, L., Borghammer, P., and Sørensen, H.T. (2015). Vagotomy and subsequent risk of Parkinson's disease. *Ann. Neurol.* **78**, 522–529.
- Unger, M.M., Spiegel, J., Dillmann, K.U., Grundmann, D., Philippeit, H., Bürmann, J., Faßbender, K., Schwierz, A., and Schäfer, K.H. (2016). Short chain fatty acids and gut microbiota differ between patients with Parkinson's disease and age-matched controls. *Parkinsonism Relat. Disord.* **32**, 66–72.
- Valera, E., and Masliah, E. (2016). Combination therapies: the next logical step for the treatment of synucleinopathies? *Mov. Disord.* **31**, 225–234.
- Vázquez-Baeza, Y., Pirrung, M., Gonzalez, A., and Knight, R. (2013). EMPERor: a tool for visualizing high-throughput microbial community data. *Gigascience* **2**, 16.
- Verbaan, D., Marinus, J., Visser, M., van Rooden, S.M., Stiggelbout, A.M., and van Hilten, J.J. (2007). Patient-reported autonomic symptoms in Parkinson disease. *Neurology* **69**, 333–341.
- Wall, R., Cryan, J.F., Ross, R.P., Fitzgerald, G.F., Dinan, T.G., and Stanton, C. (2014). Bacterial neuroactive compounds produced by psychobiotics. *Adv. Exp. Med. Biol.* **817**, 221–239.
- Walters, W., Hyde, E.R., Berg-Lyons, D., Ackermann, G., Humphrey, G., Parada, A., Gilbert, J.A., Jansson, J.K., Caporaso, J.G., Fuhrman, J.A., et al. (2015). Improved bacterial 16S rRNA gene (V4 and V4-5) and fungal internal transcribed spacer marker gene primers for microbial community surveys. *mSystems* **1**, 1.
- Wang, L., Magen, I., Yuan, P.Q., Subramaniam, S.R., Richter, F., Chesselet, M.F., and Taché, Y. (2012). Mice overexpressing wild-type human alpha-synuclein display alterations in colonic myenteric ganglia and defecation. *Neurogastroenterol. Motil.* **24**, e425–e436.
- Yano, J.M., Yu, K., Donaldson, G.P., Shastri, G.G., Ann, P., Ma, L., Nagler, C.R., Ismagilov, R.F., Mazmanian, S.K., and Hsiao, E.Y. (2015). Indigenous bacteria from the gut microbiota regulate host serotonin biosynthesis. *Cell* **161**, 264–276.
- Zhang, J., Saur, T., Duke, A.N., Grant, S.G., Platt, D.M., Rowlett, J.K., Isacson, O., and Yao, W.D. (2014). Motor impairments, striatal degeneration, and altered dopamine-glutamate interplay in mice lacking PSD-95. *J. Neurogenet.* **28**, 98–111.

Fasting-Mimicking Diet Promotes Ngn3-Driven β -Cell Regeneration to Reverse Diabetes

Chia-Wei Cheng,^{1,6,7} Valentina Villani,^{2,7} Roberta Buono,^{1,5,7} Min Wei,¹ Sanjeev Kumar,⁴ Omer H. Yilmaz,⁶ Pinchas Cohen,¹ Julie B. Sneddon,³ Laura Perin,² and Valter D. Longo^{1,4,5,8,*}

¹Longevity Institute, School of Gerontology, Department of Biological Sciences, University of Southern California, 3715 McClintock Avenue, Los Angeles, CA 90089-0191, USA

²GOFARR Laboratory for Organ Regenerative Research and Cell Therapeutics, Children's Hospital Los Angeles, Division of Urology, Saban Research Institute, University of Southern California, Los Angeles, Los Angeles, CA 90027, USA

³Diabetes Center, University of California, San Francisco, 513 Parnassus Avenue, San Francisco, CA 94143

⁴Eli and Edythe Broad Center for Regenerative Medicine and Stem Cell Research at USC, Keck School of Medicine, University of Southern California, Los Angeles, CA 90027, USA

⁵IFOM FIRG Institute of Molecular Oncology, Via Adamello 16, Milan 20139, Italy

⁶Koch Institute at MIT, 500 Main Street, Cambridge, MA 02139, USA

⁷Co-first author

⁸Lead Contact

*Correspondence: vlongo@usc.edu

<http://dx.doi.org/10.1016/j.cell.2017.01.040>

SUMMARY

Stem-cell-based therapies can potentially reverse organ dysfunction and diseases, but the removal of impaired tissue and activation of a program leading to organ regeneration pose major challenges. In mice, a 4-day fasting mimicking diet (FMD) induces a stepwise expression of Sox17 and Pdx-1, followed by Ngn3-driven generation of insulin-producing β cells, resembling that observed during pancreatic development. FMD cycles restore insulin secretion and glucose homeostasis in both type 2 and type 1 diabetes mouse models. In human type 1 diabetes pancreatic islets, fasting conditions reduce PKA and mTOR activity and induce Sox2 and Ngn3 expression and insulin production. The effects of the FMD are reversed by IGF-1 treatment and recapitulated by PKA and mTOR inhibition. These results indicate that a FMD promotes the reprogramming of pancreatic cells to restore insulin generation in islets from T1D patients and reverse both T1D and T2D phenotypes in mouse models.

INTRODUCTION

The ability of animals to survive food deprivation is an adaptive response accompanied by the atrophy of many tissues and organs to minimize energy expenditure. This atrophy and its reversal following the return to a normal diet involve stem-cell-based regeneration in the hematopoietic and nervous systems (Brandhorst et al., 2015; Cheng et al., 2014). However, whether prolonged fasting and refeeding can also cause pancreatic regeneration and/or cellular reprogramming leading to functional lineage development is unknown. β cells residing in pancreatic islets are among the most sensitive to nutrient availability.

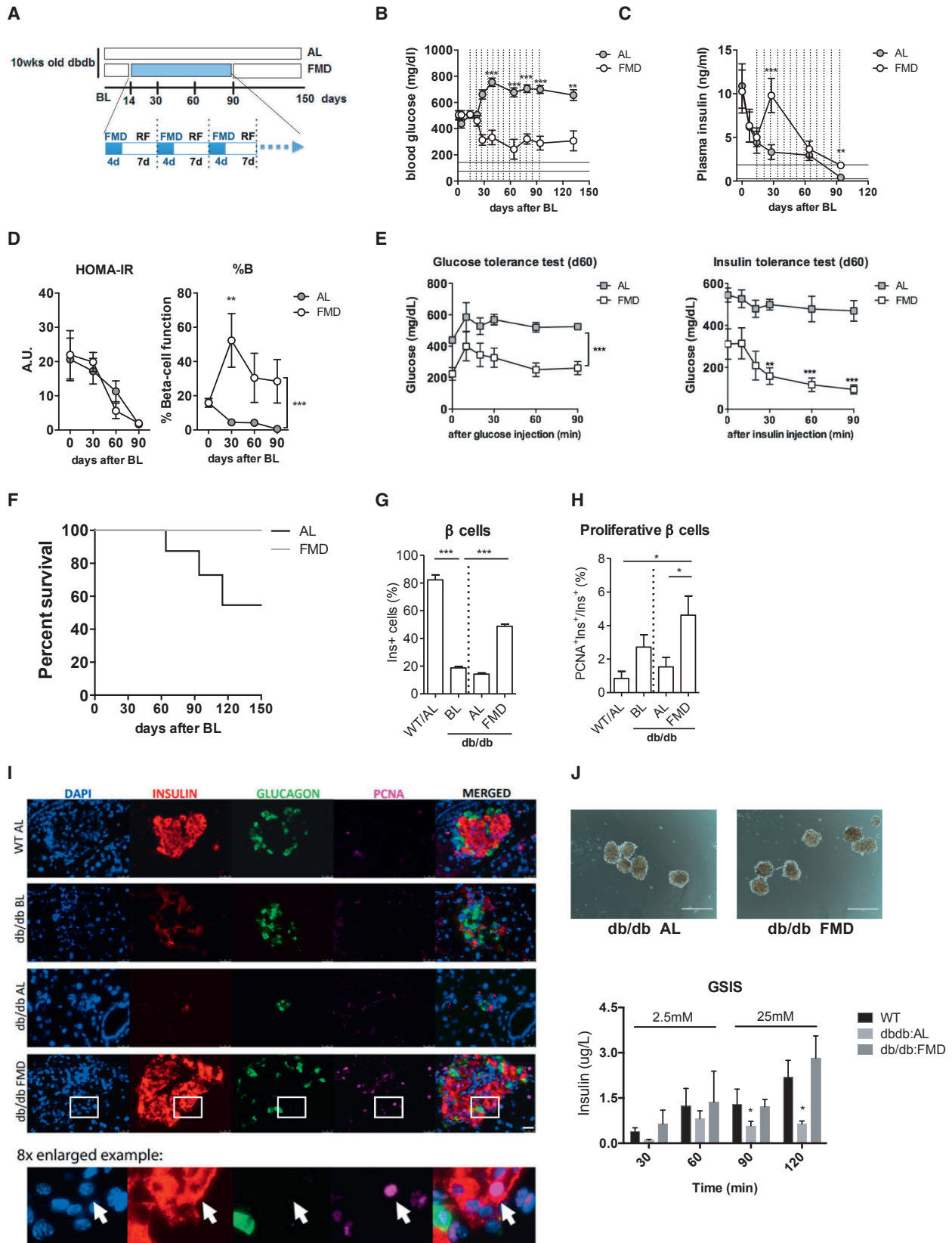
Whereas type 1 and type 2 diabetes (T1D and T2D) are characterized by β -cell dedifferentiation and trans-differentiation (Cnop et al., 2005; Dor and Glaser, 2013; Talchai et al., 2012; Wang et al., 2014), β -cell reprogramming, proliferation and/or stepwise re-differentiation from pluripotent cells are proposed as therapeutic interventions (Baeyens et al., 2014; Chera et al., 2014; Maehr et al., 2009; Pagliuca et al., 2014; Sneddon et al., 2012; Zhou et al., 2008; Ben-Othman et al., 2017; Li et al., 2017), suggesting that lineage conversion is critical in both diabetes pathogenesis and therapy (Weir et al., 2013).

Although dietary intervention with the potential to ameliorate insulin resistance and type II diabetes has been studied extensively for decades, whether this has the potential to promote a lineage-reprogramming reminiscent of that achieved by iPSCs-based engineering remains unknown. We previously showed that cycles of prolonged fasting (2–3 days) can protect mice and humans from toxicity associated with chemotherapy and can promote hematopoietic stem-cell-dependent regeneration (Cheng et al., 2014; Laviano and Rossi Fanelli, 2012; Raffaghello et al., 2008). In consideration of the challenges and side effects associated with prolonged fasting in humans, we developed a low-calorie, low-protein and low-carbohydrate but high-fat 4-day fasting mimicking diet (FMD) that causes changes in the levels of specific growth factors, glucose, and ketone bodies similar to those caused by water-only fasting (Brandhorst et al., 2015) (see also Figure S1 for metabolic cage studies). Here, we examine whether cycles of the FMD are able to promote the generation of insulin-producing β cells and investigate the mechanisms responsible for these effects.

RESULTS

Cycles of a FMD Rescue Mice from Late-Stage T2D

As a consequence of insulin resistance, the decrease in the number of functional insulin-producing β cells contributes to the pathophysiology of T2D by eventually leading to insulin deficiency (Cnop et al., 2005; Dor and Glaser, 2013). Previously, we



(legend on next page)

showed that a 4-day fasting mimicking diet (FMD) could induce metabolic changes similar to those caused by prolonged fasting and could reduce insulin and glucose levels while increasing ketone bodies and *igfbp1* (Brandhorst et al., 2015; Figure S1). Although the role of periodic fasting and fasting mimicking diets on insulin secretion is unknown, the effects of intermittent fasting and chronic calorie restrictions (CR) on insulin sensitivity have been previously reported (Barnosky et al., 2014). Here, our focus is on the putative effects of the FMD in promoting β -cell regeneration, although we have also investigated the effects of the FMD on insulin resistance.

Given that β cells replicate at an extremely low rate in the adult pancreas (Meier et al., 2008; Teta et al., 2005) and that β -cell neogenesis occurs rarely (Xiao et al., 2013), depletion of β cells and the consequent loss of insulin secretion during late-stage diabetes have often been considered conditions whose reversals require islet and stem cell transplantation (Fiorina et al., 2008; Kroon et al., 2008; Milanesi et al., 2012; Pipeleers et al., 2002; Villani et al., 2014). To determine whether the FMD could affect the β -cell deficiency associated with T2D, we studied its effect on mice with a point mutation in the leptin receptor gene (*Lepr^{db/db}*), which causes insulin resistance in the early stages and failure of β -cell function in the late stages. As reported by others, *db/db* mice developed hyperglycemia at 10 weeks of age, which we refer to as baseline (BL) (Figure 1A). The insulin levels first increased to compensate for insulin resistance but drastically declined after 2 weeks of severe hyperglycemia (Figures 1B and 1C) (Arakawa et al., 2001). As a result, *db/db* mice began to die at around 4 months of age. We attempted to reverse these late-stage T2D phenotypes by treating 12-week-old mice (14 days after the hyperglycemia stabilized, baseline) with weekly cycles of the 4-day FMD (Figure 1A). FMD cycles caused a major reduction and return to nearly normal levels of blood glucose in *db/db* mice by day 60 (Figure 1B). The FMD cycles also reversed the decline in insulin secretion at day 30 and improved plasma insulin levels at day 90 (Figure 1C). A homeostasis model assessment (HOMA) was performed to estimate steady-state β -cell function (%B) and insulin sensitivity (%S), as previously described (Hsu et al., 2013; Matthews et al.,

1985). The results indicate that the reversal of hyperglycemia was mainly caused by an induction of steady-state β -cell function (%B) (Figure 1D). Nevertheless, mice receiving the FMD showed improved glucose tolerance and insulin tolerance compared to the ad libitum (AL) fed controls (Figure 1E). Notably, although *db/db* mice on the FMD diet gained less weight compared to those on the regular diet, they maintained a weight that was ~22% higher than that of their healthy wild-type (WT) littermates during the entire experiment (Figure S2C). Altogether, these results indicate that FMD cycles rescued mice from late-stage T2D by restoring insulin secretion and reducing insulin resistance, leading to a major improvement in survival (Figure 1F, * $p < 0.05$, log-rank test for trend).

Cycles of FMD Reverse β -Cell Failure in T2D

Dedifferentiation of β cells, which results in increased non-hormone-producing cells within pancreatic islets, is a feature of diabetic β -cell failure (Dor and Glaser, 2013; Kim-Muller et al., 2014; Talchai et al., 2012). Similar to what was previously reported by others, we found an increase in cells producing neither insulin nor glucagon (i.e., non- α/β) and a decrease in β -cell number in pancreatic islets of late-stage T2D mice, but not in age-matched WT controls (Figures 1G and S2, *db/db* BL compared to WT/AL). We also found that β -cell proliferation was low in the late stage of the disease (Figure 1H, AL day 60 compared to BL). Whereas *db/db* mice fed ad libitum (*db/db*:AL) showed a 60%–80% reduction in β -cell count at day 60, *db/db* mice receiving FMD cycles (*db/db*:FMD) displayed a major improvement in the number and proliferation of insulin-generating β cells (comparing *db/db* BL, Figures 1G–1I). Pancreatic islets collected from *db/db* mice treated with FMD cycles (day 60) displayed increased glucose-stimulated insulin secretion (GSIS), compared to that of islets from *db/db*:AL mice (Figure 1J). We also determined that a longer exposure time (time point 120) was necessary to distinguish between the functionality of islets from *db/db*:AL and *db/db*:FMD group mice (Figure 1J). Overall, these results suggest that, in addition to improving insulin sensitivity, FMD induced β -cell regeneration to reverse β -cell loss, which may alleviate late-stage T2D symptoms and mortality.

Figure 1. FMD Cycles Promote β -Cell Regeneration and Reverse β -Cell Failure in T2D

(A) Experimental scheme to determine effects of the periodic FMD on T2D in the leptin-receptor-deficient (*Lepr^{db/db}*) mice. Mice were monitored for hyperglycemia and insulinemia from 10 weeks (baseline, BL) to 12 weeks and were then assigned to the dietary groups. Each FMD cycle entails 4-day FMD and up to 10 days of refeeding (RF). During refeeding, mice received a regular chow identical to that given prior to the FMD and that given to the ad libitum (AL) controls.

(B) Plasma glucose levels and (C) plasma insulin levels; vertical dashed lines indicate each cycle of the FMD, and horizontal lines indicate the range of glucose levels (mean \pm SEM) in age-matched healthy wild-type littermates. Blood samples were collected at the last refeeding day/first day of the indicated cycles. Mice were fasted for 6 hr (morning fasting) for blood glucose measurements.

(D) Homeostatic model assessment (HOMA) of insulin resistance (IR) and steady-state β -cell function (%B) at indicated time points. HOMA-B = $(20 \times \text{fasting insulin})/(\text{fasting glucose} - 3.5)\%$.

(E) Glucose tolerance test and insulin tolerance test at day 60.

(B–E) Each point represents the mean \pm SEM. * $p < 0.05$, ** $p < 0.01$, *** $p < 0.005$, two-way ANOVA.

(F) Survival curve. Mean \pm SEM, * $p < 0.05$, log-rank (Mantel-Cox) test for trend. $n \geq 16$ mice per group.

(G) Proportion of β cells per islet. $n \geq 6$ mice per group, $n \geq 15$ islets per sample.

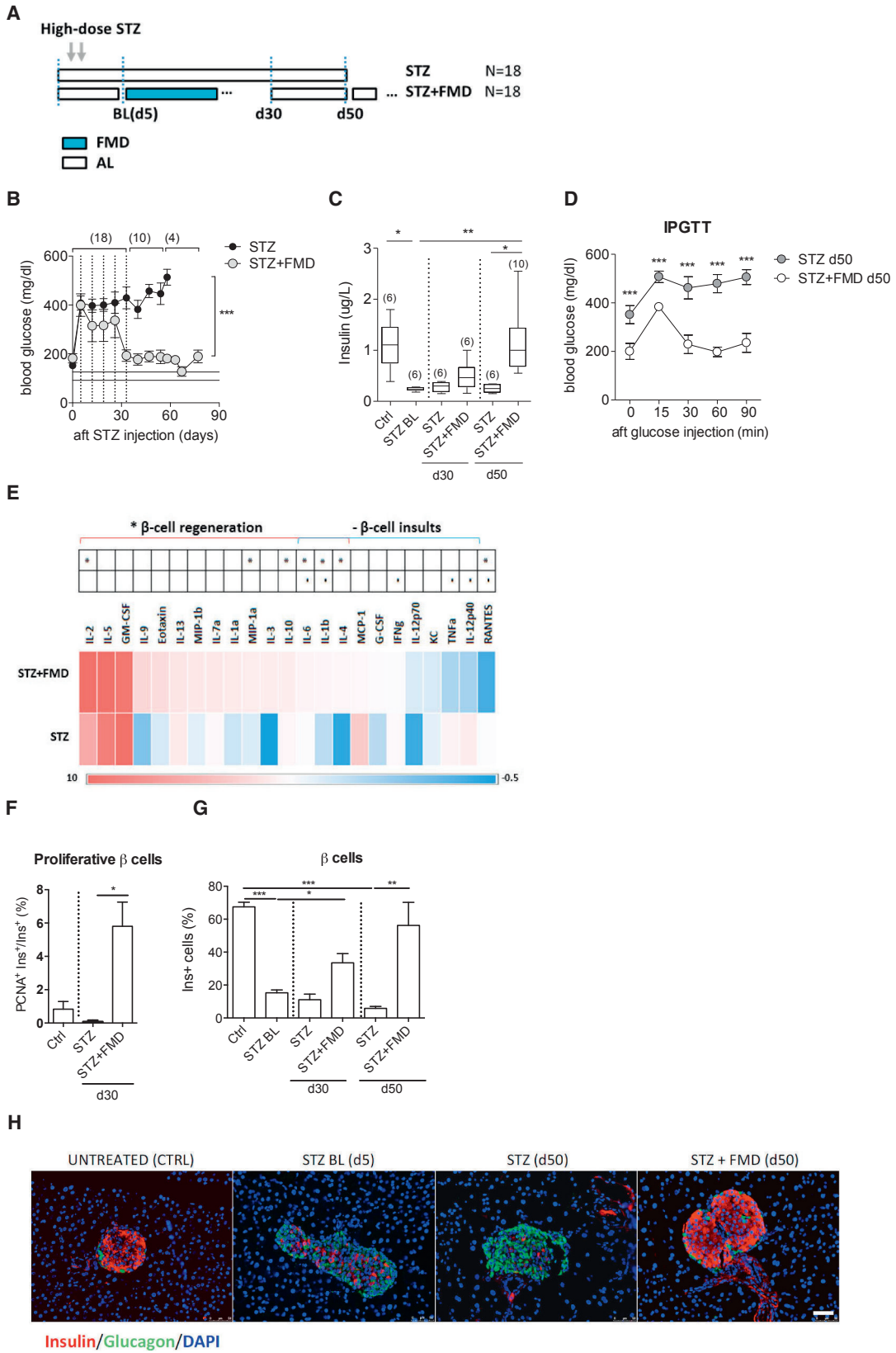
(H) Proliferative proportion of β cells per islet.

(G–I) Mean \pm SEM, * $p < 0.05$, ** $p < 0.01$, *** $p < 0.005$, one-way ANOVA. $n \geq 6$ mice per group, $n \geq 15$ islets per sample.

(I) Immunostaining of pancreatic sections from *Lepr^{db/db}* mice and their wild-type littermates at the indicated time points. Arrow in the 8x-enlarged example image indicates a typical proliferative β cell (PCNA*Insulin*). Scale bar, 50 μm .

(J) Representative images for size-matched islets isolated from AL-*db/db* and FMD-*db/db* mice and results of glucose-stimulated insulin secretion (GSIS) test in islets isolated from *Lepr^{db/db}* mice on FMD or fed ad libitum. Scale bar, 50 μm .

Mice are of the C57BL/6J background of the age indicated. In (A), mice received no additional treatments other than the indicated diet.



(legend on next page)

FMD Cycles Restore Insulin-Dependent Glucose Homeostasis in STZ-Induced T1D

To examine further the role of FMD cycles in stimulating β -cell regeneration, we applied FMD cycles on a T1D model in which high-dose streptozotocin (STZ) treatment causes the depletion of insulin-secreting β cells (Wu and Huan, 2008; Yin et al., 2006). Starting 5 days after STZ treatment, which we refer to as baseline (STZ BL), hyperglycemia (>300 mg/dl) was observed in both mice fed AL and those subjected to multiple cycles of the 4-day FMD every 7 days (4 days of FMD followed by 3 days of re-feeding, every 7 days per cycle) (Figures 2A and 2B). Levels of blood glucose continued to increase in STZ-treated mice receiving the AL diet and reached levels above 450 mg/dl at both days 30 and 50. On the other hand, in mice receiving FMD cycles, hyperglycemia and insulin deficiency were both significantly alleviated on day 30 (Figure 2B, sample size indicated in parentheses). Remarkably, the levels of these physiological parameters returned to a nearly normal range at days 50–60 after the FMD cycles (Figures 2B and 2C, sample size indicated in parentheses). Intraperitoneal glucose tolerance tests (IPGTTs) at day 50 confirmed that STZ-treated mice undergoing the FMD cycles have improved capacity to clear exogenous blood glucose (STZ+ FMD), compared to mice on the regular chow (STZ) (Figure 2D).

Levels of certain circulating cytokines have been used as indicators to determine islet pathological status in patients with recent-onset T1D (Baeyens et al., 2014; Grunnet et al., 2009; Lebastchi and Herold, 2012). We performed a 23-plex immunoassay to determine the effects of the FMD on inflammatory markers. We found that FMD cycles not only suppressed the circulating cytokines associated with β -cell damage (e.g., TNF α and IL-12), but also increased circulating cytokines associated with β -cell regeneration (e.g., IL-2 and IL-10) (Figure 2E, day 30) (Dirice et al., 2014; Rabinovitch, 1998; Zhernakova et al., 2006).

Taken together, these results indicate that FMD cycles reduce inflammation and promote changes in the levels of cytokines and other proteins, which may be beneficial for the restoration of insulin secretion and the reversal of hyperglycemia.

FMD Cycles Reverse STZ-Induced β -Cell Depletion

The characterization of pancreatic islet cells indicates a strong association between restored glucose homeostasis and the replenishment of pancreatic β cells in animals undergoing FMD cycles. STZ treatments resulted in an increase of non- α/β

cells (Figure S3) and an $\sim 85\%$ depletion of insulin-secreting β cells (Figure 2F, STZ BL). The transient increase of non- α/β cells was reversed by day 30 in both groups (Figures S2D and S2E). Mice receiving weekly cycles of the FMD showed a major increase in proliferative β cells followed by a return to a nearly normal level of insulin-generating β cells by d50 (Figures 2F–2H). In contrast, mice that received ad libitum access to regular chow remained depleted of β cells for >50 days (Figures 2F and 2H). Overall, the increase of non- α/β prior to β -cell proliferation raises the possibility that weekly cycle of the FMD might mediate the fate conversion of non- α/β cells to β cells to reverse the STZ-induced β -cell depletion, although other scenarios are possible.

FMD and Post-FMD Re-feeding Promote β -Cell Regeneration in Non-diabetic Mice

We investigated whether and how the FMD and the post-FMD re-feeding period could regulate the cell populations within the islets to promote β -cell regeneration independently of diabetes, with a focus on the non- α/β cells and proliferative β cells. To characterize cellular and hormonal changes, pancreatic samples and peripheral blood of wild-type C57Bl6 mice fed with the FMD for 4 days were collected before the diet (BL), at the end of the diet (day 4), and 1 or 3 days after mice returned to the normal diet (RF1d or RF3d). The FMD caused a trend of decrease in the number and size of pancreatic islets (Figure 3A) and reduced the proportion of β cells by 35% (Figures 3B and 3C; see also Figure S4 for absolute numbers). These effects were reversed within 3 days of re-feeding (Figures 3A and 3C). Non- α/β cells began to proliferate at the end of the FMD, and this proliferation persisted until 1 day after re-feeding (RF1d), leading to a 2.5-fold increase in non- α/β cells (proportion per islet) at RF1d (Figure S4). By RF3d, the number of non- α/β cells had dropped and that of β cells returned to basal levels (BL), although β cells remained in a much more proliferative state in the FMD group (Figure 3B and 3C). The expression of the proliferation marker PCNA was elevated in β cells, but not α cells, after re-feeding post FMD (Figures 3B and 3C and S4). Despite the number of α cells per islet remaining the same, the transitional α -to- β or β -to- α cells that co-express both α (i.e., glucagon) and β cell (i.e., Pdx-1 or insulin) markers were increased in mice that received the FMD (Figure 3D). In summary, the FMD promotes a decrease in the numbers of differentiated or committed cells, followed by the induction of transitional cells and major increases in the proliferation and number of insulin-generating β cells (Figure 3E).

Figure 2. FMD Cycles Reverse STZ-Induced β -Cell Depletion and Restore Glucose Homeostasis

(A) Experimental scheme of the periodic FMD's effects on STZ-induced T1D. Baseline measurements (BL) were performed at day 5 after STZ treatment. (B) Fasting glucose levels and (C) plasma insulin levels during and 55 days after the FMD cycles (d5 to d35). Vertical dashed lines indicate each cycle of FMD; horizontal lines (125 ± 12 mg/dl) indicate levels of blood glucose in the naive control mice. (D) Glucose tolerance test at d50. (E) Cytokine profile of mice treated with STZ or STZ+FMD at d30, compared to that in naive controls. Pancreatic samples collected at indicated time points were analyzed for: (F) PCNA+ proliferating β cells. (G) Proportion of insulin-producing β cells per islet and (H) representative micrographs with immunostaining of insulin, glucagon, and DAPI on pancreas sections of mice treated with STZ or STZ + FMD at the indicated time points. Scale bar, 50 μ m. Mice of the C57BL/6J background, age 3–6 months, received STZ treatments (150 mg/kg) as indicated in (A). For (B–G), each point represents the mean \pm SEM, and sample size (n) is indicated in parentheses. (F and G) * $p < 0.05$, ** $p < 0.01$, *** $p < 0.005$, one-way ANOVA. Ctrl, STZ-untreated control; STZ BL, baseline level of STZ treated mice at day 5. $n \geq 6$ mice per group per time point, $n \geq 15$ islets per mouse.

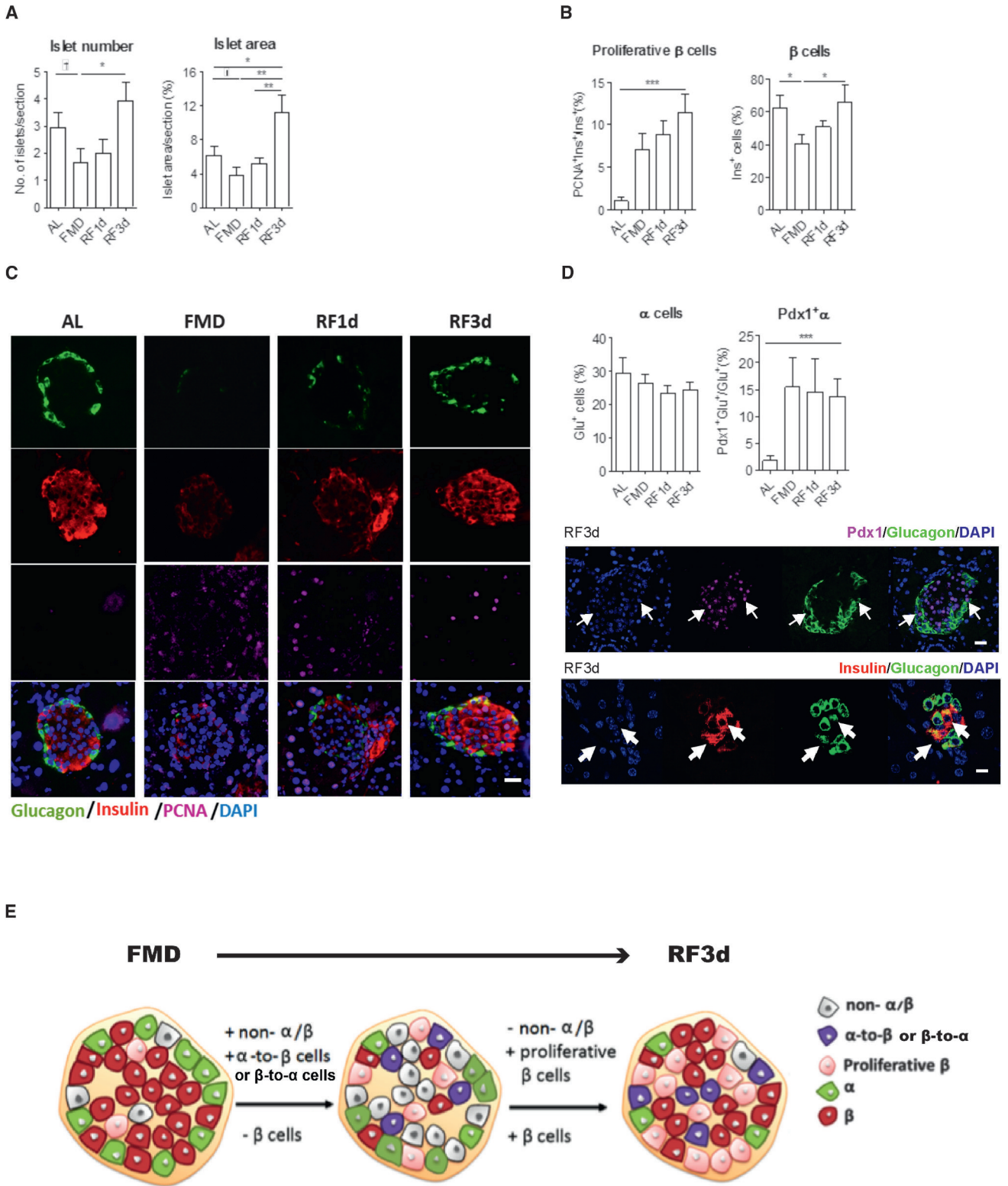


Figure 3. FMD and Post-FMD Refeeding Promote β -Cell Proliferation and Regeneration

(A) Size and number of pancreatic islets per pancreatic section.

(B) Proportion of PCNA+ proliferating β cells and of total β cells per islet.

(C) Representative images of pancreatic islets with insulin, glucagon, and PCNA immuno-staining. Scale bar, 50 μ m.

(legend continued on next page)

FMD Promotes a Gene Expression Profile in Adult Mice Similar to that Observed during Embryonic and Fetal Development

To identify the genes that may mediate the FMD-induced pancreatic regeneration, we measured gene expression in pancreatic islets at the end of the FMD and post-FMD re-feeding. At both time points, we observed a transient upregulation of *Foxo1* (6.9-fold at FMD, 5.3-fold at RF1d, * $p < 0.05$ comparing to AL) and of a set of genes that have been previously identified as dual regulators for both fat metabolism and fate determination in mammalian cells (Cook et al., 2015; Haeusler et al., 2014; Johnson et al., 2004; Kim-Muller et al., 2014; Mu et al., 2006; Stanger, 2008; Talchai et al., 2012; Talchai and Accili, 2015; Tonne et al., 2013) (Figure 4A), in agreement with the metabolic changes found in mice receiving the FMD (Figure S1). We further examined whether the metabolic reprogramming caused by the FMD affects lineage determination in pancreatic islets. In Figure 4B, the expression of lineage markers was determined by the mRNA expression of purified islets from mice fed ad libitum (AL) or the FMD. Results from the qPCR array indicate that upregulation of the following genes was statistically significant (* $p < 0.05$ comparing to AL, Figure 4B; see also Figure S5): (1) pluripotency markers (e.g., *Lefty1*, 3.0-fold during FMD, 7.0-fold at RF1d; *Podx1*, 3.9-fold during FMD, 9.8-fold at RF1d; *Nanog*, 2.6-fold during FMD and 5.4-fold RF1d, and *Dnmt3b*, 31.6-fold during FMD and 18.3-fold RF1d), (2) embryonic development markers (e.g., *Sox17*, 3.4-fold during FMD and *Gata6* 3.1-fold during FMD and 2.7-fold at RF1d), (3) pancreatic fetal-stage markers, and (4) β -cell reprogramming markers (e.g., *Mafa*, 4.7-fold at RF1d; *Pdx-1* 3-fold during FMD, 5.07-fold at RF1d; and *Ngn3*, 21.5-fold during FMD, 45.6-fold at RF1d) (Figure 4B; Zhou et al., 2008). These changes in gene expression suggest that the FMD causes either: (1) a de-differentiation of pancreatic cells toward pluripotency at the end of the diet followed by re-differentiation to pancreatic β -cell lineage during early re-feeding (RF1d) or (2) recruitment of cells with these features from outside of the pancreatic islets. The assessment of protein expression of cells within the islets was also carried out by immunostaining for key proteins associated with pancreatic development (Figures 4C and 4D). In agreement with the results of qPCR array (Figure 4B), we found that protein levels of *Sox17*, as the early lineage marker, were elevated at the end of the FMD (FMD-4d) and protein levels of *Ngn3*, a marker for endocrine progenitors, were transiently upregulated during early re-feeding (FMD-4d to RF1d) (Figure 4C).

To determine whether stepwise β -cell conversion from the de-differentiated cells occurs during early refeeding, we performed double-staining for the targeted developmental markers (i.e., *Sox17*, *Pdx-1*, *Ngn3*) across the time points of FMD treatment.

We also measured the expression of *Oct4* (*Pou5f1*), which has been previously reported to be expressed in the nucleus of adult pancreatic islets in association with *Foxo-1*-related diabetic β -cell dedifferentiation (Talchai et al., 2012; Xiao et al., 2013). *Oct4* (*Pou5f1*) mRNA expression showed a trend for an increase in mice on the FMD, which is not significant (Figure 4C, $p > 0.05$). Results of immunostaining indicate that *Oct4* (*Pou5f1*) and *Sox17* may only be co-expressed very transiently after overnight re-feeding (Figure S5B, RF12hr) followed by robust expansion of *Sox17*⁺*Pdx1*⁺ and then *Pdx1*⁺*Ngn3*⁺ cells at RF1d (Figure 4D and see also Figure S5B for all time points). Although *Ngn3*⁺ cells were also detectable in AL mice, they were mainly located outside or on the edge of the islets, in agreement with what was reported in previous studies (Baeyens et al., 2014; Gomez et al., 2015; Figure 4D). The number of *Ngn3*⁺ cells was increased both inside and outside of the islets during the FMD and re-feeding (Figure 4D).

These results suggest that, as a result of the FMD and re-feeding cycle, the pancreatic islets contain an elevated number of cells with features of progenitor cells, which may differentiate and generate insulin-producing cells.

FMD Induces *Ngn3* Expression to Generate Insulin-Producing β Cells

Ngn3⁺ cells within the pancreatic islets have been previously described as progenitor cells able to generate all lineages of endocrine cells, including the insulin-producing β cells, although the role of *Ngn3* in adult β -cell regeneration remains unclear (Baeyens et al., 2014; Van de Casteele et al., 2013; Xu et al., 2008). To investigate whether the FMD causes de novo expression of *Ngn3* and whether *Ngn3*⁺ cells may contribute to FMD-induced β -cell regeneration, we generated *Ngn3*-*CreER*;*tdTomato*^{LSL}-reporter mice to trace the lineage of putative *Ngn3*-expressing cells and their progeny in the adult mice treated with the FMD (Figure 5A). To initiate the loxP recombination for lineage tracing, low-dose tamoxifen injections (2 mg per day for 3 days) inducing the recombination (maximized at 48 hr and minimized within a week) were given to mice before or after the FMD and to mice fed ad libitum (AL control) (Figure 5A). Tissue collection time points are relative to the time of injection and to that of FMD treatments (Figure 5A). Results indicate that the FMD induces the expansion of the *Ngn3*-derived lineages (Figure 5B and 5C). Characterization of *tdTomato*⁺ cells by immunostaining indicates that *tdTomato*⁺ cells contributed 50.8% \pm 8.3% of the overall β -cell pool following the FMD (Figure 5C, group C).

To confirm the contribution of FMD-induced *Ngn3* lineages in reconstituting insulin-secreting β cells, we generated another mouse model (*Ngn3*-*CreER*/*LSL*-*R26R*^{DTA}) and performed lineage-ablation experiments in both wild-type non-diabetic mice

(D) Transitional cell populations co-expressing both the markers of α and β cells: proportion of α cells and *Pdx1*⁺ α cells. Arrows in the images with split channels indicating *Pdx1*⁺*Gluc*⁺ and *Insulin*⁺*Glucagon*⁺ cells. Scale bar, 50 μ m.

(E) Schematic of FMD and post-FMD refeeding induced cellular changes in pancreatic islets.

Mice of the C57BL/6J background at ages 3–6 months received no additional treatments other than the indicated diet. Pancreatic samples were collected from mice fed ad libitum (AL) or the fasting mimicking diet (FMD) at indicated time points: the end of the 4d FMD (FMD), 1 day after re-feeding (RF1d), and 3 days after re-feeding (RF3d). For immunohistochemical and morphometric analysis (A–E): $n \geq 6$ mice per group, $n \geq 30$ islets per staining per time point. Mean \pm SEM, * $p < 0.05$, ** $p < 0.01$, *** $p < 0.005$, one-way ANOVA. † $p < 0.05$, t test.

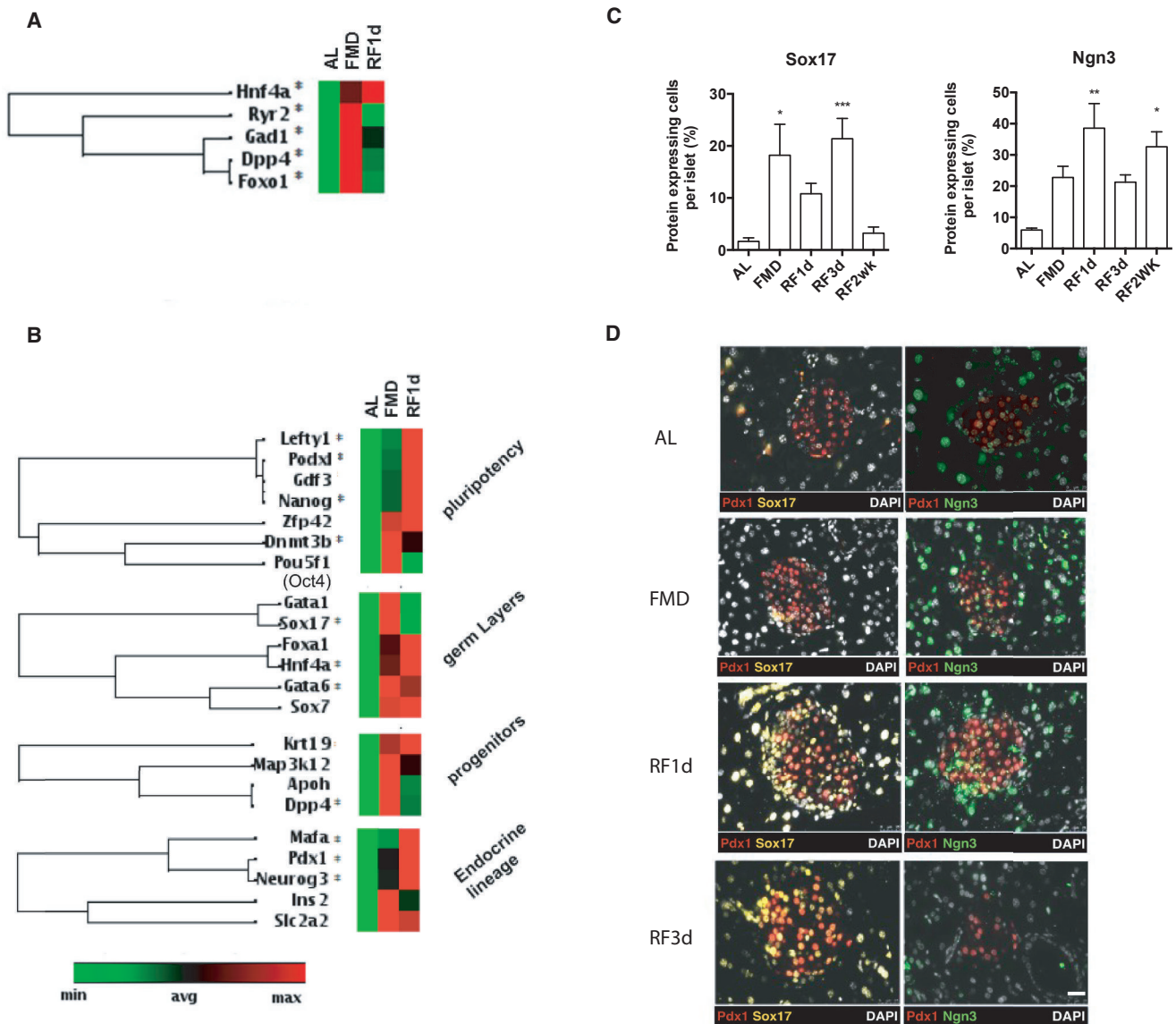


Figure 4. FMD Promotes Expression of Genes in Pancreatic Islets Characteristic of Embryonic and Fetal Development

(A) mRNA expression profile indicating changes in metabolic genes in pancreatic islets and (B) mRNA expression profile indicating changes in lineage markers in pancreatic islets at the end of 4 days FMD (FMD) and 1 day after refeeding (RF1d), comparing the ad libitum (AL) control. * $p < 0.05$, t test. Heatmap generated by QIAGEN RT² PCR array indicating a fold regulation ranging from 77 (max, red) to -4 (min, green).

(C) Quantification of protein-expressing cells of lineage markers in pancreatic islets from mice fed AL or on FMD at indicated time points. Protein expression was defined as a marker + area/total islet area. See also Figure S5B. * $p < 0.05$, ** $p < 0.01$, *** $p < 0.005$. t test comparing to AL control.

(D) Representative images of immunofluorescent staining indicating stepwise transition of Sox17/Pdx1 and Pdx1/Ngn3. Scale bar, 50 μ m.

Mice of the C57Bl6J background at ages 3–6 months received no additional treatments other than the indicated diet. Pancreatic samples were collected from mice fed ad libitum (AL) or on the FMD at indicated time points: the end of 4 days FMD (FMD), 1 day after re-feeding (RF1d), and 3 days after re-feeding (RF3d). $n = 6$ mice per group, ≥ 30 islets per marker.

and STZ-treated mice (Figure 5D). The results indicate that ablation of Ngn3+ lineage reverses FMD-induced β -cell regeneration and its effects on fasting glucose levels (Figures 5E and 5F and S5) and glucose clearance capacities (IPGTT assay) in STZ-treated diabetic mice (Figure 5G), confirming that the FMD-induced β -cell regeneration is Ngn3 dependent and suggesting a critical role for this in glucose homeostasis.

Fasting Conditions or Inhibition of Nutrient-Signaling Pathways Promote Ngn3 Expression and Insulin Production in Human Pancreatic Cells

In both mouse and humans, Ngn3 expression occurs right before and during endocrine cell generation. Ngn3 mRNA expression in the developing mouse pancreas peaks around E15.5, which is roughly equivalent to week 7–8 (Carnegie stages 21–22) in

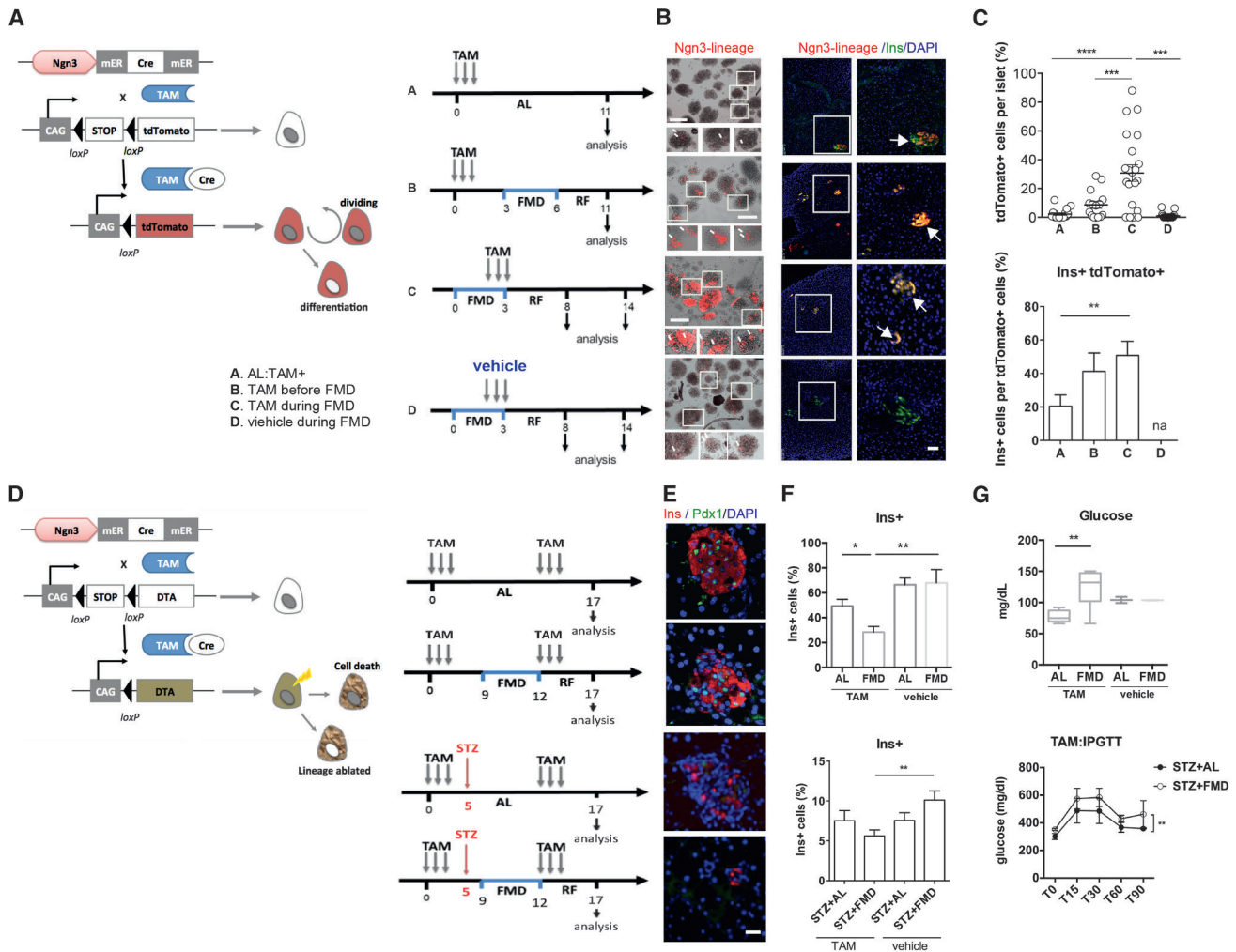


Figure 5. FMD Promotes Ngn3-Dependent Lineage Reprogramming to Generate Insulin-Producing β Cells

(A) Genetic strategy used to perform lineage tracing (tdTomato) of NGN3-expressing cells in pancreas and schematic timeline of tamoxifen (TAM) treatments for lineage-tracing experiments. (a) Mice fed ad libitum were treated with TAM. (b) Mice receiving FMD 3 days after TAM injection. (c) Mice receiving TAM and FMD concurrently. (d) Mice receiving FMD and vehicle (corn oil) concurrently. Pancreatic tissues were collected 11 days after TAM injection to analyze the effects of FMD on Ngn3 lineage generation. TdTomato+ cells (red, arrows) are Ngn3-derived cells; $n = 6$ for each group.

(B) Representative images of the labeled Ngn3 lineage cells (red, tdTomato) and insulin-producing β cells (green, Ins) at the indicated time points in pancreatic islets. (Left) Scale bar, 200 μm ; (right) scale bar, 100 μm .

(C) Quantification of total tdTomato-labeled Ngn3 lineage cells per islet (top) and proportion of labeled insulin-producing β cells (ins+tdTomato+) (bottom). Mean \pm SEM, ** $p < 0.01$, *** $p < 0.005$, t test.

(D) Genetic strategy used to perform diphtheria toxin gene A chain (DTA)-mediated Ngn3-lineage ablation in pancreas and schematic time line of tamoxifen (TAM) treatments for lineage ablation experiments (left) and results of glucose homeostasis (right). Mice were injected with TAM prior to and after the FMD to ablate Ngn3 lineage developed and/or expanded during FMD and early refeeding (RF3d). Alternatively, mice were given additional STZ injection and then assigned to the indicated dietary groups (i.e., AL+STZ or FMD+STZ), to analyze the contribution of FMD-induced β -cell conversion to glucose homeostasis.

(E) Representative images of pancreatic islets with insulin and Pdx1 immunostaining for β cells, DAPI for nuclei. See also Figure S5 for the images of vehicle controls. Scale bar, 50 μm .

(F) Quantification of insulin-producing β cells from Ngn3-lineage ablated mice of indicated groups. Mean \pm SEM, * $p < 0.05$, ** $p < 0.01$ t test, (top) paired t test (bottom). $n = 6$ for TAM and STZ, $n = 3$ for vehicle controls.

(G) Glucose levels in homeostasis and intraperitoneal glucose tolerance tests (IPGTTs) for the indicated groups. Mean \pm SEM, ** $p < 0.01$ t test, (top) paired t test (bottom). $n = 6$ for TAM and STZ, $n = 3$ for vehicle controls.

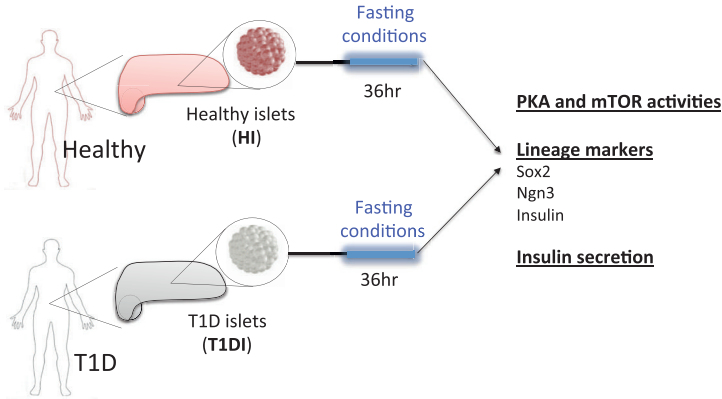
(A–C) Mice of ICR and B6;129S6 mixed background at ages 3–6 months received the diet and/or STZ treatments indicated in (A).

(D–G) Mice of ICR and B6;129S6 mixed background at ages 3–6 months received the diet and/or STZ treatments indicated in (D).

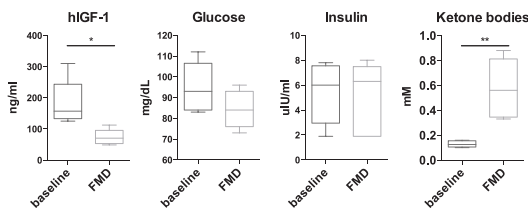
human development. Expression of Ngn3 in adult mouse islets, although rare, has been demonstrated by rigorous lineage reporter analysis (Wang et al., 2009). In agreement with results

from others, our data (Figures 5 and S5) indicate that Ngn3+ cells in adult pancreas islets are important for β -cell regeneration in mice. On the other hand, the role of Ngn3 in human islet

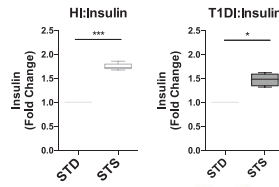
A



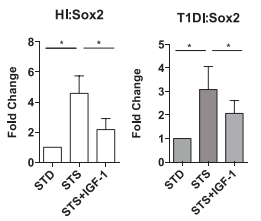
B



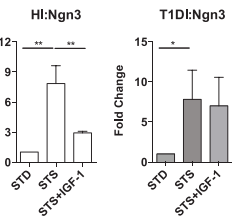
C



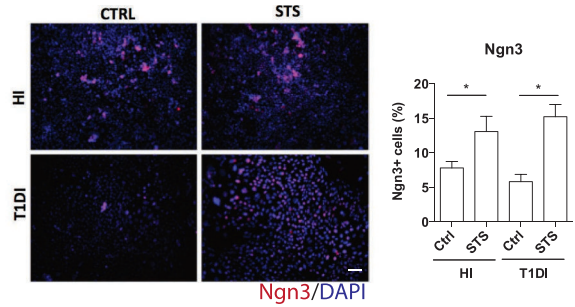
D



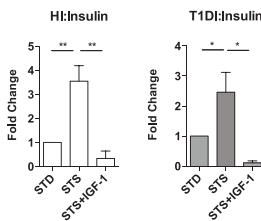
E



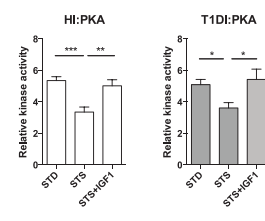
F



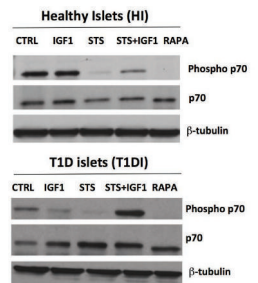
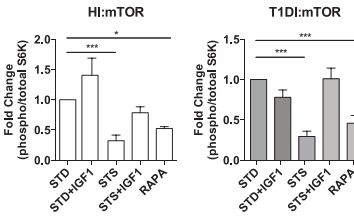
G



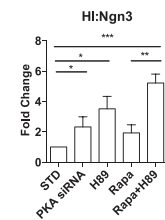
H



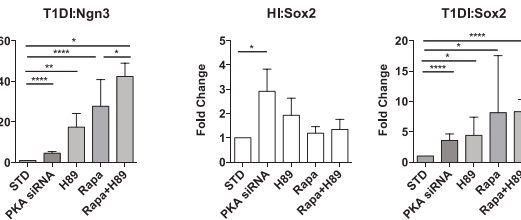
I



J



K



(legend on next page)

development and β -cell regeneration in adulthood remains poorly understood (McKnight et al., 2010).

To investigate how the fasting mimicking conditions affect Ngn3 expression and β -cell function in human pancreatic cells, we performed *ex vivo* experiments using primary human pancreatic islets (Figure 6A). Briefly, the pancreatic islets from healthy and T1D subjects (HI and T1DI, respectively) were cultured according to the manufacturer's instructions. The cultured islets were then treated with serum from subjects enrolled in a clinical trial testing the effects of a low-protein and low-calorie FMD lasting 5 days (NCT02158897). Serum samples were collected at baseline and at day 5 of the fasting mimicking diet in five subjects. We then measured IGF-1, glucose, and ketone bodies and treated human pancreatic islets with the subject-derived serum (Figure 6B and Table S1). In both healthy islets and T1D islets exposed to the serum of FMD-treated subjects, we observed a trend for glucose-dependent induction in the expression of Sox2 and Ngn3 (Figure S6A).

We then applied the low-glucose and low-serum fasting mimicking medium (STS) to the cultured pancreatic islets and found that it significantly stimulated the secretion of insulin in both HI and T1DI (Figure 6C). We further investigated the expression of lineage-reprogramming markers, which we found to be upregulated in mice as a result of the FMD-treatment (i.e., Nanog, Sox17, Sox2, Ngn3, and Ins). The results indicate that the fasting mimicking conditions had strong effects in inducing the expression of Sox2, Ngn3, and insulin in human pancreatic islets from healthy (healthy islets, HI) and T1D subjects (T1D islets, T1DI) (Figures 6D–6F). In cells from normal human subjects, these effects were reversed by IGF-1 treatment (Figure 6G). Notably, in human T1D cells, IGF-1 reversed the increased insulin and Sox 2 gene expression, but not that of Ngn3 expression caused by the STS medium (Figure 6G versus Figures 6D and 6E). Future studies are warranted to further investigate the role of circulating IGF-1 in the expression of lineage-reprogramming markers and pancreatic islet cells regeneration *in vivo*.

In both healthy and T1D human islets, STS medium significantly reduced the activity of PKA, an effect reversed by IGF-1 treatment (Figure 6H). It also dampened the activity of mTOR, which is a key mediator of amino acid signaling (Figure 6I). To further investigate the role of these nutrient-sensing signaling pathways in regulating the expression of lineage markers (i.e., Sox2 and Ngn3), we tested the role of the mTOR-S6K and PKA pathways, which function downstream of IGF-1, in the reprog-

ramming of pancreatic cells. Human pancreatic islets cultured in standard medium were treated with rapamycin, which inhibits mTOR, and H89, which inhibits PKA. mTOR and PKA were implicated by our group and others in the regeneration of other cell types (Cheng et al., 2014; Yilmaz et al., 2012). We found that, in human islets from T1D subjects (T1DI), expression of the essential lineage markers Sox2 and Ngn3 was not induced by inhibition of either mTOR or PKA but was significantly induced when both mTOR and PKA were inhibited (Figures 6J and 6K). Interestingly, the constitutive mTOR, but not PKA, activity is trending higher in HI compared to T1DI cells (Figure 6I, lane 1 for both sets for mTOR activity and Figure 6H for PKA activity), which may explain the overall differences between HI and T1DI in Sox2 and Ngn3 expression shown in Figure 6J. Taken together, these results indicate that fasting cycles may be effective in promoting lineage reprogramming and insulin generation in pancreatic islet cells, in part by reducing IGF-1 and inhibiting both mTOR and PKA signaling. Pancreatic cells from T1D subjects displayed constitutively elevated activity of mTOR-S6K and PKA, which points to the potential for inhibitors of both pathways in the induction of Ngn3-mediated lineage reprogramming. These results raise the possibility that the effect of the FMD on pancreatic regeneration in T1D subjects could be mimicked or enhanced by pharmacological inhibition of these pathways.

DISCUSSION

During mouse development, at embryonic day E8.5, pancreatic progenitor cells co-express the SRY-related HMG-box transcription factor Sox17 and the homeodomain transcription factor Pdx1. These multipotent pancreatic progenitors are then converted into bipotent epithelial cells that generate duct cells or a transient population of endocrine precursor cells expressing the bHLH factor Neurogenin3 (Ngn3). Ngn3⁺ endocrine precursors give rise to all of the principal islet endocrine cells, including glucagon⁺ α cells and insulin⁺ β cells (Arnes et al., 2012). In mice, expression of Ngn3 in the developing pancreas is transient, detectable between E11.5 and E18 (Arnes et al., 2012). Whether developmental genes, including Sox17, Pdx-1, and Ngn3, could be activated to generate functional β cells in adults was previously unknown.

Both cell-based therapy and the use of cytokines and hormones that stimulate β -cell self-replication have the potential to restore insulin-producing β cells in diabetic patients (Dirice et al., 2014). However, despite some success with transplantation-based

Figure 6. Ngn3 Expression and Insulin-Production in Human Pancreatic Islets in Response to Fasting Conditions

(A) Experimental scheme for fasting conditioning treatments on human pancreatic islet. Pancreatic islets from healthy human subjects (HI) or from T1D subjects (T1DI) were cultured separately based on manufacturer's instructions and were then exposed to fasting conditions (i.e., STS medium, mTOR and PKA inhibitors, and PKA siRNA) or control medium for 36 hr.

(B) Levels of hIGF-1, glucose, insulin, and ketone bodies in the serum from human subjects prior to (baseline) and after receiving the FMD (FMD). $n = 5$ per group.

(C) Insulin secretion capacity of HI and T1DI pre-treated with short-term starvation (STS)-conditioned medium (2% FBS and 0.5 g/L glucose) and then induced with 25 mM glucose, compared to that of islets cultured in standard medium (STD). $n = 3$ per group.

(D) Sox2 and (E) Ngn3 expression in HI and T1DI pre-treated with STS-conditioned medium with or without administration of IGF-1 (40 ng/ml). $n = 6$ per group.

(F) Immunostaining for Ngn3 protein expression in HI and T1DI. $n = 5$ per group. Scale bar, 100 μ m.

(G) Insulin gene expression, (H) PKA activity, and (I) mTOR activity in HI and T1DI pretreated with STS-conditioned medium with or without administration of IGF-1 (40 ng/ml); phosphorylated versus total p70S6K ratio was used as an indicator of mTOR activity, which was normalized to the levels of STD (standard medium); $n = 6$ per group.

(J and K) expression of lineage markers (Sox2 and Ngn3) in HI and T1DI treated with inhibitors dampening IGF-1 signaling; rapamycin, mTOR inhibitor; H89, PKA inhibitor and PKA siRNA. Mean \pm SEM, * $p < 0.05$, ** $p < 0.01$, *** $p < 0.005$, unpaired t test.

therapy, the short supply of donor pancreata plus the inefficient conversion of stem cells into specialized derivatives have represented obstacles for clinical application, suggesting that a successful β -cell regeneration might depend on the coordinated activation and re-programming of endogenous progenitors (Blum et al., 2014; Sneddon et al., 2012; Wang et al., 2009; Xiao et al., 2013). Recently, this *in vivo* lineage reprogramming or trans-differentiation has become an emerging strategy to regenerate β cells (Cohen and Melton, 2011; Heinrich et al., 2015; Abad et al., 2013; Xu et al., 2015).

In this study, we discovered that a low-protein and low-sugar fasting mimicking diet (FMD) causes a temporary reduction in β -cell number followed by its return to normal levels after re-feeding, suggesting an *in vivo* lineage reprogramming. We show that the severe hyperglycemia and insulinemia in both the late-stage *Lepr^{db/db}* T2 and the STZ-treated T1 mouse diabetes models were associated with severe β -cell deficiency in pancreatic islets. Six to eight cycles of the FMD and re-feeding were required to restore the β -cell mass and insulin secretion function and to return the 6-hr-fasting blood glucose to nearly normal levels. In non-diabetic wild-type mice, the portion of β cells per islet, as well as the total number of β cells per pancreas, were reduced at the end of a 4-day FMD, but their normal level was completely restored within 3–5 days post re-feeding. Also, insulin and blood glucose levels were reduced by 70% or more at the end of the FMD period but returned to normal levels within 24–36 hr of re-feeding. Interestingly, in diabetic mice, the majority of cells residing in the islets expressed neither insulin nor glucagon (i.e., non- α/β). This phenotype was also found in non-diabetic wild-type mice during the FMD and was accompanied by an increase of other transitional cell types (i.e., Pdx1+Glucagon+ cells and Insulin+glucagon+) followed by significant β -cell regeneration upon re-feeding. This suggests that the FMD alters the gene expression profile that normally suppresses the generation of β cells. More importantly, these results suggest that dietary-induced lineage conversion occurring prior to the β -cell proliferation may play an important role in β -cell regeneration across the diabetic and non-diabetic mouse models. One possibility is that glucagon and insulin expression are transiently suppressed in α and β cells during the FMD, followed by lineage reprogramming in committed cells. Another possibility is that the FMD may cause cell death and then stimulate progenitor or other cells to regenerate β cells.

The FMD reversed the dedifferentiated expression profile for a number of genes associated with maturity-onset diabetes of the young (MODY) and regulated by *Foxo1* (Kim-Muller et al., 2014). The FMD appears to cause pancreatic islets to first increase the expression of *Foxo1* and its transcriptional targets, then induce transitionally the expression of the progenitor cell marker *Ngn3+* upon re-feeding, leading to β -cell regeneration. We conclude that, together with the changes in a wide range of cytokines associated with β -cell regeneration, FMD and post-FMD re-feeding generate the complex and highly coordinated conditions that promote the generation of stable insulin-producing β -cells to reverse severe β -cell depletion. The key changes priming pancreatic islet cells for regeneration during the FMD appear to be the reduction of IGF-1 levels and the consequent downregulation of PKA and mTor activity, in agreement with

the role for these pathways in hematopoietic (Cheng et al., 2014) and intestinal stem-cell self-renewal (Yilmaz et al., 2012). It was proposed that transient de-differentiation of β cells may play a role in their *in vivo* dynamics (Kim-Muller et al., 2014; Weinberg et al., 2007). The capacity of these de-differentiated cells to re-differentiate fundamentally changes the therapeutic potential of existing cells in promoting β -cell regeneration and reversing T1D symptoms (Blum et al., 2014; Wang et al., 2014). Thus, our study provides an example of a potent and coordinated dietary regulation of cell-fate determination with the potential to serve as a therapeutic intervention to treat diabetes and other degenerative diseases. Our preliminary results from a pilot clinical trial also indicate that the use of periodic cycles of a prolonged FMD is feasible and ready to be tested in large randomized clinical trials for effects on both insulin resistance and pancreatic β -cell regeneration for the treatment of both T1D and T2D.

STAR★METHODS

Detailed methods are provided in the online version of this paper and include the following:

- KEY RESOURCES TABLE
- CONTACT FOR REAGENT AND RESOURCE SHARING
- EXPERIMENTAL MODEL AND SUBJECT DETAILS
 - Mouse models
 - Lineage tracing and Lineage ablation
 - Human pancreatic islets
 - Human subjects (FMD)
- METHOD DETAILS
 - Mouse fasting mimicking diet
 - Post-FMD refeeding
 - Blood glucose and insulin measurement
 - Intraperitoneal glucose tolerance testing (IPGTT) and insulin tolerance testing
 - Immunofluorescence Analysis
 - Pancreatic Islet isolation
 - Cell Lineage Identification qPCR Array
 - Glucose stimulated insulin secretion (GSIS) Assay
 - Cytokines profiling
 - Human pancreatic islet treatments and qPCR
 - Western Blotting
 - PKA activity
 - Human fasting mimicking diet
 - Ingredients
 - Supplements
 - Metabolic cages
- QUANTIFICATION AND STATISTICAL ANALYSIS

SUPPLEMENTAL INFORMATION

Supplemental Information includes six figures and two tables and can be found with this article online at <http://dx.doi.org/10.1016/j.cell.2017.01.040>.

An audio PaperClip is available at <http://dx.doi.org/10.1016/j.cell.2017.01.040#mmc2>.

AUTHOR CONTRIBUTIONS

V.D.L conceptualized and supervised the study. C.-W.C, V.V., and R.B. designed and performed experiments, analyzed data, interpreted results, and

wrote the manuscript, with input from V.D.L., M.W., S.K., P.C., J.B.S., L.P., and O.H.Y.

ACKNOWLEDGMENTS

We thank Lora Barsky (USC Flow Cytometry Core Facility) for assistance in the FACS analysis, Michael Sheard (CHLA Fluorescence Activated Cell Sorting Core) for assistance in the cytokines profiling, and Gerrardo Navarrete for preparing the diet. This study was funded in part by NIH/NIA grants AG20642, AG025135, and P01 AG034906 to V.D.L. V.D.L. has equity interest in L-Nutra, a company that develops medical food. All shares will be donated to charitable organizations.

Received: August 11, 2016

Revised: November 23, 2016

Accepted: January 30, 2017

Published: February 23, 2017

REFERENCES

- Abad, M., Mosteiro, L., Pantoja, C., Cañamero, M., Rayon, T., Ors, I., Graña, O., Megías, D., Domínguez, O., Martínez, D., et al. (2013). Reprogramming in vivo produces teratomas and iPSC cells with totipotency features. *Nature* *502*, 340–345.
- Arakawa, K., Ishihara, T., Oku, A., Nawano, M., Ueta, K., Kitamura, K., Matsumoto, M., and Saito, A. (2001). Improved diabetic syndrome in C57BL/KsJ-db/db mice by oral administration of the Na(+)-glucose cotransporter inhibitor T-1095. *Br. J. Pharmacol.* *132*, 578–586.
- Arnes, L., Hill, J.T., Gross, S., Magnuson, M.A., and Sussel, L. (2012). Ghrelin expression in the mouse pancreas defines a unique multipotent progenitor population. *PLoS ONE* *7*, e52026.
- Baeyens, L., Lemper, M., Leuckx, G., De Groef, S., Bonfanti, P., Stangé, G., Shemer, R., Nord, C., Scheel, D.W., Pan, F.C., et al. (2014). Transient cytokine treatment induces acinar cell reprogramming and regenerates functional beta cell mass in diabetic mice. *Nat. Biotechnol.* *32*, 76–83.
- Barnosky, A.R., Hoddy, K.K., Unterman, T.G., and Varady, K.A. (2014). Intermittent fasting vs daily calorie restriction for type 2 diabetes prevention: a review of human findings. *Transl. Res.* *164*, 302–311.
- Ben-Othman, N., Vieira, A., Courtney, M., Record, F., Gjernes, E., Avolio, F., Hadzic, B., Druelle, N., Napolitano, T., Navarro-Sanz, S., et al. (2017). Long-term GABA administration induces alpha cell-mediated beta-like cell neogenesis. *Cell* *168*, 73–85.e11.
- Blum, B., Roose, A.N., Barrandon, O., Maehr, R., Arvanites, A.C., Davidow, L.S., Davis, J.C., Peterson, Q.P., Rubin, L.L., and Melton, D.A. (2014). Reversal of β cell de-differentiation by a small molecule inhibitor of the TGF β pathway. *eLife* *3*, e02809.
- Brandhorst, S., Choi, I.Y., Wei, M., Cheng, C.W., Sedrakyan, S., Navarrete, G., Dubeau, L., Yap, L.P., Park, R., Vinciguerra, M., et al. (2015). A Periodic Diet that Mimics Fasting Promotes Multi-System Regeneration, Enhanced Cognitive Performance, and Healthspan. *Cell Metab.* *22*, 86–99.
- Brereton, M.F., Iberl, M., Shimomura, K., Zhang, Q., Adriaenssens, A.E., Proks, P., Spiliotis, I.I., Dace, W., Mattis, K.K., Ramracheya, R., et al. (2014). Reversible changes in pancreatic islet structure and function produced by elevated blood glucose. *Nat. Commun.* *5*, 4639.
- Cheng, C.W., Adams, G.B., Perin, L., Wei, M., Zhou, X., Lam, B.S., Da Sacco, S., Mirisola, M., Quinn, D.I., Dorff, T.B., et al. (2014). Prolonged fasting reduces IGF-1/PKA to promote hematopoietic-stem-cell-based regeneration and reverse immunosuppression. *Cell Stem Cell* *14*, 810–823.
- Chera, S., Baronnier, D., Ghila, L., Cigliola, V., Jensen, J.N., Gu, G., Furuyama, K., Thorel, F., Gribble, F.M., Reimann, F., and Herrera, P.L. (2014). Diabetes recovery by age-dependent conversion of pancreatic δ -cells into insulin producers. *Nature* *514*, 503–507.
- Cnop, M., Welsh, N., Jonas, J.C., Jörns, A., Lenzen, S., and Eizirik, D.L. (2005). Mechanisms of pancreatic beta-cell death in type 1 and type 2 diabetes: many differences, few similarities. *Diabetes* *54*(Suppl 2), S97–S107.
- Cohen, D.E., and Melton, D. (2011). Turning straw into gold: directing cell fate for regenerative medicine. *Nat. Rev. Genet.* *12*, 243–252.
- Cook, J.R., Matsumoto, M., Banks, A.S., Kitamura, T., Tsuchiya, K., and Accili, D. (2015). A mutant allele encoding DNA-binding-deficient Foxo1 differentially regulates hepatic glucose and lipid metabolism. *Diabetes* *64*, 1951–1965.
- Dirice, E., Kahraman, S., Jiang, W., El Ouaamari, A., De Jesus, D.F., Teo, A.K., Hu, J., Kawamori, D., Gaglia, J.L., Mathis, D., and Kulkarni, R.N. (2014). Soluble factors secreted by T cells promote β -cell proliferation. *Diabetes* *63*, 188–202.
- Dor, Y., and Glaser, B. (2013). β -cell dedifferentiation and type 2 diabetes. *N. Engl. J. Med.* *368*, 572–573.
- Fiorina, P., Shapiro, A.M., Ricordi, C., and Secchi, A. (2008). The clinical impact of islet transplantation. *Am. J. Transplant.* *8*, 1990–1997.
- Gomez, D.L., O'Driscoll, M., Sheets, T.P., Hruban, R.H., Oberholzer, J., McGarrigle, J.J., and Shamlott, M.J. (2015). Neurogenin 3 Expressing Cells in the Human Exocrine Pancreas Have the Capacity for Endocrine Cell Fate. *PLoS ONE* *10*, e0133862.
- Grunnet, L.G., Aikin, R., Tonnesen, M.F., Paraskevas, S., Blaabjerg, L., Størling, J., Rosenberg, L., Billestrup, N., Maysinger, D., and Mandrup-Poulsen, T. (2009). Proinflammatory cytokines activate the intrinsic apoptotic pathway in beta-cells. *Diabetes* *58*, 1807–1815.
- Haeusler, R.A., Hartil, K., Vaitheesvaran, B., Arrieta-Cruz, I., Knight, C.M., Cook, J.R., Kammoun, H.L., Febbraio, M.A., Gutierrez-Juarez, R., Kurland, I.J., and Accili, D. (2014). Integrated control of hepatic lipogenesis versus glucose production requires FoxO transcription factors. *Nat. Commun.* *5*, 5190.
- Heinrich, C., Spagnoli, F.M., and Berninger, B. (2015). In vivo reprogramming for tissue repair. *Nat. Cell Biol.* *17*, 204–211.
- Hsu, F.L., Huang, C.F., Chen, Y.W., Yen, Y.P., Wu, C.T., Uang, B.J., Yang, R.S., and Liu, S.H. (2013). Antidiabetic effects of pterisin A, a small-molecule-weight natural product, on diabetic mouse models. *Diabetes* *62*, 628–638.
- Johnson, J.D., Han, Z., Otani, K., Ye, H., Zhang, Y., Wu, H., Horikawa, Y., Misler, S., Bell, G.I., and Polonsky, K.S. (2004). RyR2 and calpain-10 delineate a novel apoptosis pathway in pancreatic islets. *J. Biol. Chem.* *279*, 24794–24802.
- Kim-Muller, J.Y., Zhao, S., Srivastava, S., Mugabo, Y., Noh, H.L., Kim, Y.R., Madiraju, S.R., Ferrante, A.W., Skolnik, E.Y., Prentki, M., and Accili, D. (2014). Metabolic inflexibility impairs insulin secretion and results in MODY-like diabetes in triple FoxO-deficient mice. *Cell Metab.* *20*, 593–602.
- Kroon, E., Martinson, L.A., Kadoya, K., Bang, A.G., Kelly, O.G., Eliazar, S., Young, H., Richardson, M., Smart, N.G., Cunningham, J., et al. (2008). Pancreatic endoderm derived from human embryonic stem cells generates glucose-responsive insulin-secreting cells in vivo. *Nat. Biotechnol.* *26*, 443–452.
- Laviano, A., and Rossi Fanelli, F. (2012). Toxicity in chemotherapy—when less is more. *N. Engl. J. Med.* *366*, 2319–2320.
- Lebastchi, J., and Herold, K.C. (2012). Immunologic and metabolic biomarkers of β -cell destruction in the diagnosis of type 1 diabetes. *Cold Spring Harb. Perspect. Med.* *2*, a007708.
- Li, D.S., Yuan, Y.H., Tu, H.J., Liang, Q.L., and Dai, L.J. (2009). A protocol for islet isolation from mouse pancreas. *Nat. Protoc.* *4*, 1649–1652.
- Li, J., Casteels, T., Frogne, T., Ingvorsen, C., Honore, C., Courtney, M., Huber, K.V.M., Schmitner, N., Kimmel, R.A., and Romanov, R.A. (2017). Artemisinin target GABA_A receptor signaling and impair α cell identity. *Cell* *168*, 86–100.e15.
- Madisen, L., Zwingman, T.A., Sunkin, S.M., Oh, S.W., Zariwala, H.A., Gu, H., Ng, L.L., Palmer, R.D., Hawrylycz, M.J., Jones, A.R., et al. (2010). A robust and high-throughput Cre reporting and characterization system for the whole mouse brain. *Nat. Neurosci.* *13*, 133–140.

- Maehr, R., Chen, S., Snitow, M., Ludwig, T., Yagasaki, L., Goland, R., Leibel, R.L., and Melton, D.A. (2009). Generation of pluripotent stem cells from patients with type 1 diabetes. *Proc. Natl. Acad. Sci. USA* *106*, 15768–15773.
- Matthews, D.R. (2001). Insulin resistance and beta-cell function—a clinical perspective. *Diabetes Obes. Metab.* *3*(Suppl 1), S28–S33.
- Matthews, D.R., Hosker, J.P., Rudenski, A.S., Naylor, B.A., Treacher, D.F., and Turner, R.C. (1985). Homeostasis model assessment: insulin resistance and beta-cell function from fasting plasma glucose and insulin concentrations in man. *Diabetologia* *28*, 412–419.
- McKnight, K.D., Wang, P., and Kim, S.K. (2010). Deconstructing pancreas development to reconstruct human islets from pluripotent stem cells. *Cell Stem Cell* *6*, 300–308.
- Meier, J.J., Butler, A.E., Saisho, Y., Monchamp, T., Galasso, R., Bhushan, A., Rizza, R.A., and Butler, P.C. (2008). Beta-cell replication is the primary mechanism subserving the postnatal expansion of beta-cell mass in humans. *Diabetes* *57*, 1584–1594.
- Milanesi, A., Lee, J.W., Li, Z., Da Sacco, S., Villani, V., Cervantes, V., Perin, L., and Yu, J.S. (2012). β -Cell regeneration mediated by human bone marrow mesenchymal stem cells. *PLoS ONE* *7*, e42177.
- Mu, J., Woods, J., Zhou, Y.P., Roy, R.S., Li, Z., Zycband, E., Feng, Y., Zhu, L., Li, C., Howard, A.D., et al. (2006). Chronic inhibition of dipeptidyl peptidase-4 with a sitagliptin analog preserves pancreatic beta-cell mass and function in a rodent model of type 2 diabetes. *Diabetes* *55*, 1695–1704.
- Pagliuca, F.W., Millman, J.R., Gürtler, M., Segel, M., Van Dervort, A., Ryu, J.H., Peterson, Q.P., Greiner, D., and Melton, D.A. (2014). Generation of functional human pancreatic β cells in vitro. *Cell* *159*, 428–439.
- Pipeleers, D., Keymeulen, B., Chatenoud, L., Hendriekx, C., Ling, Z., Mathieu, C., Roep, B., and Ysebaert, D. (2002). A view on beta cell transplantation in diabetes. *Ann. N Y Acad. Sci.* *958*, 69–76.
- Rabinovitch, A. (1998). An update on cytokines in the pathogenesis of insulin-dependent diabetes mellitus. *Diabetes Metab. Rev.* *14*, 129–151.
- Raffaghello, L., Lee, C., Safdie, F.M., Wei, M., Madia, F., Bianchi, G., and Longo, V.D. (2008). Starvation-dependent differential stress resistance protects normal but not cancer cells against high-dose chemotherapy. *Proc. Natl. Acad. Sci. USA* *105*, 8215–8220.
- Sneddon, J.B., Borowiak, M., and Melton, D.A. (2012). Self-renewal of embryonic-stem-cell-derived progenitors by organ-matched mesenchyme. *Nature* *491*, 765–768.
- Stanger, B.Z. (2008). HNF4A and diabetes: injury before insult? *Diabetes* *57*, 1461–1462.
- Talchai, S.C., and Accili, D. (2015). Legacy effect of Foxo1 in pancreatic endocrine progenitors on adult β cell mass and function. *Diabetes* *64*, 2868–2879.
- Talchai, C., Xuan, S., Lin, H.V., Sussel, L., and Accili, D. (2012). Pancreatic β cell dedifferentiation as a mechanism of diabetic β cell failure. *Cell* *150*, 1223–1234.
- Teta, M., Long, S.Y., Wartschow, L.M., Rankin, M.M., and Kushner, J.A. (2005). Very slow turnover of beta-cells in aged adult mice. *Diabetes* *54*, 2557–2567.
- Tonne, J.M., Sakuma, T., Deeds, M.C., Munoz-Gomez, M., Barry, M.A., Kudva, Y.C., and Ikeda, Y. (2013). Global gene expression profiling of pancreatic islets in mice during streptozotocin-induced β -cell damage and pancreatic Glp-1 gene therapy. *Dis. Model. Mech.* *6*, 1236–1245.
- Van de Castele, M., Leuckx, G., Baeyens, L., Cai, Y., Yuchi, Y., Coppens, V., De Groef, S., Eriksson, M., Svensson, C., Ahlgren, U., et al. (2013). Neurogenin 3+ cells contribute to β -cell neogenesis and proliferation in injured adult mouse pancreas. *Cell Death Dis.* *4*, e523.
- Villani, V., Milanesi, A., Sedrakyan, S., Da Sacco, S., Angelow, S., Conconi, M.T., Di Liddo, R., De Filippo, R., and Perin, L. (2014). Amniotic fluid stem cells prevent β -cell injury. *Cytotherapy* *16*, 41–55.
- Wang, S., Jensen, J.N., Seymour, P.A., Hsu, W., Dor, Y., Sander, M., Magnusson, M.A., Serup, P., and Gu, G. (2009). Sustained Neurog3 expression in hormone-expressing islet cells is required for endocrine maturation and function. *Proc. Natl. Acad. Sci. USA* *106*, 9715–9720.
- Wang, Z., York, N.W., Nichols, C.G., and Remedi, M.S. (2014). Pancreatic β cell dedifferentiation in diabetes and redifferentiation following insulin therapy. *Cell Metab.* *19*, 872–882.
- Weinberg, N., Ouziel-Yahalom, L., Knoller, S., Efrat, S., and Dor, Y. (2007). Lineage tracing evidence for in vitro dedifferentiation but rare proliferation of mouse pancreatic beta-cells. *Diabetes* *56*, 1299–1304.
- Weir, G.C., Aguayo-Mazzucato, C., and Bonner-Weir, S. (2013). β -cell dedifferentiation in diabetes is important, but what is it? *Islets* *5*, 233–237.
- Wu, K.K., and Huan, Y. (2008). Streptozotocin-induced diabetic models in mice and rats. *Curr. Protoc. Pharmacol.* *Chapter 5*, Unit 5, 47.
- Xiao, X., Chen, Z., Shiota, C., Prasad, K., Guo, P., El-Gohary, Y., Paredes, J., Welsh, C., Wiersch, J., and Gittes, G.K. (2013). No evidence for β cell neogenesis in murine adult pancreas. *J. Clin. Invest.* *123*, 2207–2217.
- Xu, X., D'Hoker, J., Stangé, G., Bonné, S., De Leu, N., Xiao, X., Van de Castele, M., Mellitzer, G., Ling, Z., Pipeleers, D., et al. (2008). Beta cells can be generated from endogenous progenitors in injured adult mouse pancreas. *Cell* *132*, 197–207.
- Xu, J., Du, Y., and Deng, H. (2015). Direct lineage reprogramming: strategies, mechanisms, and applications. *Cell Stem Cell* *16*, 119–134.
- Yilmaz, O.H., Katajisto, P., Lammig, D.W., Gültekin, Y., Bauer-Rowe, K.E., Sengupta, S., Birsoy, K., Dursun, A., Yilmaz, V.O., Selig, M., et al. (2012). mTORC1 in the Paneth cell niche couples intestinal stem-cell function to calorie intake. *Nature* *486*, 490–495.
- Yin, D., Tao, J., Lee, D.D., Shen, J., Hara, M., Lopez, J., Kuznetsov, A., Philipson, L.H., and Chong, A.S. (2006). Recovery of islet beta-cell function in streptozotocin-induced diabetic mice: an indirect role for the spleen. *Diabetes* *55*, 3256–3263.
- Zhernakova, A., Alizadeh, B.Z., Eerligh, P., Hanifi-Moghaddam, P., Schloot, N.C., Diosdado, B., Wijmenga, C., Roep, B.O., and Koeleman, B.P. (2006). Genetic variants of RANTES are associated with serum RANTES level and protection for type 1 diabetes. *Genes Immun.* *7*, 544–549.
- Zhou, Q., Brown, J., Kanarek, A., Rajagopal, J., and Melton, D.A. (2008). In vivo reprogramming of adult pancreatic exocrine cells to beta-cells. *Nature* *455*, 627–632.

UV Irradiation Induces a Non-coding RNA that Functionally Opposes the Protein Encoded by the Same Gene

Laura Williamson,¹ Marco Saponaro,^{1,2} Stefan Boeing,^{1,3} Philip East,³ Richard Mitter,³ Theodoros Kantidakis,¹ Gavin P. Kelly,³ Anna Lobley,³ Jane Walker,¹ Bradley Spencer-Dene,⁴ Michael Howell,⁵ Aengus Stewart,³ and Jesper Q. Svejstrup^{1,6,*}

¹Mechanisms of Transcription Laboratory, The Francis Crick Institute, Clare Hall Laboratories, South Mimms EN6 3LD, UK

²Institute of Cancer and Genomic Sciences, University of Birmingham, Vincent Drive, Edgbaston, Birmingham B15 2TT, UK

³Bioinformatics and Biostatistics

⁴Experimental Histopathology

⁵High Throughput Screening Laboratory

The Francis Crick Institute, 1 Midland Road, London NW1 1AT, UK

⁶Lead Contact

*Correspondence: jesper.svejstrup@crick.ac.uk

<http://dx.doi.org/10.1016/j.cell.2017.01.019>

SUMMARY

The transcription-related DNA damage response was analyzed on a genome-wide scale with great spatial and temporal resolution. Upon UV irradiation, a slow-down of transcript elongation and restriction of gene activity to the promoter-proximal ~25 kb is observed. This is associated with a shift from expression of long mRNAs to shorter isoforms, incorporating alternative last exons (ALEs) that are more proximal to the transcription start site. Notably, this includes a shift from a protein-coding *ASCC3* mRNA to a shorter ALE isoform of which the RNA, rather than an encoded protein, is critical for the eventual recovery of transcription. The non-coding *ASCC3* isoform counteracts the function of the protein-coding isoform, indicating crosstalk between them. Thus, the *ASCC3* gene expresses both coding and non-coding transcript isoforms with opposite effects on transcription recovery after UV-induced DNA damage.

INTRODUCTION

The efficient production and correct processing of nascent RNA polymerase II transcripts is essential for life. Factors that affect transcription and mRNA splicing, including DNA damaging agents, can thus have a dramatic effect on gene expression and cell viability. Indeed, bulky DNA lesions such as those generated by UV irradiation trigger rapid shutdown of RNA synthesis (Mayne and Lehmann, 1982; Rockx et al., 2000). They also elicit transcription-coupled repair (Gaillard and Aguilera, 2013), and, as a last resort, ubiquitylation and degradation of damage-stalled RNA polymerase II (RNAPII) (Wilson et al., 2013).

Although both transcriptional initiation and elongation are affected by UV irradiation (Rockx et al., 2000; Proietti-De-Santis et al., 2006; Andrade-Lima et al., 2015), the extent, mechanism and functional consequence of the changes occurring in these

processes remain poorly understood. UV irradiation induces global changes to RNAPII phosphorylation (Rockx et al., 2000), altered binding of TATA-binding protein to DNA (Vichi et al., 1997), and modifications to chromatin (Adam et al., 2013; Dinant et al., 2013), underscoring the complexity of the transcription-related DNA damage response. Moreover, transcription-repair coupling factor Cockayne syndrome B (CSB) is required not only for DNA repair, but also for transcription restart after DNA damage (Proietti-De-Santis et al., 2006).

The vast majority of RNAPII genes have the potential to be expressed as multiple mRNA isoforms, creating vast regulatory potential (Pan et al., 2008; Wang et al., 2008). Indeed, changes in alternative isoform expression can regulate the physiological response of cells to stress or other signals. Importantly, processing of nascent pre-mRNA occurs co-transcriptionally, so that mRNA capping, splicing, and 3' end formation are greatly influenced by the dynamics of elongation (de la Mata et al., 2003; Ip et al., 2011; Pinto et al., 2011; Fong et al., 2014). A general kinetic model has hence emerged wherein the rate of elongation governs RNA processing (de la Mata et al., 2003; Muñoz et al., 2009; Pinto et al., 2011).

To better understand the effect of UV irradiation on gene expression, we examined nascent transcription and transcript isoform expression on a genome-wide level. We hereby uncovered evidence that UV-induced alternative last exon (ALE) splicing is important for the DNA damage response, with long and short *ASCC3* ALE isoforms having opposite effects on transcription recovery after DNA damage. We also show that the short *ASCC3* isoform regulates transcription recovery in a manner that is dependent on the non-coding RNA rather than the encoded protein.

RESULTS

Transcript Elongation Rates Are Reduced Immediately after UV Irradiation

To investigate the effect of UV irradiation on transcription genome-wide, we employed 5,6-dichloro-1-β-D-ribofuranosylbenzimidazole/global run-on sequencing (DRB/GRO-seq), which

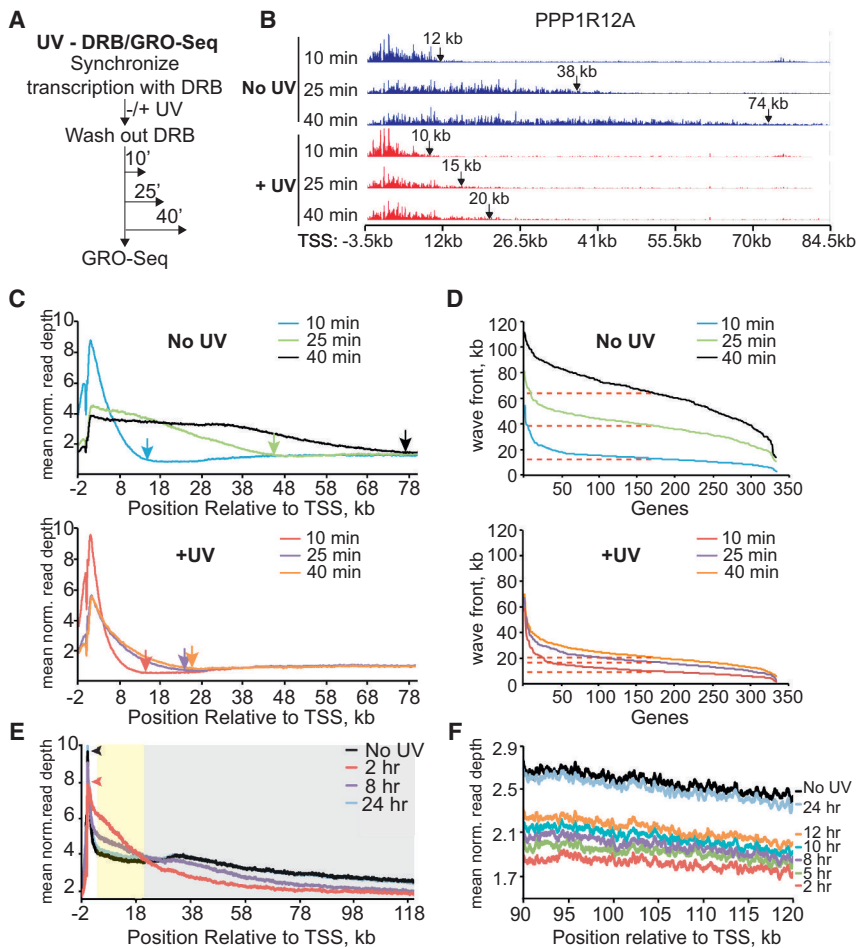


Figure 1. UV Irradiation Triggers Transcript Elongation Slow-Down

(A) Schematic of UV/DRB/GRO-seq.

(B) Profile of nascent PPP1R12A RNA reads after DRB-release \pm UV irradiation (15 J/m^2 used throughout this study). Arrows indicate transcription wave-fronts.

(C) As in (B), but meta-gene profile of normalized GRO-seq reads across 8,148 genes.

(D) Position of the GRO-seq transcription wave-front for 333 long genes over time \pm UV irradiation. Dashed lines indicate median wave-front positions.

(E) Meta-gene profile of normalized GRO-seq reads -2 kb to $+120 \text{ kb}$ relative to the TSS, \pm UV irradiation followed by 2, 8, and 24 hr recovery. Arrows indicate the height of the promoter proximal peak. Shaded areas indicate gene regions characterized by increased (yellow) or decreased (gray) GRO-seq signal 2 hr after UV exposure, normalizing over time. (F) Gradual recovery of GRO-seq reads $90\text{--}120 \text{ kb}$ downstream of the TSS following UV irradiation. See also Figure S1.

occurred, while progress further into genes was very slow or prohibited.

Meta-gene profiles of 8,148 transcripts revealed that UV irradiation generally attenuated elongation markedly, with nascent RNA wave-fronts reaching $\sim 75 \text{ kb}$ after 40 min in untreated cells (Figure 1C, upper, black arrow), but only $\sim 25 \text{ kb}$ after UV irradiation (Figure 1C, lower, orange arrow).

To calculate the UV-induced reduction in elongation rates, the nascent RNA wave-front was called for a subset of very

allows measurement of nascent RNA synthesis at a high temporal and spatial resolution (Saponaro et al., 2014). Cells were first treated with the transcription elongation inhibitor DRB to restrict RNAPII to the promoter-proximal areas (first $\sim 600 \text{ bp}$ of genes). Cells were then UV-irradiated, followed by inhibitor removal to allow synchronized transcription and its genome-wide measurement by GRO-seq (Figure 1A). Results from the PPP1R12A gene are shown as an example (Figure 1B). In untreated cells, RNAPII progressed $\sim 12 \text{ kb}$ into the gene 10 min after DRB removal and to $\sim 38 \text{ kb}$ and $\sim 74 \text{ kb}$ after 25 and 40 min, respectively. These results mirror previously published data (Saponaro et al., 2014), but were in striking contrast to those obtained when cells were UV-irradiated before DRB removal. Here, the position of the RNAPII “wave-front” was similar to that of untreated cells after 10 min. However, a dramatic reduction in RNAPII progress was observed 25 and 40 min after UV exposure, with the wave-fronts in the PPP1R12A gene moving only very slightly further forward, reaching ~ 15 and $\sim 20 \text{ kb}$ at these time points (Figure 1B). We note that little change was observed at the promoter at these times. DRB/GRO-seq only captures the activity of RNAPII molecules that incorporate 5-bromouridine-5'-triphosphate (Br-UTP) during the short run-on pulse (5 min). This suggests that initiation and transcript elongation in the promoter-proximal areas still

long transcripts ($n = 333$) (Figure 1D). In untreated conditions, the wave-front progressed to a median distance of 12.5 kb after 10 min and to 39 kb and 64.8 kb after 25 min and 40 min, respectively (Figure 1D, upper; indicated by dashed lines). This corresponds to average elongation rates of 1.77 kb/min (10–25 min) and 1.72 kb/min (25–40 min). In contrast, in UV-treated cells (Figure 1D, lower), the wave-fronts were at 10.3 kb (10 min), 17.3 kb (25 min), and 21.0 kb (40 min), respectively (Figure 1D, lower), giving rise to average elongation rates of only 0.47 kb/min (10–25 min) and 0.25 kb/min (25–40 min) (see also Figures S1A and S1B).

RNAPII Progresses Slowly during Transcription Restart after UV Irradiation

Based on experiments that measured nascent RNA synthesis by general radioactive labeling (Mayne and Lehmann, 1982; Rockx et al., 2000; Proietti-De-Santis et al., 2006), transcription levels should recover to near-normal levels over an $\sim 24\text{-hr}$ period. To analyze transcription restart genome-wide, we therefore performed GRO-seq experiments with cells that were again UV-irradiated at 15 J/m^2 , followed by recovery (Figures 1E and S1C). This dose of UV did not lead to significant cell death over the 24-hr time course (data not shown). As expected, the distribution

of active RNAPII in untreated cells was characterized by a large peak in the promoter-proximal region, followed by a marked reduction in signal further downstream (black graph). Transcription was not synchronized with DRB, so this density pattern represents the distribution of RNAPII expected for actively transcribed genes at steady state. In response to UV irradiation (2 hr time point), there was a clear reduction in the promoter-proximal peak (see arrowheads in Figure 1E), suggesting either a reduction in transcription initiation or increased promoter clearance (Ehrensberger et al., 2013). Interestingly, the GRO-seq signal increased in the region up to ~20 kb from the *transcription start site* (TSS) (Figure 1E, yellow shaded region), concomitant with depletion further downstream (Figures 1E, gray shaded region, and 1F). This suggests that while transcription initiation may be inhibited, considerable elongation activity is observed in the beginning of genes (possibly reflecting increased promoter release), and activity is dramatically reduced in regions further downstream.

As expected, RNA synthesis gradually normalized to that observed in untreated cells over the 24-hr period, with eventual restoration of activity at the 3' end of genes (Figures 1E and 1F). Interestingly, wave-front calling of a subset of very long genes indicated a rate of transcript elongation of only ~40 bases/min on average from 2 to 12 hr following UV irradiation, more than 40-fold slower than in untreated cells (Figures S1D and S1E). Mathematically determined, median transcription “wave-fronts” independently confirmed these results (Figure S1F).

Taken together, these data suggest that UV irradiation causes a rapid and dramatic reduction in transcript elongation, and even upon recovery of nascent RNA synthesis several hours after UV exposure, elongation continues to be much slower than in untreated cells. Most importantly, transcription is spatially restricted for long periods, with the promoter-proximal 20–25 kb showing much more activity than the areas further downstream.

UV-Induced Alternative Isoform Expression

Considering the dramatic change in transcript elongation and knowing that mRNA processing is tightly coupled to elongation, we now investigated the effect of UV irradiation on mRNA splicing by next generation sequencing of cDNA libraries generated from mRNA. The relative expression of transcript isoforms was quantitatively measured using the mixture of isoform (MISO) model (Katz et al., 2010). In total, we identified 435 splicing events in 298 genes that were affected either 8 or 24 hr after UV irradiation in both biological replicates (Figure 2A; Table S1).

Previous reports uncovered examples of increased inclusion of cassette exons under conditions of attenuated elongation (de la Mata et al., 2003; Muñoz et al., 2009; Fong et al., 2014). Our analysis of 131 UV-induced exon skipping/inclusion events shows only a slight bias (63% of events) for increased exon inclusion after UV irradiation (data not shown).

Interestingly, alternative last exon (ALE) splicing was the most frequent UV-induced event (Figure 2A; Table S2), accounting for more than a third of all those recorded: 156 ALE splicing events in 105 genes. ALE transcript isoforms are characterized by different 3' terminal exons and therefore inherently have different

poly-A sites. Importantly, a marked bias for expression of shorter transcript isoforms (induced ALE transcript isoforms that have terminal exons more proximal to the TSS) was observed following UV irradiation (Figure 2B), with 78% of ALE events (121 of 156) resulting in increased expression of such shorter isoforms (hereafter referred to as “ALE short” events). The majority of these (71/121) involved alternative splicing of unique terminal exons, indicating they were not solely a result of premature termination (Figure S2A). Only 35 events were characterized by increased expression of alternative longer isoforms, from 22 genes (Figure 2B, “ALE long” events).

The relative exon expression of the isoforms for two genes, *HERC4* and *INTS6*, is described in Figure 2C. The long *HERC4* pre-mRNA isoform contains 25 exons and is 153 kb, while the short *HERC4* pre-mRNA is 6.3 kb, shares the first three exons with the long isoform, but contains a fourth, unique terminal exon (Figure 2C, left, lower). Eight hours after UV irradiation, exons 1–4 (indicated by the red dashed boxes) were induced (Figure 2C, left). In contrast, expression of exons 5–26 (specific for the long isoform) was reduced, but recovered to near-normal levels after 24 hr. A similar pattern of alternative exon expression was seen at the *INTS6* gene and a large number of other genes (Figure 2C, right, and data not shown). qRT-PCR confirmed the increased expression of the short isoforms and concomitant lower expression of the long isoforms 8 hr after UV irradiation (Figure 2D).

The short RNA isoforms of *HERC4* and *INTS6* were much shorter than their long isoforms. More generally, the median length of the UV-suppressed long pre-mRNA isoforms was ~109 kb, considerably longer than that of all human genes (23 kb), whereas that of the UV-induced short isoforms was only ~32 kb. This reduction in pre-mRNA length for UV-induced ALE short events was significantly greater than expected by chance (Figure S2B), indicating a general trend for switching from particularly long isoforms to much shorter isoforms upon UV exposure. In contrast, the median length of the less common UV-induced long ALE isoforms was ~30 kb, only 9 kb longer than the median length of their corresponding, UV-suppressed short isoform (Figure 2E).

ALE Events Are Associated with Changes in RNAPII Elongation and Nascent RNA Synthesis

Because transcript elongation was attenuated after UV irradiation (Figure 1), we hypothesized that the UV-induced ALE short events resulted from preferential synthesis of the pre-mRNA producing them. Indeed, after UV-irradiation, GRO-seq read depth at *HERC4* increased over the region coding for the short isoform (Figure 2F, inset), whereas synthesis in the rest of the gene was markedly suppressed. Nascent RNA synthesis across the entire gene recovered to untreated levels 24 hr after UV exposure, correlating with the kinetics of the *HERC4* ALE splicing event. Consistent with a causative effect, the GRO-seq signal corresponding to the long isoform also remained suppressed at 24 hr for a gene in which preferential expression of the short isoform was detected not only at 8 but also 24 hr after UV irradiation (Figure S2C).

By comparing GRO-seq signals across proximal and distal terminal exons, a general, transient increase in the ratio of short

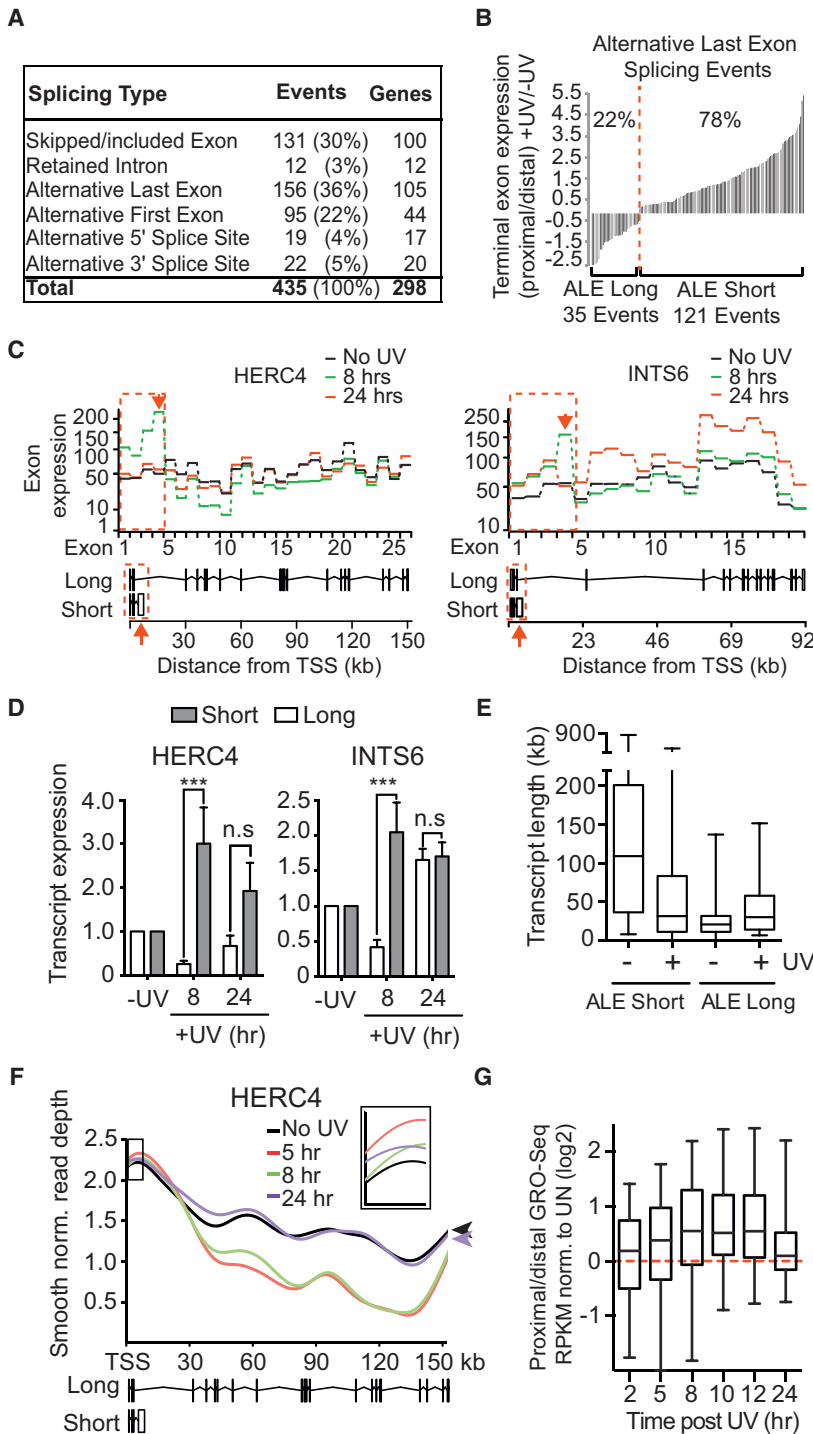


Figure 2. Splicing Analysis Reveals Frequent UV-Induced Alternative Last Exon Splicing

(A) UV-induced splicing events. (B) Relative expression of terminal exons associated with UV-induced ALE splicing events. The ratio of proximal to distal terminal exon was calculated for the UV-treated sample and normalized to the control. (C) Exon expression profiles for *HERC4* and *INTS6* upon UV irradiation. Red, dashed box indicates exons associated with expression of the short isoform. Schematic illustrations are shown below. Red arrows indicate terminal exons specific to the short isoforms. (D) qRT-PCR validation of isoform expression. GAPDH normalized data relative to untreated conditions. (E) Change in pre-mRNA length of ALE short events (left) and long events (right). Box and whisker plots with min/max/median represent pre-mRNA lengths. (F) GRO-seq signal across *HERC4* after UV exposure (boxed inset, area of short isoform). Arrowheads highlight recovery of gene synthesis at the 3' end after 24 hr. (G) Box and whisker plots (5–95 percentile with min/max/median indicated), showing relative GRO-seq read density of terminal exons following UV irradiation, normalized to untreated. Data for (D) and others like it in the following figures are mean \pm SEM, t test, * $p < 0.05$, ** $p < 0.01$, *** $p < 0.001$ and **** $p < 0.0001$. See also Figures S2 and S3 and Tables S1, S2, and S3.

slowing down and RNAPII-mediated RNA synthesis being “restricted” to the 5' end of genes. This gene-spatial restriction of transcription is associated with, or indeed causes, the preferential expression of short transcript isoforms incorporating alternative last exons.

ASCC3 Short Isoform Is Preferentially Synthesized in Response to UV

We now investigated whether the preferential expression of short ALE isoforms in response to UV irradiation is physiologically important. Gene ontology analysis of the 84 genes that undergo UV-induced ALE short isoform switching revealed that many of them are involved in transcription (Figure S3). We also cross-referenced the genes with a recently compiled database of factors that function in the transcription-related DNA damage response (Boeing et al., 2016). Interestingly, genes with short ALE events were enriched among the highest scoring genes in this database ($p = 0.0077$; Kolmogorov-Smirnoff test), with 28 of the 84 genes being among the 15% highest scorers (Table S3). Among these

to long transcript isoform expression was observed, peaking 8–12 hr after UV (Figure 2G). This increase correlated with a greater reduction in the synthesis of distal than of proximal exons and was specific for UV-induced ALE events (Figures S2D–S2F).

Together, the results presented so far indicate that UV irradiation results in a dramatic change in transcription, with elongation

factors, *ASCC3* stood out: it had the highest score in the multi-omic screening approach (Boeing et al., 2016).

The pre-mRNA giving rise to the long *ASCC3* isoform is 373.5 kb and composed of 42 exons (Figure 3A). The short *ASCC3* isoform is 25 kb in length and shares the first three exons with the long isoform, followed by a unique terminal exon

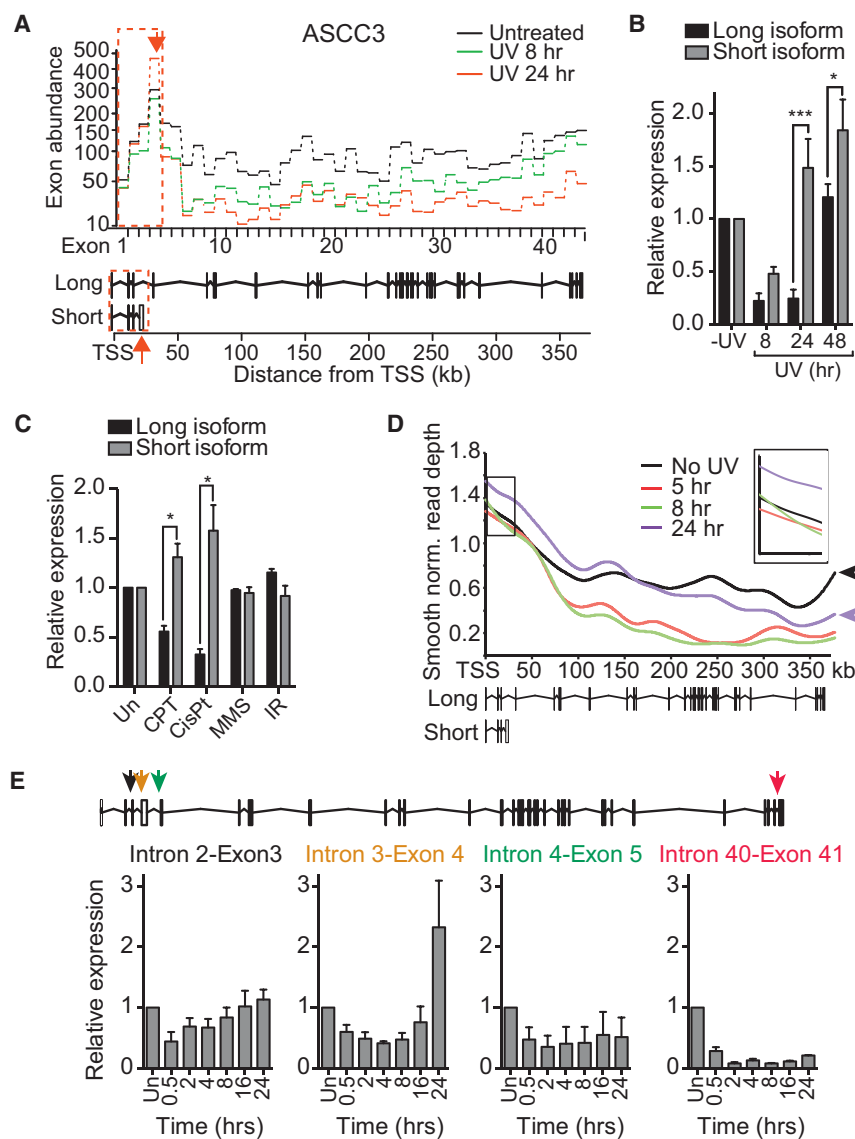


Figure 3. Bulky DNA Lesions Induce ASCC3 Alternative Last Exon Switching

(A) ASCC3 exon expression profiles, as in Figure 2C.

(B) qRT-PCR validation of the isoform switch 24 hr after UV irradiation. GAPDH normalized data relative to untreated conditions are averaged, \pm SEM.

(C) Expression, determined by qRT-PCR, of the different isoforms of ASCC3 upon exposure to 100 nM camptothecin (CPT), 20 μ M cisplatin (CisPt), 0.001% MMS, or 5 Gy ionizing radiation (IR). Untreated conditions (Un) set to 1. GAPDH normalized as in (B).

(D) GRO-seq signal across ASCC3, as in Figure 2F. (E) qRT-PCR of nascent pre-mRNA across ASCC3 after UV irradiation, using intron-exon junction primers (averaged, 18S normalized data, shown relative to untreated).

RNA synthesis across the relevant first 25 kb of the ASCC3 gene was induced at 24 hr (Figure 3D, inset; see also 3E). The transcription characteristics at ASCC3 thus again correlated with ALE switching and preferential production of the short ASCC3 isoform after UV irradiation.

ASCC3 Protein Affects Transcription after UV Irradiation

As expected from the results above, nascent RNA synthesis rapidly decreased after UV exposure as indicated by significantly reduced incorporation of ethynyluridine (EU) into nascent RNA, followed by a slow recovery (Figure S4A). In the multi-omic screening approach, we screened for nascent transcription using the EU incorporation assay to identify genes whose small interfering RNA (siRNA) knockdown affect transcription 20 hr after

UV irradiation (Boeing et al., 2016). Intriguingly, two distinct siRNA pools targeting ASCC3 scored in this screen; one resulted in high transcription while the other resulted in low transcription levels after UV irradiation. Gratifyingly, the distinct siRNA pools targeted different ASCC3 ALE isoforms (Figures 4A and 4B). ASCC3 siRNA pool-1 specifically targets the long mRNA isoform, which encodes the full-length ASCC3 protein. Knockdown with this pool resulted in high transcription levels after UV irradiation, as indicated by a reduced percentage of lowly transcribing cells and an overall increase in EU incorporation signified by a shift of the histogram to the right (Figures 4C and 4D, left histogram). ASCC3 is a component of the poorly studied activating signal co-integrator 1 complex (Jung et al., 2002). ASCC3 was also identified in a screen for genes affecting infection of West Nile virus in interferon (IFN)- β -treated human cells, with silencing of ASCC3 resulting in upregulation of certain interferon-stimulated genes (Li et al., 2013). However, a role for ASCC3 as a

(Figure 3A, last exon indicated by the red arrows). Exon expression for both isoforms was reduced 8 hr after UV treatment. However, 24 hr after UV treatment, expression of the exons of the short isoform increased while those specific for the long isoform remained repressed (Figure 3A). This result was confirmed by qRT-PCR (Figure 3B). Expression of the long isoform recovered by 48 hr after UV treatment. Exposure of cells to cisplatin and camptothecin, but not MMS or ionizing radiation, also resulted in preferential expression of the short ASCC3 isoform, indicating that this is a general response to agents inducing bulky DNA lesions (Figure 3C).

Similar to what was observed for *HERC4*, *INTS6*, and other genes, the increase in the short ASCC3 isoform was likely caused by the restriction of nascent RNA synthesis to the beginning of genes after UV irradiation (Figure 3D). Indeed, recovery of nascent RNA synthesis was only observed over the first half of ASCC3 24 hr after UV treatment. More importantly, however,

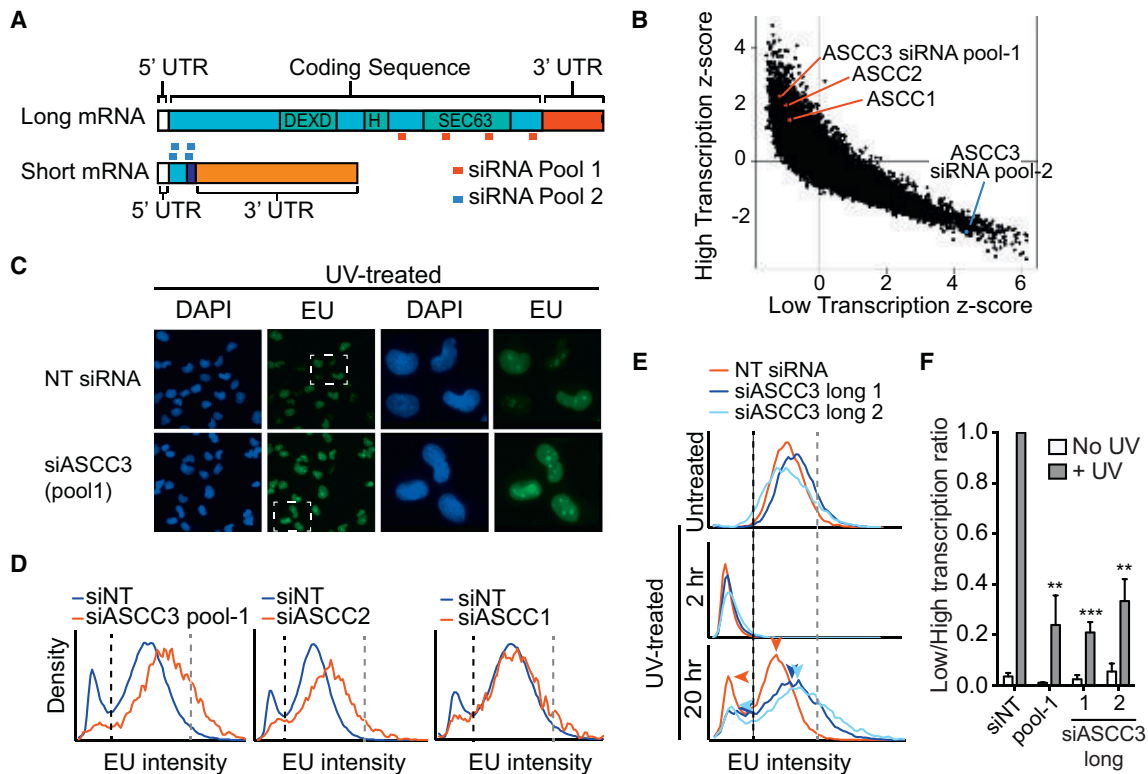


Figure 4. ASCC3 Long Isoform Knockdown Increases Global Transcription after UV Irradiation

(A) ASCC3 isoforms and siRNA-targeting regions. Ninety-three nucleotide sequence not present in the long isoform shown in dark blue. (B) Scores from the genome-wide RNAi screen (Boeing et al., 2016) with ASCC3 (pool-1), ASCC2, and ASCC1 siRNA pools highlighted in red. ASCC3 (pool-2) is highlighted in blue. (C) Representative images of cells transfected with non-targeting (NT) siRNA and the ASCC3 siRNA pool-1 20 hr after UV irradiation. Nascent EU-labeled RNA shown in green and DAPI-stained nuclei in blue. 10 \times objective image on the left, with region in white box enlarged on the right. (D) Histogram plots of average EU incorporation following knockdown of ASCC1, 2 and 3 (pool-1) 20 hr after UV irradiation. Black and gray stippled lines demarcate thresholds of lowly and highly transcribing cells, respectively. (E) EU incorporation after treatment with NT siRNA (red) or individual siRNAs targeting ASCC3 long isoform (light and dark blue), with or without UV irradiation, measured after 2 and 20 hr. Data shown as in (D). Arrowheads highlight reduced proportion of lowly transcribing cells and shift of histogram to the right in cells lacking the long ASCC3 isoform. (F) The ratio of low to high transcribing cells (cells left of the black line over cells right of the gray line in E), in untreated conditions (white bars) or 20 hr after UV irradiation (gray bars). Data were averaged and normalized relative to UV-treated control cells (set to 1), \pm SEM. See also Figure S4.

global suppressor of transcription is both unexpected and exciting. Tellingly, siRNAs targeting two other members of the ASCC complex, ASCC1 and ASCC2, also resulted in increased nascent transcription after UV irradiation (Figures 4B and 4D, center and right histogram), suggesting that the ASCC complex functions as an entity to keep transcription repressed after DNA damage. Moreover, two individual ASCC3 siRNAs, as well as stable shRNA expression targeting the long isoform increased transcription 20 hr after DNA damage, but did not affect transcription in untreated cells, or the immediate transcription shut-down observed 2 hr after UV irradiation (Figures 4E, S4B, top panel, and S4C). The differential effect at 2 and 20 hr is important, as it shows that transcription is suppressed in two distinct ways during UV-induced DNA damage, namely rapid ASCC3-independent transcriptional repression, followed by continued ASCC3-dependent suppression in the later stages of the DNA damage response. To measure the effect of ASCC3 knockdown

at 20 hr quantitatively, we calculated the proportion of cells that fail to recover transcription relative to the proportion of cells that have high levels of transcription after UV irradiation (Figure 4E, lower panel, populations to the left of the stippled black line and right of the gray line, respectively). In response to UV exposure, knockdown of the long isoform of ASCC3 significantly reduced this low/high transcription ratio (Figure 4F). We conclude that the ASCC3 protein, in the context of the ASCC complex, suppresses transcription specifically in the late stages of the cellular response to UV irradiation.

The Short ASCC3 RNA Isoform Is Required to Recover Transcription after UV Irradiation

In marked contrast to siRNA pool-1, ASCC3 siRNA pool-2 dramatically reduced transcription after UV irradiation (Figure 4B). Two of the four siRNAs in pool-2 specifically target sequences unique to the terminal exon of the short alternative

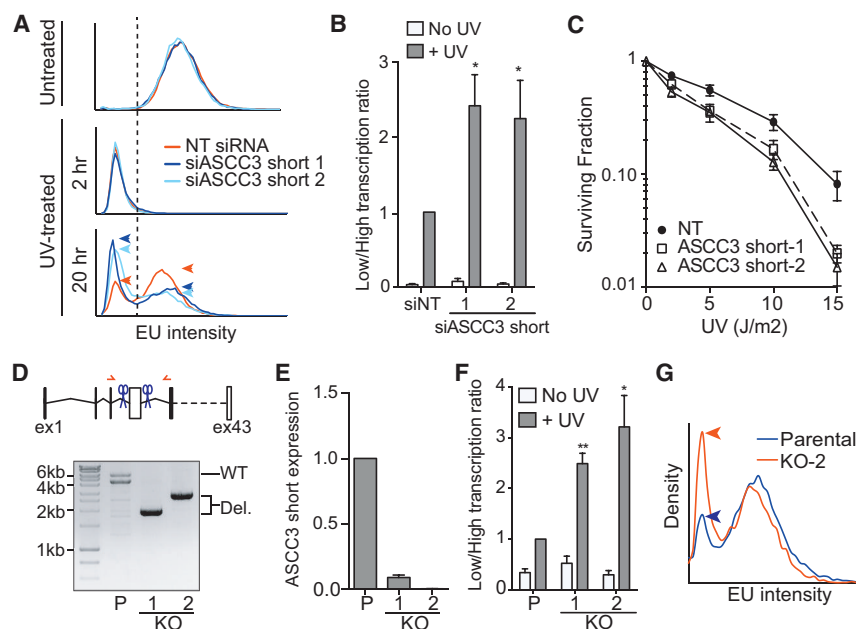


Figure 5. Cells Deficient for the Short ASCC3 Isoform Cannot Recover Transcription after UV Irradiation

(A) As in Figure 4E, but after knockdown of the short ASCC3 isoform with individual siRNAs (light and dark blue).

(B) As in Figure 4F, but after knockdown of short isoform. Data are mean \pm SEM relative to UV-treated control.

(C) UV-sensitivity measured by colony formation after knockdown with individual siRNAs targeting ASCC3 short isoform. Two-way ANOVA test: NT versus ASCC3 siRNA-1 $p = 0.0182$; NT versus ASCC3 siRNA-2 $p = 0.008$.

(D) CRISPR-Cas9-mediated knockout of the unique, terminal exon of the short ASCC3 isoform. Genomic PCR fragments isolated from parental MRC5VA cells (P) and two knockout (KO) clones are shown (red arrows, primers; blue scissors, guide RNAs).

(E) qRT-PCR analysis of short isoform RNA expression in the cell lines from (D), showing averaged GAPDH-normalized data, relative to parental cells.

(F) Transcription recovery after deletion of the short ASCC3 isoform, measured as in Figures 4F and 5B. (G) Histograms showing decreased EU intensity/nucleus in ASCC3 short isoform KO clone-2 cells compared to control cells 20 hr after UV irradiation. See also Figure S5.

transcript isoform (Figure 4A, dark blue box), reducing short isoform transcript levels 79% and 82%, respectively (Figure S4B, lower panel). Knockdown with these siRNAs neither affected transcription in untreated cells, nor did it affect global transcription shutdown immediately after UV irradiation (Figure 5A, top and middle panels). However, in a manner similar to knockdown of Cockayne syndrome B (Figures S4D and S4E), knockdown of ASCC3 short isoform inhibited transcription recovery, as indicated by a marked general change in the characteristics of nascent transcription across the cell population (Figure 5A, 20 hr panel), and consequently an increase in the ratio of lowly to highly transcribing cells after UV irradiation (Figure 5B). Furthermore, knockdown of ASCC3 resulted in increased sensitivity to UV-irradiation (Figure 5C). This indicates that UV-induced expression of the short ASCC3 ALE isoform is indeed physiologically important, in all likelihood because this isoform is required for transcription to recover after UV irradiation.

To confirm the role for the short ASCC3 isoform in transcription recovery, we also used CRISPR-Cas9-mediated gene editing to specifically remove the ALE that is specific to the short isoform, thereby abolishing short isoform expression but leaving the long isoform intact (Figures 5D, 5E, S5A, and S5C). As expected, these knockout cells, hereafter abbreviated “short knockout cells,” also showed a defect in transcription recovery in response to UV (Figures 5F and 5G).

Antagonistic Regulation by the Short and Long ASCC3 Isoforms

In the analysis above, we focused entirely on nascent RNAPII transcription. To further characterize the role of the ASCC3 isoforms in transcription after UV irradiation, we now used Illumina BeadArrays to compare their effect on stable mRNA expression

20 hr after UV irradiation. Compared to UV-treated control cells, 108 genes were differentially expressed in short knockout cells at this time-point, the majority of which (73%, 79/108) were downregulated (Figure 6A; Table S4). In contrast, 170 genes were differentially regulated in cells deficient for ASCC3 long isoform (long knockdown cell), of which 64% (107 genes) were upregulated. Interestingly, many of the genes that were downregulated in short knockout cells were upregulated in long knockdown cells (Figure 6A; p value $< 10^{-5}$, hypergeometric test on differentially regulated probes). qRT-PCR analysis of two such genes, *IL7R* and *VEGFC*, is shown in Figure 6B.

We also noticed that a subset of the genes that were most markedly affected by ASCC3 were in fact greatly induced 20 hr after UV irradiation in control cells. Indeed, the increased expression of five such genes was largely eliminated in short knockout cells (Figure 6C, upper panels). Strikingly, all of these genes were “over-induced” in long knockdown cells (Figure 6C lower panels), again pointing to opposite regulatory effects of the long and short ASCC3 RNA isoforms.

The results presented so far suggest that the long and short ASCC3 isoform are functionally antagonistic: the ASCC complex (of which ASCC3 is a component) maintains transcriptional repression after DNA damage, while the short ASCC3 isoform seems to de-repress it. This raised the intriguing possibility that transcription defect observed in ASCC3 short knockout cells might be rescued by depleting the long isoform. Strikingly, knockdown of the long ASCC3 isoform (Figure 6D), or ASCC2 (Figure S6), did indeed rescue the expression of several genes in short knockout cells following UV irradiation. Moreover, it also rescued the defect in global, nascent transcription recovery after UV irradiation, with the high proportion of lowly transcribing cells observed upon short ASCC3 knockdown (KD) or knockout

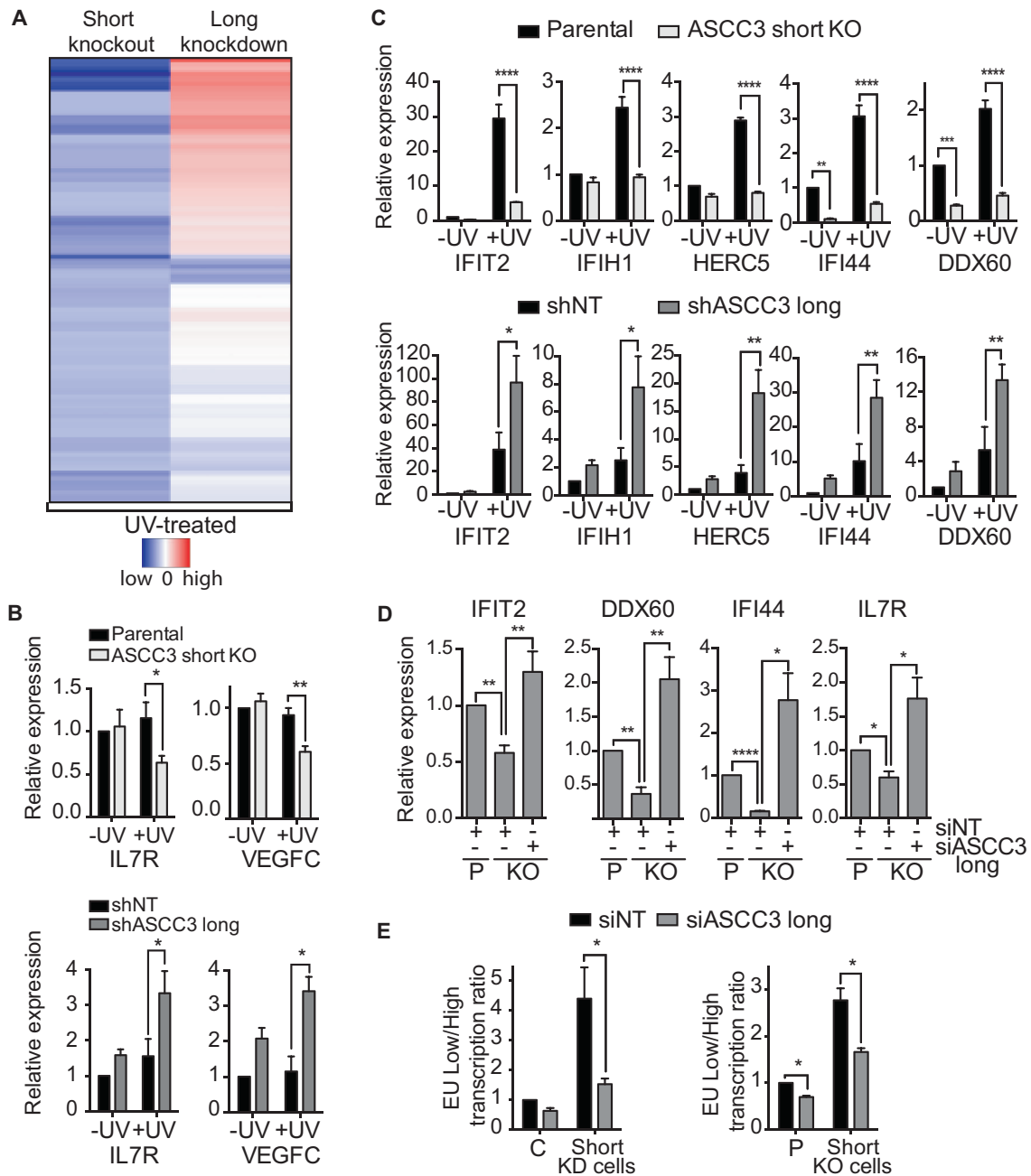


Figure 6. Numerous UV-Regulated Genes Are Antagonistically Regulated by the Long and Short ASCC3 Isoforms

(A) Hierarchical clustering of genes downregulated in UV-treated ASCC3 short knockout cells, shown alongside expression of the same genes in UV-treated ASCC3 Long knockdown cells, relative to expression in control cells. Blue and red bars indicate minimum and maximum log fold-changes, respectively.

(B) qRT-PCR analysis of *IL7R* and *VEGFC* expression in UV-treated short KO cells (light gray; top panel) compared to parental cells and in UV-treated long knockdown cells (dark gray; bottom panel) compared to NT shRNA cells (black) 20 hr after UV, shown as averaged GAPDH-normalized data, relative to untreated controls.

(C) As in (B) but analysis of genes with UV-induced expression.

(D) Rescue of gene expression in UV-treated short KO cells by transfection with siRNA targeting the long isoform. Analysis by qRT-PCR, with GAPDH-normalized data shown relative to UV-treated control cells.

(E) As in (D) but for global nascent transcription, as indicated by the low/high transcription ratio 20 hr after UV irradiation, relative to control cells. C, siNT control; P, parental control.

See also Figure S6 and Table S4.

(KO) returning to more normal levels when the long isoform was also depleted (Figure 6E). Importantly, knockdown of the long isoform did not affect expression of the short RNA isoform and vice versa (Figures S5A and S5B), showing that simple regulation of each other's expression cannot underlie the antagonistic effects observed.

Together, these results support the idea that the long and short ASCC3 isoforms have opposing regulatory roles in transcription, affecting both global nascent transcription and stable mRNA expression of several individual genes in opposite directions.

ASCC3 Short Isoform Functions as a Non-coding RNA

The UV-induced short mRNA isoform contains a 333 nt coding sequence (CDS), the protein product of which is only 13 kDa and lacks known functional domains (see Figure 4A). Frustratingly, ectopic expression of this CDS failed to suppress the low transcription phenotype of short knockdown cells (Figures S7A and S7B). Repeated, unsuccessful attempts prompted us to consider the possibility that it might not be the protein-coding function of the short isoform that is important. Interestingly, in addition to the 333 nt CDS, the endogenous ASCC3 short isoform transcript also contains a 2.8 kb 3' untranslated region (3'-UTR), which is unique to this isoform (Figure 4A). To test the hypothesis that the function of the ASCC3 short mRNA isoform required the non-coding 3' RNA sequence, we again expressed ASCC3 short isoform, this time including the 3' sequence, which does not itself contain open reading frames (ORFs) of significant length. Importantly, the 13 kDa encoded protein was expressed to similar levels irrespective of inclusion of the 3'-UTR in the transcript (Figure S7B). Remarkably, however, in contrast to the CDS alone, the transcript containing the 3'-UTR suppressed the low transcription phenotype (Figures 7A and 7B).

These results suggest that the short ASCC3 isoform promotes transcription restart via a mechanism that is mediated by RNA, not protein. To further investigate this possibility, we assessed cells for expression of the protein encoded by the short ASCC3 isoform. Although the 13 kDa protein product of this isoform could be detected following ectopic expression using an antibody targeted toward its unique C terminus (Figure S7B), the protein could not be detected in untransfected cells. We therefore generated an antibody against an N-terminal epitope of ASCC3, which is shared between the long and short protein isoforms. Immunoprecipitation using this antibody pulled down the large (251 kDa) ASCC3 protein as well as the ectopically expressed 13 kDa isoform, but the endogenous short protein isoform could not be detected, neither by immunoblotting nor targeted mass spectroscopy (Figure S7C, and data not shown).

To more conclusively test whether ASCC3 short isoform was indeed functioning as a non-coding RNA, we now used the construct expressing the CDS with its 3'UTR, but this time inserting a premature stop mutation at the beginning of the CDS. As expected, this construct failed to produce protein (Figure S7B). Nevertheless, it rescued the low transcription phenotype in cells deficient for the short isoform (Figures 7A–7D), showing that the short ASCC3 isoform must function as a non-coding RNA.

RNA in situ hybridization experiments revealed that the short ASCC3 isoform transcript is overwhelmingly nuclear with some enrichment in discrete spots within the nucleus (Figure 7E). Localization was not significantly affected by UV irradiation, and the knockout cells lost the signal, confirming that the probes for in situ hybridization were specific (Figures S7D and S7E). In contrast, probes targeting the protein-coding long ASCC3 isoform produced a signal in both the nucleus and cytoplasm (Figure 7E). Biochemical cell fractionation producing cytoplasmic (S1), nucleoplasmic (S2), and chromatin-enriched (P2) fractions (Figure 7F) further revealed that the short ASCC3 isoform is primarily chromatin-associated (Figure 7G), similar to other long non-coding RNAs (lncRNAs), including MALAT-1 (Figure S7F).

Together, these data show that the short ASCC3 isoform functions as a non-coding RNA in the nucleus of human cells.

DISCUSSION

In this report, we provide evidence for a dramatic and global effect of UV irradiation on transcript elongation, which impacts RNA processing and provides significant potential for cellular regulation. UV exposure results in spatial restriction of transcription and slower elongation, with the result that only the promoter-proximal 20–25 kb are efficiently transcribed. Together, these events underlie a switch to expression of short mRNA isoforms and preferential use of alternative last exons in a number of genes, including ASCC3. Intriguingly, the switch between ASCC3 isoforms occurs on more than one level, in that the long mRNA isoform encodes a protein, functioning in the context of the ASCC complex and required for maintaining transcriptional suppression in the late stages of the DNA damage response, whereas the short isoform functions as a nuclear non-coding RNA that is required for transcription to recover. Intriguingly, the short and long isoforms constitute an autonomous regulatory module and functionally interrelate, so that the effect of deleting one can be at least partially compensated for by deleting the other (Figure 7H).

Preferential Short ALE Isoform Expression in Response to Elongation Shutdown

The spatial restriction of transcription is surprising, but might allow some short genes to remain expressed after UV irradiation. Indeed, this phenomenon may finally explain the puzzling observation that human genes that remain expressed or are induced upon UV irradiation are invariably very short (McKay et al., 2004).

The significant spatial restriction of transcription activity and attenuation of elongation also explains the reduction in expression of long transcript isoforms, while the relative persistence of promoter-proximal RNA synthesis allows expression of short mRNA isoforms. Indeed, it seems obvious that region-restricted transcription, combined with slow transcript elongation, must underlie the increased expression of ALEs associated with these short RNA isoforms. Interestingly, data from others support the idea that recognition and inclusion of an ALE might slow transcription down even further (Kwak et al., 2013; Nojima et al., 2015) and thus promote the usage of otherwise dormant poly-A sites (Pinto et al., 2011). In this sense, ALE isoform expression might arguably also be classified as alternative termination/

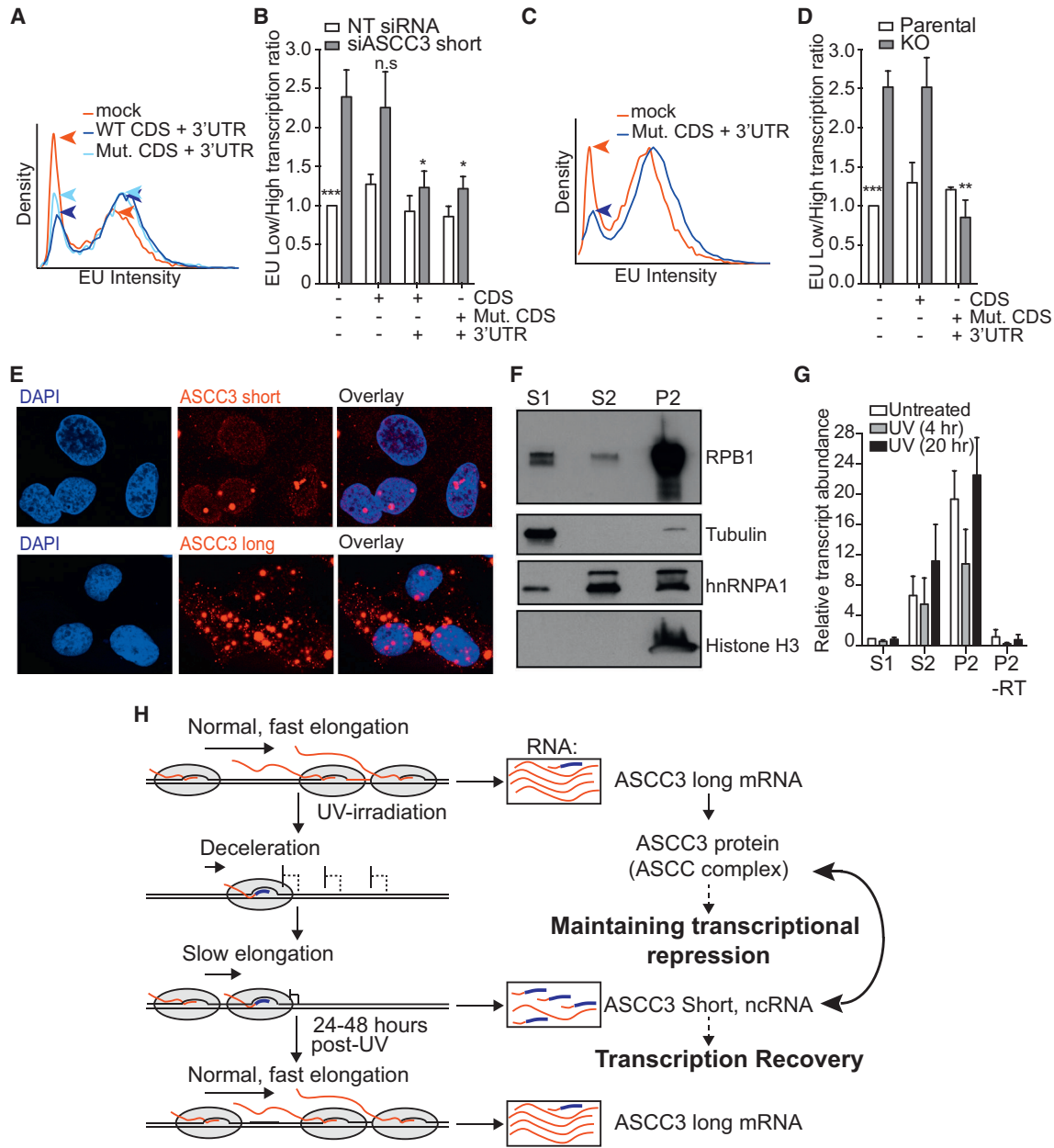


Figure 7. The Short ASCC3 Isoform Is a Chromatin-Associated lncRNA

(A and B) Histogram (A) and low/high transcription ratio plot (B), showing the effect on transcription of expressing different siRNA-resistant RNAs in ASCC3 short isoform knockdown cells. (A) Blue arrows indicate the reduction in lowly transcribing cells and concomitant increase in highly transcribing cells following rescue with ASCC3 short isoform constructs containing the 3'UTR. Data in (B) are relative to UV-treated control cells, mean \pm SEM. n.s., not significant; CDS, coding sequence; Mut. CDS, stop-containing CDS mutant.

(C and D) As in (A) and (B) but for short isoform knockout cells.

(E) RNA scope In situ hybridization signals for endogenous ASCC3 long and short isoforms. RNA scope signal (red) was overlaid with DAPI to highlight nuclear localization.

(F) Immunoblot showing localization of RNAPII (RPB1 subunit), hnRNPA1, tubulin, and histone H3 following sub-cellular fractionation. S1, cytoplasmic; S2, soluble nuclear material; P2, chromatin pellet.

(G) Enrichment of the short ASCC3 isoform in the S2 and P2 fractions as determined by qRT-PCR. As control, P2 was analyzed without reverse transcriptase (-RT). Data are relative to untreated S1 fraction, mean \pm SEM.

(H) Model showing RNAPII (gray sphere) producing nascent ASCC3 transcript (red), including the alternative last exon (thick blue line). Splicing determines exclusion/inclusion of the ALE and 3'-UTR (boxes on right). The protein-encoding long isoform mRNA and the non-coding short isoform have opposite effects on the DNA damage response and affect each other's function (indicated by double arrow on right).

See also Figure S7.

poly-adenylation (poly-A) events, due to the inherently different poly-A sites associated with these transcript isoforms.

The Transcriptional Response to UV Irradiation Is Multi-layered and Complex

The analysis presented here uncovers an unexpectedly complex transcriptional response to UV exposure, as well as novel proteins and a non-coding RNA involved in regulating it. The transcription response can be sub-divided into several distinct phases. First, the immediate response to UV irradiation is a rapid and dramatic decrease in transcript elongation rates, within minutes of exposure. Second, this is followed by a decrease in transcriptional initiation within 2 hr of exposure. Together, these events constitute the molecular manifestation of the long established “global transcription shutdown” first observed decades ago (Mayne and Lehmann, 1982).

Third, a state of slow elongation is sustained for at least 12 hr following UV irradiation, despite the fact that lesion density is greatest immediately after UV irradiation and lesion removal in genes occurs at an exponential rate with a half-life of 8 hr after 15 J/m² irradiation (Venema et al., 1990). This strongly suggests that the transcriptional response to UV irradiation is not caused solely by RNAPII stalling at DNA damage, but that UV irradiation also results in the activation of protein factors and pathways *in trans*. In support of this idea, our ongoing experiments with mutants from the screen for genes affecting transcription after DNA damage that also uncovered ASCC3 (Boeing et al., 2016), as well as recent data on *PRC1* and *UBR5* (Sanchez et al., 2016), strongly indicate that certain protein factors are indeed required for UV-induced transcription shutdown to take place. Without these factors, transcription continues even in the presence of DNA damage.

Fourth, as outlined in detail here, the widespread repression of transcription is maintained in the late phases of the UV-induced DNA damage response by a novel, separate mechanism, namely via ASCC complex-mediated transcriptional suppression. Interestingly, ASCC3 is not required for the establishment of transcriptional repression, only for maintaining it. Remarkably, this intriguing suppression mechanism is negated by the action of the short ASCC3 RNA isoform, which ultimately allows transcription to recover.

ALE Isoform Expression of ASCC3 Regulates the Transcription Response to UV Irradiation

Our data on ASCC3 comprise evidence that the UV-induced shift to expression of short ALE transcript isoforms represents physiologically important regulation. Intriguingly, knockdown of the long ASCC3 isoform rescues the transcription defect in cells lacking the short isoform, highlighting that the long and short isoforms regulate one another to control transcription after UV irradiation. This indicates that the balance between long and short isoform expression, which is temporarily altered as a consequence of UV irradiation, is critical for regulating transcription shutdown and recovery.

Despite being annotated as protein-coding, the short ASCC3 transcript isoform is nuclear and may in fact not be translated to a significant extent. Indeed, its function in transcriptional restart after UV irradiation is dependent on the non-coding 3'

UTR and is retained after its coding ability is disrupted. The short ASCC3 RNA isoform likely functions as a non-coding RNA. Long non-coding RNAs (lncRNAs) are generally bioinformatically characterized by being relatively stable, RNAPII-generated RNAs lacking ORFs of 300 nts or more (Derrien et al., 2012). However, the distinction between mRNAs and lncRNAs is often somewhat blurred (Sampath and Ephrussi, 2016), and our data show that even though the short ASCC3 isoform does contain an ORF of 333 nts, it is functionally a lncRNA (of ~3,500 bases). This points to a previously uninvestigated source of lncRNAs, namely alternative last exon (ALE)-derived, non-coding transcript isoforms produced from well-known protein-coding genes. To our knowledge, the only other example of a gene with alternative protein coding and functional lncRNA transcript isoforms is steroid receptor RNA activator 1 (*SRA*). Ironically, in contrast to ASCC3, *SRA* was long thought to encode a lncRNA, which regulates steroid hormone receptor driven transcription, but it may also produce ORF-containing alternative transcript variants that can be translated into protein. Unlike ASCC3, however, *SRA* produces alternative protein-coding splicing isoforms through mechanisms that introduce AUG codons not present in the lncRNA isoform (reviewed by Leygue, 2007).

The short ASCC3 RNA isoform appears to function, at least in part, by repressing the function of the ASCC complex, of which ASCC3 protein is a DEAD/DEAH box DNA helicase component (Jung et al., 2002; Dango et al., 2011). ASCC3/ASCC complex was identified through its role in transcriptional regulation (Jung et al., 2002; Li et al., 2013), but its biochemical mechanism of action remains unknown. We found that ASCC3 interacts with both RNAPII and CSB and it becomes highly ubiquitinated and phosphorylated upon UV irradiation (Boeing et al., 2016), suggesting a direct effect on transcription and regulation via post-translational modification. Understanding the biochemical function of ASCC complex is an important future goal, not least because it is a prerequisite for understanding the function of the ASCC3 lncRNA. Although we have so far failed to uncover convincing evidence for it, one possibility is that the chromatin-associated ASCC3 lncRNA regulates transcription through binding and regulating the ASCC complex. However, it might also function through recruitment of other factors. For example, lncRNAs such as HOTAIR and XIST both regulate transcription through recruitment of histone modification complexes and in the case of HOTAIR, even ubiquitin ligases (Bhan and Mandal, 2015; Rutenberg-Schoenberg et al., 2016). Two DNA damage-induced lncRNAs, lincRNA-p21 and PANDA, regulate p53-mediated gene expression by interacting with DNA/RNA binding proteins, resulting in gene-specific repression (Huarte et al., 2010; Hung et al., 2011). Post-transcriptional mechanisms for lncRNA function have also been described, including miRNA sequestering and regulating mRNA decay and translation (Abdelmohsen et al., 2013).

Other UV-Induced ALE Genes

Intriguingly, our analysis uncovered a number of other genes with characteristics similar to those of ASCC3. For example, *INTS6* encodes an 887 amino acid (aa) protein, which is a subunit of the Integrator complex (Baillat et al., 2005). Upon UV irradiation,

however, a much shorter RNA isoform is expressed, with the capacity to encode a 115 aa protein, which lacks the C-terminal region required for association with INTS3 and presumably the rest of the Integrator complex (Zhang et al., 2013). Likewise, *HERC4* encodes a putative ubiquitin ligase (1,057 aa), but also a short UV-induced isoform potentially encoding a 110 aa protein, which lacks the catalytic domain. Other interesting examples, such as *SUPT16H* (encoding the large subunit of the histone chaperone FACT) and *RAD51C* (involved in homologous DNA recombination) were also detected. Again, both encode very short, UV-induced isoforms, which might not result in functional proteins. Some of these short protein isoforms have been detected in a deep proteome sequencing project (Kim et al., 2014), but it is unclear whether they are functionally relevant, or whether, like for *ASCC3*, the short, stable, poly-adenylated transcript isoforms encoding them act in the form of lncRNAs. Addressing the precise function of these transcripts in the DNA damage response represents an important future goal.

STAR★METHODS

Detailed methods are provided in the online version of this paper and include the following:

- KEY RESOURCES TABLE
- CONTACT FOR REAGENT AND RESOURCE SHARING
- EXPERIMENTAL MODEL AND SUBJECT DETAILS
- METHOD DETAILS
 - Cell line manipulation and generation
 - GRO-Seq
 - RNA-Seq
 - Reverse Transcriptase Quantitative PCR
 - 5' Ethynyl Uridine transcription assay
 - Clonogenic Survival Assay
 - Gene expression array
 - Subcellular fractionation
 - Ectopic expression of *ASCC3* short isoform constructs
 - Immunoprecipitation/Immunoblotting
 - RNA in situ hybridization
- QUANTIFICATION AND STATISTICAL ANALYSIS
 - GRO-Seq analysis
 - Gene specific wave-fronts and elongation rate for DRB/GRO-Seq
 - Gene specific wave-fronts for GRO-Seq
 - Mathematically determined wave-fronts for GRO-Seq
 - Single-gene GRO-Seq profiling
 - Terminal exon synthesis analysis
 - RNA-Seq alternative isoform analysis
 - Gene ontology analysis
 - Gene expression array
 - EU Assay
- DATA AND SOFTWARE AVAILABILITY
 - Software

SUPPLEMENTAL INFORMATION

Supplemental Information includes seven figures and five tables and can be found with this article online at <http://dx.doi.org/10.1016/j.cell.2017.01.019>.

AUTHOR CONTRIBUTIONS

Conceptualization, L.W. and J.Q.S.; Methodology, L.W., M.S., S.B., and J.Q.S.; Formal Analysis, S.B., P.E., R.M., G.K., and A.L.; Investigation, L.W., M.S., T.K., J.W., and B.S.-D.; Writing – Original Draft, J.Q.S. and L.W.; Writing – Review & Editing, J.Q.S. and L.W.; Funding Acquisition, J.Q.S.; Supervision, J.Q.S., M.H., and A.S.

ACKNOWLEDGMENTS

This work was supported by the Francis Crick Institute (that receives its core funding from Cancer Research UK [FC001166], the UK Medical Research Council [FC001166], and the Wellcome Trust [FC001166]) and by grants from the European Research Council, Agreements 693327 (TRANSDAM) and 268797 (TRANSINTEG). We thank The Francis Crick Advanced Sequencing Facility, the Cell Services Facility, the High-Throughput Genomics Group at the Wellcome Trust Centre for Human Genetics (funded by Wellcome Trust grant 090532/Z/09/Z) for expression array analysis, and Yang Shi for the kind gift of *ASCC3* antibody. Peter Verrijzer and members of the Svejstrup laboratory are thanked for comments on the manuscript.

This paper is dedicated to Tomas Lindahl, and to the memory of Clare Hall Laboratories, the outstanding research institute he created.

Received: November 12, 2015

Revised: October 27, 2016

Accepted: January 18, 2017

Published: February 16, 2017

REFERENCES

- Abdelmohsen, K., Panda, A., Kang, M.J., Xu, J., Selimyan, R., Yoon, J.H., Martindale, J.L., De, S., Wood, W.H., 3rd, Becker, K.G., and Gorospe, M. (2013). Senescence-associated lncRNAs: senescence-associated long noncoding RNAs. *Aging Cell* 12, 890–900.
- Adam, S., Polo, S.E., and Almouzni, G. (2013). Transcription recovery after DNA damage requires chromatin priming by the H3.3 histone chaperone HIRA. *Cell* 155, 94–106.
- Anders, S., Reyes, A., and Huber, W. (2012). Detecting differential usage of exons from RNA-seq data. *Genome Res.* 22, 2008–2017.
- Andrade-Lima, L.C., Veloso, A., Paulsen, M.T., Menck, C.F., and Ljungman, M. (2015). DNA repair and recovery of RNA synthesis following exposure to ultraviolet light are delayed in long genes. *Nucleic Acids Res.* 43, 2744–2756.
- Baillat, D., Hakimi, M.A., Näär, A.M., Shilatfard, A., Cooch, N., and Shiekhattar, R. (2005). Integrator, a multiprotein mediator of small nuclear RNA processing, associates with the C-terminal repeat of RNA polymerase II. *Cell* 123, 265–276.
- Bhan, A., and Mandal, S.S. (2015). lncRNA HOTAIR: A master regulator of chromatin dynamics and cancer. *Biochim. Biophys. Acta* 1856, 151–164.
- Boeing, S., Williamson, L., Encheva, V., Gori, I., Saunders, R.E., Instrell, R., Aygün, O., Rodriguez-Martinez, M., Weems, J.C., Kelly, G.P., et al. (2016). Multiomic analysis of the UV-induced DNA damage response. *Cell Rep.* 15, 1597–1610.
- Dango, S., Mosammaparast, N., Sowa, M.E., Xiong, L.J., Wu, F., Park, K., Rubin, M., Gygi, S., Harper, J.W., and Shi, Y. (2011). DNA unwinding by *ASCC3* helicase is coupled to ALKBH3-dependent DNA alkylation repair and cancer cell proliferation. *Mol. Cell* 44, 373–384.
- de la Mata, M., Alonso, C.R., Kadener, S., Fededa, J.P., Blaustein, M., Pelisch, F., Cramer, P., Bentley, D., and Kornblihtt, A.R. (2003). A slow RNA polymerase II affects alternative splicing in vivo. *Mol. Cell* 12, 525–532.
- Derrien, T., Johnson, R., Bussotti, G., Tanzer, A., Djebali, S., Tilgner, H., Guernec, G., Martin, D., Merkel, A., Knowles, D.G., et al. (2012). The GENCODE v7 catalog of human long noncoding RNAs: analysis of their gene structure, evolution, and expression. *Genome Res.* 22, 1775–1789.
- Dinant, C., Ampatzidis-Michailidis, G., Lans, H., Tresini, M., Lagarou, A., Grosbart, M., Theil, A.F., van Cappellen, W.A., Kimura, H., Bartek, J., et al. (2013). Enhanced chromatin dynamics by FACT promotes transcriptional restart after UV-induced DNA damage. *Mol. Cell* 51, 469–479.

- Ehrensberger, A.H., Kelly, G.P., and Svejstrup, J.Q. (2013). Mechanistic interpretation of promoter-proximal peaks and RNAPII density maps. *Cell* *154*, 713–715.
- Fong, N., Kim, H., Zhou, Y., Ji, X., Qiu, J., Saldi, T., Diener, K., Jones, K., Fu, X.D., and Bentley, D.L. (2014). Pre-mRNA splicing is facilitated by an optimal RNA polymerase II elongation rate. *Genes Dev.* *28*, 2663–2676.
- Gaillard, H., and Aguilera, A. (2013). Transcription coupled repair at the interface between transcription elongation and mRNA biogenesis. *Biochim. Biophys. Acta* *1829*, 141–150.
- Huang, W., Sherman, B.T., and Lempicki, R.A. (2009). Systematic and integrative analysis of large gene lists using DAVID bioinformatics resources. *Nat. Protoc.* *4*, 44–57.
- Huarte, M., Guttman, M., Feldser, D., Garber, M., Koziol, M.J., Kenzelmann-Broz, D., Khalil, A.M., Zuk, O., Amit, I., Rabani, M., et al. (2010). A large intergenic noncoding RNA induced by p53 mediates global gene repression in the p53 response. *Cell* *142*, 409–419.
- Hung, T., Wang, Y., Lin, M.F., Koegel, A.K., Kotake, Y., Grant, G.D., Horlings, H.M., Shah, N., Umbricht, C., Wang, P., et al. (2011). Extensive and coordinated transcription of noncoding RNAs within cell-cycle promoters. *Nat. Genet.* *43*, 621–629.
- Ip, J.Y., Schmidt, D., Pan, Q., Ramani, A.K., Fraser, A.G., Odom, D.T., and Blencowe, B.J. (2011). Global impact of RNA polymerase II elongation inhibition on alternative splicing regulation. *Genome Res.* *21*, 390–401.
- Jung, D.J., Sung, H.S., Goo, Y.W., Lee, H.M., Park, O.K., Jung, S.Y., Lim, J., Kim, H.J., Lee, S.K., Kim, T.S., et al. (2002). Novel transcription coactivator complex containing activating signal cointegrator 1. *Mol. Cell. Biol.* *22*, 5203–5211.
- Katz, Y., Wang, E.T., Airoldi, E.M., and Burge, C.B. (2010). Analysis and design of RNA sequencing experiments for identifying isoform regulation. *Nat. Methods* *7*, 1009–1015.
- Kim, D., Pertea, G., Trapnell, C., Pimentel, H., Kelley, R., and Salzberg, S.L. (2013). TopHat2: accurate alignment of transcriptomes in the presence of insertions, deletions and gene fusions. *Genome Biol.* *14*, R36.
- Kim, M.S., Pinto, S.M., Getnet, D., Nirujogi, R.S., Manda, S.S., Chaerkady, R., Madugundu, A.K., Kelkar, D.S., Isserlin, R., Jain, S., et al. (2014). A draft map of the human proteome. *Nature* *509*, 575–581.
- Kwak, H., Fuda, N.J., Core, L.J., and Lis, J.T. (2013). Precise maps of RNA polymerase reveal how promoters direct initiation and pausing. *Science* *339*, 950–953.
- Lawrence, M., Huber, W., Pagès, H., Aboyoun, P., Carlson, M., Gentleman, R., Morgan, M.T., and Carey, V.J. (2013). Software for computing and annotating genomic ranges. *PLoS Comput. Biol.* *9*, e1003118.
- Leygue, E. (2007). Steroid receptor RNA activator (SRA1): unusual bifaceted gene products with suspected relevance to breast cancer. *Nucl. Recept. Signal.* *5*, e006.
- Li, H., and Durbin, R. (2009). Fast and accurate short read alignment with Burrows-Wheeler transform. *Bioinformatics* *25*, 1754–1760.
- Li, H., Handsaker, B., Wysoker, A., Fennell, T., Ruan, J., Homer, N., Marth, G., Abecasis, G., and Durbin, R.; 1000 Genome Project Data Processing Subgroup (2009). The Sequence Alignment/Map format and SAMtools. *Bioinformatics* *25*, 2078–2079.
- Li, J., Ding, S.C., Cho, H., Chung, B.C., Gale, M., Jr., Chanda, S.K., and Diamond, M.S. (2013). A short hairpin RNA screen of interferon-stimulated genes identifies a novel negative regulator of the cellular antiviral response. *MBio* *4*, e00385-13.
- Livak, K.J., and Schmittgen, T.D. (2001). Analysis of relative gene expression data using real-time quantitative PCR and the 2⁻(Delta Delta C(T)) method. *Methods* *25*, 402–408.
- Mayer, A., di Iulio, J., Maleri, S., Eser, U., Vierstra, J., Reynolds, A., Sandstrom, R., Stamatoyannopoulos, J.A., and Churchman, L.S. (2015). Native elongating transcript sequencing reveals human transcriptional activity at nucleotide resolution. *Cell* *161*, 541–554.
- Mayne, L.V., and Lehmann, A.R. (1982). Failure of RNA synthesis to recover after UV irradiation: an early defect in cells from individuals with Cockayne's syndrome and xeroderma pigmentosum. *Cancer Res.* *42*, 1473–1478.
- McKay, B.C., Stubbert, L.J., Fowler, C.C., Smith, J.M., Cardamore, R.A., and Spronck, J.C. (2004). Regulation of ultraviolet light-induced gene expression by gene size. *Proc. Natl. Acad. Sci. USA* *101*, 6582–6586.
- Muñoz, M.J., Pérez Santangelo, M.S., Paronetto, M.P., de la Mata, M., Pelisch, F., Boireau, S., Glover-Cutter, K., Ben-Dov, C., Blaustein, M., Lozano, J.J., et al. (2009). DNA damage regulates alternative splicing through inhibition of RNA polymerase II elongation. *Cell* *137*, 708–720.
- Nojima, T., Gomes, T., Grosso, A.R., Kimura, H., Dye, M.J., Dhir, S., Carmo-Fonseca, M., and Proudfoot, N.J. (2015). Mammalian NET-seq reveals genome-wide nascent transcription coupled to RNA processing. *Cell* *161*, 526–540.
- Pan, Q., Shai, O., Lee, L.J., Frey, B.J., and Blencowe, B.J. (2008). Deep surveying of alternative splicing complexity in the human transcriptome by high-throughput sequencing. *Nat. Genet.* *40*, 1413–1415.
- Pinto, P.A., Henriques, T., Freitas, M.O., Martins, T., Domingues, R.G., Wyrzykowska, P.S., Coelho, P.A., Carmo, A.M., Sunkel, C.E., Proudfoot, N.J., and Moreira, A. (2011). RNA polymerase II kinetics in polo polyadenylation signal selection. *EMBO J.* *30*, 2431–2444.
- Proietti-De-Santis, L., Drané, P., and Egly, J.M. (2006). Cockayne syndrome B protein regulates the transcriptional program after UV irradiation. *EMBO J.* *25*, 1915–1923.
- Ritchie, M.E., Phipson, B., Wu, D., Hu, Y., Law, C.W., Shi, W., and Smyth, G.K. (2015). Limma powers differential expression analyses for RNA-sequencing and microarray studies. *Nucleic Acids Res.* *43*, e47.
- Rockx, D.A., Mason, R., van Hoffen, A., Barton, M.C., Citterio, E., Bregman, D.B., van Zeeland, A.A., Vrieling, H., and Mullenders, L.H. (2000). UV-induced inhibition of transcription involves repression of transcription initiation and phosphorylation of RNA polymerase II. *Proc. Natl. Acad. Sci. USA* *97*, 10503–10508.
- Rutenberg-Schoenberg, M., Sexton, A.N., and Simon, M.D. (2016). The properties of long noncoding RNAs that regulate chromatin. *Annu. Rev. Genomics Hum. Genet.* *17*, 69–94.
- Sampath, K., and Ephrussi, A. (2016). CncRNAs: RNAs with both coding and non-coding roles in development. *Development* *143*, 1234–1241.
- Sanchez, A., De Vivo, A., Uprety, N., Kim, J., Stevens, S.M., Jr., and Kee, Y. (2016). BMI1-UBR5 axis regulates transcriptional repression at damaged chromatin. *Proc. Natl. Acad. Sci. USA* *113*, 11243–11248.
- Saponaro, M., Kantidakis, T., Mitter, R., Kelly, G.P., Heron, M., Williams, H., Söding, J., Stewart, A., and Svejstrup, J.Q. (2014). RECQL5 controls transcript elongation and suppresses genome instability associated with transcription stress. *Cell* *157*, 1037–1049.
- Venema, J., Mullenders, L.H., Natarajan, A.T., van Zeeland, A.A., and Mayne, L.V. (1990). The genetic defect in Cockayne syndrome is associated with a defect in repair of UV-induced DNA damage in transcriptionally active DNA. *Proc. Natl. Acad. Sci. USA* *87*, 4707–4711.
- Vichi, P., Coin, F., Renaud, J.P., Vermeulen, W., Hoeijmakers, J.H., Moras, D., and Egly, J.M. (1997). Cisplatin- and UV-damaged DNA lure the basal transcription factor TFIID/TBP. *EMBO J.* *16*, 7444–7456.
- Wang, E.T., Sandberg, R., Luo, S., Khrebtkova, I., Zhang, L., Mayr, C., Kingsmore, S.F., Schroth, G.P., and Burge, C.B. (2008). Alternative isoform regulation in human tissue transcriptomes. *Nature* *456*, 470–476.
- Wilson, M.D., Harreman, M., and Svejstrup, J.Q. (2013). Ubiquitylation and degradation of elongating RNA polymerase II: the last resort. *Biochim. Biophys. Acta* *1829*, 151–157.
- Zhang, F., Ma, T., and Yu, X. (2013). A core hSSB1-INTS complex participates in the DNA damage response. *J. Cell Sci.* *126*, 4850–4855.

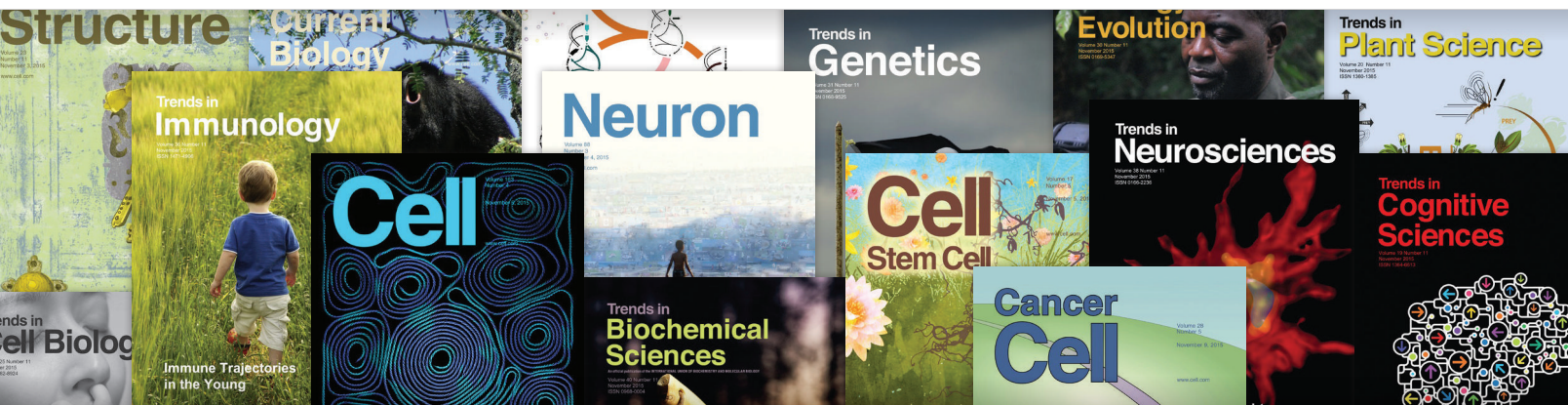


**DON'T BE THE
LAST TO KNOW**

Give your research a boost with alerts from Cell Press. You'll be glad you did.

Get first access with immediate, regular electronic table of contents (eToCs) alerts delivered directly to your desktop, free of charge, that keep you informed of breakthroughs in your field.

Exciting extra features like video abstracts, podcasts, and blog posts give you additional depth and context and you can access news and commentary, normally not accessible online, in advance of publication.



Register today
Visit cell.com/alerts

CellPress

Accelerate your neuropathology research

Identify novel interactions across 23 key pathways in less than 24 hours

nCounter[®] Neuropathology Gene Expression Panel

23 neurodegenerative pathways and processes

15 mins hands on time, publishable data in less than 24 hours

770 genes with option to add custom content

Profile disease mechanisms, response to drug treatment and biomarker characterization

View the gene list at nanosttring.com/neuro

FOR RESEARCH USE ONLY. Not for use in diagnostic procedures.
© 2017 NanoString Technologies, Inc. All rights reserved.

nanosttring



Nikon
100th
anniversary

A1ways Evolving

NEW High Definition 1K Resonant Scanner

Open up a world of new imaging strategies and possibilities with the latest upgrade to Nikon's always evolving A1R+ confocal microscope system. The all-new High Definition 1K Resonant Scanner delivers high resolution images at ultra-high speed. The new scanner also provides 4x the field of view at the same resolution usually generated by a normal 512x512 scanner. The wide dynamic range and reduced noise level raises the bar for image quality in resonant scanners.

For more information, go to www.nikoninstruments.com/a1r
or call 1-800-52-NIKON.

